# Stability and Change in Gulf of Mexico Chemosynthetic Communities

## Volume II:  Technical Report



**U.S. Department of the Interior**
**Minerals Management Service**
**Gulf of Mexico OCS Region**

# Stability and Change in Gulf of Mexico Chemosynthetic Communities

## Volume II:  Technical Report

Editor

Ian R. MacDonald

Prepared under MMS Contract
14-35-0001-30813
by
Texas A&M University
Geochemical and Environmental Research Group
833 Graham Road
College Station, Texas  77845

Published by

# Table of Contents

# LIST OF FIGURES

# LIST OF TABLES

## DISCLAIMER

This report was prepared under contract between the Minerals Management Service (MMS) and the Texas A&M Research Foundation. This report has been technically reviewed by the MMS, and it has been approved for publication. Approval does not signify that the contents necessarily reflect the views and policies of the MMS, nor does mention of trade names or commercial products constitute endorsement or recommendation for use. It is, however, exempt from review and compliance with the MMS editorial standards.

## REPORT AVAILABILITY

Extra copies of this report may be obtained from the Public Information Office (Mail Stop 5034) at the following address:

U.S. Department of the Interior
Minerals Management Service
Gulf of Mexico OCS Region
Public Information Office (MS 5034)
1201 Elmwood Park Boulevard
New Orleans, Louisiana 70123-2394

Telephone (504) 736-2519 or
1-800-200-GULF

## CITATION

MacDonald, I.R., ed. 2002. Stability and Change in Gulf of Mexico Chemosynthetic Communities. Volume II: Technical Report. Prepared by the Geochemical and Environmental Research Group, Texas A&M University. U.S. Dept. of the Interior, Minerals Mgmt. Service, Gulf of Mexico OCS Region, New Orleans, LA. OCS Study MMS 2002-036. 456 pp.

## COVER ART

Submersible sampling operations with submarine Johnson *Sea Link*.

# ACKNOWLEDGMENTS

**1.0  Stability and Change in Gulf of Mexico Chemosynthetic Communities Program**


**1.1 Introduction**

This volume is the Final Report for the research program entitled *Stability and Change in Gulf of Mexico Chemosynthetic Communities*. It describes findings obtained from natural hydrocarbon seeps on the continental slope of the northern Gulf of Mexico. This section of the report will outline the purpose and scope of the program as well as the program team jointly responsible for the results. Major milestones of the program are listed along with a compilation of technical articles and scientific presentations that have been produced while the program was underway.

The program was conducted under the auspices of the Texas A&M Research Foundation under contract (Contract No. 1435-01-96-CT-30813) to the Department of the Interior, Minerals Management Service (MMS). The contract was awarded on 31 October 1996 and has been completed over 42 months through the efforts of a multi-disciplinary team from a number of research institutions. The present research program is the second major research effort funded by the Minerals Management Service to address this topic. The *Chemosynthetic Ecosystems Study* (CHEMO I) was conducted between 1992 and 1995 as the primary assessment of the ecology of natural oil seeps on the Gulf of Mexico continental slope (MacDonald *et al.* 1995).

The continued research has been designed to aid the Minerals Management Service in the scientifically sound management of living resources found at hydrocarbon seeps on the northern Gulf of Mexico continental slope. An integrated, multi-disciplinary approach was proposed to address the complex issues associated with the protection of these biological assemblages. As such, the program encompasses ecological studies at both regional and local scales as well as an evaluation of temporal changes in these communities. Stability and change within these communities should be understood in the context of their interactions within the geological, chemical, and oceanographic setting. Knowledge of the processes that control the distribution, health, and succession of communities in these environments is necessary to forecast and forestall potential impacts derived from exploration and exploitation of fossil energy reserves on the northern Gulf of Mexico continental slope. Integrated studies were designed to collect ecological, geological, chemical, and oceanographic information related to the longevity, robustness, senescence, and recovery of chemosynthetic communities.

The team of Principal Investigators (PI) assembled to conduct this research represents some of the foremost researchers in their respective fields. The present program includes community ecological, regional geological, microbial, and site-specific chemical and oceanographic studies. Each PI and his or her associates were responsible for individual components of the program and contributed jointly to the fieldwork and overall synthesis. At the community level, efforts focus on the abiotic factors that control the distribution, abundance, and health of the major chemosynthetic and associated fauna. Investigations of the life history of these organisms are also included. At the regional level, efforts focus on the geological, chemical, and oceanographic processes that support communities including larval dispersion and circulation processes that maintain the genetic stability of these communities.

## 1.2 Key Personnel

The principal investigators, their area of expertise, and the sections of this report to which they contributed are listed in Table 1.1. A three-person Scientific Review Board has provided oversight and review of the program and is also listed in Table 1.1.

Table 1.1. Program Team and Roles. Bold-Face Text
Indicates Chapters of the Present Report to which the Team Members Contributed.

---

### Texas A&M University Investigators
#### Department of Oceanography

| | | |
|---|---|---|
| Dr. John W. Morse | Dr. Rolf Arvidson | Dr. William Sager |
| Inorganic Chemistry | Inorganic Chemistry | Geophysics |
| **Section 9** | **Section 9** | **Section 6** |

#### Geochemical and Environmental Research Group

| | | |
|---|---|---|
| Dr. Norman L. Guinasso, Jr. | Dr. Ian MacDonald | Dr. Gary A. Wolff |
| Physical Oceanography | Program Manager | Data Management |
| **Section 5** | Imaging & GIS | **Section 11** |
| | **Section 7 and editorial review** | |
| Dr. Mahlon C. Kennicutt II | Dr. Roger Sassen | |
| Deputy Program Manager | Hydrocarbon Chemistry | |
| Environmental Chemistry | **Section 10** | |
| **Section 8.5** | | |

### Principal Investigators Not at Texas A&M University

| | | |
|---|---|---|
| Dr. Steven Macko | Dr. Douglas C. Nelson | Dr. Eric Powell |
| University of Virginia | University of California, Davis | Rutgers University |
| Trophic Relationships | Microbial Ecology | Histopathology |
| **Sections 8.6 and 9.3** | **Section 8.1** | **Section 8.5** |
| Dr. Robert Carney | Dr. Paul Montagna | Dr. Samantha Joye |
| Louisiana State University | University of Texas at Austin | University of Georgia |
| Trophic Relationships | Statistical Design | Electrochemistry |
| **Section 8.6** | **Section 11** | **Section 9.4** |
| Dr. Charles R. Fisher | Dr. Steve Schaeffer | |
| Pennsylvania State University | Pennsylvania State University | |
| Physiological Ecology | Molecular Ecology and Genetics | |
| **Sections 8.3 and 8.4** | **Section 8.7** | |

### Scientific Review Board

| | | |
|---|---|---|
| Dr. James Barry | Dr. Cindy Lee Van Dover | Dr. William W. Schroeder |
| Monterey Bay Aquarium Research Institute | William and Mary University | The University of Alabama |

## 1.3 Program Milestones

Stability and Change in Gulf of Mexico Chemosynthetic Communities (hereafter abbreviated as CHEMO II) was awarded in 1996. It has progressed through planning, sampling, and analytical phases. The program now concludes with the reporting phase. The program milestones listed in Table 1.2 summarize major field efforts, workshops, and presentations of program results to public audiences.

Table 1.2 Program Milestones.

| | |
|---|---|
| October 1-8, 1996 | Program award and post-award meeting of investigators |
| June 3-15, 1997 | Geophysical survey cruise with R/V GYRE |
| July 8-31, 1997 | Community sampling cruise with submarine Johnson SEA-LINK and R/V EDWIN LINK |
| December 18, 1997 | Presentations at the MMS Information Transfer Meeting, New Orleans, LA |
| May 18-22, 1998 | Ground-truth survey with Submarine NR-1 |
| July 1-15, 1998 | Community sampling cruise with submarine Johnson SEA-LINK and R/V EDWIN LINK |
| September 1998 | Interim Report Completed |
| December 4, 1998 | Presentations at the MMS Information Transfer Meeting, New Orleans, LA |
| May 21-23, 1999 | Synthesis Workshop, College Station, TX |
| November 30, 1999 | Presentations at the MMS Information Transfer Meeting, New Orleans, LA |
| January 27, 2000 | Presentations in dedicated session at American Geophysical Union Ocean Sciences Meeting, San Antonio, TX |

## 1.4 Publications, Abstracts, and Graduate Theses

The program team has been very active in presenting and publishing technical articles concerning research results. Although the present report is intended as a definitive presentation to the Minerals Management Service, these publications, as well as follow-on articles that will continue to emerge after the report has been submitted, are critical for recording findings in the peer-reviewed literature and for offering the opportunity for critical review by the scientific community. In addition, graduate student research is vital for training the next generation of marine scientists. Table 1.4 lists open literature references produced by the program.

Table 1.3. Technical Publications Resulting from Preliminary Findings
of the Stability and Change in Gulf of Mexico Chemosynthetic Communities Program.

## Peer-reviewed articles published or in press

Bergquist, D. C., F. M. Williams, and C. R. Fisher. 2000. Longevity record for deep-sea invertebrate. Nature 403: 499-500.

Callender W. R. and Powell, E. N. 1999. Why did ancient chemosynthetic seep and vent assemblages occur in shallower water than they do today? Intl. Jnl. of Earth Sci. 88 (3): 377-391.

Callender R, Powell E.N. 2000. Long-term history of chemoautotrophic clam-dominated faunas of petroleum seeps in the northwestern Gulf of Mexico. FACIES. 43: 177-204.

Fisher, C. R., I. R. MacDonald, R. Sassen, C. M. Young, S. Macko, S. Hourdez, R. Carney, S. Joy, and E. McMullin. 2000. Methane ice worms: *Hesiocaeca methanicola* colonizing fossil fuel reserves. Naturwissenschaften 87 (4): 184-187.

Freytag, J.K., Girguis, P.R., Bergquist, D.C., Andras, J.P., Childress, J.J., Fisher, C.R. 2001. A paradox resolved: Sulfide acquisition by roots of seep tubeworms sustains net chemoautotrophy. PNAS. 98(23): 13408-13413.

Gardiner, S.L., McMullin, E., Fisher, C.R. 2001. *Seepiophila jonesi*, a new genus and species of vestimentiferan tube worm (Annelida : *Pogonophora*) from hydrocarbon seep communities in the Gulf of Mexico. Proc. of the Biol. Soc. of Wash. 114(3): 694-707.

Hourdez, S., L. A. Frederick, A. Schernecke, and C. R. Fisher. 2001. Functional respiratory anatomy of a deep sea orbiniid polychaete from the Brine Pool NR-1 in the Gulf of Mexico. Invertebrate Biology. 120(1): 29-40.

Julian, D., F. Gaill, E. Wood, A. J. Arp, and C. R. Fisher. 1999. Roots as a site of hydrogen sulfide uptake in the hydrocarbon seep vestimentiferan *Lamellibrachia* sp. J. Exp. Biol. 202; 2245-2257.

Lanoil BD, Sassen R, La Duc MT, Sweet ST, Nealson KH. 2001. Bacteria and Archaea physically associated with Gulf of Mexico gas hydrates. Applied and Env. Microbiol. 67 (11): 5143-5153.

Macavoy, S.E., Carney, R.S., Fisher, C.R., and Macko, S.A. 2002. Use of chemosynthetic biomass by large, mobile, benthic predators in the Gulf of Mexico. Mar. Ecol. Prog. Ser. 225: 65-78.

MacDonald, I.R. 1998. Habitat formation at Gulf of Mexico hydrocarbon seeps. Cahiers de Biologie Marine. 39 (3-4): 337-340.

Table 1.3. Continued

MacDonald, I. R., D. Buthman, W. W. Sager, M. B. Peccini, and N. L. Guinasso Jr. 2000. Pulsed flow of hydrocarbons from a mud volcano. Geology. 28(10): 907-910.

McMullin, E., D. C. Bergquist, and C. R. Fisher. 2000. X-metazoans: Real animals in extreme environments. Space Biol. Bull. 13: 1-12.

Nelson, K. and C. R. Fisher. 2000. Absence of cospeciation in deep-sea vestimentiferan tube worms and their bacterial endosymbionts. Symbiosis. 28(1): 1-15.

Powell, E.N., R.D. Barber, M.C. Kennicutt, and S.E. Ford. 1999. Influence of parasitism in controlling the health, reproduction and PAH body burden of petroleum seep mussels. Deep Sea Research. 46. 2053-2078.

Pruski, A. M., A. Fiala-Médioni, C. R. Fisher, and J. C. Colomines. 2000. Free amino compound composition of symbiotic invertebrates from the Gulf of Mexico hydrocarbon seeps. Mar. Biol . 136: 411-420.

Sager, W. W., C. S. Lee, I. R. Macdonald, and W. W. Schroeder. 1999. High-frequency near-bottom acoustic reflection signatures of hydrocarbon seeps on the northern Gulf of Mexico continental slope. Geo Marine Letters. 18 (4). 267-276.

Sager, W. W., I. R. MacDonald, W. R. Bryant, R. L. Carlson, and D. B. Prior, TAMU[2] digital side-scan sonar survey of Louisiana Slope areas containing active oil seeps and halokinetic sediment modification, paper 8595, Proceedings of the 1998 Offshore Technology Conference, Houston, 4-7 May 1998, 57-69, 1998.

Sager, W. W., M. C. Kennicutt II and Gas Hydrate Science Team, Proposal to the Ocean Drilling Program for Drilling Gas Hydrate in the Gulf of Mexico, paper 12111, Proceedings of the 2000 Offshore Technology Conference, Houston, 1-4 May 2000.

Sassen R, Sweet ST, Milkov AV, DeFreitas DA, Kennicutt MC. 2001. Thermogenic vent gas and gas hydrate in the Gulf of Mexico slope: Is gas hydrate decomposition significant? Geology. 29(2): 107-110.

Scott, K. M., M. Bright, and C. R. Fisher. 1998. The burden of independence: Inorganic carbon utilization strategies of the sulfur chemoautotrophic hydrothermal vent isolate *Thiomicrospira crunogena* and the symbionts of hydrothermal vent and cold seep vestimentiferans. Cah. Biol. Mar. 39: 379-382.

Smith, E. B., K. M. Scott, E. R. Nix, C. Korte, and C. R. Fisher. 2000. Growth and condition of seep mussels at a Gulf of Mexico Brine Pool. Ecology 81:2392-2403.

Table 1.3. Continued

Urcuyo, I.A., Massoth, G.J., MacDonald, I. R., Fisher, C.R.  1998.  In situ growth of the vestimentiferan *Ridgeia piscesae* living in highly diffuse flow environments in the main Endeavour Segment of the Juan de Fuca Ridge.  Cahiers De Biologie Marine 39(3-4): 267-270.

**Published abstracts**

Arvidson, R. S., and J. W. Morse. 1999. Sulfate reduction rates in chemosynthetic communities, Gulf of Mexico. EOS. 80 (49). OS242-243.

Bergquist, D. C., C. R. Fisher, and F. M. Williams. 1999. Life history characteristics and population structures of two co-occurring Vestimentiferan species at hydrocarbon seeps on the upper Louisiana Slope. EOS. 80 (49). OS243.

Buthman, D., I. R. MacDonald, M. Peccini*, W. W. Sager, and N. L. Guinasso Jr., Episodic High Temperatures and Hydrocarbon Seepage from a Mud Volcano, EOS, Trans. AGU, Ocean Sciences 2000 Meeting Supplement, OS244, 1999.

Escorcia, S. P., I. R. MacDonald, and S. B. Joye. Spatial and inter-annual variation of sulfide fluxes in chemosynthetic communities in the Gulf of Mexico. 1999. in Navigating into the next century. pp. 63, American Society of Limnologists and Oceanographers, Santa Fe, NM.

Fisher, C. R., R. T. Ward, B. Begley, and R. Kosoff. 1999. Compositional and successional patterns of cold seep communities on the Louisiana Slope of the Gulf of Mexico. eos. 80 (49). os243.

Freytag, J. K., P. R. Girguis, J. P. Andras, D. C. Bergquist, and C. R. Fisher. 1999. Sulfide uptake by buried portions of cold seep vestimentiferans can sustain autotrophic carbon fixation. EOS. 80 (49). OS5.

Guinasso, N. L., I. R. MacDonald, M. Peccini, and L. L. Lee. 1999. Near-bottom phyiscal oceanographic measurements near oil-seep sites on the Gulf of Mexico slope and their relationship to hydrate stability. EOS Supplement. 80 (49). OS242.

Kastner, M., I. R. MacDonald, A. Paytan, and S. Sweet. 1999. Isotopic and molecular composition of shallow gas hydrates from Gulf of Mexico hydrocarbon seeps. EOS Supplement. 80 (49). OS242.

MacDonald, I. R., W. W. Sager, N. L. Guinasso Jr., and E. Powell. 1999. Evidence of long-term fluctuation in fluid expulsion at hydrocarbon seeps. EOS Supplement. 80 (49). OS242.

Table 1.3. Continued

MacDonald, I. R. W. W. Sager, N. L. Guinasso, Jr. Gas in continental slope sediments, northern Gulf of Mexico: Examples from two distinct seafloor environments (extended abstract), Proceedings, International Conference on Gas in Marine Sediments, 7-11 September, 1998, Bologna, Italy.

Macko, S. A., S. E. MacAvoy, R. S. Carney, and C. R. Fisher. 1999. Stable isotope analysis of chemosynthetic and heterotrophic animals associated with hydrocarbon seeps in the Gulf of Mexico. EOS. 80 (49). OS242.

McMullin, E., J. Wood, S. Schaeffer, and C. Fisher. 1999. Genetic structure of hydrocarbon seep vestimentiferan communities. EOS. 80 (49). OS5.

Mitchell, R., I. R. MacDonald, and K. K. Kvenvolden. 1999. Estimates of total hydrocarbon seepage into the Gulf of Mexico based on satellite remote sensing images. EOS Supplement. 80 (49). OS242.

Nelson, D. C., S. C. McHatton, A. A. Ahmad, and J. P. Barry 1999. Mats of vacuolate, filamentous sulfur bacteria: adaptation to anoxia at vents and seeps? Abstracts, Annual Meeting, American Society of Limnology and Oceanography, Santa Fe, New Mexico.

Powell, E. N., K. A. Ashton-Alcox, R. D. Barber, and S. E. Ford. 1999. Parasite transmission and infection intensification in petroleum seep mussels. EOS. 80 (49). OS5-6.

Sager, W. W., and I. R. MacDonald. Long-range side-scan sonar imaging of hydrocarbon seeps and sediment mass wasting on the Louisiana continental slope, Gulf of Mexico. Society of Exploration Geophysicists, Annual Meeting, Abstracts CD, October 31 – November 5, 1999.

Sager, W. W., and I. R. MacDonald. Shallow and deep acoustic mapping of hydrocarbon seep sites, Northern Gulf of Mexico, EOS, Trans. AGU, Fall Meeting Supplement, 79, F818, 1998.

Sager, W. W., and I. R. MacDonald. Side-scan sonar survey of halokinetic and hydrocarbon seep sediment modification on the Louisiana Slope, Amer. Assoc. Petrol. Geol., Annual Meeting, April 11-14, 1999, Program with Abstracts, p. A121, 1999.

Sager, W. W., and I. R. MacDonald. Shallow and deep acoustic mapping of hydrocarbon seep sites, northern Gulf of Mexico. 1998. in American Geophysical Union Fall Meeting, San Francisco.

Sager, W. W., I. R. MacDonald, W. R. Bryant, R. L. Carlson, and D. B. Prior. TAMU[2] digital side-scan sonar survey of Louisiana Slope areas containing active oil seeps and halokinetic sediment modification. 1998. in Offshore Technology Conference. pp. OTC Paper 8595, Offshore Technology Conference, Houston, TX.

Table 1.3. Continued

Sassen, R., A. V. Milkov, D. A. DeFreitas, and S. T. Sweet. 1999. Geologic setting of Gulf of Mexico gas hydrates: significance to climate change. EOS. 80 (49). OS233.

Sassen, R., I. R. MacDonald, N. L. Guinasso Jr., S. Joye, A. G. Requejo, S. T. Sweet, J. Alcala-Herrera, D. A. DeFreitas, and D. R. Schink. 1998. Bacterial methane oxidation in sea-floor gas hydrate: significance to life in extreme environments. Geology. 26 (9). 851-854.

Sassen, R., S. Joye, S. T. Sweet, D. DeFreitas, A. V. Milkov, and I. R. MacDonald. 1999a. Thermogenic gas hydrates and hydrocarbon gases in complex chemosynthetic communities, Gulf of Mexico continental slope. Organic Geochemistry. 30. 485-497.

## **Graduate theses completed**

Bergquist, D.C. 2001. Life history characteristics and habitat-structuring by vestimentiferan tubeworms from Gulf of Mexico cold seeps. Ph.D. dissertation. Pennsylvania State University. State College, PA. 138 pp.

Davidson, N. E. 1999. Immunochemical confirmation of predation upon seep mussels and tubeworms in the Gulf of Mexico. Master of Science thesis. University of South Carolina. Columbia, SC. 67 pp.

Escorcia, S. P. 2000. Sulfide distribution in chemosynthetic communities at hydrocarbon seeps in the Gulf of Mexico. Master of Science thesis. Texas A&M University. College Station, TX. xx pp.

Macavoy, S.E. 2000. The exploitation of variable nutrient pools by aquatic predators in tidal freshwater and deep chemosynthetic communities: a multiple stable isotope and compound specific approach. Ph.D dissertation. University of Virginia. Charlottesville, VA. 233 pp.

Ward, R. T. 2000. Community composition and successional trends in Gulf of Mexico Upper Louisiana Slope seep vestimentiferan communities. Master of Science thesis. Pennsylvania State University. State College, PA. xx pp.

## 2.0 Review of Literature

### 2.1 Introduction

#### 2.1.1 Microbiology of chemosynthesis

Chemosynthesis is a mode of life practiced by numerous groups of bacteria that are able to oxidize simple compounds such as hydrogen sulfide ($H_2S$) and methane ($CH_4$) (Jannasch 1989). The sulfide-oxidizing forms use energy released by the oxidation process to drive the cellular machinery of carbon fixation. These bacteria produce carbohydrates, proteins, and other complex organic compounds starting with the basic building blocks of nutrients and water. Like photosynthetic plants, chemosynthetic bacteria are thus able to form new organic compounds at the base of the food chain. Ecologically, chemosynthetic bacteria differ from green plants because they do not need light and do require free oxygen.

In their free-living forms, chemosynthetic bacteria are found where a substrate is enriched with $H_2S$ or $CH_4$. Such conditions often occur in the anaerobic sediments of marshes or sewage treatment ponds where the decomposition of organic matter produces these chemically reduced compounds in abundance. Because they require the means for oxidizing their chemical nutrient source, chemosynthetic bacteria typically live at the interface between reduced sediments and oxygenated water. A common form is *Beggiatoa*, which lives in long filaments that form pale-colored mats on sediment surfaces (Larkin *et al.* 1994). In shallow aquatic habitats, chemosynthetic bacteria are one component of complex systems comprising numerous pathways for producing and recycling organic matter.

Below the photic zone — in depths of 300 m or more — photosynthesis is no longer possible and nutrient limits sharply constrain the possibilities for community structure. Where seepage of hydrocarbons, venting of hydrothermal fluids, or other geological processes supply abundant reduced compounds, chemosynthesis becomes the dominant component of the ecosystem. In the northern Gulf of Mexico, these conditions are met where oil and gas seep into seafloor sediments at depths of approximately 400 m and greater. Although chemosynthesis remains an exclusively microbial process at the cellular level, chemosynthetic communities in the deep sea achieve prominence because of the symbiotic partnership between chemosynthetic bacteria and invertebrate hosts (Fisher 1990).

#### 2.1.2 Symbiosis with invertebrates

Free-living chemosynthetic bacteria are limited to interfaces because they simultaneously require oxygen and reduced compounds that would spontaneously oxidize in the presence of oxygen. Symbiotic partnership with invertebrate hosts greatly extends the possible habitat for the chemosynthetic mode of life (Tunnicliffe *et al.* 1998). In basic arrangements, bacteria live within specialized cells in the host organism; however, specific adaptations can vary. The host physiology supplies oxygen and chemosynthetic substrates to the bacteria, often by means of specialized blood chemistry (Arp *et al.* 1984, Arp *et al.* 1987) and exploits the resulting bacterial productivity (Nelson and Fisher 1995).

**2.2 Discoveries of Chemosynthetic Communities**

Awareness of chemosynthetic communities in the Gulf of Mexico came in a series of steps. The initial recognition that certain locations in the seafloor might harbor dense assemblages of invertebrates occurred in 1977 when anomalous concentrations of clam shells were photographed in the vicinity of hydrothermal vents in the eastern Pacific Ocean (Lonsdale 1977). The connection between chemical enrichment and this fauna was not made until the submarine ALVIN visited the area (Corliss *et al.* 1979) and discovered assemblages of vestimentiferan tubeworms, *Riftia pachyptila* (then completely new to science), the vent mussel, *Bathymodiolus thermophilis*, and a clam from the family Vesicomyidae, which had actually first been described from material collected in the Gulf of Mexico (Boss 1968). Perhaps because the first ALVIN cruise to the vents did not include a biologist, the importance of chemoautotrophic symbionts for these species was not elucidated for at least two years (Cavanaugh *et al.* 1981, Felbeck *et al.* 1981).

Because the Gulf of Mexico is not a tectonically active region and lacks hydrothermal venting, chemosynthetic fauna were not anticipated here. Another ALVIN cruise, this time to the base of the Florida Escarpment in the eastern Gulf, unexpectedly found vestimentiferans and *Bathymodiolus*-like mussels at so-called cold seeps near the location 26° 02' N and 84° 55' W at a water depth of approximately 3200 m (Hecker 1985, Paull *et al.* 1984). This site is a continental margin brine seep, also called a cold seep, where brines formed by dissolution of the limestone Florida Platform seep out into hemipelagic sediments at the base of the Florida Escarpment (Paull and Neumann 1987). The brines are enriched in sulfides and the stable isotope signature of the source fluid can be seen in the tissue of the chemosynthetic fauna (Paull *et al.* 1985). The vestimentiferan and their symbionts depend upon this sulfide source (Cary *et al.* 1989, Cavanaugh 1985). The mussels possessed methylotrophic symbionts (Cavanaugh *et al.* 1987), which could be supported by methane dissolved in the brine. Because of the depth of occurrence, the Florida Escarpment site can only be sampled with ALVIN, which is generally occupied elsewhere. Therefore, the site has not been well sampled and was last visited during two dives in June 1992. The reader can review summaries of ALVIN dives in the Gulf of Mexico via the world wide web at the URL www.marine.whoi.edu/webpub/divelog/.

Concurrent with discoveries on the Florida Escarpment, chemosynthetic fauna were found at hydrocarbon seeps on the northern Gulf of Mexico Continental Slope. The initial discovery came as a result of sampling by otter trawl, which targeted several known oil seeps (Kennicutt *et al.* 1985). The trawl recovered vesicomyid clams (*Calyptogena ponderosa*, and *Vesicomya cordata*), a new species of mussel, *Bathymodiolus childressi* (*B. childressi* would remain undescribed for over ten years after the discovery), and two still undescribed vestimentiferan species, *Lamellibrachia* n. sp. c.f. *barhami* Webb and *Escarpia* n. sp. The first photographic evidence of these communities (Boland 1986) was obtained in the course of a research program sponsored by the Minerals Management Service (Gallaway 1988), which also sponsored the first submarine dives to Gulf of Mexico hydrocarbon seeps. These species and their associated benthic communities will be discussed in more detail below. Additional findings about hydrocarbon seep communities published during the initial discovery phase included the following:

1. Demonstration that these fauna derived their nutritional requirements from hydrocarbons (Brooks *et al.* 1987)

2. Demonstration of methanotrophy by the seep mussel (Childress *et al.* 1986)

3. Recognition of the association of the fauna with specific seep attributes (Kennicutt *et al.* 1988a, Kennicutt *et al* 1988b)

4. Description of the first submarine dives to visit a seep community (MacDonald *et al.* 1989).

Subsequently, researchers from several institutions have continued the incremental process of discovery, documentation, and scientific research at Gulf of Mexico hydrocarbon seeps. Louisiana State University (LSU) scientists have completed numerous cruises using submersible and geophysical survey methods and have developed a body of theory and documentation to explain the geological styles associated with seeps and seep communities (Roberts and Aharon 1994, Roberts *et al.* 1990a , Roberts and Carney 1997, Roberts *et al.* 1992). LSU researchers contributed heavily to two special issues of the *Journal Geo-Marine Letters* (volume 10:4, 1990 and volume 14:2/3, 1994), which offer the reader important collections of contemporary research. Pennsylvania State University scientists have completed extensive research on the life history and physiology of seep megafauna (tubeworms and mussels).

## 2.2.1 Vestimentiferan tubeworms

These highly adapted polychaetes lack a mouth, gut, and anus. They live in a tough polysaccharide tube, typically 1 cm in diameter and up to 2 m long. Gas exchange and oxygen uptake occurs via a vascularized plume (red in color) that extends 1 to 2 cm from the anterior tube end. The tube is often held 1 m or more above the seafloor. Their symbionts utilize $H_2S$, which the tubeworm absorbs from root-like structures that extend below the buried portions of the tubes. Buried tube length may be as much as one third of the body length. Two species are common to the Gulf of Mexico, *Lamellibrachia* n. sp. cf. *barhami* and *Escarpia* n. sp. The identification of the latter is currently being investigated (S. Gardener, personal communication). *Lamellibrachia* is the larger animal and typically forms bush-like clusters of several hundred individuals. These animals grow at rates typically less than 1 cm per year, so that a large adult may be 200 or more years old. A single large cluster marks a location where hydrocarbon seepage has continued unabated for several hundred years or more (Fisher *et al.* 1997).

## 2.2.2 Seep mussels

These deep-sea mussels possess methanotrophic-oxidizing symbionts that live in the linings of greatly enlarged gills (Childress *et al.* 1986). Methane and oxygen are supplied to the symbionts through the ventilation of the gills. The mussels retain functional feeding grooves and guts. Excess bacteria are sloughed out of the gills and digested normally. Because their symbionts require dissolved $CH_4$, seep mussels are restricted to locations where $CH_4$ concentrations are high, for example near active gas vents. At such sites, mussels may completely cover the seafloor in mats that are bound together by byssal threads and extend for several meters or more. The maximum length of an adult mussel is 12 to 13 cm. The growth rates are slow, with juveniles requiring at least 20 years to reach maturity and large adults frequently surviving 40 years (Nix *et al.* 1995). The most common species is *Bathymodiolus childressi*.

### 2.2.3 Vesicomyid clams

Vesicomyid clams are surface-dwelling bivalves that plow long, curving furrows across the seafloor (Rosman *et al.* 1987). The foot is thrust forward and down into anoxic soils while the siphon is extended into the bottom water with the exposed portion of the shell. This allows the animal to absorb $H_2S$ across the foot epithelium where it is transported to symbiont-lined gills via specialized blood chemistry. Adults are 75 to 90 cm long with a deep, heavy shell. The two species known from the Gulf of Mexico are *Calyptogena ponderosa* and *Vesicomya cordata.* Nothing is known of the growth rates, but deep-sea bivalves are typically long-lived. Accumulations of dead shells with clusters of live individuals suggest persistent occupation of active seep sites. These aggregations have been found on the flow fields where expulsion of oil-rich mud generates shallow anoxic layers.

### 2.2.4 Lucinid clams

Lucinid clams are possibly the most ubiquitous chemosynthetic invertebrates in the Gulf of Mexico. Living adults are almost never seen in photo-surveys, only the accumulations of dead shells. These animals live in deep, U-shaped burrows and manipulate the oxygen tension in their burrows by moving up and down in the passage to the surface. The chalky shells are subcircular, shallow, and have a small but distinct beak at the hinge. Symbionts live in enlarged gills and utilize $H_2S$. Growth rates and life spans are unknown. The most common species in the Gulf of Mexico are *Lucinoma atlantis* and *Thiasira oleophila* (Callender and Powell 1997).

### 2.2.5 Polychaete "ice worms"

The polychaete "ice worm," *Hesiocaeca methanicola,* received attention in the press following its discovery in 1997, but relatively little is published about its life history or ecology (Desbruyeres and Toulmond 1998). The worm inhabits shallow burrows on the surface of shallow gas hydrate deposits. It does not possess chemosynthetic symbionts; however, the stable carbon isotope ratios of its tissue are consistent with a diet derived from chemosynthetic production. (Fisher *et al* 2000), have recently published discovery and preliminary ecological descriptions of the ice worm.

### 2.3 Types of Chemosynthetic Communities in the Northern Gulf of Mexico

There have been several attempts by Roberts and Carney (1997) to categorize the distinguishing features of slowly seeping oil and gas seeps, rapid, mud-prone expulsion features (mud volcanoes), and quiescent, mineral-prone seeps. Reilly *et al.* (1996) categorizes complex communities that comprise a mixture of tubeworms and seep mussels, and simple communities, which consist of a single species — usually seep mussels or vesicomyid clams. MacDonald *et al.* (1998a, submitted) identified brine-pooling and sediment-diffusion habitats, noting that so-called simple and complex communities can occur in close proximity. At slow oil and gas seeps, fluids migrate to the seafloor from deep (3000-5000 m subbottom) reservoirs that are broadly distributed across the continental slope. In the upper section of the sediment column, a layer of unconsolidated hemipelagic sediment is several hundred meters thick. The upper sediment column diffuses and retains oil and gas over areas considerably larger than the fault axis (Reilly

*et al.* 1996). In the upper meter or so of the sediments, microbial degradation of the labile carbon in the oil and gas area depletes available oxygen and reduces seawater sulfate to $H_2S$. This provides chemosynthetic substrates for invertebrates with sulfide oxidizing symbionts, notably vestimentiferan tubeworms. Increased alkalinity due to microbial productivity causes extensive precipitation of carbonate. Accumulating fluid and carbonate produces low mounds with basal diameters of 10 m to over 500 m and slopes of 10% or greater. At localized vents, methane bubbles through near-bottom waters and generates sufficient local concentrations to support seep mussels. Gas hydrates form where free gas is trapped beneath layers of rock or other shallow obstructions. The result is often a patchwork of tubeworm clusters and carbonate boulders extending over the surface of the seep with the greatest concentrations along fault axes.

At mud volcanoes, formation of chemosynthetic communities is controlled by the intensity and frequency of mud discharge. Rapid fluid flux often includes abundant hydrocarbons, but burial of slow-growing fauna will limit community formation at active sites. Because the fluid flux is associated with shallow salt in most cases, halite dissolution produces concentrated brines. The increased density of these briny fluids tends to create pools or channels with distinct, stable interfaces. Seep mussels can colonize the stable edges of mud-filled craters or channels. Repeated burial over thousands of years of activity is indicated by recovery of mussels shells in cores taken at mud-prone sites.

Mineral-prone seeps occur with decreased rates of venting and formation of surface domes capped with lithified layers. Lithified surface layers and crusts represent the terminal phase of seeps regardless of whether the active seepage mode was slow, oil and gas driven, or rapid and mud prone. Lithification greatly reduces sediment porosity and limits seepage to faults and fissures in the crust. Layers of bivalve shell may remain over large areas for many years after most seepage and all chemosynthetic production has ceased. Type cases of "typical" chemosynthetic communities are given below.

## 2.4 Distribution of Chemosynthetic Communities in the Northern Gulf of Mexico

Seismic survey methods can be used to detect seeps and chemosynthetic communities by looking for migration conduits — also called seismic wipeouts — that coincide with surface mounds and low-angle faults (Reilly *et al.* 1996, Roberts and Carney 1997). Side-scan sonar has also shown promise and may be more cost-effective in some applications (Sager and MacDonald 1998). As the discussion above indicates, the timing of migration and seepage is not necessarily predicted by structures that are detected with seismic data. The geochemistry of hydrocarbon seeps has been thoroughly described (Anderson *et al.* 1983, Brooks *et al.* 1986, Brooks *et al.* 1984, Kennicutt *et al.* 1988a, Kennicutt *et al* 1988b, Kennicutt *et al.* 1987) and will reliably predict regional occurrences of chemosynthetic communities for at least the so-called "lush" communities of most concern for management (MMS 1988). However, brine-pool communities like Brine Pool NR1 (GC233) are not necessarily associated with thermogenic hydrocarbons in the surface sediments (MacDonald *et al.* 1990b). Submersible and photo-surveys have been executed haphazardly and with a definite bias toward sites greater than 1000 m in depth, this due to the cost and depth limitations of available submersibles. Surveys of chemosynthetic communities need to be evaluated critically, therefore, with an eye to the underlying limits of the

data and the motivating goals of the survey. The following sections briefly summarize different evidence for the regional distribution of chemosynthetic communities in the Gulf of Mexico.

## 2.4.1 Evidence from energy prospecting

Sassen *et al.* (1993a) demonstrated that, where data permit comparison, all major oil fields located in the deeper waters of the Gulf of Mexico are associated with chemosynthetic communities. Recent exploration and production have not been thoroughly documented by submersible observations, and there is some question as to community development in water depths between 1000 and 2000 m where data are lacking (MacDonald 1998b). However, these and other authors (Abrams, 1996 #158; Kaluza and Doyle 1998) note that salt tectonism generates migration conduits across the entire Gulf of Mexico slope. All hydrocarbon fields in the region are, therefore, highly susceptible to macro seepage. Dependence upon seeping hydrocarbons places Gulf of Mexico chemosynthetic fauna in a deep-sea locality that may be affected by human activities. The offshore energy industry has experienced several expansive episodes in the past twenty years. All of these have increased activities at ever-greater depths. The amount of seafloor influenced by seepage is quite small compared to the extent of the subbottom hydrocarbon system; therefore, industry engineers generally strive to avoid the unstable substrate at seeps (Reilly *et al.* 1996). Current interest lies in improving the capacity to predict where seep communities will occur and in understanding the processes that contribute to either stability or change in this environment so that anthropogenic changes can be distinguished from natural processes. A map of hydrocarbon discoveries and production should predict the general localities where chemosynthetic communities will be found. A good surrogate for discoveries is in active lease areas, i.e. areas where oil companies have leased development. The map in Figure 2.1 summarizes active leasing over the past 15 years. Increased leasing in the deeper waters of the Gulf of Mexico is the trend. Thus, one can surmise that abundant chemosynthetic communities will be found in these regions. However, first-hand observations are required to confirm community occurrence at scales of 1 km or less.
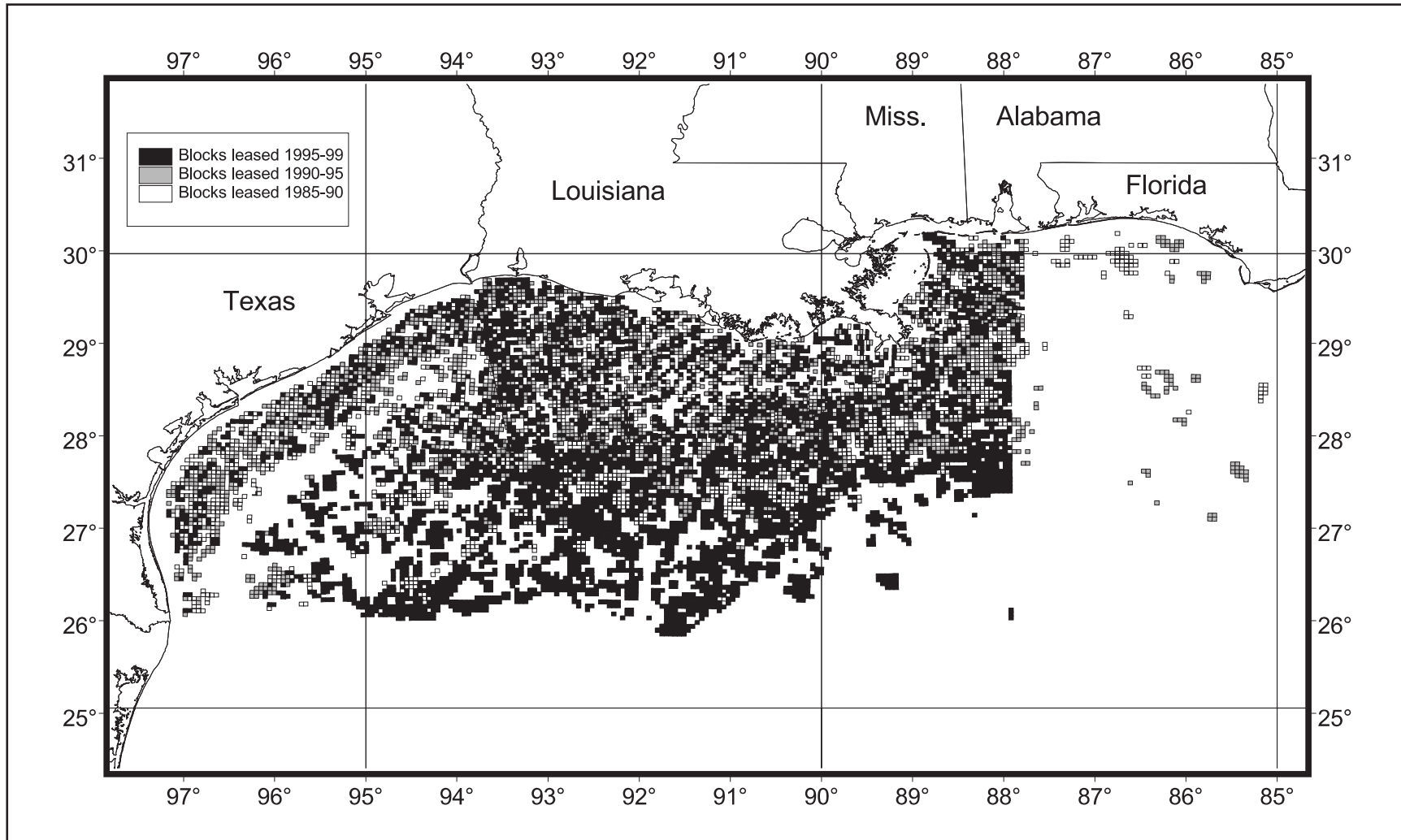
Figure 2.1.    Offshore lease holdings illustrate the trend to deeper water over the past fifteen years. Offshore leases remain active for ten years, so blocks leased in the period 1985 through 1990 but not renewed are not current while leases obtained in the 1995 through 1999 timeframe are currently under development. The southern-most lease blocks are in water depth approaching or exceeding 3000 m.

**2.4.2 Evidence from remote sensing and direct observations**

The inventory of known seep communities in the Gulf of Mexico has been developed incrementally as direct observations of chemosynthetic fauna are obtained and reported. Kennicutt *et al.* (1988b) conducted what remains as the most comprehensive exploratory survey of localities where high-molecular weight hydrocarbons were found in surface sediments when systematically sampled by trawl net. Many of these reports occur in a haphazard manner when seep fauna are discovered during the course of sampling designed for other objectives. Examples of unanticipated discoveries include the finding by Boland (1986) of tubeworms during the course of photography using a remote camera sled. Voucher collections are often not obtained from animals that live at sites found by camera sleds, and navigation is often approximate. Gallaway *et al.* (1990) were able to document several aggregations of tubeworms and vesicomyid clams with the use of a remote operating vehicle (ROV). Other ROV operations have reported sighting chemosynthetic fauna, but accurate records are often unavailable. The US Navy research submarine NR-1 has completed several broad-area surveys discovering previously unknown chemosynthetic communities (MacDonald *et al.* 1990b, Reilly *et al.* 1996). A more recent survey with NR-1 was completed in 1998 and will be described herein. Exploration in deep water (>1000 m) areas has been carried out by the submarine ALVIN at sites on the Florida Escarpment noted above, along the Sigsbee Escarpment in the central Gulf of Mexico (Brooks *et al.* 1990), and along Alaminos Canyon and Green Knoll. Most of the dives with submersibles and the vast majority of detailed sample collections have been made by the submarine Johnson SEA-LINK. SEA-LINK has a maximum depth rating of 1000 m, so there is a distinct bias in the inventory of seep communities toward sites above this depth. Aharon (1994), MacDonald *et al.* (1996), and Roberts and Carney (1997) have all published inventories or maps of known chemosynthetic communities in the Gulf of Mexico. The map shown in Figure 2.2 is derived from MacDonald *et al.* (1996).

Indirect evidence for chemosynthetic communities can be obtained by satellite remote sensing methods. Oil that escapes from most seeps floats to the surface and forms a thin (<1μm) layer that drifts downstream when driven by wind and currents. This layer dampens the capillary waves on the water's surface, thereby improving its specular reflectivity (Espedal and Wahl 1999). Electro-magnetic energy (including visible light and RADAR energy) reflected from films of this type creates areas of water that are bright or dark depending on whether the energy is reflected toward or away from the sensor (Huhnerfuss *et al.* 1989, MacDonald *et al.* 1993). This technique has been used with increasing frequency as an exploration tool in frontier basins, because it verifies the presence of source material for hydrocarbon generation as well as, pressure-charged reservoirs (Kornacki *et al.* 1994). A satellite image is a snapshot in time and other processes besides oil seepage can produce light-reflecting films on the ocean. Therefore, the rule of thumb is to look for so-called perennial slicks, that is, slicks that appear in the same location over multiple samplings. The slicks' locations, 63 in all, that are mapped in Figure 2.2 were developed by analysis of a limited number of satellite images made available for research purposes (MacDonald *et al.* 1996). Subsequent work, much of which remains proprietarily held, has greatly expanded this inventory of perennial slicks. Mitchell *et al.* (1999) document over 200 perennial slicks in a complete survey of the northern Gulf of Mexico. The northern Gulf of Mexico is potentially a very large and relatively contiguous province within which

chemosynthetic communities supported by hydrocarbon seepage will be found. It is reasonable to predict that the chemosynthetic habitat in this region has a few, basic characteristics.

**2.5 Habitat Processes at Gulf of Mexico Hydrocarbon Seeps**

At hydrocarbon seeps, reduced compounds are generated as by-products of microbial consumption of hydrocarbons in the upper few meters of the sedimentary column and are directly supplied by upward migration from deeply buried sources. Hydrogen sulfide is produced and consumed by biotic and abiotic processes at hydrocarbon seep communities at much higher rates than in normal sediments (Lin and Morse 1991). Biogenic reaction products are responsible for the formation of iron sulfide minerals and, in some cases, massive deposits of carbonate minerals at seep sites (Morse 1994). Seep sediments exhibit geochemical processes that differ from most models of normal marine sediment diagenesis in many important ways. Organic enrichment by hydrocarbon seepage is an important process in producing reduced compounds (Brooks *et al.* 1987). Hydrocarbon generation and migration occur over timeframes of millions to tens of millions of years (Sassen 1987). Chemosynthetic communities occupy areas of the seafloor that are very small compared to the extent of the hydrocarbon reservoirs that feed them. Temporally, chemosynthetic communities are ephemeral features in comparison to the overall hydrocarbon system of the Gulf of Mexico basin. The volume of hydrocarbons withdrawn from reservoirs by humans is unlikely to impact the survival of chemosynthetic communities, since this volume is insignificant when compared to the total volume of the extant hydrocarbon system. Two styles of seepage have been described at Gulf of Mexico hydrocarbon seeps: sediment diffusion and brine pooling. Much of the community-level diversity in cold seep communities can be explained by examining the environmental consequences of these two styles of seepage.
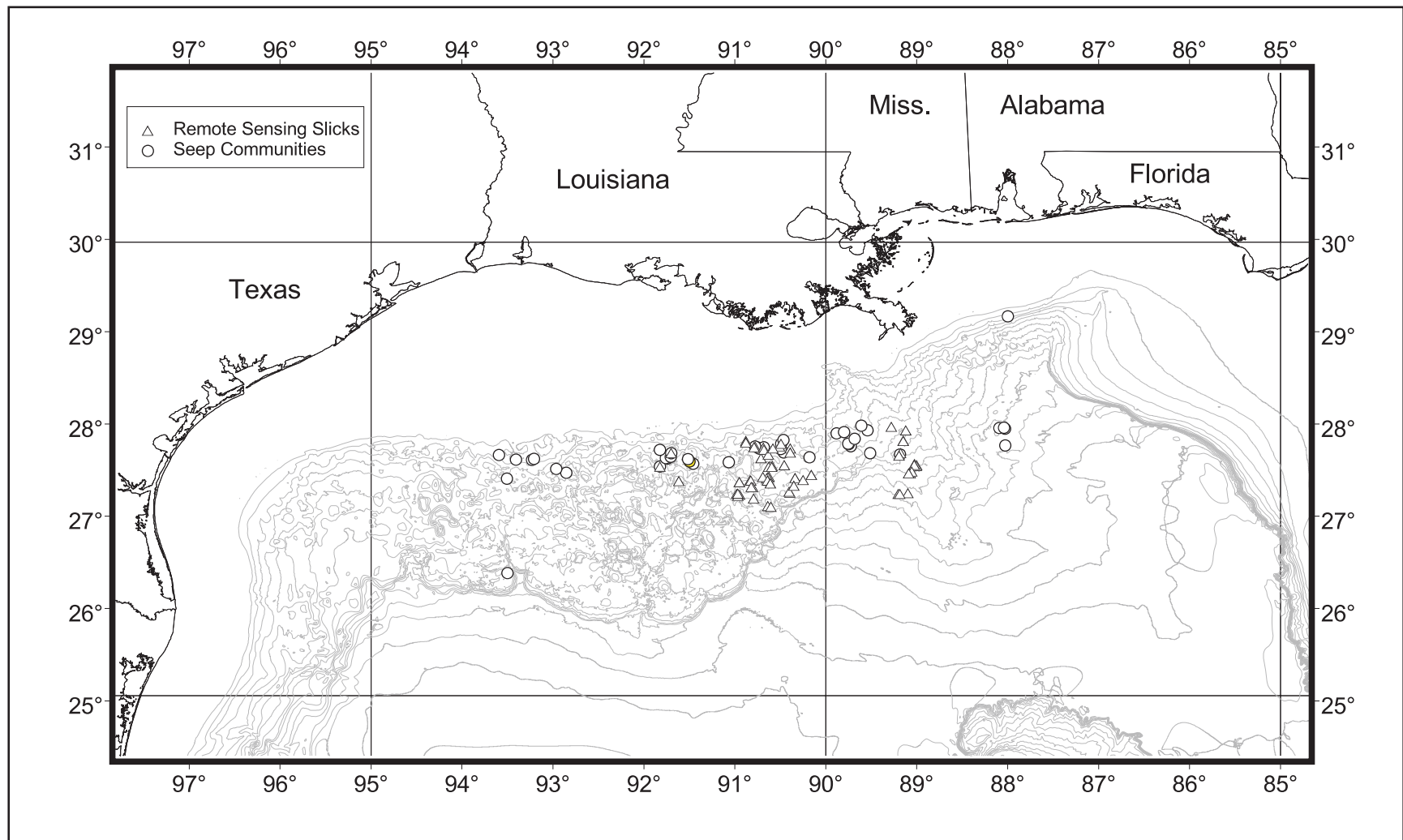
Figure 2.2.    Distribution of known chemosynthetic communities and perennial oil slicks detected in available remote sensing data (adapted from Tables 2 and 3 in MacDonald *et al.* 1996). Depth contours are at 200 m intervals.

### 2.5.1 Sediment diffusion

Sediment-diffusion hydrocarbon seeps have been discovered at many locations on the upper continental slope during energy prospecting activities. It has been widely recognized that upward migration of reservoir oils can result in high concentrations of liquid and gaseous hydrocarbons in seafloor sediments (Anderson *et al.* 1983). In these habitats mussels, clams, and tubeworms utilize reduced compounds – methane and $H_2S$ – by extending body parts into the sediment or by bathing their brachia (gills or plumes) in the steep gradients immediately above the sediment/water interface (Figure 2.3). Gas seeps and gas hydrates, ice-like solids that form when methane and water combine at high pressure, are also recognized as important components of slope seep systems (Brooks *et al.* 1984, Shipley *et al.* 1979). The important characteristics of the sediment diffusion habitat are abundant, highly altered hydrocarbons that include thermogenic gases, liquid petroleum, and tars, which are distributed throughout the sedimentary section overlying a fault or fault nexus (Behrens 1980, Kennicutt *et al.* 1987, Reilly *et al.* 1996, Roberts and Aharon 1993). At the seafloor, a complex veneer tends to entrap and further contribute to the alteration of seeping fluids. Roughly in order of greatest relative age, major components of this veneer are as follows (note that the citations provided refer to descriptions of the components, not their influence on habitat formation):

1.  Authigenic carbonates in the form of rubble and consolidated pavements (Roberts and Aharon 1994, Sassen *et al.* 1994a).

2.  Extensive aggregations of vestimentiferans, the "roots" of which extend into the upper sediment as dense tangles (Fisher *et al.* 1997).

3.  Beds of bivalves, including living mussels and/or clams and layers of shell (Callender *et al.* 1990, MacDonald *et al.* 1990a).

4.  Layers of gas hydrate, which can entrap the buoyant phases of hydrocarbons but are subject to gradual decomposition and possible catastrophic failure due to temperature fluctuations in bottom waters (MacDonald *et al.* 1994).

5.  Mats of the sulfide-oxidizing bacteria, *Beggiatoa* (Larkin *et al.* 1994), which occur in pigmented and non-pigmented forms (Sassen *et al.* 1993b).

Although there is good evidence for structural instability in rapidly forming seep habitats, particularly where mud volcanism produces massive fluid discharge (Neurauter and Roberts 1994, Roberts and Neurauter 1990), the formation of large chemosynthetic communities takes place in the context of increasing lithification and general seafloor stability (Roberts and Aharon 1994). The chemosynthetic fauna themselves will, with time, retard the escape of hydrocarbons from the sediments (Sassen *et al.* 1994b).
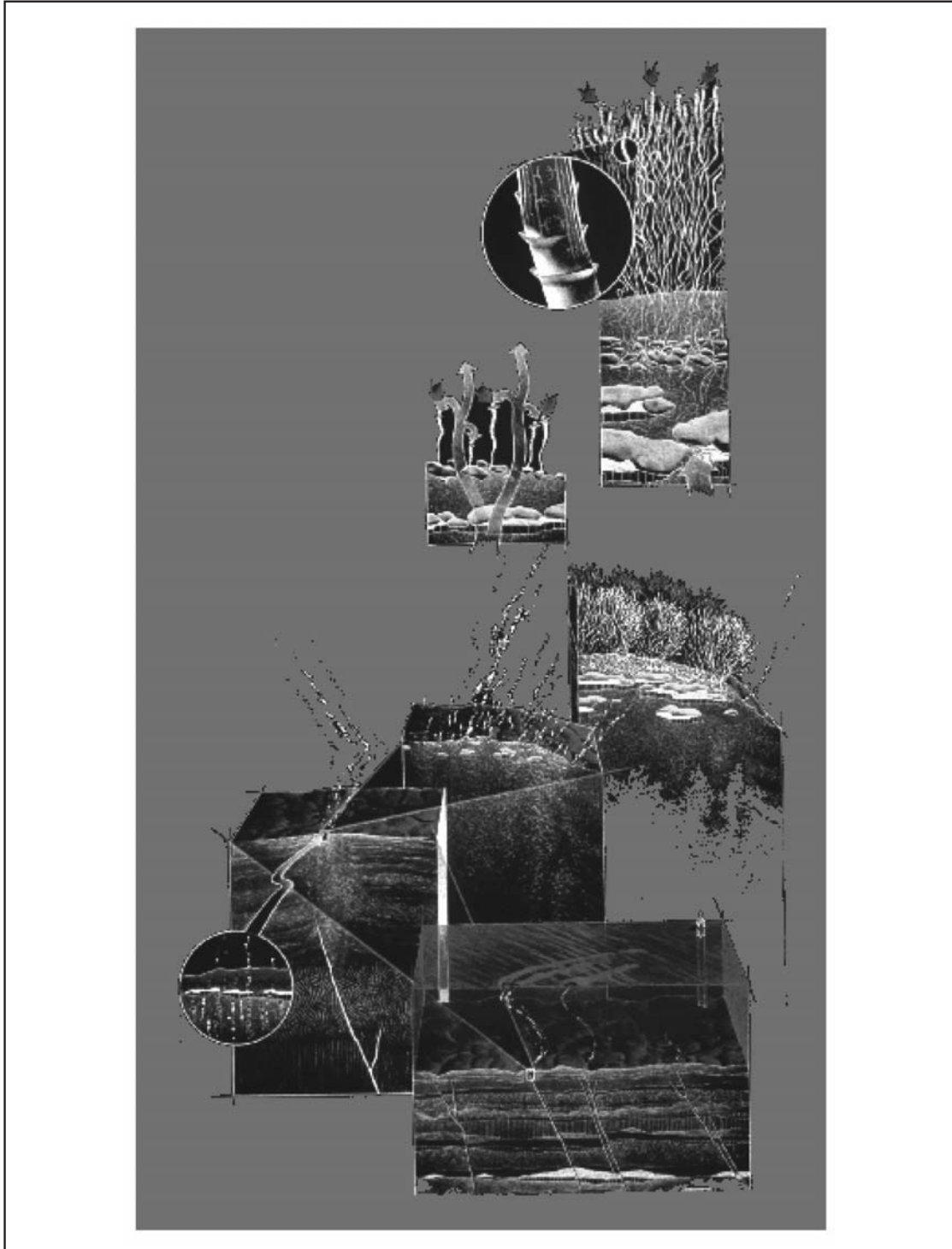
Figure 2.3.   Illustration of the chemosynthetic community formation in a sediment diffusion style hydrocarbon seep. Gas and oil migrate along fault planes that penetrate reservoirs (lower), and then diffuse through unconsolidated sediments approaching the seafloor (middle left). Formation of gas hydrate, layers of biota, and authigenic carbonate entrap hydrocarbons in uppermost sediment (middle right), facilitating microbial degradation of hydrocarbons and subsequent reduction of seawater sulfate to sulfides needed for tubeworm symbiosis (upper right). (Art by C. Bruce Morser.)

## 2.5.2 Brine pooling

Concentrated brines are often associated with petroleum migration and seepage (Behrens 1980). Where they discharge, their density allows for the formation of distinct pools on the seafloor. The discovery of brine-filled depressions in the Gulf of Mexico predates the discovery of chemosynthetic communities (Bright *et al.* 1980, Paull and Neumann 1987, Shokes *et al.* 1977). The discovery of chemosynthetic fauna on the Florida Escarpment demonstrated that brine could be a carrier of reduced compounds (Cary *et al.* 1989, Paull *et al.* 1984). The significance of the pooling process became evident when a dense colony of *Bathymodiolus childressi* was discovered around the edges of a small, brine-filled crater (MacDonald *et al.* 1990b). Where brines accumulate on the seafloor, mussels can obtain methane through the uptake of water by placing their inhalant siphons just above the brine. High concentrations of gaseous hydrocarbons are often dissolved in Gulf of Mexico brines. The defining characteristics of the brine pooling habitat are an extremely sharp (~1 cm) density-driven interface between the brine and seawater and a surface, which allows for the development of a thin layer of brine that intercepts the sediment surface. Dense colonies of mussels become established at these seawater/sediment/brine interfaces. Where the brine interface is less sharp, for example in the large brine pool filling Orca Basin that has a meters-thick separation between seawater and saturated brine (Shokes *et al.* 1977), the mussels are unable to bridge the distance between the anoxic brine and the oxygen-rich seawater; consequently, mussel communities appear to be absent (Brooks *et al.* 1990). The brine pooling habitat results from brine seeps on nearly level sea bottoms or from brine-filled pockmarks or craters that exhibit a brine/seawater interface at the edges of the depression (Figure 2.4).
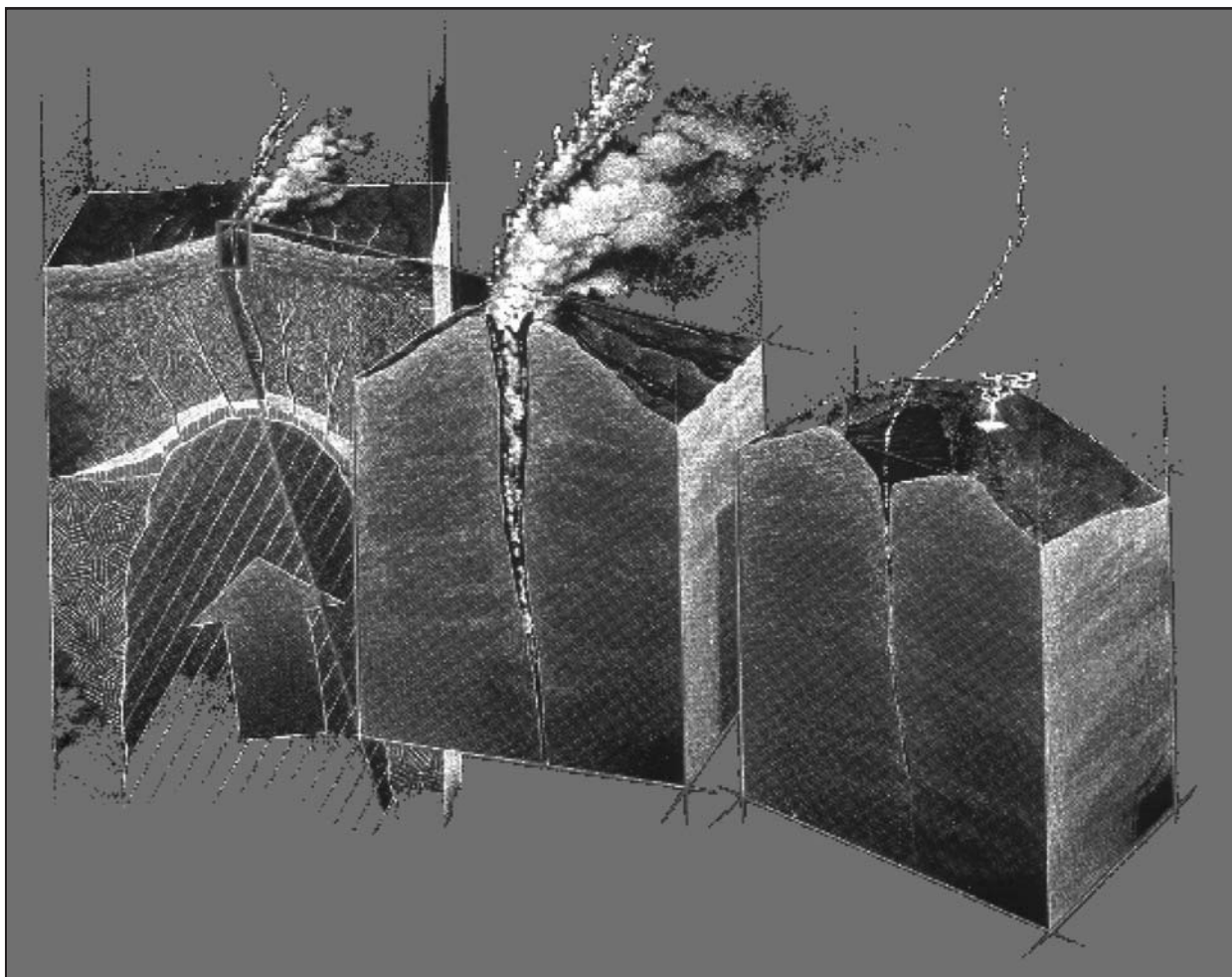
Figure 2.4.    Illustration of the chemosynthetic community formation in a brine pool style hydrocarbon seep. Salt diapir pressurizes a shallow reservoir of methane – also known as a shallow gas hazard (left). Subsequent release of gas excavates a surface crater and diatreme (middle). High concentrations of methane are available to seep mytilids around the edges of the brine pool formed by dissolution of underlying salt (right). (Art by C. Bruce Morser.)

## 2.6 Model Components and Interactions

The following sections provide a brief description of the various biological components of an overall model of chemosynthetic communities including microbial communities, mussel colonies, and tubeworm colonies. Interactions between the environmental setting and biology are also considered including change at the community level, geological stability, regional characteristics, energy flow, and food webs.

### 2.6.1 Microbial communities

Bacteria are a fundamental component of the seep community interacting with the chemical environments both as free-living bacteria and endosymbionts. The importance of bacterial occurrences and their role in mediating chemical transformations at seep sites is poorly

understood. It is believed that autotrophic microbial (sulfide oxidizing) productivity is dependent on heterotrophic microbial (sulfate reducing) productivity. *Beggiatoa* filaments can extend 8 to 12 cm down into the anoxic sediment. *Beggiatoa* mats in the Gulf of Mexico sites have the potential for competing with higher organisms for sulfide over at least the top 10 to 12 cm of these anoxic sediments. *Beggiatoa* exhibits two growth forms: pigmented and non-pigmented. Enzyme activities in the pigmented and non-pigmented forms are consistent with heterotrophic and autotrophic metabolism, respectively. *Beggiatoa* may also be facultative consumers of hydrocarbons. *Beggiatoa* and the related genus *Thioploca* are the only bacteria known to contain a central vacuole. Similar filamentous, thio-autotrophic bacteria from Guaymas Basin hydrothermal vents (Gulf of California, 2000 m depth) and the Clam Field Seeps of Monterey Canyon (Monterey Bay, depth 900 m) contain intracellular nitrate at concentrations as high as 160 mM (4,000- to 8,000-fold above ambient levels). Expanded investigations are needed to more fully understand the role microbes play in seep ecology.

### 2.6.2 Mussel colonies

*Bathymodiolus childressi*, which is the major mussel species in these habitats, has evolved in symbiosis with methanotrophic endo-bacteria (Childress *et al.* 1986, Fisher 1990). *B. childressi* was formally described by Gustafson *et al.* (1998) and had previously been given the provisional taxonomic designation Seep Mytilid I. It is often described by this name in mussel colonies and is most abundant where gaseous hydrocarbon flux is high. Compared to tubeworms, mussel colonies recruit more rapidly and are more mobile. Mussels, which inhabit the sediment diffusion habitat, experience greater variability in nutrient supply due to hydrate formation and decomposition and carbonate precipitation and are more ephemeral than mussel colonies at brine pools. Differences in the longevity, "health," and stability of mussel colonies depend on the following features of their life history and physiology:

1.  Mussels colonize a new site with motile larvae.

2.  Seep Mytilid Ia spawning is not seasonal, and recruitment is episodic.

3.  The presence of settlement substrate enhances the chances of establishment of a mussel community.

4.  Mussels require high concentrations of methane around their siphons for growth and reproduction.

5.  The final size of individuals as well as the density of the population is primarily a function of ambient methane concentrations.

6.  Mussels can grow extremely fast as well as survive over long time periods.

Mussel communities in sediment diffusion habitats may begin to die out as carbonate precipitation blocks the seepage of methane into the community. In the absence of genetic isolation, a mussel community at a sediment diffusion habitat removed by physical disturbance can resettle and mature in less than twenty years. Catastrophic mud burial is another cause for the demise of mussel communities. Mussel communities associated with brine seepage can be very long lived.

### 2.6.3 Tubeworm colonies

Tubeworms are the visually dominant biomass in sediment diffusion habitats. A significant seep community will typically contain tens of bushes distributed across several hectare of seafloor. A mature bush indicates that petroleum flux and associated microbial activity has persisted at a location for more than 100 years. However, a bush forms and declines though a series of life-history stages. Vestimentiferan bushes display distinctive growth forms, species compositions, and levels of productivity at different stages of their development (newly recruited, mature, senescent). Vestimentiferan spawning is not seasonal, and recruitment is episodic. Vestimentiferans colonize a new site with motile larvae. A larval settlement substrate is required for the establishment of a vestimentiferan colony. This substrate of choice is authigenic carbonate, which is formed in areas of active seepage. Both species of vestimentiferan recruit equally to new sites. Juveniles of both species grow relatively quickly to lengths of about 30 cm at sites where sulfide is found in the water around the plumes of the juveniles. Flow of seep fluids from the sediment column to the water column slows down as the bush matures. As a result of carbonate precipitation and sedimentation, the bases of vestimentiferan bushes become covered with an ever-increasing amount of sediment. After 10 to 20 years, the transfer of sulfide to the water column is insufficient to carry sulfide to the plumes of the vestimentiferans, and they begin to take up sulfide across the buried, terminal portion of their tube. Under these conditions, the *Lamellibrachia* out competes the *Escarpid*-like species and begins to dominate the assemblage. The *Lamellibrachia* continues to grow very slowly. Individuals can reach lengths of three meters and live for hundreds of years (Fisher *et al.* 1997). Eventually, as a result of a combination of continued authigenic carbonate precipitation and sulfide depletion by animals on the edge of the aggregation, the animals in the center of the bush begin to die. Re-channeling of seepage due to carbonate precipitation eventually cuts off the supply of sulfide to the aggregations, and the demise of the entire aggregation ensues.

### 2.6.4 Energy flow and food web

Chemical energy is converted into biomass through chemoautotrophic fixation by free-living and symbiotic bacteria. Because of the advantages inherent in multi-cellular anatomy and physiology, both mussels and tubeworms are very efficient at extracting chemicals from the environment and converting them into biomass. The endemic heterotrophic fauna rely almost entirely on seep chemosynthesis for their food. Free-living bacteria are the major source of food for most of the endemic heterotrophic fauna. Primary production of seeps finds its way into the food chain of the deep Gulf of Mexico through crustaceans, fish, and other associated fauna that feed on the seep communities.

### 2.6.5 Change at the community level

Three processes contribute to change at the community level: recruitment, succession of aggregations, and episodic instability due to localized processes (e.g., gas hydrate formation/dissociation, mud expulsion). The current model suggests that changes in chemosynthetic community structures in seep communities occur over time from a few years to tens of years. Substantial change is expected to be observed in the abundance and distribution of bacterial mats. Significant changes may occur in the abundance and distribution of mussels that are greatest for mussel communities, which occur in the sediment diffusion habitats. Lesser

changes will be evident in the tubeworm colonies, particularly among mature bushes. Catastrophic events may cause localized effects in the community, but the frequency of these occurrences is unknown. The occurrence of these "rare" events can only be determined through long-term monitoring of the community including the *in-situ* measurement of various physical/chemical variables.

## 2.6.6 Regional characteristics

The major regional feature of Gulf of Mexico communities is their prevalence across the northern continental slope. This suggests that these communities are routinely subjected to the effects of eddy-driven circulation events and variations in temperature, pressure, and sedimentation rates. Although physical oceanography is not a major focus of this program, the need for a minimum set of oceanographic observations is indicated by previous results.

Genetically isolated populations are inherently unstable and thus susceptible to extinction as a result of disturbance. In contrast, populations characterized by extensive gene flow are insulated from catastrophic decline by the capacity for resettlement. Proximity of communities on the slope and circulation characteristics of the slope suggest that the gene pool of chemosynthetic species should be well-mixed, although existing taxonomic descriptions are not sufficient to determine if this is true. Modern molecular techniques can provide the information needed by delineating corridors of gene flow.

## 2.6.7 Geologic stability

Geological evidence demonstrates that hydrocarbon and brine seepage has persisted on the northern Gulf of Mexico slope for thousands of years. Seeps are associated with migration conduits that connect the seafloor to deep sub-surface reservoirs containing gaseous and liquid hydrocarbons that were generated millions of years ago. Defining the processes that determine the geological cycle of seepage, i.e., reservoir dynamics, large-scale halokinesis, sedimentation rates, etc., is largely beyond the scope of this program. It is possible, however, to make qualitative evaluations of the relative age of the primary study sites and to identify additional sites of various ages. This will improve prediction of community presence/absence and increase the understanding of the long-term fate of communities.

# 3.0 Study Sites, Field Efforts, and Sampling Design

## 3.1 Introduction

This chapter describes the study sites where program activities were conducted and the selection criteria by which the sites and the individual sampling stations were chosen. The program was conducted in the northern Gulf of Mexico south of Louisiana where, as the previous chapter has indicated, the largest concentration of known hydrocarbon seeps is located. The program objectives called for evaluating factors that controlled the distribution of chemosynthetic communities over a large portion of the Gulf of Mexico and for detailed study of the ecology of representative communities. It was therefore necessary to conduct research at a range of different scales. At a regional scale, the seismic signatures of chemosynthetic communities were evaluated to improve detection capabilities, and a limited exploratory survey was undertaken to search for previously unknown communities. For the detailed studies, specific sites for biological and chemical samplings from submersibles were selected at the scale of individual communities. Separate field programs were conducted to accomplish detailed collections for biology and geochemistry. The community-level sites were selected based on previous information. They represent, respectively, brine pooling and sediment diffusion seeps, which are the two distinct seepage settings described in the models outlined in the previous chapter. At an intermediate level, detailed maps and geographic information system (GIS) datasets were compiled to investigate the correlation between biological and geological/geochemical components and the communities. Locations of the mega-sites and community-level sites are shown in Figure 3.1. Details of the characteristics of the sites and the rationale for their selection are given below.

## 3.2 Regional Studies

Field activities during the program included regional geophysical surveys designed to determine seismic and remote-sensing characteristics of active seeps and seep communities. Because the area of the Gulf of Mexico slope occupied by known chemosynthetic communities spans a depth range from about 500 to 2500 m, the geophysical survey was carried out within shallow- and deep-water areas. These two mega-sites were designated as survey sites for the development and testing of criteria to improve the prediction of the presence of chemosynthetic communities based on geophysical or other remote sensing data (Figure 3.1). Comparison of the geophysical signatures obtained from known or probable seeps in the two mega-sites provides a test of whether fundamental changes occur in the types of signatures when depth increases. In addition, regional-level efforts considered the geological and oceanographic processes that support communities, including larval dispersion and circulation processes that maintain the genetic stability of these communities.
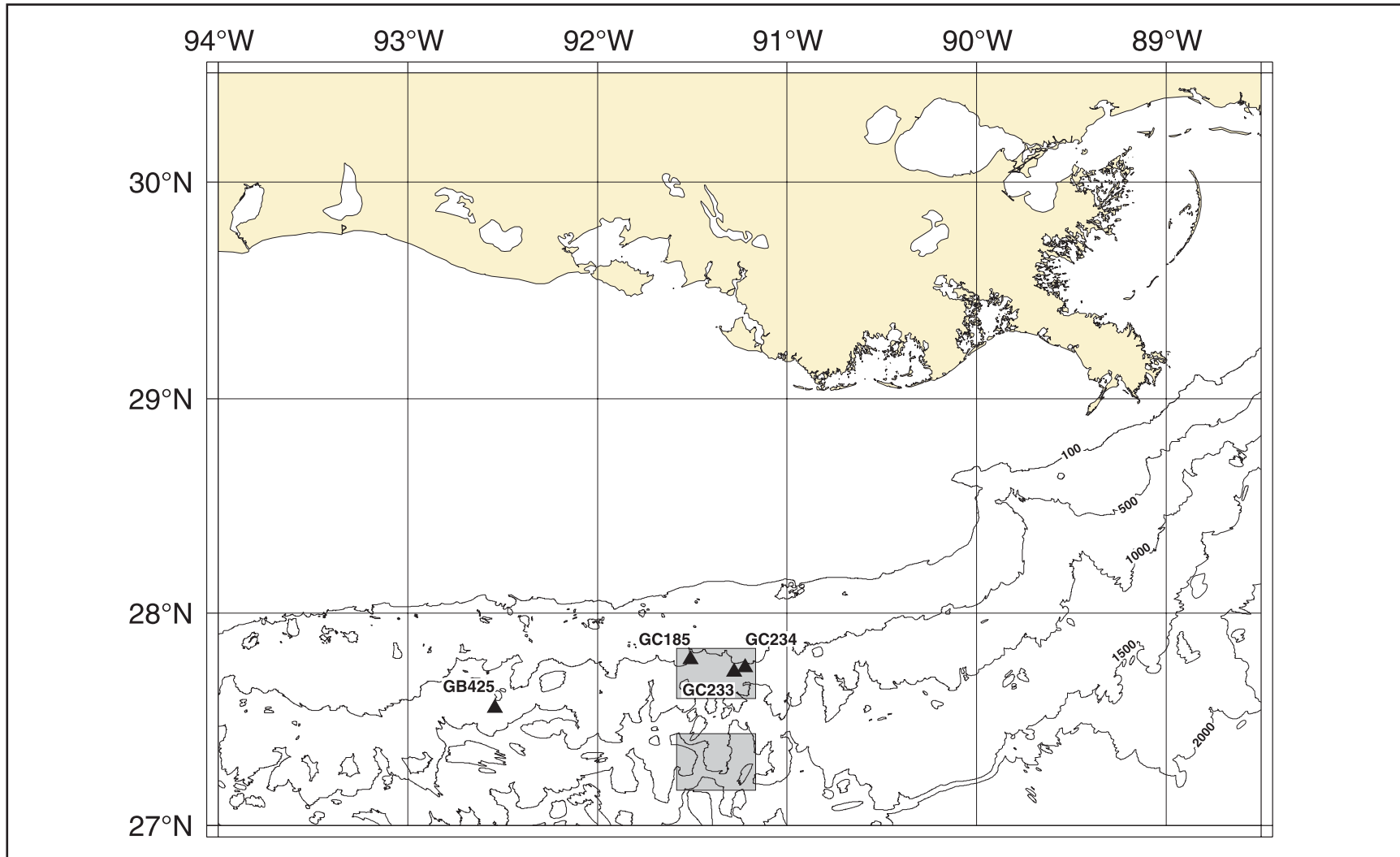
Figure 3.1.  Northern Gulf of Mexico showing study site locations for submersible operations (triangles) and mega-site areas for geophysical survey (shaded rectangles). Depth contours in meters.

The size and location of these mega-sites were designed to optimize survey operations and provide significant regional coverage. Both areas encompassed several types of geological formations. Both contained more than ten perennial sea surface slicks detected by remote sensing techniques. Both sites were surveyed with a swath-mapping sonar system (TAMU[2] System). Additional survey data were collected at the Garden Banks sampling site (GB425) in support of the community-level studies. The submarine NR-1 also visited selected targets in the shallow mega-site during 1998 in an attempt to verify the interpretations made of the TAMU[2] data. The characteristics of the two mega-sites are summarized in Table 3.1.

Table 3.1. Mega-Site Regional Survey Areas.

Mega-site 1 ("Shallow," extended 4 NM South to include GC321) - area 1214 km[2]

- Boundaries: 91°35'W-91°10'W; 27°36'N-27°50'N
- Contains GC185, GC233, and GC234 sampling sites
- Contains approximately 13 slicks
- Water depths range from 400 to 900 m

Mega-site 2 ("Deep") – area 1214 km[2]

- Boundaries: 91°35'W-91°10'W; 27°10'N-27°26'N
- Contains northern Pygmy Basin; eastern Longhorn Basin; and most of Tiger Basin (intrasalt basins)
- Contains 12 to 15 slicks
- Water depths range from 950 to 1250 m

## 3.3 Community-Level Sampling Sites

At the community level, efforts focus on the abiotic factors that control the distribution, abundance, and health of the major chemosynthetic and associated fauna. Investigations of the life history of these organisms are also included. Four principal community-level sites were designated for the intensive collection of samples and deployment of experiments and instrumentation. Two of the sites were in brine-pooling settings; two others were sediment-diffusion settings. The sites differ principally in that two sites contain significant amounts of liquid hydrocarbons in the sediments and are dominated by tubeworms (GC185 and GC234) and two sites are brine seeps and are dominated by mussels (GC233 and GB425). These sites have been the subjects of historical studies, which in most cases provided ancillary geographic data. The sites contain the major faunal groups found in chemosynthetic communities (tubeworms and mussels) and cover a range of environmental conditions so that hypotheses concerning abiotic controls on community ecology could be tested. To simplify sample identification, each site was given a unique, two-letter abbreviation. A brief description of each site's setting and community's characteristics is presented in Table 3.2.

Table 3.2. Principal Community-Level Sampling Sites and Pertinent Characteristics.

| Sampling Site (Alternate names) | Latitude, Longitude | Depth (m) | Fauna present (by dominance) | Seepage properties |
|---|---|---|---|---|
| GC185 (BH, Bush Hill) | 27°46.9' N 91°30.4' W | 550-580 | tubeworms heterotrophs mussels | high molecular weight hydrocarbons free methane to pentane gases |
| GC234 (GC) | 27°44.1' N 91°131' W | 525-560 | tubeworms heterotrophs mussels | high molecular weight hydrocarbons free methane to pentane gases |
| GC233 (BP, Brine Pool) | 27°43.4' N 91°16.8' W | 640 | mussels heterotrophs tubeworms | brine free and dissolved methane gas |
| GB425 (GB) | 27°33.2' N 92°32.4' W | 600 | mussels heterotrophs (?) tubeworms | brine free and dissolved methane gas high molecular weight hydrocarbons |

## 3.4 Sediment Diffusion Communities

### 3.4.1 GC185

The "Bush Hill" site (27°47'N, 91°30.4'W) described by MacDonald et al (1989) was the first hydrocarbon seep community to be sampled from a submersible. Reilly *et al.* (1996) describe it as the type-example of a complex chemosynthetic community. The Conoco tension legwork platform (TLWP) was installed more than 2 km west southwest from the mound and began producing oil in the late 1980's. The major seep area is a 300 m-EW by 500 m-NS mound with a crest depth of 570 m rising about 40 m above the surrounding seafloor and composed of mud, carbonate, and shallow gas hydrate (Roberts and Carney 1997). The north-south axis of the mound is situated along the surface trace of a west-dipping fault that is the conduit by which oil and gas reaches the surface from deposits located at approximately 1200 m subbottom depth. Surface sediments contain, by weight, up to 10% liquid hydrocarbons, which Kennicutt *et al.* (1988) described as having fingerprints identical to oil produced by the TLWP wells. However, reservoirs tapped by TLWP wells were located at subbottom depths of 3000 m or greater. Cook and D'Onfro (1991) suggest that the field comprises a complex of many reservoirs charged from a common source but seeping only from the shallowest strata. Sulfide concentrations in shallow sediments (<10 cm) associated with tubeworm clusters have been measured in the 100- to 250-$\mu$M range with use of a microelectrode technique (Escorcia *et al.* 1999). Methane concentrations in near-bottom waters are 30- to 60-$\mu$M in the vicinity of active gas vents, and below 1-$\mu$M elsewhere (MacDonald *et al.* 1989, Nix *et al.* 1995). Shallow gas hydrates have been recovered by coring at GC185 (Brooks *et al.* 1986). Layers of gas hydrate breach the sediment layer near the highest point of the mound (MacDonald *et al.* 1994). Tubeworm clusters extend over much of the mound crest while mussels are confined to the active gas vents.

### 3.4.2 GC234

The "Green Canyon" site is a very extensive complex of tubeworm clusters, seep mussel beds and outcropping gas hydrates located in the northeastern corner of the GC234 lease block (27°44'50"N, 91°13'30"W). The geology of this region was first described by Behrens (1980), who perceived a network of diapir crests that converge to the west of the site as an east-west trending diapir ridge. Seismic wipeouts are widespread and substantial quantities of oil are dispersed in the sediments (Brooks *et al.* 1986). The surface topography is uneven, sometimes with massive deposits of authigenic carbonate either exposed or thinly draped with sediment. Tubeworm communities appear to be restricted to terraces where the seismic reflections (25 kHz) are wiped out within approximately 3 m of subbottom, and extensional faults approach the mud-line (MacDonald *et al.* 1990a). Nix *et al.* (1995) report sulfide and methane concentrations approaching 8 and 11 mM, respectively. The type specimen of the "ice worm" *Hesiocaeca methanicola* was collected from an outcropping layer of gas hydrate at this site (Desbruyeres and Toulmond 1998, Fisher *et al.* 2000).

### 3.5 Brine-Pooling Communities

### 3.5.1 GC233

The focus of the GC233 chemosynthetic community is a small (190 m$^2$) pool of brine (salinity 121.35 psu) found near 27°43.4'N and 91°16.5'W at a water depth of 650 m (MacDonald *et al.* 1990b). Brine fills a crater at the center of an approximately 100 m wide mound. The mound rises about 6 m above the surrounding seafloor, but the crater and its diatreme extend at least 30 m below the surface. The brine contains microbial methane ($\delta^{13}C$ = -63.8) in concentrations that are supersaturated at standard temperature and pressure. Streams of $CH_4$ bubbles emanate continually from the center of the pool. The pool is ringed by a large (540 m$^2$) bed of seep mussels (MacDonald *et al.* 1990b). Mussels settled on the "shoreline" of the pool include numerous juveniles; however, the periphery of the bed comprised a single settlement class without juveniles. Sulfide levels are below levels of detection in the pool but rise sharply in fluids collected beneath the surrounding mussel bed (Fisher, personal communication). The bed of seep mussels comprises a striking example of a mono-specific aggregation of chemosynthetic fauna, but numerous other species of heterotrophic animals are also commonly observed at the site (MacDonald 1992). Recent findings challenge the Reilly *et al.* (1996) designation that this brine pool, NR-1, is a "simple" community because small but significant clusters of vestimentiferans are known to occur to the south of the pool.

### 3.5.2 GB425

GB425 is on the western edge of Auger Basin, an intraslope basin that contains economically significant hydrocarbons in the Auger, Cardamom, and Macaroni fields. Potential hydrocarbon traps in Auger Field are sealed against the up-thrown side of faults along a paleo-ridge that rises to the east and northeast of the basin, thus enabling hydrocarbon accumulation and commercial production (Shew *et al.* 1993). In the western portion of Auger Basin, the potential hydrocarbon strata are pierced by down-thrown faults along the flanks of tabular salt bodies (McGee *et al.*

1993). Geophysical records show that these faults have provided scant barriers to fluid migration. Sediment samples from this zone have recovered high-molecular weight hydrocarbons and thermogenic gas hydrate. Previous work had identified a steep-sided and flat-topped mound that extends approximately 0.7 x 1.0 km at a summit depth of 570 m located midway along the seep-affected region of Auger Basin. Active fluid expulsion has created a 50-m wide, sub-circular mud lake on the southwestern edge of the summit, which is one of two such expulsion features on the mound. Fine, fluidized mud emanates from a central diatreme, overflows the western margin of the lake, and moves down the southern flank of the mound. The mud is fluidized in hypersaline brine (133 practical salinity units) that is supersaturated with methane at standard temperature and pressure (STP). Beds of the seep mussel *Bathymodiolus childressi* rim the southern edge of the diatreme.

**3.6 Station Selection and Sample Tracking**

The objectives of the program required collection of diverse samples and deployment of in-situ growth experiments. Another important consideration was the need to compare, to the extent possible, results produced by the different disciplines. Because the program was primarily concerned with biological communities and their ecological interactions, the collection stations for detailed samples were chosen according to robust biological characteristics. That is to say, each individual station was chosen because particular species or groups of species were living in that precise location. To this degree, each station was intended as a repeatable example of the habitat for chemosynthetic species. Within the four individual sampling sites (GC185, GC234, GC233, and GB425), three major chemosynthetic habitats were studied: tubeworm dominated habitats, mussel dominated habitats, and microbial mat habitats. Control stations – locations where chemosynthetic fauna were not evident – were designated within and away from the sites. Deposits of gas hydrate constituted another habitat type, although it was somewhat problematic because it was not initially considered in the sampling design and because the extent of gas hydrate deposits in the shallow subbottom was often uncertain.

Another level of spatial variability was examined to determine the abiotic factors that control growth and development of chemosynthetic communities within a habitat. This level of spatial resolution is called the "subhabitat." In the tubeworm habitat, subhabitats are related to colony size and age. There are (small) juvenile assemblages, (large) adult assemblages, and senescent assemblages, which were thought to be relatively old. In the mussel habitat at the brine pool sites, there were mussel beds on the inner and outer edges of brine pools. There are two types of heterotrophic bacterial mats: pigmented and non-pigmented. Within the limits of program resources, stations and sites were replicated to provide statistically valid comparisons.

Considerable effort was expended to coordinate sampling activities and track samples that were distributed among the various investigators. All samples were catalogued according to a scheme that allowed investigators to determine the site and station type for each sample. As noted, each site had a two-letter abbreviation (BH, GC, BP and BH). In addition, each subhabitat type was further abbreviated. Tubeworm stations were abbreviated JT, AT, and ST, respectively for juvenile, adult and senescent aggregations. Mussel and *Beggiatoa* stations were respectively abbreviated M and B. As detailed below, each sampling dive with the submersible was given a

unique number. Thus, by recording the dive number and station number with every sample, it was readily possible to determine not only the site and subhabitat for each sample but also the time and additional details of collection. For example, a sample identified as Dive 2883 station BHAT1 is immediately identifiable as coming from GC185, from an adult tubeworm station, and from a specific collection.

## 3.7 Fieldwork

Fieldwork during the program comprised two geophysical survey cruises onboard the R/V GYRE and submarine NR-1 in 1997 and 1998, respectively, and two cruises using the submarine Johnson SEA-LINK onboard the R/V EDWIN LINK in 1997 and 1998. Although the majority of ship-time expenses were funded through MMS, significant cost sharing with other agencies and programs was an important component of the fieldwork that extended the amount of sampling that could be carried out. Contribution of ship days with R/V GYRE was received from the State of Texas/Texas A&M University ship operations program. Use of the submarine NR-1 was provided courtesy of the United States Navy. Dive days with SEA-LINK were awarded by the National Undersea Research Program (NURP) center (in grants to PIs Fisher and MacDonald) and by the Office of Naval Research. Logistic details of these cruises are briefly recapitulated below.

### 3.7.1 Geophysical survey with R/V GYRE, 1997

The geophysical survey cruise was conducted with the R/V GYRE (Cruise 97-G-4). The goal was to use the TAMU$^2$ digital side-scan sonar and a 3.5kHz echo sounder to map the character and distribution of seafloor features in three areas of the Louisiana continental slope where hydrocarbon seeps are known to occur. The three areas are as follows:

1. A 36 sq. NM (123 km$^2$) area centered on the mud mound at the border of lease blocks GB424/425 (henceforth "GB425" site).

2. A 315 sq. NM (1050 km$^2$) area on the upper slope including the intensively studied chemosynthetic community sites Bush Hill, Brine Pool NR-1, Mussel Beach, and GC234 (henceforth the "Shallow" site).

3. A 360 sq. NM (1228 km$^2$) area on the lower middle slope due south of the Shallow site (henceforth the "Deep" site). After completing the geophysical surveys, the strategy was to collect cores for 36 hours at the end of the cruise to "ground truth" the geophysical images.

The R/V GYRE departed Galveston on 3 June 1997. GB425 was surveyed from 4 to 5 June, collecting 45.5 NM (84.2 km) of trackline data. Seven north-south tracks were surveyed and were spaced 1500 m apart with the sonar swath width set at 3000 m. In addition, an east-west track was collected over the GB425 vent mound and a sub-circular feature to the west. The "Shallow" site was surveyed from 5 to 9 June with data collected on 28 north-south tracks (387.0 NM/716.0 km), spaced 1500 m apart, and 7 north-south tracks (38.5 NM/71.2 km) situated between the main lines in the northwest corner (to fill in a shallower water area). As before, the sonar swath-width was set to 3000 m. Seventeen north-south lines (272.0 NM/503.2 km) were

run at the "Deep" site on 9 to 11 June with a spacing of 2500 m and a sonar swath-width of 5000 m. All of the surveys produced high quality data showing faults, carbonate mounds, mud volcanoes, mudflows, sediment flows, and other features whose identity is uncertain. On 13 June, R/V GYRE met a crew boat to exchange technical personnel and obtain core liners. The ship returned to the "Shallow" site for coring. Thirty-one cores (16 piston cores and 15 gravity cores) were collected during a 30-hour period on 13 and 14 June. With the coring finished, the R/V GYRE returned to Galveston, docking on 15 June 1977.

### 3.7.2 Detailed sampling with submarine SEA-LINK, 1997

A 24-day cruise on board the R/V EDWIN LINK, acting as tender ship for the submersible Johnson SEA-LINK II, was completed during 8 to 13 July 1997. This cruise (JSL97) comprised a major portion of the field effort for Year 1 of the program. The goals for this cruise were to complete an extensive series of sample collections, to release marked animals for growth studies, to deploy in-situ monitoring instruments, and to map the study sites for future effort. Data produced by this effort was crucial to the success of the program. Despite a very ambitious cruise plan, all goals were achieved thanks to the dedicated efforts of the cruise participants. A total of 52 stations were occupied at four separate sites. A complete list of stations is provided in Table 3.3. All collections and observations were logged in a computerized database to facilitate data management. A detailed dive log has been issued as an Appendix to this volume.

Table 3.3. Stations Sampled According to the Experimental Design Criteria.

| Site | Habitat | Level within habitat | Stations |
|------|---------|----------------------|----------|
| GC185 Oily diffusion Station prefix = BH | Tubeworm | Adult | AT1, AT2, AT3, AT4, AT5 |
| | | Senescent | ST1, ST2 |
| | | Juvenile | JT1, JT2, JT4, JT5, JT6 |
| | Mussel | | M1, M2, M3, M4, M5 |
| | Bacterial Mat | White Mat | B1 |
| | | Red Mat | B2 |
| | Reference | Unoccupied | boxcore from ship |
| GC234 Oily diffusion Station prefix = GC | Tubeworm | Adult | AT1, AT2, AT3, AT4 |
| | | Senescent | ST1, ST2 |
| | | Juvenile | JT1, JT2, JT4, JT5 |
| | Mussel | | M1, M2 |
| | Bacterial Mat | | B |
| GC233 Brine dissolution Station prefix = BP | Tubeworm | Adult | AT1 |
| | Mussel | Inner edge | M1, M4, M7 |
| | | Outer edge | M2, M3, M5 |
| GB425 Brine dissolution Station prefix = GB | Mussel | | M1, M2 |

### 3.7.3 Geophysical survey with submarine NR-1, 1998

Submarine NR-1 and her tender M/V CAROLYN CHOUEST arrived in the sampling area and commenced operations on 18 May 1998. NR-1 was equipped with two survey instruments. a 2-12kHz subbottom profiler (EdgeTech X-Star Chirp system) and a laser line scanner (Raytheon LS4096). The subbottom profiler was used to obtain high-resolution imaging of the near-bottom sediment layers. The laser line scanner was initially used to produce high-resolution, large-area images of the seafloor. The instrument experienced difficulties and was eventually disabled due to a flooded connector. The mission continued for several days, collecting detailed subbottom data from study sites GC234 and GC233 as well as fifteen other targets that had been identified in the TAMU[2] data. After four days, a flooded connector disabled the NR-1, and the mission was cut short. Despite the abbreviated cruise, invaluable and unique data were collected in support of program objectives.

### 3.7.4 Detailed sampling with submarine SEA-LINK, 1998

A 15-day cruise on board the R/V EDWIN LINK, tender ship for the submersible Johnson SEA-LINK I was completed during 4 to 18 July 1998. This cruise (JSL98) completed the sampling effort begun in the previous year. Most of the stations sampled in the JSL97 cruise were re-sampled. Sampling efficiency was improved on the basis of experience gained during the previous year so that more samples were collected in a shorter cruise. Two ancillary dive days were added to the end of the cruise by cost sharing with the Office of Navel Research, which provided the opportunity for intensive sampling of gas hydrate deposits. A complete list of stations is provided in Table 3.3.

### 3.8 Sampling Design

The key elements of the design for the tubeworm, mussel, and microbial mat studies are similar. There are three main effects: time, subhabitat, and replicate site. The study designs differ only in that there are a different number of subhabitats for tubeworms (3) and mussels and mats (2). With the addition of the two reference stations at each site, the total number of subhabitats increases to five for tubeworms and three for mussels and mats. However, because many of the habitats occur in the same sites, the reference stations were sampled only once, and the data was used for all three statistical analyses. In addition, the mussel and mat sites have site as a design difference, because two sites contain liquid hydrocarbons and two contain brine pools.

### 3.8.1 The relationship between sites and habitats

All three habitats occur only at the sites containing liquid hydrocarbons. Therefore, most of the study can be accomplished at GC234 and GC185. The tubeworm study is to be carried out only at liquid hydrocarbon containing sites. In this case, the site is a form of replication. The mussel study is being carried out at all four sites, so site is a major design element for the mussel study. The bacterial mat study could be carried out at all four sites or at just the liquid hydrocarbon containing sites, as in the tubeworm study. Reference habitats (i.e., sediment unoccupied by mussels, mats, or worms) are used to determine the effect of biological communities on background sediment geochemistry. Unoccupied sites are available at all study sites.

### 3.8.2 Univariate statistical model for the sampling plan

A statistical model is a mathematical representation of the relationships amongst the variables in the experimental design of the study. The statistical model is used to test null hypotheses. Model development is based on the elements of the design. The following 3-way analysis of variance (ANOVA) model represents the experimental design for the common sampling plan for time, habitats, and sites that can be used to test the first three null hypotheses ($H_{o1}$ - $H_{o3}$);

$$Y_{ijkl} = \mu + \alpha_I + \beta_k + \alpha\beta_{jk} + \gamma_l + \alpha\gamma_{jl} + \beta\gamma_{kl} + \alpha\beta\gamma_{jkl} + \varepsilon_{i(jkl)} \tag{3-1}$$

where $Y_{ijkl}$ is the ith observation, $\mu$ is the overall sample mean, $\alpha_I$ is the main treatment effect for time where there are 2 levels of j, $\beta_k$ is the main treatment effect for subhabitat where there are four or five levels of k, $\alpha\beta_{jk}$ is the time-habitat interaction, $\gamma_l$ is the main treatment effect for site where there are two or four levels of one, $\alpha\gamma_{jl}$ is the time-site interaction, $\beta\gamma_{kl}$ is the habitat-site interaction, $\alpha\beta\gamma_{jkl}$ is the second order interaction for all main effects, and $\varepsilon_{i(jkl)}$ is the random error associated with each of the three replicates. Time and subhabitat are fixed effects, but site is a random effect, because the two sites sampled were only chosen to represent the generality of a larger number of actual sites available. Because this is a mixed model with both random and fixed effects, the expected mean squares for each term must be calculated, and the appropriate error term used for each null hypothesis test. The expected mean squares and F tests are the same for all habitats but differ in the number of degrees of freedom, because there is a different number of sites and subhabitats sampled (compare Tables 3.4, 3.5, and 3.6).

Post hoc multiple comparison tests, such as the Tukey Test, are used to detect differences among sample means for main effects where there are more than two levels. Subhabitat is the only main effect that falls into this category. A priori linear contrasts will also be used to test if the reference station is different from the chemosynthetic subhabitat stations. A priori linear contrasts will be used to determine if there are site differences when both the liquid hydrocarbon and brine seep sites are sampled.

Table 3.4. Experimental design for the tubeworm sampling program.Sources are Time (T), Subhabitat (H), Replicate Site (S), Degrees of Freedom (DF), Variance Components that make the Expected Mean Squares (EMS) for the mixed model and Appropriate Mean Square (MS) term used as the denominator in the F Test for each source. There are four subhabitats: young, mature, senescent, and reference. There are just two sites.

| Source | DF | EMS | Error Term |
|---|---|---|---|
| T | 2 - 1 = 1 | $\sigma$(Error) + $\sigma$(T*H*S) + $\sigma$(T*S) + $\sigma$(T) | MS(T*S) |
| H | 4 - 1 = 3 | $\sigma$(Error) + $\sigma$(T*H*S) + $\sigma$(H) | MS(T*H*S) |
| S | 2 - 1 = 1 | $\sigma$(Error) + $\sigma$(T*H*S) + $\sigma$(T*S)+$\sigma$(S) | MS(T*S) |
| T*H | (2 - 1)(4 - 1) = 3 | $\sigma$(Error) + $\sigma$(T*H*S) + $\sigma$(T*H) | MS(T*H*S) |
| T*S | (2 - 1)(2 - 1) = 1 | $\sigma$(Error) + $\sigma$(T*H*S) + $\sigma$(T*S) | MS(T*H*S) |
| H*S | (4 - 1)(2 - 1) = 3 | $\sigma$(Error) + $\sigma$(T*H*S) + $\sigma$(H*S) | MS(T*H*S) |
| T*H*S | (2 - 1)(4 - 1)(2 – 1) = 3 | $\sigma$(Error) + $\sigma$(T*H*S) | MS(Error) |
| Error | (2)(4)(2)(2 - 1) = 16 | $\sigma$(Error) | |
| Total | (2)(4)(2)(2) - 1 = 31 | | |

Table 3.5. Experimental design for the mussel program. Sources are Time (T), Subhabitat (H), Replicate Site (S), Degrees of Freedom (DF), and Variance Components that make the Expected Mean Squares (EMS) for the mixed model and Appropriate Mean Square (MS) term used as the denominator in the F Test for each source. There are two subhabitats: in the center and at the edge of the brine pool. There are four sites: two oily (liquid hydrocarbons) and two brine seeps.

| Source | DF | EMS | Error Term |
|---|---|---|---|
| T | 2 - 1 = 1 | $\sigma$(Error) + $\sigma$(T*H*S) + $\sigma$(T*S) + $\sigma$(T) | MS(T*S) |
| H | 2 - 1 = 1 | $\sigma$(Error) + $\sigma$(T*H*S) + $\sigma$(H) | MS(T*H*S) |
| S | 4 - 1 = 3 | $\sigma$(Error) + $\sigma$(T*H*S) + $\sigma$(T*S) + $\sigma$(S) | MS(T*S) |
| T*H | (2 - 1)(2 - 1) = 1 | $\sigma$(Error) + $\sigma$(T*H*S) + $\sigma$(T*H) | MS(T*H*S) |
| T*S | (2 - 1)(4 - 1) = 3 | $\sigma$(Error) + $\sigma$(T*H*S) + $\sigma$(T*S) | MS(T*H*S) |
| H*S | (2 - 1)(4 - 1) = 3 | $\sigma$(Error) + $\sigma$(T*H*S) + $\sigma$(H*S) | MS(T*H*S) |
| T*H*S | (2-1)(2-1)(4-1) = 3 | $\sigma$(Error) + $\sigma$(T*H*S) | MS(Error) |
| Error | (2)(2)(4)(2 - 1) = 16 | $\sigma$(Error) | |
| Total | (2)(2)(4)(2) – 1 = 31 | | |

Table 3.6. Experimental design for the microbial mat sampling program. Sources are Time (T), Subhabitat (H), Replicate Site (S), Degrees of Freedom (DF), and Variance Components that make the Expected Mean Squares (EMS) for the mixed model and Appropriate Mean Square (MS) term used as the denominator in the F Test for each source. There are two subhabitats, pigmented and non-pigmented, in three sites.

| Source | DF | EMS | Error Term |
|---|---|---|---|
| T | 2 - 1 = 1 | $\sigma$(Error) + $\sigma$(T*H*S) + $\sigma$(T*S) + $\sigma$(T) | MS(T*S) |
| H | 2 - 1 = 1 | $\sigma$(Error) + $\sigma$(T*H*S) + $\sigma$(H) | MS(T*H*S) |
| S | 3 - 1 = 2 | $\sigma$(Error) + $\sigma$(T*H*S) + $\sigma$(T*S) + $\sigma$(S) | MS(T*S) |
| T*H | (2 - 1)(2 - 1) = 1 | $\sigma$(Error) + $\sigma$(T*H*S) + $\sigma$(T*H) | MS(T*H*S) |
| T*S | (2 - 1)(3 - 1) = 2 | $\sigma$(Error) + $\sigma$(T*H*S) + $\sigma$(T*S) | MS(T*H*S) |
| H*S | (2 - 1)(3 - 1) = 2 | $\sigma$(Error) + $\sigma$(T*H*S) + $\sigma$(H*S) | MS(T*H*S) |
| T*H*S | (2 - 1)(2 - 1)(3 - 1) = 2 | $\sigma$(Error) + $\sigma$(T*H*S) | MS(Error) |
| Error | (2)(2)(3)(2 - 1) = 12 | $\sigma$(Error) | |
| Total | (2)(2)(3)(2) - 1 = 23 | | |

### 3.8.3 Multivariate analyses for the sampling plan

The models in the above section are univariate and can be used to test for differences among the main effects for the variables measured. The models are also used to test the first three null hypotheses concerning differences due to temporal change and spatial variability among and within specific chemosynthetic habitats. However, to test the fourth null hypothesis, about differences among the types of chemosynthetic communities, a multivariate analysis is necessary. In this case, all data collected during the study can be synthesized in one general analysis where the experiment-wide error rate is controlled. The purpose of the analysis is to identify the abiotic factors that control biotic factors among the three different chemosynthetic habitats.

In the end, the multivariate data set is a matrix consisting of rows of observations for each sample (identified with time, site, habitat, and subhabitat) and columns of values for each measurement taken at each station. Many of the columns of data in this matrix are auto correlated, or co-vary; therefore, a simple bivariate test, such as calculation of correlation coefficients for all possible combinations of variables, is inappropriate and introduces multiple testing errors. Multivariate analysis is used so that important relationships are not ignored among the variables and to control the experiment-wide error rate.

Principal Components Analysis (PCA) is the multivariate technique of choice. PCA is a transformation of the data set to create another data set with two desirable attributes – the principal components are mutually orthogonal (which means that the columns are now uncorrelated), and the components are extracted in order of decreasing variance. This gives a

data set that has a reduced number of variables but still contains most of the information in the original data set. The reduced number of variables is used to test hypotheses or make predictions about how abiotic factors are related to biotic factors. Hypotheses are tested by visualizing plots of PCA scores for each row (i.e., observation) where the various elements of the experimental design are plotted as the symbols for the observation. This technique has been used successfully in many environmental studies.

# 4.0 Field Methods

## 4.1 Introduction

Extensive sampling of the community stations was completed with the use of the submersible Johnson SEA-LINK during research cruises in 1997 and 1998. The logistics and sampling design for these cruises was presented in the previous chapter. Many of the sampling methods, equipment, and procedures were developed expressly for this program and related research. This chapter provides a description of the field methods and procedures used and details the unique aspects of the effort.

## 4.2 Submarine Johnson SEA-LINK

SEA-LINK is a four-person, battery-powered vehicle that operates to a maximum depth of 1000 m (Figure 4.1A). The SEA-LINK typically carries two crew members and two scientists or observers. The pilot and one observer sit forward in an acrylic sphere. One other observer and a safety officer ride in a second chamber in the aft of the vehicle. SEA-LINK is launched from the deck of the tender, which during this program was R/V EDWIN LINK, by use of a heavy-lift A-frame. Launch and recovery operations can be carried out in moderately heavy seas. Loss of dive due to weather was minimal during this program. In normal operations, SEA-LINK dives twice per day and remains on the bottom for approximately 2.5 hours each dive. The monitoring equipment, which is standard to the SEA-LINK, includes video and still cameras. The video camera is mounted on a pan-and-tilt assembly under the control of the forward observer. The still camera is either fired manually or by an interval-trigger. A macro-focus camera system is also available for detailed documentation. Samples are collected by use of a seven-function mechanical arm that can be equipped with a clamshell-type scoop. Additional sampling equipment includes a suction-sampler that feeds into as many as 12 discrete containers. Samples of the ambient water can be collected through several intake lines that are plumbed into the aft chamber.

A sampling plan for a typical sampling day was agreed to during a series of pre-dive conferences and the observers were provided with detailed check lists of stations to survey, samples to collect, and other tasks to be accomplished. The sequence of collections would be planned to accommodate the sample-processing schedule during the morning and afternoon activities. The SEA-LINK was generally launched so that it would reach bottom at or near the stations that comprised the sampling objectives for the dive. Once on bottom, the forward observer would start recording video sequences and audio notes on a high-band 8-mm recorder connected to the SEA-LINK video camera, recording that continued uninterrupted throughout the dive. These videos, along with written notes, comprised the scientific documentation for the samples collected during the dive. When the dive finished and the SEA-LINK was recovered, the observers would compare and combine notes to ensure an accurate record of the collections was taken. Problems that required immediate attention were discussed with the chief scientist so that missed tasks could be completed in the second dive of the day. Science meetings were held each

evening after the dives and immediate sample processing had been completed. During these meetings, the observers who had dived that day would recount their experiences and shared any difficulties that had been encountered. The lists of samples would then be reviewed to determine the priorities and tasks for the sampling activities to be accomplished the next day. The following sections detail significant aspects of collection and other field methods.

## 4.3 Navigation

During the 1997 and 1998 sampling cruises with SEA-LINK, the tender ship R/V EDWIN LINK was navigated with differentially corrected global positioning system (GPS) (accurate to approximately 5 m). The position of the submarine on the bottom was determined by use of a short base-line acoustic system. An estimate of the submarine's absolute position was obtained from the offset between the two vessels. Although this method is adequate for reoccupying stations, it was sensitive to factors such as how the submarine was oriented and changes in the water column that affect acoustic transmission. Consequently, the navigation system might indicate that the submersible was occupying a particular station, while the estimated position of the station was only accurate to about 10 m. In many cases, errors of as much as 30 m apparently occurred. Efficient submarine sampling at multiple stations requires the pilot and scientists to know the relative bearings between stations. Putting this in perspective, the study sites encompass areas on the order of 100 x 100 m and include from 5 to 15 sampling stations. If station positions are only known with an error of 10 m, then bearings between stations will not be accurate enough for reliable navigation. Consequently, valuable bottom time is expended and replication of samples is difficult to achieve. Acoustic pingers were also placed at prominent points at the stations. By homing on these pingers, the submarine pilots were usually able to find sampling stations with minimal searching.

## 4.4 Markers and Sketch Maps

To maximize spatial control, pragmatic operational procedures during the dives and image processing and geographic information system (GIS) methods were combined and applied to the best available information on the study sites. The pragmatic methods included standard markers for the stations and a set of simple sketch maps designed to be used by the submersible scientist and pilot during the dives.

Each station was marked with a combination float and visual scale (Figure 4.2). The float, which was painted with reflective paint, provides high-visibility marking from the vantage point of the submersible. The marker, a 30 x 30 cm square painted with a black and white checker pattern, provides a marking for an over-head vantage point and a convenient scale for future visual survey efforts. Each marker was labeled with an abbreviated form of the station name, e.g., AT1 for BHAT1. Hand-drawn sketch maps included locations of individual stations and relative bearings between stations (Figure 4.3). These sketches were continually updated and modified as stations were marked and occupied, or as better information became available about station locations, adjacent landmarks, etc.
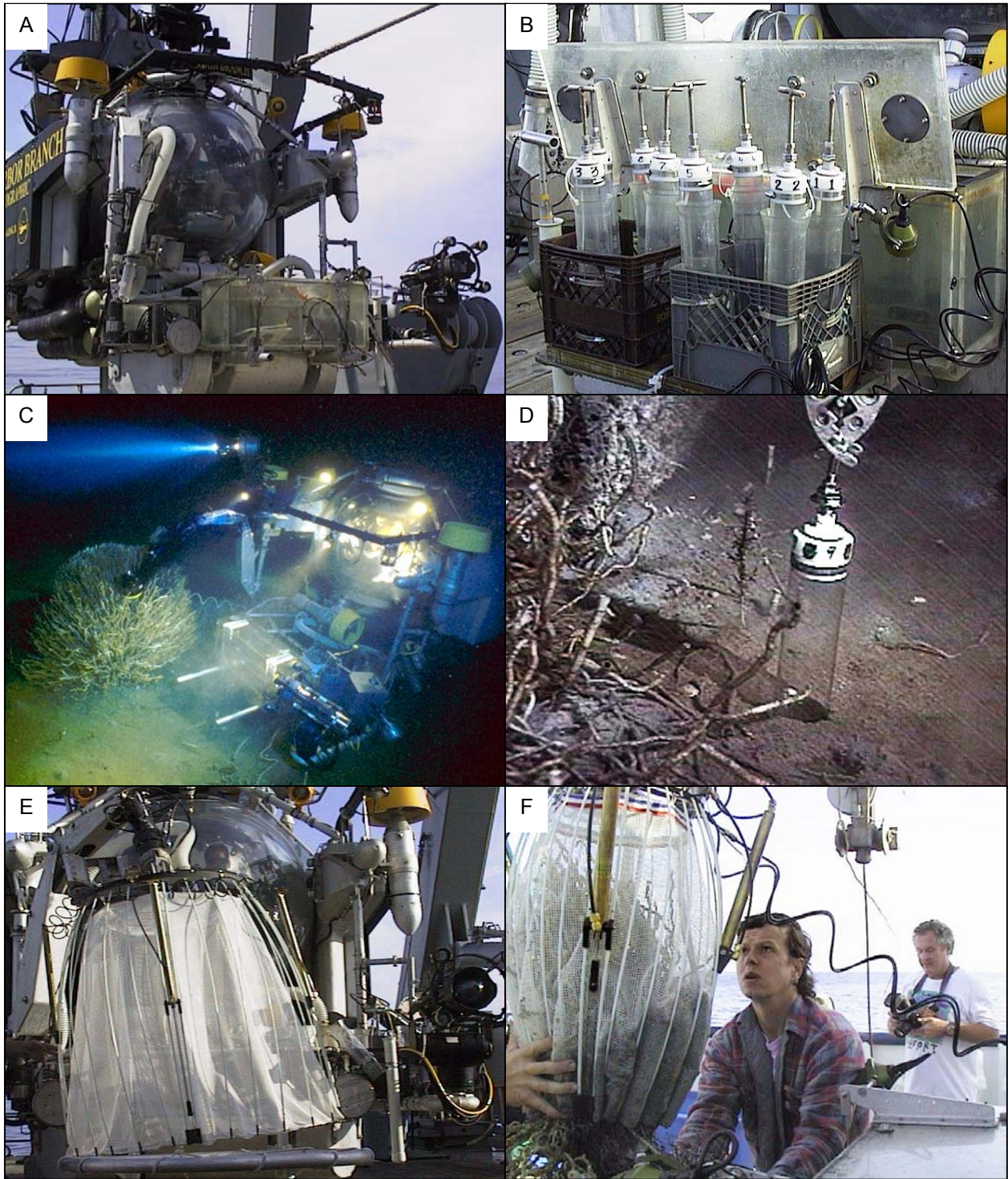
Figure 4.1. Submersible sampling operations with submarine Johnson SEA LINK. SEA LINK is launched from the deck of the tender (A). Plexiglass box is used for recovering mussels and other animals at bottom temperatures (A and B). Push cores are used for sediment collection (B). On the bottom, SEA LINK collects samples with use of a mechanical arm shown deploying the tubeworm-staining device (C) and a push core (D). Tubeworms were collected with use of large (E) and small (F) bushmaster devices.

## 4.5 Sediment Collection

An important component of the sampling program was to collect sediment from the stations defined by the study design. The majority of sediment samples were taken with so-called push cores. These were butyrate tubes with 7 cm internal diameter and 40 cm length. The cores were mounted on nylon plugs fitted with tee-handles and one-way valves. The tee-handle allowed the mechanical arm of the SEA-LINK to grasp the core and force it into the sediment. The valves allowed water displaced by sediment to escape from the tube. Typically, SEA-LINK carried eight push cores on a rack mounted of the front of the work platform (Figure 4.1B). Each core was marked with a sequence number that was clearly visible to the forward observer. When collecting a core, the observer would note the station number, the placement of the core relative to the station marker and to faunal clusters, the core sequence number, and any other peculiarities of the collection. An important distinction was the relation of cores to tubeworm clusters. Cores could not be collected within a tubeworm cluster because of the interference from the tube mass. Cores were collected as close as possible to the base of the cluster (Figure 4.1D) often under the overhang of the longer worms. Other cores were collected through or adjacent to bacterial mats. Whenever possible, core collection was recorded with the video camera. As the pilot slowly pushed the core tube into the sediment, ideally in a vertical orientation, the observer closely monitored the circle of sediment inside the tube. The pilot would continue to push down until the circle began to move below the level of the surrounding sediment, at which point insertion was stopped to avoid compacting the sample. Push cores generally recovered 20 to 25 cm of sediment. When the submarine was recovered, the core tubes were quickly removed from their holders, capped, taped and labeled, and then stored in a shipboard cold room until processed by the individual investigators. In 1998, each core was photographed prior to processing to retain a record of sediment visual characteristics.

A series of control sediment samples was collected using a Gulf of Mexico box core deployed from the surface by R/V EDWIN LINK. These cores were taken within the approximate boundaries of the sampling stations or at approximately 2 km distances from the stations. Because they did not sample tubeworm clusters or mussels, they were deemed control samples of the seep area un-colonized by chemosynthetic fauna. When the box cores were brought onboard the ship, sediments were sub-sampled from within the core by manually inserting a core tube, which was then treated like a standard push core. Limited sediment samples were also collected by use of the clam-shell scoop on the SEA-LINK mechanical arm.

Figure 4.2.    Combination float and bottom marker used to mark sampling stations.

## 4.6 Mussel and Associated Fauna Collection and Shipboard Processing

Quantitative collections ("ring collections") of mussels and associated fauna were made from each mussel bed to assess mussel density and size-frequency distributions, to characterize the faunal associates, and to provide samples for other investigators. Two different shapes of "rings" were used over the course of this study. Both "rings" were constructed of 20 cm wide and 2 mm thick stainless steel. One, a 0.5 m diameter circular ring, was used previous to 1997 and again in 1998 (described by Nix *et al.* 1995). At the suggestion of the submersible pilots a new 0.5 m square ring was built and used in 1997. This "ring" had the advantage that the SEA-LINK collection scoop, which has a square footprint, goes right up to the edge of the "ring," making it more efficient for pilots to clear out the ring. However, it was discovered while at sea that it had the significant disadvantage of sinking mussel aggregations over very soft substrate (at the Brine Pool) rather than cutting out an area to subsample. Therefore, none of the quantitative (density)

data on Brine Pool collections from 1997 is considered reliable, and we have substituted data Brine Pool collections made in 1995 to allow comparison to the other study sites. The other collections made with the square ring in 1997 appeared satisfactory based on submersible observations and video records, and the data is included here.

The placement of the rings for these collections was not random; the sub pilots were instructed to place the rings in an undisturbed portion of the mussel bed that appeared representative of the general area and amenable to collection. The ring was placed firmly in the mussel bed and all fauna within the inside of the ring were collected first by scooping into the insulated box on the front of the submersible and then by suctioning into other containers. Video documentation of the ring was taken during and after collection to record animals that "escaped" or were not collected (left behind); later, counts were corrected for these missing animals. After recovery of the submarine, the entire collection was transferred to chilled water for separation and enumeration of the fauna. The lengths of all living mussels collected were measured. An average of about 6% of the living mussels were damaged during the collections. These damaged mussels were counted, and the best possible estimate of their length was made. After measurement, mussels were removed from the collection for other studies, including genetic analyses, histopathology, determination of hydrocarbon loads, stable isotope determinations, and determination of condition indices. The associated fauna was subsampled at sea for stable isotope analyses and the remainder placed in 10% formalin in seawater for transport back to the laboratory.

Six to twelve mussels from each collection were sampled for determination of physiological condition. The shell length of each mussel was measured. The shell was then opened a few millimeters to drain seawater from the mantle cavity. The abductor muscles were cut over a pre-weighed sample bag, collecting all internal fluids, and the tissue scraped into the sample bag and stored at -20°C. The empty shell was cleaned, dried, and marked for later determination of shell volume. The samples were transported back to Pennsylvania State University on dry ice and stored at -70°C until further analysis.

Figure 4.3.    Hand-drawn sketch maps of locations for individual stations and the relative bearings between stations.

## 4.7 Mussel Growth and Transplant Studies

One hundred and fifty mussels collected at GBM1 in 1997 were measured and marked as described below for a growth study of mussels at this newly discovered site. The marked animals were re-collected in 1998 and re-measured.

For the reciprocal transplant studies, ring collections from a site were augmented with several scoops of mussels (into a separate recovery container) to assure sufficient material for the study. In a cold room (8°C) on board the ship, the length of each mussel was measured. Then a commercial, color-coded and numbered larval fish tag (6.9 x 3.2 mm) was glued to the umbo for identification (Nix *et al.* 1995). Three hundred individuals of a representative size range from each location were marked in 1997 and half redeployed at their original collection site (marked controls) while the other half were deployed at the transplant site. Immediately before the launch of the submersible, the marked mussels were placed in temperature insulated deployment containers filled with chilled seawater (8°C). Upon arrival at the experimental site, the lids of the deployment containers were removed and the mussels were re-deployed.  All mussels were deployed within 24 h of their collection. Approximately one year later, the marked mussels were re-collected, and their lengths re-measured. Ten additional mussels were processed at sea for later determination of condition index from each of the collection and deployment sites in both 1997 and 1998 (unmarked controls).

A short-term transplant experiment was conducted in 1997 to provide information on the time course of change in condition index, water content, and glycogen content in mussels removed from a favorable environment. Mussels were collected from the inner zone of the Brine Pool and placed in boxes constructed of one-half inch mesh plastic coated fence wire that were designed such that the lid could be shut on the bottom by the submersible.  Between 8 and 14 mussels were placed in each of four boxes, and an additional 12 mussels were brought to the surface after the dive. Two of the boxes were returned to the original collection site (controls), and two were transplanted onto bare mud substrate about 100 meters from the Brine Pool. One box from each location was picked up at the end of the cruise (after a 13-day deployment), and the other two were collected after a 42-day deployment during another cruise. After collection, the mussels were sampled for determination of physiological condition as described above.

## 4.8 Tubeworm and Associated Faunal Collections and Shipboard Processing

Intact vestimentiferan aggregations were collected along with all associated fauna using the so-called bushmaster devices, which were designed specifically for this collection and required by this program. Each collection device consists of an outer mesh net suspended in a frame of fiberglass rods and four hydraulic pistons (Figure 4.1E, F). The first deployment of the bushmasters in the 1997 SEA-LINK cruise made use of nets lined with 1 cm mesh, which allowed many smaller animals to escape. During the 1998 SEA-LINK cruise, the mesh was lined with 4 mm nylon netting. The frame provides support during deployment and keeps the net open while it is positioned over a vestimentiferan aggregation. The four hydraulic pistons are attached to a steel "draw-string" cable that is threaded through the open end of the net so that it can be

closed hydraulically, and an intact aggregation can be securely contained during collection and recovery. The large bushmaster has a maximum open diameter of 150 cm and a height of 120 cm (Figure 4.1E). The small bushmaster has a maximum open diameter of 70 cm and a height of 67 cm (Figure 4.1F). When closed, the bottom portion of the devices can be cinched to a diameter of less than 10 cm. These devices have also been used to collect tubeworm aggregations from hydrothermal vents on the Juan de Fuca Ridge allowing direct comparison between these habitats.

Immediately after collection, samples of the major associated macro fauna were removed and frozen for isotopic analysis, samples of tubeworms were removed for genetic and physiological studies, and some stained tubeworms were removed for the processing described below. The intact aggregation with the remaining associated fauna was preserved in 10% formaldehyde-seawater, bagged and stored in a 55-gallon drum for transportation to the laboratory for subsequent processing.

## 4.9 Tubeworm Growth Studies

Staining the anterior ends of their tubes and monitoring the deposition of new tube material above this stain mark followed growth of over 600 tubeworms from 22 aggregations. The tubes were stained using an *in-situ* staining apparatus manipulated by the SEA-LINK submersible. The apparatus used a 20-liter collapsible plastic reservoir to hold the stain, which was plumbed through a reversible hydraulic pump to a 25 cm diameter clear plastic dome. The dome was placed over a group of vestimentiferans (normally 20 to 40 individuals) in an aggregation, and the hydraulic pump delivered a positively buoyant saturated solution of the dye Acid Blue 158 (in 40% seawater) from the reservoir into the dome (Figure 4.1C). The tubeworm tubes inside the device were continuously exposed to this staining mixture for approximately five minutes. Then the staining mixture was redirected from the dome back to the reservoir by reversing the flow of the hydraulic pump. Up to six groups of vestimentiferans were stained during a single dive. During the staining process, the tubeworms retracted inside their tubes and were therefore not directly exposed to the dye solution. The tubeworms appeared healthy during follow-up dives to the sites. There was no evidence of mortality due to staining or of differential tube growth compared to adjacent unstained tubeworms. Subsequent anterior tube growth is readily apparent the following year as white tube increments above the blue-stained tube section (Bergquist *et al.* 2000). To confirm that tube growth does not occur in the middle region of the tubes of these species, several aggregations of smaller tubeworms were stained entirely, either in situ or in buckets on board ship, and then re-deployed. When appropriate and possible, aggregations containing stained individuals were collected intact using one of the bushmaster devices described above. In other cases, the stained animals were collected using the manipulator arm of the SEA-LINK and recovered in a temperature-insulated box mounted on the front of the submarine (Figure 4.1A, B).

When time allowed, ten stained worms from each collection were processed at sea for calculation of growth rate, determination of biomass, and subsequent calculation of condition index. In some collections, ten additional tubeworms were taken as back-up samples. These animals were placed in a recirculating water bath (~8°C), and the tube length prior to staining,

new tube growth, and anterior tube diameter of each individual were measured. Each animal was removed from its tube, dissected and placed into two separate sample bags: one containing the vestimentum, plume, and upper body wall and the other containing the trophosome and lower body wall. All samples were individually labeled and frozen on board the ship and returned to Pennsylvania State University on dry ice for further processing. All remaining stained tubeworms were fixed in formalin and returned to the Pennsylvania State University.

# `5.0 The Physical Environment at the Seep Sites[*]

## 5.1 Background

Chemosynthetic communities are found in the Gulf of Mexico at depths greater than 500 m. Several sites in Green Canyon and Garden Banks were investigated during two cruises in 1997 and 1998.  The study region is sandwiched between these two well-studied areas.

To the north, a large anti-cyclonic gyre dominates the Texas-Louisiana Shelf. Currents along the coast are predominantly southerly resulting from the prevailing wind stress and buoyancy forcing of the Mississippi River outflow water. A return flow brings water east along the shelf break (Cochrane and Kelly 1986). The Louisiana-Texas Shelf Circulation Study confirmed this general scheme, although it still remains uncertain as to whether or not the easterly flow returns to the Louisiana coast to fully close the coastal gyre (Nowlin *et al.* 1998).

To the south, the currents of the waters of the deep northern Gulf of Mexico are dominated by the passage of anti-cyclonic, warm-core eddies or rings that break off the Loop Current. These large, circular, baroclinic structures, 250 to 300 km in diameter, transit slowly to the west along the continental slope losing their energy as they interact with the slope off the eastern coast of Mexico (Forristall *et al.* 1992, Kirwan *et al.* 1984, Lewis and Kirwan 1987). These warm-core eddies are often associated with cyclonic, cold-core eddies. Interactions between the cyclonic and anti-cyclonic rings can produce very large currents capable of moving large amounts of water on or off of the shelf (Biggs and Muller-Karger 1994, Brooks 1984).

Although the circulation of the overlying waters is fairly well understood, surprisingly little is known about the physical environment of the sea floor at these sites. Knowledge of the deep currents, temperature, and salinity is important in understanding how the environment affects the ecosystems found in the study region. Ocean currents give clues to the dispersal pathways taken by larvae of chemosynthetic species. Ocean temperatures can affect the reproductive cycling of organisms present.  Ocean temperature also affects the stability of gas hydrate deposits.

During this program we made a series of measurements to help characterize the temperature and current regimes that affect the chemosynthetic communities. We sought to characterize the temperature range and variability and acquire measurements of near-bottom current speed and direction.

## 5.2 Methods

To learn more about the physical environment at the study sites, we made physical measurements as part of the two submersible cruises carried out during this program on the R/V EDWIN LINK. A current meter mooring was deployed in GC185 during the August 1997 cruise and recovered about nine months later on the May 1998 cruise. During these two cruises,

---

[*] This section was authored by Norman L. Guinasso, Jr.

measurements with a recording conductivity, temperature, and depth instrument (CTD) were made from the support ship, R/V EDWIN LINK, as well as from the SEA-LINK itself.

The mooring, described in more detail in MacDonald (1998b, Figure 3.8), consisted of two Oregon Environmental Inc. 9407 vector-averaging current meters. These current meters were selected mainly on the basis of cost as were the plastic fishing floats used for buoyancy. Again to lower cost, the mooring used a single Benthos 866A acoustic release and incorporated a weak link that could have been cut by the Johnson SEA-LINK if the release had failed. Table 5.1 gives details of the mooring deployment. The mooring was planned to observe temperature currents near the top of the water column and near the bottom as well. The top meter, located at a depth of 250 m, was intended to pick up any currents associated with the passage of rings. The bottom meter was placed about 10 m above the bottom raising it above most of the bottom Ekman layer that might be present. The units were set to record a 10-minute average each hour allowing them to record up to a year of data.

Table 5.1. GC185 Current meters.

| Location | 27° 46.95' N; 91° 30.28' W |
|---|---|
| Water depth | 547 m |
| Depth of bottom meter | 537 m (10 m above bottom) |
| Depth of top meter | 247 m (300 m above bottom) |
| Sampling interval | 10-minute average every hour |
| Deployed | 9 August 1997 |
| Recovered | 22 May 1998 |

The CTD instruments used were a Seabird SBE19 (serial #1992) owned by Texas A&M and a Seabird SBE25 (serial #254334-0041) owned by the Harbor Branch Oceanographic Institute. Both recorded temperature depth and conductivity internally. The times and type of CTD measurements made during the two cruises are given in the appendix volume. During the 1997 cruise, nine CTD profiles were made from the R/V EDWIN LINK.  Other profiles were collected from CTD instruments mounted on the submarine or, in the case of lowering into the brine pool or mud volcano, from a small winch mounted on the submarine.

## 5.3 Measurements of Currents and Temperature

The current meter mooring was successfully recovered during the 1998 SEA-LINK cruise. After recovery of the mooring, data was downloaded from both meters and provided records for a duration of 286 days for both temperature and current. Table 5.2 shows the speed and direction statistics for the top and bottom meters. The values in the body of the table are the fraction of the time the current had a particular speed and direction.

For the top meter, the right-hand column shows that the current was less than 10 cm/sec 55% of the time. The bottom row shows the number of measurements in each octant centered at the

direction shown. Currents were about twice as likely to be toward the eastern or western octant

than in the other six direction groupings. For the bottom meter, currents were below 10 cm/second 93% of the time and predominantly to the north.

Table 5.2. The frequency, in percent of time, that currents had a particulate range of speed and direction for the top and bottom meters. The column at the left summarizes the speed ranges for all directions. The row at the bottom summarizes the percent of time for octant of direction for all speeds.

| Speed (cm/sec) | N | NE | E | SE | S | SW | W | NW | Total |
|---|---|---|---|---|---|---|---|---|---|
| | | | | CHEMO Top CM | | | | | |
| < 2 | 7.48 | 0.17 | 0.35 | 0.06 | 0.15 | 0.25 | 0.41 | 0.41 | 9.28 |
| 2 - 10 | 5.01 | 4.87 | 5.29 | 3.52 | 3.84 | 3.79 | 11.03 | 8.05 | 45.40 |
| 10 - 20 | 1.48 | 2.47 | 5.20 | 2.92 | 1.16 | 2.46 | 10.74 | 3.57 | 30.00 |
| 20 - 30 | 0.26 | 0.71 | 3.44 | 0.57 | 0.03 | 0.45 | 3.91 | 0.25 | 9.62 |
| 30 - 40 | 0.00 | 0.33 | 2.89 | 0.01 | 0.01 | 0.17 | 1.05 | 0.01 | 4.47 |
| > 40 | 0.00 | 0.01 | 1.15 | 0.01 | 0.01 | 0.01 | 0.01 | 0.01 | 1.21 |
| Total | 14.23 | 8.56 | 18.32 | 7.09 | 5.20 | 7.13 | 27.15 | 12.30 | |

| Speed (cm/sec) | N | NE | E | SE | S | SW | W | NW | Total |
|---|---|---|---|---|---|---|---|---|---|
| | | | | CHEMO Bottom CM | | | | | |
| < 2 | 24.32 | 1.70 | 3.28 | 2.00 | 1.12 | 0.68 | 3.19 | 1.68 | 37.97 |
| 2 - 10 | 8.60 | 6.16 | 7.87 | 10.90 | 6.03 | 3.06 | 5.60 | 8.70 | 56.92 |
| 10 - 20 | 1.02 | 0.57 | 0.77 | 0.75 | 0.01 | 0.09 | 0.12 | 1.65 | 4.98 |
| 20 - 30 | 0.00 | 0.01 | 0.01 | 0.01 | 0.01 | 0.01 | 0.01 | 0.01 | 0.07 |
| 30 - 40 | 0.00 | 0.00 | 0.00 | 0.00 | 0.00 | 0.00 | 0.00 | 0.00 | 0.00 |
| > 40 | 0.00 | 0.00 | 0.00 | 0.00 | 0.00 | 0.00 | 0.00 | 0.00 | 0.00 |
| Total | 33.94 | 8.44 | 11.93 | 13.66 | 7.17 | 3.84 | 8.92 | 12.04 | |

Table 5.3 from DiMarco (2000) has provided the amplitudes of the tidal components derived from the analysis of these two current meter records using the method of cyclic descent in the manner of DiMarco and Reid (1998). Shown is the period in hours for each of the tidal constituents, the amplitudes of the semi-major and semi-minor axes, and the orientation of the tidal ellipse. Negative values indicate clockwise "rotation." The amplitudes of the tidal components are generally less than about 1 cm/sec at the top meter and less than 0.6 cm/sec at the bottom meter.

Figure 5.1 shows the power spectra from the top and bottom current meter data. Evident are significant peaks near 12 and 24 hours. The inertial period at 27.7N is 25.7 hours so the peak near one cycle per day can be expected to contain inertial as well as tidal signals.

Inertial currents can be expected to rotate clockwise. Figure 5.2 shows rotary power spectra from the top and bottom current meter records calculated by the method of Gonella (1972). The

top meter shows a predominant clockwise rotation as would be expected from inertial currents. Rotary spectra from the bottom meter do not seem to have a rotational preference.

Table 5.3. Tidal analysis of the two current meters showing magnitudes of the semi-major and semi-minor tidal constituents and the direction of the resulting tidal ellipse.

| | | Top Meter | | |
|---|---|---|---|---|
| | Period (hours) | Major (cm/s) | Minor (cm/s) | Direction (N) degrees |
| M2 | 12.42 | 1.02 | -0.12 | 1117.9 |
| S2 | 12.00 | 0.19 | 0.01 | 131.5 |
| N2 | 12.66 | 0.34 | 0.01 | 120.5 |
| K2 | 11.97 | 0.07 | -0.02 | 85.1 |
| K1 | 23.93 | 0.99 | -0.30 | 174.1 |
| O1 | 25.82 | 0.98 | 0 | 145.8 |
| P1 | 24.07 | 0.28 | 0.06 | 65.7 |
| Q1 | 26.87 | 0.47 | -0.02 | 179.0 |

| | | Bottom Meter | | |
|---|---|---|---|---|
| | Period (hours) | Major (cm/s) | Minor (cm/s) | Direction (N) degrees |
| M2 | 12.42 | 0.27 | 0.07 | 20.9 |
| S2 | 12.00 | 0.12 | 0.02 | 51.8 |
| N2 | 12.66 | 0.15 | -0.08 | 139.6 |
| K2 | 11.97 | 0.09 | 0.02 | 83.9 |
| K1 | 23.93 | 0.56 | 0.20 | 185.4 |
| O1 | 25.82 | 0.54 | 0.09 | 133.8 |
| P1 | 24.07 | 0.40 | -0.33 | 19.1 |
| Q1 | 26.87 | 0.34 | 0.10 | 239.0 |

## 5.4 Temperature Records

Temperature was measured along with current speed and direction by the sensors in the current meters. A long-term temperature record in this region was also collected by Ian MacDonald from December 1993 through August 1995 using a recording thermistor located about one meter off the bottom. This recording thermistor was first deployed in GC185, recovered in September 1994, and then moved to a nearby site in GC234.

The top and middle panels in Figure 5.3 shows the temperature time series collected at GC185 in 1993 and 1994 and at GC234 in 1994 and 1995. The bottom panel in Figure 5.3 shows the temperature time series from the bottom and top meters during the 1997-1998 deployments. The range of temperatures in the bottom meter and the near-bottom thermistor deployment are shown in Table 5.4. Considerable variability is evident in the records from both the top and bottom meter.
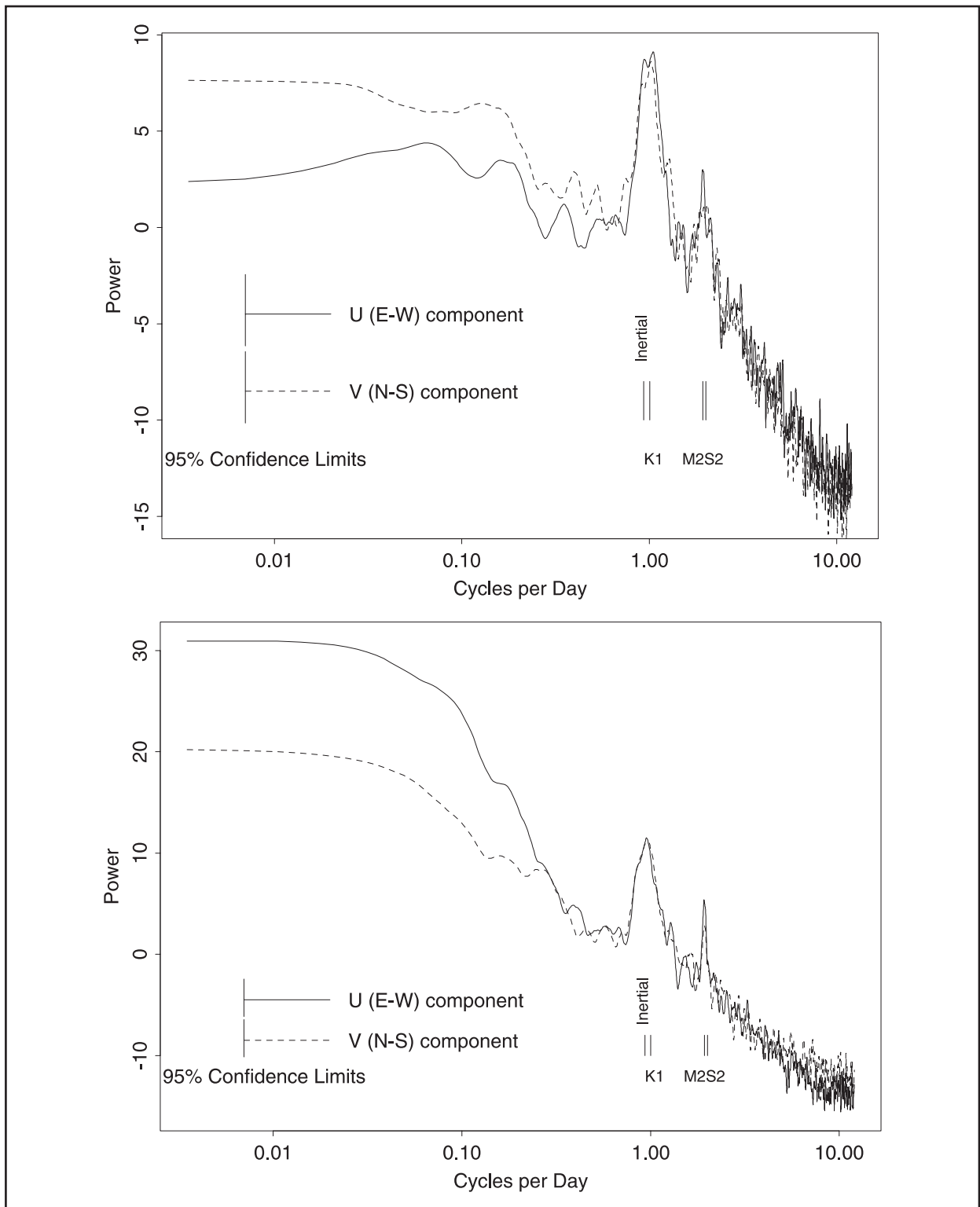
Figure 5.1. Power spectra of the current speed from the top and bottom meters on the GC185 meter mooring. The bar shows 95% confidence limits of the spectral estimates. Vertical lines mark the period of the M2 and K1 tides. The vertical line labeled "Inertial" is the inertial period at the mooring site.
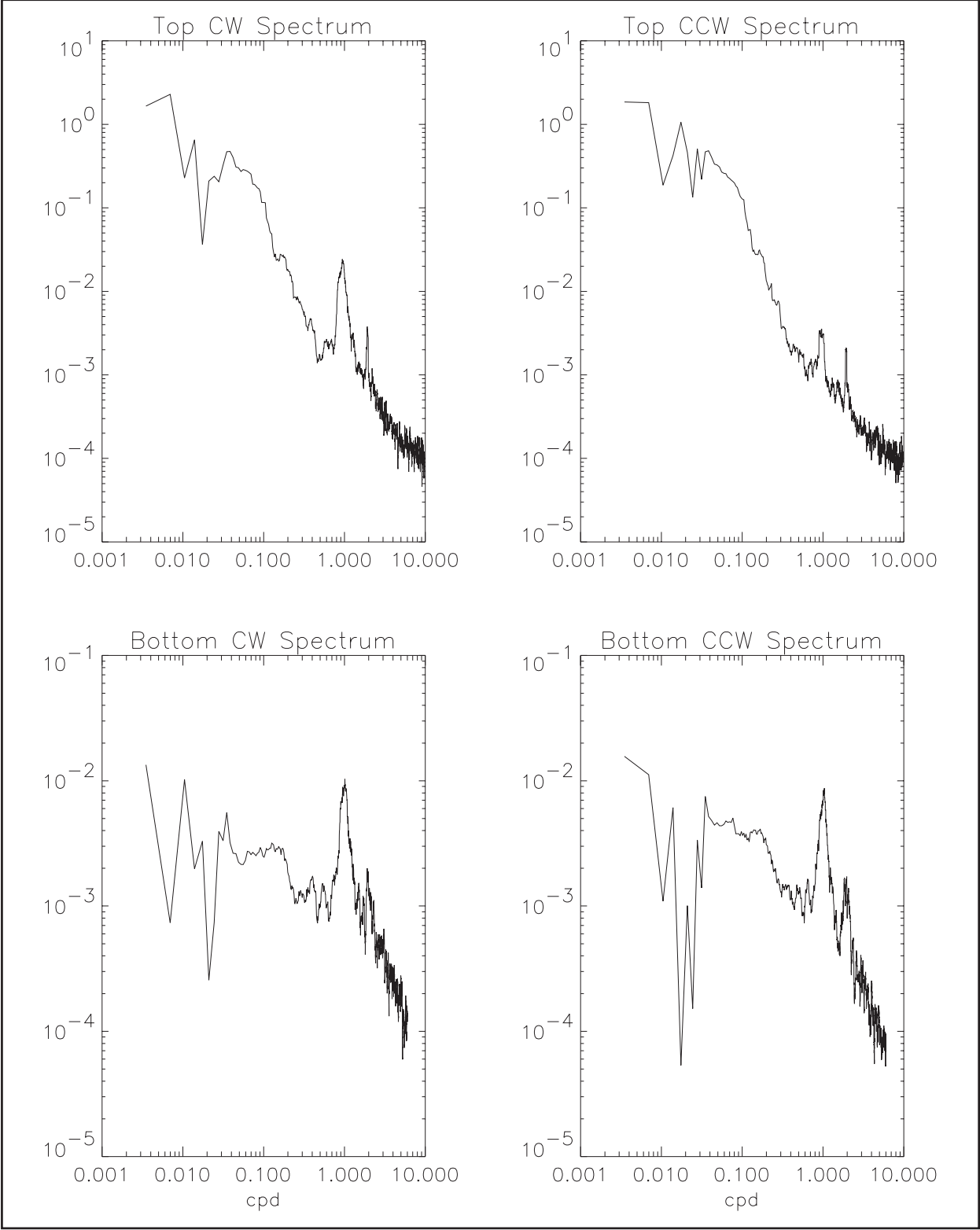
Figure 5.2. Rotary spectra from the GC185 current meters. The left panel for each meter gives the clockwise spectra; the right panel gives the counterclockwise spectra.
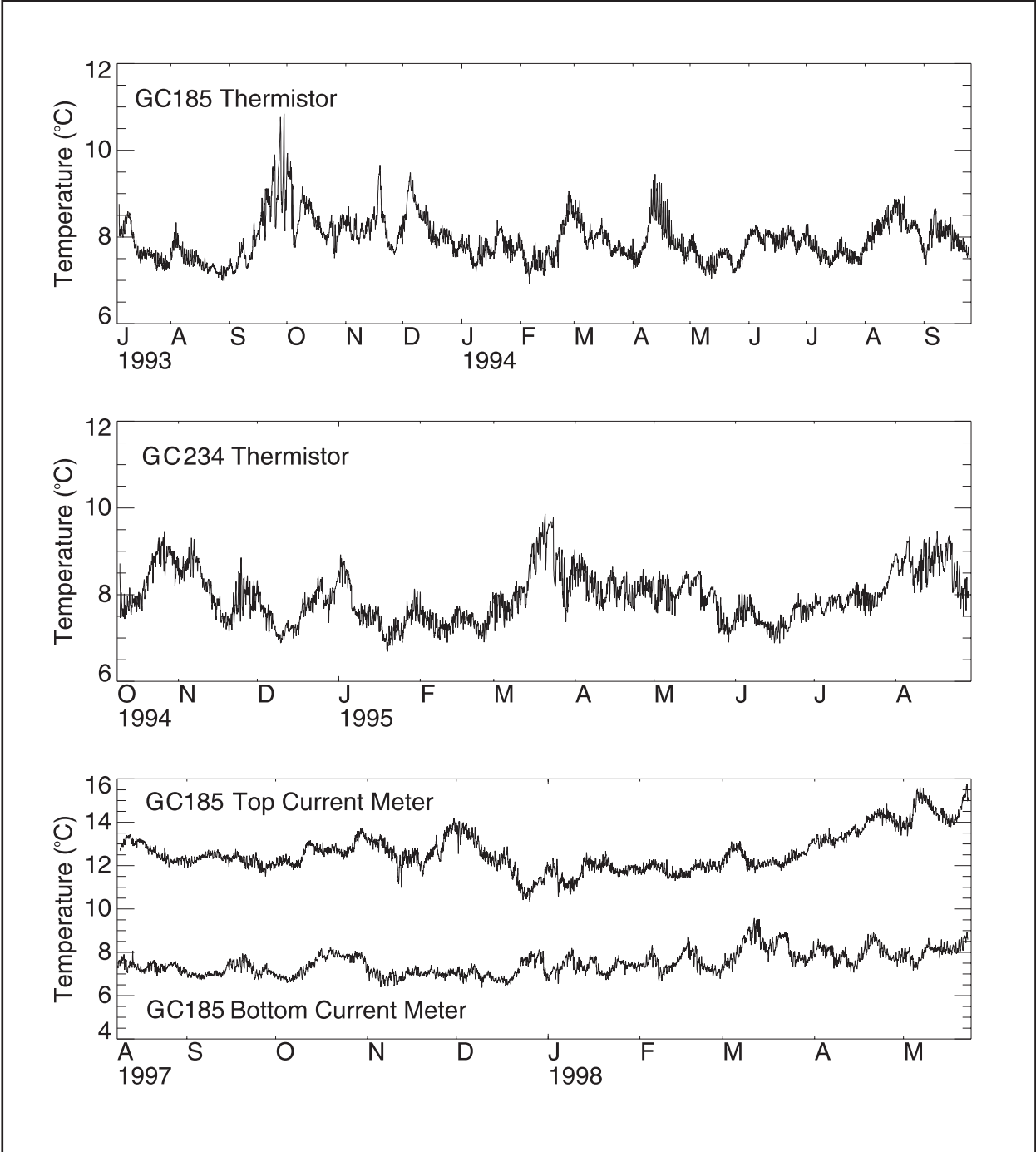
Figure 5.3. Time series of temperatures recorded by thermistors at GC185 and GB425. Time series of temperature collected at GC185 at the top and bottom current meter.

Table 5.4. Statistics of recorded bottom water temperatures.

| Location | Deployed | Recovered | Temperature | | | |
|----------|----------|-----------|------|---------|---------|-----------|
| | | | Mean | Minimum | Maximum | Standard Deviation |
| GC185 | January 1993 | September 1994 | 7.9° | 6.9° | 10.8° | 0.49° |
| GC234 | October 1994 | August 1995 | 8.0° | 6.9° | 9.9° | 0.58° |
| GC185 | August 1997 | May 1998 | 7.5° | 6.4° | 9.6° | 0.50° |
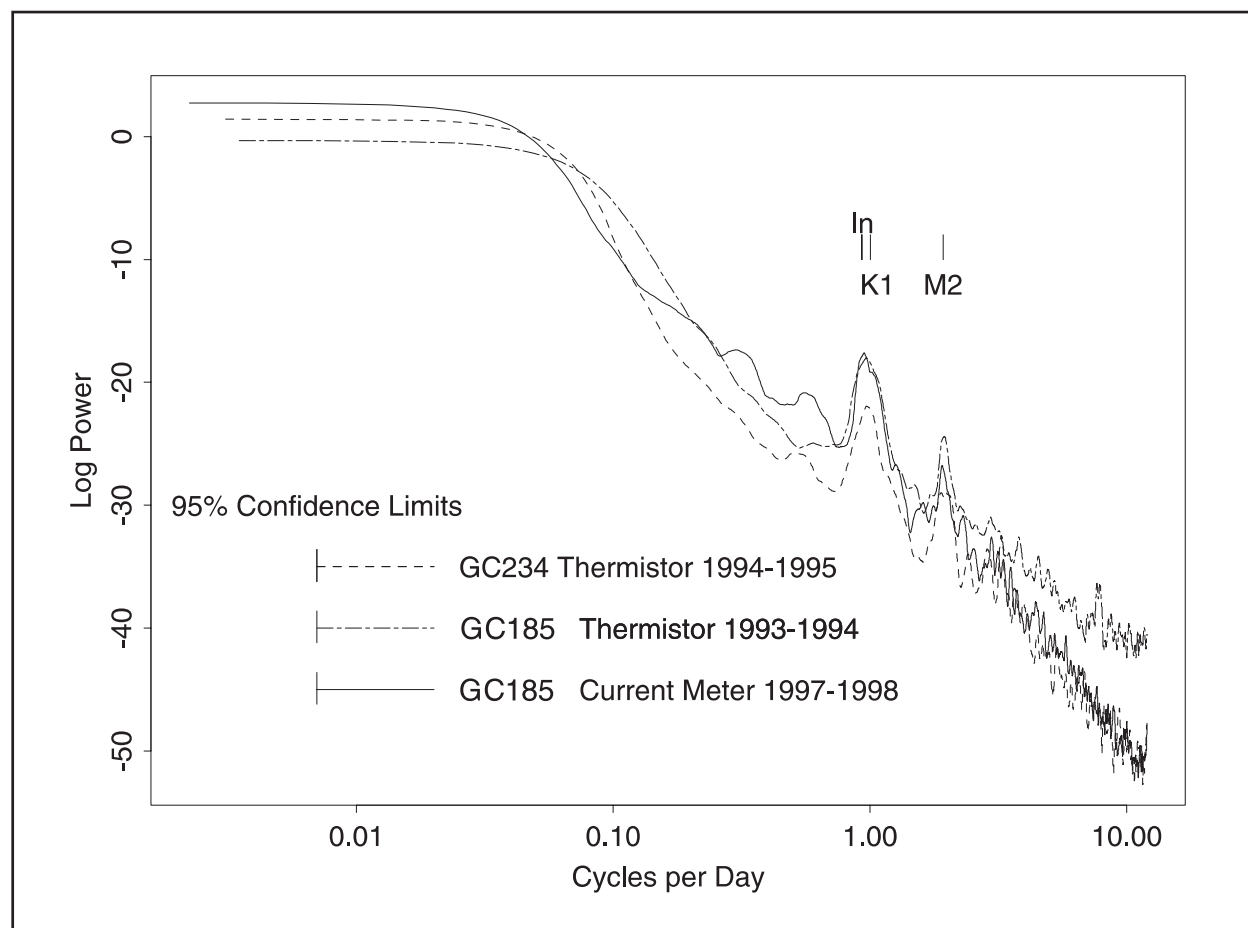


Figure 5.4.    Power spectra from near bottom temperature sensors showing pronounced peaks near the 12- and 24-hour period.

Figures 5.5A-E show stick plots of currents along with temperature time series for the entire GC185 mooring deployment. Current speeds are greater at the top meter and show considerable mesoscale variability. The diurnal and semi-diurnal periods are in evidence in the bottom record. In September and October 1997 much of the flow seems to be directed along a north-south or northwest-southeast line.   This is most likely due to the larger scale topographic features as

shown in Figure 6.11, referenced in section six of this report. A large mound rises up to about 250 m depth about 5km to the NW of the current meter site. A northeast-southwest canyon-like feature is formed between the surrounding topography and this mound. Flows up and down the axis of this feature would direct currents at the mooring site north-south or northwest-southeast as observed. It is particularly interesting that the large near-bottom currents observed during November and December 1997 tend to align with the canyon direction. This is particularly evident the first week in November, the period from November 22 to December 6, 1997, and throughout most of January, February and early March of 2000.

Much of the variability of currents in the region results from the propagation of mesoscale eddies. These eddies or rings are largely driven by density gradients in the water column, which in turn produce changes in elevation of the sea surface of the Gulf of Mexico. These elevation changes are observed by microwave radar altimeters deployed in satellites orbiting the earth (Leben and Born 1993, Leben *et al.* 1990). Figures 5.6a-d show a series of maps of a sea surface height anomaly for the period of deployment produced by Leben (2000) and downloaded from his web site http://www-ccar.colorado.edu/. In the Gulf of Mexico, currents flow clockwise around regions of positive sea surface anomaly and counterclockwise around negative regions.

A prominent feature in the data is Eddy El Dorado, which moves westward toward the current meter sight during September through December 1997. By the end of December 1997, Eddy El Dorado was directly south of the current meter mooring at GC185. Strong westward currents and elevated temperatures in December 1997 at the top meter may be the result of the approach of Eddy El Dorado. Of interest is the sharp temperature drop accompanied by the reversal to westerly flow at the top meter. This is the result of a cold-core cyclone associated with Eddy El Dorado. Near the beginning of 1998, Eddy Fourchon breaks off from the Loop Current and begins heading west toward the GC185 mooring. In March, the top meter and associated temperature rise indicates the arrival of the effects of Eddy Fourchon at the mooring. Current velocities at the top meter in April and May are more complicated and may be associated with the cold-core feature to the northwest of Eddy Fourchon.

Currents at the bottom may intensify during some of the stronger current episodes higher in the water column. Strong easterly and northeasterly currents in early November 1997, for example, are associated with increased north-south fluctuations of water velocity at the bottom. High currents in December 1997 at the top meter are associated with large fluctuations directed northwest-southeast in the bottom meter. Currents at the bottom may intensify during some of the stronger current episodes higher in the water column. Strong easterly and northeasterly currents in early November 1997, for example, are associated with increased north-south fluctuations of water velocity at the bottom. High currents in December 1997 at the top meter are associated with large fluctuations directed northwest-southeast in the bottom meter.
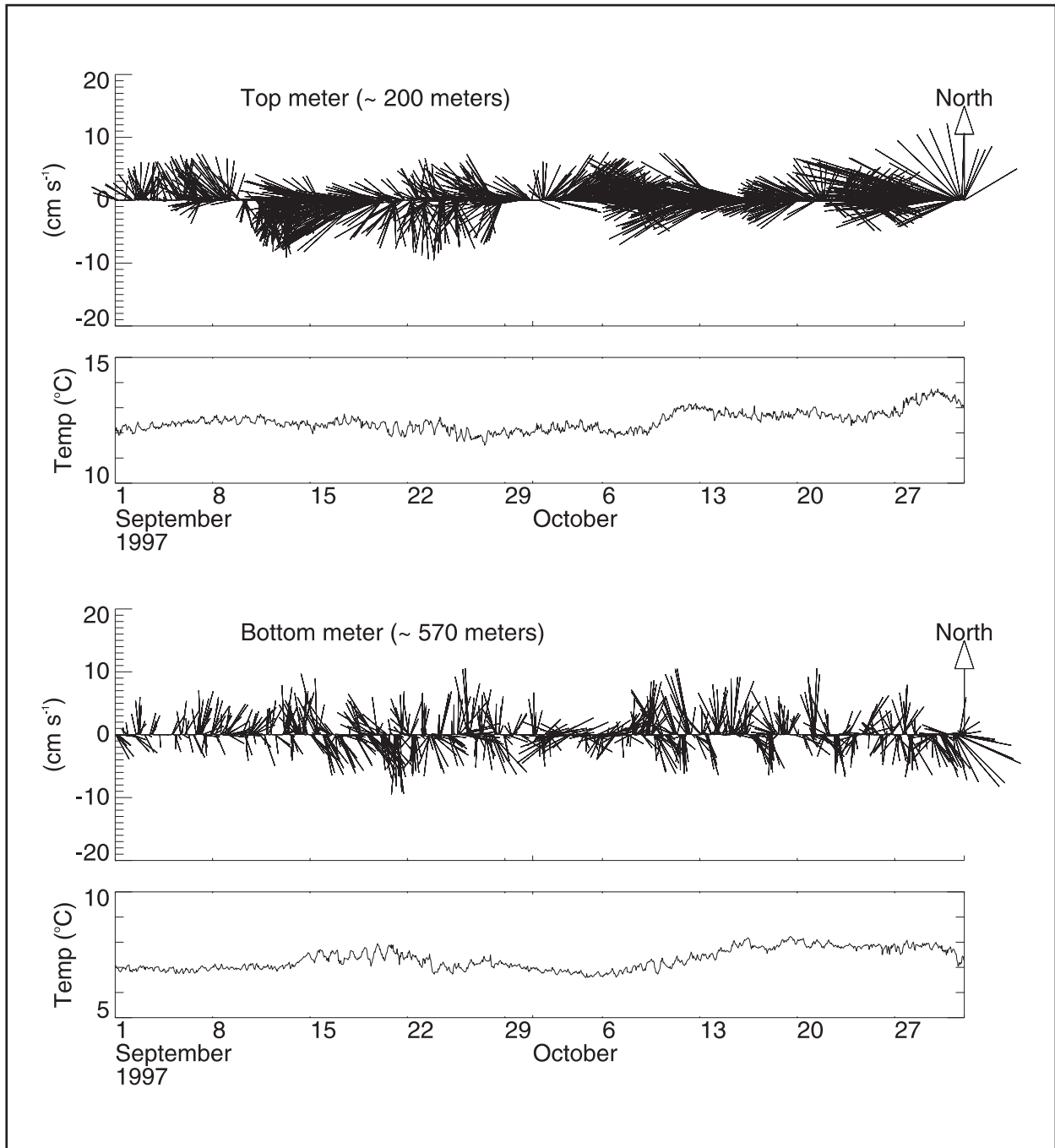
Figure 5.5A. Stick plots of currents at GC185 from September and October 1997 together with the associated temperature measurement at each meter. The top panel shows the record from the current meter at a depth of 247 m. The bottom panel shows the record from the current meter 10 m off the bottom.
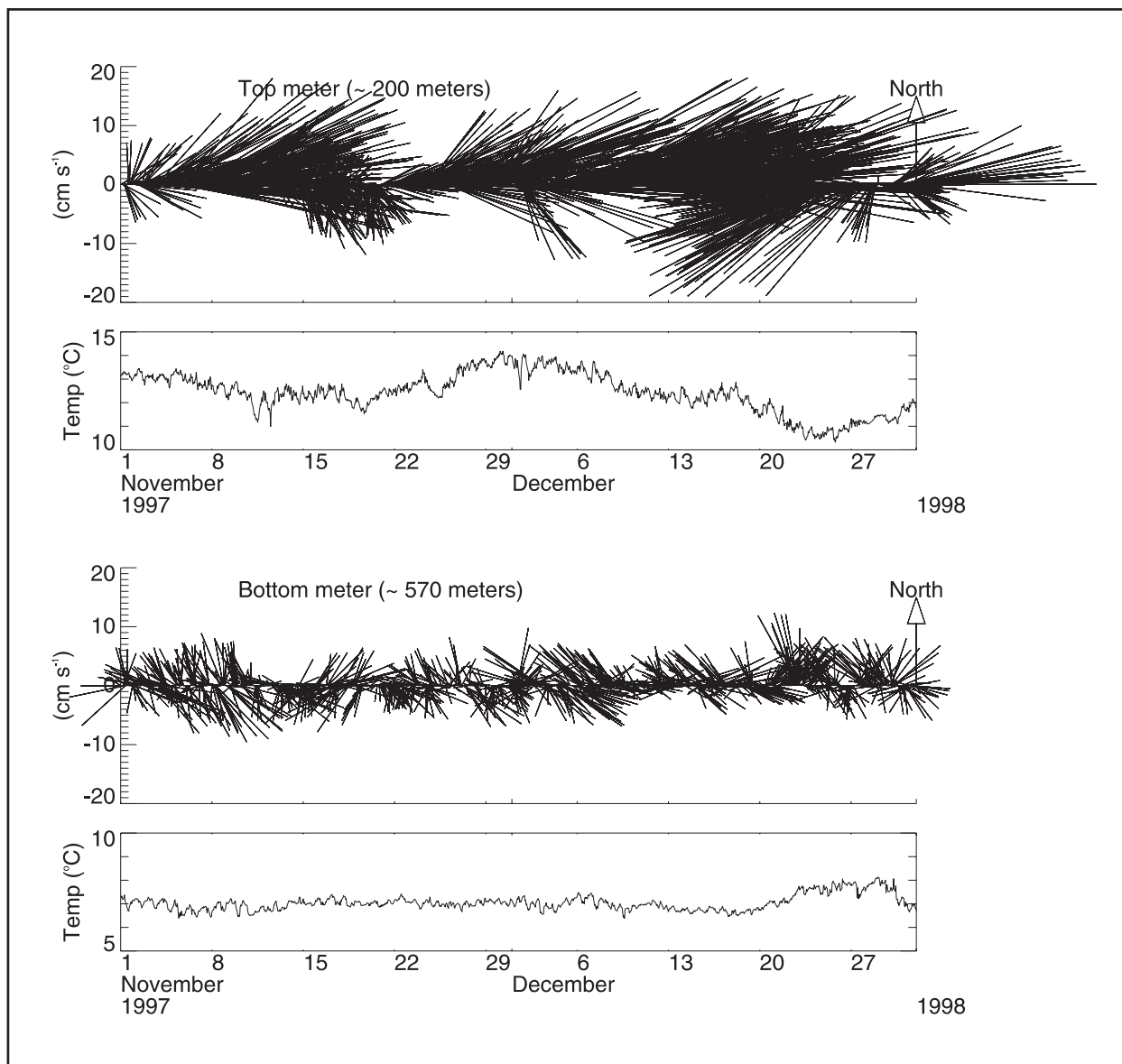
Figure 5.5B. Stick plots of currents at GC185 from November and December 1997 together with the associated temperature measurement at each meter. The top panel shows the record from the current meter at a depth of 247 m. The bottom panel shows the record from the current meter 10 m off the bottom.
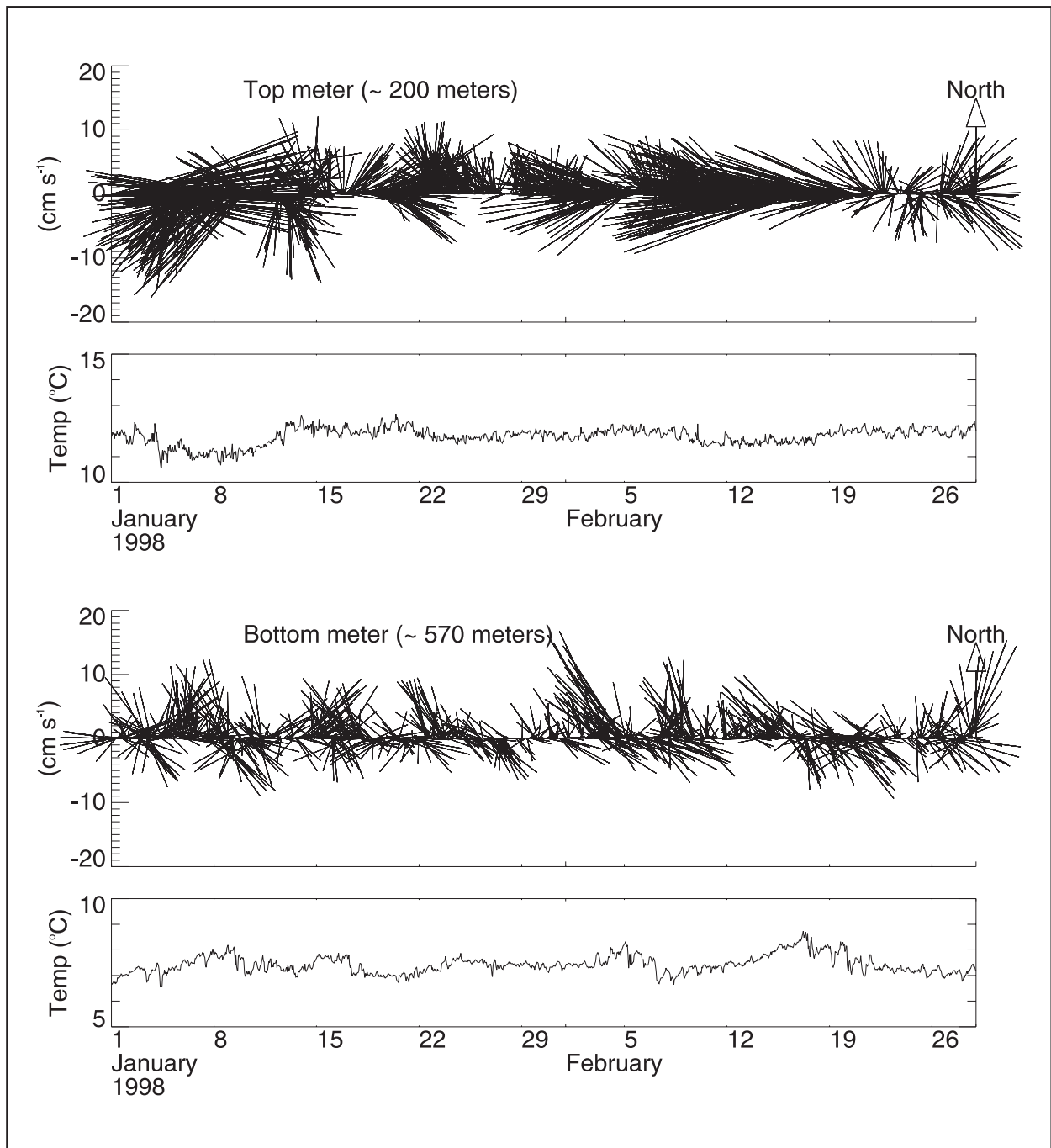
Figure 5.5C. Stick plots of currents at GC185 from January and February 1998 together with the associated temperature measurement at each meter. The top panel shows the record from the current meter at a depth of 247 m. The bottom panel shows the record from the current meter 10 m off the bottom.
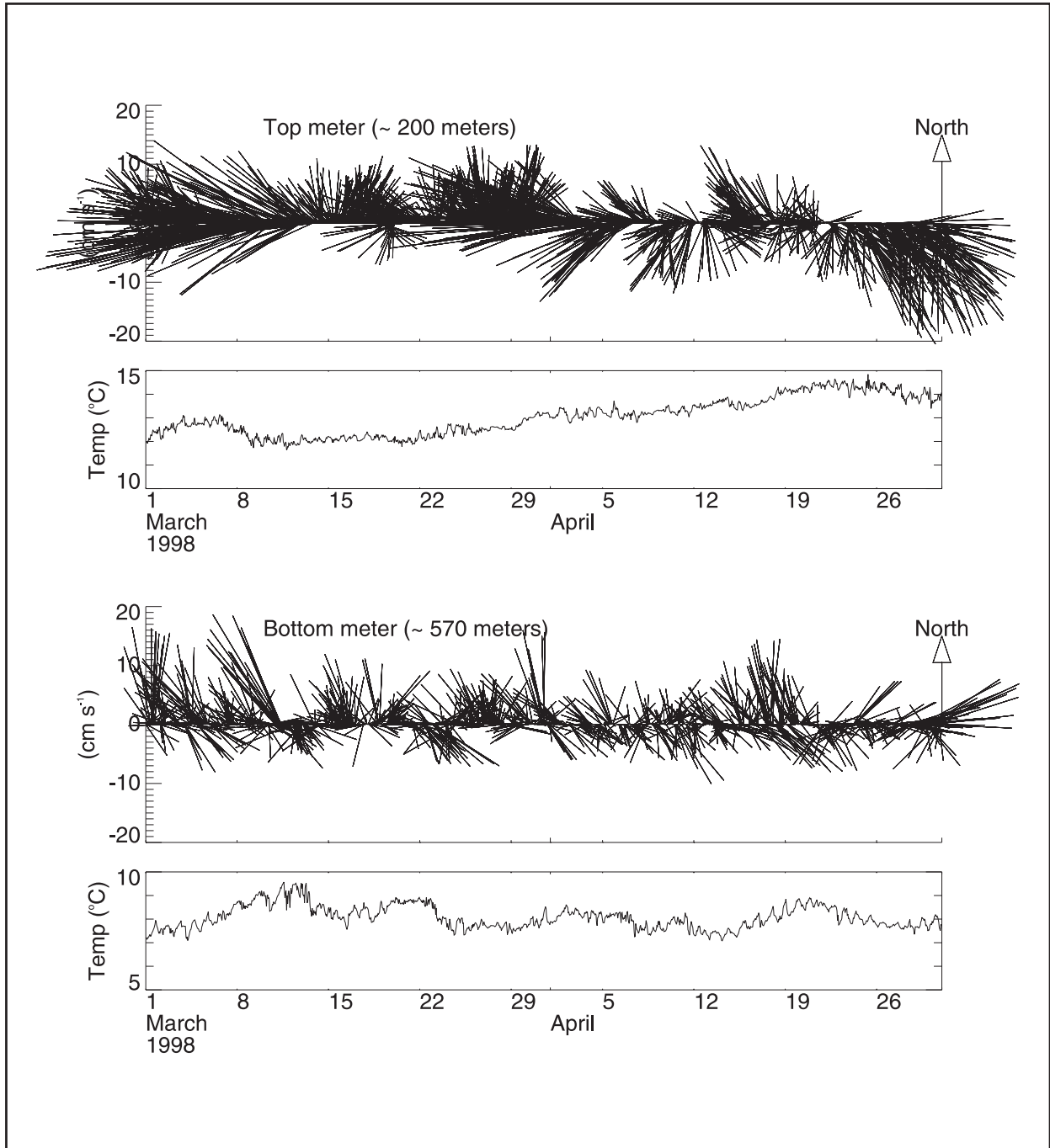
Figure 5.5D. Stick plots of currents at GC185 from March and April 1998 together with the associated temperature measurement at each meter. The top panel shows the record from the current meter at a depth of 247 m. The bottom panel shows the record from the current meter 10 m off the bottom.
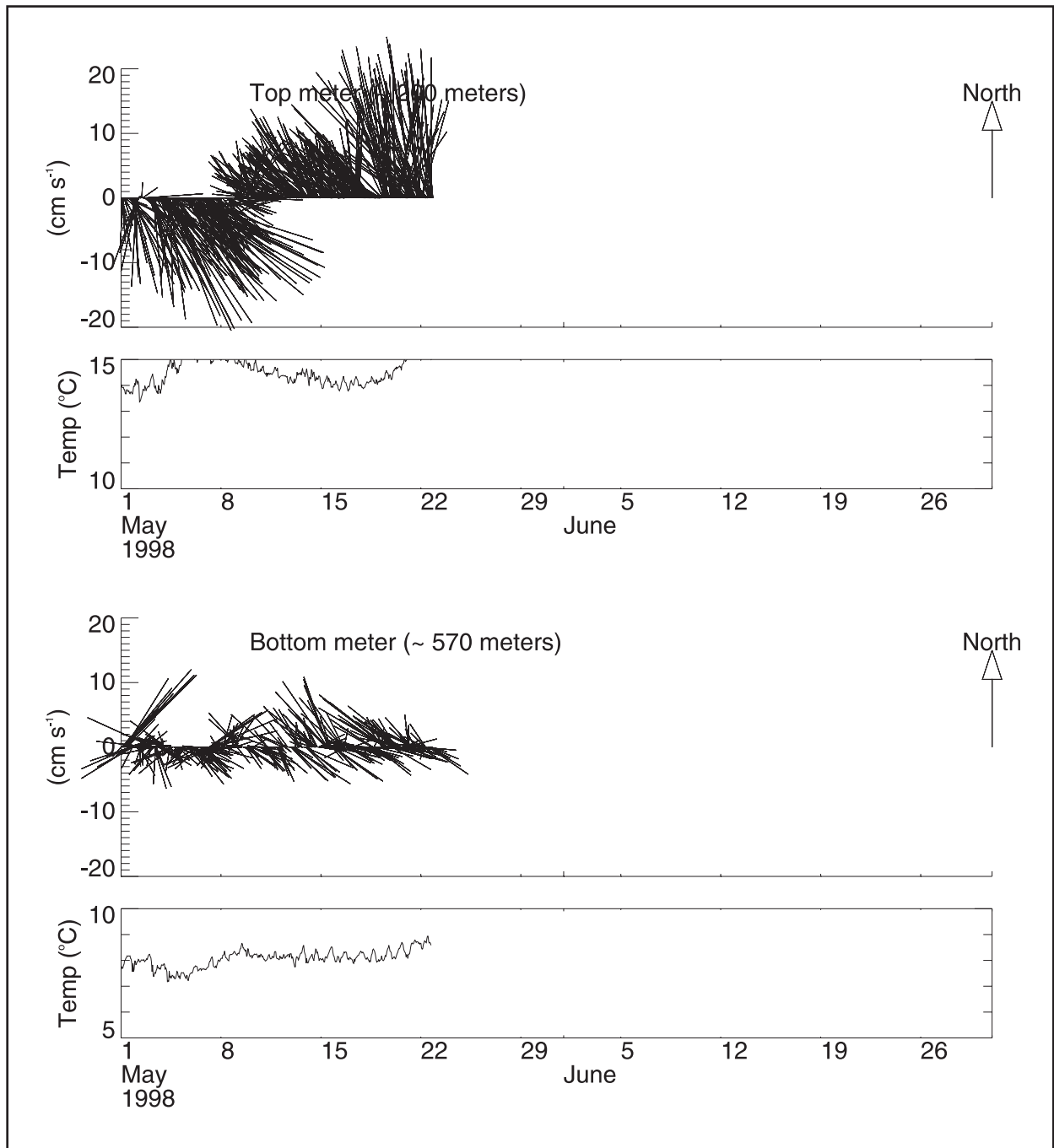
Figure 5.5E. Stick plots of currents at GC185 during May 1998 together with the associated temperature measurement at each meter. The top panel shows the record from the current meter at a depth of 247 m. The bottom panel shows the record from the current meter 10 m off the bottom.
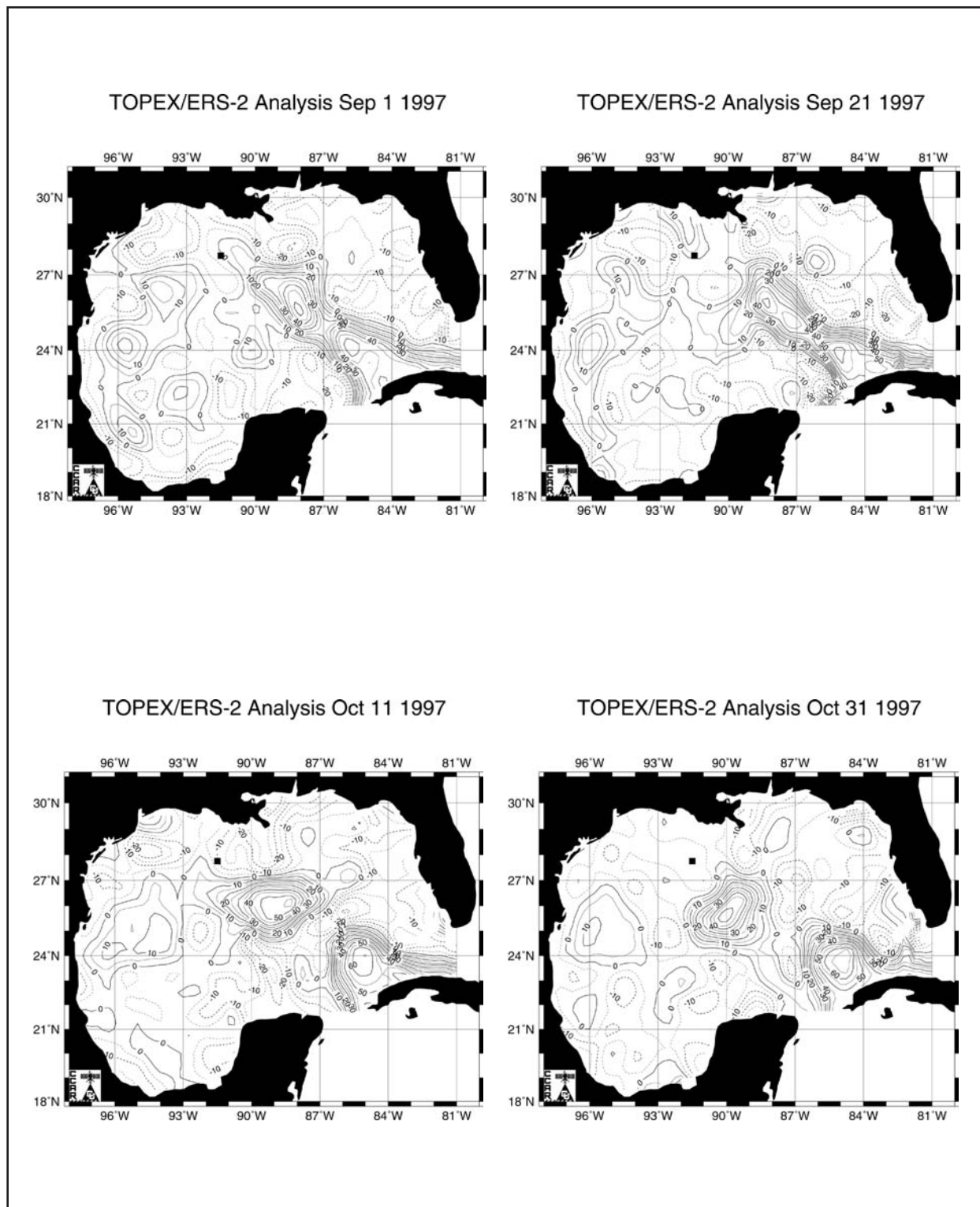
Figure 5.6A. Charts of sea surface height anomaly every 20 days during the 1997-1998 current meter deployment (Sept.-Oct. 1997).

## TOPEX/ERS-2 Analysis Nov 20 1997

## TOPEX/ERS-2 Analysis Dec 10 1997

## TOPEX/ERS-2 Analysis Dec 30 1997

## TOPEX/ERS-2 Analysis Jan 19 1998
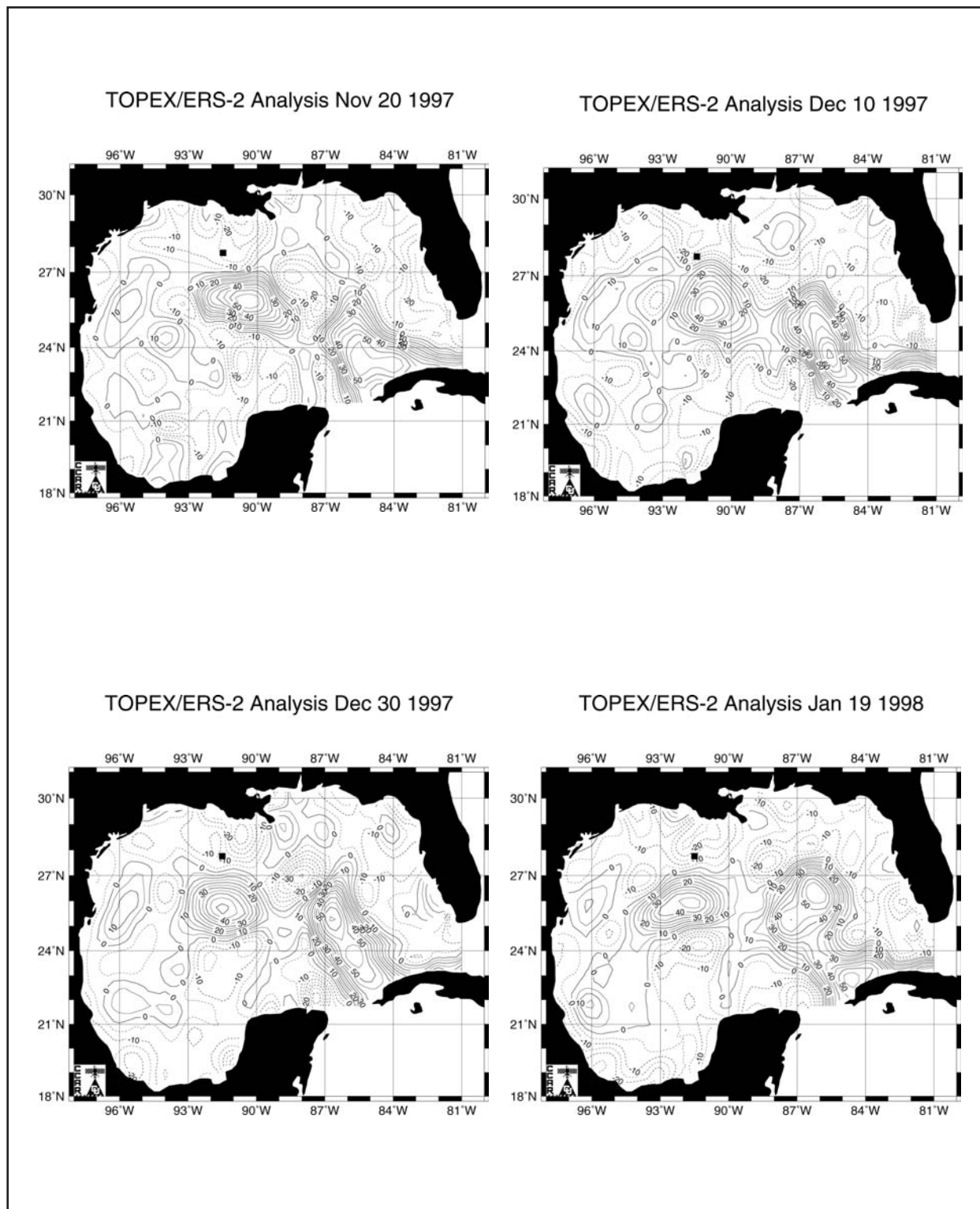
Figure 5.6B. Charts of sea surface height anomaly every 20 days during the 1997-1998 current meter deployment ( Nov. 1997-Jan. 1998).
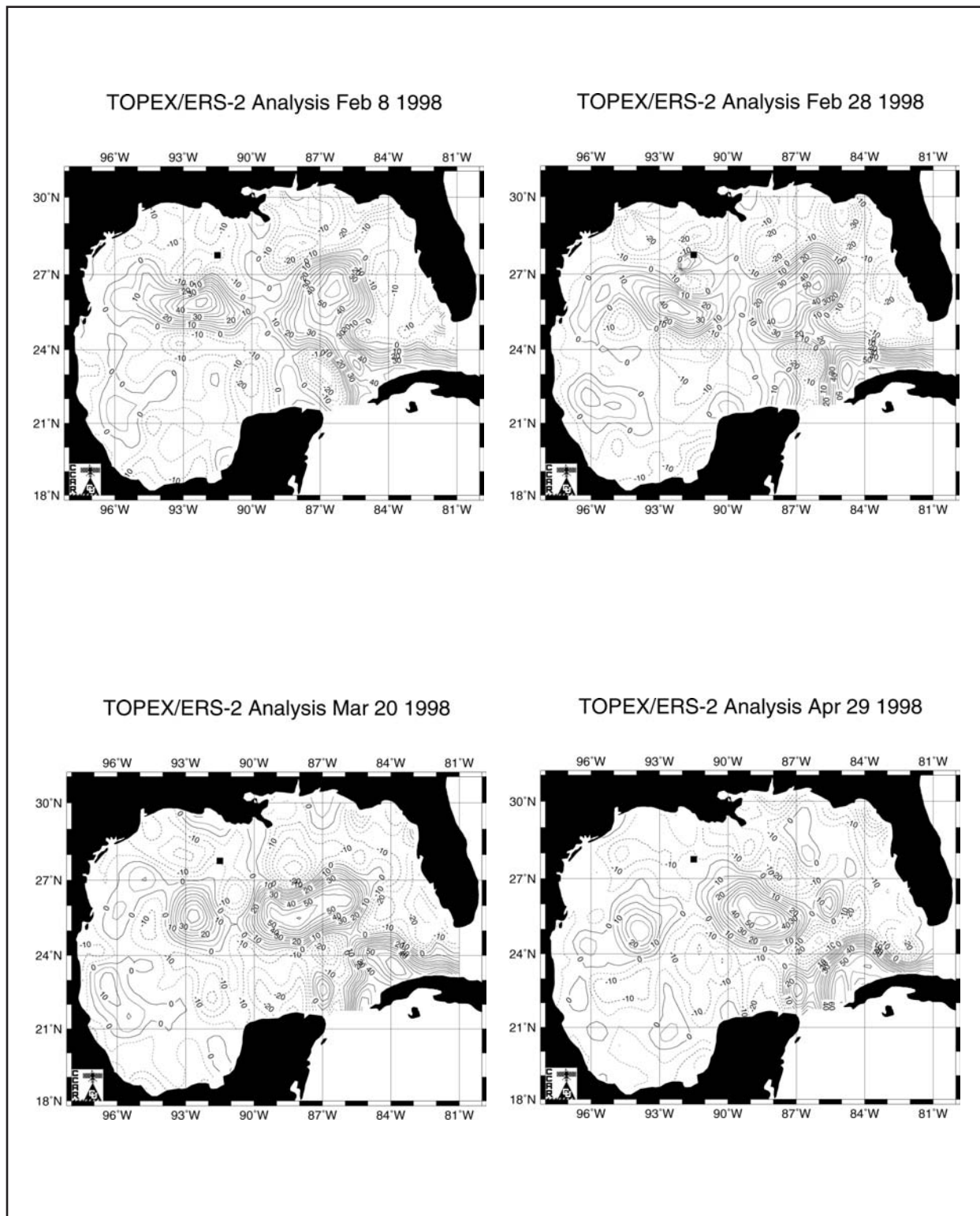
Figure 5.6C. Charts of sea surface height anomaly every 20 days during the 1997-1998 current meter deployment (Feb.-April 1998).
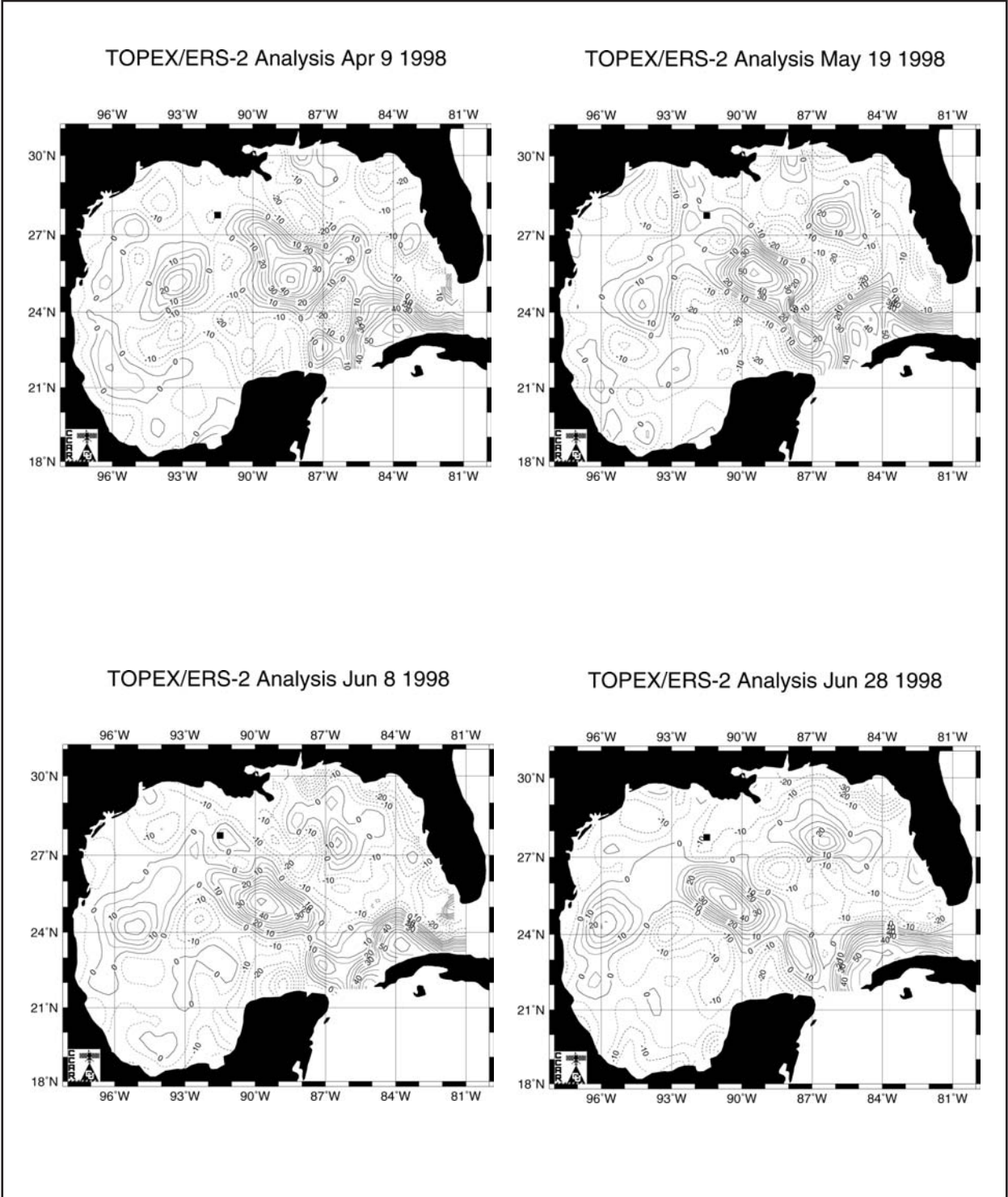
Figure 5.6D. Charts of sea surface height anomaly every 20 days during the 1997-1998 current meter deployment (April-June 1998).

## 5.5 Effects of Bottom Water Fluctuation on Hydrate Stability

A major goal of the program of physical measurements was to learn how temperature fluctuations at the sites of chemosynthetic communities affect the stability of gas hydrates outcropping and buried in the sediments (Brooks *et al.* 1994). Figure 5.7 shows a chart of Pressure-Temperature stability fields, calculated using the 1998 version of CSMHYD, the Colorado School of Mines Hydrate Stability Program (Sloan 1989) for several types of gas hydrates that might occur at the near bottom near GC185.

The dotted curve is the stability line for a structure II gas hydrate. Structure II hydrates contain methane and significant amounts of $C_2$-$C_4$ hydrocarbons. These hydrates are stable at temperatures and pressures beneath and to the left of the dotted line.

The dashed curve is for pure methane structure I hydrate. Again this hydrate is stable to the left and beneath the dashed line. Finally, the solid line shows a stability curve for structure H hydrate. This hydrate, postulated to exist in nature in the Gulf of Mexico (Sassen and MacDonald 1994), can contain significant amounts of isopentane in addition to the smaller hydrocarbon gas molecules.

Shown for comparison using a box is the range of pressures and temperatures measured during this program (Table 5.4). Structure II hydrate is calculated to be stable over the entire temperature range measured at the GC234 canyon sites. Structure I hydrate is stable only part of the time at these sites and the measured temperature fluctuations would lead to the disassociation of structure I hydrate. The calculations show that structure H hydrate is not stable at the pressures and temperatures found at the GC185.

## 5.6 Conclusions and Recommendations for Future Measurements

This examination of the oceanic environment at chemosynthetic communities, although limited in scope, found that current speed and direction and water temperatures varied dynamically. A strong diurnal periodicity in water temperature and current speed is clearly demonstrated in the long-term temperature records that were collected and analyzed. This periodic fluctuation is undoubtedly a predictable feature of sea floor habitats in the depth range of the study sites (500-600 m). Also evident from the temperature records are regular, but non-periodic episodes of temperature variations that tend to recur on a monthly or sub-monthly basis. These episodes result are evident as gradual fluctuations of the temperature baseline over a range of 2 to 3°C. Coupling between Loop Current eddies and transient deep-water currents are indicated, but the data are not extensive enough to define the mechanisms. Because chemosynthetic organisms are quite temperature sensitive ([Fisher, 1990 #100), the range and consistency of diurnal and longer-term temperature variations constitutes an environmental signal. This is noteworthy because the deep sea, which is devoid of sunlight, is often described as being temporally constant and unchanging. Moreover, because slight temperature increases can have an immediate and significant effect on the rates of venting from gas hydrate deposits (MacDonald, 1994 #187), a rise in temperature can influence the availability of nutrients in methanotrophic organisms such

as seep mussels. These observations have been quite limited geographically and in terms of water depth. Future work should prioritize obtaining temperature time-series from deeper sites to determine whether the diurnal periodicity and longer term fluctuation continues to be present as one moves further offshore. Determining the relationship between Loop Current processes and deep-water circulation will require a much more ambitious program than the present, limited, observations can support. However, findings to date clearly indicate that events driven by Loop Current can have biological and possibly geochemical significance on the outer continental slope of the Gulf of Mexico.

## GC185 Hydrate Stability Curves

Figure 5.7. Plot of the stability fields in Structure I, II, and H hydrate. The box shows the pressure temperature region measured at GC185. Structure II hydrate is most likely the only stable hydrate species at the site.

Figure 5.7. Plot of the stability fields in Structure I, II, and H hydrate. The box shows the pressure temperature region measured at GC185. Structure II hydrate is most likely the only stable hydrate species at the site.

## 6.0 Geophysical Detection and Characterization of Chemosynthetic Organism Sites[1]

### 6.1 Introduction

Chemosynthetic organisms flourish at oil seeps, deep beneath the ocean surface in an environment that is difficult for humans to explore. As a result, much of our knowledge of chemosynthetic ecosystems in the Gulf of Mexico comes from a small number of sites, most found by chance. Gulf of Mexico chemosynthetic sites are found in water depths from several hundred meters to more than two thousand meters (MacDonald *et al.* 1996). They seem to exist wherever there are hydrocarbon seeps on the continental slope. Despite the apparently large depth range, the distribution of such organisms is poorly known owing to sparse data. A fundamental unanswered question is whether lush chemosynthetic sites are rare and fragile or ubiquitous and robust. Although chemosynthetic organisms cover only a tiny fraction of the seafloor, they have the potential to cause the offshore energy industry to spend large sums of money to make sure that drilling rigs, pipelines, and other production equipment do not blunder into community sites and cause irreparable harm.

Because chemosynthetic organisms are small, they are difficult to detect using geophysical methods. Even near-bottom geophysical records do not readily show chemosynthetic organisms. This means that confirmation of chemosynthetic organisms at a given site depends on near-bottom optical imaging, for example, submersible observations or bottom photography, or recovery of physical samples, such as coring or trawling. Nevertheless, geophysical techniques can detect hydrocarbon seeps because the seeps change the physical properties of surface and near-surface sediments (Roberts *et al.* 1990). Thus, the task of remotely locating chemosynthetic organism sites becomes one of defining the small percentage of the seafloor affected by seepage and then checking within that area for chemosynthetic habitation.

In this study, our goal was to compare and contrast geophysical methods of detecting and characterizing hydrocarbon seep sites inhabited by chemosynthetic organisms. Because of this focus, we ran the risk that the small number of sites that were studied are not entirely representative and are insufficient in number to make significant tests of hypotheses. Nevertheless, the results of this study are consistent with what is known about seeps and chemosynthetic organisms. Our overarching conclusion is that there is no one method of detecting chemosynthetic sites that is always accurate. Ultimately, confirmation of the existence of chemosynthetic organisms at a given location depends on actually seeing the organisms, by submersible, deep-camera platform, or recovery of recently live specimens in trawl or core. Defining areas of the seafloor that have been affected by seepage is more straightforward. This can limit the area of seafloor that must be considered to a fraction of the deep slope. Making the next step, to document whether a chemosynthetic site exists by remote techniques, is a process of collecting sufficient evidence to make a reasonable conclusion as to their presence or absence.

---

[1] This section was authored by William W. Sager.

### 6.1.1 Overview of continental slope geology

The continental slope and rise of the northern Gulf of Mexico technically fits into the category of "passive margin," (i.e., it contains no plate boundary) and is very active owing to salt tectonics. This activity is reflected in the physiography of the slope. The seaward incline is broken by uplifts caused by rising salt diapirs or massifs and basins caused by salt withdrawal (Bryant *et al.* 1990; 1991; Bouma and Bryant 1994). Indeed, the base of the slope is an escarpment (Sigsbee Escarpment) resulting from the seaward migration and coalesence of large salt sheets (Amery 1969; Humphris 1979). Salt movement has caused the slope to be broken by numerous regional and local growth faults and related structures (Worrall and Snelson 1989). Topographic gradients are much higher than is the norm for passive margins, with slope angles often greater than 40° (Bryant *et al.* 1995).

Modern-day salt tectonism in the Gulf of Mexico has its roots in the early geologic history of the Gulf. The basin first opened with the rifting of North and South America during the Jurassic (e.g., Pindell 1985). A thick salt sheet was deposited on syn-rift sediments in the young basin, and the salt was buried in turn by Late Jurassic continental sediments, carbonate-dominated Cretaceous sediments, and finally siliciclastic Tertiary sediments (Worrall and Snelson 1989). The Neogene saw huge volumes of sediment poured into the northern Gulf of Mexico, ultimately creating a thick (up to 16 km) continental-margin sedimentary wedge (McGookey 1975). Salt is incompressible, so the weight of Neogene sediments caused the salt layer to deform and mobilize, moving upward and toward the south (Humphris 1979). Today the salt is found high in the sediment column where it has taken on a variety of morphologies, two of the principal being diapirs and sheets (Seni and Jackson 1983; Jackson and Talbot 1986).

The rough topography of the northern Gulf of Mexico slope reflects the deformation caused by salt tectonics. Salt diapirs are common on the shelf and upper slope, but the middle and lower slope are characterized by laterally extensive salt sheets stretching south to the Sigsbee Escarpment (Humphris 1979). Atop this sheet, the slope character is dominated by small subcircular to elongate basins and salt massifs, the former occurring where the salt is thin or absent (Bryant *et al.* 1991). The mobile salt has extensively fractured the overlying sediments with regional growth (normal) faults and associated fault types (Rowan *et al.* 1999). These faults act as conduits for the migration of hydrocarbons, which ascend from older, deeper layers to shallow reservoirs at 2-3 km depths and from there to the seafloor (Kennicutt *et al.* 1988).

Late Cenozoic to Recent sedimentation in the Gulf of Mexico has occurred at a moderate to high rate, especially during sea level lowstands when rivers emptied onto the shelf edge and upper slope (Lowrie 1987; Coleman *et al.* 1991). Given this situation, a blanket of Pleistocene to Holocene sediments is expected at the seafloor. Although the northern Gulf of Mexico slope is indeed generally draped by recent sediments (Coleman *et al.* 1991), salt tectonics and deep currents have caused mass wasting, erosion, and sediment reworking (Bryant and Roemer 1983; van den Bold *et al.* 1987; Bryant *et al.* 1999). As a consequence, it is difficult to predict the age and texture of seafloor sediments at an arbitrary location.

## 6.1.2 Overview of seep geophysical signatures

Active seeps are often visible owing to their release of oil and gas in the water. Slicks on the water surface can be imaged from space (and presumably lower altitudes), using photography or synthetic aperture radar (SAR), because oil alters the roughness of the sea surface (MacDonald *et al.* 1993; 1996). It is not clear, however, how continuous such slicks are because analysis of SAR data at one Gulf of Mexico site suggests intermittent activity (MacDonald *et al.*, in press). Gas released into the water column by seeps can scatter sound waves and give rise to a vertical plume on records from high-frequency echo-sounders (Anderson and Bryant 1990). Such plumes are not always observed over active seeps, perhaps because the gas plume must reach a large volume before enough sound is scattered to register on the echo-sounder.

More often, seeps are recognized by their effects on the physiography of the seafloor and acoustic characteristics of near-surface sediments. Seeps are a result of tensional faulting of continental margin sediments allowing upward migration of hydrocarbons and other formation fluids from buried reservoirs (e.g., Kennicutt *et al.* 1988). In recent times active faults have often broken the seafloor, leading to rough topography caused by fault scarps, horsts and grabens, and mass wasting of sediments (Roberts *et al.* 1990b). Fluids and gas expelled from vents along the faults cause a number of "fluid expulsion features" including mud volcanoes, mud diapirs, and pock marks (Behrens 1988; Neurauter and Bryant 1990; Roberts *et al.* 1990a; 1990b; Neurauter and Roberts 1994; Kaluza and Doyle 1996). In addition, authigenic carbonate buildups, up to tens of meters in size, occur at the seafloor as a result of microbial oxidation of hydrocarbons by bacteria and the subsequent release of carbon dioxide and bicarbonate that catalyze the production of carbonate in near-surface interstitial waters (Roberts *et al.* 1990).

Seeps give rise to several distinct signatures on high-frequency echo-sounder profiles and seismic reflection profiles. In echo-sounder records, seeps cause acoustic "wipeout," which is the absence of subsurface reflectors. This can be a result of the near total reflection of sound owing to a hard ground at the seafloor or attenuation owing to dispersion of the sound waves by gas bubbles within the sediment (Behrens 1988; Anderson and Bryant 1990). Generally, two types of wipeout are noted on echo-sounder records: simple wipeout (subsurface layers vanish) and reverberant wipeout (a prolonged bottom echo). The former probably results simply from attenuation owing to gas and the latter may occur because of reverberation caused by gas bubbles, carbonate, biogenic debris, or other seep-related material (Behrens 1988). Evidently, gas may cause either simple wipeout or reverberation, depending on gas bubble size and density (Anderson and Bryant 1990).

Similar effects were noted in ultra-high frequency echo-sounder records acquired over seeps from near the seafloor (Sager *et al.* 1999). Seafloor acoustic characteristics ranged from total reflection from hard bottoms, to limited reflection penetration in shallow buried hard bottom regions, to acoustic reverberation, to wipeout. Because of rapid attenuation of sound at high frequency, such records can only be obtained from deep-tow vehicles or submersibles. Consequently, such data are rare and typically lack wide lateral coverage.

The effects of seepage are often noted on seismic reflection data, in particular the 2D and 3D multi-channel seismics often used for hydrocarbon exploration by the energy industry. The seafloor topographic expression of a seep is often not well represented because marine seismic

systems are designed for imaging deep reflectors rather than the seafloor. The low sound frequency has poor vertical resolution because the long wavelength and the geometry of long streamers do not image the near-surface well. However, the high lateral data density afforded by 3D seismic data sets often makes up for these problems. As a consequence, an interpreter can usually recognize seafloor mounds and craters if they are large (tens of meters vertically and hundreds of meters laterally). The most common seismic signature of a seep is a signal loss akin to the wipeout in higher frequency reflection records. Typically, this appears as a columnar region for up to 1-2 seconds (two-way travel time) beneath the seep in which reflectors are weak or absent owing to signal attenuation. These features are commonly called "gas chimneys," although it is uncertain whether the effect is caused solely by gas or whether other factors related to seepage also contribute (Abrams 1996; Roberts *et al.* 1999). Although gas chimneys are often nearly vertical, sometimes they are inclined, following the path of an inclined fault that acts as a conduit for gas and formation fluids. In some instances, reflectors at the edges of these chimneys appear to turn downward ("pull-down") as a result of lower seismic velocities in the sub-seep sediments caused by significant volumes of gas (Corthay 1997).

Using modern seismic workstations, digital multi-channel seismic data can be processed in many ways to enhance certain signal characteristics. As a result there are many different characteristics that can be used to define regions with anomalous signal characteristics, including seeps. One technique is to extract the amplitude of the seafloor reflection. The seafloor signal strength depends on the reflection coefficient, which in turn depends on characteristics of the near-surface sediments, so seafloor amplitude anomalies have been used to define seep areas (Roberts 1996; Roberts *et al.* 1996). Using this technique, the high lateral density of 3D data is especially useful in showing the geometry of anomalous sediments, which often provides clues about the nature of the geologic cause (Roberts *et al.* 1996). In addition, the sign of the amplitude anomaly can be used to infer whether significant volumes of gas are present. Positive amplitude anomalies indicate an increase in density or seismic velocity, which suggests a hard bottom, such as that caused by carbonate crusts, gas hydrate, or other dense material accumulation (Roberts *et al.* 1996; Reilly *et al.* 1996). Positive amplitude anomalies are the most common. In contrast, negative amplitude anomalies indicate lower velocity and density, which can occur when significant concentrations of gas are present (Roberts *et al.* 1996; Reilly *et al.* 1996). Low signal anomalies in 3D data time slices can also be used to identify gassy regions in the subsurface, using similar logic (Corthay 1997). Other signal characteristics can be used to define anomalous regions, either at the surface or in the subsurface. Virtually any attribute that is used to highlight anomalous signal characteristics, such as amplitude-velocity-offset (AVO), coherency, signal envelope, or rms deviation, can be used to define areas affected by seeps.

A similar digital seismic technique that has the potential to delineate seep-affected areas is high-resolution 3D seismic data. Some energy companies reprocess standard exploration 3D data to maximize the resolution and frequency content. Only the first hydrophone group in the streamer, or first several groups of hydrophones, are used to mitigate the adverse geometry caused by the lengths of modern exploration streamers. The data are also high-pass filtered to improve resolution. The result is a 3D data set with about twice the near seafloor resolution of the original data. Another similar technique is to acquire short-offset, high-resolution 3D multi-channel data. Such data sets are acquired with short streamers (typically 100-m in length) and higher-frequency sound sources. Furthermore, they are processed to more carefully position the streamers. The result is a data set with three to five times better resolution than exploration 3D

data. Because of their high resolution and dense data coverage, these data sets are very useful for interpreting seep geology (Corthay 1997). Unfortunately, few of these data sets exist, because they represent additional field expenses.

Side-scan sonars also have the ability to show differences in surface sediment properties and thus may be useful in imaging seeps. Such sonars construct an image by displaying the amplitude of sound returned from the seafloor perpendicular to the sonar transducer arrays. Unlike seismic reflection profiling, which relies on vertical-incidence reflection, the side-scan sonar makes an image from sound that is "backscattered" from the seafloor. Backscatter depends on scattering of sound from surface roughness and particles within the near-surface sediment (Johnson and Helferty 1990), so side-scan sonars are often used to examine variations in sediment type at the seafloor. Around seeps, side-scan sonars typically show enhanced backscatter owing to the physical disturbance of seafloor sediments by seepage (Kaluza and Doyle 1996; Vogt *et al.* 1997; Roberts 1998; Sager *et al.* 1998). The processes that cause enhanced backscatter have not been widely investigated. In addition, large side-scan sonar image mosaics are not common because extensive side-scan sonar mapping is also not frequently done for hydrocarbon exploration and production.

### 6.1.3 Geologic controls on chemosynthetic communities

It is clear that chemosynthetic communities occur along faults where hydrocarbons seep to the surface. To have hydrocarbon seeps, two ingredients must be present: (1) hydrocarbons in subsurface sediment layers and (2) conduits for the hydrocarbons to reach the sea floor. In the Gulf of Mexico, rapid sedimentation buried copious amounts of organic matter and turned it into hydrocarbons by the right combination of elevated temperature and pressure. Conduits are faults which are a result of the mobilization of a Jurassic salt layer by the accumulation of a thick post-Jurassic sediment pile.

In virtually every geophysical data set in which seeps, faults, and chemosynthetic organisms can be mapped, the chemosynthetic communities occur along the surface expressions of active faults (Behrens 1988; Roberts 1995; Reilly 1996; Sager *et al.* 1999). In the northern Gulf of Mexico, many of these faults have developed in response to rapid sedimentation in Pliocene and Pleistocene time and resultant adjustment of the unstable sediment pile (Worral and Snelson 1989; Cook and D'Onfro 1991). Although much research has gone into the faulting in the Gulf of Mexico and its relation to structure and morphology (e.g., Worral and Snelson 1989; Rowan *et al.* 1999), our understanding of the mechanics of seepage is poor. Recent research suggests that fluid flux at seeps varies with time on time scales that range from months (MacDonald *et al.*, in press) to centuries or longer (Reilly *et al.* 1996; Roberts and Carney 1997), but the forcing mechanisms are uncertain.

Reilly *et al.* (1996) hypothesized that faulting style and salt activity are two major controls. They maintain that the faults that yield the most consistent long-term flux of hydrocarbons are antithetic faults rooted on regional growth faults (they term these "fault-dominated" seeps). Such faults are generated by fracturing and adjustment of the continental slope sediment pile in response to downslope gravity sliding and regional salt movements. Alternatively, they argue that faults that root into salt diapirs may cause seeps, but that these seeps ("salt-dominated" seeps) are not continuous enough for colonization by complex chemosynthetic communities.

Their reasoning is that rotational shear on the hanging wall of regional growth faults continually produces tension consistent with the sustained rapid flux of hydrocarbons needed by complex chemosynthetic communities. In contrast, they contend salt diapir faults are only intermittently active in response to the upward movement of the salt diapir.

### 6.1.4 Finding chemosynthetic communities using geophysics

Although geologists working for energy companies frequently use geophysical data to define seep and potential chemosynthetic organism sites, few publications exist on the subject. Dr. Harry Roberts has published a series of papers describing submersible dives to chemosynthetic community sites, which were based on geophysical data and other knowledge (e.g., Roberts and Aharon 1994). Many were based on high-frequency echo-sounder profiles showing fluid expulsion mounds, bathymetry, or multi-channel seismic data. Roberts did not examine the process of finding the chemosynthetic sites using these geophysical data. However, he did suggest that seismic amplitude data rendered at the seafloor may be useful for locating seep sites hospitable to chemosynthetic organisms if the data show low amplitude, phase reversal spots caused by gas (Roberts *et al.* 1996; Roberts and Doyle 1998).

Reilly (1995) tackled the issue directly and developed a protocol for identification of chemosynthetic organism sites (Figure 6.1). He suggested using satellite imagery to detect a sea surface slick, and if no slick was detected a chemosynthetic site was unlikely because they are only likely to form at continuous seeps. The next decision was whether the site showed prolonged, high strength returns from the seafloor on multi-channel seismic data. If so, and the reflection coefficient is negative, further investigations were warranted. A positive coefficient was deemed to be indicative of hard bottom development and unlikely to be a chemosynthetic organism site. At the negative reflection coefficient location, the next observation was to acquire piston cores and examine the geochemical signature of the sediments. If significant $C_1$-$C_5$ hydrocarbons were found, especially elevated $C_5$, the organic matter for chemosynthetic organisms are present and additional consideration is needed. The next step is to consider the geologic model. First fault conduits need to be traced and then correlated to a model of fault development. Reilly contends that faults directly related to salt dome uplifts are too intermittently leaky to sustain lush chemosynthetic organism sites, whereas inter-domal faults are more likely to be continually active. If the site in question is on the latter, he recommended either avoiding the site, imaging the seafloor with cameras, or making an observation with a submersible or ROV.

### 6.1.5 Study overview and rationale

A complete examination of the geophysical characteristics of hydrocarbon seeps and their relation to chemosynthetic organism sites is a project of such large magnitude as to be beyond the grasp of the present study. Instead, we chose to focus on a few data types in limited areas. Prior chemosynthetic organism site studies have focused on areas typically restricted to a few kilometers on a side or less; consequently, we thought it important to investigate a larger area to

see how much is affected by seepage and how many chemosynthetic organism sites are located there. Three study areas were chosen, all on the Louisiana continental slope (Figure 6.2). The two larger areas were chosen to be representative of the upper and lower slope morphologic regions. In addition, both contain seeps as shown by about 10 slicks in each (Figure 6.3) on the images studied by MacDonald *et al.* (1993; 1996). The third area was much smaller and centered on a known chemosynthetic organism site.

# Chemosynthetic Community
## Search Protocol
### Reilly (1995)

**Surface slick** → none → no chemos

(aerial/space photo)

**Wipeout zone** → none

(sea surface, high-res)

**Reflection coefficient** → positive (hardbottom)

(multichannel seismics)

negative
(Low velocity zone)

**Piston Cores** → No C1-C5 hydrocarbons

(hydrocarbon signature)

C1-C5 hydrocarbons

**Geological model** → salt dome fault

regional fault

**Optical observations** confirm
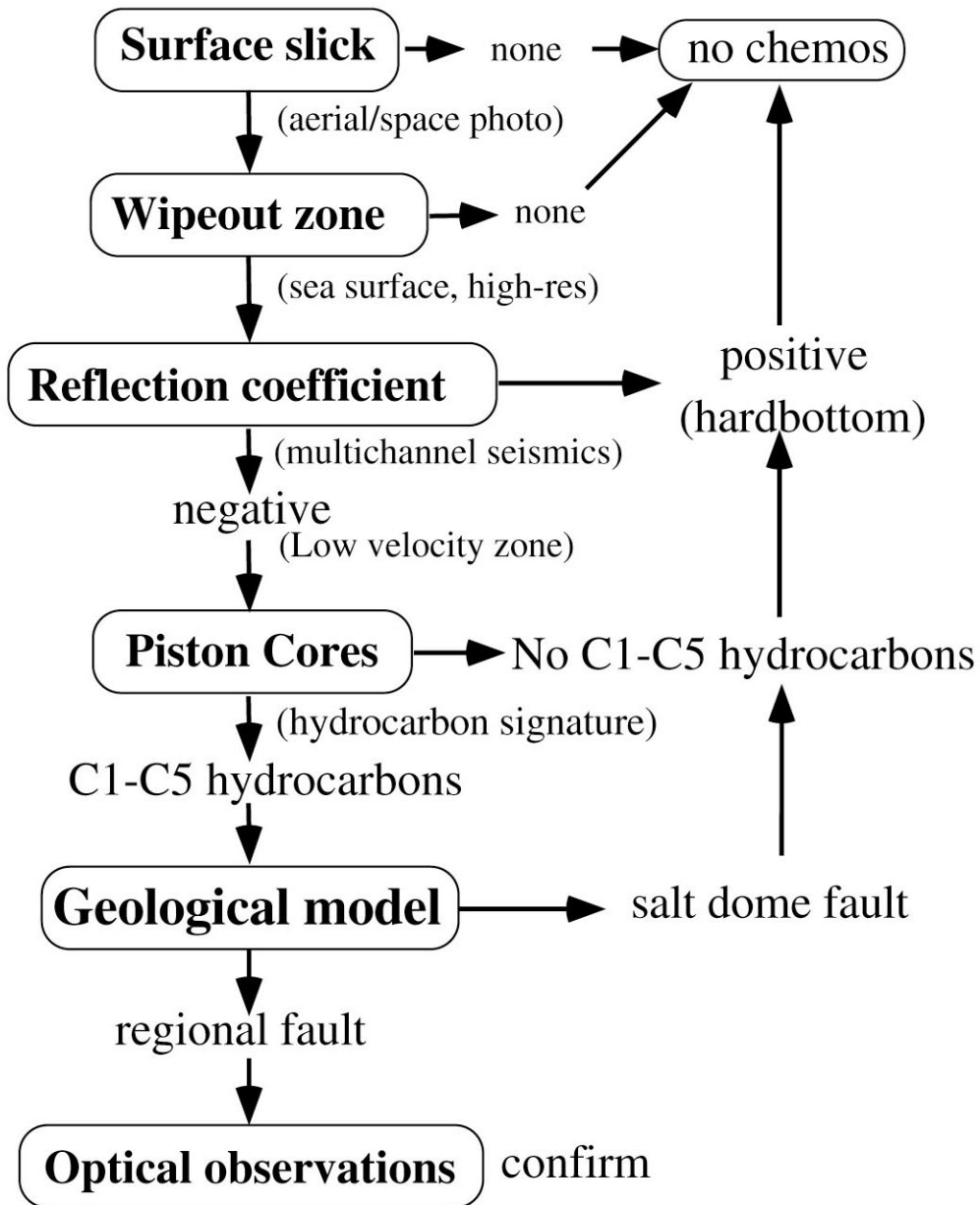
Figure 6.1.    Chemosynthetic site search protocol proposed by Reilly (1995).
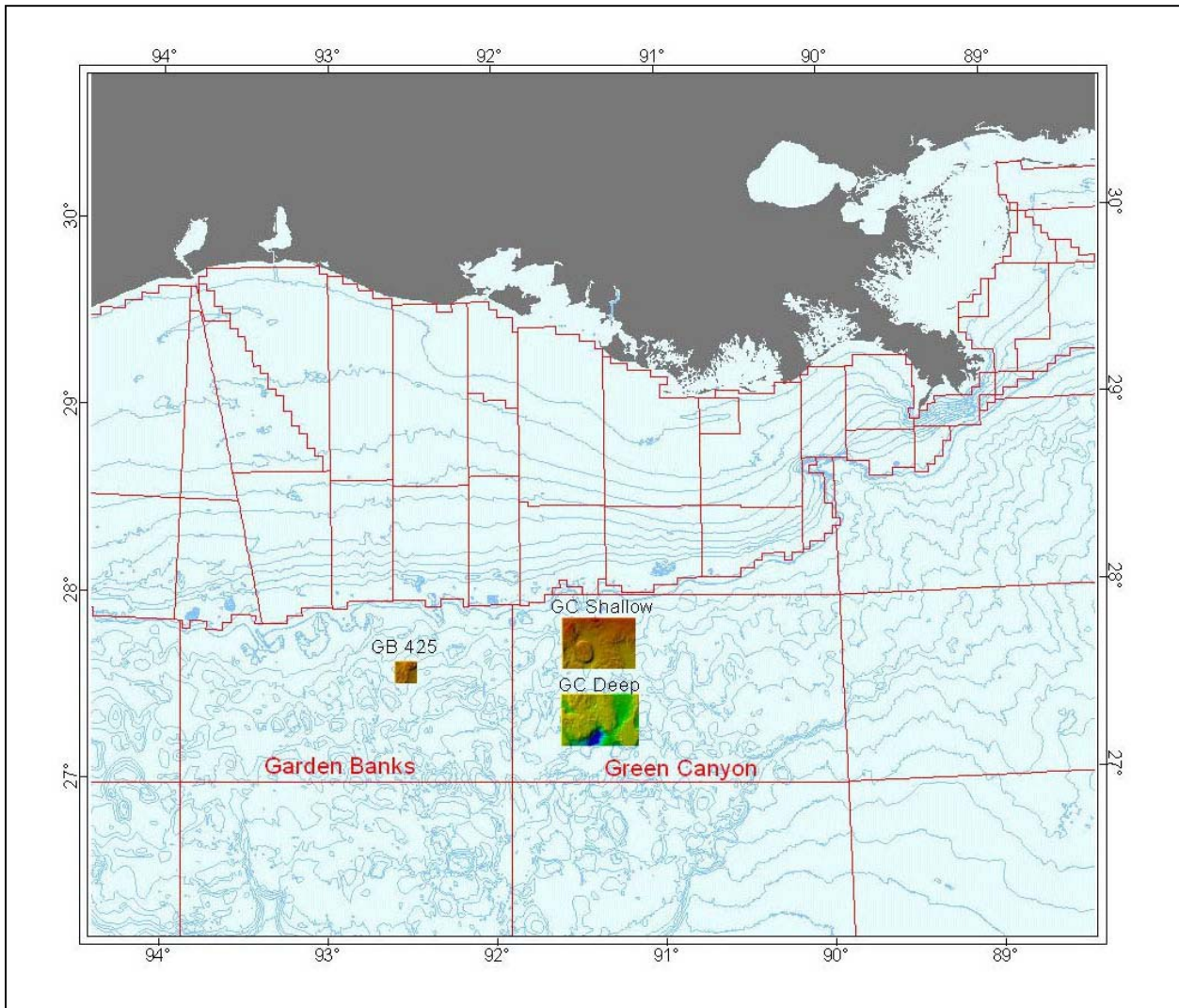
Figure 6.2. Location map of study sites on the Louisiana continental slope. Dark gray shading shows land area. Light lines show bathymetry contours and leaseblock areas. Boxes with shaded bathymetry denote study areas.

The rationale of the study was to collect a high-resolution geophysical data set in these known seep areas and compare it with other geophysical and geologic data. For the high-resolution data coverage, we surveyed using long-range side-scan sonar because seepage affects the physical properties of surficial sediments providing a contrast that can be imaged with side-scan sonar. In addition, side-scan sonars yield detailed acoustic images akin to aerial photographs in which much can be learned about the geometry and spatial characteristics of seafloor features owing to the high data density. The side-scan images provided a data set that could be compared to pre-existing geophysical and submersible data. In addition, as a part of the project, we planned to collect piston cores with a surface ship as well as deep geophysical data and observations with submarine NR-1 from selected targets in the sonar images. We hoped that with NR-1 we could learn how many of the sites that appeared to be seeps in the geophysical data were actually inhabited by chemosynthetic organisms.

6-9
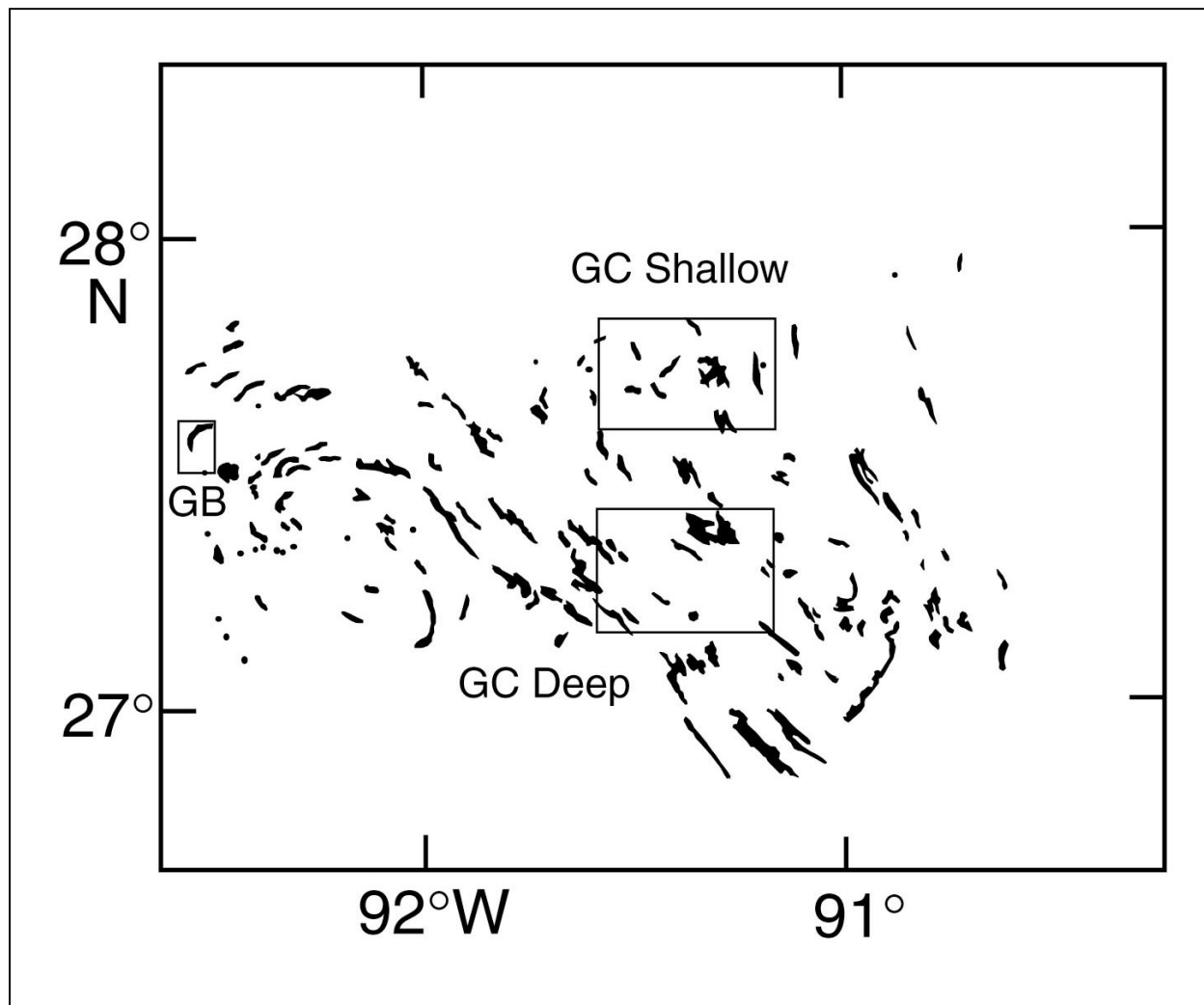
Figure 6.3.  Oil slicks on the sea surface over the Louisiana slope, imaged from Space Shuttle photography and synthetic aperature radar images. Boxes show study areas. Redrawn from MacDonald *et al.* (1993; 1996).

## 6.2 Surveys

### 6.2.1 Study sites

The two larger study areas are in the Green Canyon leaseblocks. The "GC Shallow" area is 25 x 41 km in size and includes water depths from 300 to 1050 m on the upper slope (Figure 6.4). It covers all or parts of 54 lease blocks. This area contains several chemosynthetic organism sites that have been the subject of ongoing studies (GC185, GC233, and GC234) in addition to other locations known as seeps (GC139-GC140, Roberts and Aharon 1994; GC272, Roberts 1996). This area was chosen because it is one in which prior data from seep sites could be used to better understand regional geophysical data.
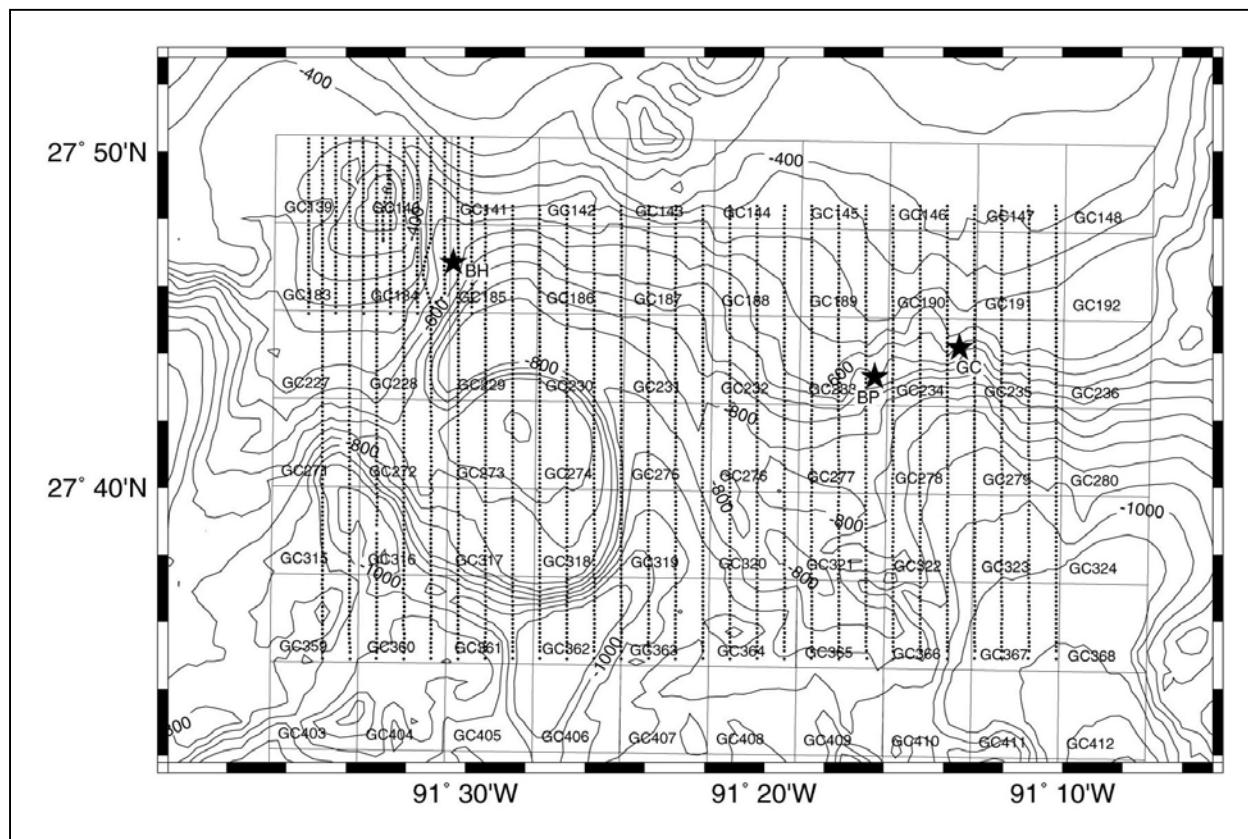
Figure 6.4.     Bathymetry, lease blocks, and ship tracks for the GC Shallow site survey. Bathymetry contours are shown at 50-m intervals from NOAA multibeam soundings. Dots show shotpoints along ship tracks for the TAMU[2] side-scan sonar survey of cruise 97G4 on R/V GYRE. Squares represent lease block boundaries. Stars show chemosynthetic community sites GC185 (BH), GC233 (BP), and GC234 (GC).

The second large study area, "GC Deep," is nearly the same size as the GC Shallow site (30 x 41 km), but is located directly south of the shallow site on the deeper continental slope in water depths of 1000 to 2250 m (Figure 6.5). It contains approximately the same number of sea surface slicks as GC Shallow (Figure 6.3) and covers all or parts of 63 lease blocks. Although little is known about the specific geology of this area, other than bathymetry, we studied the GC Deep area for comparison with GC Shallow. GC Deep is representative of the deeper slope where salt massifs and intra-salt basins characterize the topography, whereas GC Shallow has a smoother topography less perturbed by salt tectonics.

The third survey site is located on the upper slope in the Garden Banks lease blocks. It is smaller, only 12 x 13 km, and centered on an active mud volcano, which is a chemosynthetic organism site, at the border of blocks GB424 and GB425. Water depths in this study area range from 550 to 850 m.
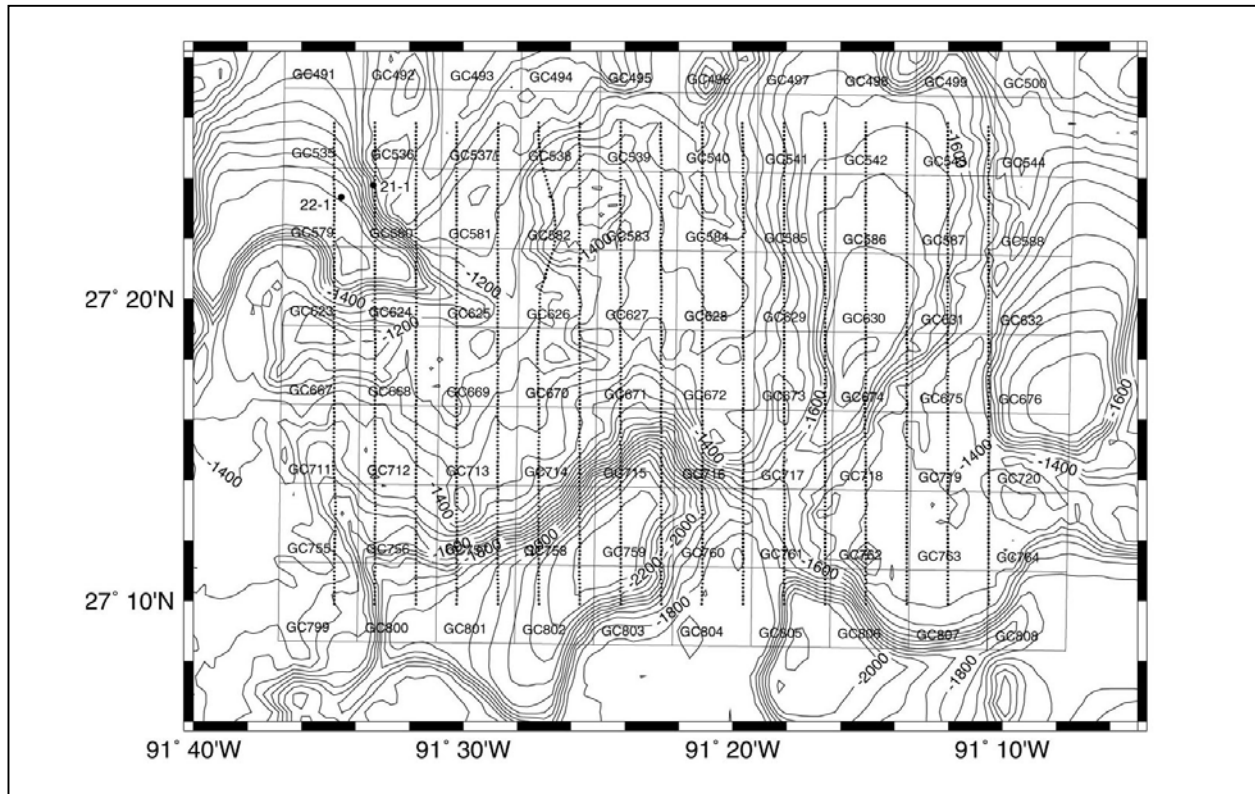
Figure 6.5.    Bathymetry, lease blocks, and ship tracks for the GC Deep site survey. Conventions as in Figure 6.4. Small filled circles show locations of cores 21-1 and 22-1.

## 6.2.2 Cruise 97G4: side-scan sonar survey and coring

Cruise 94G4 occurred from 3 to 15 June 1997 on board the R/V GYRE. The three study sites were surveyed using the TAMU$^2$ side-scan sonar, which uses frequencies of 11 and 12 kHz (Hilde *et al.* 1991). In all, a total area of approximately 2400 km$^2$ was surveyed. The sonar body was towed behind the GYRE at a depth of approximately 50 m and with a layback of about 240 m. The ship itself was positioned using a differential global positioning system (DGPS), with an accuracy of <5 m, and the tow body was located relative to the ship using an ultra-short base line (USBL) acoustic ranging system. A 3.5 kHz echo-sounder was run simultaneously with all lines to collect subbottom profiler records along the tracks.

Survey lines were run north-south (N-S) at a speed of 5 to 6 knots. In the GC Shallow and GB sites, ship tracks were spaced 1500 m apart, and the sonar swath width was set at 3000 m. This provided 200% coverage, allowing each area of the seafloor to be insonified from two different angles and allowing the zone beneath the sonar (which is poorly imaged) of one track to be filled by data from adjacent tracks. With this swath width, pixel sizes of about 1.5 m were achieved on the original sonar swaths. Seven N-S lines were run in the GB area (Figure 6.6) and one cross-line was made to look at the mud volcano from a different angle and to run the subbottom profiler across the crater in the western part of the study area. In the GC Shallow study area, 21

N-S lines were run across the entire extent of the survey box (Figure 6.4). Additionally, 21 short lines were run in between the original lines on the north side of the survey. These were fill lines designed to fill bathymetry coverage in the shallow parts of the survey. Fill lines were needed because it is only possible to calculate bathymetry to a distance of 3.5 times the water depth with the TAMU$^2$ sonar and this left gaps with a track spacing of 1500 m.
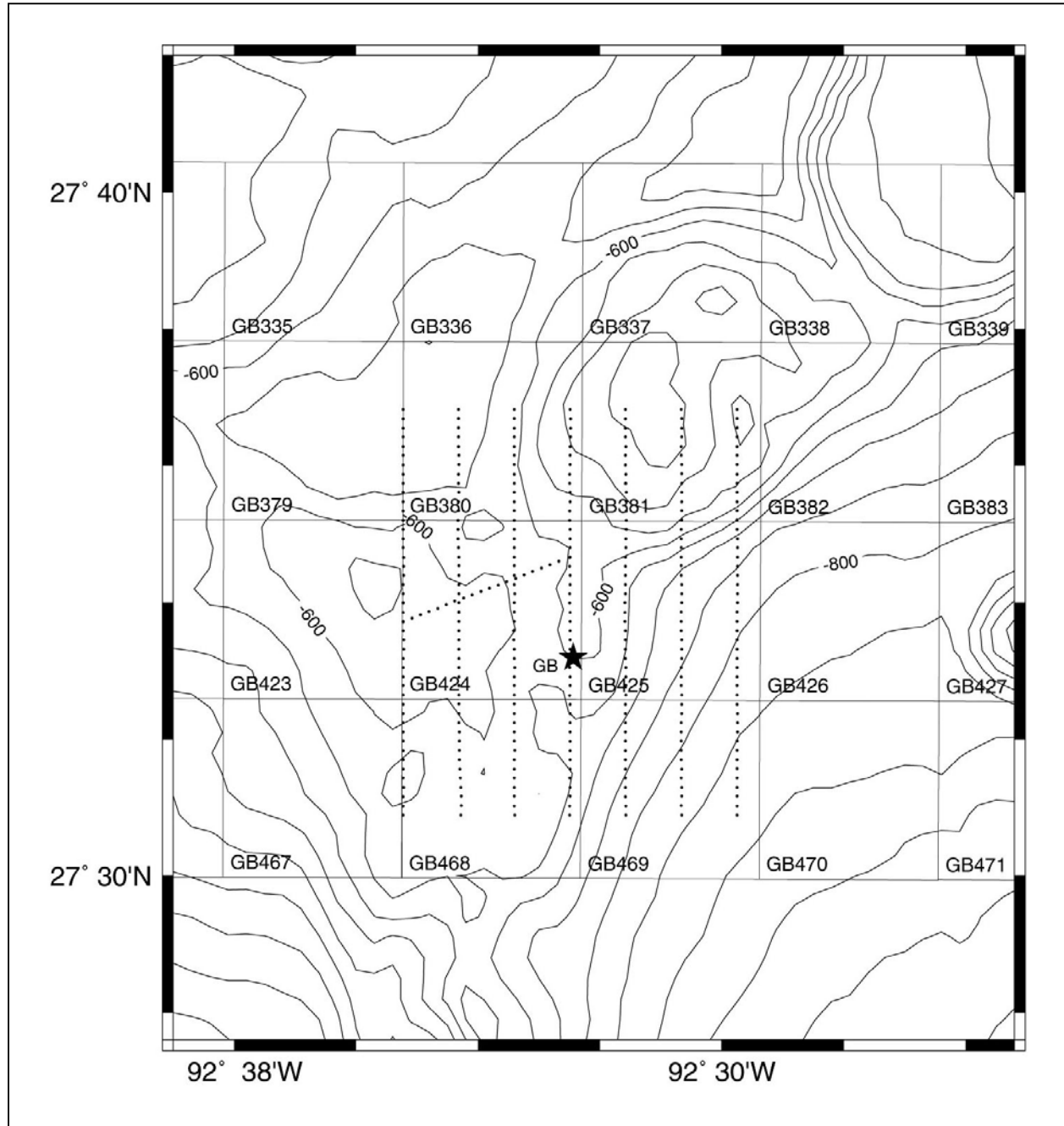


Figure 6.6.   Bathymetry, lease blocks, and ship tracks for the GB site survey.   Star labeled "GB" shows chemosynthetic community site on a mud volcano.  Conventions as in Figure 6.4.

In the GC Deep area, the swath width and track spacing were increased to make the survey shorter. Seventeen N-S lines were run, spaced 2.5 km apart (Figure 6.5). A 5500-m swath width was used, giving a pixel dimension of about 2.7-m on the original sonar swaths.

After the side-scan sonar surveying, 31 gravity and piston cores were collected from features thought to represent seeps in the sonar images (Table 6.1). Core penetration ranged from 4 cm to 5.2 m. Most cores were taken in the GC Shallow survey area (Figure 6.7) because it was believed better to concentrate on one study area rather than to spread the ground truth data too thin.

Table 6.1. Cruise 97G4 Core Locations

| Core | On Bottom Date | Time (UT) | Depth (m) | Latitude (d) | (m) | Longitude (d) | (m) | Length (m) | Lease Block | Type* |
|---|---|---|---|---|---|---|---|---|---|---|
| GC1-1 | 13-Jun-97 | 13:32 | 420 | 27 | 48.097 | -91 | 13.025 | 4.61 | GC146 | P |
| GC1-2 | 13-Jun-97 | 14:12 | 420 | 27 | 47.832 | -91 | 13.370 | 1.42 | GC146 | G |
| GC2-1 | 13-Jun-97 | 14:52 | 405 | 27 | 46.351 | -91 | 12.471 | 5.20 | GC191 | P |
| GC2-2 | 13-Jun-97 | 15:33 | 407 | 27 | 46.363 | -91 | 12.475 | 0.04 | GC191 | G |
| GC3-1 | 13-Jun-97 | 16:18 | 519 | 27 | 44.277 | -91 | 11.337 | 5.51 | GC235 | P |
| GC3-2 | 13-Jun-97 | 16:51 | 519 | 27 | 44.228 | -91 | 11.513 | 1.47 | GC235 | G |
| GC4-1 | 13-Jun-97 | 17:55 | 641 | 27 | 43.475 | -91 | 15.560 | 5.43 | GC234 | P |
| GC4-2 | 13-Jun-97 | 18:20 | 641 | 27 | 43.469 | -91 | 15.644 | 1.03 | GC234 | G |
| GC5-1 | 13-Jun-97 | 19:04 | 809 | 27 | 42.401 | -91 | 15.661 | 4.27 | GC278 | P |
| GC6-1 | 13-Jun-97 | 19:53 | 832 | 27 | 42.425 | -91 | 15.193 | 4.16 | GC278 | P |
| GC7-1 | 13-Jun-97 | 20:50 | 559 | 27 | 43.762 | -91 | 18.052 | 2.18 | GC233 | P |
| GC7-2 | 13-Jun-97 | 21:10 | 575 | 27 | 43.729 | -91 | 17.946 | 1.34 | GC233 | G |
| GC8-1 | 13-Jun-97 | 21:42 | 639 | 27 | 43.436 | -91 | 17.050 | 4.57 | GC233 | P |
| GC8-2 | 13-Jun-97 | 22:16 | 592 | 27 | 43.371 | -91 | 17.417 | 1.30 | GC233 | G |
| GC9-1 | 13-Jun-97 | 22:55 | 688 | 27 | 43.457 | -91 | 20.950 | 4.20 | GC232 | P |
| GC9-2 | 13-Jun-97 | 23:38 | 688 | 27 | 43.542 | -91 | 21.004 | 1.48 | GC232 | G |
| GC10-1 | 14-Jun-97 | 0:36 | 766 | 27 | 38.859 | -91 | 20.906 | 4.25 | GC320 | P |
| GC10-2 | 14-Jun-97 | 0:57 | 766 | 27 | 38.906 | -91 | 20.684 | 1.36 | GC320 | G |
| GC11-1 | 14-Jun-97 | 1:46 | 766 | 27 | 38.910 | -91 | 20.473 | 4.00 | GC320 | P |
| GC12-1 | 14-Jun-97 | 2:39 | 795 | 27 | 38.320 | -91 | 20.340 | 4.08 | GC320 | P |
| GC13-1 | 14-Jun-97 | 3:34 | 890 | 27 | 35.779 | -91 | 23.133 | 4.08 | GC363 | P |
| GC14-1 | 14-Jun-97 | 5:29 | 985 | 27 | 39.972 | -91 | 33.805 | 3.78 | GC315 | P |
| GC15-1 | 14-Jun-97 | 6:44 | 726 | 27 | 40.363 | -91 | 32.215 | 3.93 | GC272 | P |
| GC16-1 | 14-Jun-97 | 15:36 | 676 | 27 | 41.574 | -91 | 32.398 | 0.74 | GC272 | G |
| GC17-1 | 14-Jun-97 | 16:17 | 630 | 27 | 43.054 | -91 | 32.108 | 1.41 | GC228 | G |
| GC18-1 | 14-Jun-97 | 17:26 | 279 | 27 | 49.369 | -91 | 33.055 | 1.28 | GC140 | G |
| GC19-1 | 14-Jun-97 | 17:52 | 327 | 27 | 49.234 | -91 | 33.256 | 1.92 | GC140 | G |
| GC19-2 | 14-Jun-97 | 18:46 | 263 | 27 | 48.396 | -91 | 33.129 | 0.25 | GC140 | G |
| GC20-1 | 14-Jun-97 | 19:21 | 401 | 27 | 47.947 | -91 | 35.434 | 1.33 | GC139 | G |
| GC21-1 | 14-Jun-97 | 10:37 | 1152 | 27 | 23.764 | -91 | 33.345 | 1.50 | GC580 | G |
| GC22-1 | 14-Jun-97 | 11:43 | 1542 | 27 | 23.365 | -91 | 34.530 | 1.67 | GC579 | G |

*Type: P = piston; G= gravity
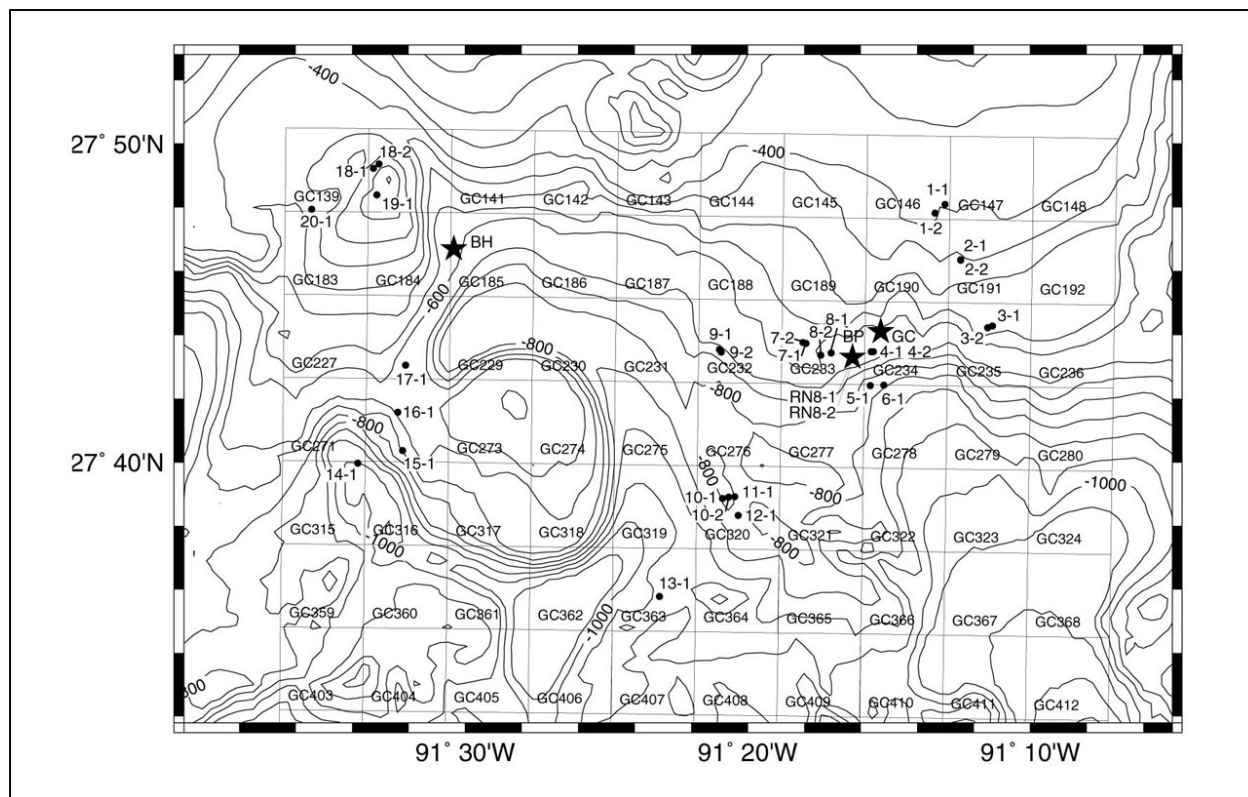
Figure 6.7.    Core locations in GC Shallow survey area (small filled circles). Conventions as in Figure 6.4.

### 6.2.3 Submarine NR-1 cruise

In the summer of 1998, we were scheduled for three weeks of time on the submarine NR-1 in the Gulf of Mexico. Two weeks of that time was to be spent investigating sites within the GC Shallow and GB study sites. Two remote sensing tools were installed on the submarine for the cruise, X-Star 2-12 kHz chirp sonar for making near-bottom echo-sounder profiles and a Raytheon laser line-scanner for making optical images. Submarine positions were obtained using inertial navigation tied to daily fixes provided by acoustic ranging to the tender ship, which was itself navigated with P-code global positioning system (GPS).

Owing to technical difficulties, the NR-1 was late leaving port, and the available survey time was decreased. The submarine reached the GC Shallow study area on 18 May 1998 and operations were commenced. For the next several days, repeated problems with the laser line-scanner and its data storage unit made it necessary to return to the surface several times. Eventually the laser line-scanner developed a short in a cable through the hull and was unusable for the rest of the survey. Although there were problems with a preamplifier on the chirp sonar, it performed well near the sea bottom and delivered good data. Seventeen targets from the side-scan sonar mosaics were investigated in four days (Figure 6.8). These included dense grids of X-star lines over the GC234 chemosynthetic organism site and the GC233 site. Finally on 22 May, the NR-1 developed problems with a thruster and the cruise was terminated.
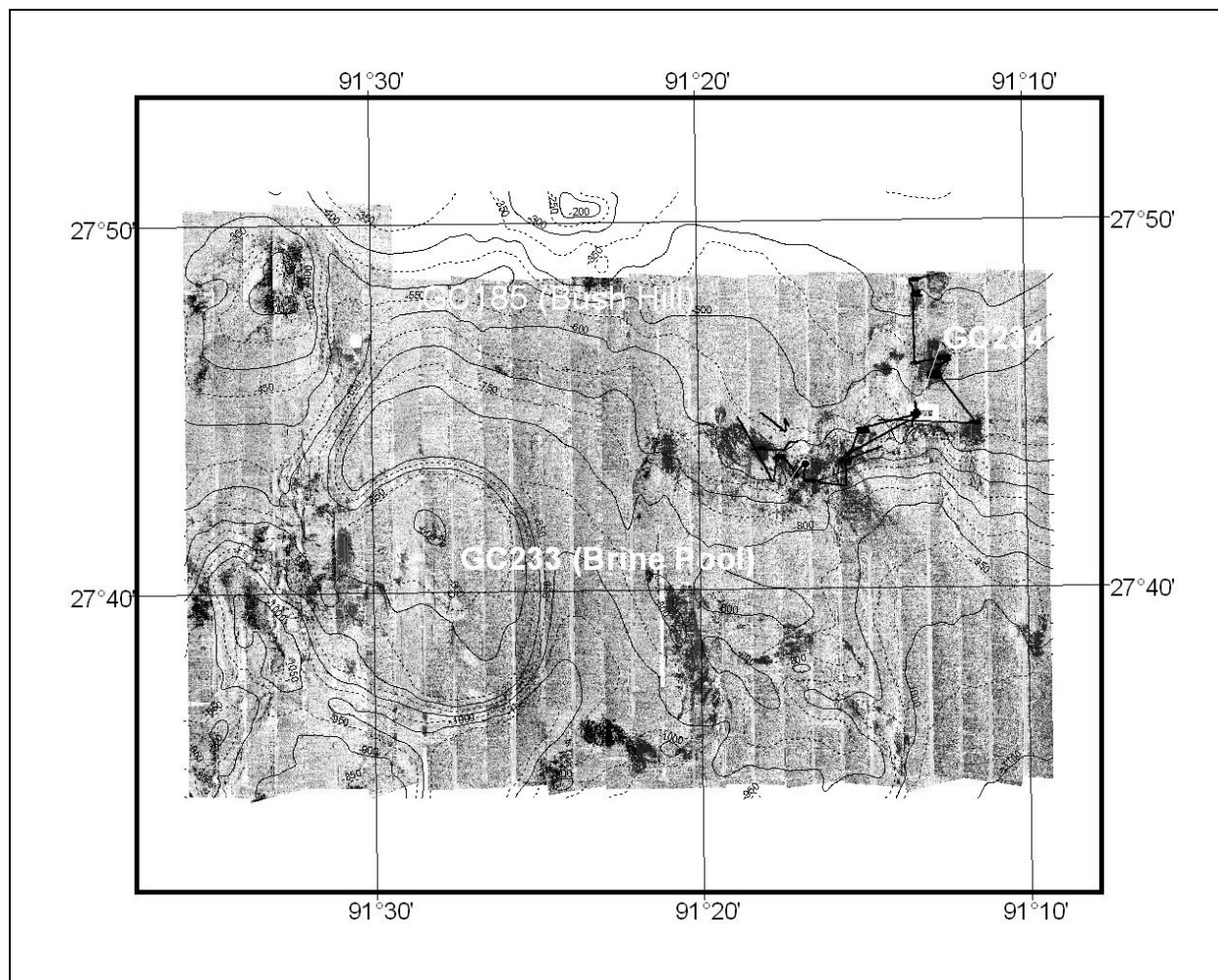
Figure 6.8.    Tracks of the 1998 submarine NR-1 dives.  Background is the TAMU[2] side-scan sonar mosaic.  Thin
               dark lines are 50-m bathymetry contours.  Light lines are submarine tracks.

## 6.3 Data and Methods

TAMU[2] side-scan sonar swaths were georeferenced and combined to make mosaics by C&C
Technologies, Inc., using proprietary software. The result was a side-scan sonar image of the
whole of each survey area with pixel resolutions of 4 m for the GC Shallow and GB sites and 8
m for the GC Deep site. For comparison with other data, such as core locations and NR-1
surveys, the mosaics were entered into two GIS computer programs, ERMapper and ArcView.
Interpretations for features in the side-scan mosaics were made from inference using the two-
dimensional geometry and reference to the 3.5 kHz subbottom profiles collected along ship
tracks, cores, and submersible observations. In many ways, the mosaic interpretation is similar to
that of aerial photographs in which the interpreter attempts to recognize features from their shape
and morphology using results from limited ground-truth data to extrapolate into other similar
areas. Comparison with 3.5 kHz echo-sounder data was useful because these subbottom profiles
give the show geometry in the vertical plane as well as detail within the sediments. For example,

the 3.5 kHz data were critical in recognizing faults from the offset of buried layers and confirming mounds from the change in seafloor elevation.

Chirp sonar data from the NR-1 cruise were plotted from tapes recorded during the cruise. Navigation data were corrected for offsets occurring between fixes from the mother ship. Tracks from the dense surveys over the GC233 and GC234 chemosynthetic organism sites were entered into ArcView for more detailed spatial analysis and comparison with pre-existing data. Seafloor acoustic signature maps were constructed using criteria similar to those of Lee (1995) and Sager *et al.* (1999), developed from higher frequency subbottom profiler data from submarine NR-1. Submarine tracks were plotted for surveys over individual site surveys and areas of similar acoustic reflection characteristics were plotted and contoured. The result was a series of micro-surveys, typically a few hundred meters across, similar to those in Sager *et al.* (1999).

Cores were sectioned and capped at sea. On shore, the cores were split across a diameter to expose the interior for description. All cores were photographed and described using techniques and sedimentological terminology similar to that used by the Ocean Drilling Program at Texas A&M University. The description produced a graphical representation that shows layering, color, and large objects such as shells and nodules. For a subset of the cores, a 1-cm slab was cut from the core split face and X-rayed to look for variations in density and structure. The X-radiographs often show layering, structure, and textural features not evident to the naked eye.

Several geophysical data maps were gathered from outside sources for comparison with the side-scan sonar and NR-1 profiler data. A map of wipeout zones from 3.5 kHz profiles, published in Behrens (1988), was obtained for the eastern half of the GC Shallow area. Two seafloor amplitude anomaly maps, derived from exploration 3D multi-channel data, were obtained for lease blocks GC184, GC185 and GC272. In addition, a shallow geohazard map, derived from 3.5 kHz subbottom profiler data, was obtained for lease blocks GC233, GC234, and GC235.

3D multi-channel seismic data sets were also procured from Western Geophysical, Inc., for several blocks in the GC Shallow and GB sites. Data from lease blocks GB424 and GB425 were acquired from the GB site, whereas data from blocks GC184, GC185 and GC233, GC234 were obtained from the GC Shallow site. These data were examined using PC workstations running Kingdom Suite interpretation software. Because these data were received late in the project, only limited interpretation was possible. The seafloor horizon was picked on all data sets, and bathymetry maps and seafloor amplitude extractions were made. A few lines within each block were examined in comparison to existing knowledge of the structure of each of the seep areas.

### 6.4 Results

The TAMU[2] side-scan sonar mosaics yielded wonderfully detailed images of the seafloor that show areas disturbed by faulting, seepage, and mass wasting. Areas of dark and light on the mosaics are determined by the strength of the acoustic pulse returned to the side-scan sonar from the seafloor. Unlike reflection profiling methods, which show variations in reflection coefficient across interfaces, side-scan sonar images represent the amount of signal scattered back to the sonar from the seafloor. This "backscatter," as it is called, depends on topography, surface

texture and roughness, and acoustic scattering within the near-surface sediments (Johnson and Helferty, 1990). On the mosaics shown in this report, dark areas represent high backscatter ("sonar bright") and light gray areas, low backscatter ("sonar dim").

### 6.4.1 GB site mosaic

The predominant feature on the GB site mosaic is a sonar bright zone running from the northeast corner to the center and from there south (Figure 6.9). A second zone of sonar bright returns occurs several kilometers to the west of the first. Both zones represent seep alterations of sediments along normal faults (Figure 6.10). The faults themselves are particularly evident in the sharp, linear sonar bright zones in the south center and central west parts of the mosaic. The area to the east of the central sonar bright zone is a slope that inclines southeastward (Figure 6.6). From the central bright zone westward is a plateau of rough bathymetry caused by faulting. The north part of the mosaic covers the south side of a salt dome, notable in the bathymetry contours (Figure 6.6).

Several subcircular sonar bright zones, approximately 500 to 700 m in diameter, are evident in the mosaic. One is located in the northeast corner, two are in the center, and a fourth is in the west central part of the survey. These features are typical of mud mounds formed by fluid expulsion at hydrocarbon seep vents (e.g., Neurauter and Bryant 1990; Kaluza and Doyle 1996). The southern of the two mounds in the center has been visited during several dives of the submarine NR-1 and submersible Johnson SEA-LINK. It has active gas and oil vents on its northeast and southwest sides but little activity is evident over its flat summit. The vent on the southeast side is also the site of a brine pool, filled with warm, sediment-rich fluid. Around this vent, chemosynthetic organisms have been noted, in particular a mussel bed near the brine pool. Submersible observations of the seafloor reveal extensive flow-like features suggesting ongoing expulsion of fluidized mud.

An interesting feature of this active mound is a small spot atop the mound, no more than about 100 m in diameter, that gives little or no sonar return. Such a sonar "dead" spot has been noted on several other mounds that have active vents with brine pools. This dead spot may result from absorption of the sonar energy by extremely gassy sediments or by specular reflection of the sonar waves away from the sonar.

The subcircular features on the west and northeast sides of the survey are not well known. The northeastern feature appears to be a fluid expulsion vent described by Roberts and Carney (1997, their Figure 6.11). The feature in the western part of the mosaic appears to be a crater that has been partly filled by sediments. On three sides it is a depression, but on its east side, the flat floor is raised. Features that look like sediment faulting, failure and collapse appear on its western side, implying the feature was originally a crater. Because the sonar bright zone in the center of the crater corresponds to acoustic wipeout in 3.5 kHz profiles, the sediments filling the crater appear gassy.

In several locations, linear sonar bright streaks run down slope. Based on their geometry and where they start, these are probably sediment flows. A large flow appears to emanate from the area between the two central mounds and may be from the vent on the northeast flank of the large, southern mound. Streaks emanate from other locations along the main fault in the center of

the survey area, implying fluid expulsion from many points in and along the fault. Seafloor with mottled backscatter appears to the north central area of the mosaic. This zone corresponds to the steeper flanks of the salt diapir. Thus, the variegated backscatter may represent tectonic disturbance and slope failure on the side of the diapir.
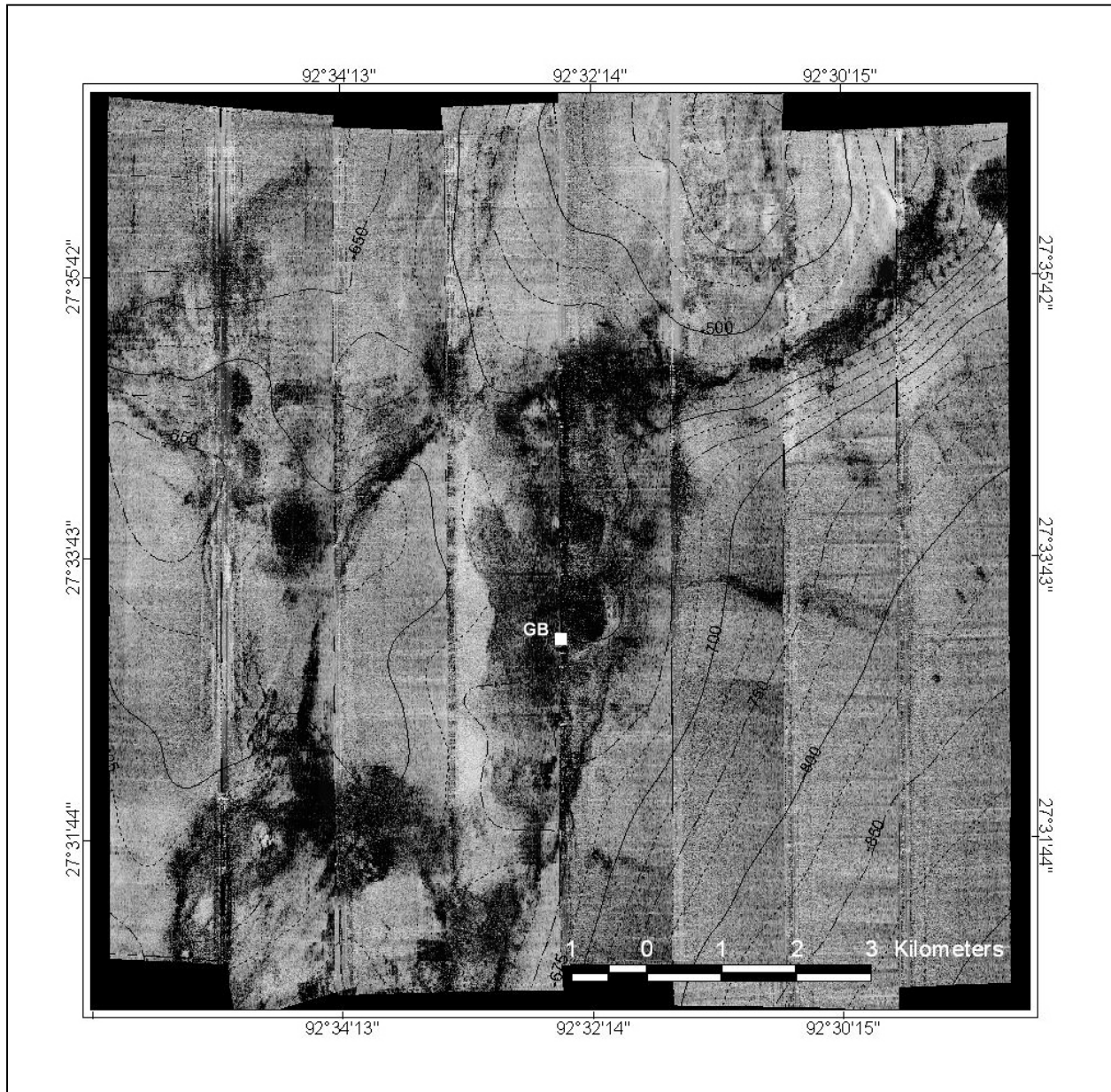


Figure 6.9.    *TAMU²* side-scan sonar mosaic of GB site.  Dark shades indicate areas of high acoustic backscatter, whereas lighter shades represent low backscatter.  Thin lines are bathymetry contours at 25-m intervals with multiples of 50 shown as solid.  Square labeled GB shows the location of the chemosynthetic community on the mud volcano.
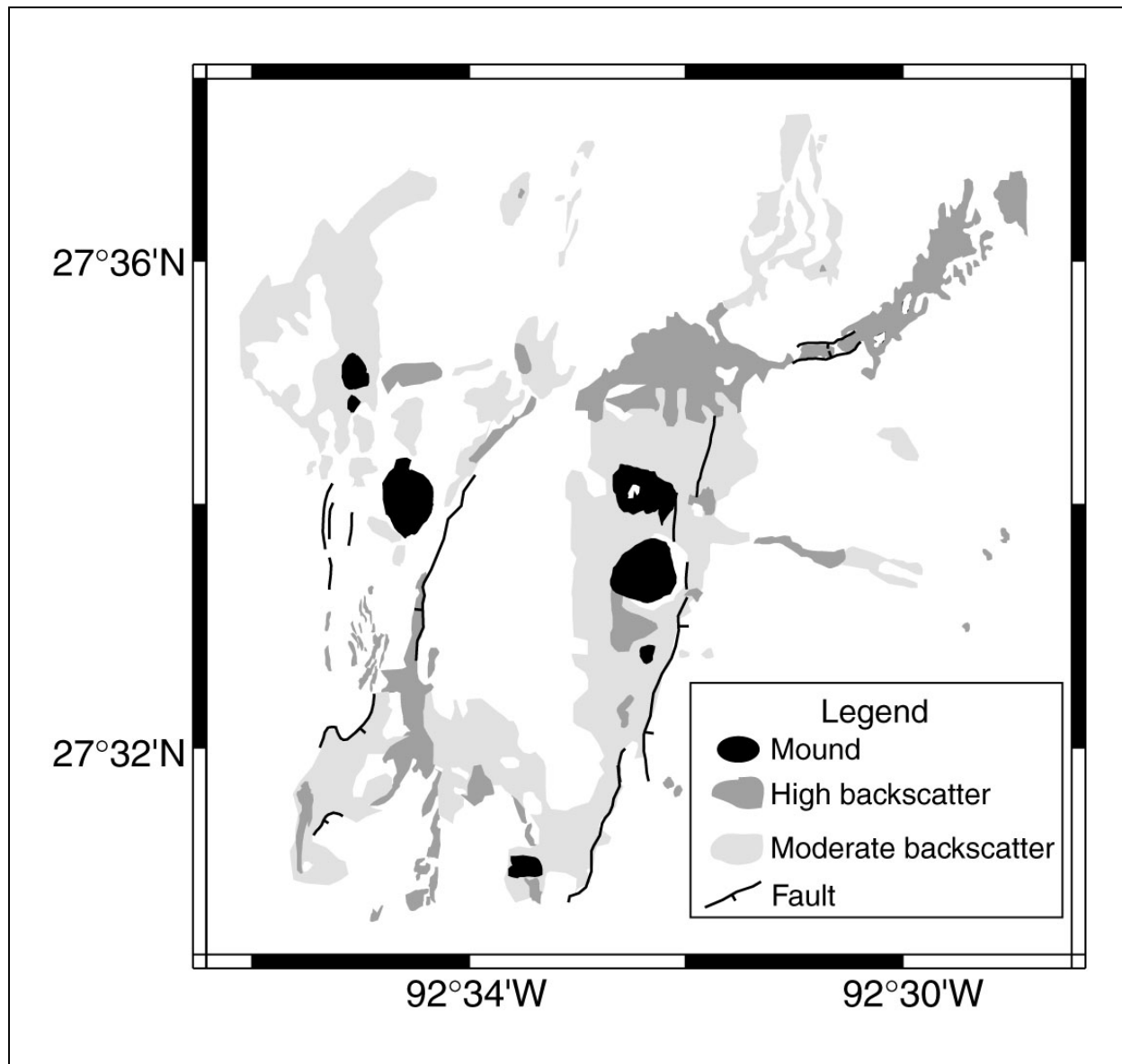
Figure 6.10.    Surface geology interpretation map of GB site.  Geologic interpretation was developed using *TAMU²*
                side-scan sonar mosaic and 3.5 kHz echo-sounder profiles along ship tracks.

## 6.4.2 GC Shallow mosaic

Seepage along faults and large salt domes characterizes the GC Shallow mosaic. On the west side of the survey, two large salt diapirs cause domes, both associated with sonar bright patches (Figure 6.11). The northern diapir, in GC139 and GC140, is conical in shape (Figure 6.4) and has faults radiating to its southwest and southeast sides (Figure 6.12). Its summit has a mottled, sonar bright appearance caused by a cap of reflective material. In detail, the sonar bright zones contain many small, subcircular features, some with shadows on the side away from the sonar (Figure 6.13). These are likely mounds constructed from precipitated carbonate material that have been described on this mound by Roberts and Aharon (1994). In some places, these mounds form lineaments that likely indicate seepage and mound formation along a fault.
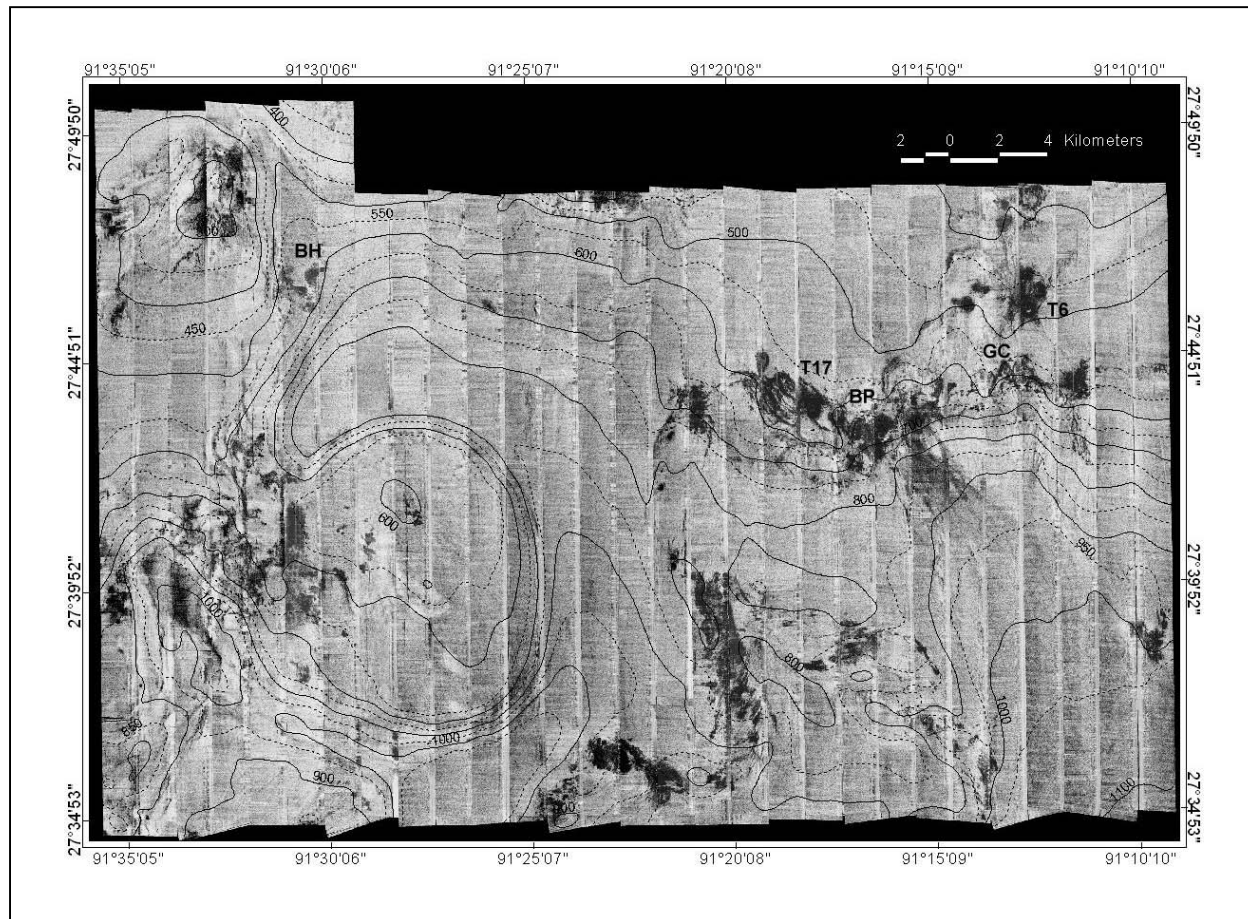
Figure 6.11.   *TAMU²* side-scan sonar mosaic of GC Shallow site.   Dark shades indicate areas of high acoustic backscatter, whereas lighter shades represent low backscatter.   Thin light lines are 50-m bathymetry contours, with multiples of 100 m shown as solid lines.   Known lush chemosynthetic community sites are labeled (BH= Bush Hill, T17=TAMU-17, BP=Brine Pool *NR-1*, GC=GC234, T6=TAMU-6).

GC185 is located on the southeast flank of this dome. It appears as a comma-shaped sonar bright patch (Figure 6.14), of which the large subcircular portion corresponds to the mound mapped in prior work (Sager *et al.* 1999). Nearby mottled sonar bright zones imply that seepage has occurred in other spots near GC185. Particularly interesting is a dark, subcircular sonar bright patch about 2 km south of GC185. Like the active mud volcano in the GB425 survey, this mound has a light, sonar dead spot in its center. This mound is Bush Lite, an active vent and chemosynthetic organism site that has been visited by previous submersible dives (H. H. Roberts, personal communication 1995).

The southern diapir has a circular, pancake shape with steep sides and a relatively flat, rounded top (Figures 6.4, 6.11). Steep sides on the dome circumference appear to be fault scarps. Only a few sonar bright patches are seen on the top of this dome but on its northeast side are numerous highly reflective areas. Those sonar bright patches occur where a fault complex appears to connect this dome with one farther north with faults that trend out the southern side of the survey area. Within this zone of sonar bright patches are several different types of sonar features. Linear
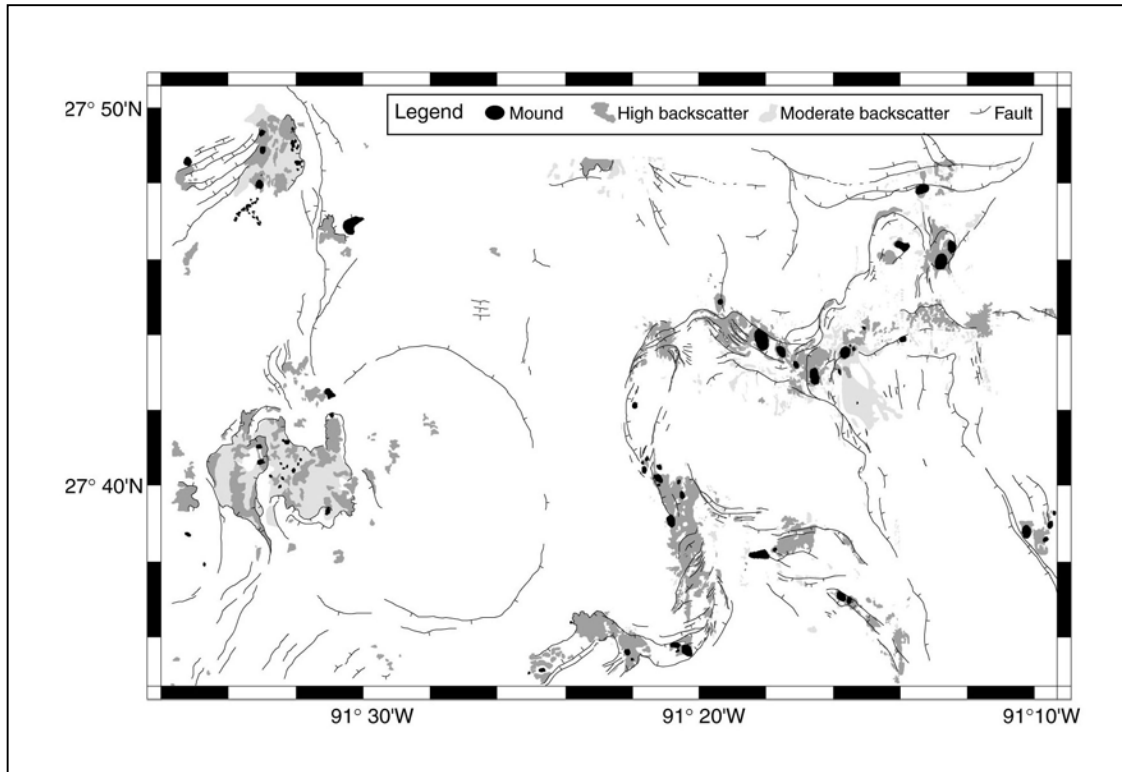
Figure 6.12. Surface geology interpretation map of GC Shallow site. Geologic interpretation was developed using *TAMU*² side-scan sonar mosaic and 3.5 kHz echo-sounder profiles along ship tracks.
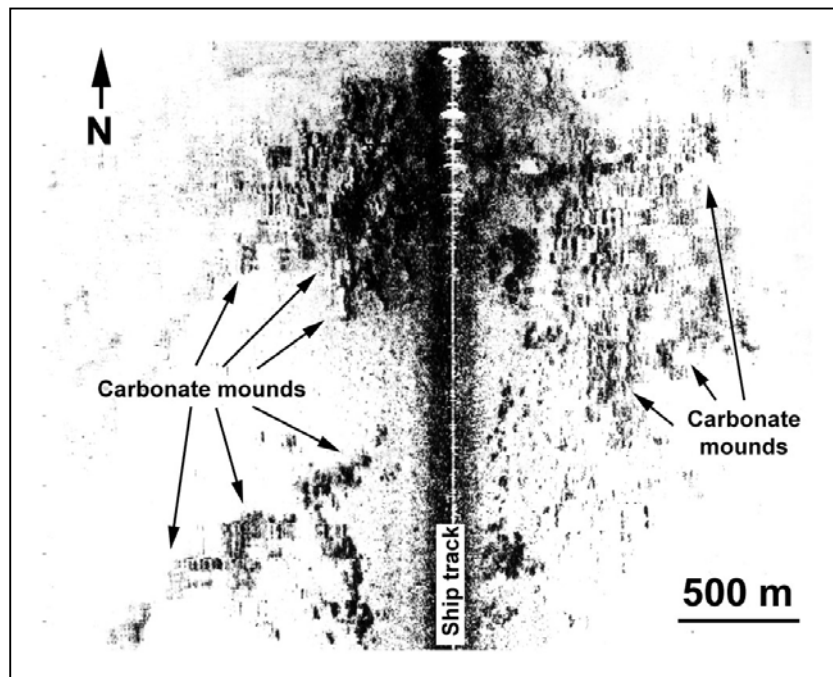


Figure 6.13. Side-scan sonar image of carbonate mounds in Green Canyon lease block 139. The mounds appear as small subcircular features with strong backscatter toward the ship track and weak backscatter (or shadow) away. Many mounds occur in lineaments that possibly indicate formation along a fault.
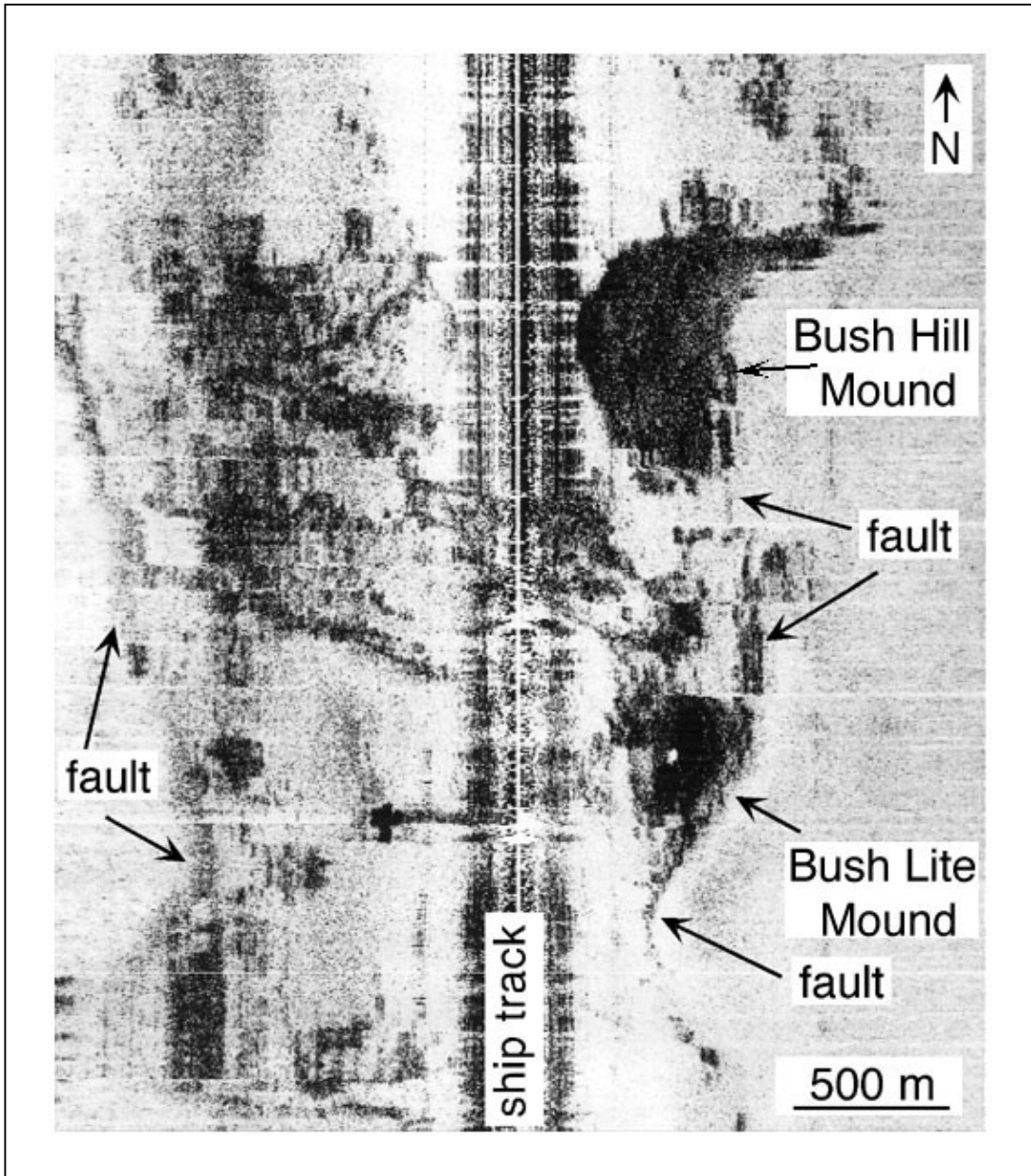
Figure 6.14. Side-scan sonar image of the Bush Hill and Bush Lite chemosynthetic community sites. Both appear as subcircular, high backscatter features that correspond to the mud mounds at each site. Bush Lite has a "dead spot" near its center from which there is no sonar return. Image is from Green Canyon lease blocks 184 and 185.

or curvilinear sonar bright areas correlate to faults and evidently show faults on which seepage has occurred. In one location to the northwest of the dome, a lobate sonar bright patch trends downslope from the faults (Figure 6.15). This feature may be a sediment flow that has emanated from the fault. In the southwest part of this sonar bright area is a dark area that has streaks oriented downslope (Figure 6.16). Some of these streaks appear to radiate from certain spots. This sonar bright zone appears to be a broad sediment flow (or multiple flows) that has been emitted from vents along the faults. Several active mud volcanoes and oil/gas seeps have been discovered in the area to the north and east of the vents during previous submersible dives (Roberts 1996; Roberts and Carney 1997).
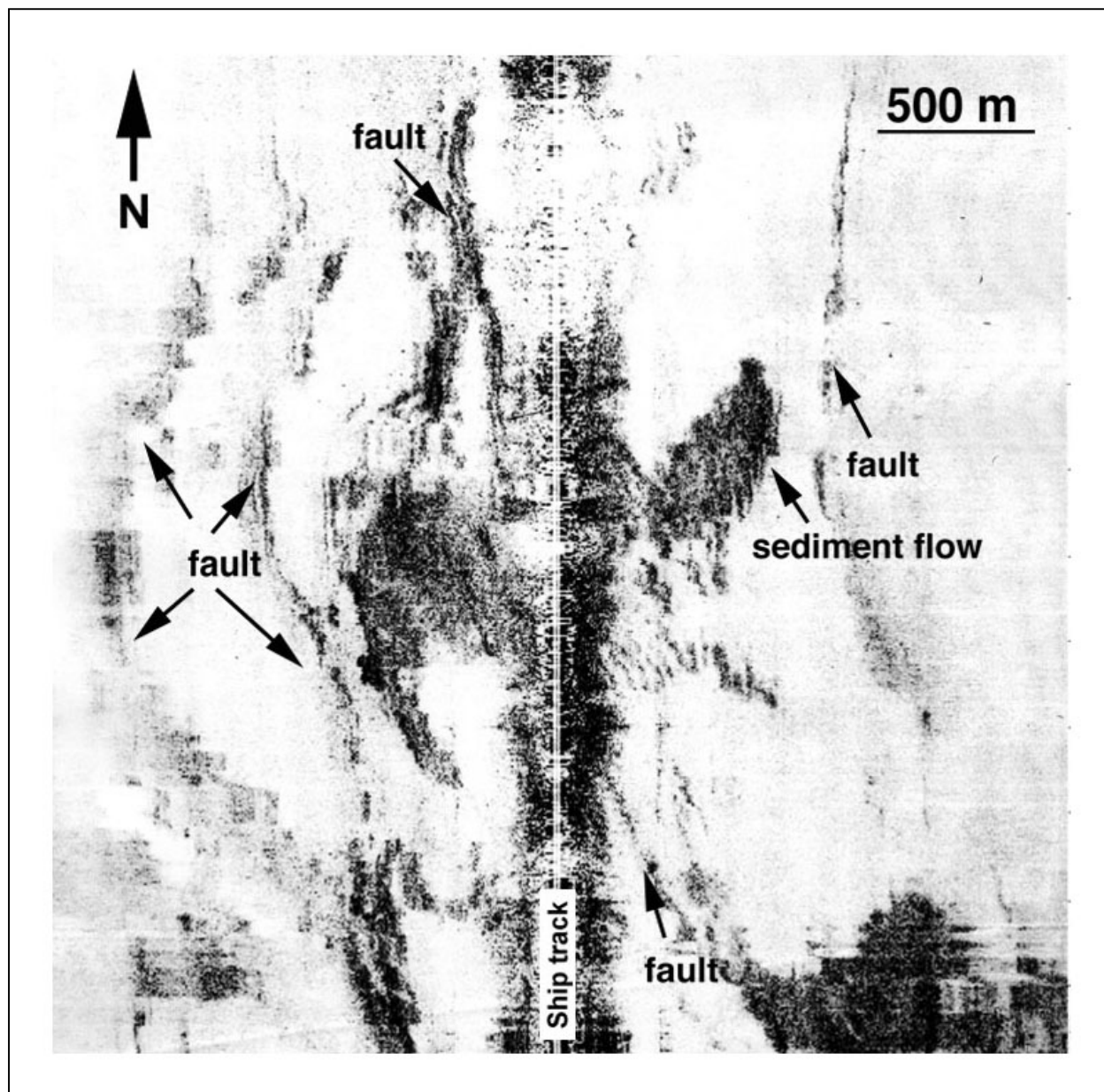
Figure 6.15.   Side-scan sonar image of faults and probable sediment flow caused by seepage from fault.  Image is from Green Canyon lease block 228.

The east side of the GC Shallow mosaic is dominated by sonar bright patches associated with a fault system that rings the head of a shallow canyon that trends southeastward out of the study area (Figures 6.4, 6.11, 6.12). Particularly notable is the fault zone located in the eastern central part of the survey. Along this fault are located several chemosynthetic organism sites: GC233, GC234, Mussel Beach, and two that were discovered during the NR-1 dives, TAMU-17 and GC191 (Figure 6.17). In this fault system, most of the sonar bright patches occur very near the faults. Indeed, many are located in grabens, i.e., downdropped zones between normal faults.
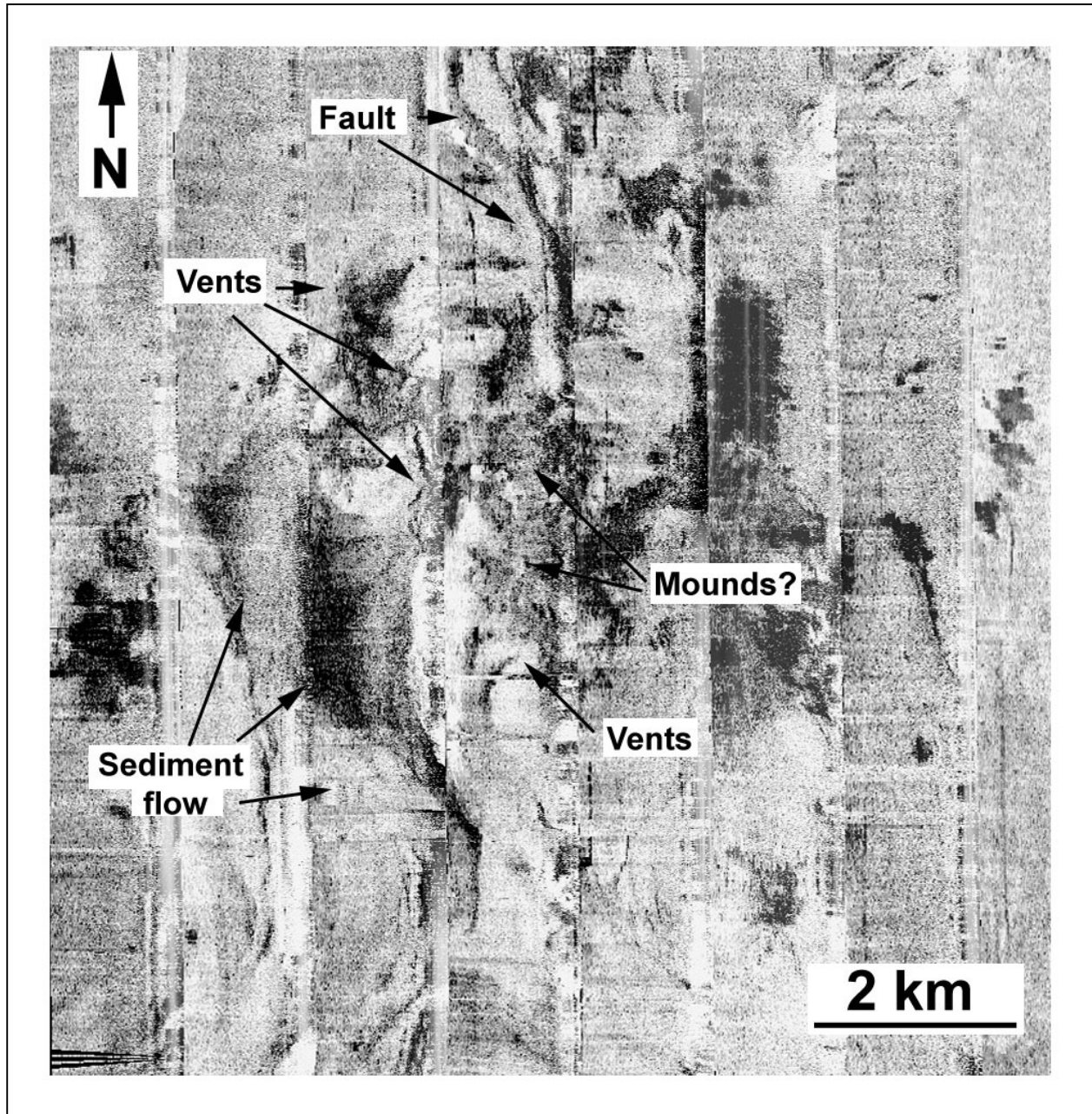
Figure 6.16.  Side-scan sonar mosaic of vents and sediment flows in Green Canyon leaseblocks 271, 272, 315, and 316.  Dark, high-backscatter patches indicate pervasive seepage in area along faults at flank of large salt dome.  A dark area with features trending downslope indicates a large sediment flow or flows that appear to emanate from several vents.

As in the western part of the survey, the eastern fault complex contains many subcircular sonar bright patches ranging in size from a few hundred meters to about a kilometer across. These appear to be mud mounds constructed by fluid expulsion. With further examination, several classes of mound were noted. Some are uniformly dark (sonar bright) and some are uniform, but

lighter. A number of mounds have brighter centers surrounded by less bright haloes. These were dubbed "bulls eye" mounds owing to their appearance. Also noted were two mounds that are sonar bright with sonar dead spots in their centers. These differences are likely related to the degree of mud volcano activity and the progressive buildup of hard material, such as carbonate or gas hydrate, atop these mounds. Mound appearances will be discussed in more detail in a later section.
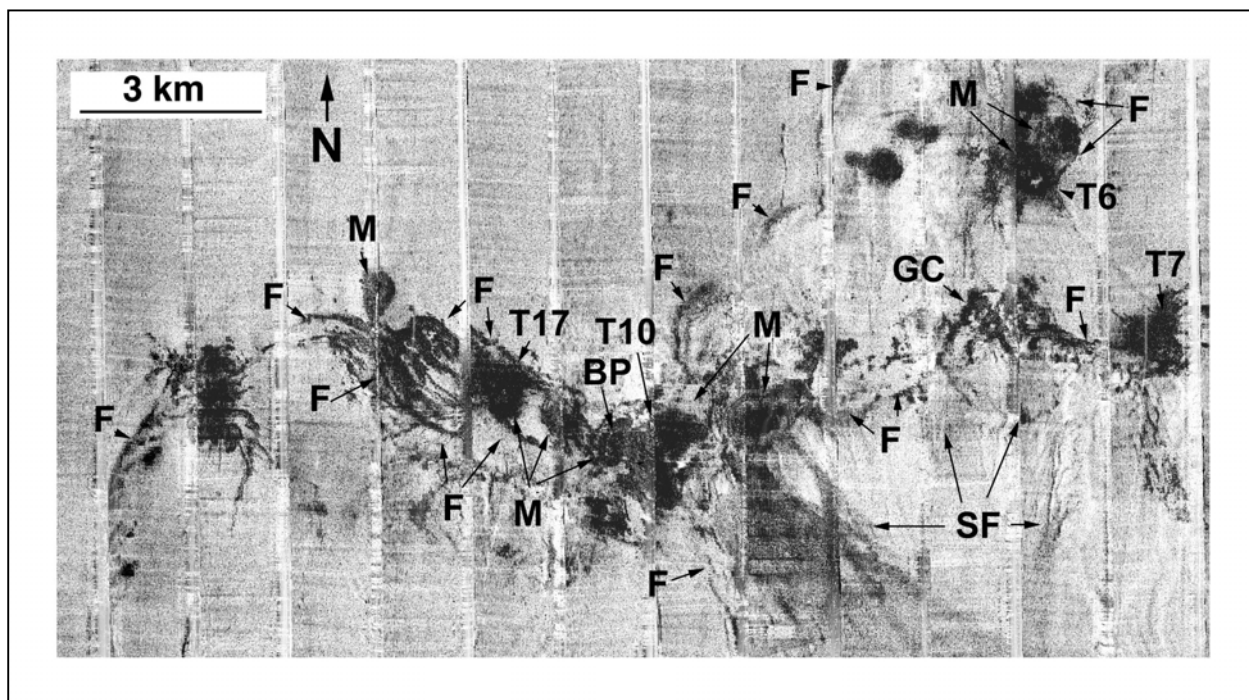


Figure 6.17.  Side-scan sonar mosaic of area including Green Canyon leaseblocks 232 to 236.  A fault system trends east-west across the center of the image and is the locus of much seepage.  Feature labels as follows: F=fault, M=mound, SF=sediment flow.  Known chemosynthetic community sites are labeled (T17=TAMU-17, BP=Brine Pool NR-1, T10=TAMU-10, GC=GC234, T7=TAMU-7, T6=TAMU-6).

At the head of the canyon is a broad, fan-shaped sonar bright area with streaks trending downslope. This bright area appears to emanate from a mound at the intersection of three sets of faults in the western part of GC234. The geometry of the fan-shaped bright zone implies that it is a large sediment flow or series of sediment flows that have originated from a vent at the location of the mound. Elsewhere along the faults that ring the head of the canyon are curvilinear sonar bright streaks trending downslope. These may be smaller sediment flows caused either by fluid expulsion or mass wasting.

In several places along the eastern fault zone, linear and curvilinear sonar bright features are seen along the faults (Figures 6.12, 6.17). These features probably result where faults experience a small amount of seepage. At other spots along these faults, small lobate sonar bright zones are

seen trending downslope, probably indicating sites where greater seepage has occurred, leading to small sediment flows.

The fault zone along the eastern central part of the survey area contains four known significant chemosynthetic organism sites. Two have similar appearances – dark, subcircular sonar bright mounds with dead spots (TAMU-17 and GC191). The two others are remarkable in that their locations do not stand out in the mosaic (Figure 6.17). Both GC233 and GC234 are in broad, sonar bright zones that do not stand out among the many sonar bright patches in this area. The geophysical signatures of these sites are discussed in more detail below.

### 6.4.3 GC Deep mosaic

The appearance of the GC Deep site mosaic is startlingly different than the GB and GC Shallow mosaics (Figure 6.18). Sonar bright patches in the shallow mosaics cover a small percentage of the total area and are arrayed along faults, mainly resulting from seepage. The GC Deep mosaic has a more chaotic appearance with many sonar bright areas scattered throughout the survey area. Although little ground truth data is available from the GC Deep area, many features can be interpreted from a combination of bathymetry, geometry, and character on subbottom profiles.
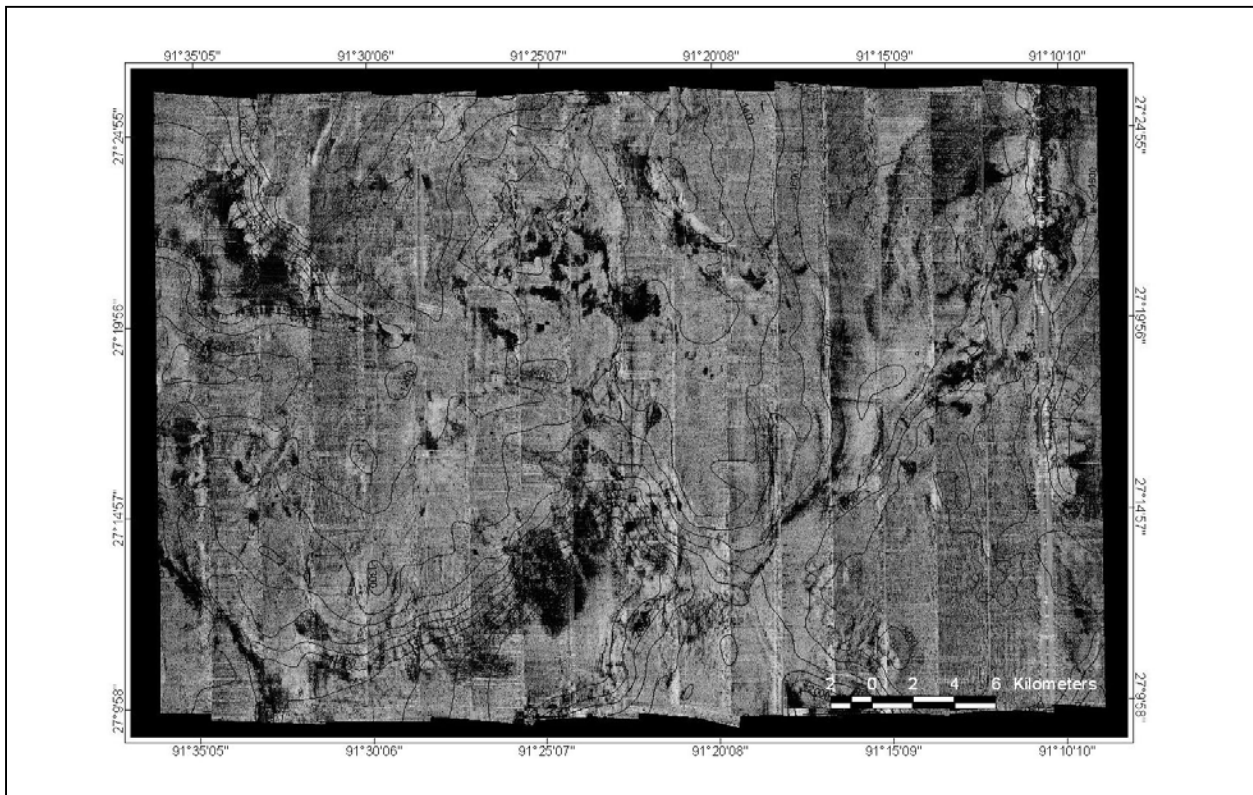


Figure 6.18. *TAMU²* side-scan sonar mosaic of GC Deep site. Dark shades indicate areas of high acoustic backscatter, whereas lighter shades represent low backscatter. Thin light lines are 50-m bathymetry contours.

Many of the sonar bright features in the GC Deep area appear to be a result of sediment mass wasting caused by slumping related to uplift and subsidence between salt withdrawal basins and salt massif highs. Three salt withdrawal basins are seen in the study area: Longhorn Basin in the northwest corner, Pygmy Basin on the south edge, and Tiger Basin in the northeast (Figure 6.5).

Many of the features in the sonar images appear to be related either to faulting or tectonic disturbance of the sediments. Longhorn Basin, in the northwest corner of the survey, has steep flank slopes that display sharp headwall scarps where sediments have failed and cascaded down into the basin. The flanks appear rough as is expected for faulted, failed slopes. Similar features are seen on the northern flank of Pygmy Basin and the eastern flank of Tiger Basin. In fact, faults appear to rim the sides and upper flanks of many of the salt massifs between basins (Figure 6.19).
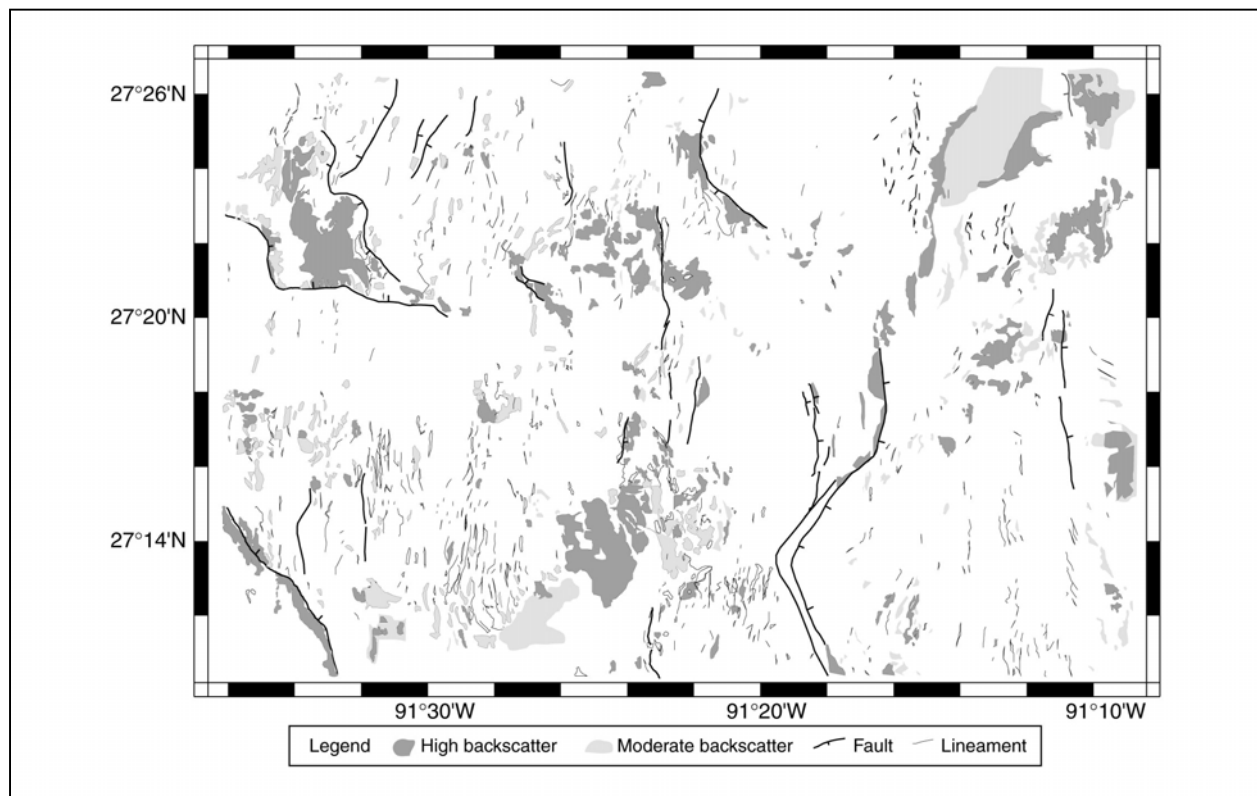


Figure 6.19.   Surface geology interpretation map of GC Shallow site.  Geologic interpretation was developed using *TAMU²* side-scan sonar mosaic and 3.5 kHz echo-sounder profiles along ship tracks.

Broad sonar bright patches occur on the floor of all three basins where sediments have accumulated owing to slope failure. In Longhorn Basin, such sonar bright sediments ring the edge of the basin. Similar sediments are evident in on the northeast side of Pygmy Basin. On the floor of Tiger Basin is an especially interesting sonar bright zone. Its shape on the floor of the basin is lobate and appears to have curved from east-west to north-south trending (Figure 6.20). Furthermore, it terminates on the eastern basin flank and appears to emanate from two small

sources. This bright zone appears to be a large sediment flow that cascaded down the basin flank, turned to follow the slope toward the south, and ponded in the basin. The fact that this flow traces back to two possible vents suggests that it may have resulted from fluid expulsion, rather than slope failure.
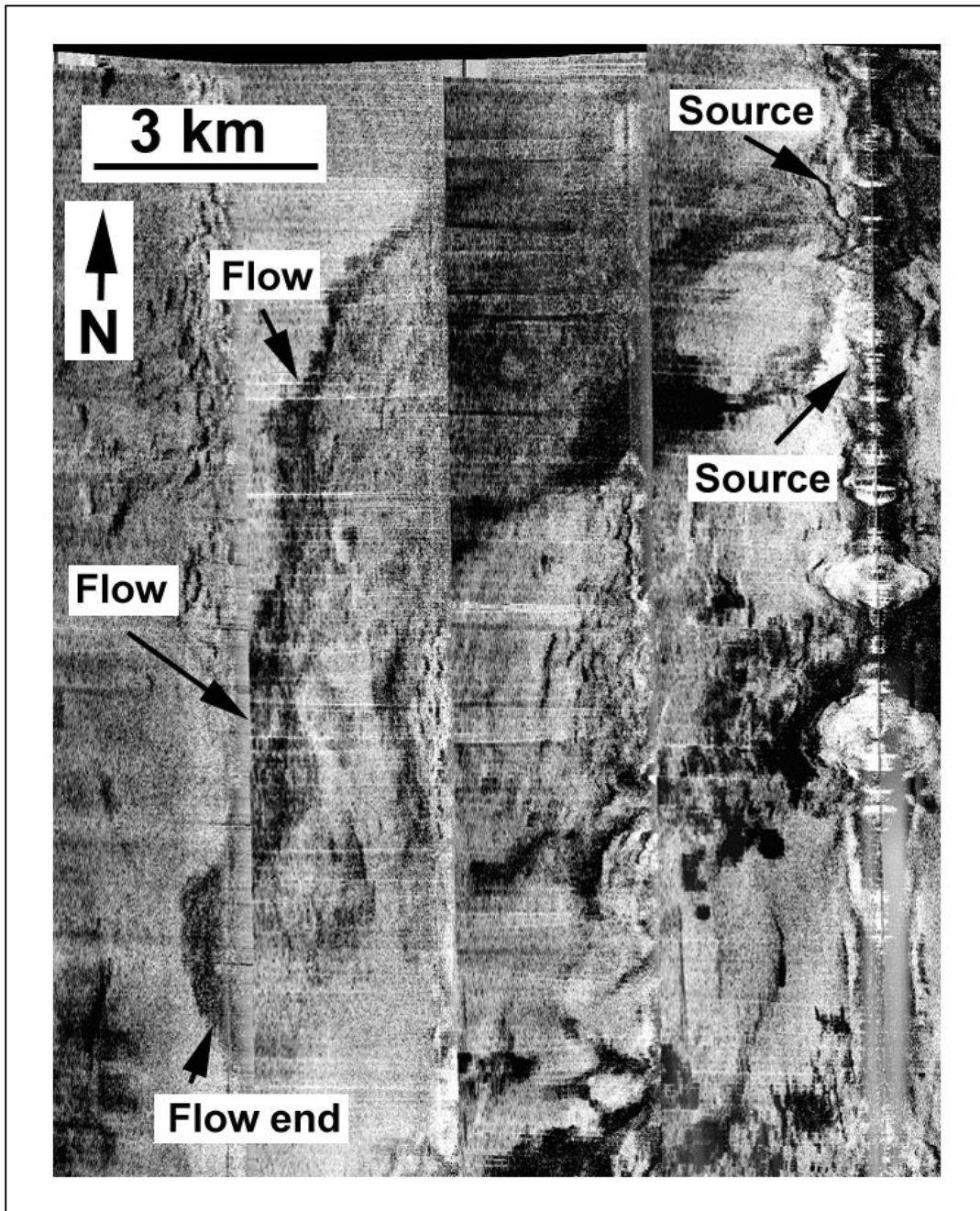


Figure 6.20.   Side-scan sonar mosaic of large sediment flow on the floor of Tiger Basin in the GC Deep survey area.   Dark, lobate feature is flow, which has emanated from sources on the salt uplift flanks that border the basin.   Lobate flow end suggests ponding on basin floor.   Image includes Green Canyon leaseblocks 586, 587, 630 and 631.

The side-scan sonar images also show many zones with parallel linear or curvilinear features that have the appearance of grooves from the geometry of shadows and bright returns. Typically, these grooves trend downslope on the flanks of the salt massifs. These features may be erosion gullies caused by rapid downslope transport of sediments on the massif flanks.

Because of the greater complexity, fewer 3.5 kHz profiles, fewer ground truth data, and lack of known seeps in the GC Deep area, it is difficult to pinpoint seeps in this area. Dark, irregular sonar bright patches occur in places, such as the north central part of the survey, and these may indicate the effects of seepage. Likewise, the flow in Tiger Basin may result from seeps. However, it is clearly much more difficult to find seeps with side-scan sonar in the more highly tectonized area of the lower slope than on the upper slope.

**6.4.4 Submarine NR-1 dives**

During the NR-1 cruise, the submarine visited 17 targets defined from the side-scan sonar mosaic and made detailed mini surveys over 12 sites (Figure 6.8). Two of the mini surveys provided extensive mapping of subbottom characteristics from known chemosynthetic organism sites, GC234 and GC233. The other sites were previously unexplored.

One of the goals of the submarine observations was to see which sites are inhabited by chemosynthetic organisms. Depauperate communities of chemosynthetic organisms were found in numerous locations. These might have included one or a few small, stunted tubeworm bushes, bacterial mats, or a collection of chemosynthetic bivalve shells. This observation implies that there are many places in the sonar bright zones where hydrocarbons are available near the surface in small amounts, insufficient to support lush communities. Clusters of chemosynthetic organisms were observed at six new locations during the NR-1 survey. Two sites had particularly large concentrations of tubeworms. One is at site TAMU-6 in the southwest corner of GC191 ($27^o$ 45.8'N, $91^o$ 12.7'W). The other is site TAMU-17, located in the west central part of GC233 ($27^o$ 43.7'N, $91^o$ 18.1'W). In the side-scan sonar mosaics, both appear as subcircular sonar bright areas 500 to 700 m in diameter. Furthermore, both have sonar dead spots near their centers. From the submarine, the seafloor at both sites was characterized by extensive sediment flows, indicating recent and ongoing fluid expulsion. In addition, brine pools were found at both locations. Both sites contained abundant tubeworm bushes. The other sites are TAMU-7 ($27^o$ 44.1'N, $91^o$ 11.5'W), TAMU-9 ($27^o$ 44.6'N, $91^o$ 14.9'W), TAMU-10 ($27^o$ 43.4'N, $91^o$ 15.6'W), and TAMU-14 ($27^o$ 42.9'N, $91^o$ 16.6'W). TAMU-9 and TAMU-14 both appear to be medium diameter (200-400 m) mud mounds, although the former is a bulls eye mound whereas the latter is more homogeneous in appearance. TAMU-10 is the large mound that appears to be the source of the large sediment flow seen in the mosaic. In contrast, TAMU-7 displays no obvious mound but is a circular high backscatter feature within a large aureole of moderate backscatter.

Subbottom profiler records in the mini surveys show characteristics that include normal, unaffected sediments, acoustic turbidity, acoustic wipeout, hard bottoms, and buried hard bottoms (e.g., Sager *et al.* 1999). In general, the highest backscatter zones correspond to hard bottoms. At least one bulls eye feature appears to have a chirp sonar reflection pattern (a central buried hard bottom surrounded by acoustically turbid sediments) that matches its side-scan sonar image. Other mini surveys are more difficult to interpret because lateral heterogeneity in chirp sonar profile character is high. Most sites have combinations of hard bottoms, buried hard

bottoms, turbidity, and wipeout. Interestingly, the relief of the subcircular sonar bright zones ranges from nothing to tens of meters, implying that not all circular features are mounds. The consistent aspect of these surveys is that these features occur over sites that have the appearance of seeps in the side-scan mosaic (usually a subcircular sonar bright feature), whereas other zones have lesser evidence of seep disturbance or undisturbed sediments.

Although observations from the submarine NR-1 found chemosynthetic organism communities at several of the hypothesized seep sites, it is notable that many sites appeared barren. Many of the mini surveys were limited in extent, so it is possible that by chance chemosynthetic communities were missed at some sites where they exist. However, it appears that many of the apparent seeps are dormant. In particular, some sites have extensive hard bottoms but no obvious vents and chemosynthetic communities. These may be older sites whose lack of evident activity or chemosynthetic organisms may reflect the "paving over" of these sites by authigenic carbonate precipitation with time (e.g., Sager *et al.* 1999). This implies that side-scan sonar, or indeed any geophysical exploration tool, may have difficulty recognizing which seep sites are active, because the geophysical techniques are affected by anomalous physical properties in the upper few meters of sediment, which have been deposited over a few thousand years.

### 6.4.5 Core data

Twenty-nine of the 31 cores recovered on cruise 97G4 were examined for evidence of seepage or chemosynthetic organisms. The other two were short cores containing copious amounts of oil that were given over to chemical analysis. Two additional cores from GC233 were also studied.

Physical characteristics of the cores were extremely variable. A few showed little evidence of seep disturbance (Table 6.2). Typically these were cores that missed high backscatter zones or were at their edges. Most cores showed one or two of several types of disturbance and few were highly disturbed. The following were disturbances noted in these cores: dense layers, high degree of consolidation, gas expansion cracks, strong hydrogen sulfide ($H_2S$) smell, carbonate (and clay/carbonate) nodules, crusts, or gravels, shells, and oil. Often the highly disturbed cores showed multiple types of disturbance and these cores are typically from near known or suspected seep vents. The stiffening, formation of dense layers, and carbonate nodules all probably come from precipitation of authigenic carbonate within the pores of the sediment owing to the byproducts of microbial degradation of hydrocarbons. Gas cracks are caused by the expansion of gas within the pore space as the pressure is relieved from the core; some gas expansion voids may result partly from gas hydrate decomposition as well. The strong $H_2S$ smell comes from the production of that gas in near surface sediments driven to anoxic conditions by microbial activity. In sum, it appears that surface sediments from sonar bright zones typically show disturbances related to seepage. However, the properties of these sediments show high lateral variation, so it is difficult to predict the degree and type of core disturbance from the side-scan sonar mosaic.

Table 6.2. Core disturbance properties.

| Core | Back-scatter | Disturbances | Feature |
|------|--------------|--------------|---------|
| No disturbance | | | |
| GC5-1 | M | | sediment flow in GC278 |
| GC9-1 | H | | south edge high BS, vent-like zone |
| GC19-1 | L | | near high BS on top of salt dome |
| | | | |
| Low-moderate disturbance | | | |
| GC1-1 | L | gas cracks, oil at bottom | between high BS features |
| GC1-2 | M | clay/carbonate nodules, highly consolidated | small bulls eye |
| GC2-2 | | carbonate pebbles | large bulls eye |
| GC3-2 | H | H$_2$S smell | high BS vent-like feature |
| GC4-2 | M | clay/carbonate nodules, highly consolidated | south flank, large flow-source mound |
| GC6-1 | M | dense layers | sediment flow in GC278 |
| GC8-2 | H | highly consolidated | south edge of high BS zone |
| GC10-1 | M | dense layers | west edge of high BS zone |
| GC10-2 | M | highly consolidated | patchy high BS zone |
| GC11-1 | H | clay/carbonate nodules, gas cracks | patchy high BS zone |
| GC12-1 | H | clay/carbonate nodules, dense layers | high BS zone between faults |
| GC13-1 | L | dense layers | near south edge of high BS zone |
| GC14-1 | H | dense layers | sediment flow in GC215-316 |
| GC15-1 | M | clay/carbonate nodules | patchy high BS zone |
| GC17-1 | M | highly consolidated | edge of high BS near fault |
| GC18-1 | M | carbonate nodules, gravel, highly consolidated | patchy high BS zone atop salt dome |
| GC19-2 | M | highly consolidated | patchy high BS zone atop salt dome |
| GC20-1 | M | highly consolidated, H$_2$S smell | high BS zone near mound |
| GC21-1 | L | highly consolidated | failed basin flank in GC Deep area |
| GC22-1 | H | highly consolidated | basin floor in GC Deep area |
| | | | |
| High disturbance | | | |
| GC2-1 | H | clay/carbonate nodules, H$_2$S smell, oil stain | large bulls eye |
| GC3-1 | H | clay/carbonate nodules, H$_2$S smell, oil | edge of high BS vent-like feature |
| GC4-1 | M | clay/carbonate nodules, oil stain, gas expansion | south flank, large flow-source mound |
| GC7-1 | H | carbonate gravel, shells | center of active mud volcano w/chemo |
| GC7-2 | H | oil, highly consolidated | SE edge of active mud volcano w/chemo |
| GC9-2 | H | abundant oil, tar | south edge high BS, vent-like zone |
| GC8-1 | H | Oil | high BS area near mound |
| GC16-1 | H | abundant oil, gas expansion, carbonate nodules | high BS area near mound |
| RN8-001 | H | oil, gas cracks, clay/carbonate nodules, shells | GC233 |
| RN8-002 | H | oil, gas cracks, clay/carbonate nodules, shells | GC233 |

## 6.4.6 Comparison with other geophysical data

**Wipeout zones.** Wipeout on high-frequency echo-sounder profiles is a reflection character frequently interpreted as indicating the presence of shallow gas (Hovland and Judd 1988). It is also a common characteristic of mud mounds and mud volcanoes (e.g., Neurauter and Bryant 1990). This characteristic is frequently used to define shallow seeps. The term wipeout actually encompasses two slightly different acoustic reflection characters. With true wipeout, subsurface

reflectors disappear laterally, leaving an apparent "void" (Behrens 1988). Acoustic turbidity, which is a prolonged bottom echo owing to scattering and reverberation, is often accompanied by the loss of subbottom reflectors, so it is sometimes called wipeout (Behrens 1988). Both may be caused by free gas because the reflection character of gas depends on the bubble concentration and size (Anderson and Bryant 1990). However, acoustic turbidity may also be caused by scattering resulting from introduced matter, such as carbonate nodules and shell fragments (Sager *et al.* 1999).

Comparison of wipeout zones in the GB and GC Shallow sites with the side-scan sonar mosaics shows that there is a correlation between wipeout and high backscatter. This is to be expected as both are a result of seepage. The cause of the correlation is likely a link between the cause of the high backscatter and gas. The cores suggest that carbonate precipitates are common in the high backscatter zones and form due to bacterial utilization of the hydrocarbons.

Examined in detail, the wipeout zones are slightly more extensive than the sonar bright areas (Figures 6.12, 6.21). This is likely caused by the fact that high frequency echo-sounders penetrate through tens of meters of sediment, and wipeout may occur within that zone, whereas sonar backscatter is dependent on the properties of surficial sediments. Calculations indicate that most of the returned sonar energy at 12 kHz comes from the upper 1 to 2 m of sediment (Liu 1997).
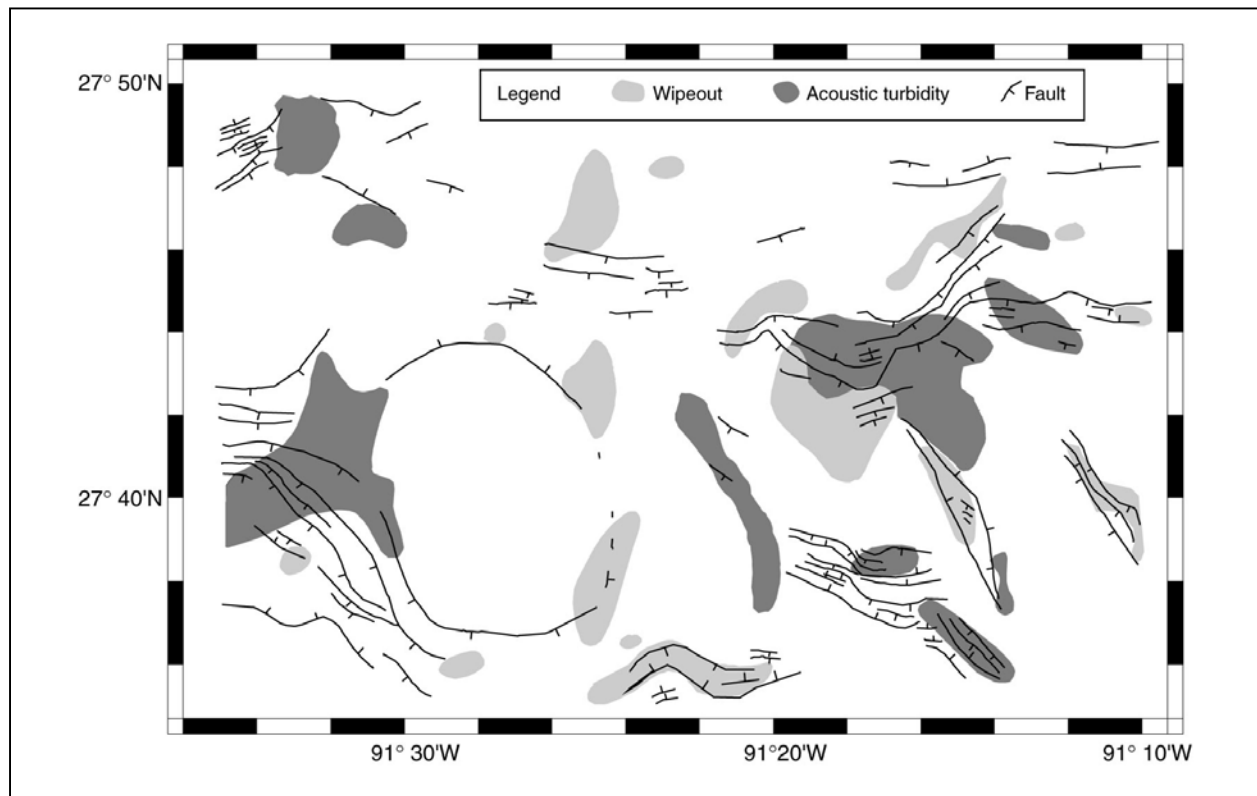


Figure 6.21.   Zones of acoustic wipeout and turbidity in GC Shallow survey area.  Interpretation made from 3.5 kHz echo-sounder profiles collected on cruise 97G4 of the R/V *Gyre*.

Another difference is the amount of detail in the two types of records. Side-scan sonar mosaics show far more detail in surface features than do the wipeout maps (Figures 6.12, 6.21). In part, this is a result of the difference in resolution, which is determined by the way the data are collected. Wipeout is interpreted from single profiles, so the lateral resolution is defined by the ship track spacing. In contrast, the side-scan sonar insonifies all of the seafloor and the resolution is dependent on the pixel size and the footprint of the sonar (Blondel and Murton 1997). For the GC Shallow and GB site mosaics, the pixel size is 4 m, and variations in seafloor backscatter are recognizable at a resolution of about 2 pixels. Closely spaced reflection profiles might be able to attain similar resolution, as is suggested by modern high-resolution 3D geohazard surveys, but at substantially greater cost. The side-scan sonar also achieves greater detail by its dynamic range. Wipeout is typically interpreted as present or not, whereas the side-scan sonar can distinguish differences in backscatter amplitude, which add detail to the image for interpretation.

High frequency echo-sounder data do have one distinct advantage over side-scan sonar data in defining seeps. Topography and faults are more easily recognizable in the profiler records. The topography affects side-scan sonar images but not to the extent of seafloor texture differences. On profiler records, topography is simply the undulation in the level of the seafloor return. Faults show up on echo-sounder records as offsets in the layering and sometimes the seafloor, if the fault is active. On the side-scan sonar images, faults are not evident unless they cause significant topography that gives rise to a strong return off a scarp face or a shadow or if there is disturbance of the physical properties of the sediments at the fault trace. In the GC Shallow and GB site mosaics, many faults were visible. Faults that were not visible do not break the seafloor or display significant seepage.

The best interpretation can be made with a combination of side-scan sonar and echo-sounder records, one to show seafloor property variations and the other to show topography and faults. This combination was used to make the detailed interpretations shown in Figures 6.10, 6.12, and 6.19.

**Surface amplitudes from 3D multi-channel seismic (MCS) data.** The energy industry and support companies have spent considerable time and energy devising ways to use multi-channel 3D seismic data to highlight small differences in sediment geometries and physical properties. With modern seismic workstations, it is often possible to look at numerous signal attributes to enhance variations in properties. One readily available attribute is the amplitude of the reflected signal at the seafloor. Obviously, this will correlate with the reflection coefficient of the seafloor interface, which depends on the change in seismic velocity and elastic parameters (i.e., stiffness). Because seeps affect those properties, they should be evident in maps of reflection amplitude rendered at the seafloor. This has been suggested as a method of finding seeps and the chemosynthetic communities that inhabit them (Roberts 1996; Roberts *et al.* 1996; Reilly 1996). Specifically, these authors suggest that chemosynthetic community sites are characterized by a negative reflection coefficient (and consequent phase reversal of the seafloor reflector) owing to the presence of near surface gas.

In this study, the author visited William Shedd at the Minerals Management Service to view the results of his study of the correlation of chemosynthetic sites with multi-channel seismic amplitude anomalies at dozens of Gulf of Mexico sites. In addition, amplitude anomalies were compared with the locations of several known chemosynthetic organism sites in the GB and GC

Shallow survey areas (GB mud volcano, GC185, GC233, GC234, TAMU-17, and TAMU-6). The conclusion is that the situation is more complicated than just simply finding a circular anomaly with the right coefficient.

At the very first, it is necessary to note differences in data. Not all multi-channel data are created equal. Standard exploration multi-channel data were collected with long streamers and low frequencies and are optimized for deep penetration. This limits resolution near the seafloor. Indeed, with many exploration data, the seafloor return can be difficult to recognize, especially where topographic features intervene. Reprocessed multi-channel data are better (Roberts 1996). These are derived from signals from only a small part of the seismic streamer and have been filtered to raise the frequency content. Better still are high resolution, short-offset 3D multi-channel data optimized for near seafloor imaging (Corthay 1997; Sonnier and Gerlach 1999; Campbell 1999).

Examination of the many study areas in Shedd's study indicate that in some areas, chemosynthetic organism-inhabited seeps are visible as subcircular amplitude anomalies that probably reflect a mud volcano. However, in many places there are widespread surface amplitude anomalies making it difficult to determine where the inhabited seeps occur. In the data from the GB and GC Shallow sites, there was much variation in amplitude signature. None of the known chemosynthetic organism sites clearly showed a phase reversal at the seafloor; however, this may have been partly a result of the limited resolution of the exploration 3D multi-channel seismic data at our disposal. GC185 shows a subcircular, negative amplitude anomaly that corresponds to the well-known mud mound (Figure 6.22). With better data, this mound may show a phase reversal. The GB mud volcano shows little amplitude anomaly at the seafloor (Figure 6.23), despite the fact that it is an active mud volcano. Small features in the amplitude image may or may not reflect actual differences owing to the limited resolution of the 3D seismic data. Interestingly, the GB mud volcano has a large reflection contrast in the upper few tens of milliseconds below the seafloor, as evidenced by strong seabottom multiples (Figure 6.24). However, this is not evident at the seafloor itself as seen in Figure 6.23.

In GC233 and GC234 there are three chemosynthetic sites – TAMU-17, GC233, and GC234. Surface amplitude anomalies are highly variable and show features such as flows and bright spots around the TAMU-10 mound on which only a few chemosynthetic organisms were found. The TAMU-17 site shows up as a strong, bright spot, but GC233 and GC234 do not stand out (Figure 6.25). In addition, we also compared a low-resolution surface amplitude anomaly map of GC272 with the side-scan sonar map and published figures (Roberts 1996). This is a complicated area with many sonar bright features, many amplitude anomalies, and several known mud volcanoes (Roberts 1996). Owing to the complexity and number of anomalies, it appears difficult to sort out which anomalies result from active seeps that might be inhabited.
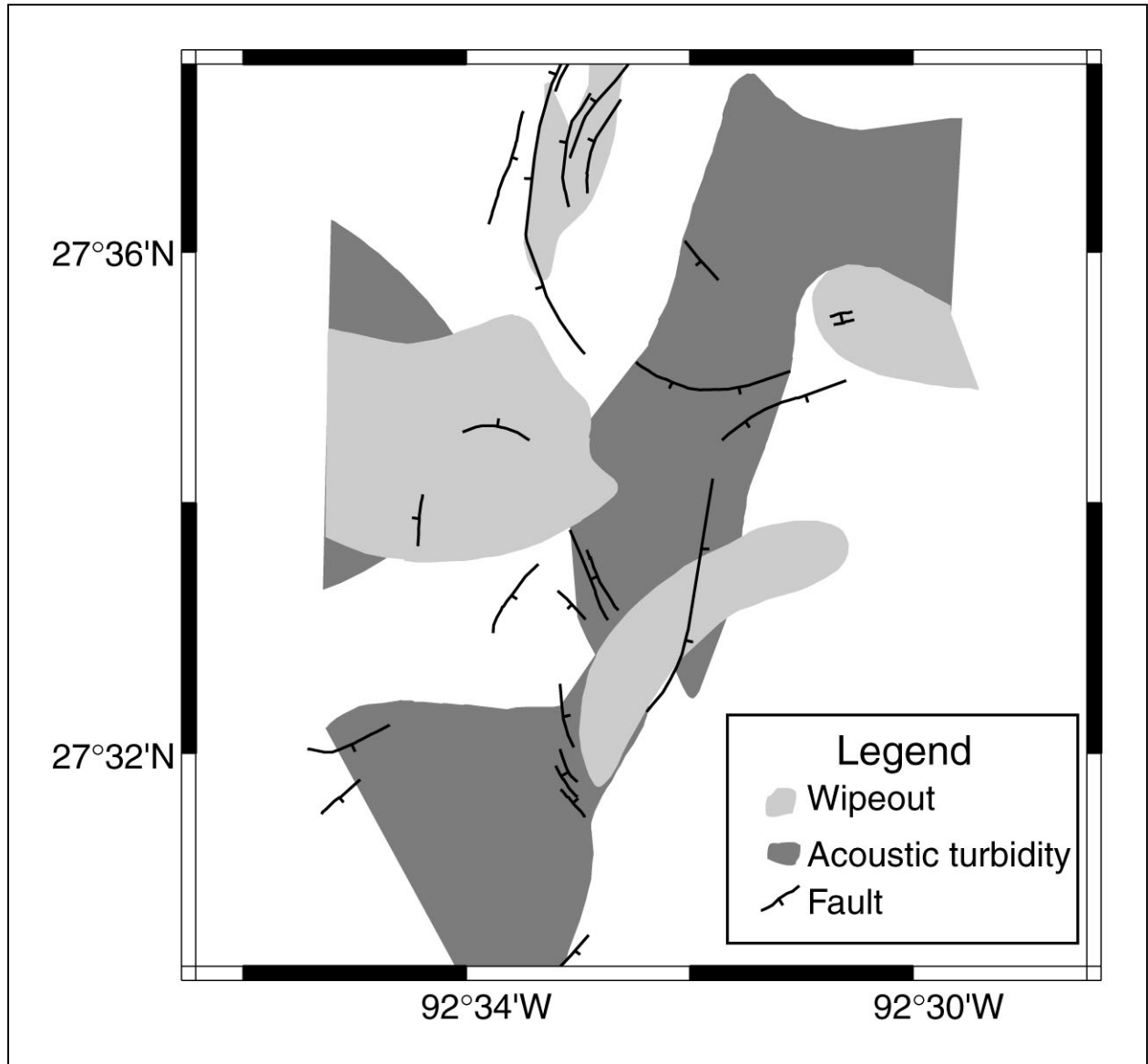
Figure 6.22.   Zones of acoustic wipeout and turbidity in GB survey area.  Interpretation made from 3.5 kHz echo-sounder profiles collected on cruses 97G4 and 92G14 of the R/V *Gyr*e.

## 6.5 Discussion

### 6.5.1 Geophysical signature of seeps

Probably the most significant result from this study relative to the geophysical characterization of seeps is an increased awareness of their complexity in geophysical data. The near-bottom NR-1 profile data reiterate prior interpretations that the lateral variability of seep effects is high at
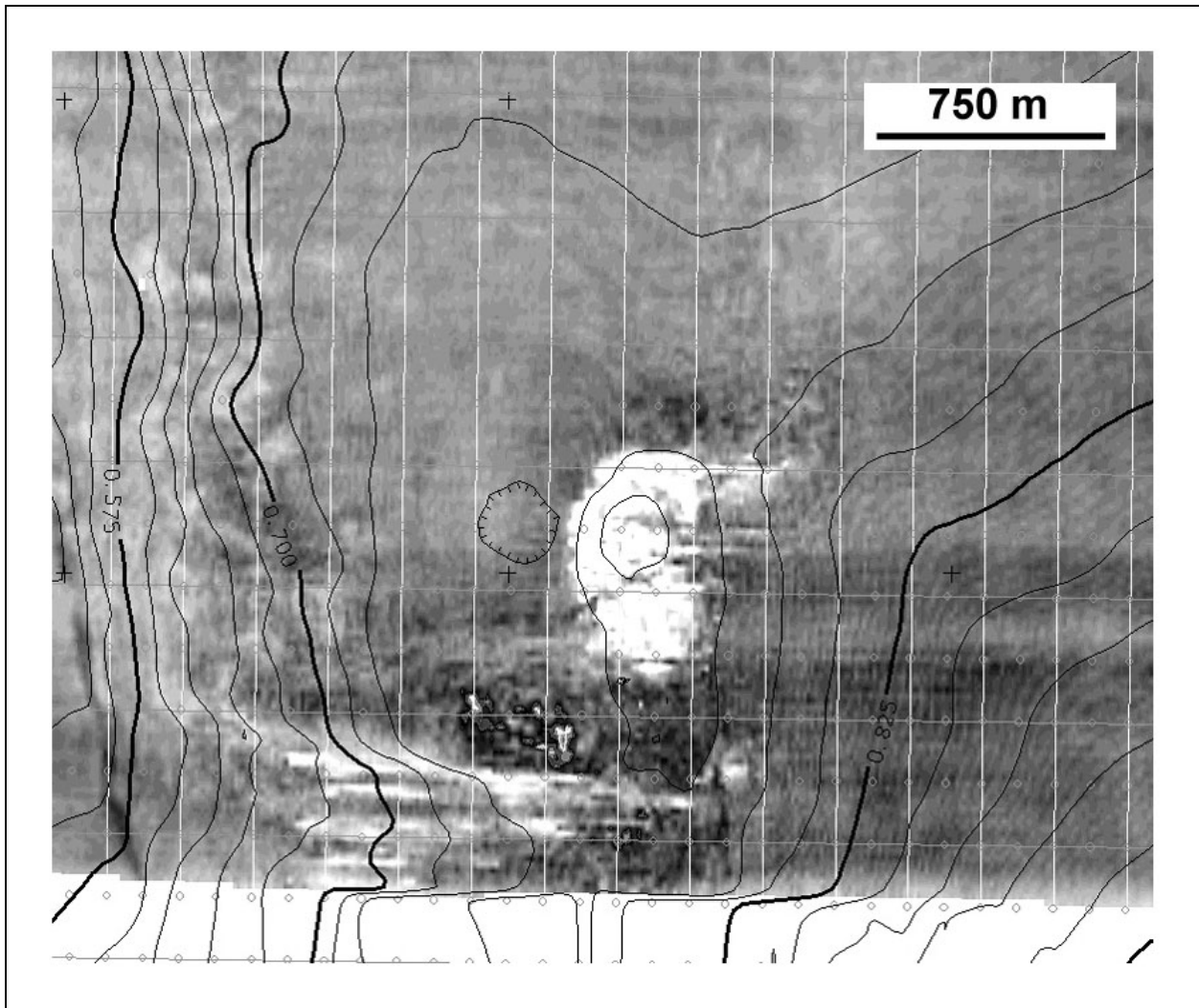
Figure 6.23.  Seismic amplitude rendered on the seafloor from 3D multi-channel seismic data over Bush Hill.  Dark shades are high amplitude, whereas low amplitudes are light.  Bush Hill is at center and displays a low amplitude anomaly coincident with the mound.  Depth contours in two-way travel time are shown at 25 millisecond intervals (18.8 m).

seeps and chemosynthetic organism sites (e.g., Sager *et al.* 1999). Often only meters to centimeters separate areas with little or no alteration from areas replete with carbonate rock outcrops, gas hydrate mounds, gas and oil vents, and chemosynthetic organisms. When one attempts to characterize such spatial heterogeneity with an acoustical technique from afar, particularly from the sea surface, the resultant signature depends in large part on the type of technique and its resolution. Even long range side-scan sonar data and 3D multi-channel seismic data, with resolutions of several (side-scan) to several tens (3D) of meters, tend to give a blended, average signature that belies the true complexity shown by near-bottom data.

Despite the uncertainties, we can nevertheless make some general statements. One thing that is abundantly clear from our study is the tight link between faults, seeps, and chemosynthetic
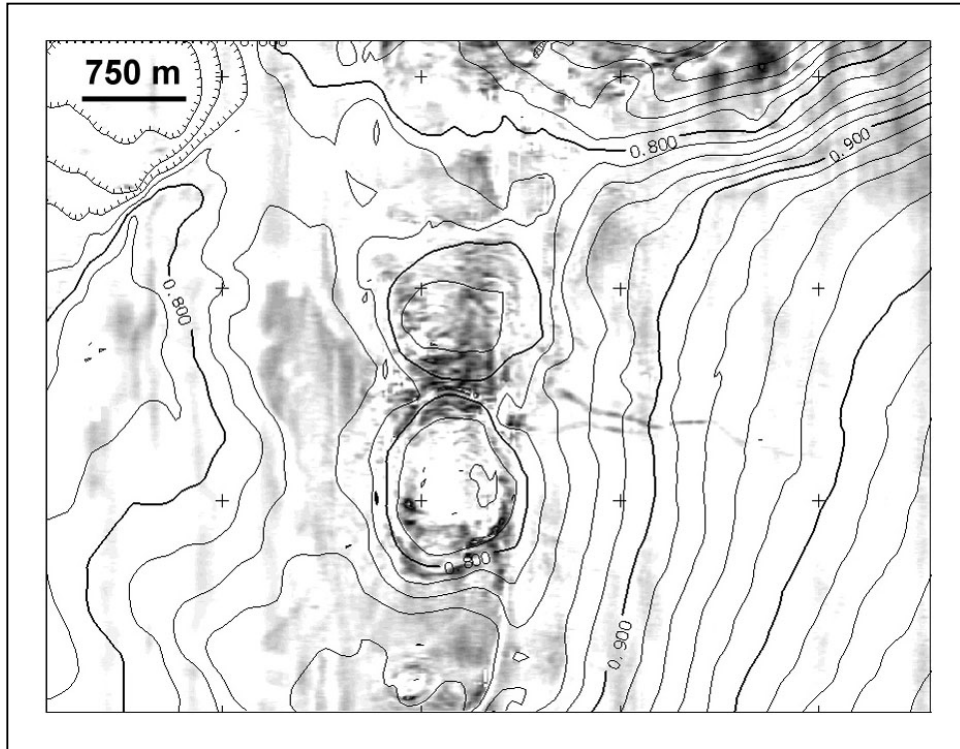
Figure 6.24.  Seismic amplitude rendered on the seafloor from 3D multi-channel seismic data over the Garden Banks 425 mound.  Dark shades are high amplitude reflections from the seafloor, whereas low amplitudes are light.  High amplitude returns are seen over the flanks of the flat-topped mud volcano.  A sediment flow, trending downslope to the east, also displays high amplitude returns.  Depth contours in two-way travel time are shown at 20 millisecond intervals (15 m).
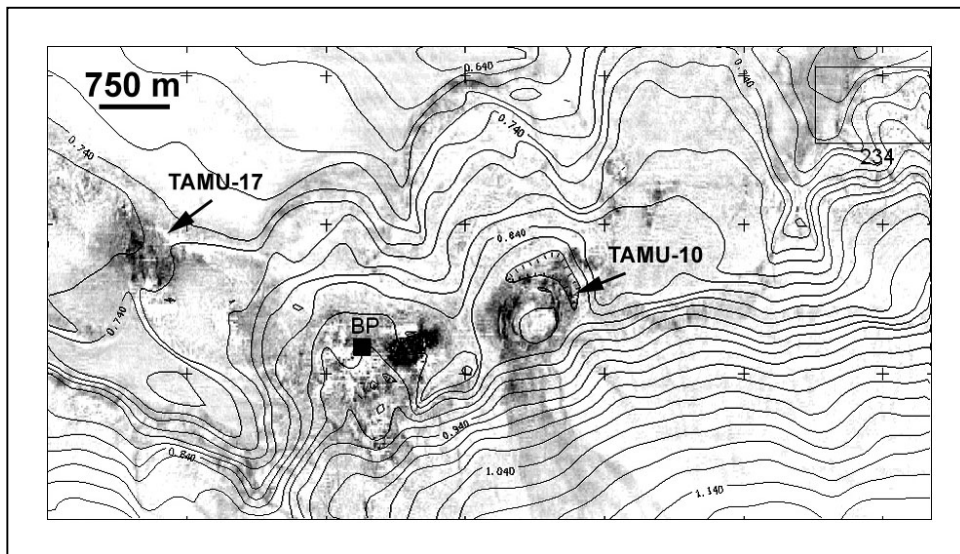


Figure 6.25.  Seismic amplitude rendered on the seafloor from 3D multi-channel seismic data over Green Canyon lease blocks 233 and 234.  Dark shades are high amplitude reflections from the seafloor, whereas low amplitudes are light.  High amplitude anomalies are seen in a ring around the TAMU-10 mound and in elliptical patches over two low mounds to the west, including the TAMU-17 site.  Neither the Brine Pool NR-1 (BP) or GC234 (234) sites stand out in this amplitude anomaly map.  Depth contours in two-way travel time are shown at 20 millisecond intervals (15 m).

organism sites. We have no example of a significant chemosynthetic community site that is not on a significant, active fault. Indeed, all of the large chemosynthetic sites that we have studied are on large regional faults or regional fault complexes (a series of related, nested faults). Along these faults the intrusion of gas and oil into the shallow sediment column changes the acoustic reflection properties in ways that can be exploited by acoustic remote sensing.

Seeps appear to be associated with the classic high-frequency echo-sounder wipeout signature, which is thought to result from attenuation and reverberation owing to free gas bubbles (Behrens 1988; Hovland and Judd 1988). This is true of the GB425, GC185, Bush Lite, TAMU-17, GC234, and TAMU-6 chemosynthetic sites. From the sea surface, most of these sites are characterized by large columnar wipeout zones that lie beneath the seep mounds. In near-bottom profiler records, the wipeout zones are patchier, reflecting the greater resolution of having the acoustic sensor near the seafloor. The same may also be true of the GC233 site, but this site is more difficult to interpret from sea surface records because it is small and lost in a geologically complex zone. From near the seafloor, the brine pool mound only shows a slight wipeout directly beneath the crater lake. This may be a result of the main gas reservoir being deeper than the penetration of the chirp sonar.

In side-scan sonar data, seep related faults show high acoustic backscatter. Cores from the affected areas do not always show the same geologic characteristics, but are typically altered from normal hemipelagic property in a number of ways (Table 6.2). Changes include overconsolidation (stiff clays), formation of hard layers, formation of authigenic carbonate nodules, gas and oil charging, and the introduction of chemosynthetic biogenic debris. Another potential disturbance is the formation of gas hydrate, but because any hydrate in our cores would have dissociated before reaching the surface or shortly thereafter, we have not been able to document it. With the exception of free gas bubbles, all of these disturbances should increase the amount of acoustic reflection, primarily as a result of scattering. We note that many of the cores exhibited carbonate nodules or layers, suggesting that much of the acoustic scattering in seep affected areas may result from authigenic carbonate material. Strong reflections might be caused, in particular, by carbonate crusts and gas hydrate bodies.

A feature of special importance to seep geology is the subcircular mud mound. In older surveys, with widely spaced high-frequency echo-sounder profiles, these were found primarily when a mound was crossed by a ship track (e.g., Neurauter and Bryant 1990). Increasingly, with swath bathymetry, side-scan sonars, and 3D multi-channel data, this is no longer necessary. Many such mounds appear to be mud volcanoes formed at high flux seep vents. Often they rise several tens of meters above the surrounding seafloor and have widths from hundreds of meters to kilometers. In side-scan sonar data they appear as subcircular sonar-bright zones, sometimes with high-backscatter features indicative of sediment flows emanating from their centers. In multi-channel 3D seismic data, mud mounds often show anomalous reflection properties at the seafloor. Typically, they have strong reflections, often with a positive reflection coefficient (Roberts 1996), but sometimes with a negative coefficient indicative of gas (Reilly 1995).

In the side-scan sonar mosaics, we imaged many subcircular, sonar-bright patches in the GB and GC Shallow areas. In general, there were three different signatures: (1) uniformly high-backscatter (Figure 6.26), (2) a high-backscatter center with a halo of lesser backscatter intensity ("bulls eye," Figure 6.26), and (3) high-backscatter with a central spot having little or no

backscatter ("dead eye," Figure 6.27). Some of the uniformly high backscatter patches were mud mounds, although none that we visited with submarine NR-1 was obviously active. A few subcircular sonar-bright patches were merely areas of the seafloor that appear to have had moderate seepage sometime in the past, but not enough to build a mound or support chemosynthetic communities. At several bulls eye sites, the near-bottom chirp sonar records from submarine NR-1 imply that the central high-reflectivity zones are hard-bottoms, which we interpret as either carbonate or gas hydrate layers. The surrounding haloes seem to be wipeout areas (either attenuation or turbidity) caused by lesser seep-related disturbances to the sediments
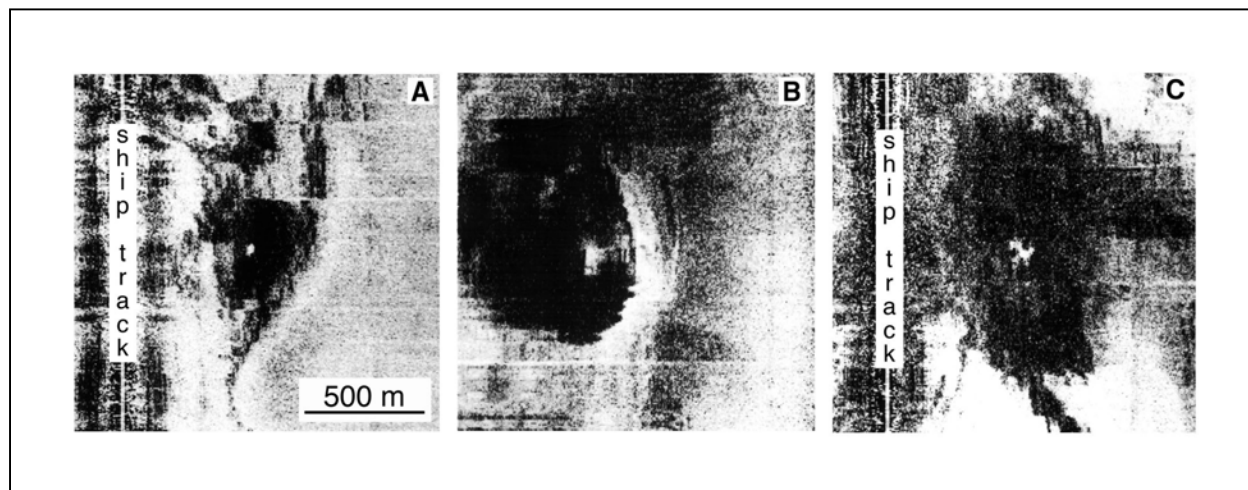


Figure 6.26.    Side-scan sonar image of different mound backscatter characteristics.  This record shows several subcircular high backscatter patches, a large bulls eye mound, and another mound that has a dead spot (which shows better on another overlapping swath).  The dead eye mound is the TAMU-6 site where chemosynthetic organisms were found.  This record is from Green Canyon lease block 191.

and introduction of gas. Interestingly, none of the bulls eye mounds visited with submarine NR-1 appeared to have significant chemosynthetic communities or evidence for high-flux seepage. We speculate that these mounds may be older and have become inactive or sites for only limited seepage, perhaps because of plugging of the vents by carbonate or hydrate formation. Dead eye mounds in all cases were the site of active brine discharge or brine pools (GB425 mud volcano, Bush Lite, TAMU-17, and TAMU-6). We think the dead eye feature may result either from the specular reflection of sonar signals away from the sonar off a brine pool interface (recall that the sonar "sees" objects by backscatter) or from the near total absorption of sonar signals by extremely gassy, fluid-sediment slurries in these brine vents.

An interesting aspect of our examination of seep mounds is the recognition that many of the mounds appear presently inactive when visited by submarine NR-1. This is important because it suggests that there are limits to our ability to infer active seep sites from sea surface exploration geophysics alone. That active and inactive mounds would appear much alike in side-scan sonar, high-frequency echo-sounder, and multi-channel 3D data is reasonable because all of these techniques respond to the physical properties of the upper several meters or more. Thus a

recently active, but now dormant mound may appear geophysically very similar to an active mound. This implies that other evidence is necessary to decide whether a particular mud mound is inhabited by chemosynthetic organisms.
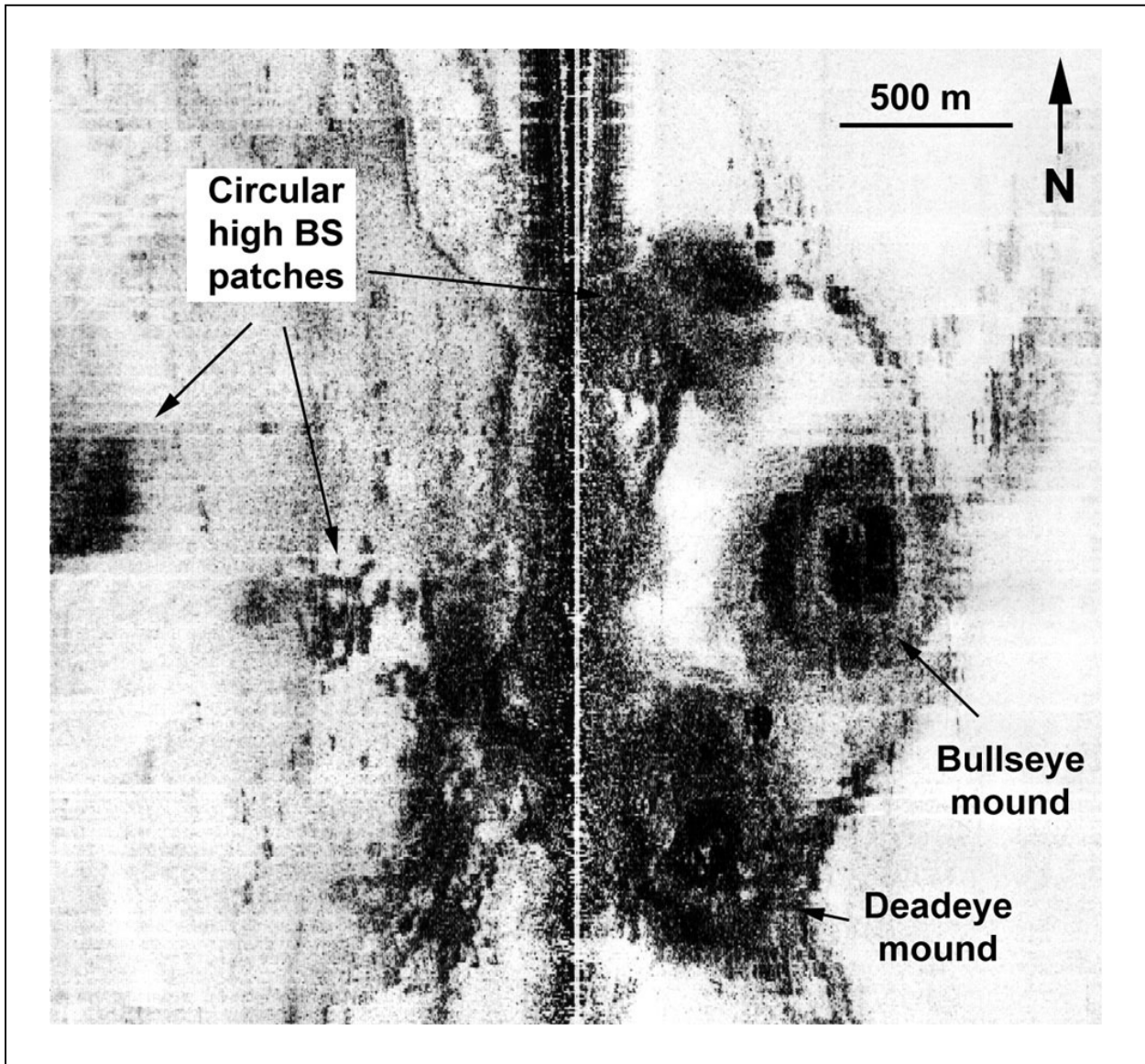


Figure 6.27    Dead eye mounds.  Partial side-scan sonar swaths are shown with three dead eye mounds in different parts of the study areas.  (A) Bush Lite mound, Green Canyon lease block 184; (B) GB425 mound, Garden Banks lease block 425; (C) TAMU-17 mound, Green Canyon lease block 233.

Another important finding from this study is the realization that the geophysical signatures of the upper and lower slopes are so different. On the upper slope, disturbances to the seafloor sediments are largely a result of seepage, so seep affected regions stand out. In contrast, on the lower slope, seep affected regions are almost lost in a complex tapestry of disturbances that mainly result from mass wasting owing to salt tectonics around intra-salt basins and salt massifs. These severely limit the effectiveness of side-scan sonars to image seeps on the lower slope. In

addition, high-frequency echo-sounders are almost useless in the same areas owing to the poor resolution caused by the large separation of source and reflector (and consequent beam spreading). In addition, the geologic complexity also adds to the problem by the reflection of sound off rough topography. Although we had no lower slope 3D multi-channel data to examine in our lower slope study region, we suspect that such data also are inadequate to the task of finding seeps in similar terrains. One reason is the same spreading of sound waves with long distances from source to receiver. Another is that the same disturbances to surficial sediments that show up on side-scan sonar records will also cause reflection anomalies. In sum, the usual geophysical methods that have worked well on the upper slope may be limited in their ability to detect seeps on the lower slope.

## 6.5.2 Geologic controls on chemosynthetic communities

The present study has not greatly changed our picture of the geologic factors that constrain chemosynthetic community locations. This is not unexpected given that many of the sites studied here are those examined by prior workers (Reilly *et al.* 1996). If anything, this study has cemented the link between complex chemosynthetic sites and faults, which is especially evident in the geophysical data from the shallow sites (e.g., Figures 6.10, 6.12). In the GB and GC Shallow study sites, the known, large chemosynthetic communities are found along regional faults. What is less clear is whether all of these sites occur on antithetic faults because we did not have the data to map the faults in detail or at depth. Furthermore, we recognize that it is very difficult to delineate faults in complex structural terrains, especially when the acoustic perturbations caused by seepage interfere. Defining faults near the sea floor with exploration 3D multi-channel data is difficult owing to the low resolution. High-resolution high-frequency data is often limited in its subsurface penetration and by acoustic wipeout. As a result, we still cannot make detailed maps of faults in the shallow subsurface and this limits our ability to understand how faults control seepage.

One thing made clear by the chirp sonar data collected near the seafloor by submarine NR-1 is the high lateral variability of seep effects along the fault zones that were investigated. The high variability implies that small-scale structure is important in determining the location, intensity, and duration of seepage. While large-scale faults likely determine where seeps occur in the broad sense, the small scale structure of seep sites is likely controlled by near surface faulting and modification of the conduits by seep products, such as gas hydrate and authigenic carbonate. In several locations in our study area, it appears that large faults are modified near the seafloor by breakage of the near-surface sediments into small blocks by slope instabilities (Reilly *et al.* 1996). The result is that the distribution of seeps is controlled in part by the system of near-surface faults that develop.

The side-scan sonar data from the GC Deep survey area suggest a somewhat different picture than do the shallow data. In the deep area we have been hampered in understanding seep occurrence by having few ground truth data and by the fact that high-resolution is difficult to achieve using geophysical data collected at the sea surface. Nevertheless, the structural style of the GC Deep survey area is very different because much of the surface is disturbed by sediment mass wasting owing to slope failure caused by salt uplift and because many of the faults are directly related to the boundaries between salt massifs and salt-withdrawal basins. Others have suggested that most seepage occurs along faults ringing the basins (Sassen *et al.* 1999) and this

seems to fit our data. Current data sets available to us are inadequate for comparison of these faults to the shallower structures and test models such as that proposed by Reilly *et al.* (1996). Furthermore, because energy companies have only recently begun exploration of the deep slope, few studies have been done about seeps in this environment. This is clearly an area needing future research.

**6.5.3 Searching for chemosynthetic community sites**

One of the primary motivations for this study was to consider how geophysical remote sensing methods may be used to find chemosynthetic community sites. The good news is that geophysical methods can identify a small fraction of the seafloor that might be inhabited by chemosynthetic organisms by finding evidence of seep-related disturbances to surficial sediments. The bad news is that seeps are geologically complex and have high lateral variability, so there is no geophysical method that unequivocally and reliably identifies the inhabited seep sites.

It is useful to compare our data and knowledge to the chemosynthetic community site identification protocol proposed by Reilly (1995, Figure 6.1). The present study cannot provide a definitive test of Reilly's approach because the number of sites that were studied is small. Nevertheless, our data suggest certain shortcomings.

The topmost level of Reilly's search is to look at the sea surface for an oil slick using high-altitude or space-platform aerial photography, radar imagery, or a similar method (e.g., MacDonald *et al.* 1993; 1996). The slick map published by MacDonald (1996) shows slicks that emanate from the area of GC185, TAMU-17, and GC234. In addition, slicks have been detected over the GB site (MacDonald *et al.*, in press). While this is encouraging, it is difficult to trace a given slick to a particular chemosynthetic community site because the slicks are large, the chemosynthetic community sites small, and there is likely some drift of the slick as the hydrocarbons ascend through the water column. Furthermore, as noted by MacDonald *et al.* (1996), the correspondence of slicks with chemosynthetic community sites is good, but not universal. This may occur because the flux of hydrocarbons at the seafloor is variable. MacDonald *et al.* (1996) suggest that the most robust slicks are those that emanate from high flux vents, such as mud volcanoes. Additionally, the flux may change with time owing to changes to the hydrocarbon supply to the vent. At the GB site, which has shown active venting on several visits by submersible, it was noted that a prominent slick is sometimes present, but at other times is absent (MacDonald *et al.*, in press). In short, it appears that the absence of a slick does not mean the absence of a chemosynthetic community, but the presence of a slick greatly increases the chance that such a community exists on the seafloor somewhere in the vicinity of the upwind end of the slick.

Wipeout zones constitute the second level indicator in Reilly's protocol. He specifically mentions this signature on high-frequency echo-sounder profiles, such as 3.5 kHz sonars, but wipeout may also occur on records at other frequencies. In addition, Reilly does not distinguish between the two different types of wipeout signature, attenuated signal and turbidity. Since we have no example of a Gulf of Mexico chemosynthetic community site that does not display wipeout in its environs, this appears to be a reliable indicator. However, it was observed that wipeout zones are typically much more extensive in area than the chemosynthetic sites (for

example, Figs. 6.21, 6.22). Thus, it is usually not possible to use the wipeout signature to define the exact location of a chemosynthetic community site.

Reilly (1995) contends that chemosynthetic community sites are indicated by negative amplitude anomalies at the seafloor in multi-channel seismic data. The negative anomalies are recognized by a phase reversal at the seafloor and are a result of low acoustic velocities in the surficial sediments owing to gas. Furthermore, he contends that amplitude anomalies characterized by a positive reflection coefficient (i.e., no phase reversal) are indicative of hard bottoms and are unlikely to be the sites of significant chemosynthetic communities. Although the present study has only a limited amount of multi-channel data over a small number of sites for comparison, it appears that this indicator is unreliable. A phase reversal is not evident at the seafloor at known chemosynthetic organism sites GB, GC, GC185, and TAMU-17. Part of the problem may be that the data we examined is exploration 3D multi-channel data in which the long acoustic streamers used make for a poor geometry to define the seafloor. As a result, it is often difficult to see a phase reversal over a small patch of seafloor. High-resolution data collected for seafloor geohazards studies might work better. However, given the results of our limited analysis, it appears that the reflection coefficient is not diagnostic.

The occurrence of $C_2$-$C_5$ hydrocarbons in piston cores is suggested by Reilly (1995) to be another indicator of lush chemosynthetic community sites using the logic that if a higher-molecular weight hydrocarbon signature is present, it is likely that the full range of chemosynthetic organisms are also present. We could not do an adequate test of this hypothesis in the present study because only a small number of the cores were analyzed for geochemistry. Oil or oil stains were found in cores GC1-1, GC2-1, GC3-1, GC4-1, GC7-2, GC8-1, GC9-2, GC16-1, RN8-001 and RN8-002. Of these, cores GC1-1, GC2-1, and GC8-1 were obtained from sites where no significant occurrence of chemosynthetic organisms was noted during the 1998 NR-1 dives. Cores GC3-1 and GC4-1 were recovered from sites where only small, limited chemosynthetic sites were found (TAMU-7 and TAMU-10, respectively). Although it is possible that significant concentrations of chemosynthetic organisms exist at these locales, but were missed by the NR-1, the indication is that higher-molecular weight hydrocarbon occurrence in the surficial sediments is more widespread than the occurrence of lush chemosynthetic communities. Chemosynthetic communities seem to require sustenance by sustained, robust seeps, but it is probable that heavier hydrocarbons appear in locations along lower flux seeps where the hydrocarbon availability is insufficient to support a lush community. Thus, the appearance of higher molecular-weight hydrocarbons in a piston core is a necessary, but not sufficient, indicator of chemosynthetic community occurrence.

Reilly (1995; 1996) recognized the importance of faults in controlling the location of seeps and chemosynthetic community sites. Implied in his protocol is the assumption that all chemosynthetic sites occur on faults. He went one step farther, distinguishing two types of fault: (1) a regional fault, typically connecting uplifted salt masses, and (2) a local, salt dome fault, usually directly above a rising salt diapir. According to Reilly (1995; 1996), only the regional faults are sufficiently active to produce the continuity of seepage needed to support lush chemosynthetic communities. In contrast, he proposed that salt dome flank faults leak hydrocarbons intermittently and are too intermittent for the development of large, multi-species chemosynthetic communities. Our data are not inconsistent with this view. GC185 and Bush Lite are on an antithetic fault rooted in a regional growth fault connecting diapirs (e.g., Cook and

D'Onfro 1991). Several chemosynthetic communities occur in GC232 to GC236 (TAMU-17, GC233, TAMU-10, GC234, TAMU-7, and TAMU-6) along a set of regional faults that occur around the rim of an intra-salt basin and which connect the crests of buried salt bodies (Figure 6.17; e.g., Behrens 1988). In addition, the seep site on the mud volcano at the boundary of GB424 and GB425 also occurs on a major regional growth fault. While this dichotomy seems to apply to the limited data set in this study, caution is probably in order for a broader application. In many cases, local salt dome flank faults may connect with or grade into larger regional faults, making a distinction between the two problematic. Furthermore, there are few examples of seeps on salt dome flanks, so a generalization may be premature.

The final step in Reilly's (1995) chemosynthetic community search protocol is confirmation of inhabitation by sea bottom photography or submersible observations. Given the complexities of seeps and the patchiness of chemosynthetic communities, direct observation is probably the only method of absolute confirmation.

Reilly's approach to locating chemosynthetic community sites was to make a cascading flow chart of increasingly detailed observations (Figure 6.1). Virtually all of these observations are cogent, but the representation as a decision tree, in which certain observations lead to a rejection of a given location as a potential site, has some suspect elements and should be used with caution. Because of the uncertainties in our knowledge of chemosynthetic community sites, deciding whether a site is likely to be inhabited should be a process of gathering evidence either for or against (Table 6.3). Unless data exists that directly confirms habitation, such as bottom photographs of chemosynthetic organisms, submersible observations of the same, or cores or trawls containing chemosynthetic organisms, one must consider the preponderance of geologic and geophysical evidence and decide whether there are sufficient indicators that are consistent with the presence of chemosynthetic organisms. Mostly these are indicators of a robust seep.

For many purposes, it may be sufficient to define seep-affected areas along surficial faults as potential chemosynthetic community sites to be avoided in offshore production operations. In the GC Shallow area, these areas cover about 11% of the total seafloor, although some lease blocks are covered 50% or more (e.g., GC139, GC140, GC232-GC235, GC272, GC320-GC321, and GC363-GC364). Definition of seep-affected area might be approached with 3.5 kHz data by looking for wipeout signatures, with side-scan sonar images by looking for high backscatter areas, or with multi-channel 3D seismic data by looking for anomalous reflection at the seafloor or shallow subsurface. If an area apparently affected by seepage is deemed important enough for operations, more detailed investigations, including high-resolution geophysics, coring, ROV photography, or submersible observations can be made.

### 6.5.4 Directions for future research

Knowledge about the geologic controls of chemosynthetic communities still has several significant gaps. Most research to date has focused on a small number of sites, so conclusions about chemosynthetic community occurrences, even on the upper slope, is limited by the generality of those sites. We had hoped that the submarine NR-1 dives on many targets in the shallow seep study areas would illuminate the distribution of chemosynthetic sites, but bad luck dictated that only a small number of sites was visited. Increasing the number of seep sites investigated should be a high priority. This should include investigations into the number within

Table 6.3. Chemosynthetic community site indicators.

| Indicator | Data type | Likelihood |
|---|---|---|
| Deep rooted fault | Multi-channel 2D or 3D seismic data | M |
| Acoustic wipeout | High frequency echo-sounder profiles | M |
| Strong amplitude anomaly | Multi-channel 2D or 3D seismic data | M |
| Mound along fault | Swath bathymetry; 3D multi-channel seismics, geohazard survey | M |
| Confluence of regional faults | Multi-channel 2D or 3D seismic data | H |
| Sea surface oil slick | Aerial photography; space photography; synthetic-aperature radar | H |
| Gas stream in water column | High frequency echo-sounder profiles | H |
| High backscatter along fault | Side-scan sonar | H |
| Chimney-shaped acoustic wipeout | Multi-channel 2D or 3D seismic data | H |
| Strong amplitude anomaly along fault coincident with mound | Multi-channel 2D or 3D seismic data | H |
| High backscatter along fault coincident with mound | Side-scan sonar | VH |
| Strong amplitude anomaly along fault, negative reflection coefficient, coincident with mound | Multi-channel 2D or 3D seismic data | VH |
| Presence of small mounds | Near bottom high frequency echo-sounder profiles | VH |
| Presence of small mounds | Near bottom side-scan sonar swaths | VH |
| Oil, gas | Cores | VH |
| Chemosynthetic shell debris | Cores | C |
| Images of chemosynthetic organisms | ROV video, camera sled, submersible | C |

*Likelihood of chemosynthetic community code: M = moderate, H = high, VH = very high, C = confirmed

a given area, so that we have better knowledge about the density of sites. It should also include an effort to obtain a broader picture of chemosynthetic sites in different structural settings. To date, most investigations have been on the Louisiana upper slope. The morphology of the lower slope is different from the upper slope, suggesting that controls on seeps may be different. In addition, the style of faulting changes from west to east across the continental slope and this may change the controls on seep occurrence. Because a large amount of geophysical data already exists for the Gulf of Mexico, collected by the energy industry, it would be prudent to consider obtaining geophysical data on seeps from a variety of settings and using computer GIS and database technology for assimilation and study.

## 7.0 Spatial and Temporal Patterns in Seep Communities*

### 7.1 Introduction

Questions about the distribution and persistence of chemosynthetic communities in the northern Gulf of Mexico have to be posed in terms of scale. Over distances that span the Western and Central Lease areas, occurrences of chemosynthetic communities are determined by the presence of hydrocarbon reservoirs. Leasing and production trends demonstrate conclusively that a massive hydrocarbon system extends across virtually the entire continental slope (Figure 2.1). The tendency of this system to produce viable chemosynthetic habitats is confirmed, to the limits of exploration, by direct observation and collection of the fauna (Figure 2.2). Likewise, the prevalence of mineral deposits formed by biologically mediated processes (Roberts and Aharon 1994, Roberts and Aharons 1993, Sassen *et al.* 1989) and the abundant fossil remains of chemosynthetic species (Powell *et al.* 1998) convincingly show the persistence of chemoautotrophic processes in the Gulf of Mexico throughout recent geologic time and probably the entire Pleistocene. Therefore, chemosynthetic fauna supported by hydrocarbon seepage are a broadly distributed and well-established component of the continental slope ecosystem.

However, effective management of this ecological component requires the capacity to predict where and in what configuration individual chemosynthetic communities occur and to detect unusual changes in these communities; this capacity must be scaled to the activities under management, that is energy exploration and production. The various components of this program address different ranges of this scale. Findings concerning the physical oceanography of the shallow mega-site (Chapter 5) document circulation patterns and temperature ranges that typify much of the central slope. Geophysical surveys (Chapter 6) identify seep-affected zones and show the influence of geological features such as salt diapirs and growth faults. The surveys also indicate major differences in seepage style between the shallow and the deep zones — differences that have a largely undetermined effect on community formation. At the other end of the scale, the ecological and geochemical investigations (Chapters 8, 9, and 10) are largely directed toward processes within individual clusters of chemosynthetic species, although site-to-site comparisons certainly apply, particularly in the results from the trophic and the genetic studies.

At an intermediate scale, however, a major management concern remains the so-called lush chemosynthetic community. What constitutes a lush chemosynthetic community? How large an area does it cover? What densities of chemosynthetic species and what sorts of normal variation do such communities experience over a multi-year timeframe? The program study sites were chosen because they typify lush communities. Quantifying the dimensions, densities and faunal composition of these sites provides a baseline against which communities newly discovered can be compared. Mapping the fine-scale limitations posed by seep geology at each site creates a template that can be used to refine the search for lush communities in future surveys. Temporal change is problematic because observations have been sporadic, due to the availability of sampling platforms, and because the time-scales over which observations have been carried out

---

* This section was authored by Ian R. MacDonald.

are relatively short. Case studies of evidence for variability or persistence can nonetheless identify general tendencies or processes that are relevant to management timeframes.

This chapter will marshal evidence for spatial and temporal patterns at the four principal sites. Available data includes surveys conducted during the present program and data gathered during previous efforts and reanalyzed with use of updated techniques. Clearly, having a small number of sampling sites limits the generality of these results. However, the four sites represent two pairs of communities supported by distinct styles of seepage: sediment diffusion versus focused flow and the pooling of hypersaline fluids. The specific objectives of this work are as follows:

1.  To provide a general description of the relative locations of sampling stations within the four sites, along with the overall dimensions and bathymetry of the sites;

2.  To demonstrate the clustered distribution of tubeworms and mussels within the study sites and quantify the spatial coverage of these fauna;

3.  To detail the evidence for geological processes, such as faults, gas hydrate deposits, or fluid flows, that facilitate or limit the ability of chemosynthetic fauna to colonize the sites;

4.  To examine evidence of temporal change within the sites by use of geological interpretation, time-series observations, and satellite remote sensing of oil venting.

## 7.2 Materials and Methods

Datasets and other materials discussed in this chapter are summarized in Table 7.1. All data were compiled as GIS data layers to facilitate comparison over multiples scales or time periods. The individual datasets and analytical methods are described in further detail below.

### 7.2.1 Survey results from submarine NR-1

Submarine NR-1 provides unique capabilities for surveying chemosynthetic communities. NR-1 is nuclear powered and can remain submerged in continuous operation for tens of days. Compared with other scientific submarines, it is a very stable platform from which to deploy optical and acoustic imaging systems. It employs a precise inertial navigation system that tracks its relative position during near-bottom operations. Notably, it continually records operational data such as its position, heading, and altitude above bottom, which makes it possible to reproduce highly accurate tracklines and to mosaic data collected along track into large area images or interpreted maps. NR-1 has been used for several surveys of chemosynthetic communities in the Gulf of Mexico beginning in 1987 and continuing through the cruise made in 1998 under the auspices of the CHEMO II program. Survey methods and capabilities employed with NR-1 have been described in several publications (MacDonald *et al.* 1990b, MacDonald *et al.* 1997, Reilly *et al.* 1996, Sager and MacDonald 1998). In addition, detailed bathymetric maps and side-scan sonar mosaics from study sites GC185, GC234, and GB425 were presented in the previous program, The Chemosynthetic Ecosystem Study (MacDonald *et al.* 1995). Wherever possible, these datasets were re-analyzed and co-referenced, geographically, with newer results to provide continuity and synergy with previous work (Table 7.1).

Table 7.1. Summary of datasets analyzed and discussed in this chapter.
Datasets are organized by study site, with collection details in parentheses.

**GC185**
–   Laser line-scan mosaic and bathymetric data (collected with NR-1, 1994).
–   Time-lapse video sequence of surface gas hydrates
      (recorded Sept. 1995 through Jan. 1996).
–   Ground-truth observations and photo-mosaics
      (collected with SEA-LINK, 1997 and 1998).
–   Piston cores (collected from surface ship June 1998).

**GC234**
–   Side-scan sonar mosaic and bathymetric data
      (collected with NR-1, 1990, revised for present work).
–   X-Star subbottom profiles (collected May 1998).
–   Ground-truth observations and photo-mosaics
       (collected with SEA-LINK, 1997 and 1998).
–   Piston cores from surface ship (collected June 1998)
–   3D seismic survey data (obtained from Western Geophysical, Inc.).

**GC233**
–   CTD profiles of brine pool (collected with SEA-LINK, 1991, 1992, and 1998).
–   Laser line-scan mosaic and bathymetric data (collected with NR-1, 1994).
–   Ground-truth observations and photo-mosaics
       (collected with SEA-LINK, 1997 and 1998).
–   Piston cores from surface ship (collected June 1998).
–   X-Star subbottom profiles (collected May 1998).

**GB425**
–   Laser line scan mosaic and bathymetric data (collected with NR-1, 1994).
–   Ground-truth observations and photo-mosaics
       (collected with SEA-LINK, 1997 and 1998).
–   CTD profiles of brine pool (collected with SEA-LINK, 1997 and 1998)
–   Temperature time-series from brine pool (recorded 1997-1998)
–   Satellite synthetic aperture radar images (collected by RADARSAT, 1997-1998)

## 7.2.2 Laser line-scan mosaics

Laser line-scan system (LLSS) technology uses a solid-state laser and a rotating mirror to illuminate individual scan-lines. By passing the device across the bottom in a track perpendicular to the scan-lines, a LLSS can image a swath of the seafloor up to 30 m wide with centimeter resolution. During a cruise in 1994, Submarine NR-1 was used for collection of contiguous LLSS images that could be assembled into a geo-rectified mosaic covering thousands of square meters of the seafloor. Construction of mosaics requires ER-MAPPER and PV-WAVE computational programs on UNIX workstations and additional image-processing routines on PC workstations. The methods are described in detail by MacDonald *et al.* (1997).

During a research cruise in 1994, data were collected for large-area mosaics of three of the four sampling sites: GC185, GC233, and GB425. The mosaics for these sites were completed prior to the 1997 SEA-LINK cruise. At three of the four study sites, the sketch maps were based on laser line-scan mosaics covering all or most of the site. These mosaics provided detailed information about the location of prominent landmarks and faunal clusters. Mosaics also provided an accurate distance and bearing scale for locating individual sampling stations.

To combine the information in the laser line-scan mosaics with the selection of sampling stations accomplished during the submersible cruise, the following procedure was adopted. First, the mosaics were geo-rectified in the ER-MAPPER software environment. Each image was registered, without warping, to the best available coordinates of some prominent feature within the site, preserving the scale and rotation information calculated when the mosaic was constructed. Latitude and longitude for any point in the mosaic was then available through the software. The video information and notes from the scientists in the submersible's sphere were used to locate each sampling station within the mosaic. Details of the mosaic are adequate for this in most cases. Finally, the geo-rectified images were queried in ER-MAPPER to determine the interpolated coordinates of each sampling station. Comparison of the interpolated coordinates with coordinates obtained by the SEA-LINK acoustic navigation system confirmed that there was general agreement between the two methods.

### 7.2.3 Subbottom profiling

Subbottom profiles and large-scale visual reconnaissance were conducted in May 1998 from submarine NR-1. The profiler was a 2-12 kHz chirp system (Edgetech X-Star), which employed a deep-ocean transducer array hard-mounted on the submarine's box keel. Operation of the instrument and data logging was done from inside the submarine. During subbottom profiling, the submarine was steered at a constant depth along a straight trackline – generally east-west or north-south. Navigation was accomplished with the submarine's inertial positioning system, regularly updated with fixes from a short baseline acoustic tracker operated by the support vessel (DSR CAROLYN CHOUEST). The subbottom profiles were recorded digitally and could be replayed, filtered, and contrast-enhanced during analysis.

### 7.2.4 Geographic co-registering

Extensive information was collected and compiled from the GC234 site during a 1990 cruise with submarine NR-1. Although positions recorded by the inertial navigation system were precise, this cruise pre-dated availability of GPS and acoustic positioning data for NR-1 and her tender. A small but unknown bias, therefore, offset the grid of side-scan, bathymetric, and visual observations made during this cruise. To co-register these data with the grid of observations recorded during the 1998 cruise, the bathymetric data generated by both surveys were fitted to surfaces or digital elevations models (DEM) with a grid size of 1 m. The two surfaces were then iteratively compared until an alignment was found that produced the minimum difference between the two surfaces. The 1990 data were then shifted by the offset required to bring the two surfaces into alignment.

## 7.2.5 Satellite image processing and interpretation

SAR images that were obtained from RADARSAT (a Canadian satellite operator) and were analyzed to monitor oil venting in the vicinity of the GB425 site have the following reference numbers and acquisition dates: COO115630 wide 1 (19 May 1997), 8374-1219180 wide 1 (5 June 1997), MO120437 wide (29 June 1997), M0193062 SN1 (6 Aug. 1997), M0192826 wide 1 (27 Nov. 1997), C0014225 wide 1 (24 Feb. 1998). This is the complete inventory of images that were archived after collection and were collected under weather conditions compliant with visualizing floating oil.

Wind speeds in surface areas examined in the SAR images were in the range of 2 to 7 m s$^{-1}$, based on estimates provided by Enfotec Technical Services Inc. Surface current speeds were in the range of 0.1 to 0.3 m s$^{-1}$ as estimated from satellite altimetry. Radar signals received from layers of floating oil have a low backscatter coefficient and appear "dark" compared to adjacent radar "bright" areas. Natural layers of floating oil—so called oil slicks—are distinguished from biogenic surfactants by having a few broad and parallel bands, which have distinct termini and often describe acute-angle curves as floating oil drifts with wind and current (Espedal and Wahl 1999).

## 7.3 Results and Discussion

## 7.3.1 GC185

The GC185 site is one of two study sites that were defined in the sampling design as sediment diffusion sites. The second sediment diffusion site is GC234. A chemosynthetic community at GC185, which is also known as Bush Hill, has been very widely studied since its discovery in 1986 (MacDonald *et al.* 1989). It has become a de facto type specimen for the so-called lush chemosynthetic community defined by management concerns (MMS 1988). Notably, the community has, since 1989, coexisted with an energy production in Jolliet Field, where the world's first tension leg well platform was installed in 536 m of water. The field consists of multiple, stacked reservoirs that formed in association with a major growth fault and slump block. The gravity slide occurred when sediment was tilted by a salt diapir rising to the west-northwest during Lower Pleistocene (Cook and D'Onfro 1991). Regional bathymetry in the vicinity of the GC185 site clearly shows it to be situated on the flank of a canyon created by this slide (Figure 6.4). Part of the secondary or antithetic fractures emanating from the growth fault intersects the seafloor along a north-south trace that defines the GC185 community, as well as a smaller seep (Bush Lite) to the south (Figure 7.1). Reilly *et al.* (1996) consider the site to be a clear example of the "fault-dominated" seepage style that, these authors assert, uniquely supports complex communities of tubeworms, mussels and associated species. Roberts and Carney (1997) describe the setting as an example of a transitional seep, and cite it as "the most extensive [known] development of a chemosynthetic community." Additionally, the influence of shallow gas hydrate deposits upon the surface geology and chemosynthetic community development has been widely noted and discussed (Carney 1994, MacDonald *et al.* 1994, Reilly *et al.* 1996, Roberts and Carney 1997, Sassen *et al.* 1994b). In this context of previous results, a careful re-examination of the biological and geological features of the site serves to refine and extend understanding of Gulf of Mexico chemosynthetic communities.
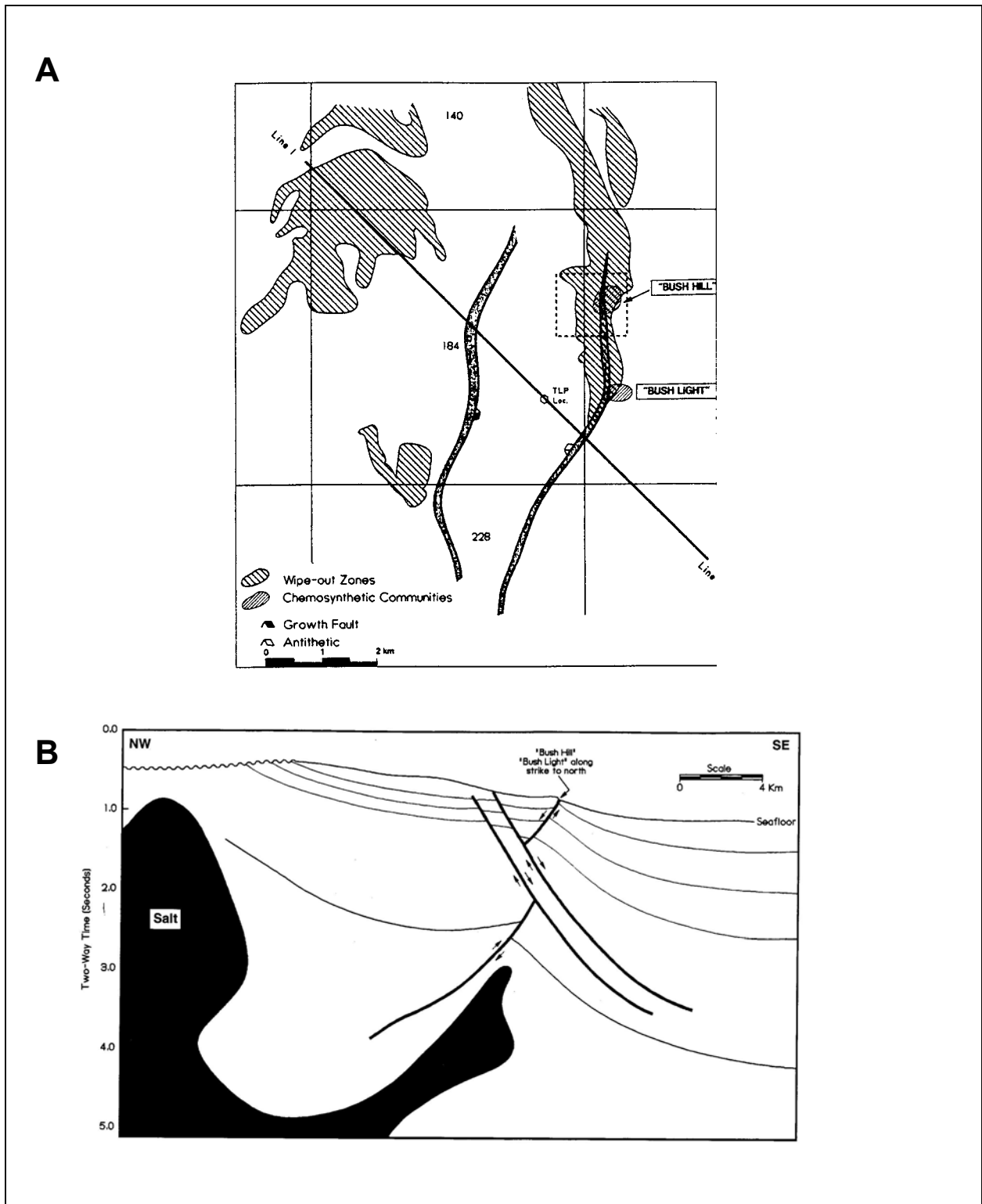
Figure 7.1.    Generalized view of fault system and mound formation at the GC185 site (adapted from Reilly *et al*. 1996). (A) Plan view of fault trace and mound location.  Chemosynthetic community labeled Bush Hill corresponds to the GC185 study site. (B) Schematic diagram of subsurface faulting and salt structures in the region near GC185 site.  Note the high-angle or antithetic fault that forms the principal migration conduit for hydrocarbons reaching the community.

Use of laser line-scan survey data, processed with satellite image processing techniques, yields a definitive map of the major community components extending over an area of 27,650 sq. m, which is more than 80% of the mound (Figure 7.2). The laser line-scan survey was completed with coverage of virtually the entire mound, omitting only the steep escarpments on the western margin where imaging was problematic. Review of the raw data revealed that much of the area was unoccupied by the larger chemosynthetic animals (tubeworms and mussels). These portions of the survey were not processed for inclusion in the final map. Interpretation of the image was greatly enhanced by ground-truth observations of the fauna during the 1997 and 1998 SEA-LINK cruises. Tubeworm clusters and mussel beds were quite evident, for the most part, in this image. Components could be quantified in terms of the area each feature occupied (Table 7.2). Tubeworm clusters, a major component of the community were categorized according to their densities. Questions of identification were resolved, for the most part, by review of the video and photographs taken by SEA-LINK.

One very abundant component of the community was bacterial mats, which were evident as mottled patches virtually throughout most of the mosaic, becoming less abundant to the eastern side of the area. Mats tend to be ephemeral and are therefore impossible to verify. Bacterial mats were not quantified. Another problematic feature component was areas of dead mussel shells and rubble that were often found on the margins of living assemblages. Figure 7.3 shows this mixture of living and dead components near the juvenile tubeworm station BHJT1. Difficulties distinguishing the defunct remains of former aggregations from living animals posed a minor source of uncertainty regarding the total areas affected by seepage and occupied by chemosynthetic animals.

Despite these difficulties, the laser line-scan mosaic of GC185 probably represents the largest area over which a comprehensive census of a deep-sea community has been completed. Analysis of this product shows that chemosynthetic animals occupied less than 2% of the total area of the mosaic. Authigenic carbonate, an additional indicator of hydrocarbon seepage (Roberts and Aharons 1993), occupies only an additional 2.2% of the area. Most of the area of the community consists of soft sediments that are widely colonized by *Beggiatoa*. The distribution of chemosynthetic animals and carbonate describes a distinctly linear pattern that closely parallels the fault trace described by Reilly *et al.* (1996). Tubeworms were the most dispersed component of the community (apart from bacterial mats), while most of the mussels and all of the outcropping gas hydrate, both of which are dependent on rapid gas flux, were focused in two small areas near the crest of the mound. This result is qualitatively similar to the original mapping of the GC185 community by MacDonald *et al.* (1989). However, owing to limited navigation and sampling, that work failed to discern the linear, north-south alignment of the community. Additionally, the previous mapping used a kernel smoothing routine to predict a broad, smoothly extended region over which tubeworms would be found. Discontinuities in the occurrence of tubeworms distinguished in the laser line-scan data contradict this finding. Carbonate, although it occupied the largest area of the community, was also largely restricted in distribution to the western margin of the site. Much additional carbonate structure could be found on the western slope of the mound. This region comprises the active margin of the fault, and the offset from the surrounding seafloor indicates protracted activity of this fault margin. The active biological community, however, is displaced 20 to 30 m easterly from this margin.
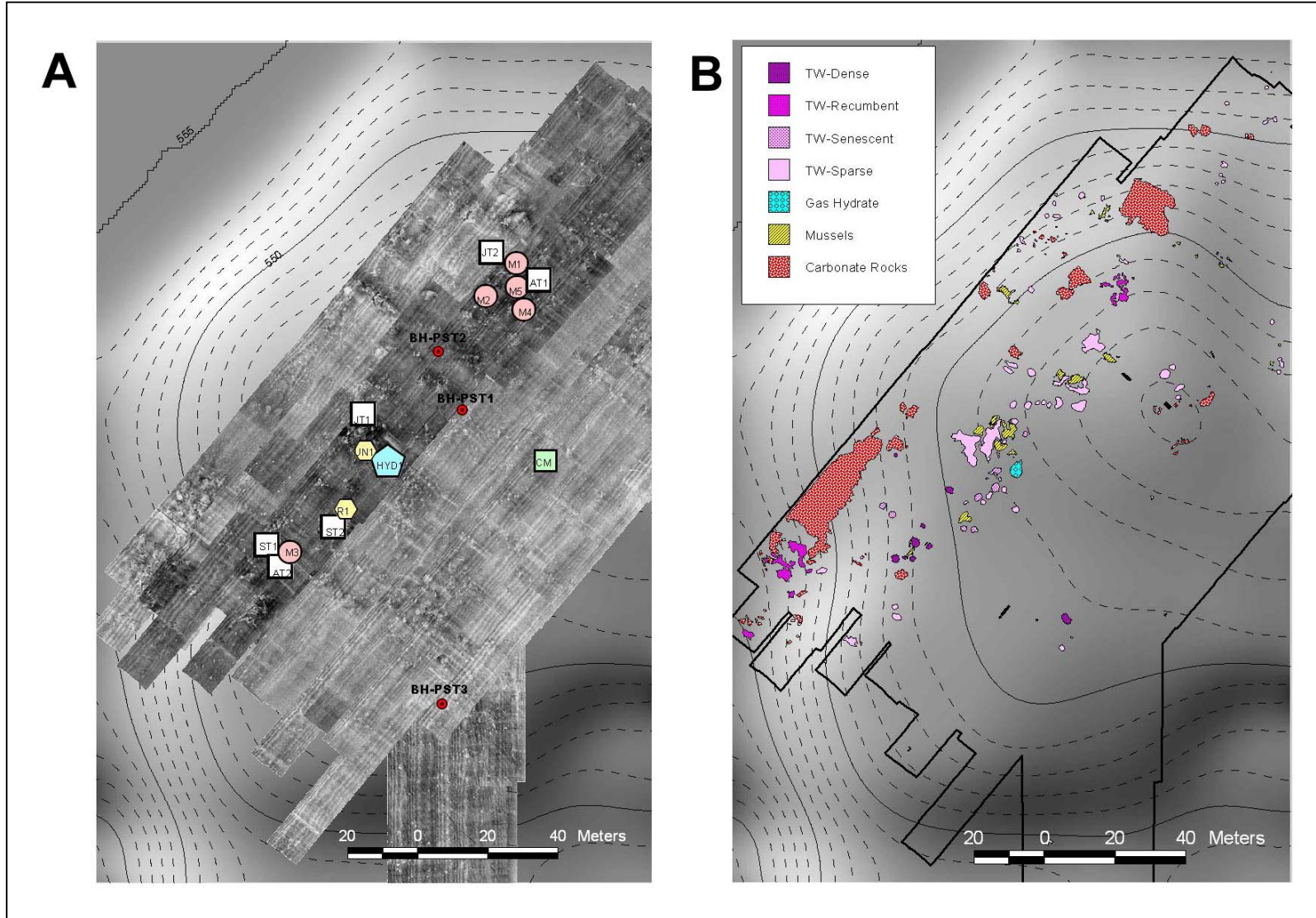
Figure 7.2.    Detailed bathymetry (1-m contours) of the GC185 site (see Fig. 6.4 for regional bathymetry).  (A) Mosaic of 18 laser line-scan tracks GC185 mound overlaid with sampling stations, current meter mooring, and piston core sites (BHPST1-3). (B) Areas of individual clusters of tubeworms, mussels, and carbonate outcrops are plotted based on interpretation of the full-scale mosaic
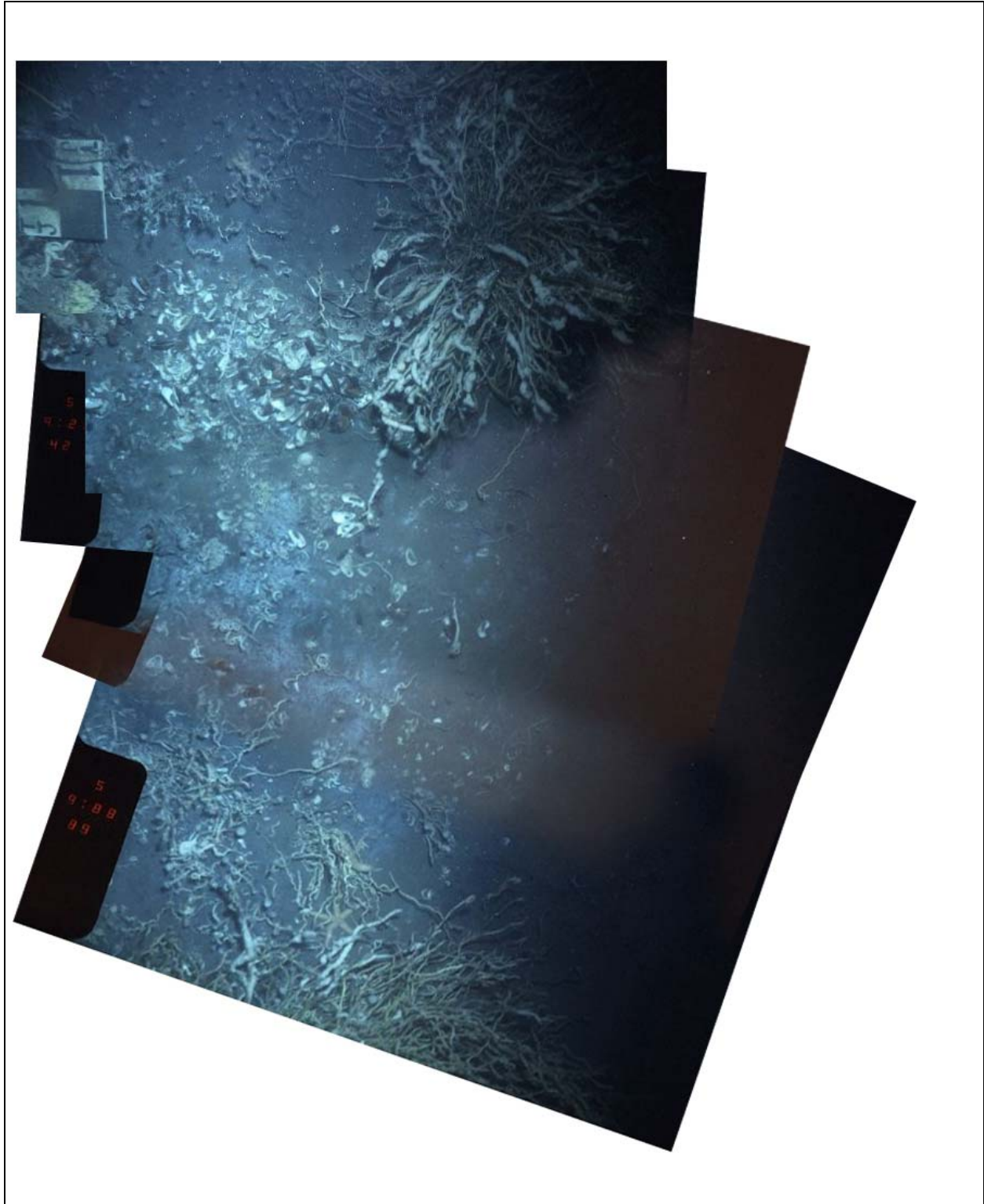
Figure 7.3. Detailed photomosaic of station JT1 in GC185 shows scattering of dead shells and live mussels, sparse tubeworms and carbonate rubble. Black and white marker is 30 cm wide. Juvenile tubeworms have a coiled growth form and have settled on hard substrate next to the marker.

The outcropping deposit of gas hydrate near the center of the community (point HY1 in Figure 7.2A) has been the source of much discussion in the literature. MacDonald *et al.* (1994) noted the tendency of the mound to change radically in shape from one year to the next and speculated that pieces of the deposit may break free and float away. Sassen and MacDonald (1994) found pentane in the sediments overlying this mound and speculated that the hydrate might include structure-H crystal forms. Although this was not confirmed by subsequent work (Sassen *et al.* 1998), the proximity of tubeworm aggregations to the hydrate outcrop was noted. In a general sense, Carney (1994) has suggested that gas hydrate might act as a buffer that would retain hydrocarbons in surface sediments and extend the possibility for biological interactions. The dynamics of gas hydrate at the site and possible interaction between it and the biological community is therefore of interest.

Table 7.2. Areas occupied by components of the chemosynthetic community at GC185 that were identified in laser line-scan mosaic.

| Community Component | Area (sq. m) |
|---|---|
| Tubeworms, Dense | 22.7 |
| Tubeworms, Recumbant | 69.0 |
| Tubeworms, Senescent | 24.6 |
| Tubeworms, Sparse | 215.3 |
| Gas Hydrate Outcrop | 11.9 |
| Seep Mussels | 71.9 |
| Carbonates | 610.0 |
| Total Area of Mosaic | 27,650 |

Compiled results show that gas hydrate deposits are a perennial feature of this specific location; markers and dropped objects confirm this placement. The outcrop forms on the sloping southern margin of a large mussel bed, which is surrounded on three sides by recumbent tubeworms (Figure 7.2). The location is offset from the top of the mound on a gradual slope. The surrounding tubeworms are numerous, but by no means the densest aggregation in the community. Exposed hydrate appears on the downslope side of the deposit, which evidently extends laterally underneath the mussels.

A time-lapse camera positioned to monitor this hydrate outcrop recorded 1-sec video sequences at hourly intervals over a 132-day deployment (Figure 7.4). Beginning as a prominent mound, with approximately 30 cm of relief above the surrounding seafloor and patches of exposed gas hydrate clearly visible, the mound gradually deflated over the monitoring interval. By the end, the exposed hydrate had completely disappeared and the mound was leveled. Biological activity was high on and around the mound, with fish and invertebrates appearing in numerous video sequences. Visible in the video images was a bacterial mat, which covered the mound and the sediment directly in front of the mound. During the monitoring interval, this mat was repeatedly disturbed by the activity of crabs and bivalves. The animals would appear in several of the hourly images, where they could be seen plowing through the surface sediments until the

bacterial mat had been completely obscured and overturned. Subsequently, over the course of several days the mat would re-establish itself. A similar pattern was observed during most disturbance events.

Piston cores provide additional information on gas hydrate and basic sediment characteristics of the site (Table 7.3). Significant recoveries of gas hydrate were made from 1 m subbottom depths at a location 70 m south of the outcropping deposit (Figure 7.2A, BHPST-3). The core closest to the outcropping deposit (BHPST-1) recovered carbonate and oily mud, but no intact hydrate. Both of these cores were short, indicating a hard substratum at shallow subbottom depths. The third core, which was collected closest to the rocky margin of the mound, failed to penetrate a rocky bottom location. Interestingly, the recovery of gas hydrate came from a locality well removed from the major concentrations of chemosynthetic animals. This demonstrates that, although shallow gas hydrate deposits may be associated with tubeworm aggregations, presence of shallow gas hydrate does not guarantee that tubeworms will occur at a location. The rocky substratum encountered by the BHPST-2 core is consistent with the observation of carbonate outcrops in the laser line-scan mosaic.

Table 7.3. Field notes on piston cores taken at sites GC185 (BHPST1-3:
See Figure 7.2 for locations.) and GC234 (GCPST1-3: See Figure 7.7 for locations).

| Core ID Number | Length (m) | Description |
|---|---|---|
| BHPST-1 | 1.2 | Soft, liquid-rich clay. Oil vugs and veins mixed with small carbonate nodules. Strong odor of $H_2S$. |
| BHPST-2 | 0.1 | Oil-rich carbonate rubble and small pieces of tubeworm tube in tip of core. |
| BHPST-3 | 1.2 | Upper 90 cm comprise soft, olive gray clay with oil veins. Small carbonate nodules at 60 cm subbottom. Lower 20 cm of core comprise a solid cylinder of gas hydrate, laced with veins of oil and sediment nodules. |
| GCPST-3 | 0.1 | Recovery from tip only, which contained carbonates and vestimentiferan pieces. |
| GCPST-2 | 2.4 | Firm clay with multiple oil stains, veins, and vugs. Strong odor of $H_2S$. Color olive gray. Hydrates from 0.5 to 8 cm in sections 4, 5, and 6. Extremely gassy with gas cuts and fractured in all sections. |
| GCPST-1 | 0.8 | Liquid filled core. Strong odor of $H_2S$ with oil staining throughout. Hydrates from 0.5 to 3.0 cm in diameter in section 3. Gassy and bubbling. |

In summary, the present compilation of results portrays the GC185 site as a broad, low mound, roughly hemispherical in cross-section, the rocky western margin of which aligns with high angle faulting. The biological community is concentrated in a relatively small portion of the mound, in a 40-m wide band that is offset, but largely parallel with, the axis of the fault. Gas hydrate outcrops on the eastern-most margin of this band, furthest from the fault, and appears to be a plug that waxes and wanes at the orifice of an active gas vent. The outcropping deposits of

gas hydrate are dynamic structures in terms of their size, but occur persistently at predictable locations. Shallow deposits of gas hydrate extend from the community to locations well away from the principal axis of biological activity. Although these characteristics result from mapping a single site, which we previously defined as a sediment diffusion site, comparison of similar attributes at the program's second sediment diffusion site, GC234, provide a means for evaluating their generality.

**7.3.2 GC234**

The GC234 site is the locality where the first documented collections of sediments containing thermogenic hydrocarbons were made in the Gulf of Mexico (Anderson *et al.* 1983). The geology of the region has been described by Behrens (1988) and Reilly *et al.* (1996). The extensive chemosynthetic community is situated on a slump block within a half-graben. Steep escarpments rise above the community on three sides, with extensive lithification on the western slope, and the bottom slopes away to the south. In 1990, the site was thoroughly surveyed with submarine NR-1, which completed a series of east-west oriented tracks through the site at a line spacing of about 30 m over a total area of approximately 1200 by 700 m (Figure 7.5). Video records of the chemosynthetic animals, bathymetric soundings, and side-scan sonar records comprise a baseline description of the site. The side-scan sonar mosaic, which was assembled digitally from scanned paper-chart records, delineates several broad areas of high-reflectance seafloor (Figure 7.5). Visual survey confirms abundant carbonate hardground and outcroppings across the western escarpment. Several large, solitary promontories are visible as isolated hard targets in the side-scan image; these include a massive structure approximately 15 m wide and 5 m tall that is situated in the center of the side-scan mosaic. Visual survey confirmed that the remaining regions of high reflectance comprise large colonies of tubeworms situated on an undulating terrain. Notably there are two broad bands that trend northwest-southeast across the center of the image. Within these regions, tubeworms colonies occur at densities ranging from sparse aggregations, to bushes measuring 1 to 2 m across, to continuous stands that extend for 10 m or more (MacDonald *et al.* 1990a, MacDonald *et al.* 1995, Reilly *et al.* 1996).

On the basis of this information, the array of sampling stations for the present program were established within a sub-area of the seep that measured approximately 300 x 200 m (Figure 7.6). Operations during the 1997 cruise with SEA-LINK deployed permanent markers at these stations and provided detailed descriptions of the features present at each station (see Chapter 3, this volume). When the site was surveyed in 1998, with submarine NR-1, these markers were used as benchmarks to align NR-1 survey results with station locations. NR-1 completed a dense array of north-south and east-west tracklines. Depth soundings along these tracks were used to compile an independent bathymetric surface. The side-scan sonar mosaic and the visual observations from the 1990 NR-1 cruise were aligned with the recent data on the basis of this surface. Piston cores, collected after the NR-1 cruise, used a coring device that dropped marker buoys at the location of each core (Table 7.3). These markers were located with SEA-LINK during its 1998 sampling cruise. Buoy locations were confirmed by use of the SEA-LINK's acoustic navigation system. Thus, it is possible to compare numerous layers of geographic information from the site.
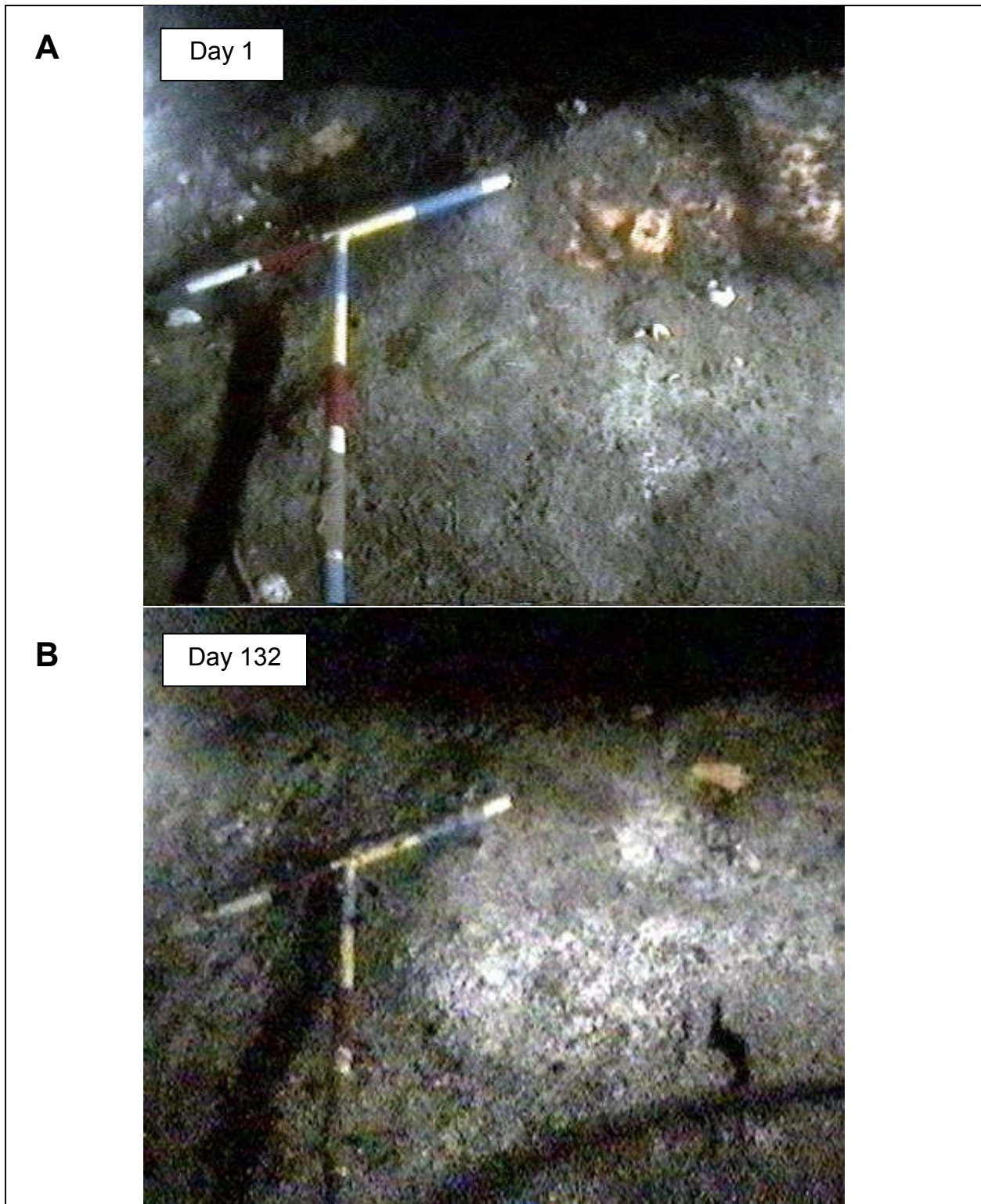
Figure 7.4. First (A) and last (B) frame from a time-lapse series recorded at the HYD1 station. Exposed hydrate is clearly visible in the first image as an outcropping patch on a low mound. During the intervening time the mound gradually deflated and the hydrate entirely disappeared. Crossbar is 40 cm wide.
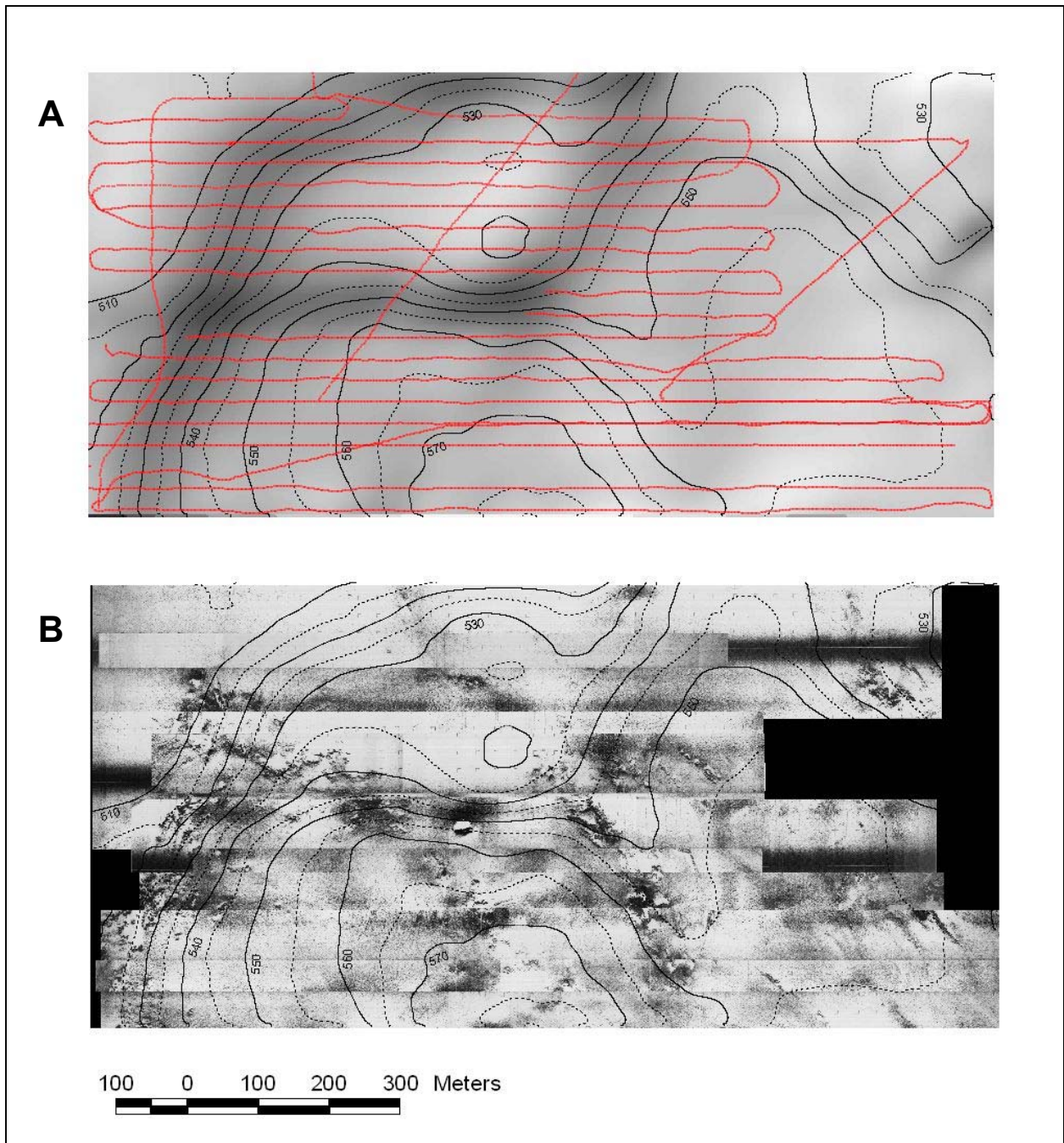
Figure 7.5.   Overview of the GC234 study site, situated in the head of a canyon formed between active fault lines. (A) Bathymetry of canyon overlaid with the trackline of submarine NR-1 during 1992 cruise. (B) Side-scan sonar mosaic of site compiled from data collected by NR-1 in 1992. Note regions of high surface reflectivity.
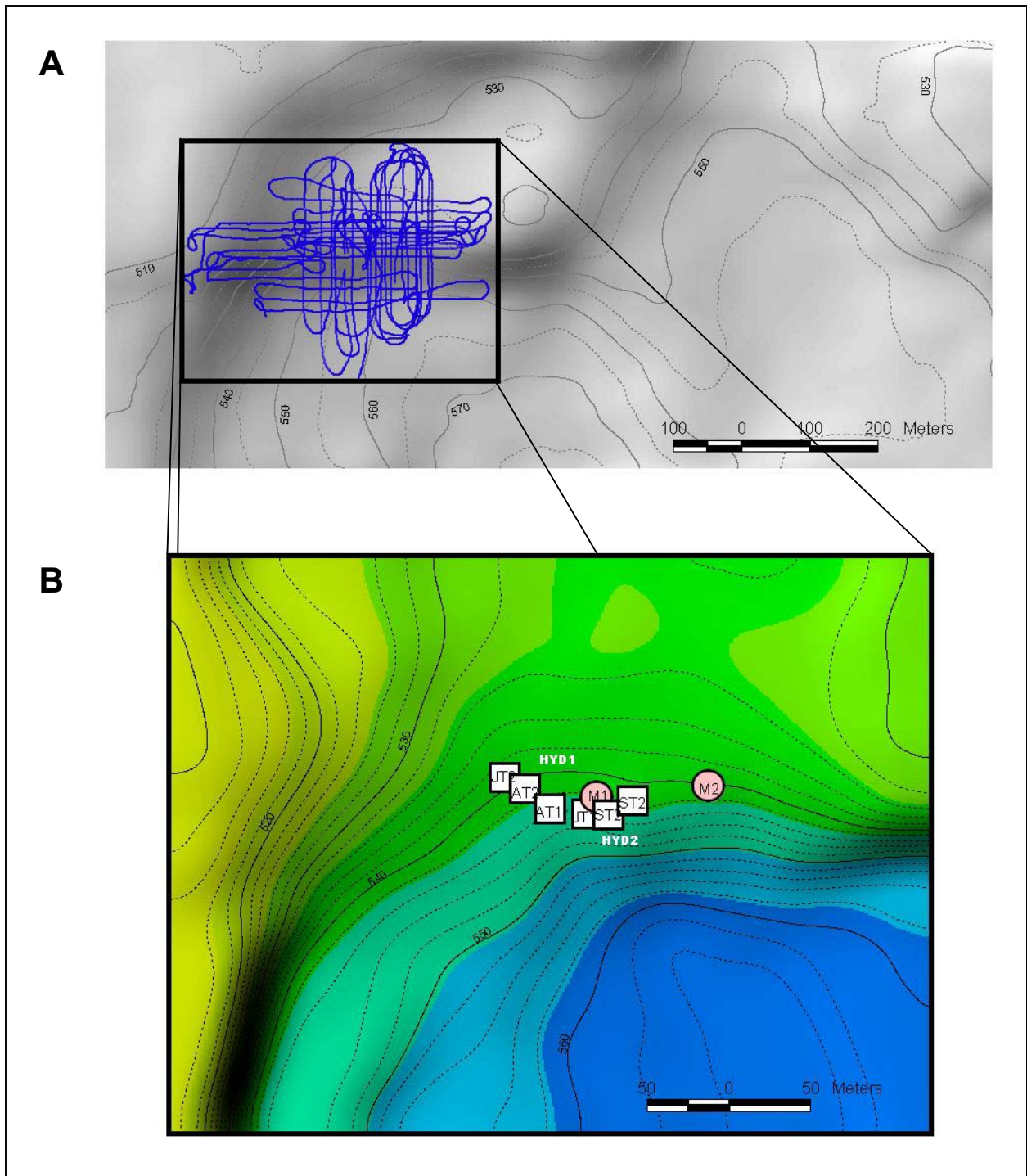
Figure 7.6.  Merger of 1990 survey data with 1998 survey data and sampling stations.  (A) Inset box overlaid on GC234 bathymetry shows detailed trackline followed by NR-1 in 1998 cruise. (B) Bathymetry of X-Star survey area generated from 1998 depth data and GC234 sampling station locations.  The 1990 a and 1998 datasets were co-located by shifting the 1990 data to match the 1998 bathymetric contours.

Subbottom profiles from the 1998 survey revealed complex and abrupt transitions from regions in which surface strata appear as distinct, closely spaced layers to areas in which the strata were blanked by continuous, moderate-intensity returns. These so-called wipeout zones have been described in previous investigations of Gulf of Mexico seeps (Sager and MacDonald 1998) and are accepted as indicators of gassy surface sediments that dampen or obscure high-frequency seismic reflections. The present data, however, made it possible to trace the transitions between normally stratified sediments and the wipeout zone (Figure 7.7). The wipeout zone begins abruptly, over a distance of less than 10 m, and describes a zigzag margin that bisects the study area. East-west tracks show a series of faults that appear to be separating along this line direction. These faults evidently begin as slight offsets in the alignments of substrata (e.g., Fault A in Figure 7.7) and open into larger conduits. The north-south track indicates an equally abrupt transition to the wipeout zone that begins where the slope increases (Figure 7.8). The wipeout zone is not homogeneous. Distinct, arc-shaped reflectors were detected at numerous points within the wipeout zone, usually at levels 2-3 m subbottom (e.g., Track M2-12, Figure 7.7).

Within the wipeout zone and adjacent to the normally stratified strata, the seafloor had a distinctively undulating profile along many of the tracks (e.g., Track M2-8, Figure 7.6). This seafloor irregularity was lacking in the regions where the subbottom was visibly stratified. By comparing adjacent tracklines, these irregularities were resolved as a series of mounds with base areas 15 to 20 m across and relief of 1 to 3 m. The reflection intensity at the seafloor was not consistent among all the mounds. Most of the sampling stations occupied during the program were on or adjacent to these mounds (Figure 7.8). Some mounds had distinct, intense reflections at the seafloor. However, the prominent mound at station M2 had a very indistinct seafloor reflector.

Visual observations from the SEA-LINK cruises at GC234 conclusively link several of the mounds with shallow deposits of gas hydrate. Notably, the HYD1 station, when first observed in the 1997 cruise, was a prominent outcrop of gas hydrate that exposed a broad expanse of gas hydrate on its downslope margin (Figure 7.9). The polychaete *Hesiocaeca methanicola* (Desbruyeres and Toulmond 1998) was first observed on the exposed portion of this gas hydrate outcropping (Fisher *et al.* 2000). A similar exposure of gas hydrate was seen at the HYD2 station. The gas hydrate deposit at HYD1 completely disappeared between the 1997 and 1998 SEA-LINK cruises, while the HYD2 deposit was reduced to a small remnant. Gas hydrate deposits were also observed immediately beneath the surface at the M2 station, where small pieces of the substance were dislodged by push core collections. Piston core recovery of gas hydrate from the M2 station (Table 7.3) confirmed that the visible deposit observed from SEA-LINK was part of a larger, buried deposit that extended down the flanks of the mound.

From these results, it is evident that gas hydrate forms in the upper few meters of the sediment column and produces broad mounds. As at GC185, it was seen that individual deposits might expand to breach the seafloor on the margin of steeper slopes (MacDonald *et al.* 1994). This exposes patches of gas hydrate, which subsequently dissolves so that the localized relief gradually deflates. It appears that a cycle of exposure, dissolution, re-growth and re-exposure repeats at fixed localities within individual mounds. It also appears that the mounds are concentrated along the margin between the wipeout zone and the region in which shallow sedimentary strata are visible.
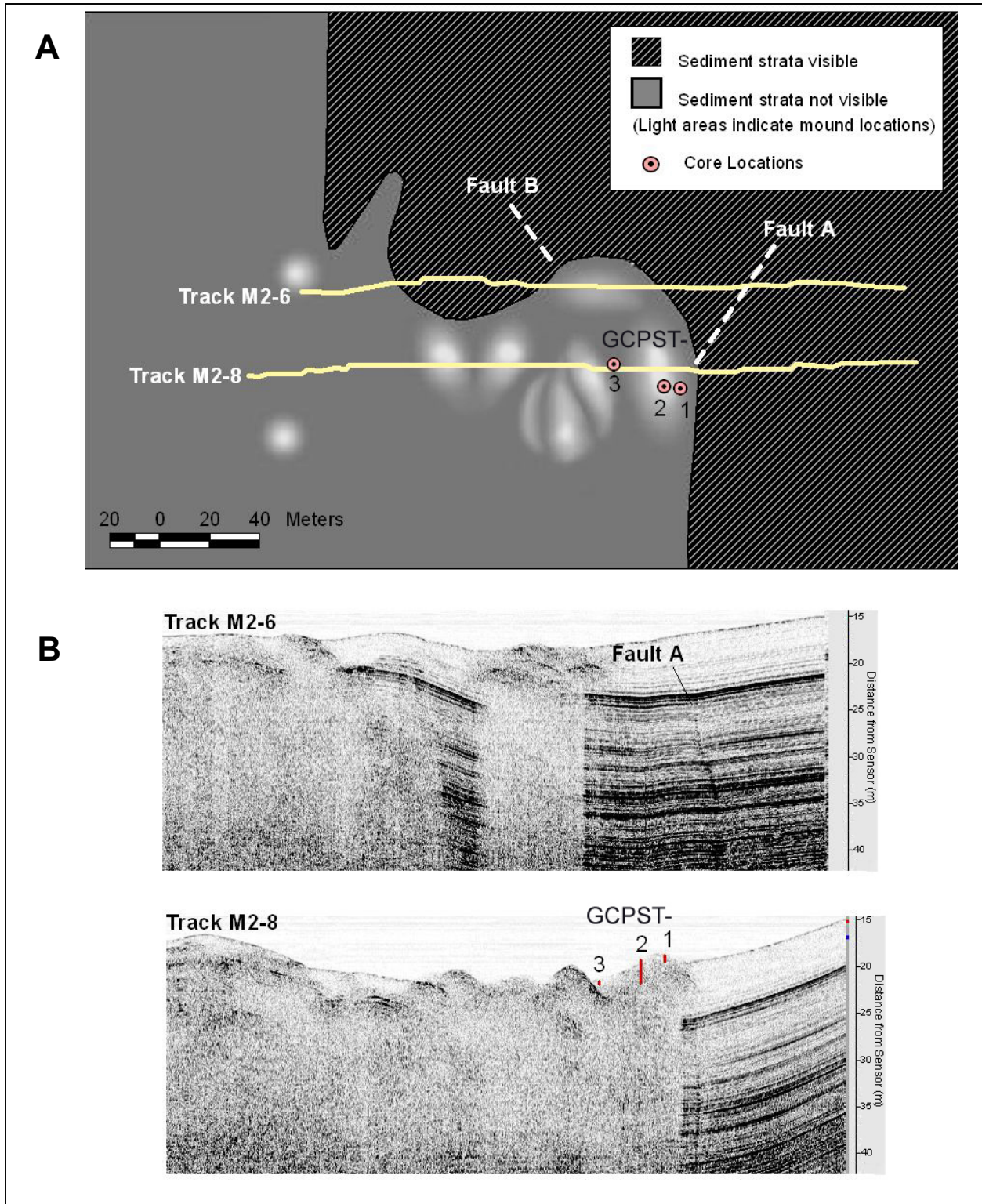
Figure 7.7.  Results of X-Star subbottom profile survey. (A) East-west tracklines overlaid on sediment style showing location of hydrate mounds, faults and ground-truth piston cores. (B) X-Star subbottom profiles showing abrupt transition between stratified and un-stratified sediments, faults, mounds, and piston core locations.
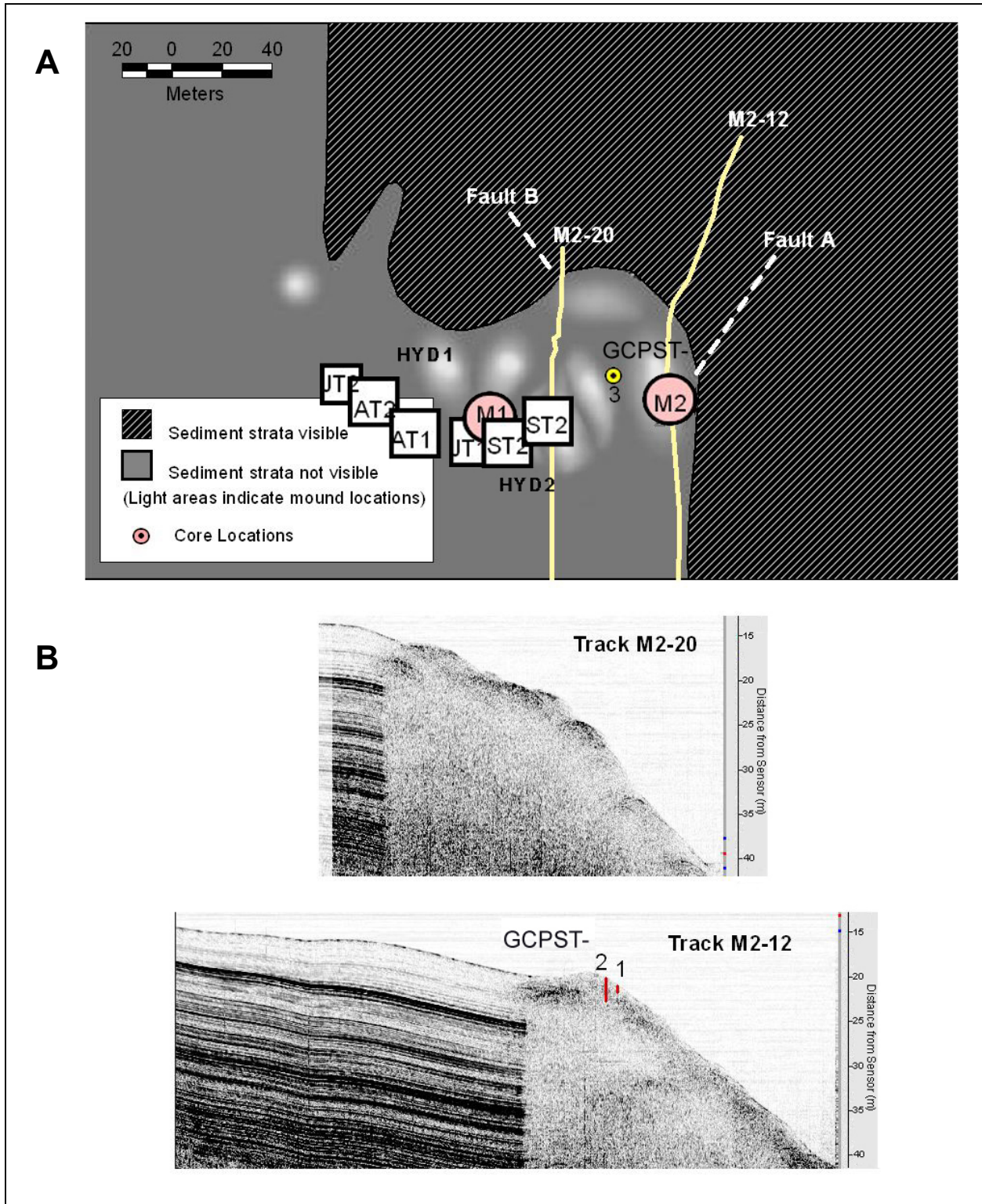
Figure 7.8. Results of X-Star subbottom profile survey with station locations. (A) North-south tracklines overlaid on sediment style showing location of hydrate mounds, faults, and sampling station locations. (B) X-Star subbottom profiles showing abrupt transition between stratified and un-stratified sediments, faults, mounds and piston core locations.
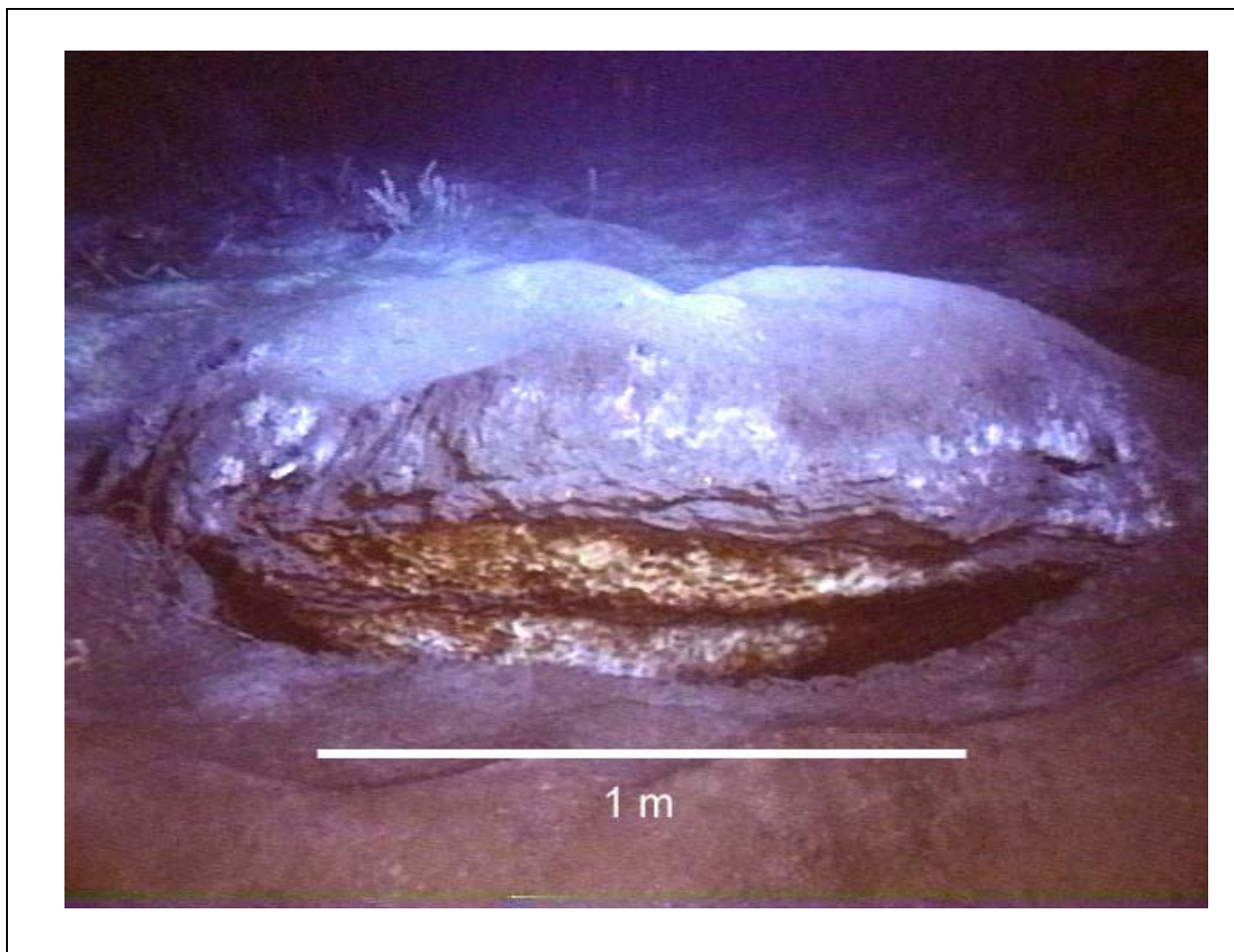
Figure 7.9. Exposed gas hydrate at the HYD1 station in GC234 site, 1997. Location where the ice worm (*Hesiocaeca methanicola*) was first collected. This deposit disappeared between the 1997 and 1998 SEA-LINK cruises. Note the band of sediment sandwiched between two layers of hydrate.

The clustering of chemosynthetic animals within the site is apparent from characteristics observed at the sampling stations during SEA-LINK dives (Figure 7.7). As was the case at the GC185 site, sampling stations defined by juvenile, adult, and senescent tubeworms were readily located, as were stations defined by mussels and bacterial mats. Though tubeworm colonies were abundant in the immediate vicinity of the sampling stations, there were large areas that were unoccupied by tubeworms and other chemosynthetic animals. As was also seen at the GC185 site, the association between tubeworm aggregations and gas hydrate at the site was consistent, but not deterministic. Dense aggregations of tubeworms extended beyond the limits of the hydrate mounds (e.g., Station AT1, Figure 7.7). Conversely, the prominent hydrate outcrop at HYD1 occurred in an area locally devoid of tubeworm colonies (Figure 7.9). To examine the discontinuities in distribution of tubeworms in light of the subbottom profiles and other geological data, the visual survey data obtained in the 1990 survey with NR-1 were reanalyzed as a layer in the GIS dataset (Figure 7.10).
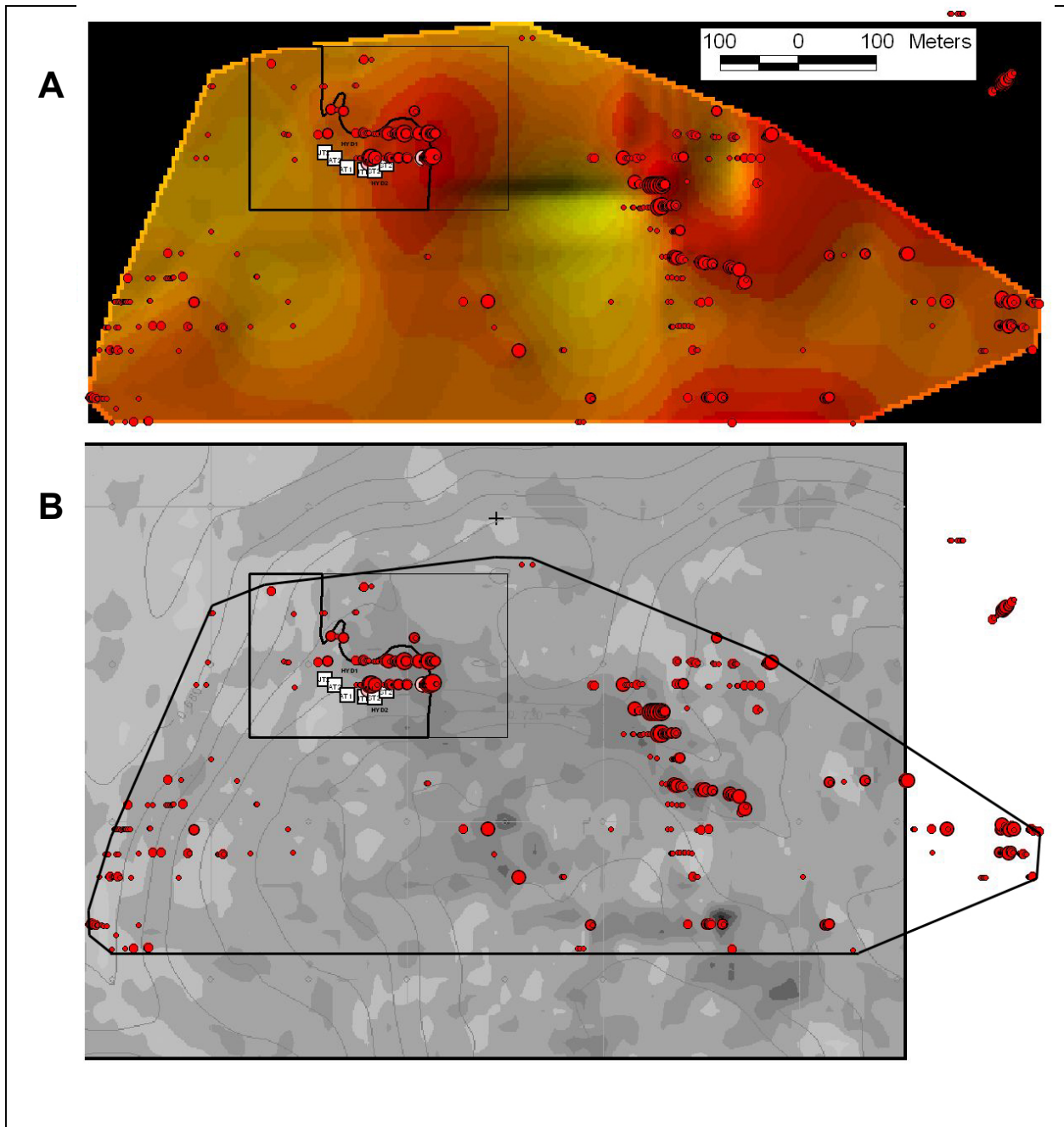
Figure 7.10. Tubeworm abundance at GC234. (A) Tubeworm clusters scaled according to area occupied and relative density of each cluster; analysis was based on visual survey done by NR-1 in 1990. Cluster locations are overlaid on a krige surface calculated from log-transformed tubeworm abundance with use of software routines in the S-Plus spatial statistics package. Dark areas in krige surface indicate areas of greater predicted abundance for tubeworms; black areas show limits of interpolated data. (B) Surface amplitude map from 3D seismic data for area. (Low amplitude areas are plotted in dark shades.) Rectangular outline delineates 1998 subbottom survey area and stations from Figures 7.7 and 7.8.

The first step was to fit a continuous surface to the tubeworm abundance estimates calculated from the NR-1 survey data from 1990 (Figure 7.10A). Kriging is a statistical technique for spatial prediction frequently used by geologists to delineate the distribution of ore deposits or other features that have a relatively continuous distribution, but are sampled at discrete locations (Cressie 1991). In calculating the krige surface, scales of spatial auto-correlation, threshold levels, and nugget effects (tendency to occur in large isolated concentrations) were estimated from the survey data using standard techniques (Kaluza and Doyle 1998); the parameters for the krige surface fit were adjusted accordingly. Least-square error values were calculated and several surfaces were produced until a minimum error was obtained. The resulting surface delineates several zones of high abundance, which are separated by larger areas in which tubeworms were evidently vacant. As expected, the predicted regions of high abundance correspond closely to the observed tubeworm clusters. However, the best fit predicts high abundance in areas where no tubeworms were observed. Notably, in the region of the program sampling sites, the krige surface predicts a zone of high abundance centered on the M2 station and extending over an ovoid approximately 200 m by 150 m. To the northeast of station M2, the predicted surface extends over the area in which the subbottom survey found normally stratified sediments (little evidence of seepage) and where the 1990 visual survey with NR-1 failed to detect tubeworm colonies.

The second treatment of the tubeworm survey data was to compare the observed tubeworm clusters to available surface amplitude values from a 3D seismic survey (Figure 7.10B). Surface amplitudes process the first return from a 3D-processed dataset. They are standard products that would be available to operators assessing a region prior to siting exploration or production facilities (See Chapter 6 for details). The data are coarse, spatially, because of array limits and the present plot distinguishes only 8 levels of return. Nonetheless, the correspondence between tubeworm abundance and low surface amplitude is striking. Table 7.4 summarizes the surface amplitudes observed along the 1990 survey tracklines and at the locations where tubeworm clusters were encountered. Discounting area where amplitude data were missing, this analysis shows that approximately 81% of the tubeworm population was found in that 25% of the surveyed area having low to moderate seismic amplitude. A goodness-of-fit test on these results indicates that the probability this distribution would arise by random chance is less than 5%. Examining the zone around the sampling stations, an area of low amplitude clearly contains much of the observed tubeworm population. Unlike the krige surface, however, the low amplitude zone does not extend to the northeast. Instead it appears roughly conformal to the wipeout zone delineated by the independent subbottom survey. Low surface amplitudes appear to be a good predictor of tubeworm abundance.

It is evident from the results at GC234 that sharp discontinuities in seepage are prevalent within the study area. A probable cause of these discontinuities is ongoing fracturing of the sediment column during the movement of the slump block and the expansion of the graben found at the site. The subbottom data delineate distinct zones generated by these small-scale faults or fractures. In areas where subbottom strata are obscured, one finds abundant evidence of active fluid and gas migration, including widespread colonies of tubeworms and shallow gas hydrate deposits. Results of surface fitting to a detailed survey of chemosynthetic animals tended to overestimate the occurrence of the animals. The reason for this is probably that the surface fitting routines used do not deal well with sharp discontinuities. This result suggests that an evaluation

of the extent of chemosynthetic animals in a seep-affected region should make use of seismic amplitude data combined with visual surveys.

Table 7.4. Comparison of surface amplitudes from 3D seismic data to tubeworm abundance (Figure 7.10). For details on the 1990 NR-1 survey tracklines see Figure 7.5.

| Surface amplitude levels: increasing intensity | Proportion 1990 survey area along trackline | Proportion total tubeworm abundance |
|---|---|---|
| no data | 0.07680 | 0.01460 |
| 1 | 0.00046 | 0.00190 |
| 2 | 0.00184 | 0.03420 |
| 3 | 0.06839 | 0.28030 |
| 4 | 0.17458 | 0.47800 |
| 5 | 0.55663 | 0.12340 |
| 6 | 0.16920 | 0.05330 |
| 7 | 0.00799 | 0.00670 |
| 8 | 0.01322 | 0.00750 |

### 7.3.3 GC233

The brine-filled pockmark and mussel bed at GC233 is a notable example of a chemosynthetic community supported by focused flow and methane dissolved in pooled hypersaline fluid (MacDonald *et al.* 1990b). This pool is situated on a low mound, which is elevated 6 to 8 m above the surrounding seafloor and has a basal diameter of approximately 100 m (Figure 7.11). The fluid filling the pool has a salinity of 130 practical seawater units and is supersaturated in biogenic methane. Samples of fluid, decanted from ambient pressure into one atmosphere, will boil vigorously as gas comes out of solution. The solids dissolved in the fluid are primarily NaCl, derived from halite deposits at depth. Added density due to the excess salt is what maintains the brine as a distinct fluid in the pool. However, the salinity of the brine is grossly out of equilibrium with seawater. Brine is certainly mixing with seawater by molecular and turbulent diffusion. The elevation of the mound, sediment slides, and bacterial mats on the downslope (southern) end of the pool, and a raised dike around the upslope (northern) edge of the pool are among the abundant visual evidence that the pool was excavated by a vigorous discharge of fluid. The persistence of a mussel community, developed in the present day to a continuous band that completely surrounds the pool on the level margins of the crater, is strong evidence for conditions that have favored chemosynthetic animals over an extended time (Table 7.5). The probable age of the larger seep mussels in this population exceeds 100 y (Nix *et al.* 1995). Stability of the level of brine filling the pool is essential because the brine is anoxic in addition to being hypersaline. Therefore, it would be fatal for mussels to be submerged in the brine. Examination of the inner edges of the pool, however, reveals that the mussel hold their siphons less than half their body lengths (about 4 cm) above the brine. The outer edges are less than 15 cm higher than the inner edges. Because mussels are sessile and bound in place by the byssal

threads of their neighbors, even the slightest increase in the brine level would produce widespread stress or mortality. This site and its strikingly dense population represent an equilibrium state between the violent forces of formation and continual processes (e.g., dissolution of the brine) that are eroding the present conditions. Perception of stability in the face of potentially destabilizing forces is intuitively clear. The purpose of this section is to present the basic evidence for change during the past and stability during the present at the GC233 site. In the final section of this chapter, this evidence will be contrasted with a site in a much more active state.

Table 7.5. Relative areas of GC233 brine pool (Brine Pool NR-1)
as calculated from laser line-scan mosaic (Figure 7.11).

| Site Characteristic | Area (sq. m) |
| --- | --- |
| Contiguous mussel bed | 434 |
| Peripheral mussel beds | 214 |
| Open brine | 253 |
| Total area of mosaic | 1658 |

To investigate the sedimentary evidence for the formative history of Brine Pool NR-1, a thorough subbottom survey was completed with submarine NR-1 during the 1998 cruise (Figure 7.12A). Two piston cores were also taken at locations intended to penetrate the downslope edge of the pool and the periphery of the mound (Figure 7.12A). As with piston cores at other program sites, the coring device was rigged to drop markers, which were relocated to confirm positions. Subbottom records revealed considerable complexity in the mound and pool. On the flanks of the mound, indurate layers underlie layers that gave weak seismic reflections (Figure 7.12B), suggesting surface flows of loosely consolidated material over hardened ground. A narrow dike, raised about 25 cm, forms a rim that surrounds three sides of the pool outside of the mussel bed. The mussels appear as a layer distinct from the brine, which forms a very level reflecting surface. Below the brine, sediments are homogeneous and contain a large, irregular reflector near the bottom of the record. The most regular subbottom features were a sequence of regular layers buried under the present day mound. Distances between these layers were greatest in the center of the mound and least around the edges. The deepest layer formed a funnel shaped base to the outline of the mound.
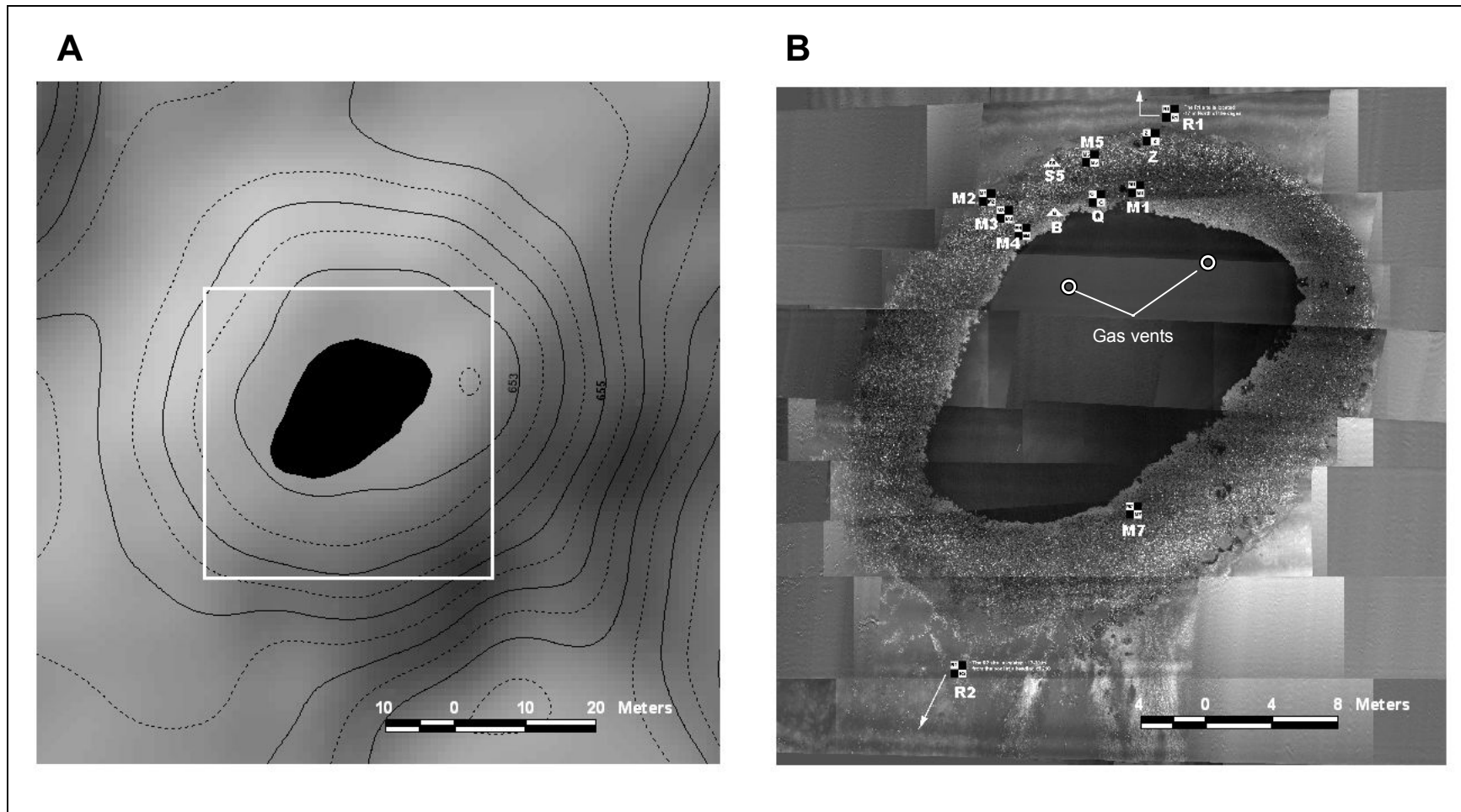
Figure 7.11. Brine Pool NR-1 in the GC233 study site (north is topmost). (A) Local bathymetry of site (contours in meters) showing placement of pool on a low, circular mound. Inset box shows outline of laser line-scan mosaic. (B) Laser line-scan mosaic of brine pool and surrounding mussel bed at GC233 site. Marked points show sampling station locations. Gas vents mark persistent bubble streams that emerge from brine; western vent is location of temperature profiles.
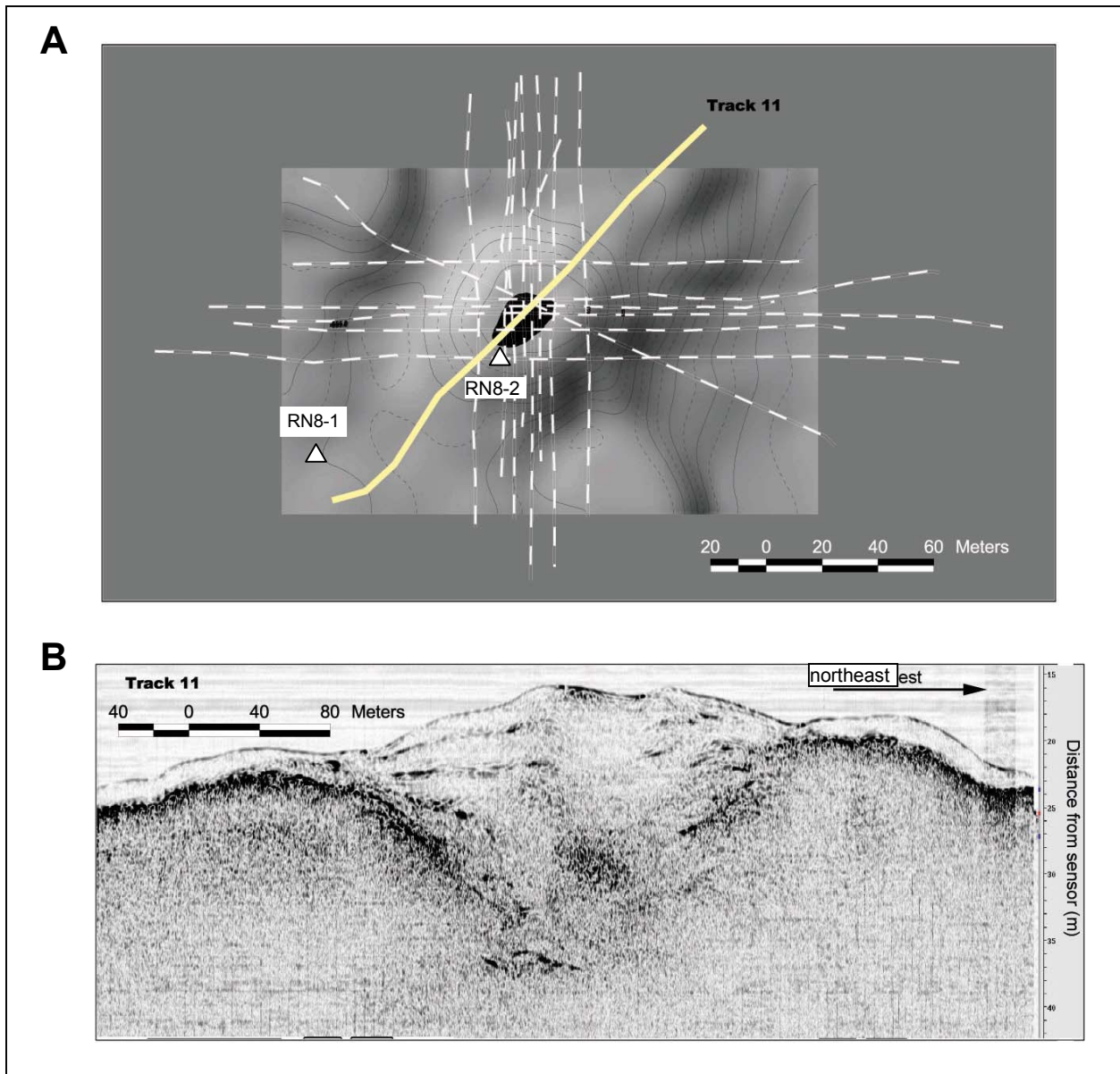
Figure 7.12. Subbottom profile survey of GC233 brine pool. (A) Plan of site showing trackline and piston core locations (Δ). (B) Example subbottom record from Track 11 taken along southwest to northeast track. Water depth of submarine was held constant (within < 1 m) along trackline, so bottom profile is accurate.

From the bathymetric and subbottom records, it is evident that the pool and mound have a complex three-dimensional structure. Two separate studies were completed to quantify this structure. The depth of the brine pool was measured by a series of lead-line casts into the brine. These were accomplished by lowering a weight from the SEA-LINK by use of a small winch and by counting depth markings on the line. The position of each cast was estimated by sighting from the submarine to markers visible around the pool edge. These sightings were then compared to a copy of the laser line-scan mosaic to mark the position of each cast. Depths from the completed

series of 30 casts was interpolated by hand and then fit to a continuous bathymetric surface (Figure 7.13A). The survey reveals the pool is a shallow shelf, pierced by two deep and narrow diatremes. In plan view, the pool is broadest at its northern end. The two diatremes are positioned in the two ends of this broad portion of the pool (Figure 7.11B) and can be recognized by the continual streams of bubbles that escape from the pool at these points. The other effort to delineate the three-dimensional structure of the site was to georectify the individual subbottom profiles, to trace out the subbottom layers visible within the mound, and to fit these layers into continuous surfaces for enumeration. This was successfully competed for the surface of the mound, including the brine-water interface, and three additional subbottom layers (Figure 7.13A). Additional reflectors were visible between the deepest layer and the second layer, but were not distinct enough to trace them through multiple records. The total volume between the deepest layer and the mound surface was 63,530 cu. m. The surface, middle, and bottom layers contributed 20,410 cu. m, 7,712 cu. m, and 35,410 cu. m, respectively to this total.

What these data show is a mound formed by repeated eruptions of fluidized mud through two distinct vents. The present-day diatremes have evidently closed in to a fraction of their greatest diameter, but remain open well below the deepest visible layers in the mound. Examining Figure 7.12C, it is clear that the maximum depth recorded in the deepest diatreme (28 m) would extend from the pool surface to below the deepest extent of the subbottom profile. The surface properties of each layer evidently hardened enough to appear as distinct reflectors. Additional data from the GC233 site were examined to determine whether these hardened layers supported chemosynthetic communities and to gauge the recent stability of the feature.

The two piston cores that were taken from the pool edges provided strong evidence for continual chemosynthetic communities at the site (Figure 7.14). Core RN8-1 was collected at the outer edge of the mound. Mudstones and stiff clay in the upper sections are consistent with the strong reflector seen in the upper portion of the subbottom record. A lucinid shell recovered from 1 m subbottom indicates circumstances favorable to chemosynthetic animals in this stratum. Notably, at 3.7 m subbottom a seep mussel shell indicates presence of a mussel colony at a position about 80 m, laterally, from present mussel colonies. Core RN8-2 was recovered immediately south of the pool and mussel bed. Fragments of lucinid shell and mud stones at 0.5, 2, and 4 m subbottom are consistent with the depths of the upper layers in the subbottom profile. However, gas expansion pockets in the core make measurements problematic and this result should be regarded with caution.
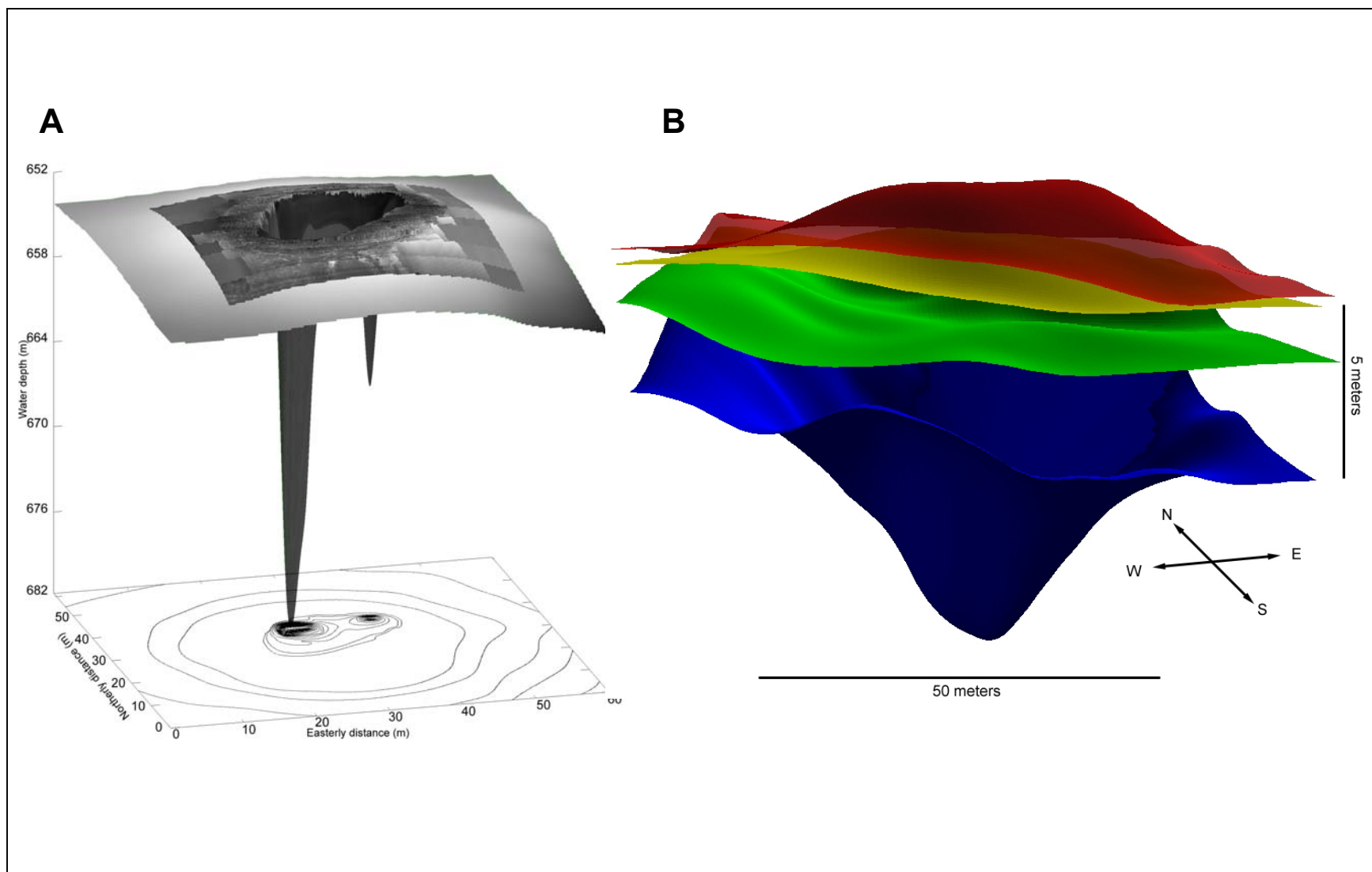
Figure 7.13. Three-dimensional interpretations of combined data for GC233 brine pool. (A) Laser line-scan mosaic draped over a bathymetric surface comprising the mound and the measured depth of the brine pool. (B) Individual surfaces interpolated from subbottom profiles of the mound trace contiguous reflectors, which are interpreted as relic mound surfaces.
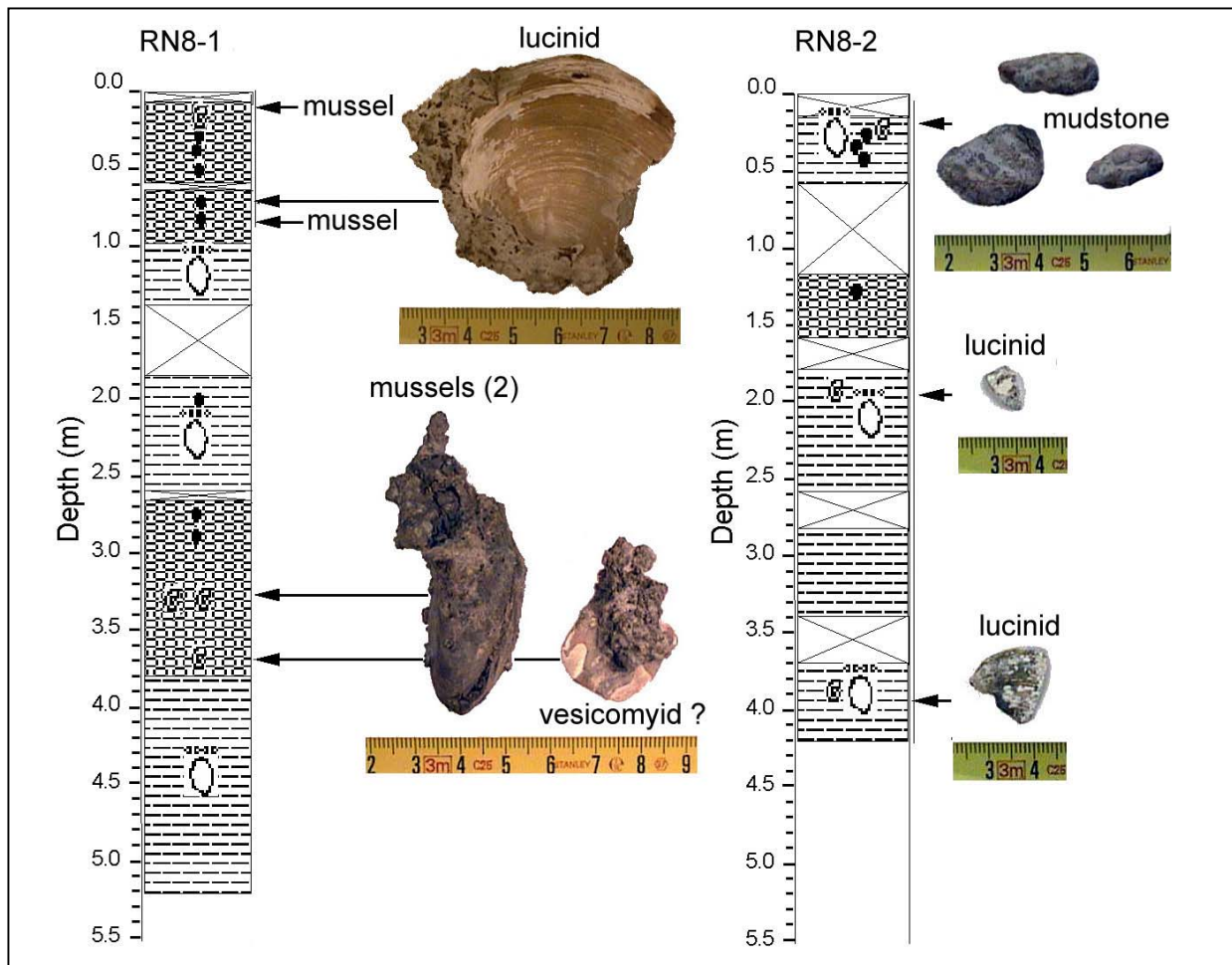
Figure 7.14. Descriptions of piston cores collected at GC233 study site (see Figure 7.12 for locations). The larger shells or shell fragments are depicted with their positions within the cores indicated. See Table 7.6 for 14C ages of shells. Sediments comprised stiff clay or looser mud.

The cores do show layering and chemosynthetic occupation at the site. Carbon dating of the recovered shell material provides an indication of the ages of substrata around pool (Table 7.6). However, interpretation is somewhat problematic due to contamination with ancient carbon that is depleted in $^{14}$C. To have a baseline for comparison, shell samples were taken from living specimens at GC233 and GC185. Each shell from the living specimens was sub-sampled from the umbo and the ventral margin to determine ages for the oldest and youngest parts of the shells, respectively. These results show $^{14}$C "age" at settlement of 2020 y BP for a 120 mm mussel from GC233 and 1760 y BP for a 91 mm mussel from GC185. Because a zero age mussel could not have had an age of approximately 2000 y, these values indicate incorporation of bicarbonate from a source depleted in $^{14}$C. The result is somewhat problematic because the slightly negative $\delta^{13}$C values do not appear to balance the dilution of modern carbon if one assumes that living mussel soft tissue will have strongly negative $\delta^{13}$C values. Also there is a fractionation with age of about one per mill between the young and old values. However, it is highly suggestive that both specimens are near the asymptotic lengths found in their respective populations and should therefore represent the maximum age of the population. Strikingly, carbonate from the ventral (youngest) margin of both specimens exhibited $^{14}$C ages about 200 y older than the umbo. This is

consistent with the maximum ages estimated from previous growth studies of seep mussels (Nix *et al.* 1995). Additional analysis and modeling would be required to model the carbon pools utilized by mussel shell growth. The apparent ages do provide a minimum age, which could be subtracted from fossil material to approximate a more accurate age.

Table 7.6. Shells collected from living mussels (SEA-LINK) at GC233 and GC185 sites and in piston cores from GC233 site. Shell samples from living specimens were taken from the umbo and ventral margin to compare, respectively, the oldest and youngest portions of the shell. Living mussel from GC233 (BP outer) was 120 mm; living mussel from GC185 was 91 mm. Figure 7.14 shows relative positions within cores — at least three bivalve species were found. Ages estimated by $\Delta^{14}C$ (accelerator mass spec. determination). Stable carbon isotopes ($\delta^{13}C$) are a check on carbonate source.

| Site (Station) | Collection Method | Stratum depth m (specimen type) | $^{14}C$ Age (y BP) | Error (y) | $\delta^{13}C$ |
|---|---|---|---|---|---|
| GC233 (BP outer) | SEA-LINK | 0.0 (umbo) | 2020 | 35 | -6.77 |
| GC233 (BP outer) | SEA-LINK | 0.0 (margin) | 2220 | 35 | -7.77 |
| GC185 (BHM1) | SEA-LINK | 0.0 (umbo) | 1760 | 40 | -1.66 |
| GC185 (BHM1) | SEA-LINK | 0.0 (margin) | 1950 | 35 | -2.46 |
| | | | | | |
| GC233 (RN8-2) | piston core | 2.80 (lucinid) | 13750 | 35 | -2.78 |
| *GC233 (RN8-2) | piston core | 2.80 (lucinid) | 13750 | 30 | -2.65 |
| GC233 (RN8-2) | piston core | 4.00 (lucinid) | 14850 | 35 | -1.55 |
| | | | | | |
| GC233 (RN8-1) | piston core | 0.05 (mussel) | 7270 | 40 | -1.97 |
| GC233 (RN8-1) | piston core | 0.70 (lucinid?) | 17450 | 55 | -22.89 |
| GC233 (RN8-1) | piston core | 0.85 (mussel) | 12200 | 35 | -1.11 |
| GC233 (RN8-1) | piston core | 3.40 (mussel) | 15800 | 40 | -2.3 |
| GC233 (RN8-1) | piston core | 3.40 (mussel) | 16200 | 50 | -5.16 |
| GC233 (RN8-1) | piston core | 3.69 (vesicomyid ?) | 16800 | 45 | 6.07 |

*replicate

With these caveats, the apparent ages of the fossil shell material from the cores show reasonably consistent trends. The strata in core RN8-2, closest to the brine pool and mussel community, have ages of 13750 y BP at 2.8 m subbottom and 14850 y BP at 4 m subbottom. These ages are in excess of what could be explained by burial through sedimentation at rates typical of the upper slope (10 cm per 1000 y). Similarly, strata in core RN8-1 show increasing age with depth. One outlier in the trend has excessively negative $\delta^{13}C$ values. Radiocarbon ages in shell material from the cores suggest prolonged occupation of this site by chemosynthetic animals over the past 10 to 13 x $10^3$ y. Relative differences in the apparent ages of the strata, and the depth of the strata, are consistent with episodic burial events related to discharges from the brine pool feature. Brine Pool NR-1 appears from these data to be an ancient site, continually occupied by chemosynthetic bivalves, but subject to major perturbations over time. The length of time that the pool

community has been in its present state cannot be estimated from the core stratigraphy. The best evidence for recent stability comes from the properties of the brine and the age structure of the mussel population.

Seepage of gas is continuous through the northern end of the pool at the GC233 site, but has been reduced to a few sparse streams of bubbles. Temperature profile through the upper part of the pool (Figure 7.15A) shows a fluid column that is sharply stratified by salinity and temperature. Fluid samples indicate that the maximum conductivity values correspond to a salinity of 130 PSU. The abrupt increase at the brine water interface indicates a fluid volume that is at near equilibrium with the overlying seawater. Mass and thermal fluxes across the interface appear to be dominated by diffusive rather than advective processes. A second, sharper thermocline beginning about 2 m below the brine surface corresponds to an abrupt decrease in conductivity and to a marked increase in amount of suspended sediment in the fluid column. The conductivity effect is an artifact upon the CTD instrument produced by the suspended sediment. Similar temperature profiles in the pool have been measured in 1991, 1992, and 1998, indicating recent stability of the pool's density structure. The persistence of a colony of methanotrophic mussels and their uniform distribution around the pool is further evidence for long-term stability of the feature. The presence of a mussel whose age may be as great as 200 y on the outer portion of the mussel bed surrounding the pool suggests that the pool has not erupted or overflowed in recent history. However, if the supposition of episodic eruptions is valid, examples should exist of brine-filled pools with much more dynamic behavior. As an example of a more active brine pool and mud volcano, we turn to the final study site examined in this program, namely GB425.
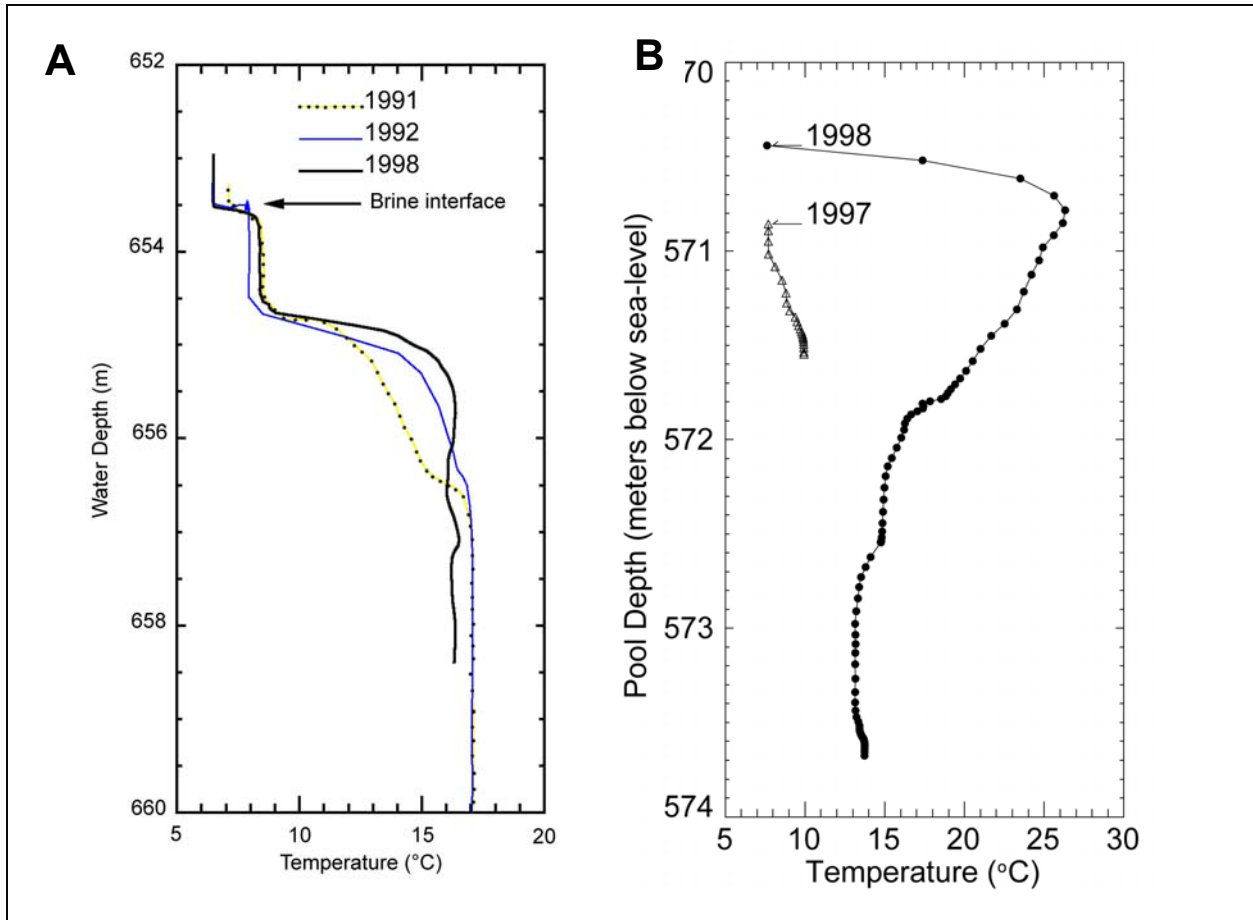
Figure 7.15. Temperature profiles of two brine pools. (A) Temperature profiles in Brine Pool NR-1 (GC233 site) taken at three times over an eight year time span. (B) Temperature profiles in mud-filled crater at GB425 site taken in 1997 ()) and 1998 ( ● ). Temperature profiles shown are from points where oil and gas venting was most evident. Pool depths are relative to sea level. Depths of interface (arrows) were derived from conductivity response of CTD and comparison of pictures that showed change in the height of mud on thermistor mooring tether.

## 7.3.4 GB425

The GB425 site is a mud volcano located at the edge of Auger Basin (Figure 17.16A), an intraslope basin that contains economically significant hydrocarbons in the Auger, Cardamom, and Macaroni fields and is bordered to the west by tabular salt bodies (McGee *et al.* 1993). A tension-leg platform installed at Auger Field is producing from an estimated 100 million barrels of extractable oil (Shew *et al.* 1993), but large quantities of pressurized fluid have evidently escaped through anticline faults along the flanks of the salt at the basin margin. Sediment cores from this zone have recovered high-molecular weight hydrocarbon and thermogenic gas hydrate. Fluids migrating up these faults disturb surface sediments due to the formation of carbonate nodules, oil and gas pockets, and biogenic debris. These anomalies are readily detectable by seismic and acoustic imaging (Figure 17.16B).
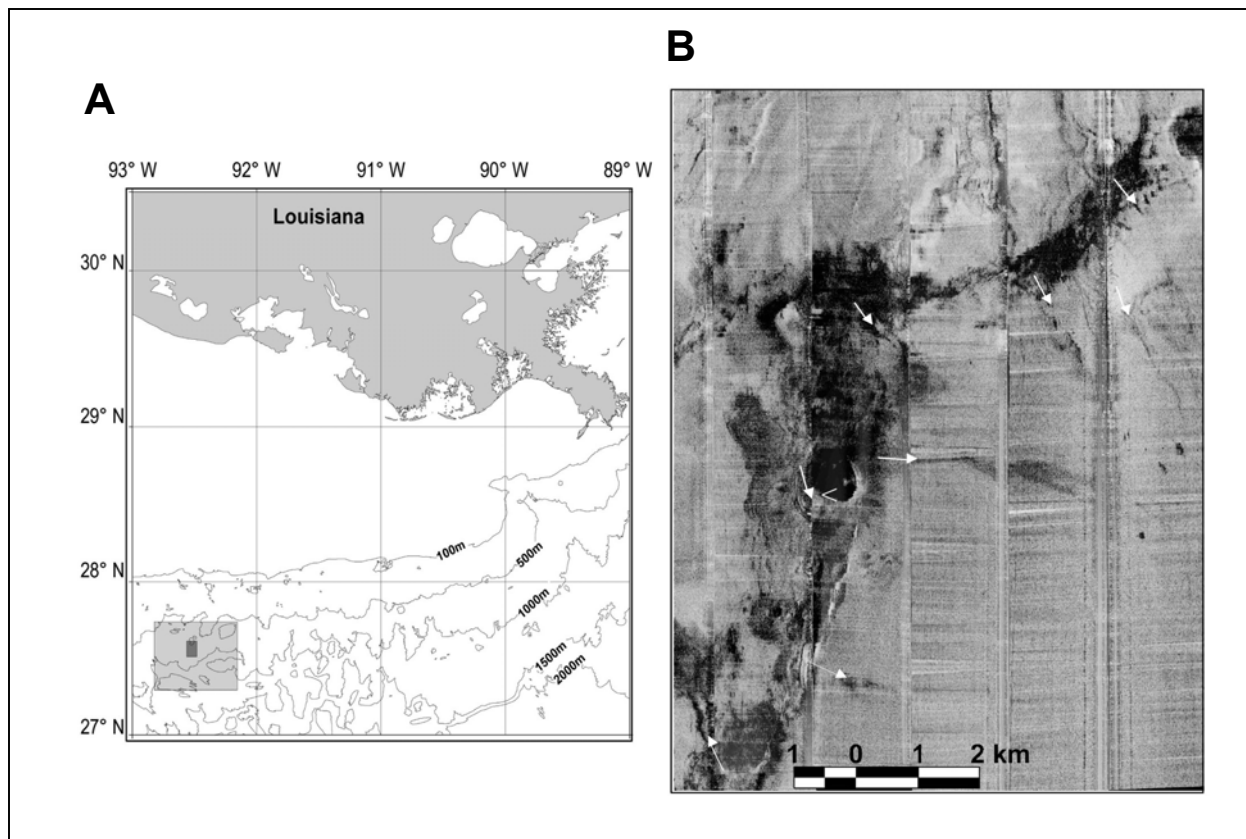
Figure 7.16. Regional setting for study site in GB425. (A) Larger stippled box shows the area that was covered in satellite remote sensing (SAR) images (Figure 7.19) while the inner stippling shows coverage of a side scan sonar mosaic and of SAR sub-scenes (Figure 7.20). (B) Mosaic of 75 kHz side-scan sonar tracks shows acoustic texture of western Auger Basin. Production facilities for Auger oil field are centered approximately 6 km to the east. A salt wall and fault system border the basin to the west and northwest. Migration of fluid along the flanks of this salt unit provides natural release of pressures accumulated within the basin. Seafloor mounds, mud flows (arrows), and slump scars indicate dynamic material fluxes at numerous points along the fault. The study site is situated at a small, active diatreme on the southern margin of a flat-topped mound located mid-way along the fault (<).

Active fluid expulsion is localized in a 50-m wide, sub-circular crater on the southwestern edge of the summit, which is one of two such vents on the mound (Figure 7.17A). Fine, fluidized mud overflows the northeastern margin of the crater and moves down the southern flank of the mound. The mud is fluidized in hypersaline brine (133 practical salinity units) that is supersaturated with methane at STP. Beds of the seep mussel rim the southern edge of the crater (Figure 7.17B).

The mud lake at GB425 was sampled with use of the SEA-LINK on 29 July 1997 and 11 July 1998. On the first visit a thermistor was suspended below a float anchored on a short tether. It recorded a reading every 20 min. The anchor was attached to a 75 by 75 cm plate to prevent it from sinking in the soft mud of the crater bottom. Samples of brine and mud were collected with use of a chamber that the SEA-LINK positioned below the fluid-seawater interface and sealed for recovery. The brine had a salinity of 133 practical salinity units. The fluid degassed violently

when the collection chamber was opened on the surface, indicating that gases were super-saturated with respect to sea level temperature and pressure. The gas that evolved was less than 99% $CH_4$. Solvent extractions of sediments suspended in the brine contained high-molecular weight hydrocarbons, as did sediments collected in short cores. Exposed deposits of gas hydrate were observed around a gas vent (M2) that was located about 150 m northeast of the lake.

Visual observations indicated that gas and oil discharges were minor in 1997 and the feature appeared less active than had been previously noted. In 1998, however, a continual stream of small gas bubbles and drops of oil emanated from the central diatreme, while bursts of larger bubbles, oil drops, and suspended sediment periodically escaped from the surrounding mud. Although drops of oil were observed reaching the sea surface, this flow did not generate a conspicuous slick. In 1997, a thermistor was suspended 30 cm below the interface at a position about 15 m west of the apparent vent. When the thermistor was recovered in 1998, the apparent level of mud in the pool, as measured by its height on the mooring tether, had risen by 50 cm (Figure 7.18).

On both occasions, a temperature profile was recorded by lowering a CTD into the fluid. The 1997 profile penetrated only 0.7 m into the muddy fluid (Figure 7.15B). In 1998, however, active venting pointed the way to a deeper part of the lake and the CTD was lowered 3.2 m below the interface (Figure 7.15B). Changes in characteristics of pooled fluid over the ~1 year interval demonstrate increased flow. In both profiles, abrupt increases in conductivity demarcated a ~1 cm interface between the fluid mud and overlying seawater. In 1997, convective cooling across this interface produced the monotonic 2.7°C decrease in temperature between the pool bottom and the interface. In 1998, a subsurface maximum temperature of 26.7°C at 34 cm below the interface and the apparent rise in the level of mud in the pool, provide evidence for discharge of warm mud that spread in a surficial layer, eventually flowing downslope from the mud lake outlet. Similar sheet-flows of mud would have been required to form the flow-fields evident in the side-scan sonar (Figure 7.16B).

Changes in the fluid properties of the mud lake over a one-year period indicated episodic activity related to fluid discharge. The geologic evidence of mud slides and the formation of large flat-topped structure points to ongoing and massive fluid expulsion. Episodic events are difficult to capture with sampling cruises of a few days separated by months or years. To provide independent data on fluid discharge at GB425 and from the region as a whole, available satellite synthetic aperture radar (SAR) data were reviewed in collaboration with scientists from Unocal Corporation. Satellite SAR readily detects layers of floating oil that form over active seeps. It provides a means to survey the numbers of hydrocarbon seeps across oil-producing regions and to estimate the rates at which seeps are flowing. Comparison of SAR images collected in the Gulf of Mexico (Figure 7.16A) indicates large differences in the amount of oil seepage over short time lags (Figure 7.19). These changes are too great to be attributed to different sea surface conditions. Seafloor measurements from the mud volcano explain how large short-term differences in seepage might occur.
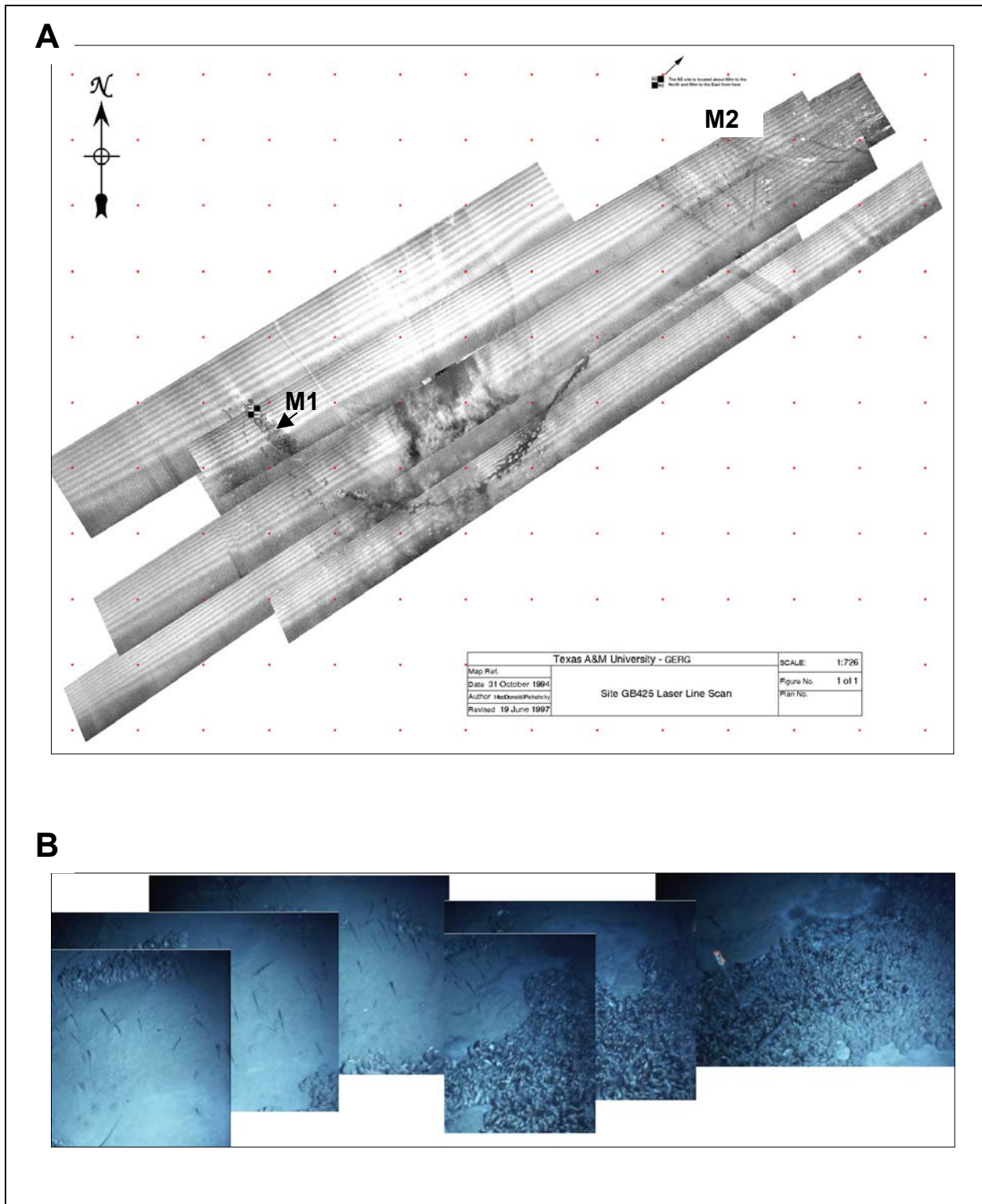
Figure 7.17. Mud-filled crater at GB425. (A) Laser line-scan mosaic of GB425 brine pool, showing location of M1 sampling station (grid points are at 10 m centers). M1 station is located approximately 150 m to the northeast. Mussel beds are restricted to southwestern (upslope) end of pool. (B) Photomosaic of M1 station looking south. Note marker float.
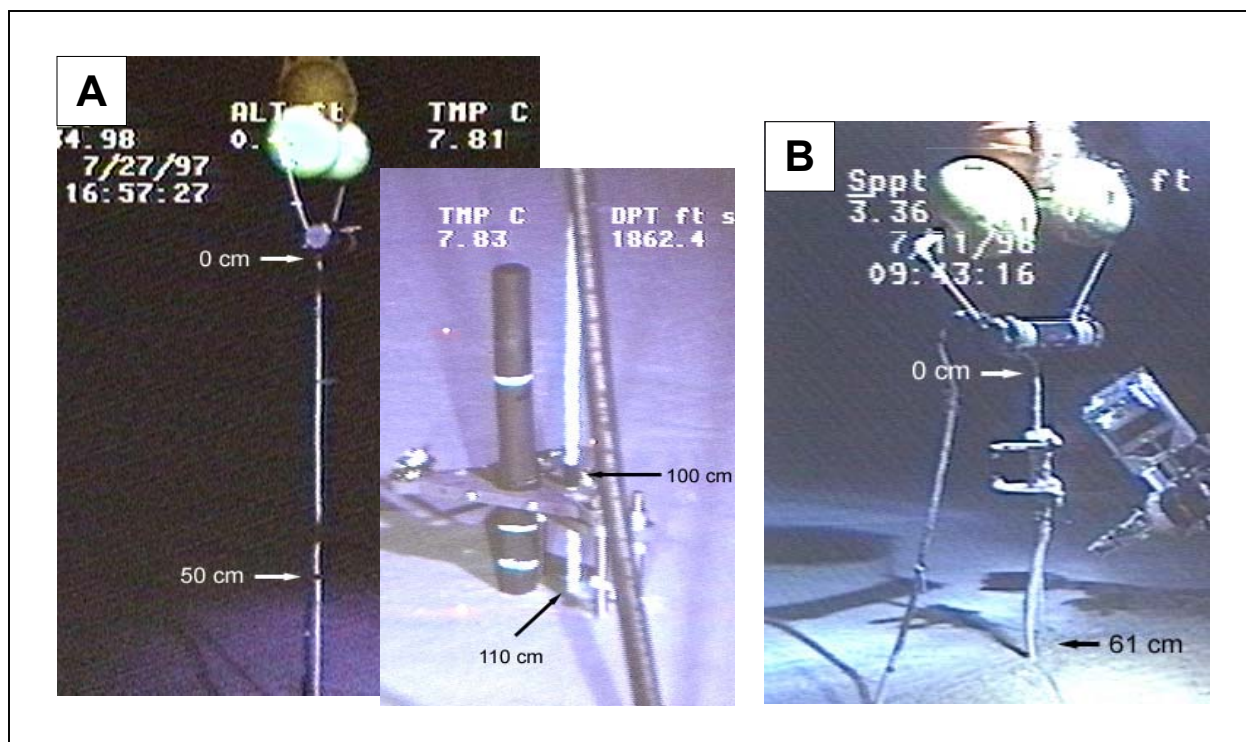
Figure 7.18. Thermistor array deployed in mud filled crater at GB425. (A) Distance between float and mud interface was 110 cm eight hours after deployment. (B) Distance was reduced to 61 cm when device was recovered one year later, apparently due to an increase in the level of mud in pool.

Available time-series data from the 1997 through 1998 periods at GB425 comprised six SAR images and the records from the thermistor (Figure 7.20). Three of the SAR images were collected in May and June 1997, prior to deployment of the thermistor; three were concurrent with the deployment. The area of oil slicks overlying the fault zone repeatedly underwent order of magnitude changes between the May 1997 and the February 1998 observations (Figure 7.20B). During the 349-day thermistor deployment, fluid temperatures varied between 6.1° and 48.3°C with a mean of 26.1°C and standard deviation of 9.07.

Some fresh oil can be seen surfacing in SAR images near the location of the diatreme (Figure 7.19 inset). Although lateral offsets of ~1000 m are typically seen between a sea-floor vent and the location where rising oil reaches the sea surface (MacDonald et al. 1996), only a portion of the oil slicks that were detected could have originated from this specific source, because the analyzed portions of the SAR images covered a much wider area than the vent. Much additional oil presumably came from other discharge points along the seep-affected zone (Figure 7.16B); some may have drifted into the scene from sources external to the study area. Temperature data confirm pulsed flow at a point source within the zone. SAR data indicate that these flows were part of a regional pattern of discharge. Active seepage has not been identified in this region during remote sensing surveys (MacDonald et al. 1996, Mitchell et al. 1999). Therefore, the floating oil detected by satellite SAR during 1997-98 represents a higher level of seepage activity than was previously known from the locality.
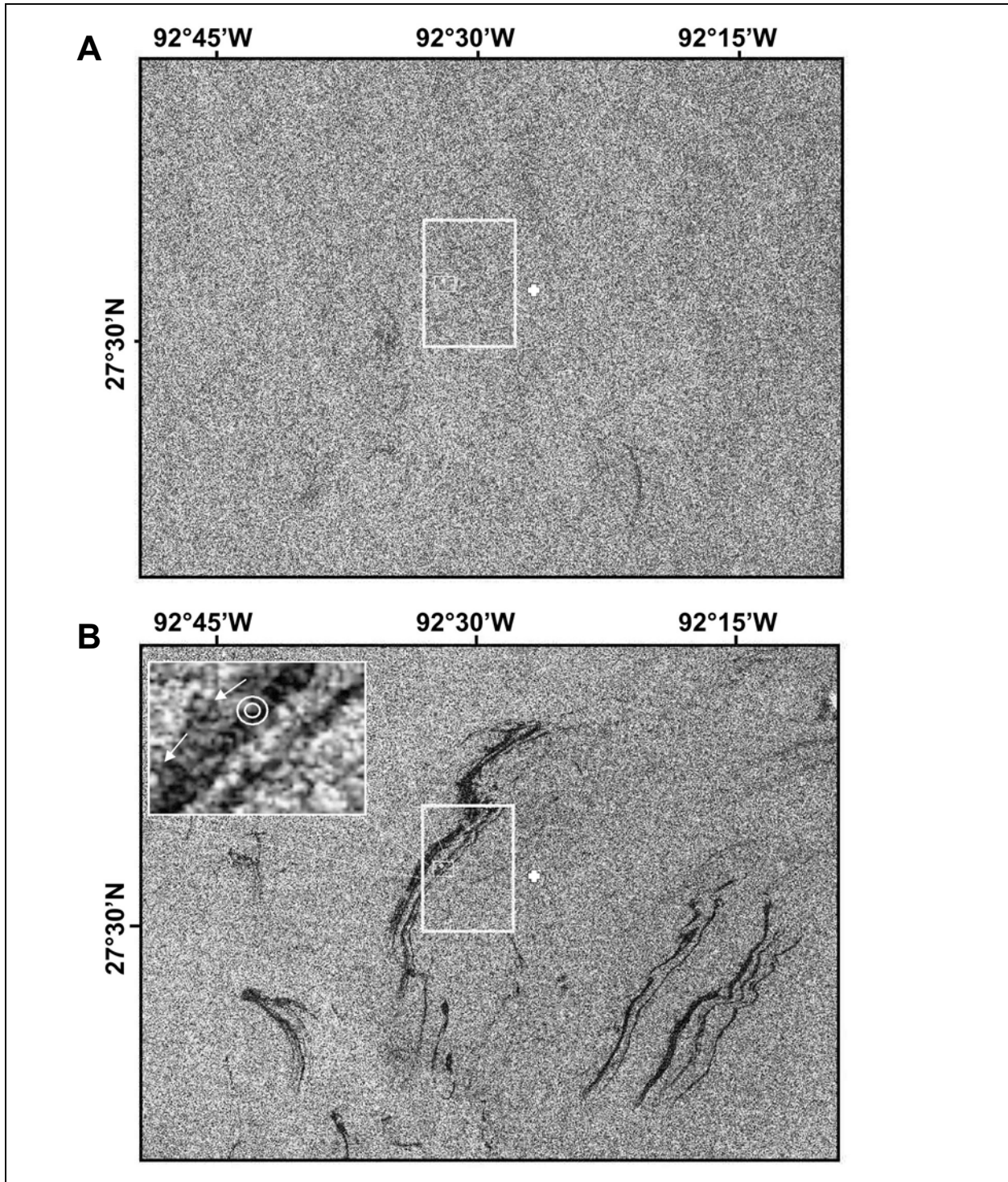
Figure 7.19. Synthetic aperture radar (SAR) images (collected by RADARSAT) provide a means to compare the size of natural oil slicks on 29 July (A) and 11 August 1997 (B) on the sea surface immediately above the GB425 site. Outlines in both images indicate area overlying Auger Basin fault (Figure 7.19B) that was analyzed in detailed studies of slick area (Figure 7.20) and show the location of mud volcano. Inset image details fresh oil surfacing close to the seafloor location of the site. Cross-marks indicate location of Auger platform.
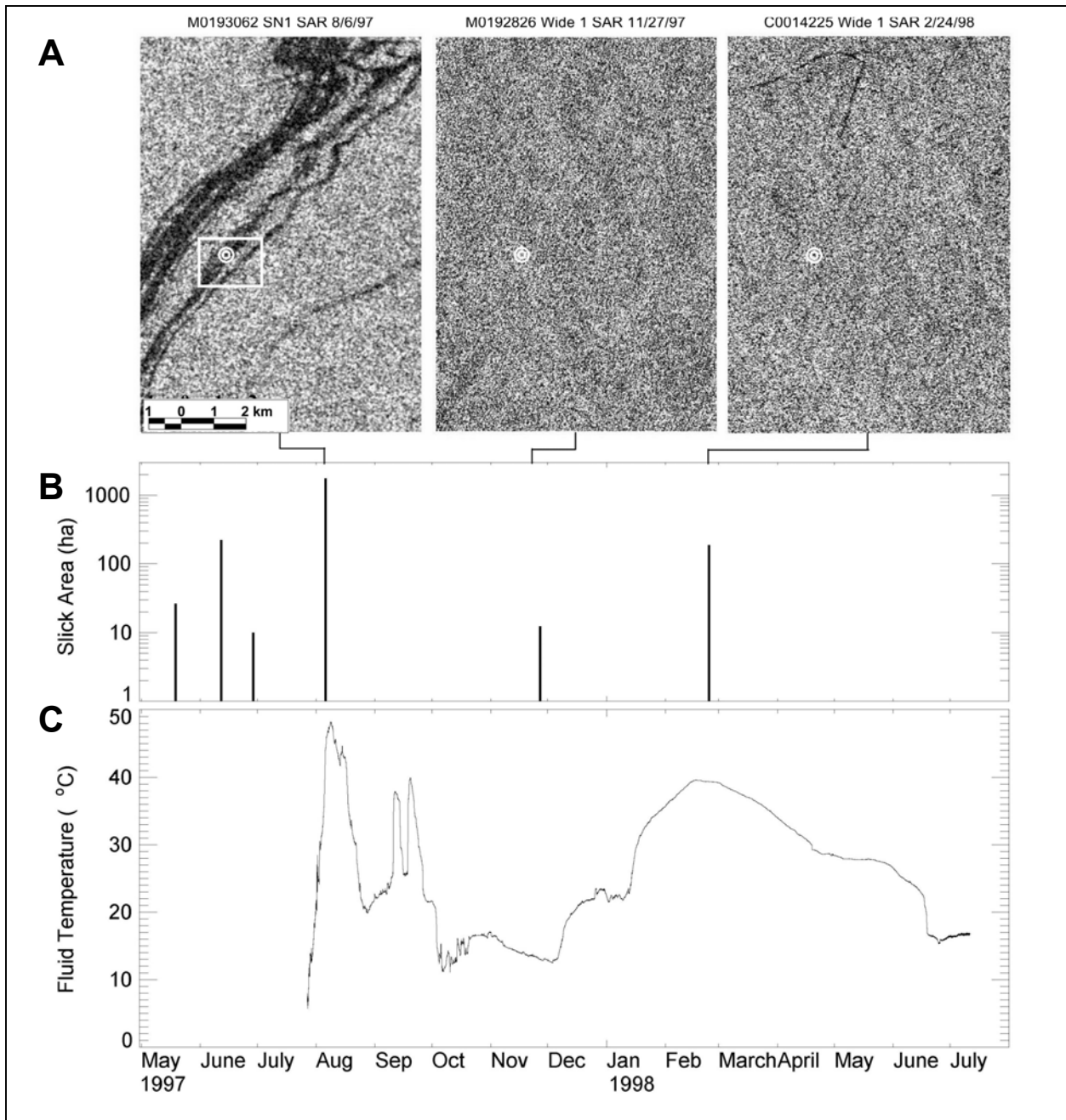
Figure 7.20. Comparison of temperature time series to abundance of floating oil above site. (A) Three sub-scenes of SAR data are reproduced to show, from left to right, large-, small-, and medium-size oil slicks. (B) Time series of slick areas (in hectares) imaged by available SAR. Slick areas were compiled for an 18.7 by 13.1 km region overlying the Auger Basin fault zone (Figure 7.19). (C) Temperature time series from fluid in diatreme recorded between 27 July 1997 and 11 July 1998.

Previous studies of mud volcano systems have identified pulsed flow in sealed boreholes based on temperature increases of at most 4°C over periods of months (Carson and Screaton 1998). Seafloor temperature anomalies recorded in diatremes have been ascribed to shallow convection within mud-filled chambers, perhaps driven by dissociation of gas hydrates (Henry *et al.* 1996). The extreme, rapidly fluctuating temperature of pooled fluids reported here, and the coincidence of large oil slicks, demonstrate energetic flow from considerable subbottom depth. Vertical transfer of geothermal heat is intensified in the presence of subbottom halite (McBride *et al.* 1998), so the rate of increase in subbottom temperature is likely to be greater in the vicinity of the salt unit bounding Auger Basin. The temperature in a borehole, located approximately 8 km northwest of the mound over shallow salt, was 48°C at 2309 m subbottom. This suggests that fluids with temperatures recorded at 48°C in the diatreme would have leaked from at least this depth.

Present results mitigate against two processes that could explain occurrence of pulsed flow in this fluid expulsion feature. Gas hydrate layers trap large quantities of free gas in marine sediments (Dickens *et al.* 1997). In the Gulf of Mexico, where massive gas hydrates occur near the seafloor, precipitous failure of these deposits will release quantities of oil and gas (MacDonald *et al.* 1994). Although gas hydrate has been collected from the flank of the mound peripheral to the mud vent, it cannot act as a fallible seal in the diatreme because, at pressures of ~5 to 20 megapascal, the high temperature and salinity of the fluidized mud would prevent gas hydrate from forming (Sloan 1989). Some evidence suggests that earthquakes stimulate the activity of marine hydrocarbon seeps (Macgregor 1993). Although the continental slope of the northern Gulf of Mexico is not a seismically active region, many faults on the slope intersect and offset the seafloor (including the fault on which this fluid expulsion mound lies), which indicate ongoing activity (Rowan and Weimer 1998). There is no record, however, of significant seismic activity in the northern Gulf of Mexico during 1997-1998.

The expulsion episodes described by the present data are part of an ongoing process that has prevented formation of commercial hydrocarbon reservoirs in the western portion of Auger Basin. Rejecting the possibility of gas hydrate dissociation or seismic activity, one can speculate that pulsed flows result when ongoing filling of hydrocarbon traps in western Auger Basin induces the failure of the permeable seals in the fault zone, injecting gas, oil, brine, and mud into surface strata and the ocean. Previous remote sensing surveys have depended on repeated detection of floating oil to confirm flowing seeps (Kornacki *et al.* 1994, MacDonald *et al.* 1993, MacDonald *et al.* 1996, Mitchell *et al.* 1999). This criterion would have overlooked seeps like the one described here. These results suggest that the time-dependence of seepage rates should be considered when remote sensing results are used for evaluating the hydrocarbon potential of a new basin or extrapolating to estimate a regional seepage rate. Such studies are needed to constrain the balance of hydrocarbon generation, entrapment, and natural seepage into the biosphere.

## 7.4 Conclusions

This chapter examined the distribution of chemosynthetic animals and geologic features associated with hydrocarbon seepage and fluid discharge at the four study sites. Results indicated

that temporal and spatial variability in chemosynthetic communities have distinct styles and characteristic scales. Temporally, the main process that causes short-term variation at the sediment-diffusion style sites (GC185 and GC234) appears to be formation and dissociation of gas hydrate outcrops. These features can wax and wane over periods of a few months and cause major upheavals to local sediment. Mounds, pockmarks, and small fissures are local and transient features that can be ascribed to gas hydrate formation and dissociation. There is little data resulting from this study to constrain the variability of sediment-diffusion communities over longer timeframes — although the extreme longevity of tubeworms described elsewhere in this report (Chapter 8) is clear evidence of longer-term stability. A much broader spectrum of temporal variability was found in the brine-pooling sites. Satellite evidence of oil venting and temperature fluctuations in the GB425 mud volcano indicates rapid cycling of fluid expulsion activity over periods of days or weeks. Brine pools are also able to come to a dynamic equilibrium between gas venting, fluid mixing, and molecular diffusion, as the temperature profiles from GC233 demonstrate. The result is establishment of extremely steep gradients that evidently persist relatively unperturbed for years or tens of years. Over geologic time, fluid expulsion can remain focused in zones a few meters across.

Spatially, communities at the so-called brine pooling sites were tightly constrained by the discharge and pooling properties of expelled fluids. The mussel beds at these sites exhibited markedly higher densities — at a community scale — than were found in the sediment diffusion sites. Mussels were concentrated along gradients defined by the edges of standing bodies of methane-saturated fluids. Overflow patterns sharply constrain the habitable area around brine pools. The result is communities focused into a few large and dense patches with well-defined boundaries. Sediment-diffusion sites are characterized by generally smaller and more widely dispersed patches scattered over much greater areas. Although boundaries defined by fluid migration processes are evident (for example, the transition between stratified sediments and wipeout zone in GC234), they are blurred by the distribution of chemosynthetic animals. Linear trends were evident at GC185 and GC234, reflecting alignment with fault traces. However, the bulk of the chemosynthetic biomass was displaced away from the high-amplitude regions above the most active regions of the faults and showed a distinct prevalence for sediment with low seismic amplitude. The across-trend dimension of the two sites studied was on the order of 50 to 100m, while the along-trend dimension was several-fold greater.

For management concerns, these patterns indicate that different approaches should be used to evaluate the regions requiring protection depending on whether the seepage style is dominated by focused flow in mud volcano-like features or by diffuse migration along fault planes. In the former case, chemosynthetic communities could be effectively avoided by defining the axes of discharge and, from available evidence, the total area of concern would be relatively small. In the latter case, geophysical evidence could be used to help define zones where chemosynthetic animals could occur, but these zones will be larger and may lack distinct boundaries.

# 8.0 Ecology of Seep Fauna

## 8.1 Introduction[*]

The Gulf of Mexico seep communities exist as a direct consequence of the biological oxidation of the energy-rich pore fluids seeping from the sea floor and the concomitant production of biomass. The organisms responsible for this production are chemoautotrophic and methanotrophic bacteria. These bacteria exist as free-living cells throughout the seep environment and also occur as thick mats on the sediment or other surfaces. Chemoautotrophic sulfide-oxidizing bacteria also occur as symbionts in several different invertebrates, most notably vestimentiferan tubeworms and several species of mussels and clams. The dominant mussel at these sites, *Bathymodiolus childressi*, harbors symbiotic methanotrophic bacteria. In each of these cases, the symbiotic bacteria provide the overwhelming bulk of the host's nutritional needs, making the animals themselves chemoautotrophic in a sense.

Three overlapping types of communities are present in the primary areas that were a focus for this study. Bacterial mat communities are apparent both separated from and immediately adjacent to aggregations of other types of seep fauna. These mats can be quite extensive in both size of individual mats and abundance of mats at a site. Because the mats produce organic biomass and oxidize potentially toxic substrates, they are potentially important primary producers and detoxifiers for the seep ecosystem. Tubeworms and mussels, because of their autotrophic lifestyle, gregarious settlement behavior, and relatively large size, are ecosystem engineers. As such, they create substantial areas of habitat for numerous other species of endemic and non-endemic animals. Tubeworm and mussel communities can be relatively small or can completely cover areas up to thousands of square meters. Each can occur where the other is absent, or they can co-occur, each literally growing on one another.

One of the long-term goals of the Minerals Management Service's programs to study seep communities has been to develop an understanding and appreciation of these relatively poorly known and recently discovered communities. The hope is to provide the knowledge base for well-informed management decisions. Over the past fifteen years, many other projects have also contributed to the database on these and related communities. However, only recently has there been available sufficient information to put together a cohesive picture of the biology and ecology of the seep animals. The present study specifically built on what was known about the physiology, genetics, and ecology of the three key faunal groups (bacteria, tubeworms and mussels) to build and test working models of the animal's life histories and the communities they form. In some cases, studies were designed to address very fundamental physiological or genetic questions important to understanding the animals. In other cases, studies were designed to test system-level concepts arising from developing models of community succession, larval dispersal, or niche differentiation.

To the greatest extent possible, experimental design included integrated sampling between the different components of the overall project. For example, before a mussel bed was sampled, water samples were taken from beneath and over the mussels for chemical analysis. The bed

---

[*] This section was authored by Charles R. Fisher

was then sampled in a quantitative approach that allowed the biomass and size of all inhabitants to be determined and the biomass of the entire bed to be calculated from photographs or mosaics. Each collection was further sub-sampled for all appropriate components (i.e., condition analyses, PAH tissue load determination, histopathology, population genetics, stable isotope food-web studies, and in some cases growth or transplant studies). This greatly enriched the interpretation and future usefulness of each individual study and is also an ecologically sound approach to obtaining the maximum amount of knowledge with minimal impact on the populations.

Over the course of the program, numerous discoveries were made that fundamentally changed the views of the animals and the working models of these communities. Many of the studies remain ongoing because early results led to new directions and/or development of new techniques. Finally, as discovery usually does, the results of these studies spawned new and important questions that were not anticipated when the program was initiated.

Each of the separate studies presented in this chapter produced findings that have important implications for management decisions even when considered in isolation. These findings and studies are briefly highlighted here. More discussion of these discoveries and the related studies that have contributed to the working models are contained in the synthesis chapter of this report (Chapter 11).

Section 8.4 details the key discovery that the two species of tubeworms are extremely long-lived, in fact, the longest lived animals known to exist on the planet. This is in direct contrast to the hydrothermal vent tubeworms, which are a very fast-growing, opportunistic species. Because the tubeworms produce the framework for a complex ecosystem, the seep tubeworms are much more analogous to trees in the sense of being long-lived and ecosystem-structuring. As a result, activities that damage well-established communities may have an impact that would last for centuries. In fact, consideration of their long life in light of the non-persistent size distributions in the aggregations suggests that old communities might never recover from serious damage because the time window for vestimentiferan recruitment to the site would have passed.

A second discovery discussed in Section 8.4 is that at least one of these species can acquire sulfide from buried sources and therefore may not require surface expression of seepage (into the water column). This may explain how the tubeworms live for centuries and also why the diversity of non-endemic fauna in these communities is much higher than at hydrothermal vents. It also suggests that the sulfide supporting these communities must be present at depths considerably greater than the depths of sulfide generation from seawater sulfate reduction (see Chapter 9). Thus, hydrocarbon seepage alone (with attendant production of sulfide in very shallow sediments) may not be sufficient for maintenance of large and long-lived tubeworm colonies. Therefore, the source of sulfide necessary to support these communities may be more patchily distributed than hydrocarbon seepage in general.

Section 8.5 demonstrates that the mussel beds in some areas of the Gulf of Mexico were so severely infected with parasites that mussels in these areas are effectively sterile and therefore cannot contribute to larval pool of the *Bathymodiolus childressi* in the Gulf of Mexico. By comparison, mussel populations at other sites were quite healthy. Thus, some populations may be key to the maintenance of the Gulf-wide meta-population, while other sites are inconsequential. The life history of seep mussels is further detailed in Section 8.3.

A finding with implications for heterotrophic fauna is presented in Section 8.6. Results from stable isotope studies show that seep primary production not only supports a higher diversity of animals that are seep endemics or colonists than previously demonstrated, but also that significant amounts of seep primary production are being transferred into the surrounding deep-sea benthos. Of the eight species of larger mobile predators captured and analyzed for this study, individuals of six contained a significant amount of seep carbon and nitrogen in their tissues, indicating continued consumption of seep animals or bacteria over a significant period of time. Thus the seeps are not small islands of productivity inhabited by unique animals to be managed in isolation, but rather they are affecting and being affected by the surrounding deep-sea fauna.

Related to this finding is the discovery that significant numbers of the mat forming bacteria are present in situations when the mats are not visually apparent, and the strong implication that most of the fauna found among the tubeworms are not deriving their nutrition from tubeworm primary production. This finding, which is detailed in Section 8.2, suggests that primary production from free-living seep microbes may be much more important to the communities than usually recognized and underlies how little we know about the microbial ecology of these systems.

The molecular genetics studies, which are presented in Section 8.7, are still underway due to a combination of unforeseeable complications in the samples themselves and in the methodology. However, this work to date indicates that over the areas sampled for this study, the tubeworm and mussel populations are exchanging larvae between sites and therefore can be managed as single, large, meta-populations. Genetic diversity is not at risk through anthropogenic activities in this region. Another key finding is that the symbionts of four Gulf of Mexico tubeworm species are not specific to the host species, but rather to the geographic region where they are found. This strongly supports the hypotheses that the symbionts are not transmitted directly (rather they must be acquired de-novo each generation) and that niche-differentiation between species at a site is not a function of symbiont differences, and further suggests site-specific differences in the bacterial populations at different sites. All of this information contributes to our working models of these species.

Based on our current level of understanding of the biology of the key ecosystem engineers and of the community ecology of the seep ecosystem, we have refined our working model of these communities. It is important to note that in the regions of the Gulf of Mexico where the seep communities occur the larval population is well mixed, and based on other studies, we know that the larvae of key species spend weeks or more in the water column. Thus, colonization and evolution of a new site will follow the same general pattern as colonization and evolution of patches of organisms within an established site, although the increased abundance of mobile consumers at established sites will likely influence the process through biological interactions.

## 8.2 Bacterial Mats[*]

### 8.2.1 Objectives

This section addresses the following objectives:

1. To characterize and compare of the morphology of Gulf of Mexico *Beggiatoa* to ascertain their affinity to ecologically similar groups elsewhere;

2. To examine the dominant energy motifs of *Beggiatoa* with respect to their vertical distribution, their change in internal nitrogen ions, and their impact on sediment sulfide;

3. To verify that *Beggiatoa* are capable of consuming energy sources (e.g., sulfide or methane) at sediment depths up to 10 cm;

4. To assay bacterial mats for diagnostic enzymes.

### 8.2.2 Introduction

Colonies of the bacteria *Beggiatoa* spp. are prominent indicators of hydrocarbon seepage in the outer continental shelf and slope of the Gulf of Mexico. They are among the earliest known chemoautotrophs, and their ability to synthesize new carbon by use of chemical energy obtained by oxidizing $H_2S$ was suspected as early as the late 1880s (Brock and Schlegel 1989). *Beggiatoa* are members of a diverse group of sliding and gliding bacteria that occupy large filaments and have the ability to position themselves along chemical gradients in the upper-most sediments (Larkin *et al.* 1994, Larkin and Strohl 1983, Nelson *et al.* 1989). *Beggiatoa* are very common in Gulf of Mexico seeps. Indeed the present work found that individual filaments were nearly ubiquitous among sediment samples from the study sites and often infiltrated the upper 5-10 cm of sediment cores. *Beggiatoa* are most visible when they form thick surface aggregations, often termed "bacterial mats," on the periphery of seep habitats occupied by tubeworms and mussels (MacDonald *et al.* 1989, Nikolaus 1995). These mats usually extend well beyond the immediate vicinity of tubeworm or mussel aggregations. They are highly visible due to their white or yellowish color and will frequently be encountered in visual surveys of seep localities.

Recently, several studies have been published on natural populations of morphologically diverse marine chemoautotrophic, sulfur-oxidizing bacteria belonging to the genera *Thioploca*, *Beggiatoa*, and *Thiomargarita* (Fossing *et al.* 1995, McHatton *et al.* 1996, Nelson *et al.* 1989, Otte *et al.* 1999, Schulz *et al.* 1999). Individual cells of these uncultivated bacteria are unusually wide ranging from 12 to 750 μm in diameter versus a typical bacterial cell dimension of approximately 1 μm. Each of the wide sulfur-oxidizers examined has been found to contain a central vacuole as the majority of the vital volume of each cell and whenever examined these bacteria have been observed to accumulate nitrate at intracellular concentrations ranging from 40 to 800 mM – roughly 10,000-fold higher than the corresponding ambient concentration. The possession of vacuoles is an extremely unusual bacterial trait, and until the work of Fossing *et al.* (1995) accumulation of nitrate by bacteria was unknown. The physiological role of nitrate, which is presumably stored in the vacuole, has been fairly well characterized for two natural

---

[*] This section was authored by Douglas C. Nelson and Sarah C. McHatton.

populations (McHatton 1998, McHatton *et al.* 1996, Otte *et al.* 1999). It appears these bacteria employ nitrate as an electron acceptor that allows them to fuel their metabolic processes via oxidation of hydrogen sulfide even in the absence of oxygen. This respiratory process, which converts sulfide to elemental sulfur plus sulfate and nitrate to ammonia, allows the studied populations of *Beggiatoa* and *Thioploca* to dominate the top 10 to 20 cm of marine sediments and to reach biomass densities exceeding 1.0 kg wet wt./m$^2$. When dense mats of these bacteria are observed at the sediment/water interface, they are at the one point in their migration cycle where it is possible for them to take up and store nitrate. All of the vacuole-containing, nitrate-accumulating bacteria that have been characterized to date by molecular analysis (Ahmad 1999, Ahmad *et al.* 1999, Teske *et al.* 1999) fall into a very restricted evolutionary affinity group (Cluster 3, Figure 8.2.1), suggesting that they also share numerous other metabolic properties.

### 8.2.3 Results

Based on samples from a number of sediment cores, the dominant Gulf of Mexico *Beggiatoa* populations are in two main width classes, averaging approximately 40 and 80 μm in diameter (Table 8.2.1). Any core taken in the vicinity of the hydrocarbon seeps, regardless of whether a surface mat was present, contained significant biomass of these bacteria distributed over the upper 3 to 5 cm of the sediment (Table 8.2.1). There is some tendency for the depth-integrated *Beggiatoa* biomass to be lower for the sites where no surface mat was present (Figure 8.2.2), but the no-surface-mat core designated GCB3 C9 (Table 8.2.1) has a total biomass and vertical distribution typical for those of the orange and white mats (Table 8.2.1, Figure 8.2.2). For representative samples of the narrower (ca 40 μm) Gulf of Mexico *Beggiatoa* tested, the protein to vital volume ratio (Table 8.2.2) indicates that they contain a non-cytoplasm-filled vacuole as approximately 80% of their vital volume. That is, like the vacuolate strain from Monterey Canyon, they contain only about 20% of the protein predicted if their vital volume was occupied by typical bacterial cytoplasm.

Table 8.2.1. Depth distribution of *Beggiatoa* filaments in Gulf of Mexico cores, 1998.

| Sample | Cell Width (um) | *Beggiatoa* (grams wet wt./ m sq.) by depth interval | | | | | | |
|---|---|---|---|---|---|---|---|---|
| | | 0–1 cm | 1–2 cm | 2–3 cm | 3–4 cm | 4–5 cm | Total | Comments |
| BPB2 C5 | 40 | 1.4 | 0.7 | 0.1 | 0 | 0 | 202 | **No surface mat** |
| BPB2 C7 | 37 | 2.2 | 1.8 | 0.3 | 0 | 0 | 4.3 | dense Orange mat |
| BPB3 C7 | 40, 81 | 6.1 | 3.5 | 2.3 | 0.7 | 0 | 12.6 | Orange mat |
| GCB1 C3 | 38 | 4.7 | 2.9 | 2.3 | 1.1 | 0.7 | 11.7 | White/Orange mat |
| GCB1 C4 | 44, 80 | 8.4 | 1.5 | 1.5 | 0.2 | 0.2 | 11.8 | great Orange mat, **harvested** |
| GCB2 C7 | 41 | 4.1 | 2 | 1.5 | 0.5 | 0 | 8.1 | Orange mat, **harvested** |
| GCB3 C1 | 42 | 9.2 | 5.3 | 2.6 | 1.4 | 0.7 | 19.2 | great Orange mat, **harvested** |
| GCB3 C2 | 42, 81 | 7.6 | 3.8 | 2.1 | 0.8 | 0.5 | 14.8 | White/Orange mat |
| GCB3 C9 | 40 | 4.8 | 3.2 | 1.8 | 1.3 | 0.3 | 11.4 | **No surface mat** |
| GCBXC1 C3 | 37 | 2.6 | 0.4 | 0.4 | 0 | 0 | 3.4 | **No mat, box core** |

Table 8.2.2. Evidence that 37 – 44 μm wide *Beggiatoa*
from Gulf of Mexico have vacuoles that lack typical bacterial cytoplasm.

| Beggiatoa sample | Filament Diameter | Central Vacuole? | Protein Vital volume $(mg/cm^3)$ |
|---|---|---|---|
| <u>Control</u> strain MS-81-6 (pure culture) | 4 μm | No | $121 \pm 17$ (n = 12) |
| GCB2 C7 Gulf of Mexico Seeps | 43 μm | Yes | 25 – 27 |
| Monterey Canyon Seeps | 75 μm | Yes | 24 |
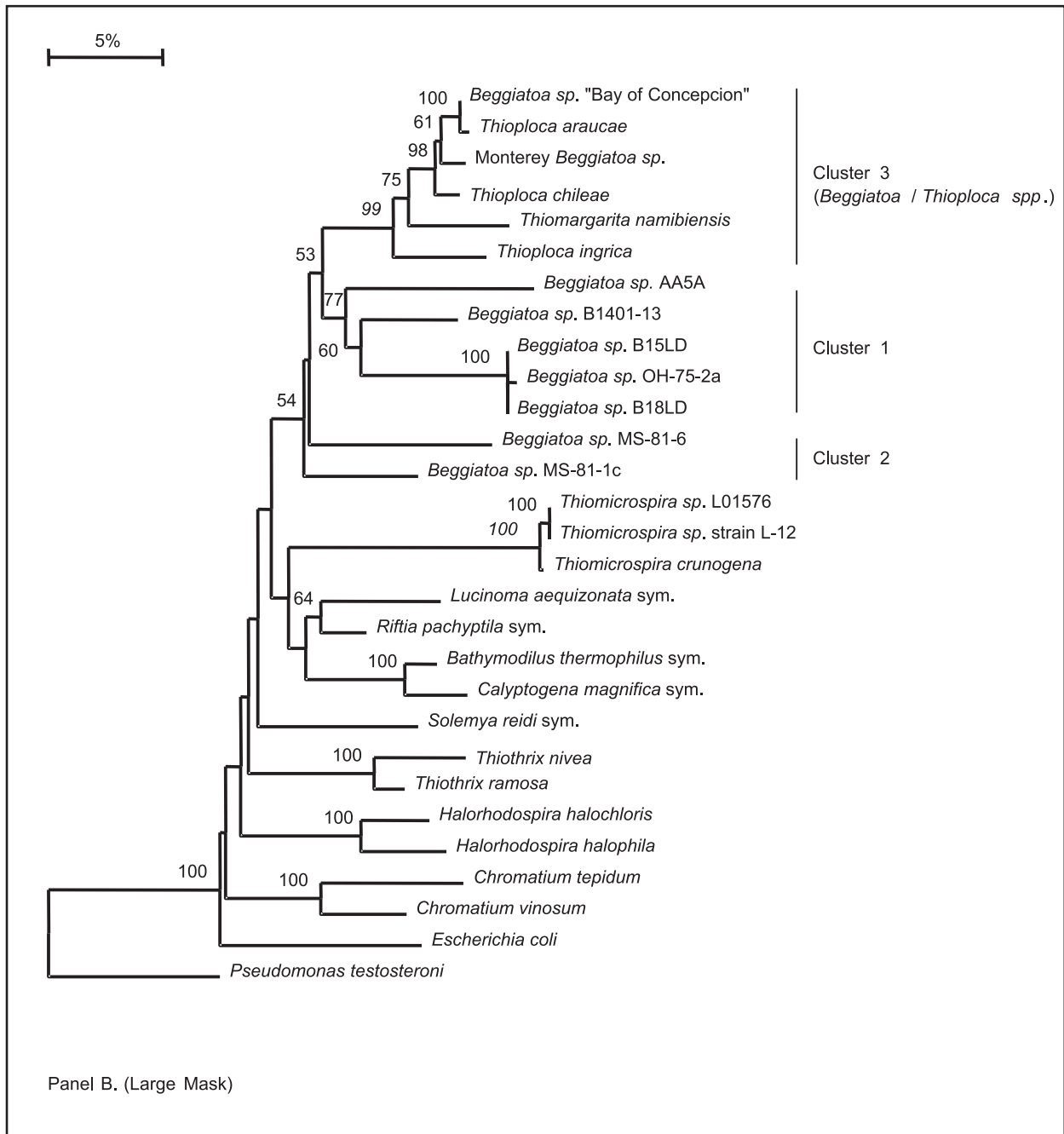
Figure 8.2.1.    Evolutionary relationships among selected members of the gamma *roteobacteria* as determined by 16S rRNA sequencing (Ahmad 1999, Ahmad *et al.* 1999). The majority of the strains shown are autotrophic sulfur bacteria. Cluster 3 includes all vacuolate sulfur bacteria known to accumulate intracellular nitrate. Clusters 1 and 2 include all known sequences for, respectively, non-vacuolate freshwater and non-vacuolate marine pure cultures of *Beggiatoa* spp.
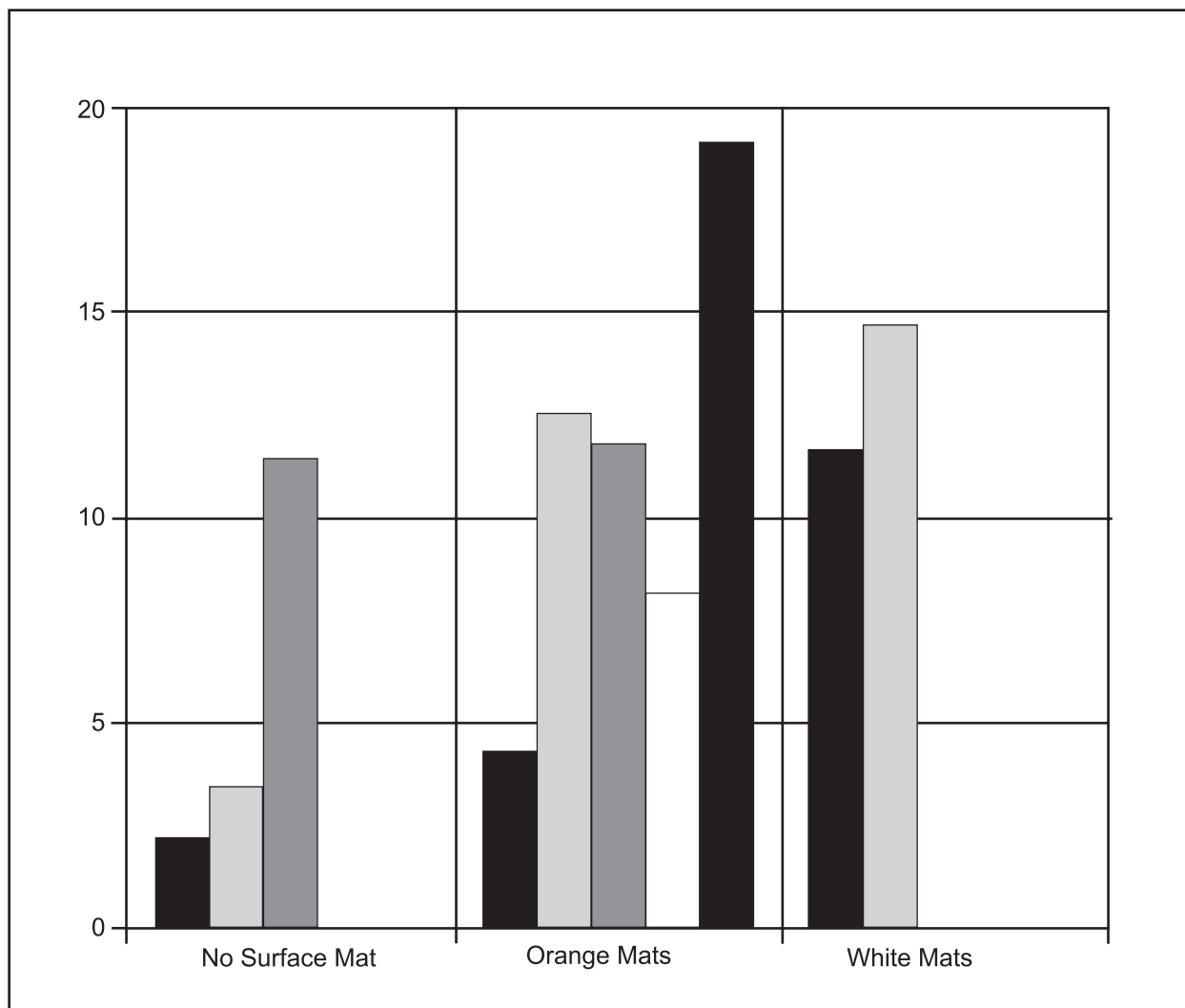
Figure 8.2.2. Depth integrated *Beggiatoa* biomass (0 to 5 cm) for 10 representative cores from Gulf of Mexico hydrocarbon seeps. Groupings depend on color of surface *Beggiatoa* mat or its absence. Sites and biomass versus depth details are presented in Table 8.2.1.

Table 8.2.3 summarizes the physiological properties for surface *Beggiatoa* populations taken from various Gulf of Mexico cores. All populations tested accumulated nitrate to internal concentrations of 8 to 110 mM when averaged over their entire vital volume (cytoplasm plus vacuole). Activity of the enzyme alpha-ketoglutarate dehydrogenase (AKGdH), indicative of the ability to oxidize organic matter by the Kreb's cycle (also called the citric acid cycle or TCA cycle) was present in three of the eight samples tested. It was present in some, but not all, orange mats tested and in the one mixed orange/white mat tested. However, it was not detected in the only pure white mat tested (Table 8.2.3). The enzyme ribulose-1,5-bisphosphate carboxylase/oxygenase (RuBPC/O), diagnostic for carbon dioxide fixation via the Calvin cycle, was present in 9 of the 11 samples tested. Although the highest RuBPC/O activity was observed for a white mat (BHB3 C1, Table 8.2.3), other white mats had less activity than some orange mats, and one white

mat had no detectable activity. No pure orange mat that was assayed had zero detectable RuBPC/O activity (Table 8.2.3).

Several 80-μm wide Gulf of Mexico filaments hybridized with a 16S rRNA oligonucleotide probe specific to Monterey Canyon *Beggiatoa* sp. (Ahmad *et al.* 1999).

Table 8.2.3. Seep *Beggiatoa*, Gulf of Mexico. Enzyme activities and internal nitrate concentrations.

| Core/Subcore | RuBPC/O (nmol min$^{-1}$ mg$^{-1}$ prot) | AKGdH (nmol min$^{-1}$ mg$^{-1}$ prot) | Int. NO$_3^-$ (mM) | *Beggiatoa* Color |
|---|---|---|---|---|
| BHB1 C3 | 0 | 1220 | 22 | Orange/White |
| BHB3 C1 | 4.8 | - | 110 | White |
| BPB2 C1 | 0.22 | 125 | - | Orange |
| BPB2 C5 | - | 1270 | - | Orange |
| BPB2 C7 | slight. Activity | - | - | Orange |
| BPB3 C7 | 0.16 | below detection limit | 12 | Orange |
| GCB1 C3 | 0 | - | 19 | White |
| GCB1 C4 | - | below detection limit | 26 | Orange |
| GCB1 C7 | 0.35 | below detection limit | - | White |
| GCB1 C8 | 0.44 | below detection limit | - | Orange |
| GCB2 C2 | 0.066 | - | 36 | Orange |
| GCB2 C7 | 0.11 | - | 8 | Orange |
| GCB3 C4 | 0.05 | below detection limit | - | Orange |

## 8.2.4 Discussion

Compared to Monterey Canyon *Beggiatoa* populations, the Gulf of Mexico *Beggiatoa* mats have shallower deep distributions in the sediment and lower overall biomass densities (Figure 8.2.3). Monterey Canyon *Beggiatoa* sp. and *Thioploca* spp. appear to consume sulfide completely over the zone they occupy while respiring internal nitrate stores to ammonia (McHatton 1998, Otte *et al.* 1999, see figure 8.2.3). It is assumed, based on possession of a nitrate-filled vacuole and the close evolutionary relationships of all vacuolate filamentous bacteria (Figure 8.2.1), that the dominant Gulf of Mexico *Beggiatoa* spp. will have similar metabolic properties with respect to sulfide oxidation and nitrate reduction. By hypothesis, their oxidation of sulfide or stored elemental sulfur to sulfate at depths of up to 5 cm in the sediment will serve to re-supply this electron acceptor to the very active sulfate reducing bacterial populations present there (see Section 9). Their relatively low internal nitrate stores (Table 8.2.4) may reflect either low availability of this compound or rapid consumption of nitrate to drive the oxidation of reduced-sulfur substrates.
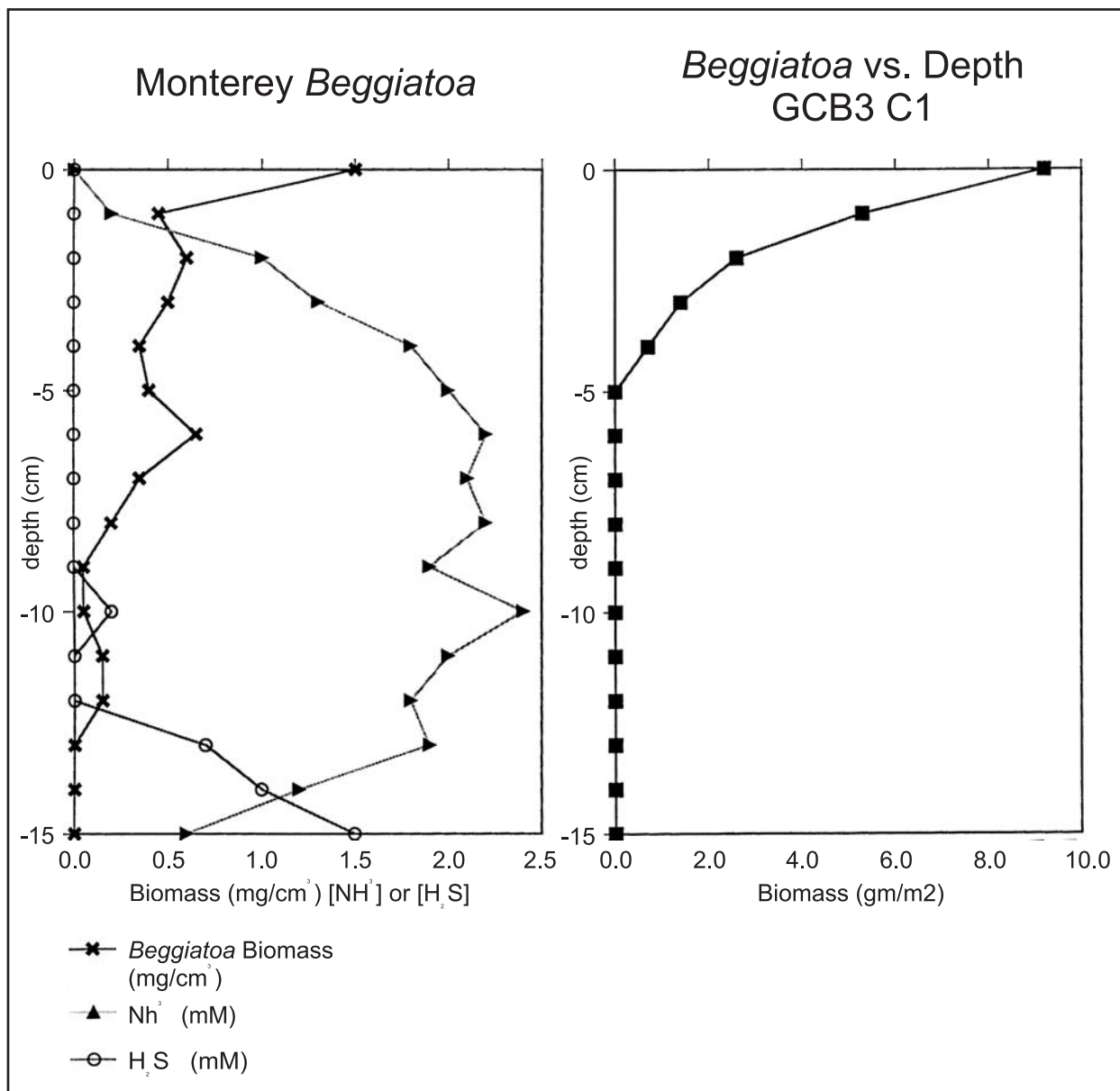
Figure 8.2.3.    Comparison of sediment depth distributions of (A) Monterey Canyon *Beggiatoa* sp. (75-μm cell diameter) at a cold seep (900-m depth) and (B) a representative Gulf of Mexico *Beggiatoa* sp. (42-μm cell diameter) at a hydrocarbon seep (600 m depth). For panel A, note the absence of free $H_2S$ throughout the range occupied by *Beggiatoa* and the ammonia maximum centered in the same region. These chemical signatures are assumed to be due to energy conserving bacterial oxidation of sulfide to sulfate at the expense of the reduction of internally stored nitrate to ammonia. Although the scale is compressed for panel B, similar metabolism is assumed. For panel A biomass is measured in mg dry wt. per $cm^3$; for panel B it is in gm wet wt. per $m^2$ over a 1.0-cm depth interval.

The enzyme ribulose-1,5-bisphosphate carboxylase/oxygenase (RuBPC/O), diagnostic for carbon dioxide fixation via the Calvin cycle, was present in 9 of the 11 samples tested. Although one white *Beggiatoa* mat (BHB3 C1) had high activity of this enzyme (Table 8.2.3), the average value for these populations (Table 8.2.4) is 3- to 30-fold lower than the corresponding activity found in chemoautotrophic populations from Monterey Canyon seeps and the Guaymas Basin hydrothermal vents. Conversely, certain Gulf of Mexico *Beggiatoa* populations contain alpha-ketoglutarate dehydrogenase activity, an enzyme diagnostic for the ability to oxidize organic matter in the process of energy generation. This is the first such demonstration of this activity for any native *Beggiatoa* population (Table 8.2.4). Obligate chemoautotrophic *Beggiatoa* strains and facultative strains grown as chemoautotrophs lack this activity (Table 8.2.4). Among chemoautotrophs, only facultative strains grown as chemoheterotrophs (e.g., strain 81-6 in the presence of acetate, Table 8.2.4, see also McHatton *et al.* 1996) possess this activity, which is essential for oxidizing organic matter to carbon dioxide in energy conserving reactions. Thus, although we did not completely confirm the finding of Nikolaus (1995) that orange *Beggiatoa* mats lack Calvin cycle activity while white mats possess it, it seems that the Gulf of Mexico mats are, on average, less autotrophic and more heterotrophic than any natural *Beggiatoa* mats previously studied. Given the high organic content of the sediments they occupy, this should not be surprising. These high enzyme activities associated with organic respiratory processes do not preclude the possibility that sulfide oxidation rates are also high.

Table 8.2.4. Comparison of Gulf of Mexico *Beggiatoa* spp. with
non-vacuolate, narrow *Beggiatoa* cultures and other native populations of vacuolate bacteria.

| Non-Vacuolate *Beggiatoa* Controls | Source | RuBisC/O Activity (nmol min$^{-1}$ mg$^{-1}$ prot) | α KDGH Activity (nmol min$^{-1}$ mg$^{-1}$ prot) | Internal [NO$_3^-$] (mM) | Fil. Width (µm) |
|---|---|---|---|---|---|
| strain 81-1c (obligate chemoautotroph) | sulfide medium | 20 ± 2.5 | 0 | 0.0003 | 2 |
| | sulfide+acetate | 14 ± 1.6 | 0 | | |
| strain 81-1c (facultative chemoautotroph) | sulfide medium | 23 ± 9.2 | 0 | not tested | 4 |
| | sulfide+acetate | 3.3 ± 0.2 | 153 ± 11 | | |
| **Vacuolate Bacterial Genus** | | | | | |
| **Beggiatoa spp.** | Gulf of Mexico seeps (this study) | 0.56 (n = 11) | 330 (n = 8) | 32 (n = 8) | 40 & 80 |
| *Beggiatoa* sp. | Monterey Canyon seeps | 7.5 - 15 | 0 | 160 (n = 5) | 75 |
| *Beggiatoa* spp. | Guaymas Basin hydrothermal vents | 1.47 (n = 8) | not tested | 130 (n = 3) | 24 - 32 40 - 42 116 - 122 |
| *Beggiatoa* sp. | Bay of Concepion | not tested | not tested | 42 ± 27 (n = 16) | 35 – 40 |
| *Thioploca* spp. | Chilean oxygen minimum zone | not tested | not tested | 150 - 500 | 12 – 20 30 – 43 |
| *Thiomargarita namibiensis* | Namibian oxygen minimum zone | not tested | not tested | 100 – 800 | 100 – 750 |

## 8.3 Mussel Community Ecology[*]

### 8.3.2 Objectives

The overall objectives of the mussel community ecology study fall into five general categories as follows:

To characterize the primary MMS study sites with respect to the biomass and numerical density of mussels, the size frequency of mussel populations, methane concentrations in water among the mussels, physiological condition of the mussels, and biomass and species composition of the associated fauna;

To characterize in a more general sense the species richness and biomass of associated fauna supported by this type of chemosynthetic community at the shallow Gulf of Mexico seep sites;

To determine the growth rate of mussels from GB425 for comparison to previous studies;

To determine the time course of changes in condition of mussels after removal from a favorable habitat in order to provide increased interpretive power in the previous and current transplant experiments;

To conduct reciprocal transplant experiments to test the hypotheses that differ in growth rates, condition, and maximum size of the mussels in different study sites found in the previous MMS study that are due to habitat characteristics;

### 8.3.3 Laboratory methods

**Measures of physiological condition in mussels.** Three analyses were initially employed to document variations in the physiological condition of mussels in the short-term transplant experiment. After evaluation of that data and data from previous studies (Nix *et al.* 1995; Smith *et al.* 2000), it was determined that glycogen content provided little or no additional information on the physiological condition of the mussels from different sites, so that analysis was not performed on animals from other collections. Water content (as a percent of wet weight) and standard bivalve condition index (CI, the ratio of ash free dry tissue mass to shell volume) were determined on 6 to 12 mussels from all treatments of the reciprocal transplant experiment and for 6 to 12 mussels from each primary MMS study site. Two techniques were used to determine the dry and ash free dry weights of the mussel tissue, depending on whether the mussels were also analyzed for glycogen content. For mussels also analyzed for glycogen content (primarily the short-term transplant mussels), the mussel tissue was first homogenized in nine times its mass of deionized water. Ten mm of the homogenate was dried at 60°C to constant weight (usually 48 hours) and then ashed at 500°C to obtain an ash weight. Animals not analyzed for glycogen were diced in a glass petri dish, and three non-uniform tissue samples were dried and then ashed. Tissue water content was calculated from the wet weight and dry weight. Shell volumes were calculated from the weight of sand needed to fill the shells and an empirically determined relationship between sand weight and volume. Glycogen content of the tissue of the short-term

---

[*] This section was authored by Charles R. Fisher and Tracie Ward.

transplant treatment mussels was measured using a modified spectrophotometric enzyme assay (Nix *et al*. 1995) and references therein on a subsample of the primary homogenate further diluted to a final concentration of 1:499 with deionized water.

**Separation and biomass determination of associated fauna.** In the laboratory, the faunal specimens were transferred from formalin into a 70% ethanol solution. They were then sorted into provisional taxonomic groups, hereafter called morphospecies. Members of the same morphospecies from each location were counted and sorted by size. A random subsample was then selected for biomass analysis from the size classes that represented the majority of the collection.

The *subsample*d individuals were weighed (wet weight) and placed in a 60°C oven until a consistent weight was obtained (dry weight), usually about 30 hours. The samples were then ashed at 500°C for six hours to obtain an ash weight. From these measurements, ash free dry weight (AFDW) was calculated by subtracting the ash weight from the dry weight, and the ash free wet weight (AFWW) was calculated by subtracting the ash weight from the wet weight. To obtain the biomass for an entire morphospecies of a site, the overall wet weight of the morphospecies collection was recorded and multiplied by the average percent-AFWW of the collection in question. Percent-AFWW was calculated as ash free wet weight divided by wet weight. An estimate of a morphospecies with many individuals across the same site was found using the average percent-AFWW for the subgroup of the site in question. For less well-represented individuals, percent-AFWW from all collections in which the morphospecies was present was averaged. The average percent-AFWW was then used for all biomass estimation of the under-represented species at all sites.

Mussel lengths were used to estimate biomass using the empirically determined equation,

$$W = 2.88 \times 10^{-5} \times L^{3.1862} \tag{8.3-1}$$

where W is tissue wet weight in grams, and L is shell length in millimeters (Fisher, 1993).

**Preliminary statistical analyses.** Significant differences between the size-frequency distributions in the different zones and years were detected using a continuity-adjusted chi-squared test to correct for small sample sizes (SAS Institute, 1989). If all years of the same zone were not significantly different ($p > 0.05$), then the size-frequency distributions for all years were combined and used to test for differences between zones.

Due to the nature of the condition indices data (percentages and ratios), the data for all three condition measurements were transformed using an arcsine function to approximate a normal distribution prior to statistical analysis. Significant differences between zones and years were tested using ANCOVA with length as the covariate (SAS Version 6.07, Proc GLM). If the model was significant ($p < 0.05$), then differences between specific sites and years were tested using Tukey's pairwise comparisons (SAS Version 6.07, Proc GLM).

The von Bertalanffy growth parameters of $L_\infty$ (maximum size) and $k$ (the rate at which $L_\infty$ is approached) were estimated from mark-recapture data using Fabens' method (Fabens, 1965) and asymptotic standard errors were obtained for these estimates (SAS Version 6.07, Proc NLIN). However, the estimation of von Bertalanffy growth parameters from mark-recapture data when the recapture interval of each individual is the same is not straightforward. Simulation studies have shown that when individual variability in growth parameters exists, the parameter estimates obtained may be extremely biased even when Fabens' method, the best method available at this time, was used (Smith *et al.* 1997). Therefore, although the estimates provided here are internally consistent and consistent with size-frequency data, they may be biased from the true population parameters.

Due to the potential bias in parameter estimates obtained for the von Bertalanffy growth model, it is not possible to test with adequate power for differences between populations using standard t-tests on these estimates (Smith *et al*. 2000). Therefore, it is necessary to use alternative techniques such as nonlinear regression with indicator variables (modified from Juliano and Williams 1985). First, Equation 8.3.1 (for comparing two sites or years)

$$L_{t+1} = (L_\infty + \delta I) \times (1 - e^{-(k + \beta I)\,dt}) + e^{-(k + \beta I)\,dt} \times L_t \qquad (8.3\text{-}2)$$

where $L_{t+1}$ is the recapture length (mm), $L_t$ is the initial length (mm), $dt$ is the recapture interval (years), and $I$ is the indicator variable with a value of 0 for the first site or year, or 1 for the second site or year, was fit for the two sites or years of interest. Then standard F-tests were used to test for significant differences between the full model (Equation 8.3.1) and the reduced model with no indicator variables and for the significance of the model parameters ($\delta$ and $\beta$), which would indicate significant differences between the growth parameters. This technique provides adequate power in testing for differences in growth between populations in spite of the potential bias in parameter estimates. However, tests for the significance of individual parameters, either $L_\infty$ or $k$, using this method does not provide adequate power in most cases (Smith *et al*. in preparation). Therefore, this nonlinear regression technique can detect differences in growth between two populations, but it cannot adequately assign this difference to either $L_\infty$ or $k$.

### 8.3.4 Results

**Site characterizations and differences.** Methane was consistently detectable at the Brine hosted sites but was only detected at three of the eight mussel beds at GC185 and GC234 (Table 8.3.1). The detection of methane was correlated with the presence of recent recruitment events at a site as reflected in the size frequency distribution of mussels (Figure 8.3.1). Recent recruitment had occurred at the BHM3, GCM2, and GC233 (Figure. 8.3.1) but not at BHM1 where methane was consistently detected in 1997.

Table 8.3.1. Methane levels in water samples from among mussels at MMS stations.

| Station | Year | n | Min $\sum$CH4 (mM) | Max $\sum$CH4 (mM) | Mean $\sum$CH4 (mM) |
|---|---|---|---|---|---|
| | | | | Range | |
| BHM1 | 1997 | 4 | 0.009 | 0.101 | 0.039 |
| | 1998 | 4 | 0 | 0.055 | 0.0014 |
| BHM2 | 1997 | 3 | 0 | 0 | 0 |
| BHM3 | 1997 | 3 | 0 | 0.010 | 0.003 |
| | 1998 | 3 | 0 | 0 | 0 |
| BHM4 | 1997 | 0 | 0 | 0 | 0 |
| BHM5 | 1997 | 3 | 0 | 0 | 0 |
| BHM6 | 1998 | 3 | 0 | 0 | 0 |
| GCM1 | 1997 | 3 | 0 | 0 | 0 |
| | 1998 | 2 | 0 | 0 | 0 |
| GCM2 | 1997 | 3 | 0.016 | 0.068 | 0.035 |
| | 1998 | 2 | 0 | 0 | 0 |
| GBM1 | 1997 | 3 | 0.253 | 0.797 | 0.452 |
| | 1998 | 6 | 0 | 4.496 | 1.359 |
| BPM1 (middle) | 1997 | 8 | 0.021 | 0.162 | 0.077 |
| | 1998 | 3 | 0.049 | 0.061 | 0.055 |
| BPM2 (outer) | 1997 | 3 | 0.690 | 0.926 | 0.794 |
| BPM3 (middle) | 1997 | 3 | 0.690 | 2.162 | 1.483 |
| BPM4 (inner) | 1997 | 3 | 0.142 | 0.937 | 0.433 |
| | 1998 | 4 | 1.052 | 0.356 | 0.141 |
| BPQ (inner) | 1997 | 3 | 0.015 | 0.028 | 0.019 |
| BPR (outer) | 1997 | 3 | 0 | 0 | 0 |
| BPT (inner) | 1998 | 6 | 0.132 | 0.475 | 0.245 |
| BPV (inner) | 1998 | 3 | 0 | 0.058 | 0.019 |
| BPW (outer) | 1998 | 3 | 0.077 | 0.240 | 0.155 |

The wide variation in the density and area-specific biomass of mussels in the different collections provides a picture of the range in these parameters found in this type of chemosynthetic community around shallow seep sites in the Gulf of Mexico (Figure 8.3.2 and 8.3.3). No consistent difference between types of sites, or sites, is apparent in this data set that emphasizes the variability within a site and even within a large mussel bed.

The variation in the condition indices (percent-water and CI) also reflects significant bed-to-bed variation (Table 8.3.2). The two beds at GB425 are significantly different with respect to both CI ($p < 0.01$) and percent-water ($p < 0.005$). The two beds at GC234 are significantly different with respect to CI ($p < 0.001$). Similarly, GC185 bed M5 had a significantly lower CI than any other BH bed, and M4 was also significantly lower than M1. At GC233, the M1 and M2 collections had significantly different CI values and were significantly lower than the M3 and M4 collections. However, the large sample size of this data s*et al*so allows robust comparisons

between types of sites and sites. Both indices indicate that, overall, mussels at the brine dominated sites are in better condition than mussels from petroleum dominated sites (CI, p < 0.001; percent-water, p < 0.005) and that the mussels at GC233 are in better condition than mussels from GC234 or GC185 (CI p < 0.001; percent-water, p < 0.05).

**Associated fauna.** The gastropod, *Bathynerita naticoides*, and the Alvinocarid shrimp were present in all mussel beds sampled and were often abundant (Table 8.3.3). The undescribed orbinid polychaete was very abundant in most collections from GC233 and both collections from GC234 but was absent in the collection from GB425. Only a single individual was found in a single collection from GC185. The galatheid crab, *Munidopsis* sp. 1, and the gastropods, *Provanna sculpta, Cantrainea meroglypta,* and *Buccium canetae,* were abundant in GC185 collections but absent or very rare in GC233 collections.
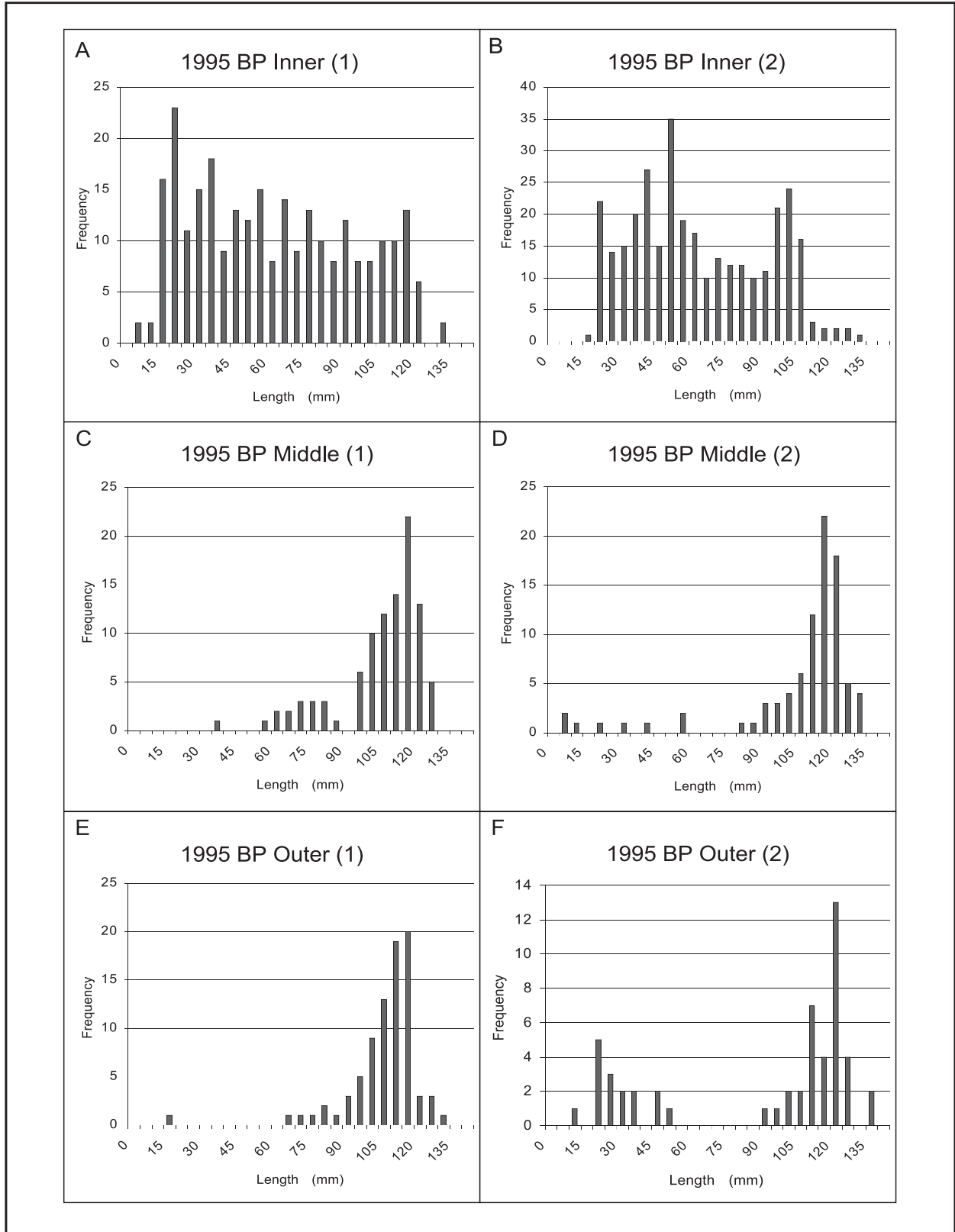
Figure 8.3.1A.　Size frequency distribution of mussels from six collections at the GC233 in 1995.
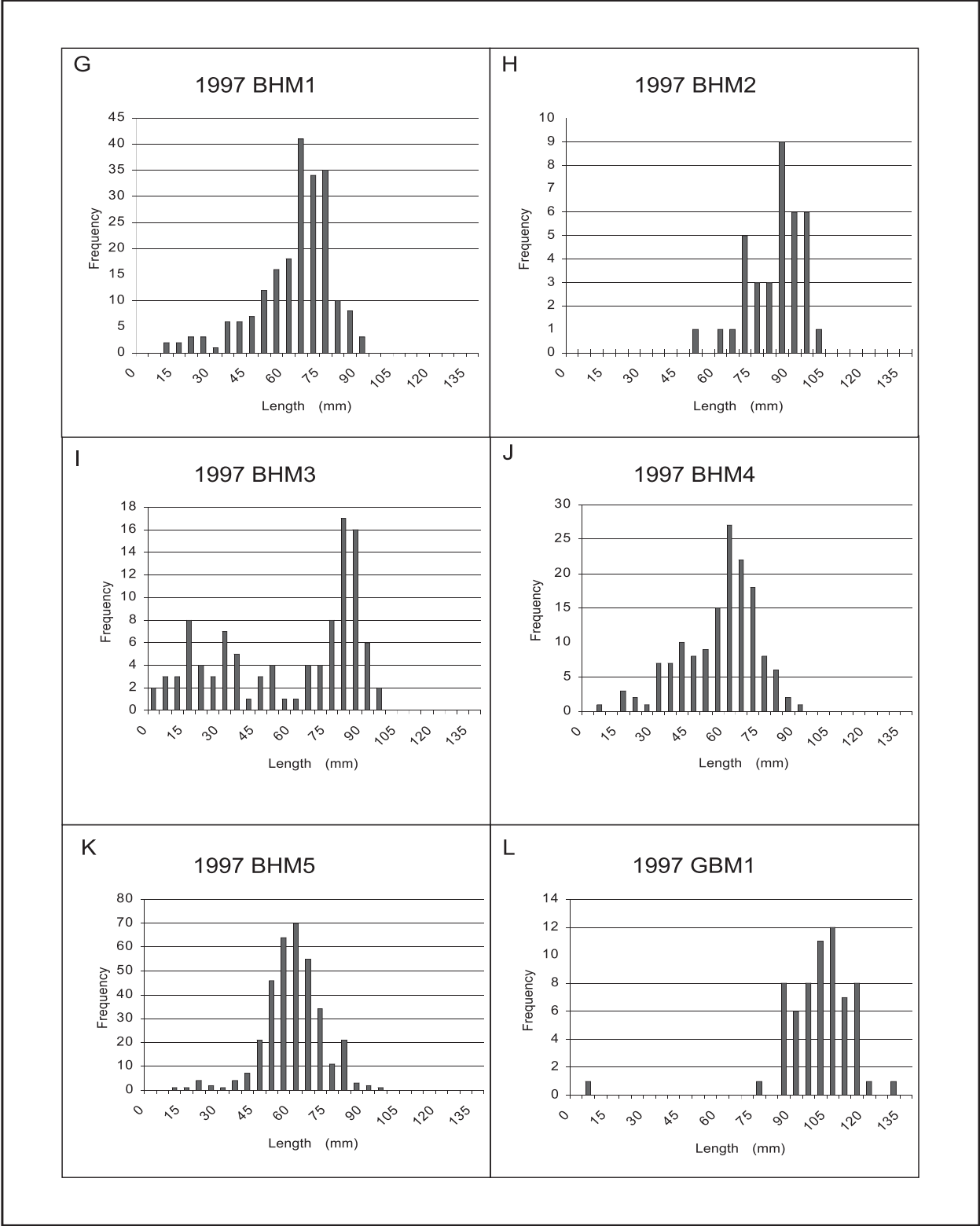
Figure 8.3.1B.    Size frequency distribution of mussels in each of the MMS primary study sites (G-L).
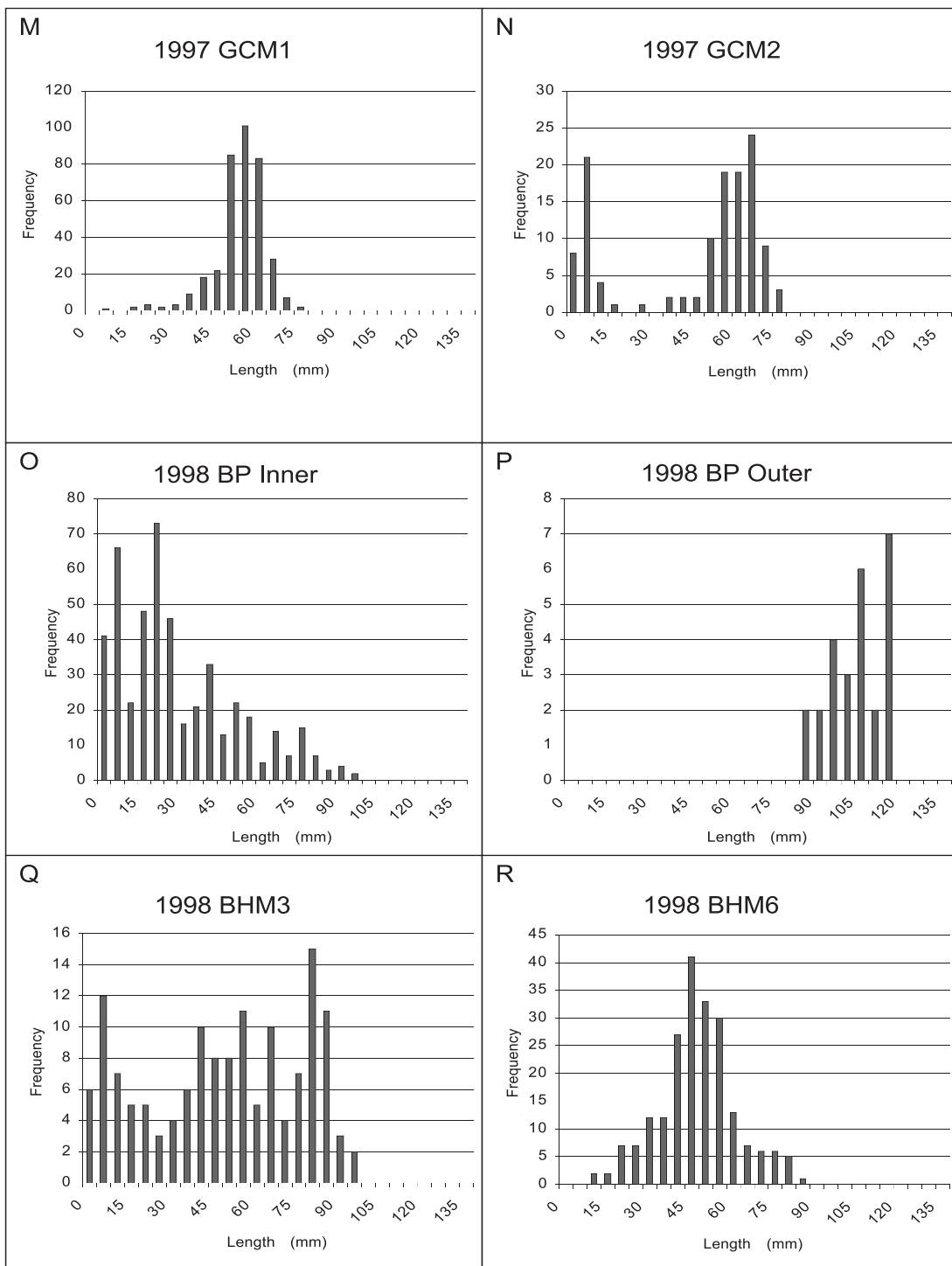
Figure 8.3.1C.    Size frequency distribution of mussels in each of the MMS primary study sites (M-R).
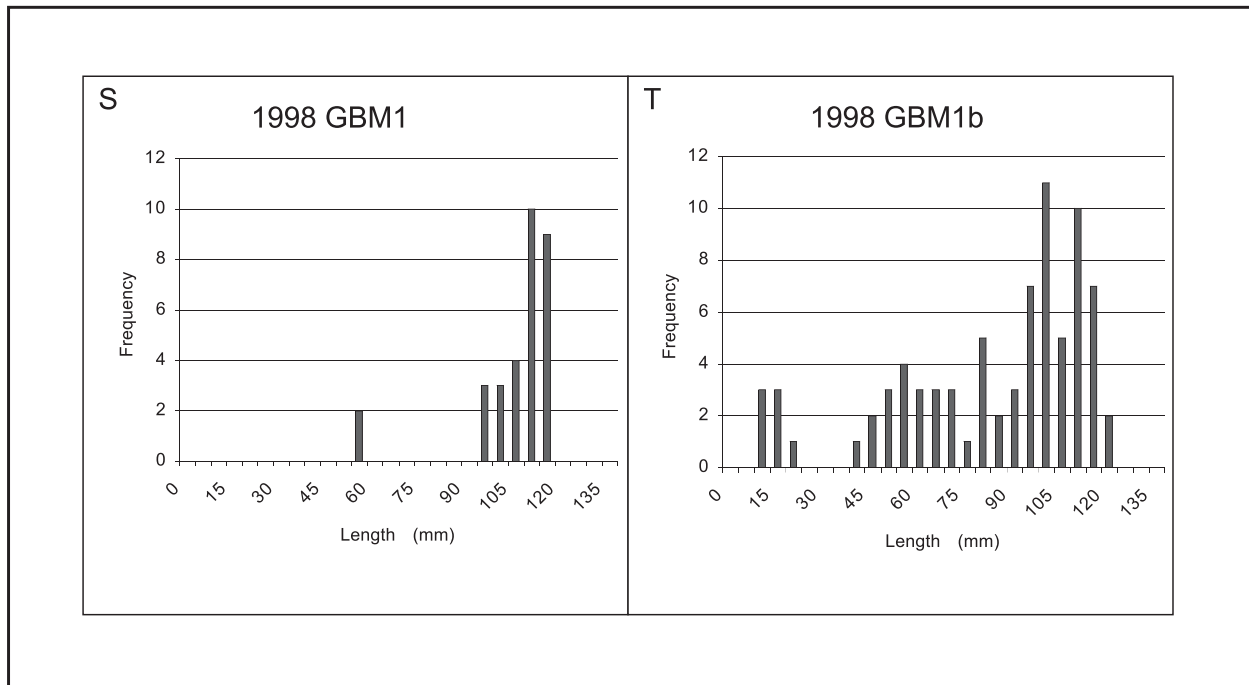
Figure 8.3.1D.     Size frequency distribution of mussels in each of the MMS primary study sites (S-T).

**Short-term transplant experiments.** Water sampling data showed non-detectable levels of methane ($< 2$ μM) at the short-term transplant location while the inner edge of GC233 (BP I) had moderately high levels of methane (Table 8.3.4). Both sites were similar in oxygen concentration; however, the oxygen at the short-term transplant site could potentially be much higher as the highest observed concentration here was over two times as high as the maximum observed at GC233. The three physiological condition indices showed no significant differences between the inner zone mussels and either the 13- or 42-day transplants (Table 8.3.4). Only the 13-day control mussels were found to have significantly lower CI and higher water content from all other samples, indicating that the mussels in this control box sustained damage through manipulation or were placed in a very stressful microhabitat at GC233. Glycogen content in all of the mussels sampled including the original population was highly variable (Table 8.3.5), possibly obscuring differences between transplant groups. However, this variability did not correspond with any experimental factor, such as order run or assay date, in the assay protocol, indicating that the variability was most likely present in the inner zone mussel population and was not a result of the transplant experiment.
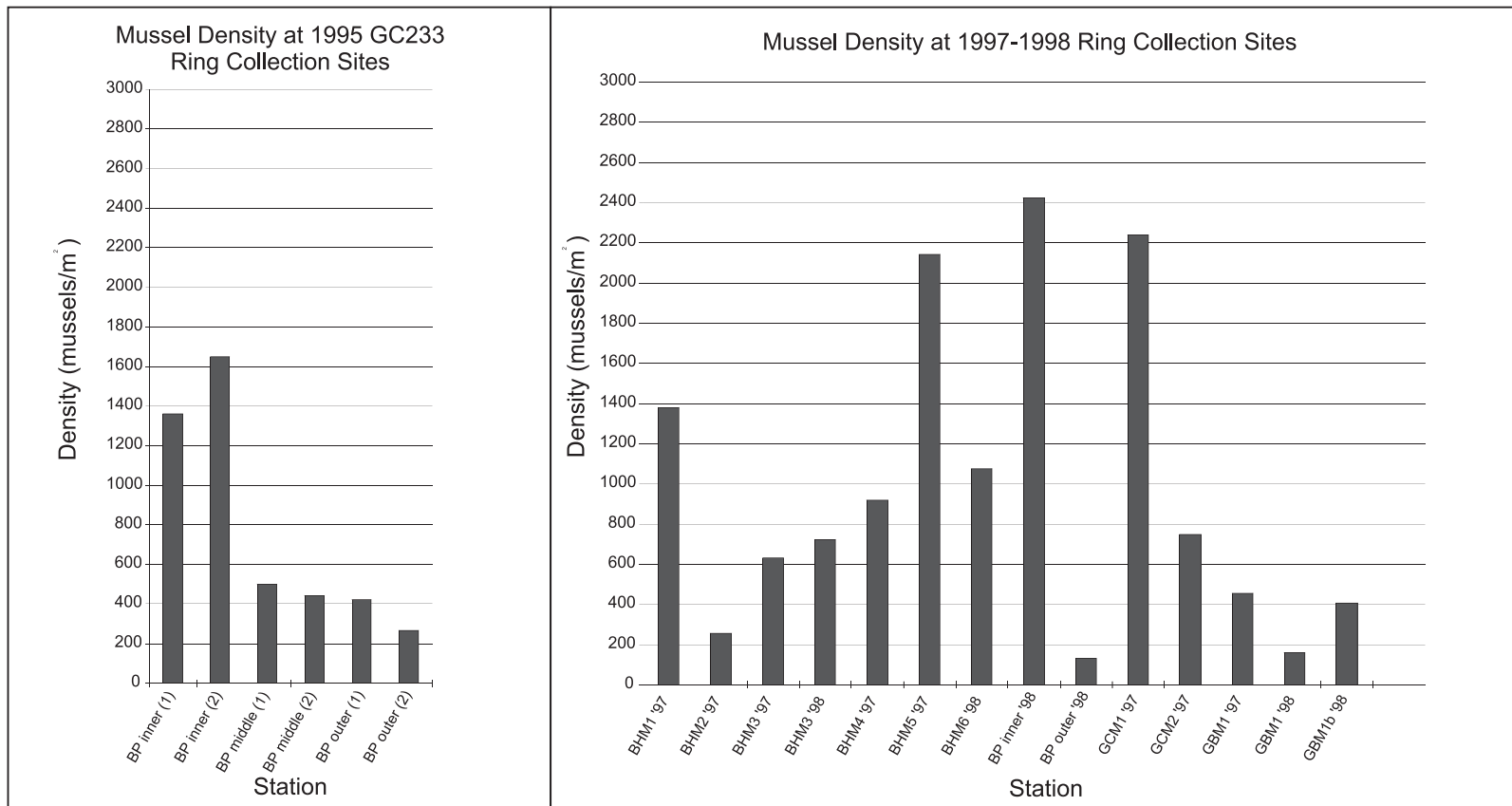
Figure 8.3.2.     Density of mussels, as individuals per sq. m, in each of the MMS primary study sites and from six collections at the GC233 in 1995.
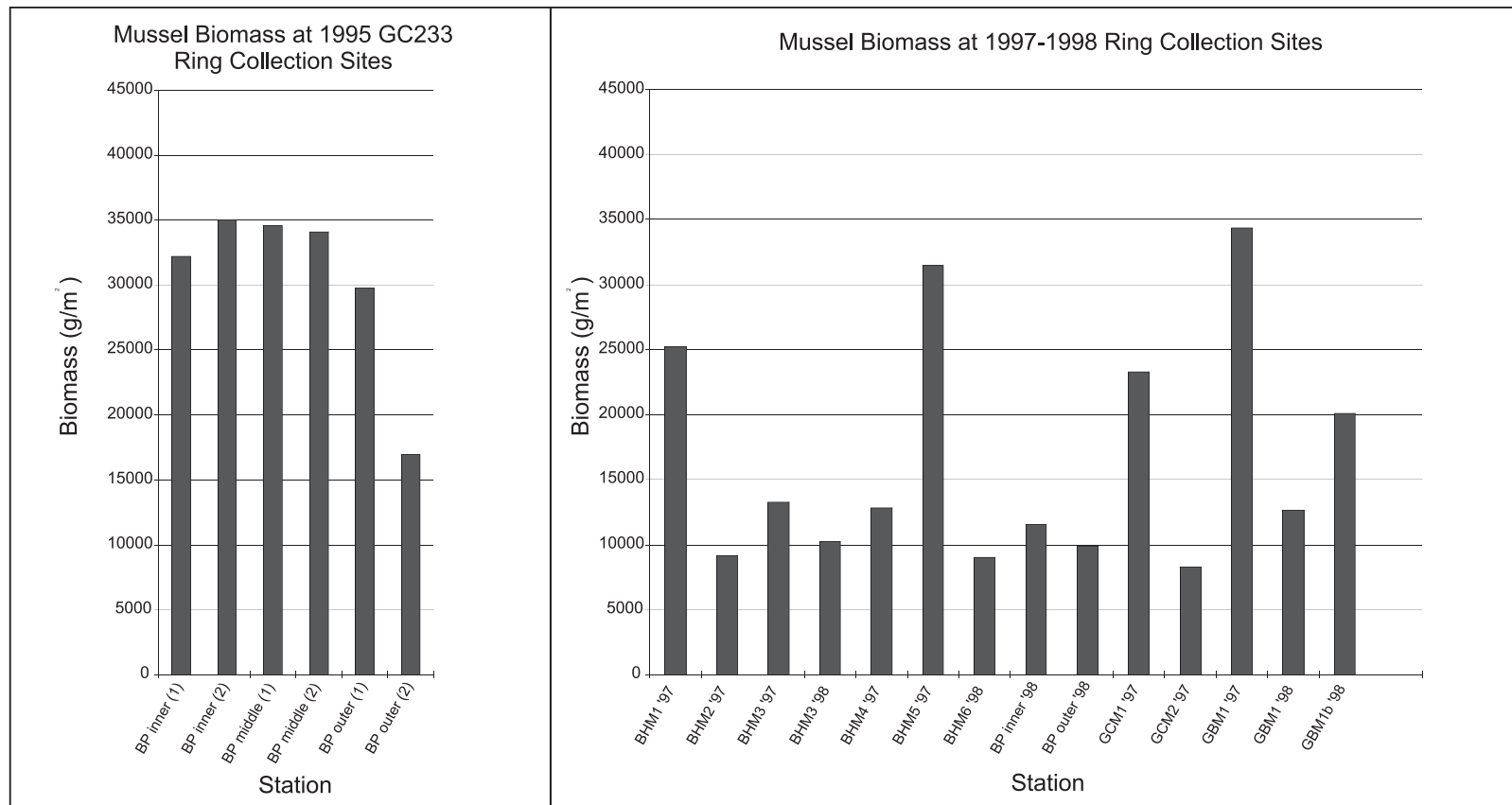
Figure 8.3.3. Biomass of mussel soft tissue in each of the MMS primary study sites and from six collections at the GC233 in 1995.

Table 8.3.2. Characteristics of mussel collections from each primary MMS study site and GC233 in 1995.

| Year | Dive | Station | L max (mm) | L min (mm) | L mean (mm) | | L median (mm) | Density (indiv/sq. m) | Biomass (g/sq. m) | Mean Condition Index | Mean Percent-Water |
|------|------|---------|-----------|-----------|-------------|--|---------------|------------------------|-------------------|----------------------|--------------------|
| 1995 | 2626 | BP-inner | 128.8 | 2.4 | 58.2 | (±32.9) | 53.9 | 1360 | 32210 | ND | ND |
| | 2630 | BP-inner | 130.0 | 14.9 | 59.5 | (±28.1) | 53.7 | 1650 | 34990 | ND | ND |
| | 2628 | BP-middle | 125.0 | 31.0 | 101.3 | (±18.0) | 106.7 | 499 | 34550 | ND | ND |
| | 2630 | BP-middle | 127.3 | 2.5 | 102.2 | (±27.2) | 110.5 | 443 | 34100 | ND | ND |
| | 2626 | BP-outer | 125.2 | 13.4 | 102.8 | (±15.3) | 106.6 | 423 | 29730 | ND | ND |
| | 2630 | BP-outer | 134.5 | 8.3 | 86.2 | (±42.0) | 109.0 | 265 | 16950 | ND | ND |
| 1997 | 2852 | BHM1 | 93.4 | 13.3 | 65.5 | (±15.1) | 67.5 | 1380 | 25213 | 0.131 | 91.4 |
| | 2857 | BHM2 | 100.7 | 53.8 | 84.4 | (±11.2) | 86.7 | 255 | 9148 | 0.107 | 94.1 |
| | 2865 | BHM3 | 79.7 | 10.5 | 59.8 | (±27.1) | 75.5 | 632 | 13259 | 0.101 | 93.5 |
| | 2868 | BHM4 | 93.4 | 16.1 | 59.2 | (±15.6) | 62.2 | 918 | 12832 | 0.065 | 87.0 |
| | 2873 | BHM5 | 97.4 | 14.6 | 61.6 | (±11.9) | 61.3 | 2140 | 31488 | 0.036 | 92.4 |
| | 2851 | BPM1 | 117.7 | 27.5 | 73.9 | (±23.0) | 72.5 | ND | ND | ND | ND |
| | 2870 | BPM2 | 128.9 | 9.5 | 75.0 | (±36.7) | 81.3 | ND | ND | 0.107 | 85.1 |
| | 2870 | BPM3 | 125.8 | 5.0 | 81.4 | (±24.2) | 78.7 | ND | ND | 0.142 | 80.9 |
| | 2876 | BPM4 | 124.1 | 7.4 | 82.2 | (±24.1) | 81.9 | ND | ND | 0.146 | 80.4 |
| | 2877 | GCM1 | 78.9 | 9.6 | 55.8 | (±9.1) | 56.5 | 2237 | 23298 | 0.068 | 87.6 |
| | 2883 | GCM1 | 134.5 | 75.2 | 103.7 | (±11.1) | 103.4 | 456 | 34362 | 0.090 | 886.9 |
| | 2889 | GBM2 | 77.9 | 3.8 | 51.8 | (±21.8) | 60.0 | 748 | 8258 | 0.099 | 86.3 |
| 1998 | 4038 | BP-inner | 95.5 | 2.2 | 30.5 | (±22.4) | 24.1 | 2424 | 11560 | 0.148 | 79.9 |
| | 4038 | BP-outer | 119.9 | 86.9 | 105.7 | (±10.4) | 107.8 | 132 | 9890 | 0.123 | 81.9 |
| | 4342 | BHM3 | 96.6 | 1.5 | 50.6 | (±28.1) | 53.7 | 723 | 10230 | 0.115 | 85.0 |
| | 4342 | BHM6 | 85.2 | 11.1 | 49.6 | (±13.9) | 49.1 | 1075 | 9020 | 0.100 | 84.7 |
| | 4040 | GBM1 | 118.4 | 58.5 | 107.3 | (±14.5) | 112.4 | 158 | 12630 | 0.092 | 85.9 |
| | 4041 | GBM1b | 122.2 | 13.2 | 85.2 | (±30.0) | 96.5 | 408 | 20110 | 0.106 | 85.5 |

ND – Not determined

Table 8.3.3. Density (number of individuals per sq. m) of associated fauna in mussel beds.

| Year | Dive | Station | *Bathynerita naticoidea* | *Alvinocaris stactophila* | *Alvinocaris stactophila affinis* | Bersilliidae sp. | Orbiniidae | *Munidopsis* n. sp. 1 | *Provanna sculpta* | *Cantrainea* sp. | Buccinidae sp. | Polynoidae sp. | Xanthidae sp. | *Phascolosoma turnerae* | *Lamellibrachia* sp. | Escarpid-like sp. | Nudibrancha sp. | Whelk | Misc. Polychaete species |
|---|---|---|---|---|---|---|---|---|---|---|---|---|---|---|---|---|---|---|---|
| 1995 | 2626 | BP-inner | 87 | 346 | 31 | 0 | 5265 | 0 | 0 | 5 | 0 | 15 | 0 | 0 | 0 | 0 | 5 | 0 | 0 |
| | 2630 | BP-inner | 26 | 87 | 15 | 0 | 3657 | 0 | 0 | 0 | 0 | 5 | 0 | 0 | 0 | 0 | 0 | 0 | 0 |
| | 2628 | BP-middle | 51 | 138 | 5 | 0 | 52 | 0 | 0 | 0 | 0 | 0 | 0 | 0 | 0 | 0 | 0 | 0 | 0 |
| | 2630 | BP-middle | 31 | 51 | 5 | 0 | 1323 | 10 | 0 | 0 | 0 | 0 | 0 | 0 | 0 | 0 | 0 | 0 | 0 |
| | 2626 | BP-outer | 76 | 82 | 0 | 0 | 3631 | 0 | 0 | 0 | 0 | 0 | 0 | 0 | 0 | 0 | 0 | 0 | 0 |
| | 2630 | BP-outer | 66 | 10 | 5 | 0 | 1219 | 0 | 0 | 0 | 20 | 0 | 0 | 0 | 0 | 0 | 5 | 5 | 5 |
| 1997 | 2852 | BHM1 | 827 | 24 | 49 | 0 | 6 | 30 | 67 | 0 | 0 | 0 | 0 | 0 | 0 | 0 | 0 | 0 | 0 |
| | 2865 | BHM3 | 2674 | 176 | 0 | 0 | 0 | 0 | 55 | 30 | 6 | 0 | 0 | 0 | 0 | 0 | 0 | 0 | 0 |
| | 2868 | BHM4 | 2273 | 164 | 30 | 0 | 0 | 18 | 760 | 711 | 24 | 0 | 6 | 0 | 0 | 0 | 0 | 0 | 6 |
| | 2873 | BHM5 | 1106 | 97 | 12 | 6 | 0 | 97 | 590 | 6 | 140 | 0 | 0 | 0 | 0 | 0 | 0 | 0 | 0 |
| | 2851 | BPM1 | 6 | 650 | 6 | 6 | 1167 | 24 | 0 | 0 | 0 | 0 | 0 | 0 | 0 | 0 | 0 | 0 | 30 |
| | 2870 | BPM2 | 280 | 511 | 0 | 0 | 0 | 6 | 0 | 0 | 24 | 0 | 0 | 0 | 0 | 0 | 0 | 0 | 0 |
| | 2870 | BPM3 | 201 | 37 | 0 | 0 | 0 | 12 | 0 | 0 | 0 | 0 | 0 | 0 | 0 | 0 | 0 | 0 | 12 |
| | 2876 | BPM4 | 67 | 201 | 67 | 0 | 0 | 0 | 0 | 0 | 0 | 0 | 0 | 0 | 0 | 0 | 0 | 0 | 0 |
| | 2877 | GCM1 | 979 | 286 | 18 | 0 | 693 | 6 | 55 | 0 | 0 | 0 | 0 | 0 | 0 | 0 | 0 | 0 | 6 |
| | 2889 | GCM2 | 1787 | 565 | 37 | 0 | 2383 | 0 | 164 | 213 | 0 | 0 | 0 | 0 | 0 | 0 | 0 | 0 | 0 |
| | 2883 | GBM1 | 468 | 225 | 12 | 0 | 0 | 24 | 12 | 6 | 0 | 0 | 0 | 0 | 0 | 0 | 0 | 0 | 6 |
| 1998 | 4042 | BHM3 | 1253 | 158 | 0 | 0 | 0 | 20 | 316 | 5 | 10 | 5 | 0 | 46 | 0 | 15 | 0 | 0 | 0 |
| | 4042 | BHM6 | 2241 | 285 | 5 | 0 | 0 | 20 | 234 | 31 | 0 | 20 | 0 | 5 | 10 | 10 | 0 | 0 | 0 |

**Growth studies and long-term reciprocal transplant experiments.** Growth was monitored in four mussel beds, three of which were used for the reciprocal transplant experiments. Very large mussels dominated the newly discovered mussel bed at GB425 (GBM1), so an experiment was initiated to monitor growth in that population. Although the limited size range and small number of marked mussels recovered limits the conclusions that can be drawn from this study, the fact that larger animals are clearly still growing is apparent (Figure 8.3.4) Two reciprocal transplant experiments were conducted. In this section, changes in growth and condition indices of the transplanted mussels with respect to the host populations are reported. Differences in the histopathology and hydrocarbon loads of the mussels are discussed in section 8.5. Tagged mussels were compared to untagged mussels (controls) at the end of the experiment to test for an effect of the tagging process. There was no significant difference in either percent-water or CI between tagged and untagged mussels at any of the four sites, indicating no detectable effect of the tagging process.

Table 8.3.4. Concentrations of Methane ($CH_4$) and Oxygen ($O_2$)
at GC233 inner zone and the short-term transplant locations for 1997.
Sampling depth was 2.5 cm.

| Sample | | CH, (µM) | O, (µM) |
|---|---|---|---|
| GC233-inner | mean | 48 | 67 |
| | median | 32 | 46 |
| | low | 12 | 30 |
| | high | 101 | 120 |
| Short-term transplant | mean | ND | 66 |
| | median | ND | 45 |
| | low | ND | 34 |
| | high | ND | 285 |

ND – non-detectable

The first experiment was a transplant between the GC185 mussel bed, BHM1, and the GC233 collection site BPM1. The growth of the two populations over the period of the transplant experiment (marked controls) was significantly different ($p < 0.001$, Table 8.3.6, Figure 8.3.4). Growth of the transplanted mussels was significantly different from growth of their populations of origin ($p < 0.001$) but not significantly different from the mussels they were transplanted among. The condition indices (percent-water and CI) of the two host populations were not significantly different in the year of collection, precluding analysis of transplant induced changes in condition in this experiment (Figure 8.3.4).

Table 8.3.5. Mean (standard deviation) condition index, glycogen content, water content, and
length for the inner zone of the GC233, the control boxes and the short-term transplant boxes in 1997.

| | Inner Zone | 13-day Control | 42-day Control | 13-day Transplant | 42-day Transplant |
|---|---|---|---|---|---|
| CI $(g/ml^3)$ | $0.13^A$ (0.01) | $0.06^B$ (0.03) | $0.13^A$ (0.03) | $0.11^A$ (0.03) | $0.10^A$ (0.02) |
| Percent-Glycogen | $1.6^A$ (1.3) | $1.0^B$ (0.9) | $1.6^A$ (0.6) | $1.3^{A,B}$ (1.0) | $1.4^A$ (0.8) |
| Percent Water | $83.7^{A,C}$ (2.6) | $92.6^B$ (4.1) | $80.8^A$ (2.3) | $85.5^C$ (2.5) | $82.7^{A,C}$ (2.4) |
| Length (mm) | 74 (32) | 75 (25) | 94 (20) | 81 (27) | 90 (21) |
| N | 6 | 7 | 6 | 12 | 12 |

[A,B,C] Categories with different letters indicate a significant difference ($p < 0.05$) between them.


The second transplant was between the GC234 M1 mussel bed and another collection site in GC233, BPM4. Growth of the marked controls at each site was significantly different ($p < 0.0001$, Table 8.3.6, Figure 8.3.4). Growth of both transplanted populations was significantly different from their populations of origin and the mussels they were transplanted among, with patterns intermediate between the two extremes of the host populations (Figure 8.3.5). The condition indices of the two host populations were significantly different in 1997 and 1998. The condition indices of the transplanted populations were significantly different from their populations of origin but not significantly different from the mussels they were transplanted among (Figure 8.3.6).


Table 8.3.6. von Berltalanffy growth parameter estimates
For GC233, GCM1, BHM1, and GBM1 mussel populations.

| | Parameter Estimates | |
|---|---|---|
| Station | $L_{max}$ | k |
| BPM1 | 124.48 (116.52, 138.43) | 0.16 (0.11, 0.21) |
| BPM4 | 103.78 (92.02, 115.49) | 0.24 (0.14, 0.35) |
| BHM1 | 94.47 (85.10, 103.84) | 0.17 (0.10, 0.23) |
| GCM1 | 66.60 (57.18, 76.02) | 0.08 (0.01, 0.14) |
| GBM1 | 124.02 (106.40, 141.64) | 0.05 (0.01, 0.08) |
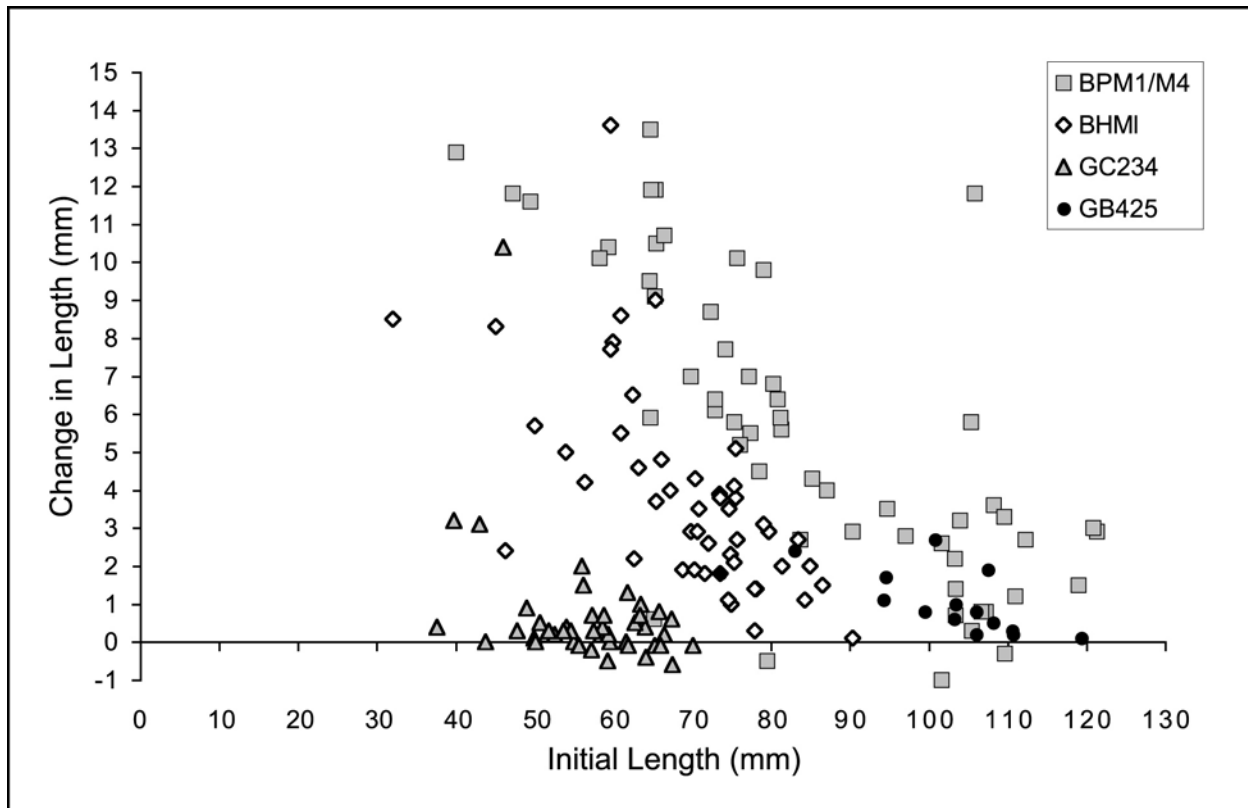
Figure 8.3.4.    Growth of mussels between 1997 and 1998 field seasons at the GC233 and at MMS study stations BHM1, GCM1, GBM1, and BPM1/M4.


## 8.3.5 Discussion

There was considerable heterogeneity between collections of mussels with respect to all of the "community ecology" parameters. Care should be exercised in interpreting the differences because there is also considerable heterogeneity within a single mussel bed. The scientists and pilots in the submarine for each collection were asked to make the collections from "typical appearing" regions of the bed they were sampling. However, review of photo mosaics and video records of each collection site confirms the heterogeneity present within most mussel beds. For example, in many of the beds there were regions where no juveniles were present, but disarticulated shells were abundant. Other regions had no juveniles or disarticulated shells apparent while yet in other regions, all the large mussels were literally covered with juveniles. Nonetheless, all analyses reported in this section were conducted on collections from within a 0.5-meter ring or square, so correlation between parameters such as mussel population characteristics, condition, faunal associates, and chemistry are appropriate. Also, because of the replication within some sites (notably GC185 and GC233), comparisons between faunal associates are appropriate.
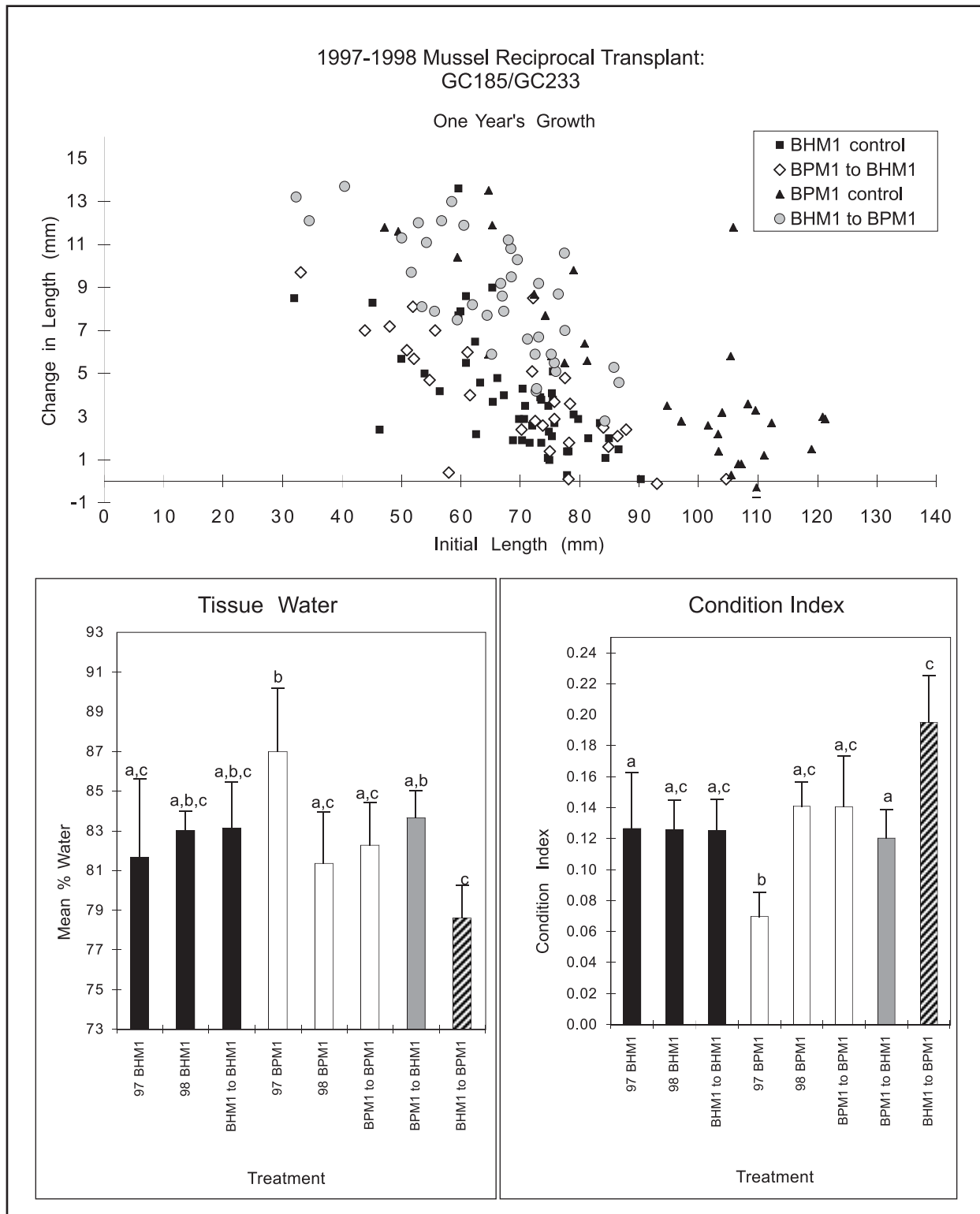
Figure 8.3.5.    Growth and condition of transplant and control mussels from GC185 – GC233 reciprocal transplant study. Bars with different letters over them are significantly different from each other.

Mussel density at the sites ranged from 255 to 2424 individuals m$^2$ and from 8.3 to 35 kg m$^2$ of mussel tissue in mussel beds at these sites. This is, of course, a very high biomass compared to

the rest of the deep Gulf of Mexico and would be expected to be a source of nutrition for numerous other animals from the nutrient limited background fauna. In fact, the greatest species richness found in any single collection was only eight species, and the total species richness for this type of community at any one site was 13 species (from a total of six collections at GC185). The overwhelming bulk of the biomass of the associated fauna is from seven species, five of which are endemic to the seeps. This is in contrast to the communities associated with tubeworm aggregations, which have a much higher species richness and host significant numbers of non-endemic species. Although the identity of the associated fauna is quite variable between sites, the total biomass of associated fauna between sites is remarkably constant.

Two species were always found associated with mussel beds – the gastropod, *Bathynerita naticoides*, and the Alvinocarid shrimp, suggesting that these endemic species have excellent dispersal abilities and can tolerate a wide range of conditions. A different pattern was seen with the undescribed orbinid polychaete that was very abundant in most collections from GC233 and both collections from GC234 but was absent in the collection from GB425. Only a single individual was found in the single collection from GC185. Its abundance in one of the oil and salt dominated sites and absence in the others suggests that dispersal abilities rather than physiological tolerance may limit its distribution. The fact that *Bathynerita naticoides* was found in much lower abundance at GC233, and the other gastropods were absent or rare, suggests that this habitat may not be suitable for these gastropods, perhaps because of the steep gradients in dissolved gases and brine among the mussels (Smith *et al*. 2000).

The short-term transplant experiment found a very high level of individual variation in glycogen content between each of the treatments, which would mask moderate differences between sites. Because this is also a very time-consuming assay, we decided not to use this assay for the other studies but instead increased the number of animals assayed for condition by other methods. Neither CI nor percent-water was significantly different between the control animals and the animals transplanted off site, with the exception of one control cage whose animals crashed in condition and are not considered for this analysis. This indicates that it takes a minimum of months for changes to occur in these conservative indices of animal condition and that they are, therefore, reliable indicators of average environmental conditions experienced over at least the previous several months and not sensitive to short-term fluctuations in environmental conditions.

The two reciprocal transplant experiments indicate a significant effect of environment on animal growth and condition but also suggest that mussels moved into very different environments may take more than one year to fully feel the effects of the new environment. In the GC185-to-GC233 experiment, the initial populations had similar (but significantly different) growth patterns and physiological condition that were not significantly different between populations (Figure 8.3.5). When transplanted, the mussels showed the same growth pattern as the mussels they were transplanted among and were significantly different from their bed of origin. There was no evidence of a historic effect on the mussels' growth pattern after transplantation, but the initial populations were very similar. In the second experiment, the initial populations had very different growth parameters and physiological condition indices. After transplantation, the mussels were in the same condition as those around themselves (and different from their bed of origin), but the growth characteristics were significantly different from either population (Figure. 8.3.6). Sample size and limitations in statistical power for analysis of growth parameters prevent conclusions concerning where the differences in growth parameters occur, but visual examination of the data suggests that the growth characteristics of the transplanted mussels were

intermediate between the two host populations. Hypothetically, this could reflect either genetic differences between the populations, a residual effect of their original physiological condition affecting growth for at least the first few months of the experimental interval or some other carry-over condition such as a pathology or lack thereof. The other studies reported here indicate that genetic differences are unlikely to contribute to this effect. Pathology and condition are likely contributors.
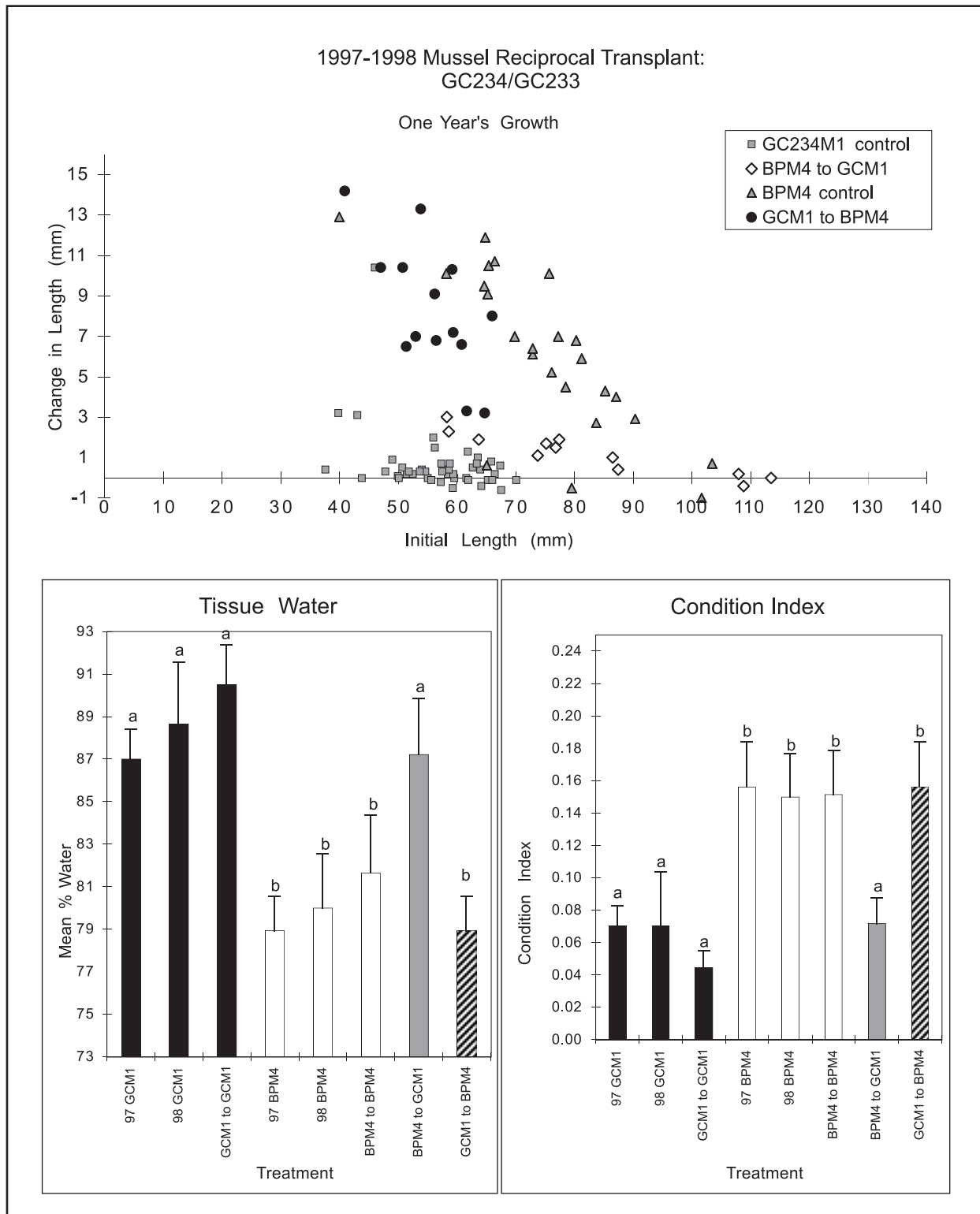
Figure 8.3.6.    Growth and condition of transplant and control mussels from the GC234 – GC233 reciprocal transplant study. Bars with different letters over them are significantly different from each other.

## 8.4. Vestimentiferan Community Ecology[*]

### 8.4.1 Introduction

Vestimentiferan tubeworms are the biomass dominant fauna at many Gulf of Mexico hydrocarbon seeps and are undoubtedly the best known chemosynthetic species occurring in the region. Within the program study sites, tubeworms are prevalent at the sediment diffusion sites, GC185 and GC234, and occur in reduced abundance on the margins of the two brine-pooling sites, GC233 and GB425. The Gulf of Mexico species are taxonomically and functionally similar to *Riftia pachyptila*, the tubeworm species first discovered at hydrothermal vents in the eastern Pacific Ocean. Both forms lack any alimentary apparatus and live by harboring sulfide-oxidizing bacteria in a symbiotic and chemosynthetic partnership. Both forms occur in prominent clusters of hundreds of individuals. These clusters offer habitat substrata to diverse, non-chemosynthetic invertebrates and fishes. Environmental evidence has suggested that the Gulf of Mexico species are distinguished from their hydrothermal vent analogs by their ability to subsist on sulfides dissolved in the sedimentary pore fluids instead of an actively venting fluid source. The molar strength of MMS demonstrated that tubeworms grew at rates of less than one centimeter per year and lived in excess of one hundred years (Fisher *et al.* 1997).

### 8.4.2 Objectives

The tubeworm community ecology study comprised six overall objectives as follows:

To characterize the principal sampling stations for integration with data collected by other investigators. Each primary tubeworm aggregation was characterized with respect to growth rate and physiological condition of the tubeworms. Seven of these aggregations were collected intact and were also characterized with respect to tubeworm species composition, size frequency and biomass. Four of those aggregations were collected with a bushmaster device that recovered associated fauna. Biomass and species composition of the associated fauna were quantified for these four aggregations. Data on sulfide levels above and below the sediment water interface are available for most aggregations.

To characterize generally the species richness and biomass of associated fauna supported by this type of chemosynthetic community at the shallow Gulf of Mexico seep sites.

To determine precisely the growth rates of tubeworms over their life cycle and calculate ages for animals of representative sizes.

To study the differences in occurrence and life history of the two co-occurring species of tubeworms to refine working models of their interactions.

To investigate the hypothesis that adult tubeworms take up sulfide from their buried posterior ends.

---

[*] This section was authored by Derk Bergquist and Charles R. Fisher

To develop new life history models for the tubeworms and the communities of fauna associated with tubeworm aggregations.

### 8.4.3 Materials and Laboratory Methods

**Tubeworm growth measurement and bulk collection of tubeworm aggregations.** The length and anterior tube diameter were measured for all individuals of the two co-occurring vestimentiferans, *Lamellibrachia* cf *luymesi*. and the *Escarpia*-like species, in seven aggregations collected intact. This allowed the construction of size frequency histograms for these populations.

**Condition and biomass of vestimentiferans.** Subsamples taken at sea for determination of physiological condition and biomass were thawed in the laboratory and dried to a uniform weight (60°C). Individual samples were then ashed at 500°C for at least six hours and weighed again for calculation of ash-free dry weight (AFDW). The tube of each of these animals was cut into segments of 10 cm or less, and the diameters of the ends of each segment were measured to +/- 0.05 mm for diameters less than 4 mm and +/- 0.1 mm for diameters larger than 4 mm using a precision-machined device similar to a ring-sizer. The volume of each tube was calculated as the sum of the volumes of each segment estimated as the frustrum of a cone:

$$V = (1/3)(\pi l)(r_1^2 + r_1 r_2 + r_2^2) \tag{8.4-1}$$

where $l$ is the section length, $r_1$ is the radius of one end of the section and $r_2$ is the radius of the opposite end of the section. Condition was then calculated as the ratio of tissue-AFDW to tube-volume. The relationship between individual biomass and total tube length for each species was determined using linear regression. This was used to estimate the biomass of whole aggregations based upon their size distributions.

**Associated fauna.** During the July 1997 cruise, three trial collections were made using the large and small bushmaster devices. At this time, the bushmaster devices did not have linings, and the openings in the mesh bag were four millimeters. These collections were analyzed for studies on the tubeworm populations, but associated fauna was not quantified. In 1998, four collections were made using the bushmaster devices lined with 64-µm mesh. These four collections were analyzed with respect to composition, density, and biomass of associated fauna. Tubeworm aggregations at stations BHJT2, GCAT1, and BHAT2 were collected in their entirety. Approximately 50% of the aggregations at station GCST1 was enclosed in the bushmaster device and recovered intact with its associated fauna. Because the data were analyzed on the basis of the density of the associated fauna, this collection is treated the same as the others.

Contents of the mesh-lined bag were filtered sequentially through a 240-µm and 64-µm sieve. Fauna retained on the sieves was stored in 70% ethanol. The formalin from each preserved tubeworm aggregation (bush) was also sieved and the retained fauna transferred to 70% ethanol. Each aggregation was rinsed twice with 25% to 50% ethanol, preserved in 50% ethanol (because

of fire danger) in glass aquaria where they were carefully searched, and the remaining associated fauna removed. All animals removed from the aggregation were pooled, sorted to the lowest practical taxonomic level, and enumerated.

A haphazard sample of up to 30 individuals of each species in a collection was measured for length with calipers. In some collections, all individuals of a species were measured. Crustaceans were measured from the tip of the rostrum to the tip of the telson. Mussel lengths were measured from the longest points of the shell edge. For clams, shell length was measured from the umbo to the maximum shell distance. Pulmonate gastropod shells were measured from the spiral tip to the base of the apex. Minimum, maximum, and average lengths were determined for each species in each collection. A complete presentation of these data are made in Appendix Table 8.4.1. The trends and modes are discussed in this section.

Wet weights and ash-free dry weights were determined for a subsample of six to 15 individuals of each species measured for length. Weighed samples were placed in pre-ashed aluminum pans and dried at 60°C. The samples were then ashed at 500°C for a minimum of six hours and weighed. A conversion factor for wet weight to AFDW was calculated from this data and total species wet weights per collection were then converted to total AFDW for each species in a collection.

Species residency status (endemic versus nonendemic) was determined from the literature where possible. Specimens not identified by the tubeworm ecology group were sent to specialists for classification (see appendix volume for species identifications).

The number of vestimentiferans in each aggregation and total surface area of tubeworm tubes in each aggregation was estimated from haphazard sub-sampling of aggregations. The length of each tubeworm tube above the root ball and the outside diameters of the posterior and anterior tube ends were used to calculate tube surface area using the equation for the surface area of a frustrum:

$$\pi \times l \; (r_1 + r_2) \tag{8.4-2}$$

where l is the length of the tube, and $r_1$ and $r_2$ are the radii of the two ends.

**Statistical analyses.** Non-linear regression was used to fit a variety of growth models, including the von Bertalanffy, Gompertz, Richards, Logistic, Negative Exponential, and various linear transformations, to the relationship between growth rate and tube length. The best model was chosen based upon visual inspection and analysis of residuals. The

age of each individual, $i$, was determined by integrating the growth model and solving over the definite integral (0, length of $i$).

In three aggregations, growth data was successfully collected on both *Lamellibrachia* cf *luymesi* and the *Escarpia*-like species found within the aggregation. To test for within-aggregation growth rate differences between the two species, individual t-tests were employed and the sequential Bonferroni method was used to correct for multiple comparisons (Rice 1989).

Additionally, comparisons between and within aggregations of different developmental stages (juvenile–JT, adult–AT, and senescent–ST) were performed using analysis of variance and linear regression to determine whether growth and physiological condition vary according to the previously proposed model of bush development (Simpkins 1994). Because growth rate is known to vary with animal length, length was incorporated as a covariate (ANCOVA, Minitab 12) in all models involving growth rate; when length was not found to be significant it was removed and an analysis of variance was performed (ANOVA). All multiple comparisons were corrected using the Tukey-Kramer method, and all p-values shown are adjusted.

### 8.4.4 Results

**Growth rates and ages.** Data from over 600 individual *Lamellibrachia* cf *luymesi*, including both data collected as part of the study and data from animals stained previously to this study, were combined for a statistically robust analysis of their growth and calculation of age for this species. A simple negative exponential model of the form,

$$dL/dt = ae^{-bL} \tag{8.4.3}$$

where *a* and *b* are parameters and L is the standardized animal length, consistently provided the best and most robust fit to the relationship between yearly growth rate and tube length in *Lamellibrachia* cf *luymesi* (Figure 8.4.1). For this species, our results indicate the ages of animals in the upper range of sizes collected for this study (greater than two meters in length) are in excess of 170 to 250 years (Bergquist *et al.* 2000, Figure 8.4.2). These results provide a minimum age for individuals of various lengths. For example, assuming a two-meter long tubeworm grew at the maximum rate throughout its life (a very unlikely scenario), its minimum age would be 80 years.

Because the *Escarpia*-like species grows very close to the sea floor, only juvenile aggregations were successfully stained. Within the limited size range sampled, no significant relationship was found between growth rate and standardized tube length in this species (Figure 8.4.3). The mean overall growth rate for all the *Escarpia*-like species collected in this study was 2.19 cm/yr (SE = 0.20, n = 80) and was significantly less than the mean growth rate for *Lamellibrachia* cf *luymesi* of the same size range (mean = 2.92, SE = 0.09, n = 373; *df* = 116, t = 1.98, P = 0.0012). The mean growth rate of *Lamellibrachia* cf *luymesi* was greater than that of the *Escarpia*-like species at two of the three stations for which we had data on both species (Figure 8.4.4). Mean growth rates were only significantly different between the two species at one of the stations (BHJT2; t-test, P = 0.0154; sequential Bonferroni method).
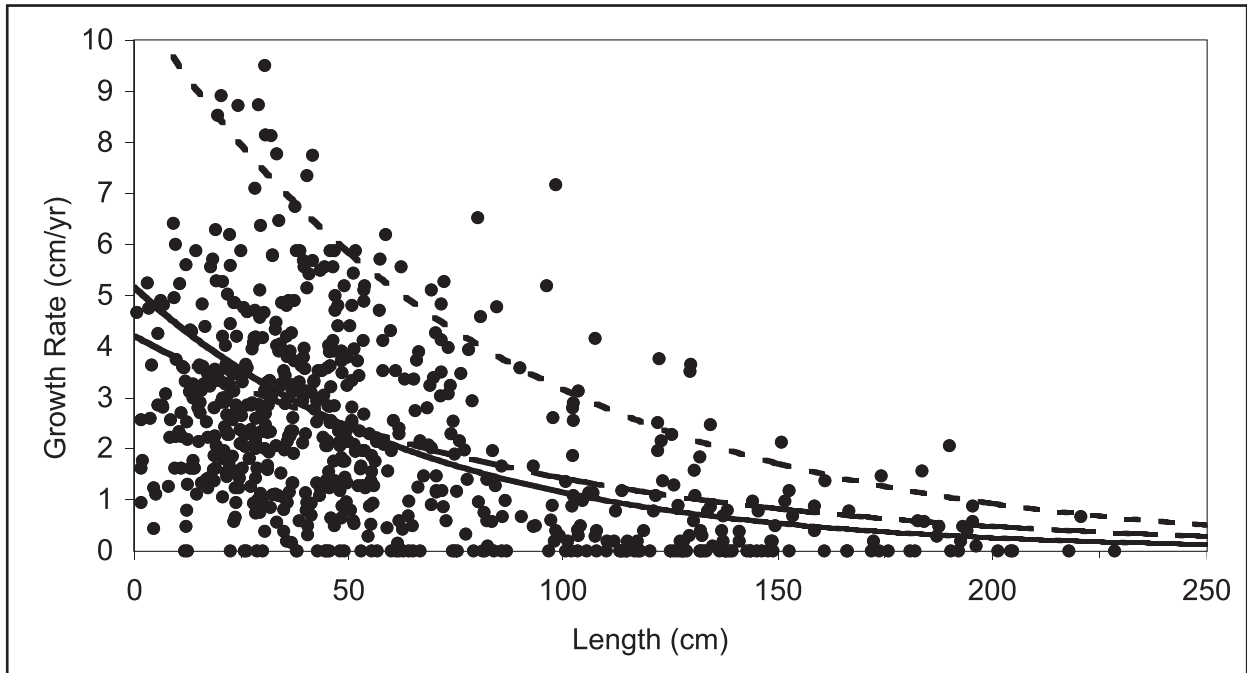
Figure 8.4.1.  Size specific growth rate in *Lamellibrachia* sp. Negative exponential model fit to data collected in 1998 (solid line), all data collected between 1995 and 1998 (broken line) and the upper bound of the 1998 data (dotted line). (Modified from Bergquist *et al.* 2000.)
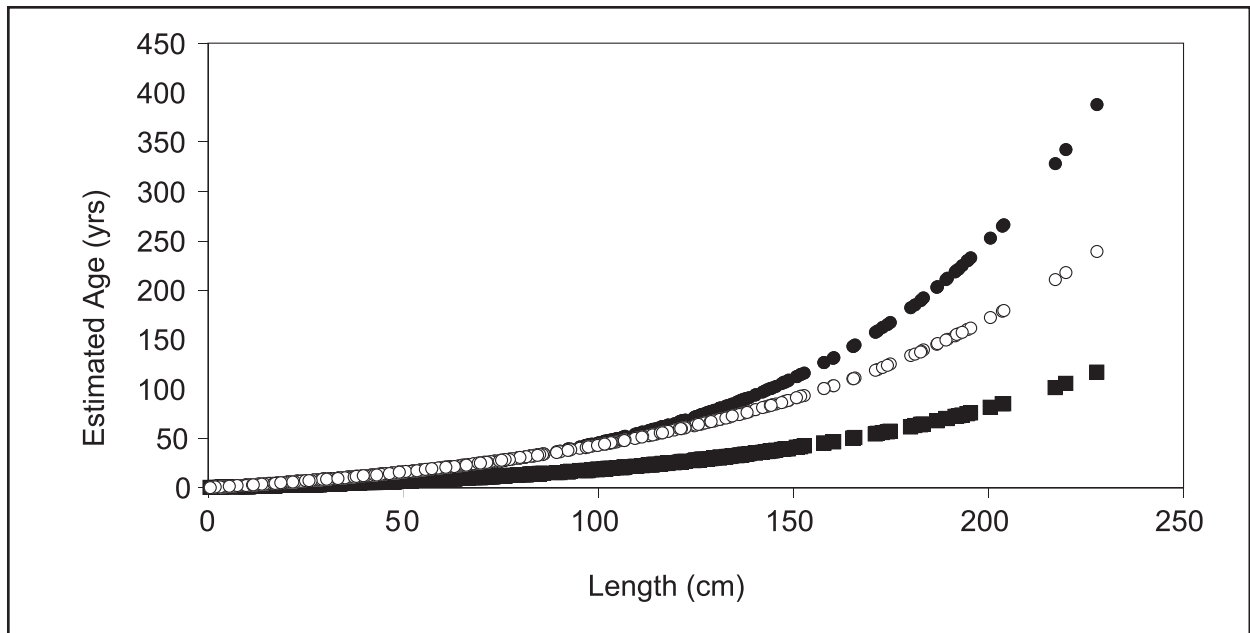


Figure 8.4.2.  Individual ages predicted from tube length using the negative exponential model. The 1998 data set (solid circles) and the 1995-1998 data set (open circles) predict the average expected age of an individual. The upper bound of the 1998 data set (closed squares) predicts the minimum theoretical age of an individual constantly growing at the maximum growth rate of the species throughout its life.
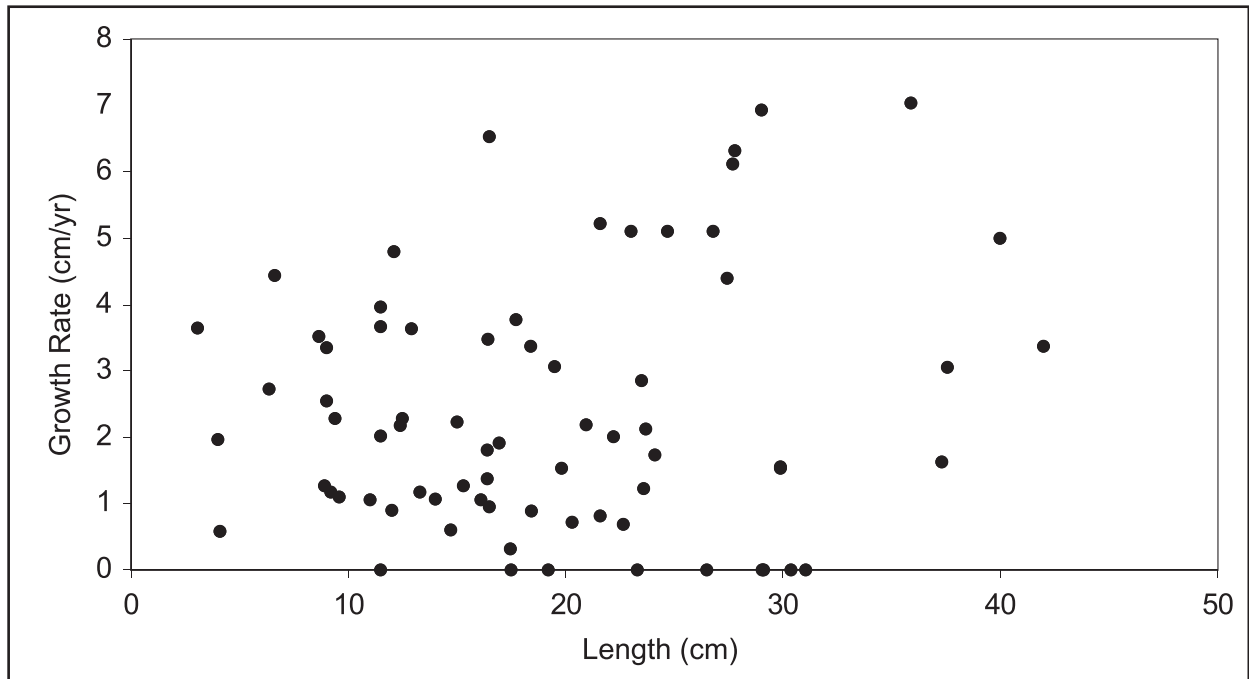
Figure 8.4.3.    Size-specific growth rate in the *Escarpia*-like species. All data collected between 1995 and 1998 are shown.
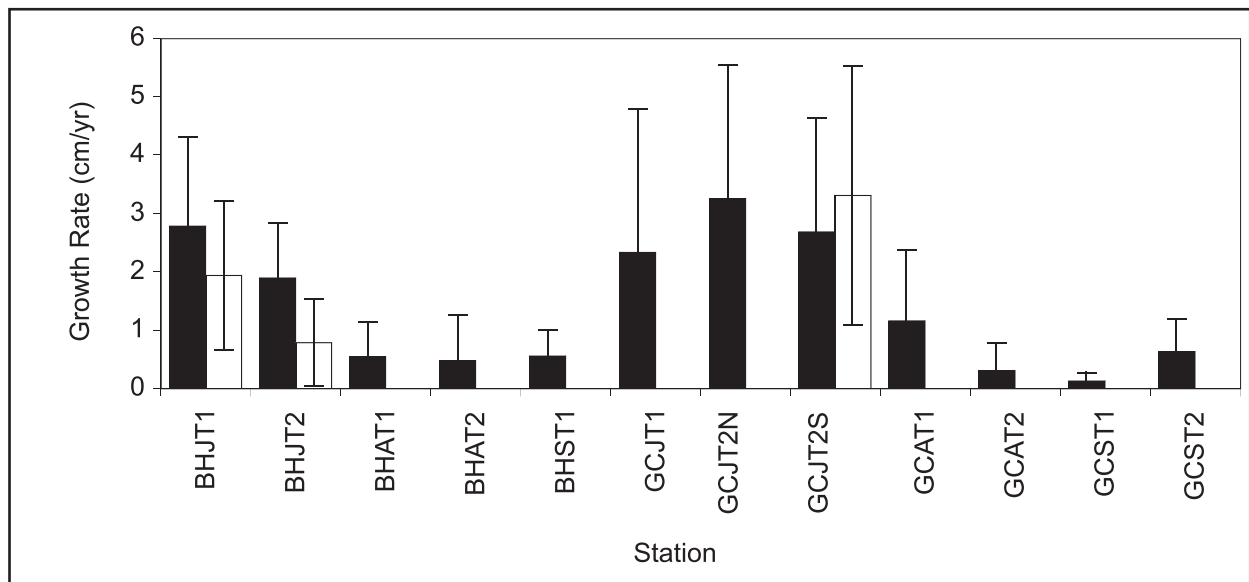


Figure 8.4.4.    Mean growth rates (±s.d.) of *Lamellibrachia* sp. (solid bars) and the *Escarpia*-like species (open bars) at all principal sampling stations. As sample size was low and growth rates were not significantly different, they were pooled to decrease sample variance.

**Site-specific comparisons.** Table 8.4.1 summarizes the length, growth rate, and condition of *Lamellibrachia* cf *luymesi* and the *Escarpia*-like species of the three vestimentiferan community developmental stages collected in this study. The mean growth rates of *Lamellibrachia* cf *luymesi* at each principal sampling station are shown in Figure 8.4.4. As expected, growth rates of *Lamellibrachia* cf *luymesi* in the juvenile aggregations were significantly greater than the growth rates in both adult and senescent aggregations (ANCOVA; $P < 0.0001$ and $P = 0.0485$, respectively), but unexpectedly, there was no significant difference in growth rates between adult and senescent aggregations ($P = 0.9083$). The growth rates of *Lamellibrachia* cf *luymesi* varied significantly between different juvenile and adult aggregations (ANCOVA; $P < 0.001$ and $P = 0.002$, respectively), but growth rates did not vary significantly between different senescent aggregations ($P = 0.245$). Among the juvenile stations, BHJT1 and BHJT2 showed significantly less growth than GCJT2N and GCJT2S ($0.0003 \leq P \leq 0.0346$). Among the adult stations, GCAT1 showed significantly more growth than BHAT1 and BHAT2 ($P = 0.0193$ and $P = 0.0229$, respectively). The growth rates of the *Escarpia*-like species varied significantly between different juvenile aggregations (ANOVA, $p = 0.028$) with GCJT2S growing faster than BHJT2 ($P = 0.0270$).

Table 8.4.1. Characteristics of *Lamellibrachia* sp. and the *Escarpia*-like species in juvenile, adult and senescent aggregations. Included are the number of individuals of each species and the number of stations from which individuals were sampled from each developmental stage. Length, growth rate, and condition are all given as means and standard deviation (s.d.).

| Species | Stage | Stations | Count | Length in cm (s.d) | Growth rate in cm/yr (s.d.) | Condition in $g/cm^3$ (s.d.) |
|---|---|---|---|---|---|---|
| *Lamellibrachia* sp. | Juvenile | 6 | 244 | 36.3 (16.8) | 2.75 (1.94) | 0.131 (0.031) |
| | Adult | 4 | 136 | 119.5 (37.7) | 0.61 (0.91) | 0.094 (0.026) |
| | Senescent | 3 | 59 | 155.5 (121.2) | 0.59 (0.56) | 0.119 (0.045) |
| *Escarpia*-like | Juvenile | 5 | 57 | 24.5 (10.4) | 2.84 (2.22) | 0.148 (0.055) |
| | Adult | 2 | 20 | 41.7 (8.3) | ------- | 0.144 (0.025) |
| | Senescent | 1 | 5 | 53.6 (21.5) | ------- | 0.165 (0.037) |

The condition of *Lamellibrachia* cf *luymesi* and the *Escarpia*-like species at each station is shown in Figure 8.4.5. Overall, the relationship between condition and growth rate in *Lamellibrachia* cf *luymesi* is positive and significant ($P < 0.001$, Pearson's $r = 0.359$), indicating that growth rate reflects relative animal health over a large size range. No such relationship was found for the *Escarpia*-like species ($P = 0.473$). In a two-way ANOVA, the interaction between site and developmental stage was significant ($P < 0.001$), so the two sites were analyzed separately with two one-way ANOVAs. At BH, juvenile and senescent aggregations has higher condition indices than adult aggregations ($P = 0.002$ and $P < 0.001$, respectively), but juvenile and senescent aggregations did not have significantly different condition indices ($P = 0.261$). At GC, juvenile aggregations had significantly higher condition indices than adult or senescent aggregations ($P < 0.001$ in both cases), but senescent and adult aggregations were not

significantly different (P = 0.78).  No similar trends were apparent in the *Escarpia*-like species, but less data were available for this species because of collection methods. The condition of *Lamellibrachia* cf *luymesi* differed significantly between aggregations within all developmental stages (ANOVA; P ≤ 0.033 for all), but in the *Escarpia*-like species only varied significantly between aggregations within the juvenile stage (P < 0.0001). Among juvenile aggregations, the condition of *Lamellibrachia* cf *luymesi* was significantly higher at GCJT2N than at BHJT2, GCJT1a and GCJT1b (P < 0.001 for all); at GCJT2S condition was significantly higher than at BHJT2 or GCJT1b (P = 0.006 and P = 0.002, respectively). The condition of *Lamellibrachia* cf *luymesi* among adult stations was higher at BHAT1 than at BHAT2 (P = 0.038) and among senescent stations was lowest at GCST2 (P < 0.0001), the lowest condition found in any aggregation collected. The condition of the *Escarpia*-like species was significantly lower at BHJT2 than at any other juvenile station except GCJT1a (ANOVA; P ≤ 0.0005 for all) and was significantly lower at GCJT1a than at BHJT1 and GCJT2S (P = 0.0231 and P = 0.0438, respectively). The condition of *Escarpia*-like species did not vary significantly among adult stations. The mean lengths of all the vestimentiferans subsampled from each of the primary stations for growth rate and condition are shown in Figure 8.4.6. Mean lengths varied significantly between the three developmental stages in both species (P < 0.001 for both) and varied significantly between stations within all developmental stages in *Lamellibrachia* cf *luymesi* (P < 0.001 for all) and between stations within the juvenile stage in the *Escarpia*-like species (P < 0.001).

**Vestimentiferan population composition and size structure.** Both the *Escarpia*-like species and *Lamellibrachia* cf *luymesi* were present in every aggregation that was collected intact. The *Escarpia*-like species was the less abundant of the two vestimentiferans in six of the seven aggregations (Figure 8.4.7) and, overall, was significantly less abundant within the aggregations than *Lamellibrachia* cf *luymesi* (Paired t-test, *df*=6, P = 0.032). *Lamellibrachia* cf *luymesi* was significantly longer than the *Escarpia*-like species in all of these aggregations (paired t-tests, p < 0.001 in all cases, sequential Bonferroni method).

The size distributions of both species in all but one aggregation (BHJT2) were non-persistent (Figure 8.4.8a-g). The smallest size classes were present in aggregations of only small animals indicating that new recruitment was occurring or had recently occurred (Figure 8.4.8a, b).  In these aggregations the two species show similar modes in their size distributions.  The smallest size classes were present in only one aggregation of larger individuals (GC-AT1); when collected, a cluster of smaller individuals was partially entangled with one edge of this aggregation. With the exception of GC-AT1, aggregations of larger individuals in the smallest size classes were not represented indicating that recruitment to these sites had ceased (Figure 8.4.8c-g). In addition, the modes of the *Lamellibrachia* cf *luymesi* size distributions were much higher than the *Escarpia*-like species.
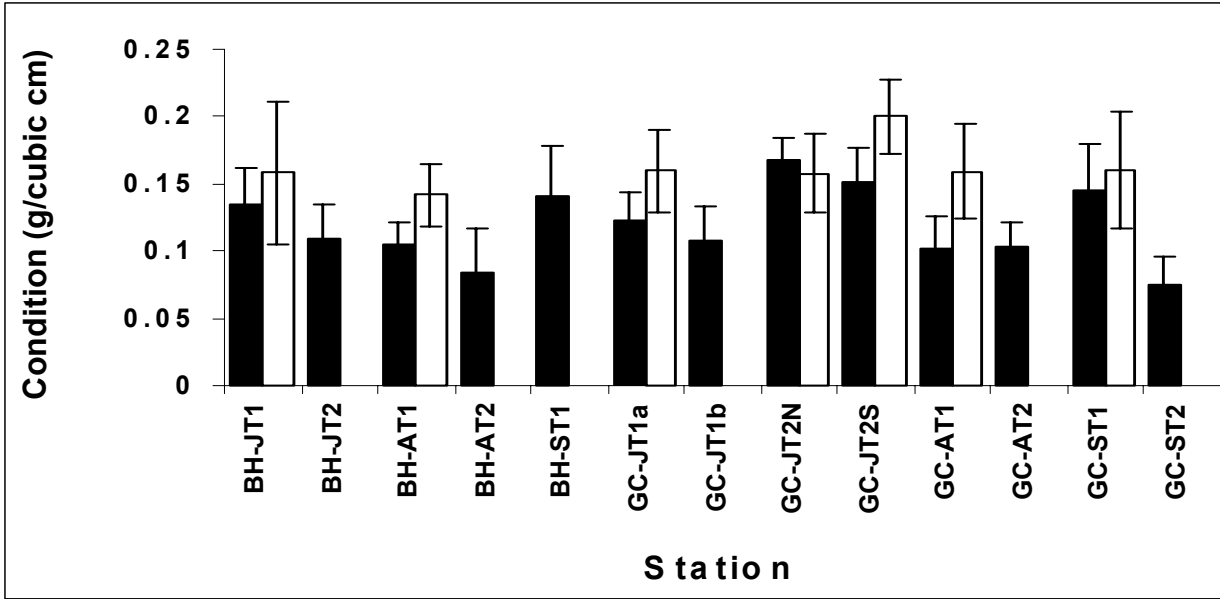
Figure 8.4.5.    Mean condition indices (±s.d.) of *Lamellibrachia* sp. (solid bars) and the *Escarpia*-like species (open bars) at all principal sampling stations.
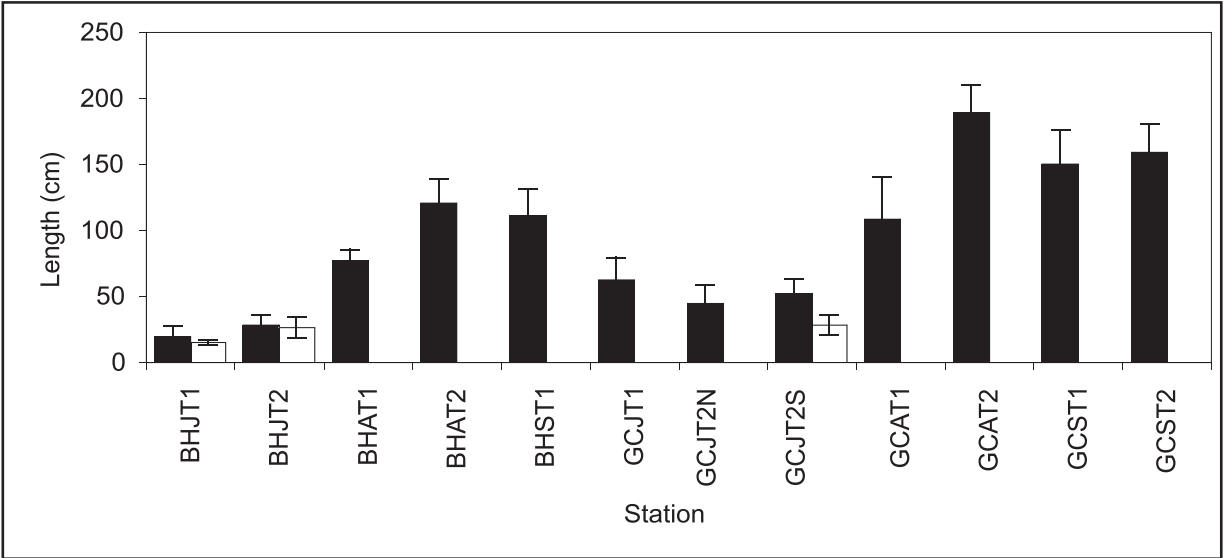


Figure 8.4.6.    Mean tube lengths (±s.d.) of subsamples of *Lamellibrachia* sp. (solid bars) and the *Escarpia*-like species (open bars) taken from the principal sampling stations for determination of growth rate and condition.
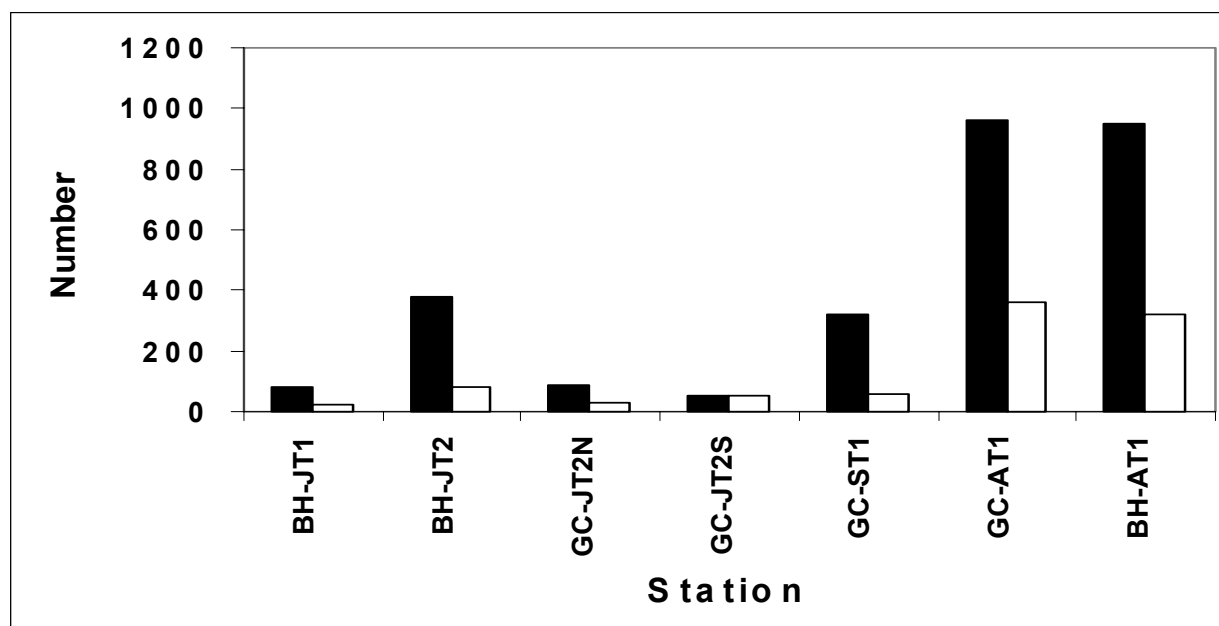
Figure 8.4.7.    Abundances of *Lamellibrachia* sp. (solid bars) and the *Escarpia*-like species (open bars) at seven principal sampling stations from which all vestimentiferans were collected and measured.

**Associated faunal collections.** The complete list of species collected with the four bushmaster collections is presented in appendix volume. The resident status (endemic, non-endemic, or unknown) is given in this table as well. A total of 60 species of animals from 11 phyla (4,624 individuals) was collected with the four aggregations. Thirty-five species had not been documented from previous collections of seep fauna and many of those may turn out to be new species. Eight species were present in all collections. Four of these species, the shrimp *Alvinocaris stactophila*, the crab *Munidopsis* sp. 1, the annelid *Nicomache* sp., and the sponge *Ectyomyxilla methanophila* are thought to be endemic to the seeps. The four other species, the nemertean *Lineus* sp., the hydroid *Acryptolaria* sp., the amphipod *Stephonyx* sp., and the polychaete *Harmothoe* sp., are likely endemic but confirmation of this awaits complete identification by experts.

A collection of juvenile tubeworms yielded 19 species of associated fauna, and the highest biomass of associated fauna of any collection (Table 8.4.2). Most of this biomass was a result of the very high numbers of a few species of endemic animals (Figure 8.4.9). Communities associated with adult aggregations are much more diverse, with about twice the species richness of the juvenile community (Table 8.4.2). The communities are still dominated by endemic species, but numerous species of non-endemic animals are present in small to moderate numbers (Figure 8.4.10 and 8.4.11). The biomass of associated fauna in the adult aggregations is almost one order of magnitude less (per unit area) than in the juvenile aggregation. A single collection of a senescent aggregation contained 20 species, half of which were represented by a single individual (Figure 8.4.12). This aggregation was supporting about 20% of the biomass of the adult aggregations (Table 8.4.2). Even endemic fauna was only present in small numbers if present at all in the senescent aggregation.
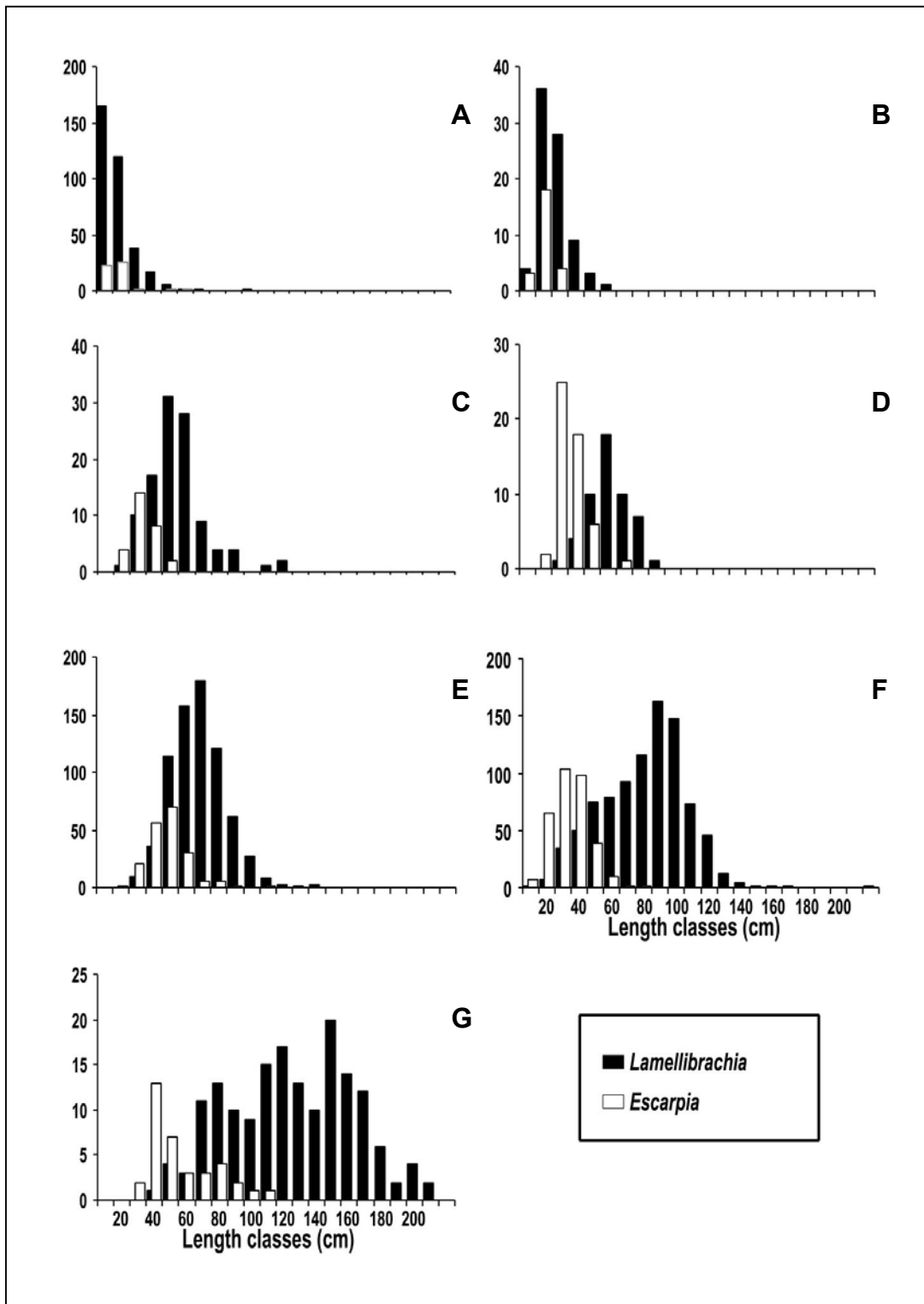
Figure 8.4.8.    Size frequency histograms of *Lamellibrachia* sp. (solid bars) and the *Escarpia*-like species (open bars) at the seven principal sampling stations from which all vestimentiferans were collected and measured. Histograms ordered by increasing *Lamellibrachia* sp. modal size: a) BHJT2*, b) BHJT1, c) GCJT2N, d) GCJT2S, e) BHAT1*, f) GCAT1*, g) GCST1**. (*Size frequencies presently based on subsamples; **one half of the aggregation was collected and all individuals in that half were counted and measured.)

Table 8.4.2. Characteristics of 1998 bushmaster collections.

| Aggregation Name | Volume ($m^3$) | Number | Tube SA ($m^2$) | No. Species | No. Individuals Ind/$m^2$ | Density gAFDW/$m^2$ | Biomass |
|---|---|---|---|---|---|---|---|
| BHJT2 | 0.02 | 1236 | 1.3 | 19 | 3263 | 2453 | 100 |
| GCAT1 | 0.1 | 1112 | 6.2 | 34 | 323 | 52 | 15 |
| BHAT2 | 0.3 | 800 | 5.3 | 37 | 976 | 185 | 20 |
| GCST1 | 0.4 | 306 | 4.7 | 20 | 64 | 14 | 3 |

**Pore water and wand samples associated with tubeworm aggregations.** Water samples taken above the sediment and associated with tubeworm bushes were analyzed using a method that allowed detection of sulfide at concentrations as low as 0.1 µM (Table 8.4.3). Sulfide was never detected in control samples taken by the submarine between 100 and 300 meters above the bottom. Sulfide was only detected in 2 of 25 samples taken at plume level among tubeworm aggregations and both of these samples were taken in juvenile aggregations. Sulfide was detected in 4 of 23 samples taken at a point approximately half way between the sediment and the plumes of the tubeworms in the middle of aggregations. Even at the sediment water interface sulfide was below the limits of detection in 15 of 22 samples. Of the 13 samples with detectable sulfide, eight were associated with juvenile aggregations and four with a senescent aggregation station found to be in close proximity to a juvenile aggregation.

Table 8.4.3. Seawater sulfide concentrations among hydrocarbon seep tubeworm bushes.

| Sample Location | Range of [$H_2S$] (µM) | Samples Taken | Samples with No Detectable Sulfide | % ND |
|---|---|---|---|---|
| Water Column | ND | 24 | 24 | 100 |
| Plume Level | ND – 0.7 | 25 | 23 | 92 |
| Mid-Bush | ND – 1.9 | 23 | 19 | 83 |
| Sediment Level | ND – 3.7 | 22 | 15 | 68 |

Using the deep probe, interstitial water samples were taken from beneath the tubeworm aggregations. Depth of the sample was determined by the depth where the probe met solid substrate; in some cases this was likely the top or edge of the carbonate rock the aggregations were attached to. Juvenile aggregations tended to be attached to shallowly buried rocks, and the larger aggregations to much deeper buried rocks. Distribution of sulfide in the interstitial spaces was very patchy. In one case "replicate" samples taken from the same depth beneath an aggregation yielded 0 and 2.75 mM sulfide. Because of the patchiness and the relatively small number of samples taken in association with each aggregation it is not appropriate to use this data to draw conclusions about the exposure of individual aggregations to sulfide. Nonetheless it is apparent from the data set that high levels of sulfide are often present in interstitial pools and that high levels of sulfide are found at least to 70 cm depth, the deepest depth sampled (Table 8.4.4).

Table 8.4.4. Interstitial sulfide levels beneath vestimentiferan aggregations in the Gulf of Mexico. Included are depth ranges from which the samples were taken, the number of those samples in which sulfide was not detected (ND), the range of quantified sulfide concentrations, and the mean sulfide concentration (+/-1 s.d.).

| Bush Type | Depth Range (cm) | Number Samples | Number ND | Sulfide-Range (mM) | Sulfide Concentration (mM) |
|---|---|---|---|---|---|
| Juvenile | 10-40cm | 9 | 5 | 0.000-2.725 | 0.5610 (+/-1.097) |
| Adult | 15-70cm | 12 | 2 | 0.000-0.6865 | 0.1682 (+/-0.2451) |
| Senescent | 27.5-65cm | 12 | 6 | 0.000-7.885 | 0.6644 (+/-2.2739) 0.0080 (+/-0.0106)* |

*mean sulfide concentration when the single very high value (7.885 mM) was removed

**Sulfide uptake by posterior extensions (roots).** Using the new bushmaster collection devices, it was confirmed that root-like extensions were present on all intact individuals examined from larger aggregations and even most individuals from juvenile aggregations. Permeability studies on these and other translucent buried tubes, "roots," confirmed that they are quite permeable to sulfide and that this increased permeability is not due solely to the thickness of the root tubes (Figure 8.4.13, Julian *et al*. 1999a). Incubation of live animals in split respirometers demonstrated unequivocally that *Lamellibrachia* cf *luymesi* is capable of taking up sulfide across its posterior end (root) at rates sufficient to fuel net $CO_2$ uptake (autotrophy) (Table 8.4.5, Freytag *et al*. submitted).

Table 8.4.5. Plume $CO_2$ flux
prior to, during, and after root $H_2S$ exposure*

| Experimental Conditions | $CO_2$ Flux (μmoles/gm./hr.) |
|---|---|
| Pre-$H_2S$ Exposure | - 2.36 ± 0.76 (n = 73) |
| 500 μM $H_2S$ in posterior chamber | 2.13 ± 0.98 (n = 78) |
| Post-$H_2S$ Exposure (17 hrs) | - 4.87 ± 1.81 (n = 38) |

*From Freytag *et al.* submitted
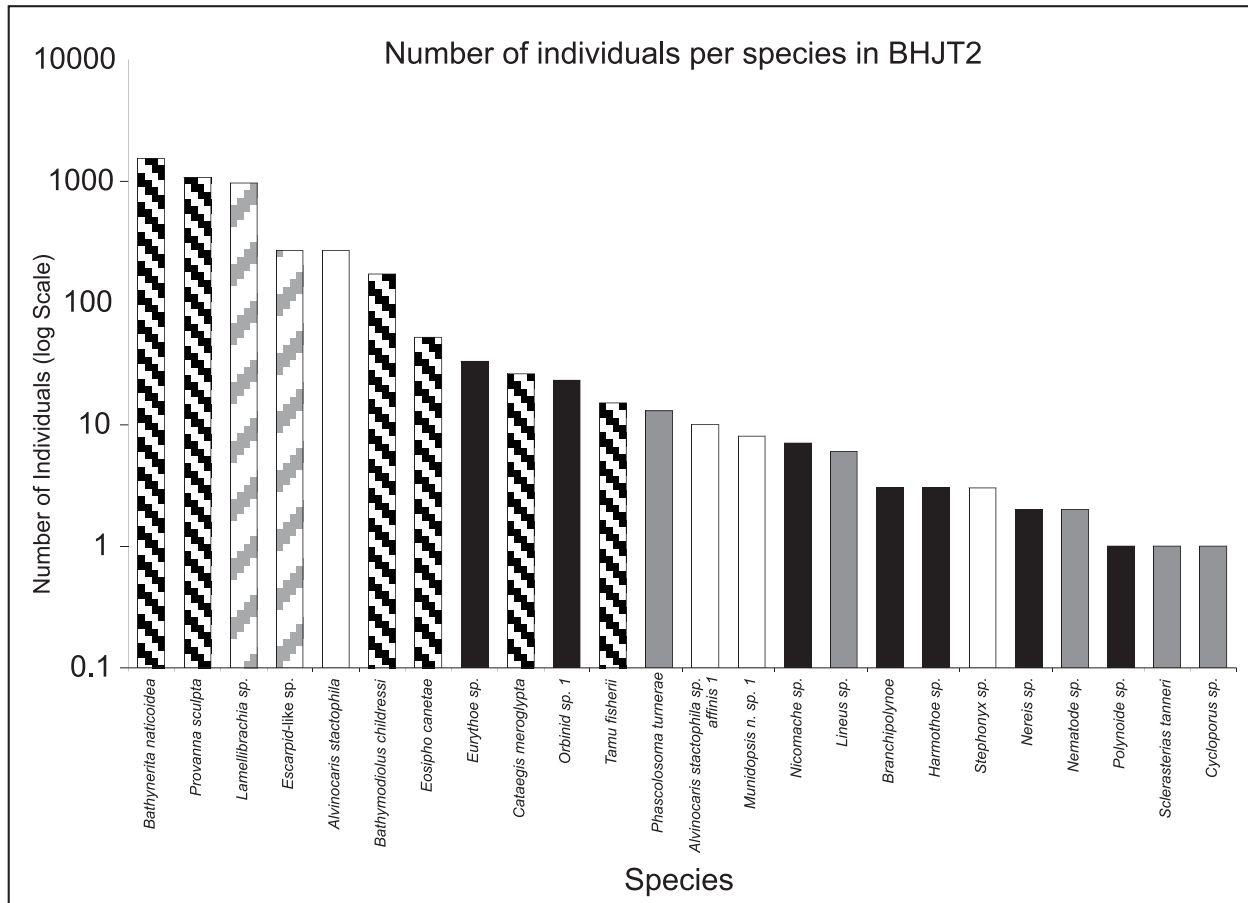
Figure 8.4.9.    Species richness and abundance in Bushmaster Jr. Collection of BHJFIGURE 8.4.2. Vestimentiferans are indicated by the bars with ascending hash marks, mussels by bars with descending hash marks, arthropods with white bars, annelids by black bars, and all other fauna by gray bars.
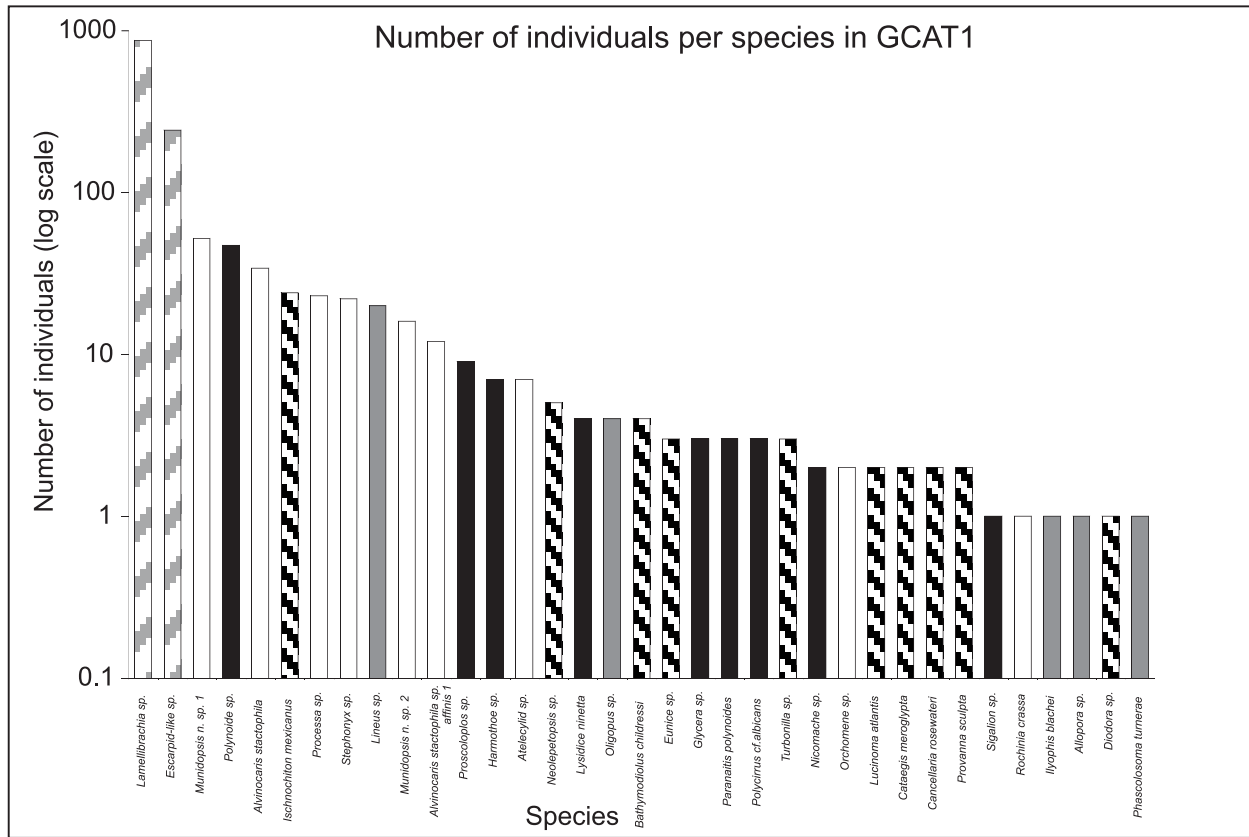
Figure 8.4.10.    Species  richness  and  abundance  in  Bushmaster  Sr.  Collection  of  GCAFIGURE  8.4.1.
Vestimentiferans  are  indicated  by  the  bars  with  ascending  hash  marks,  mussels  by  bars  with
descending hash marks, arthropods with white bars, annelids by black bars, and all other fauna by
gray bars.
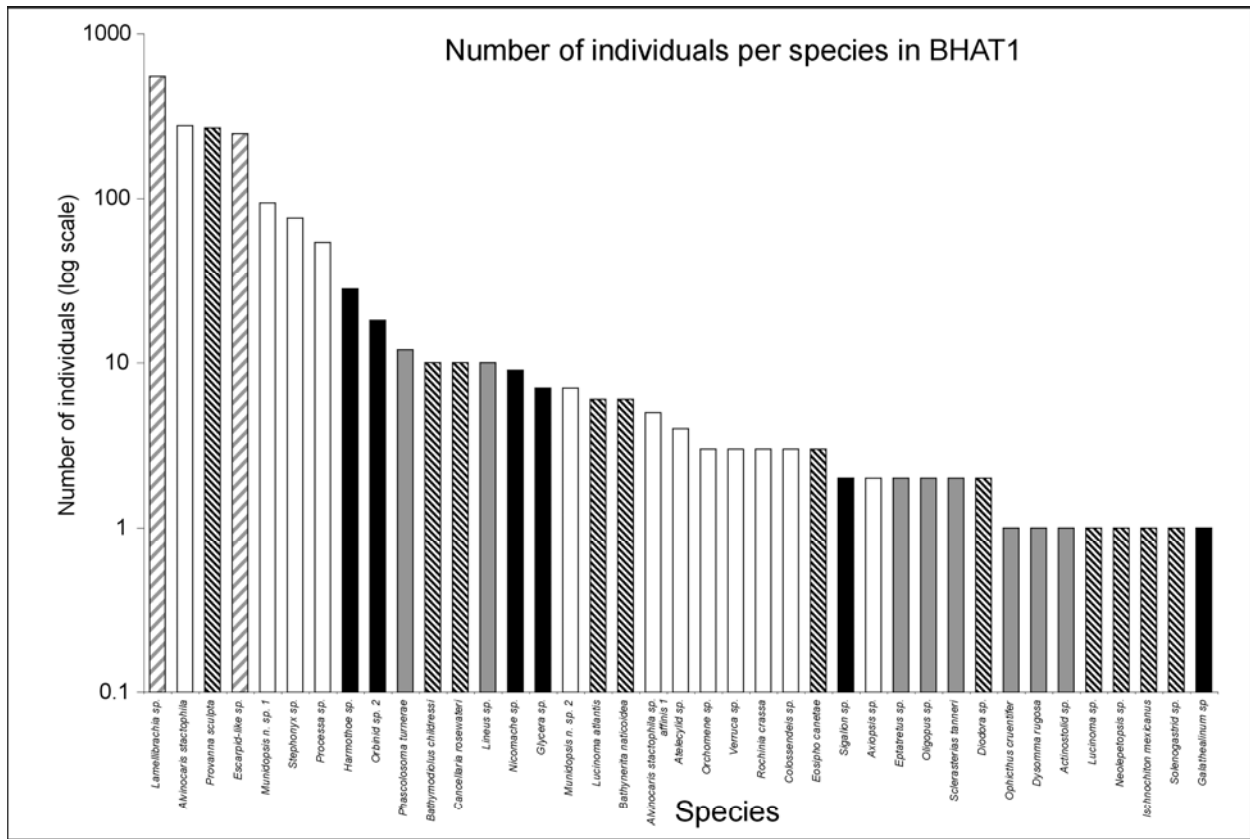
Figure 8.4.11. Species richness and abundance in Bushmaster Sr. Collection of BHAFIGURE 8.4.1. Vestimentiferans are indicated by the bars with ascending hash marks, mussels by bars with descending hash marks, arthropods with white bars, annelids by black bars, and all other fauna by gray bars.
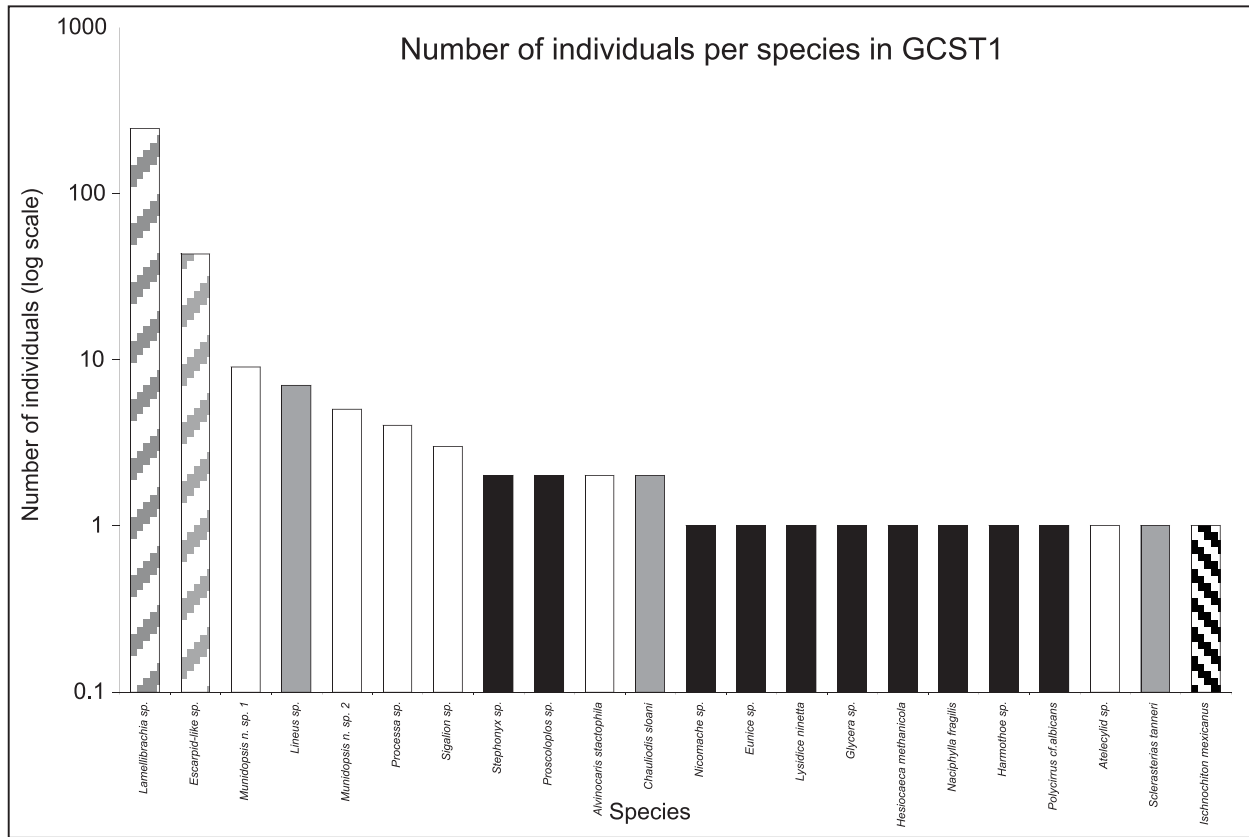
Figure 8.4.12.    Species richness and abundance in Bushmaster Sr. Collection of GCSFIGURE 8.4.1.
Vestimentiferans are indicated by the bars with ascending hash marks, mussels by bars with
descending hash marks, arthropods with white bars, annelids by black bars, and all other fauna by
gray bars.
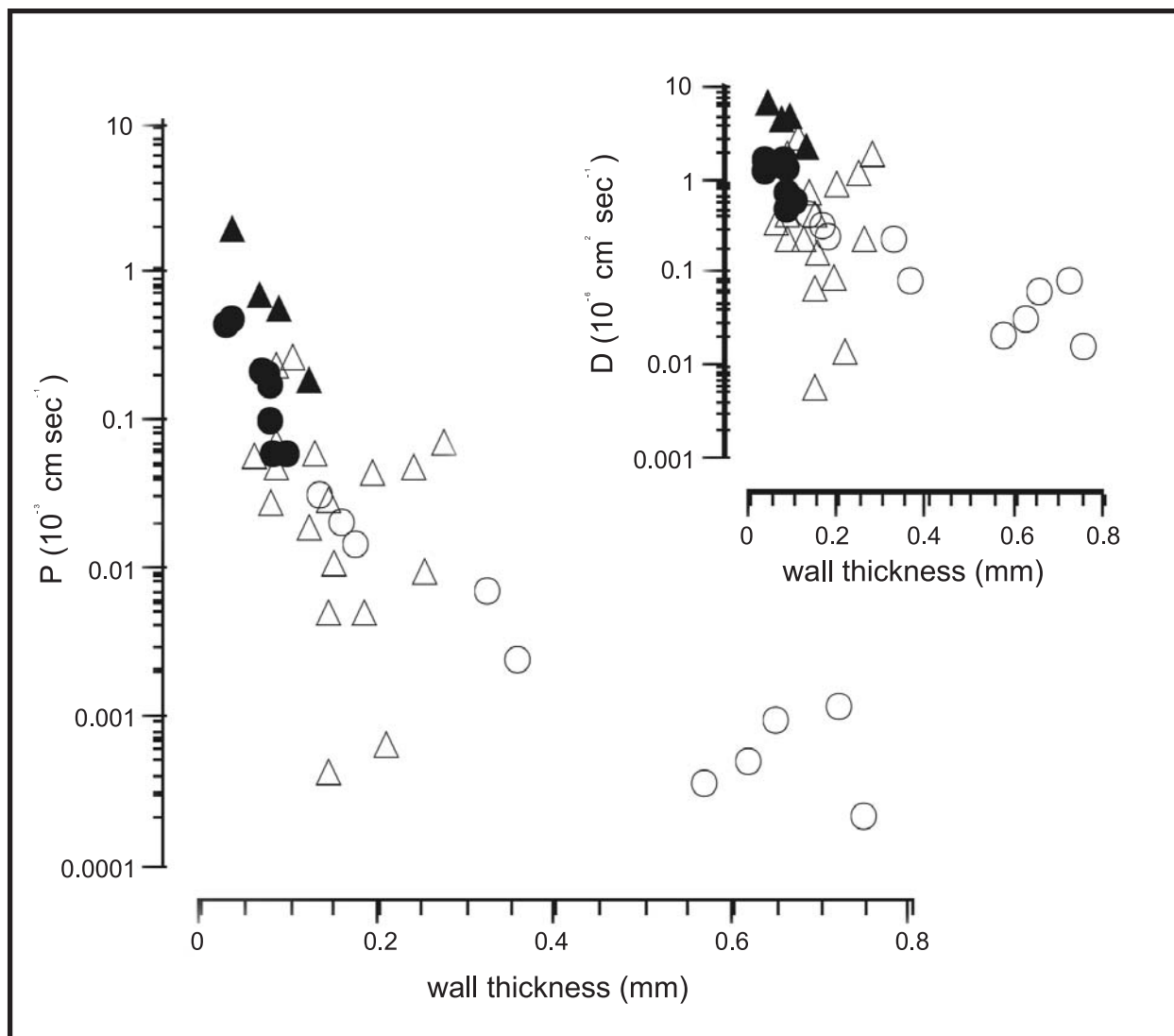
Figure 8.4.13.    Sulfide permeability of *Lamellibrachia* sp. tubes. Closed symbols represent root tube sections, open symbols represent trunk tube sections. Circles represent flow-through measurements, and triangles represent recirculating measurements. The diffusion coefficient (D, inset) was calculated by multiplying P by the wall thickness. (Julian *et al.* 1999a)

## 8.4.5 Discussion

Two key discoveries from this study have profound implications to the understanding of the tubeworm communities in the Gulf of Mexico.  One is the presence and function of the long posterior extensions of the tubeworms, their roots. It is now known that *Lamellibrachia* cf *luymesi* at least, and most likely the *Escarpia*-like species as well, can take up sulfide from interstitial fluids, which are tens of centimeters deep in the sediment. This adaptation provides the tubeworms access to a stable and longer lasting source of sulfide and provides the explanation for the growth and abundance of tubeworms in areas where sulfide is not detectable in the water above the sediments. It also has significant implications for the structure of the associated faunal communities. Tubeworm communities can flourish in areas where very little

potentially toxic seep fluid is present in the water above the sediments. Access to a stable and long-lived source of sulfide may also be a key factor in explaining the longevity of tubeworms, which was the second key discovery of this study. When the current study began, it was known that the tubeworms could live in excess of one hundred years, but we had no proof that they could live much beyond a century. The current data set clearly indicates that *Lamellibrachia* cf *luymesi* lives in excess of 170 to 250 years (Bergquist *et al.* 2000) making them one of the longest lived non-colonial animals we know of. The data was interpreted conservatively (Bergquist *et al.* 2000) because those estimates were based on a maximum size of two meters, and animals up to three meters have been collected at these sites and are presumably much older. It is conceivable that they can live considerably longer still.

There are a variety of lines of evidence that suggest *Escarpia*-like species lives at least as long as *Lamellibrachia* cf *luymesi* and perhaps even longer. Because both species appear to settle simultaneously over a period of time before recruitment to a substratum ceases, the presence of the *Escarpia*-like species in every aggregation recovered, particularly in aggregations with the largest *Lamellibrachia* cf *luymesi*, strongly suggests that this species is living at least as long as *Lamellibrachia* cf *luymesi*. The fact that aggregations comprising only large *Escarpia* were observed and that aggregations comprising only *Lamellibrachia* cf *luymesi* were not observed suggests that *Escarpia* might outlive *Lamellibrachia* cf *luymesi*. If this is in fact the case, the *Escarpia*-like species may be living significantly longer than *Lamellibrachia* cf *luymesi*.

Characteristics of the vestimentiferan populations varied significantly between different stations. As was expected, vestimentiferans display the highest growth rates in juvenile aggregations, but the variation found between different juvenile aggregations and the lack of any difference in growth rates between the adult and senescent aggregations clearly suggest that developmental phase is not the only factor driving growth rate. The positive relationship between growth rate and condition in *Lamellibrachia* cf *luymesi* and the fact that those juvenile aggregations showing the lowest growth rates typically had the lowest condition index values indicate that the ability of this vestimentiferan to grow is tied to its physiological health. This is particularly interesting when considering the high condition index of juvenile and BH senescent aggregations as compared to the relatively low condition of the adult aggregations. One possibility is that in juvenile aggregations, the local seepage rate can support the relatively low vestimentiferan biomass, but as the populations and the individuals within those populations grow to the adult phase, standing-stock biomass increases and competition begins to play an important role. As the population size decreases as a result of competition, the aggregation enters the senescent phase where fewer individuals are vying for the limited local seepage. The large number of individuals occupying a very limited space at BHJT2 may be reflecting this competition dynamic in their low growth rate and condition relative to the other juvenile aggregations.

The bushmaster collections yielded an unexpected wealth of associated fauna. A total of 59 different species were collected in association with these four aggregations of tubeworms. Thirty-five species had not been documented from previous collections of seep fauna and many of those may turn out to be new species. Many of these species were found in more than one collection indicating that their occurrence was not unusual. Since 17 of the species were represented in only a single collection it is likely that we have only begun to scratch the surface of the species richness of fauna associated with vestimentiferans at these sites. One discovery of special relevance to the study that also emphasizes the superiority of this new collection method over previous methods was the association of the chemosynthetic mussel *Tamu fisheri* with the

bases of some vestimentiferan aggregations. A significant effort was made during CHEMO I to collect this species, but its natural habitat was unknown (like the new species of *Escarpia*-like vestimentiferan discovered during this study, only a few individuals of *Tamu fisheri* were collected during the CHEMO I project). A second surprise was the consistent collection of fish and eels in the aggregations.

The limited number of collections precludes a statistical comparison of bushes of different ages, but several trends stand out in the data. The juvenile aggregation had the highest biomass of any aggregation even though it also had the lowest surface area of exposed tube for colonization. Species richness was about half of the adult aggregations and dominated by known endemic species. Mollusks dominated the associated fauna as they do in mussel beds and the fauna in general was similar to that found associated with mussel beds. All of these observations are consistent with juvenile aggregations occurring in the areas of most active seepage colonized by vestimentiferans and with a high level of productivity in the aggregations. The abundance of grazers suggests an abundant food source for this feeding group, which is likely to be free-living bacteria.

Both adult aggregations had about twice the species richness of the juvenile and senescent aggregations. However, the biomass supported by the adult aggregations was 15 – 20% of that supported by the juvenile aggregation. Although mollusks are still abundant in these aggregations, arthropods are more dominant. Even though the two collections were from different sites, the six most abundant species (morphotypes) of arthropod were the same. Although many of the species in these aggregations are endemic to the seeps, the presence of many known vagrant species suggests this habitat is tolerable by a wider range of fauna. The moderately high biomass suggests that there is still significant primary productivity associated with the adult aggregations.

The senescent aggregation was notable for the very low biomass of associated fauna, 69% of which was accounted for by a crab and two fish. Mollusks were rare in this aggregation (a single individual) and non-endemic species abundant. Over half of the species present were represented by a single individual, and the density of associated fauna was less than 1% of that found in the juvenile aggregation. All of this is consistent with a habitat of low productivity and low toxicity.

The model for seep tubeworm life history and community succession that results from the present work is as follows: Tubeworm aggregations begin with larval tubeworms settling in areas of active seepage where the precipitation of carbonates forms the hard substrate they need for recruitment. In some cases, this is in areas where mussels are also settling or have previously colonized. For a few years, the high level of seepage is maintained at this point, the carbonate the first recruits have settled on may continue to grow, and recruitment to this aggregation continues as long as sulfide is released from the seafloor and the carbonate remains exposed. Because the young aggregation is in a microhabitat of active seepage, only fauna that can tolerate these conditions are associated with the young aggregations. These fauna include the animals found in mussel beds and is dominated by endemic seep animals that can occur in large numbers with significant biomass. During this time the very young tubeworms obtain sulfide across their plume, grow a posterior extension of their tube (a "root"), and begin to supplement their sulfide uptake from interstitial pools. Over the next century or two, the tubeworms continue to grow while seepage of sulfide from the sediment into the water column progressively decreases. During this period, there is sufficient primary production associated with the aggregation to

maintain a moderately high biomass community and yet the toxicity of the habitat has decreased to the point that a wide variety of non-endemic fauna can colonize or visit the aggregations. At this point, the analogy between the tubeworms and long-lived ecosystem-structuring plants is quite strong. Although the tubeworms may not be the prime food source for most of the associated fauna, they provide a habitat for numerous species and stable isotope data suggests most of the fauna is incorporating seep primary production. As the aggregation continues to age, flow of sulfide into the water column continues to decrease and some thinning of the aggregation occurs. Non-endemic and non-mobile fauna often colonizes the tubes heavily, primary production by free-living bacteria associated with the aggregation decreases significantly, and the biomass of the associated faunal community drops significantly. This stage in their life history may also last a very long time, because the tubeworms in these less dense old aggregations continue to grow and are in very good condition, presumably in part because of reduced competition from the remaining vestimentiferans.

## 8.5 Histopathy and Health of Seep Mussels[*]

### 8.5.1 Introduction

Petroleum seep mussels (*Bathymodiolus childressi*) are often exposed to high hydrocarbon concentrations in their natural habitat. And, like many mollusks, they are susceptible to parasitism and disease. Thus, they offer the opportunity to examine the relationship between parasitism, disease, and contaminant exposure under natural conditions. Because petroleum seep mussels are closely associated with hydrocarbon seepage, the prevalence and infection intensity of parasites, diseases, and tissue pathologies may vary with site chemistry and, as a consequence, may provide a useful early warning signal of long-term changes in the health of seep communities that may eventually result in local extinction. Discriminating populations that are in decline from those that are healthy is a key component to understanding the processes controlling the structure and persistence of seep communities.

This is the first report on the histopathology of cold-seep mussels. The goals of this study were as follows:

1. To document the parasite body burdens in petroleum seep mussels;

2. To determine whether parasite body burdens varied spatially between nearby populations and between populations separated on larger scales;

3. To evaluate the degree to which parasites might impact population dynamics and the persistence of seep communities;

4. To document the rapidity with which parasite infections and physiological condition respond to changes in host population structure and environment;

---

[*] This section was authored by Evic N. Powell.

5. To examine the relationship between parasites levels and polycyclic aromatic hydrocarbon (PAH) body burdens.

The importance of parasitism and disease in seep mussel populations has not been studied. Mussels commonly harbor parasites and diseases of a variety of types (Gee and Davey 1986; Kent *et al.* 1989; Kim *et al.* 1998) and, in some cases, these parasites and diseases can significantly affect their health and fecundity (Bierbaum and Ferson 1986; Coustau *et al.* 1991; Pérez *et al.* 1997). The concept that reduced health, which is brought on by pollutants, limitations in food availability, and other stressors, results in increased susceptibility to a range of parasites and diseases in mollusks was initially propounded by Laird (1961) and has received support from a wide array of subsequent studies (Kim and Powell 1998).

Understanding the role that parasites might play in mussel population dynamics and health requires an understanding of the rapidity with which parasite infections respond to changes in host population structure and environment. Parasite transmission rates vary substantially between parasite types. Some oyster parasites, such as *Perkinsus marius* and *Haplosporidium nlesoni*, can reach 100% prevalence in less than six months (Hofmann *et al.* 1995; Ford *et al.* in press). Other parasites, including many trematodes, have very slow rates of transmission (Sousa 1990; Curtis 1996, 1997). Proliferation of parasite infection also varies according to the response time to environmental change and physiological limitations on parasite growth.

In this report, we examine these processes in populations of the seep mussel, *Bathymodiolus childressi*. Following the methods section, we will first discuss the results of the population survey in year one and then address the specific process-oriented questions studied in year two.

## 8.5.2 Methods

The Johnson SEA-LINK collected seep mussels, *B. childressi*, from the primary study sites GC185, GC233, and GC234. Additional limited collections were taken from GB425 and a fifth site designated as TAMU-17. Table 8.5.1 lists the sampling stations and the 1997 and 1998 collections for the study. For most collections, sampling focused on the largest mussels in the population. This permitted sufficient tissue for PAH analysis and provided a direct comparison between PAH analysis and parasite body burden. In theory, this sampling protocol focused on the most heavily parasitized fraction of the population. At selected sites, the importance of size on parasitism was evaluated by taking a wider range of size classes for analysis.

Collected mussels were fixed in Davidson's fixative immediately after surfacing following the NOAA Status and Trends (NS&T) protocols (Ellis *et al.* 1998a). Dissection, embedding, sectioning, and staining procedures followed the same protocol. All assessments were based on quantitative measures or semi-quantitative scales so that reproductive stage and parasite/pathology infection intensity could be rigorously statistically evaluated. Direct appraisal of this approach during the MMS GOOMEX program (Wilson-Ormond *et al.*, in press) showed the power of using quantitative scales of infection intensity rather than just prevalence. Nearly all statistically significant relationships were observed using quantified measures. Earlier work in the NS&T program had indicated that this approach would be advantageous (Wilson *et al.* 1990, 1992). Friedman *et al.* (1997) provides a recent comparison example for abalone.

Reproductive stage and certain pathologies like digestive gland atrophy were assigned semi-quantitative scales describing stage of development or severity of the effect, respectively. Most

parasites were quantified by tallying the number of specimens in standardized tissue cross-sections (Ellis *et al.* 1998b; Sericano *et al.* 1993). The exception was widespread, ramifying, or invasive parasites such as certain trematode infections. These were also quantified using a semi-quantitative infection scale. Table 8.5.1 describes the scales used for these evaluations.

Table 8.5.1. Semi-qualitative scales used for evaluation of gonadal stage (Ellis *et. al* 1998a), gill and digestive gland atrophy, and Bucephalus infection (Ellis *et al* 1998b).

| Variable | Scale description | Scale values |
|---|---|---|
| Gonadal Stage | Resting | 0 |
| | Developing to fully ripe | 1 to 5 |
| | Spawning to spent | 4 to 1 |
| Gill and Digestive- gland atrophy | No atrophy to severe, widespread tissue degeneration | 0 to 3 |
| Parasitic infestation | Uninfected to complete or near complete filling of organism | 0 to 4 |

Mussels used for PAH analysis were frozen immediately after collection. PAHs were analyzed using the NS&T Mussel Watch protocol (Wade *et al.* 1993). In order to permit easy comparison to Mussel Watch data, a series of 18 PAHs were summed and reported as total PAHs (Wade *et al.* 1988; Jackson *et al.* 1994). These PAHs were naphthalene, 2-methylnaphthalene, 1-methylnaphthalene, biphenyl, 2,6-dimethylnaphthalene, acenaphthalene, fluorene, phenanthrene, anthracene, 1-methylphenanthrene, fluoranthene, pyrene, benz[*a*]anthracene, chrysene, benzo[*e*]pyrene, benzo[*a*]pyrene, perylene, and dibenz[*a,h*]anthracene.

In addition, the experimental design included a reciprocal transplant between pairs of populations, which were located at separate study sites. These populations generally correspond to mussel beds or mussel stations (e.g., BHM1) which are described elsewhere and are generally referred to by their study site descriptor. Mussels (*B. childressi*) were collected from one site (e.g., GC184), hereinafter termed the donor population, by submersible and brought to the surface in a temperature-controlled container. Mussels were kept onboard ship for up to 18 hr at *in situ* temperatures. Each mussel was marked with a numbered tag affixed with epoxy. Half of each collection, hereinafter termed the control site, was returned by submersible to the donor population from which the collection was made. The remainder, hereinafter termed the transplant population, was deployed by submersible at a second site (e.g., GC233) into a population hereinafter termed the receiver population. At the same time, mussels from the natural population at this second site were collected, returned to the surface, and marked as before. Once again, one group was returned to the same population, and a second group was transplanted into the population from which the first transplant was obtained. Thus, each population in the reciprocal pair had mussels of three types. They are as follows:

1.  The natural population untouched by the experimental protocol;

2.  The control mussels taken to the surface and returned into the same population;

3.  The mussels transplanted from the reciprocal site.

In addition, each population served as both donor and receiver depending on the direction of transplant. The reciprocal transplant pairs were GC185-GC233 and GC234-GC233. The two GC233 collections came from different, albeit nearby, stations (BPM1 and BPM4). One year later, each of these stations was revisited and samples of each of the three groups were collected – the natural mussels, the controls, and the transplanted mussels.

Statistical analyses used non-parametric analysis of variance (ANOVA) (Kruskal-Wallis) and Tukey's Studentized Range Test on ranked data to identify significant differences within the ANOVA. In some cases, a principal components analysis (PCA) was run first, and the first three or four PCA factors were used as variables in the ANOVA.

For parasite prevalence, data were initially encoded as 1 (infected) or 0 (uninfected). For semi-quantitative variables, data were encoded as their scores. For quantitative variables, data were normalized in two ways. First, parasite counts per section were normalized to an estimate of cross-sectional area using $L^2/4.75$ as the divisor. The latter was deemed sufficient because a regression of anterior-posterior length (L) against dorsal-ventral height (H) or left-right width (W) did not yield a significant slope. That is, mussel shape did not change significantly with size and, hence, cross-sectional area bore a simple relationship to length (L/H = 2.5, L/W = 1.9). The term "whole body" cross-sectional area is used because the divisor ($L^2/4.75$) is not an actual measure of the tissue section cross-sectional area but simply a normalizing tool to put animals of varying sizes into a common frame of reference. In the second normalized treatment method, wet-weight (gr) was divided by length (mm) to obtain the condition index. Although some measure of mantle cavity volume is typically used for condition indices (Rainer and Mann 1992; Smith 1995), the regular growth form of *B. childressi* permitted the simpler measure of normalized length to be used.


### 8.5.3 Results: the parasitic fauna of seep mussels

**Description of parasites found.** Collections and assays completed during the first year of the program demonstrated significant parasite infestations of seep mussels. These results provided a characterization of the parasitic fauna and comparisons of the intensity of parasitic infestations among the program study sites. Five types of parasites were identified in sectioned preparations: gill rosettes, gill inclusions, gill ciliates, body inclusions, and *Bucephalus*-like trematodes. Figure 8.5.1 illustrates these parasites. They are described below.
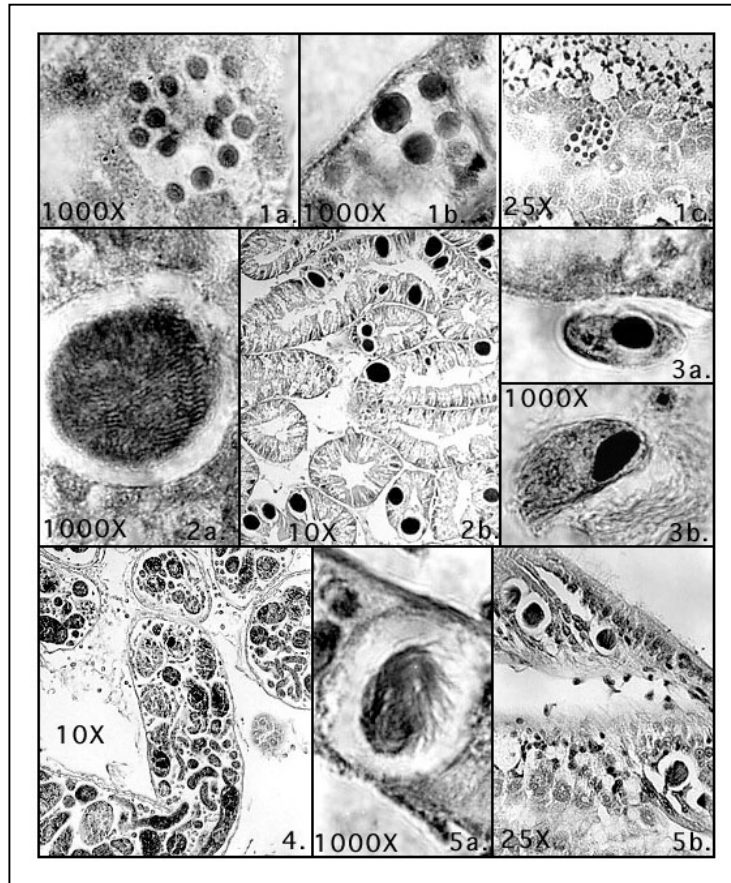
Figure 8.5.1.   Plate 1.   Gill rosettes -- 1a, b: 1000x; 1c: 25x. Plate 2. Rickettsial-like bodies in the digestive tubules and diverticula -- 2a, b: 1000x.   Plate 3.   Gill ciliates between the demibranches -- 3a, b: 1000x. Plate 4.  *Bucephalus* in the gonad -- 10x. Plate 5. Rickettsial-like bodies in the gill -- 5a: 1000x; 5b: 25x.

**Gill rosettes.** Gill rosettes of unknown affinity are associated with the bacteriocytes in the gill. Bacteriocytes are the specialized cells in *B. childressi* that harbor methanotrophic symbionts (Fisher 1990). The cells show no internal structure at the light microscope (Figure 8.5.1: Plates 1a, 1b, and 1c). Each rosette is characterized by a group of 12 to 28 variably sized (2 to 5 $\mu$m) rounded cells within or breaking through the gill. Except where the rosette breaks through the gill surface, no tissue pathology was observed. Gill rosettes resemble the free inclusion bodies observed by Johnson and Pennec (1995) (their Figures 1 through 4) in *Loripes lucinalis*.

**Gill inclusions and body inclusions.** Gill inclusions and body inclusions are similar to chlamydia/rickettsia inclusions (Buchanan 1978; Meyers 1979; Fries *et al.* 1991) but have a more visible structure and often appear as a group of tightly compacted strands that are usually in a swirled configuration. For simplicity, they are hereinafter referred to as rickettsia. These rickettsia-like bodies were usually located at or near the distal end of the thickened tissue of the gill filaments that surround the water tubes (Figure 8.5.1: Plates 5a and 5b). Their average size is 9.9 $\mu$m by 15 $\mu$m; however, they can vary greatly in size.

Body inclusions are also chlamydial/rickettsial-like inclusions but have a more visible structure, often appearing as a group of tightly compacted short rods that are in multidirectional groups. Occasionally, similar bodies are observed that appear smooth, without internal structure. Johnson and Pennec (1995) observed a very similar organism in *Loripes lucinalis* (their Figures 1 through 3), which they believed to be a *Chlamydia*. For simplicity, they are herinafter referred to as rickettsia. These rickettsia are found in the digestive diverticula or the digestive tubules (Figure 8.5.1: Plates 2a and 2b). Size is highly variable but averages 26.6 μm by 20.9 μm, about twice the size of the rickettsia in the gills. Besides the substantial size difference, significant differences in the distribution pattern among sites strongly suggest that body and gill rickettsia are distinctive organisms. No obvious tissue pathology was observed.

**Gill ciliates.** Extracellular gill ciliates, averaging 21 μm by 11.4 μm, are found between the gill filaments or near the base of the gill demibranches (Figure 8.5.1: Plates 3a and 3b). The ciliates appear to be freely mobile on the gill surface. Whether these ciliates are parasitic or adventitious commensals has not been determined.

***Bucephalus*-like trematodes.** *Bucephalus*-like trematodes (e.g., Hopkins 1957, 1958; Wardle 1990) were observed invading the gonadal material and, in heavier infections, other body compartments. The sporocysts are very similar to the *Bucephalus* trematodes found in shallow-water oysters and mussels, except that the mature cercariae are very large (Figure 8.5.1: Plate 4). Hereinafter, these will be referred to as *Bucephalus* for simplicity although, we caution the reader that the trematodes observed in these mussels have not been unequivocally assigned to that genus.

Results of the population survey in the first year showed that infection intensity of gill parasites was significantly higher at GC233 than at the other sites (Tables 8.5.2 and 8.5.3). Much of this difference was due to a significantly higher prevalence and infection intensity of gill rickettsia. Gill parasites were not observed at GC234 or at three of four GC185 sites but were present in over half of all GC233 specimens. Body rickettsia was prevalent at all sites and in all

Table 8.5.2. Prevalences and infection intensities in year one for the five types of parasites identified for each of the 4 primary sites.  In cases where sites were sampled more than once, each sample came from a discrete mussel bed. Infection intensities are counts per tissue cross-section, except for *Bucephalus* which is rated on a 0-to-4-point scale.

| Location | N | Gill Rosettes Prevalence | Gill Rosettes Infection Intensity | Gill Inclusions Prevalence | Gill Inclusions Infection Intensity | Gill Ciliates Prevalence | Gill Ciliates Infection Intensity | Body Inclusions Prevalence | Body Inclusions Infection Intensity | *Bucephalus* Prevalence | *Bucephalus* Infection Intensity |
|---|---|---|---|---|---|---|---|---|---|---|---|
| **GC-233** | | | | | | | | | | | |
| M1 | 10 | 30% | 4.3 | 30% | 0.9 | 30% | 0.5 | 80% | 28.9 | 0% | 0.0 |
| M2 | 3 | 0% | 0.0 | 67% | 25.3 | 0% | 0.0 | 67% | 19.7 | 0% | 0.0 |
| M3 | 8 | 88% | 22.6 | 100% | 51.5 | 25% | 0.6 | 88% | 30.9 | 0% | 0.0 |
| **GC-184** | | | | | | | | | | | |
| M1 | 11 | 0% | 0.0 | 0% | 0.0 | 0% | 0.0 | 100% | 58.0 | 18% | 0.5 |
| M2 | 8 | 0% | 0.0 | 13% | 0.1 | 13% | 0.1 | 88% | 4.9 | 100% | 3.8 |
| M4 | 10 | 0% | 0.0 | 0% | 0.0 | 0% | 0.0 | 90% | 46.0 | 70% | 2.0 |
| M5 | 10 | 0% | 0.0 | 0% | 0.0 | 0% | 0.0 | 90% | 7.7 | 40% | 1.2 |
| **GC-234** | | | | | | | | | | | |
| M1 | 10 | 0% | 0.0 | 0% | 0.0 | 0% | 0.0 | 90% | 46.0 | 80% | 1.9 |
| M2 | 10 | 0% | 0.0 | 0% | 0.0 | 0% | 0.0 | 100% | 24.1 | 20% | 0.3 |
| **GB-425** | | | | | | | | | | | |
| M1 | 7 | 29% | 0.6 | 86% | 3.7 | 0% | 0.0 | 100% | 30.3 | 0% | 0.0 |

Table 8.5.3. Comparison of sites for which greater than one sample was available in year one. Like letters indicate no significant difference at α = 0.05 using Tukeys Studentized Range Test. Totals do not include *Bucephalus*.

|  | GC233 | GC185 | GC234 |
|---|---|---|---|
| **Gill Rosettes** |  |  |  |
| Prevalence | A | A | A |
| Infection Intensity | A | A | A |
| **Gill Chlamydia/Rickettsia** |  |  |  |
| Prevalence | A | B | B |
| Infection Intensity | A | B | B |
| **Gill Ciliates** |  |  |  |
| Prevalence | A | A | A |
| Infection Intensity | A | A | A |
| **Total Gill Parasites** |  |  |  |
| Infection Intensity | A | B | B |
| **Body Chlamydia/Rickettsia** |  |  |  |
| Prevalence | A | AB | B |
| Infection Intensity | A | A | A |
| **Total Parasites** |  |  |  |
| Infection Intensity | A | A | A |
| ***Bucephalus* sp.** |  |  |  |
| Prevalence | A | B | B |
| Infection Intensity | A | B | AB |
| Gonadal Stage | A | A | A |
| Gill Tissue Atrophy | A | A | A |
| Digestive Gland Atrophy | A | A | A |
| PAH Body Burden | A | A | A |

populations, never less than 67%; however, prevalence at GC234 was significantly higher than at GC233 (Table 8.5.3). Prevalence of *Bucephalus* was much higher at GC185 than at the other sites. *Bucephalus* was not recorded at GC233 or GB425 but reached prevalence as high as 100% at GC185 and 80% at GC234. Mussel bed-to-bed variation within a site was high. All gill parasites recorded from GC185 were recorded from only one of the four GC185 samples. *Bucephalus* prevalence ranged from 18% to 100% GC185. Body rickettsia infection intensity ranged from 4.9 to 58 at GC185 (Table 8.5.2).

Prevalence and infection intensities of the three gill parasites were normally highly correlated. That is, mussel beds having high prevalence or infection intensities for one gill parasite normally had high prevalence or infection intensities for all gill parasites (Tables 8.5.4 and 8.5.5). The only exception was gill ciliates, an extra cellular commensal that was not correlated with gill rickettsia, an internal parasite. The two body parasites, body rickettsia and *Bucephalus*, were essentially uncorrelated with each other or with any gill parasite, with the exception of *Bucephalus* prevalence, which was weakly correlated with gill rickettsia prevalence.

**Comparison with shallow-water mussels.** Gill ciliates were commonly observed in *Mytilus edulis* and *Mytilus californianus* at nearly every locale on both coasts. Overall, in comparison to shallow-water mussel populations, parasite infection intensities were higher by a factor of 10 in seep mussels than in shallow-water populations sampled by the Mussel Watch program.

Table 8.5.4. P values ($\alpha = 0.05$) for Spearman's Rank correlations for parasite prevalence and measures of general health, based on year one samples.  Parentheses indicate negative correlations.

| | Gill Inclusions | Gill Ciliates | Body Inclusions | *Bucephalus* | Gonadal Stage | Gill Atrophy | Digestive Gland Atrophy | PAH Body Burden |
|---|---|---|---|---|---|---|---|---|
| **Gill Rosette** | .009 | .02 | — | — | — | — | — | — |
| **Gill Inclusions** | | — | — | (.05) | .05 | — | — | — |
| **Gill Ciliates** | | | — | — | — | — | — | (.04) |
| **Body Inclusions** | | | | — | — | — | — | .03 |
| ***Bucephalus*** | | | | | | — | — | — |
| **Gonadal Stage** | | | | | | (.01) | (.01) | — |
| **Gill Atrophy** | | | | | | | .0003 | — |
| **Digestive Gland Atrophy** | | | | | | | | — |

Table 8.5.5. P values ($\alpha = 0.05$) for Spearman's Rank correlations for parasite infection intensity and measures of general health based on year one samples.  Parentheses indicate negative correlation.

| | Gill Inclusions | Gill Ciliates | Total Gill Parasites | Body Inclusions | Total Parasites | Gonadal Stage | Gill Atrophy | Digestive Gland Atrophy | PAH Body Burden |
|---|---|---|---|---|---|---|---|---|---|
| **Gill Rosette** | .001 | .002 | .0001 | — | .02 | — | — | — | — |
| **Gill Inclusions** | | — | .0001 | — | .008 | — | — | — | — |
| **Gill Ciliates** | | | .02 | — | — | — | — | — | — |
| **Total Gill Parasites** | | | | — | .005 | — | — | — | — |
| **Body Inclusions** | | | | | — | — | (.02) | (.03) | — |
| **Total Parasites** | | | | | | — | (.04) | (.01) | — |
| ***Bucephalus*** | | | | | | (.002) | — | .03 | — |
| **Gonadal Stage** | | | | | | | (.01) | (.01) | — |
| **Gill Atrophy** | | | | | | | | .0003 | — |
| **Digestive Gland Atrophy** | | | | | | | | | — |

**Implications for reproduction.** *Bucephalus* infections are initiated in the gonadal tissue of a mollusk (infection intensity 1). As the sporocysts grow and the infection spreads, the gonadal tissue is completely consumed, and the parasite begins to invade the body tissue (infection intensity 2). Although mortalities have rarely been recorded (see Allen 1979 for an example), the loss of reproductive potential in infected animals is well known (Hopkins 1957). The evidence presented here indicates that *Bucephalus* exerts a significant influence on seep mussel population dynamics. Entire populations at the study sites are no longer reproductively active. Seep mussel populations were often found to have parasite prevalence exceeding 70% and infection intensities as high as 3.8 on the four-point scale (Table 8.5.2). Of even more interest is the fact that 50% to 75% of populations at the two primary sites, GC185 and GC234 (Table 8.5.2), are heavily impacted by this parasite. Thus, the populations of seep mussels at certain primary sites

may have insufficient fecundity to maintain themselves. Very likely, only a fraction of petroleum seep mussel populations are maintaining the entire beta-level population structure of this species.

**Measures of tissue atrophy.** Measures of tissue atrophy (Table 8.5.6) were inversely correlated with gonadal stage, which was determined, in large measure, by *Bucephalus* infection. Healthy mussels, those with low atrophy scores, were reproductively active, averaging a 3 or 4 on the five-point scale for gonadal stage. Unhealthy mussels with high atrophy scores rarely advanced in reproductive condition. Furthermore, gill tissue atrophy was negatively correlated with gonadal stage, which suggests that tissue atrophy in seep mussels, as we measured it, is a pathological condition. Body rickettsia was most common in animals with low atrophy scores, which possibly indicates that healthy tissue is required for infection intensification in this parasite. Generally, rickettsia/chlamydia are not thought to be harmful in mollusks (Otto *et al.* 1977; Elston and Peacock 1984; Cajaraville and Angulo 1991); however, mortality is frequently associated with infections in crustaceans (Johnson 1984; Sparks *et al.* 1985; Bower *et al.* 1996) and occasional reports of pathologies associated with high prevalence are seen in bivalves (Le Gall *et al.* 1988).

Table 8.5.6. Health indices and PAH body burden (ppb) in year one for mussels taken from each of the 4 primary sites.  In cases where sites were sampled more than once, each sample came from a discrete mussel bed.

| Location | Gonadal Stage | Gill Tissue Atrophy | Digestive Gland Atrophy | PAH Body Burden |
|---|---|---|---|---|
| **GC233** | | | | |
| M1 | 3.5 | 0.7 | 0.5 | 565 |
| M2 | 3.0 | 0.7 | 0.7 | — |
| M3 | 4.4 | 0.5 | 0.1 | 214 |
| | | | | |
| **GC185** | | | | |
| M1 | 3.1 | 0.0 | 0.3 | 1346 |
| M2 | 0.0 | 2.1 | 2.4 | 283 |
| M4 | 0.5 | 0.7 | 1.1 | 697 |
| M5 | 0.0 | 2.7 | 2.4 | 1135 |
| | | | | |
| **GC234** | | | | |
| M1 | 0.8 | 1.1 | 0.5 | 614 |
| M2 | 3.8 | 0.5 | 0.5 | 1065 |
| | | | | |
| **GB425** | | | | |
| M1 | 4.0 | 0.6 | 1.0 | 1160 |

**PAH body burden.** PAH body burden was high in petroleum seep mussels, exceeding 1 ppm in four of nine seep populations sampled in 1997 (Table 8.5.6). Variation in two parasites, gill ciliates and *Bucephalus*, explained most of the variation in PAH body burden between mussel populations. Although the data are admittedly few, so that relationships of this sort must be considered with caution, the amount of variation explained (81%) is extremely high by NS&T standards – where the infection intensity of any three parasites rarely explains more than 40% of the PAH body burden (Kim *et al.* 1998). The higher average body burdens in seep mussels may

be responsible for this greater predictability, as many Mussel Watch locales were characterized by low PAH body burdens (<400 ppb).

The partial regressions for gill ciliates and *Bucephalus* on PAH body burden indicate that PAH burden decreases with increased infection of both parasites. The data do not permit a determination of causality, but the size and infection intensity of gill ciliates do indicate that ciliates are a surrogate for some other physiological variable that would decrease sequestration of PAH. In the case of *Bucephalus,* the probable cause of decreased PAH burden is more apparent. At infection intensities of one or higher, *Bucephalus* replaces a substantial fraction of the host tissue, including all of the gametic tissue. PAHs are known to be sequestered in lipid-rich gametic tissue at much higher concentrations than somatic tissue (Friocourt *et al.* 1985; Ellis *et al.* 1993) in some bivalves. This is due to the increased lipid concentration of the gametes. The relationship holds true for both eggs and sperm (Ellis *et al.* 1993). *Bucephalus* would be expected to reduce overall body burden, at high infection intensities, by replacing gametic tissue.

The three highest PAH body burdens came from populations without *Bucephalus* and with few gill parasites. The simplest explanation for the observed relationship between PAH and parasites is that PAH body burden was low in some mussels due to the absence of gametic tissue and *that* PAH body burden was low in other mussels in which overall health was low, accounting for the frequency of gill ciliates that would not have been found in healthier animals. This result leads to the unanticipated conclusion that higher body burdens are found more frequently in healthy petroleum seep mussels. The generally high PAH body burdens found in all seep mussel populations and the finding of highest PAH burdens in the healthiest population is evidence that seep mussels are not as sensitive to PAH exposure as are the shallow-water mytilids.

### 8.5.4 Dynamics of parasitism

Sampling in the second year (1998) was designed to confirm certain conclusions made in the first year (1997) and to investigate the dynamics of parasitism in mussel populations. The results from 1997 collections suggested that the parasite species and infection intensities differ significantly in mussel populations at separate sites. A larger survey was conducted in 1998 to determine the validity of this conclusion (Table 8.5.7). No additional parasite types were recognized in 1998 collections, which suggest that the five parasite types already described comprise the overwhelming majority of all parasites plaguing *B. childressi*. A more extensive sampling of mussel beds in the study sites confirmed the absence of *Bucephalus* in GC233, its relative rarity at GC234 and its abundance at GC185. *Bucephalus* was also found at TAMU-17 and at one site at GB425. More extensive sampling confirmed the absence of gill rosettes at GC185 and GC234, and the ubiquity of this parasite at GC233. (One light infection at GCM1 may have occurred by introducing this parasite to this site via the transplant experiment.) Gill rickettsia were once again not observed at GC234 (One light infection at GCM1 may have occurred by introducing this parasite to this site via the transplant experiment.).

Table 8.5.7. Mean prevalences, infection intensities, and physiological indices for mussel populations sampled in year two. For gill rosette, gill ciliate, gill rickettsia, and body rickettsia infection intensities, parasite counts per section were normalized to an estimate of cross-sectional area using, as the divisor, $L^2/4.75$. N is the number of individuals used to generate the mean in this table and used in most statistical analyses. (N) is the number of additional individuals used in the size-frequency analyses.

| Location | N | Gill Rosettes Prevalence | Gill Rosettes Infection Intensity | Gill Inclusions Prevalence | Gill Inclusions Infection Intensity | Gill Ciliates Prevalence | Gill Ciliates Infection Intensity | Body Inclusions Prevalence | Body Inclusions Infection Intensity | *Bucephalus* Prevalence | *Bucephalus* Infection Intensity | Indices Gonadal Stage | Indices Condition Index | Atrophy Scores Gill Tissue | Atrophy Scores Digestive Gland | Species Richness |
|---|---|---|---|---|---|---|---|---|---|---|---|---|---|---|---|---|
| **GC-233** | | | | | | | | | | | | | | | | |
| M1 | 15 | 13.3% | 0.024 | 73.3% | 0.253 | 26.7% | 0.017 | 80.0% | 1.508 | 0.0% | 0.000 | 3.733 | 0.338 | 0.267 | 1.067 | 1.933 |
| M4 | 9 | 33.3% | 0.033 | 33.3% | 0.216 | 11.1% | 0.005 | 100% | 2.610 | 0.0% | 0.000 | 3.444 | 0.266 | 0.667 | 0.556 | 1.778 |
| AT1 | 5 | 0.0% | 0.000 | 0.0% | 0.000 | 0.0% | 0.000 | 100% | 3.404 | 0.0% | 0.000 | 0.000 | 0.103 | 1.000 | 1.200 | 1.000 |
| IBP | 10(10) | 50.0% | 0.099 | 60.0% | 0.128 | 40.0% | 0.042 | 100% | 4.990 | 0.0% | 0.000 | 3.800 | 0.244 | 0.000 | 1.000 | 2.500 |
| OBP | 3 | 33.3% | 0.018 | 100% | 6.323 | 0.0% | 0.000 | 100% | 3.715 | 0.0% | 0.000 | 3.000 | 0.341 | 0.000 | 1.000 | 2.333 |
| **GC-184** | | | | | | | | | | | | | | | | |
| M1 | 9 | 0% | 0.000 | 0.0% | 0.000 | 0.0% | 0.000 | 100% | 4.936 | 77.8% | 1.556 | 2.667 | 0.233 | 0.556 | 0.778 | 1.778 |
| M2 | 10 | 0% | 0.000 | 0.0% | 0.000 | 10.0% | 0.008 | 80.0% | 2.001 | 100% | 3.000 | 0.000 | 0.270 | 1.100 | 1.200 | 1.900 |
| M3 | 10(9) | 0% | 0.000 | 0.0% | 0.000 | 20.0% | 0.012 | 100% | 3.567 | 40.0% | 1.200 | 1.400 | 0.208 | 0.100 | 1.000 | 1.600 |
| M4 | 8 | 0% | 0.000 | 0.0% | 0.000 | 0.0% | 0.000 | 100% | 11.442 | 87.5% | 2.625 | 0.250 | 0.138 | 0.125 | 0.500 | 1.875 |
| M5 | 6(10) | 0% | 0.000 | 50.0% | 0.048 | 16.7% | 0.006 | 100% | 1.521 | 33.3% | 1.000 | 2.333 | 0.400 | 0.000 | 0.833 | 2.000 |
| M6 | 10(13) | 0% | 0.000 | 0.0% | 0.000 | 0.0% | 0.000 | 100% | 1.823 | 70.0% | 2.100 | 0.900 | 0.151 | 0.000 | 0.400 | 1.700 |
| JT2 | 8(7) | 0% | 0.000 | 0.0% | 0.000 | 0.0% | 0.000 | 100% | 4.529 | 62.5% | 1.875 | 0.750 | 0.121 | 0.125 | 1.000 | 1.625 |
| **GC-234** | | | | | | | | | | | | | | | | |
| M1 | 10 | 10.0% | 0.010 | 10.0% | 0.787 | 0.0% | 0.000 | 100% | 5.361 | 20.0% | 0.600 | 1.300 | 0.100 | 0.700 | 1.000 | 1.400 |
| M1A | 10 | 0.0% | 0.000 | 0.0% | 0.000 | 0.0% | 0.000 | 100% | 6.419 | 40.0% | 1.200 | 0.800 | 0.107 | 0.000 | 0.700 | 1.400 |
| M2 | 13 | 0.0% | 0.000 | 0.0% | 0.000 | 7.7% | 0.013 | 92.3% | 3.273 | 15.4% | 0.308 | 1.846 | 0.156 | 0.692 | 1.154 | 1.154 |
| **GB-425** | | | | | | | | | | | | | | | | |
| M1 | 13 | 23.1% | 0.020 | 76.9% | 0.515 | 23.1% | 0.011 | 92.3% | 5.584 | 7.7% | 0.231 | 3.462 | 0.338 | 0.308 | 0.462 | 2.231 |
| M1A | 4 | 0.0% | 0.000 | 25.0% | 0.088 | 0.0% | 0.000 | 100% | 1.769 | 0.0% | 0.000 | 3.000 | 0.390 | 0.250 | 1.000 | 1.250 |
| M2 | 12 | 0.0% | 0.000 | 58.3% | 0.446 | 8.3% | 0.004 | 100% | 7.428 | 0.0% | 0.000 | 2.417 | 0.277 | 0.000 | 1.167 | 1.667 |
| **TAMU-17** | 8 | 0.0% | 0.000 | 37.5% | 0.053 | 0.0% | 0.000 | 100% | 2.691 | 50.0% | 1.250 | 1.875 | 0.302 | 1.000 | 0.375 | 1.875 |

Thus, an extended survey conducted in 1998 confirms the endemic nature of many of the parasites in *B. childressi* populations. Program study sites differ significantly in their parasite complement. The similarity in parasite burden between GB425 and GC185 and the dissimilarity between the much closer GC185 and GC233 suggest that environmental effects are the likely cause of these differences.

A high force of infection combined with either short parasite lives or rapid adult mortality could sustain the parasite prevalence and infection intensities seen in seep mussel populations. The first alternative is rare among invertebrates, while the second alternative is not consistent with the long life spans observed in *B. childressi* (Nix *et al.* 1995). Therefore, it is most likely that the parasite prevalence and infection intensity observed resulted from the slow, persistent accumulation of infection.

We investigated the dynamics of transmission, proliferation, and loss in two ways: by transplanting mussels from one place to another and by examining the influence of host size on prevalence and infection intensity.

**Results of Transplant.** Donor and receiver populations varied significantly in prevalence and infection intensity for most parasites and in physiological condition for most physiological indices. Therefore, the infection intensity and/or prevalence (typically both) of transplanted populations had to rise or fall significantly over one year in order to come into equilibrium with receiver populations. Transplanted populations came into equilibrium with the receiver populations much faster in cases where a decrease in infection intensity or prevalence was required (Table 8.5.8). Quite the opposite was true for cases where the transplanted population had to gain infections or increase in infection intensity to come into equilibrium with the receiver population. Very few cases reached equilibrium after increased infection. In many cases, the transplanted population retained the donor population condition for relatively uninfected populations. In most of the remainder, the transplanted population clearly fell between the donor and receiver population condition. All transplant results are summarized in Table 8.5.8. Overall, the single-celled rickettsia responded more rapidly to the environment of the receiver population than did the multi-celled *Bucephalus*.

In cases where the transplant was made to a receiver population of lower prevalence and infection intensity, infection intensity and prevalence rapidly declined so that the transplanted mussels were indistinguishable from the receiver population after one year. The data strongly suggest that rickettsial infections are rapidly lost without a constant source of infective elements renewing infections and the force of infection as well as factors controlling within-host proliferation probably significantly influences that infection intensity.

The rapid loss rates explain why gill rickettsial prevalence is maintained well under 100% in the GC233 populations despite the long life span of *B. childressi*. This suggests that the same rates for body rickettsia are distinctly lower, perhaps because the life span of a rickettsial body is significantly longer, and as a result prevalence hovers around 100%. The information clearly suggests that a more effective method of transmission exists at GC233 (both sites) than at GC234 or GC185 for gill rickettsia and that conditions for proliferation are equally superior there. What precisely these conditions are we do not yet know.

Table 8.5.8. Relationship of the transplanted individuals to the donor and receiver population in cases where a nonparametric ANOVA identified a significant population effect. Brackets indicate situations where a Tukey's Studentized Range Test did not resolve the source of the variation. In each case the transplant population is listed under the population of greatest affinity.

***Receiver Population Significantly Greater than Donor Population***
Change required an increase in the variable value

| **No Change**<br>(Donor Population<br>Not Significantly Different) | **Moderate Change**<br>(Donor and Receiver Population<br>Not Significantly Different) | **Complete Change**<br>(Receiver Population<br>Not Significantly Different) |
|---|---|---|
| *Bucephalus* prevalence (GC184) | Gill rickettsia infection intensity (GC233M1) | Gonadal stage (GC233M4) |
| *Bucephalus* infection intensity (GC184) | Gonadal stage (GC233M1) | Gill rickettsia prevalence (GC233M4) |
| Gill rickettsia prevalence (GC233M1) | Digestive gland atrophy (GC233M1) | Gill rickettsia infection intensity (GC233M4) |
| Gill tissue atrophy (GC233M1) | Condition index (GC233M4) | |
| Condition index (GC233M1) | [ *Bucephalus* prevalence (GC234)] | |
| | [ *Bucephalus* infection intensity (GC234)] | |
| | [Body rickettsia prevalence (GC184)] | |
| | [Body rickettsia infection intensity (GC184)] | |

***Receiver Population Significantly Lower than Donor Population***
Change required a decrease in the variable value

| **No Change**<br>(Donor Population<br>Not Significantly Different) | **Moderate Change**<br>(Donor and Receiver Population<br>Not Significantly Different) | **Complete Change**<br>(Receiver Population<br>Not Significantly Different) |
|---|---|---|
| *Bucephalus* prevalence (GC233M4) | Gonadal stage (GC184) | Gill rickettsia prevalence (GC184) |
| *Bucephalus* infection intensity (GC233M4) | Condition index (GC184) | Gill rickettsia infection intensity (GC184) |
| | | *Bucephalus* prevalence (GC233M1) |
| | | *Bucephalus* infection intensity (GC233M1) |
| | | Gill tissue atrophy (GC184) |
| | | Digestive gland atrophy (GC184) |
| | | Condition index (GC184) |
| | | Body rickettsia infection intensity (GC233M1) |
| | | Gonadal stage (GC234) |
| | | [Gill rickettsia prevalence (GC234)] |

The multi-celled *Bucephalus* shows precisely the opposite condition. Again, transmission rates could be estimated in two cases because *Bucephalus* was not found in either GC233 population. Rates were 0.12 to 0.25 $y^{-1}$. These transmission rates are surprisingly high given the prevalence observed in mussels transplanted to GC234 but are in accordance with the high prevalence observed in mussels transplanted to GC185. This suggests that loss rates are much higher at GC234. Observations support the potential for rapid loss of infections, but are ambiguous overall. Mussels transplanted from GC234 to GC233-BPM1 retained donor population prevalence. Infections were not lost measurably over one year. Mussels transplanted from GC185 to GC233-BPM1 lost about 75% of their infections in one year.

*B. childressi* is considered to have a life span measured in decades. Measured transmission rates are relatively high, yet measures of population prevalence are often well below 100%. The strong suggestion is that these trematode sporocysts have life spans considerably less than their hosts, a fact that is of some consequence since, while infected, the mussels lose any capacity to reproduce. From these arguments, however, we cannot explain the persistence of *Bucephalus* in mussels transplanted from GC234 in comparison to those originating at GC185.

The simplest explanation for the high parasite prevalence is the slow, steady accumulation of infections over a long life span. However, transplanted mussels rapidly approached the condition of the receiver population in most instances, both in prevalence and infection intensity. Clearly, the parasite body burden in these mussels is a dynamic process, rapidly responding to changes in infection pressure in the environment. The rates of proliferation and loss must also be relatively rapid. This infection milieu must be dramatically different from that experienced by shallow-water mussels on the east and west coast of the United States, where low prevalence and infection intensities are the norm (Kim *et al.* 1998).

**Local versus regional control on parasitism.** Nearby populations were as different, in many respects, as populations from the different major sites (e.g., GC233, GC185). This observation, made after 1997, was confirmed by the more extensive sampling in 1998 (Table 8.5.7). Thus the dynamics controlling parasite acquisition, proliferation, and loss are predominately determined by local environmental and/or biological conditions varying from population to population, not major site to major site. The single exception is the absence of certain parasite types from certain major sites. Some of the within-major-site patchiness may be ascribed to the size and remoteness of populations within the major sites. For example, both samples of mussels from tubeworm-designated collections (BPAT1 and BHJT2) had prevalence measures of zero for all gill parasites. On the other hand, two neighboring collections at GB425 (GBM1 and GBM1A) differed considerably in gill parasite infection intensity, as did some of the samples from the extensive mussel bed surrounding the brine pool at GC233 so that within-population patchiness is also likely to be responsible.

Gill parasites, all of which probably have a nearest neighbor type of transmission, exhibit the greatest degree of patchiness, in comparison to *Bucephalus*, which infects from what is likely a mobile definitive host. Transmission of the nearest-neighbor kind would sustain patchiness and limit transmission to remote, small populations. Of course, the same type of transmission might be ascribed to the ubiquitous body rickettsia, yet its ubiquitously high prevalence would demand a more efficient mode of transmission.

**PAH Body Burdens.** PAH body burdens averaged lower in 1998 than in 1997. Nevertheless, 8 of 21 populations had body burdens exceeding 500 µg (g dry wt) and two exceeded 1 µg (g dry wt) in animals collected in 1998. Body burden was not related to major site. Some populations were high and some were low at each major site (Figure 8.5.2). Body burden depended upon small-scale processes. The same could be said when the proportional contribution of individual PAHs to the total was examined. A major-site dependency did not exist. However, local populations differed substantially (Figure 8.5.3). As examples, mussels from GCM1 and BHM6 were relatively depleted in naphthalenes. Mussels from BPOBP and BPM1 were relatively enriched in methylnaphthalenes. Mussels from TAMU-17 were relatively enriched in chrysenes.

Transplanted populations came into equilibrium with receiver populations in PAH body burden after one year, in cases where body burden was higher in the receiver population. Body burden remained high in the one case of mussels transplanted to populations with lower body burden (Figure 8.5.4). However, an examination of the proportional contribution of 44 PAHs to the PAH body pool indicated that proportions came into equilibrium in all cases (Figure 8.5.5). Therefore, the retention of high body burdens in the case where mussels were transplanted to a population with lower body burden was not due to low depuration rates. Likely, it was due to an inherently higher storage capacity in mussels obtained from populations with high body burden. What biological process is responsible is not yet clear. Changes in total lipid, for example, did not explain the pattern.

In 1998, the in-depth analysis of a larger data set confirms the conclusions made in 1997 that parasites are much more closely related to PAH body burden than physiological indices such as condition index or tissue atrophy scores. They further confirm that gill ciliate prevalence and infection intensity and *Bucephalus* infection intensity explain much of this relationship. *Bucephalus* certainly changes the tissue composition of the host. Gonadal tissue is reduced or absent, and trematode tissue attains a relatively high proportion of total tissue. It seems likely that a differential capacity for PAH sequestration may most easily explain the relationships observed. Gill ciliates are likely too small and infection intensities too low to themselves damage the host in any way. Gill ciliates probably are symptomatic of some exposure or physiological process impacting the animal, recalling the original proposal of Laird (1961). Regardless, the comparisons identify an important relationship between PAH body burden and parasitism in petroleum seep mussels and raise the question of using caution in accepting PAH body burden as a simple measure of exposure in these populations.
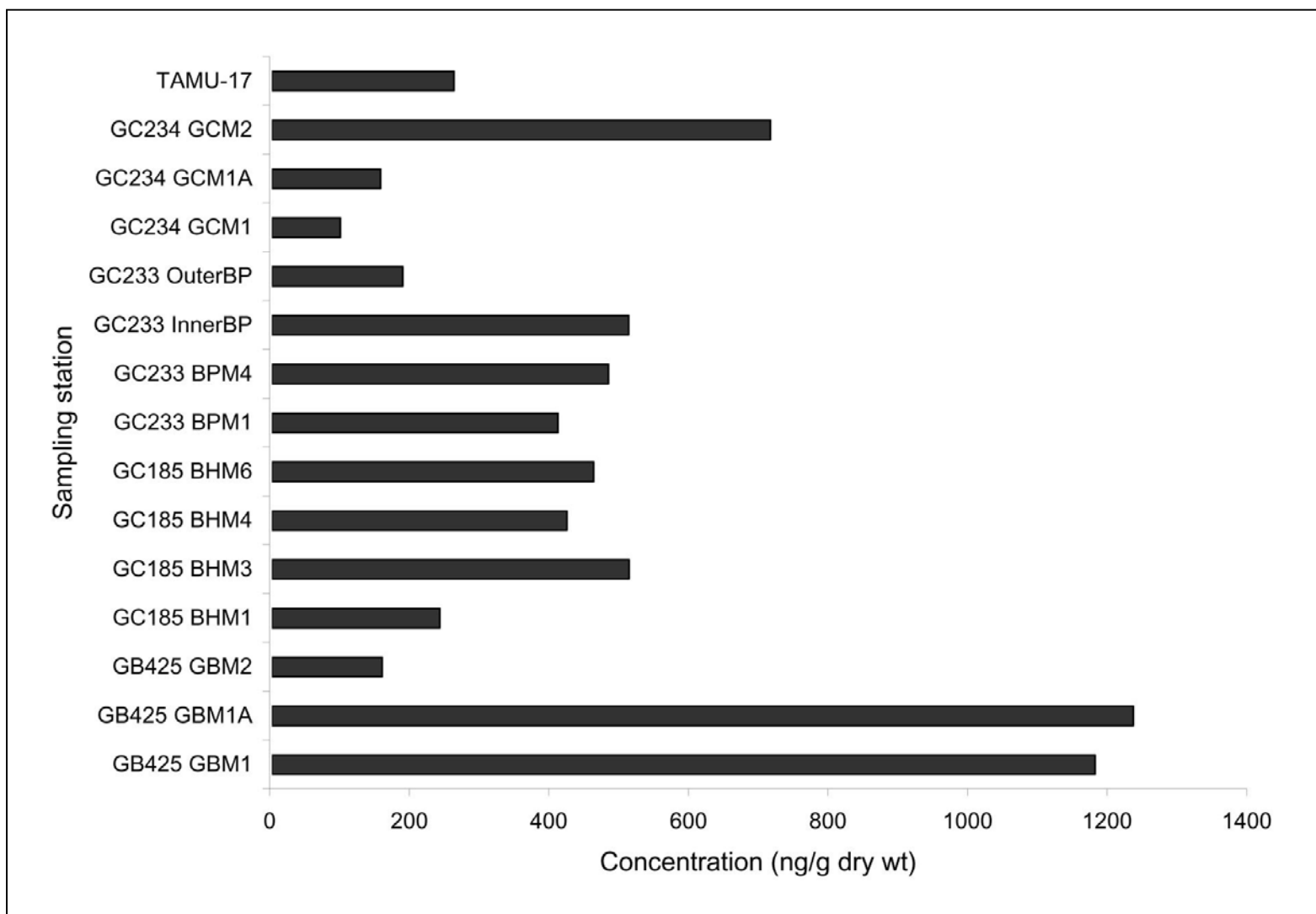
Figure 8.5.2. Plot of total PAH body burden versus population for *B. childressi* populations from 5 major sites. The PAHs summed for this measurement are listed in Figure 8.5.3.
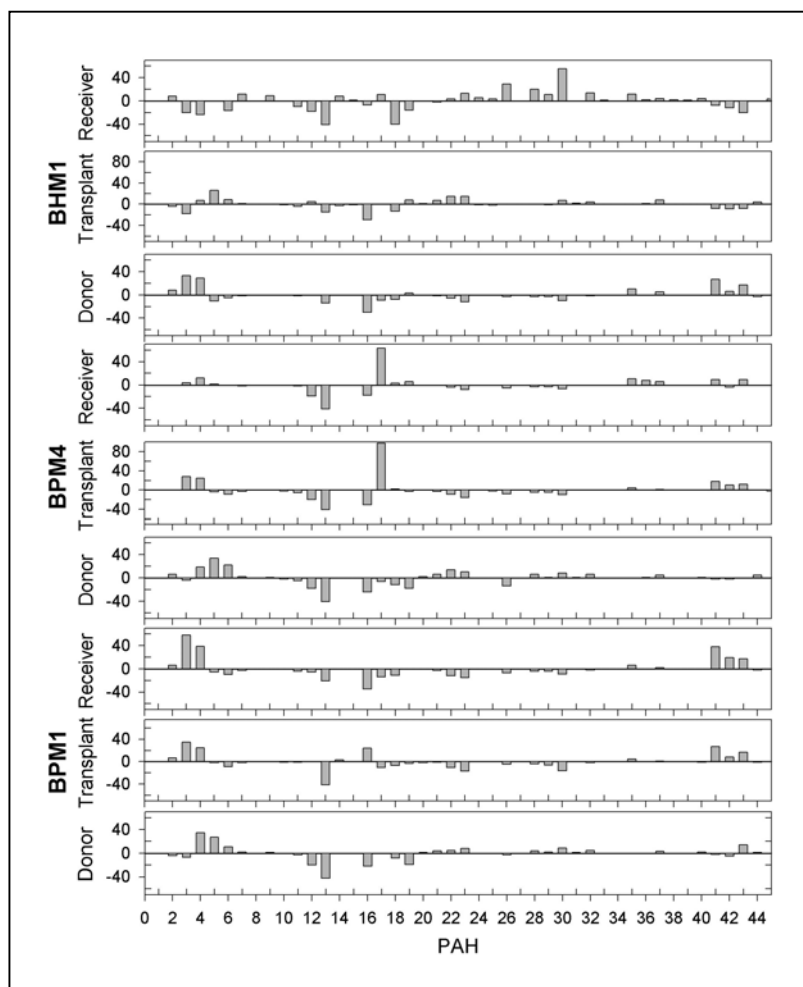
Figure 8.5.3. Proportional differences between the sample mean and the global mean for each compound in the PAH compound series. For this calculation, each mean variable value for each sample was standardized to parts per thousand, as was the global mean value for the variable for all samples. The difference between the global mean standardized value and the sample mean standardized value was calculated and these mean standardized differences were plotted. The PAH compound series is as follows: 1, naphthalene; 2, c1-naphthalenes; 3, c2-naphthalenes; 4, c3-naphthalenes; 5, c4-naphthalenes; 6, biphenyl; 7, acenaphthylene; 8, acenaphthene; 9, fluorene; 10, c1-fluorenes; 11, c2-fluorenes; 12, c3-fluorenes; 13, phenanthrene; 14, anthracene; 15, c1-phenanthrenes/anthracenes; 16,c2-phenanthrenes/anthracenes; 17, c3-phenanthrenes/anthracenes; 18, c4-phenanthrenes/anthracenes; 19, dibenzothiophene; 20, c1-dibenzothiophenes; 21, c2-dibenzothiophenes; 22, c3-dibenzothiophenes; 23, fluoranthene; 24, pyrene; 25, c1-fluoranthenes/pyrenes; 26, benzo[a]anthracene; 27, chrysene; 28, c1-chrysenes; 29, c2-chrysenes; 30, c3-chrysenes; 31, c4-chrysenes; 32, benzo[b]fluoranthene; 33, benzo[k]fluoranthene; 34, benzo[e]pyrene; 35, benzo[a]pyrene; 36, perylene; 37, indeno[1,2,3-c,d]pyrene; 38, dibenzo[a,h]anthracene; 39, benzo[g,h,i]perylene; 40, 2-methylnaphthalene; 41, 1-methylnaphthalene; 42, 2,6-dimethylnaphthalene; 43, 1,6,7-trimethylnaphthalene; 44, 1-methylphenanthrene.
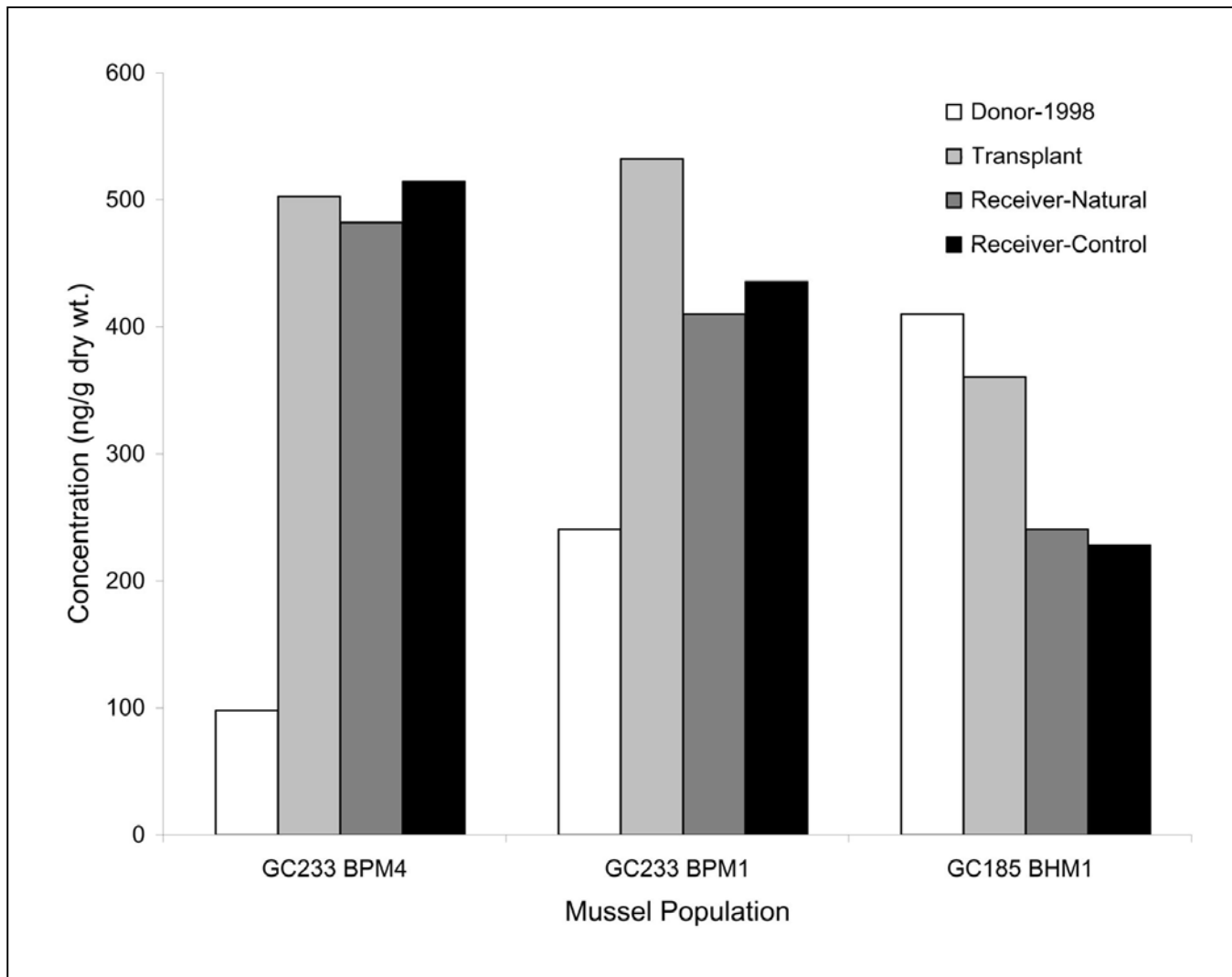
Figure 8.5.4.    Plot of total PAH body burden for mussels in the transplant experiment.  The donor population for the GC233M1 transplant was GC185M1. The reciprocal was true for the GC185M1 transplant. The mussels transplanted to GC233M4 came from GC234M1.  The PAHs summed for this measurement are listed in Figure 8.5.3.
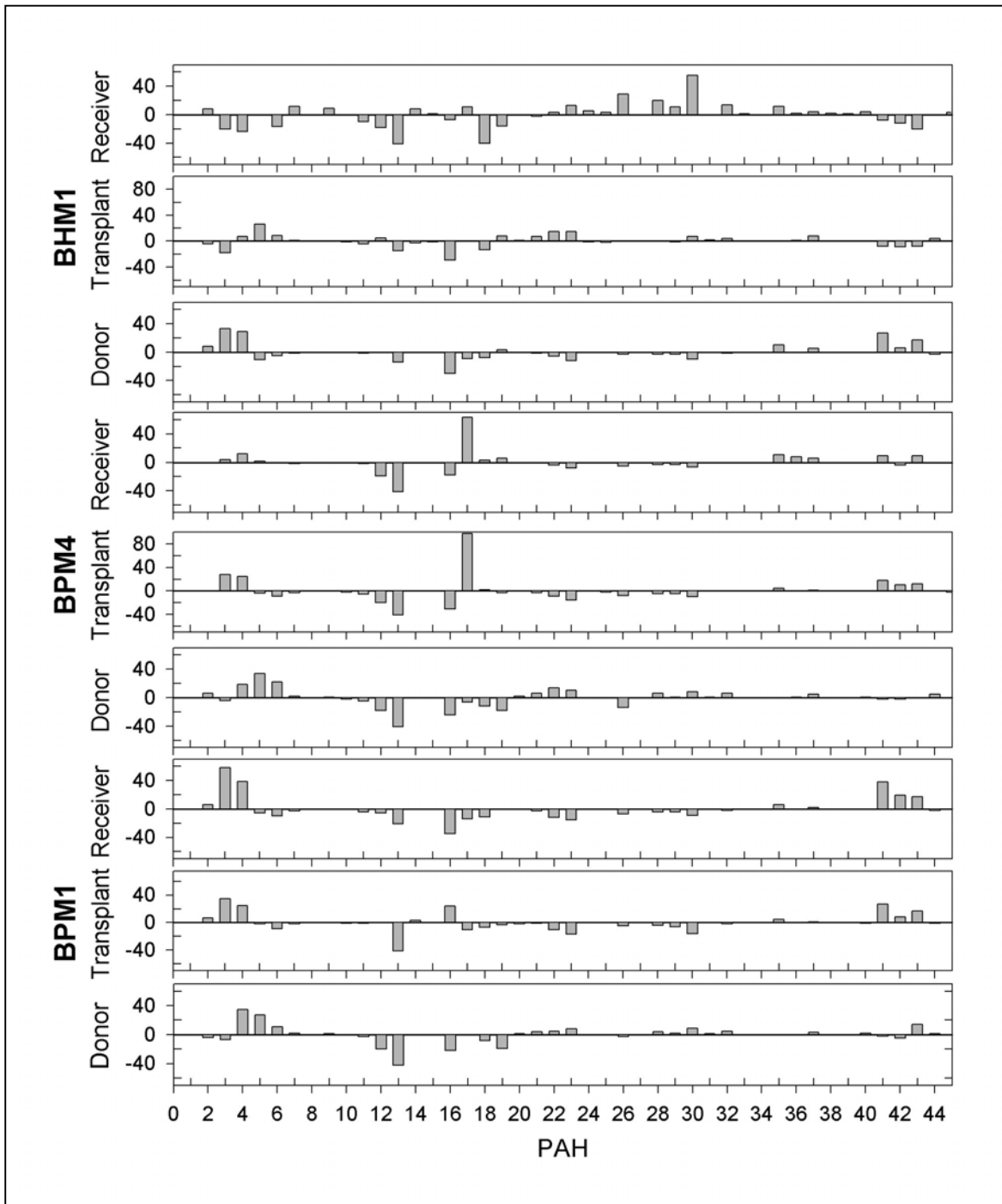
Figure 8.5.5. Proportional differences between the sample mean and the global mean for each compound in the PAH compound series for the three transplant experiments. For this calculation, each mean variable value for each sample was standardized to parts per thousand, as was the global mean value for the variable for all samples. The difference between the global mean standardized value and the sample mean standardized value was calculated and these mean standardized differences were plotted. Donor populations are identified in Figure 4 and the PAH compound series in Figure 8.5.3.

## 8.6 Food Chain Dynamics[*]

### 8.6.1 Introduction

There is an obligate relationship between the habitat-forming chemosynthetic hosts—tubeworms (vestimentiferans), mussels (modiolids), and clams (vesycomids)—and seafloor emissions of hydrogen sulfide and/or methane. This relationship is so obvious and strong that declaration of these ecosystems to be chemically and physically controlled would meet with little debate. Uncritical acceptance of the position that a special geochemical environment is both necessary and sufficient for the establishment and persistence of chemosynthetic communities is unwise from the management perspective. As in most ecosystems, seeps are likely to experience both abiotic and biotic control, which renders the geochemical environment necessary but insufficient for community establishment and persistence. If this is the case, effective management to protect seep environments must consider the role of biotic control.

Rigorous demonstration of biotic control, starting with models and progressing into field situations, has dominated much of theoretical and practical ecology for the past fifty years. Unfortunately, strict requirements of experimental design, replication, and use of controls may make it impractical formally to identify the nature and extent of biotic control in any deep-sea system, especially seeps and vents. This is the case when non-lethal competition among species is a factor in biotic control. It is possible, however, to gauge the nature and extent of predation through analyses that determine the dietary history of a sampled organism. This section presents results from this investigation.

There are two basic questions about seep trophic relations that are of both scientific and management importance: within-seep feeding patterns and interactions between the seep and background systems. The background system is defined as the surrounding deep-sea environment. It is established that the numerous consumer organisms associated with seeps and vents derive all or some nutrition from chemosynthetic sources. If the details of feeding indicate that the habitat-forming species are being preyed upon, then predatory-mediated population control could impact system stability and persistence. Similarly important are seep-background interactions. If the background fauna exploits the seep system or the seep somehow exploits the background, then the zone of interaction must extend beyond the confines of the special geochemical environment. Regulatory policies, therefore, need to protect such a larger area.

### 8.6.2 Background: expected seep-background interactions

**The oasis of seeps versus the desert of the background benthos.** In spite of different geological settings, deep-sea chemosynthetic communities at continental margin cold seeps and seafloor spreading sites share ecological features. Both are known to have high standing stock biomass levels of producer and consumer organisms in spatially compressed areas. Interactions of these productive systems with the comparatively meager background of typical deep-sea benthic fauna are poorly known. Observations within seep and vent systems support the view that only a very small fraction of background species actually exploit the chemosynthetic production (Carney 1994).

---

[*] This section was authored by Robert S. Carney, Steven Macks and Stephan Macavoy.

**Initial observational evidence of linkage.** Analysis of stable isotope content in tissues from hot vent and hydrocarbon seep organisms has been instrumental in confirming the chemosynthetic nature of productivity and apparent trophic linkages within the producers and consumers community (Fisher *et al.* 1994; Kennicutt *et al.* 1992; Rau 1981; Rau and Hedges 1979; Vandover and Fry 1989, 1994). Successful trophic tracing requires unambiguous end points. With some cautions, this condition is met at the hydrocarbon seeps. For most non-seep fauna, phytodetritus will be the ultimate food source and sole organic carbon pool. Phytodetritus is organic material created photosynthetically in the euphotic zone. Depending on the species composition of the phytoplankton and various oceanographic conditions, the isotopic composition of the phytodetritus reflects fractionation of the available seawater inorganic carbon pool (Degens *et al.* 1968a; Degens *et al.* 1968b; Goericke and Fry 1994; Goericke *et al.* 1994). In the Northern Gulf of Mexico, the non-seep deep benthic fauna has a very well defined $\delta^{13}C$ value 17.7‰ ±1.2 (Carney *et al.* unpublished manuscript). For consumers in and near seeps, the abundant biomass of the symbiont-hosting organisms is a possible food source. In the methanotrophic mussels at Gulf of Mexico seeps, the methane source affords a pool of carbon distinguishable by the stable carbon isotope signature of methane (Kennicutt *et al.* 1992). Studies of the isotope composition of Gulf of Mexico seep biota have been undertaken since the earliest discoveries of the systems and have proven extremely informative. They served to identify methane as an energy and carbon source for the methanotrophic mussels, proved some degree of trophic dependence by the heterotrophic seep residents upon chemosynthetic productivity, and suggested that certain mobile fauna caught away from seeps, notably large crabs like *Chaceon* and fish like *Synaphobranchus* had foraged in the seep areas at some time (Carney *et al.* unpublished manuscript).

However, as results accumulated, it became evident that the carbon pools available to the seep organisms are complex and do not always have distinguishing isotopic signatures. Therefore, interpretation has been more speculative than desired. This was most noticeable for the seep-resident gastropods and crustaceans that displayed isotope values from (-45‰ up to -17‰). This wide range can be interpreted in many ways. Falling between mussel tissue and phytodetritus, it simply could be a mixture of sources. But, how could the animals get so much phytodetritus at those depths? Alternately, there could be multiple carbon pools, which are essentially chemosynthetic but mimic chemo-phyto mixed sources. Such mimics could be tubeworms that have been found to have very wide ranges (Kennicutt *et al.*, 1992) or free-living bacteria that have yet to be effectively sampled. A similar suggestion of a confounding bacterial carbon pool has been put forward by VanDover and Fry (1989, 1994).

Whether seeps and vents are trophically open or closed is fundamental in respect to how both those systems and the deep-sea background function. There is a prevalent idea in deep-sea ecology that the deep benthos is food limited (reviewed in Gage and Tyler 1991). Food limitation means that the inventory of sustained species populations is more impacted by food supply than other factors. This condition is assumed to have persisted over very long time periods giving rise to considerable foraging specialization (Jumars *et al.* 1990). If the deep background were food limited, then one would predict a high level of exploitation of seep/vent systems. This investigation examines the interaction of these two systems by looking for evidence of trophic links in samples from the background rather than the seep or vent site. Inquiry directed at the background is a necessary complement to site-directed work and may prove to be a better means of assessing larger-scale effects of seep and vent systems.

### 8.6.3 Objectives

The objective of this work is to provide a trophic component to the study of interdependencies and interrelationships between chemosynthetic and non-chemosynthetic organisms. The task is intended to improve upon preliminary findings and is intended to provide the following:

A definitive means of determining which seep-dwelling species actually exploit chemosynthetic production rather than some other habitat value of seep-related topographic features;

A definitive means of determining if mobile deep-sea species found adjacent to seep communities exploit chemosynthetic production;

A definitive means of identifying prey-predator pairs, which might indicate predatory control on seep populations.

### 8.6.4 Methods

**Field methods.** The animals examined in this study were collected during the summers of 1997 and much more extensively in 1998. Mobile predatory fauna within seep communities were collected either with small (~75x75x50 cm) wire mesh traps deployed within and around tubeworm and mussel beds at GC185, GC234, and GC233 by the Johnson SEA-LINK submersible or directly by the submersible. Mobile predators were caught off-site with surface deployed Z-frame traps, which measured approximately 150x200x75cm, and were deployed roughly 2 km off the location of the seep communities in areas known from prior surveys to lack active seep communities. Both small and Z-frame traps were intended to capture fish and crustaceans. Both were constructed of 1-in trap mesh, equipped with two 20-cm entry mouths, and baited with menhaden in a wire bait cage to minimize consumption. Trap soak time (duration of deployment) was determined by cruise logistics and ranged from one to six days.

**Isotope analysis.** Tissue samples were taken from captured organisms and frozen until shipment to the stable isotope laboratory. Samples were dried at 60°C for three days and homogenized. The dried tissues were then ground to powder and, if they contained carbonate, were acidified with 10% HCl, and re-dried. The powder was placed in a tin cup and weighed (typically 0.5 mg was used). The isotope compositions were determined using a high temperature combustion system that incorporated a Carlo-Erba CHN analyzer interfaced to an OPTIMA stable isotope mass spectrometer using a continuous flow interface. The samples were combusted in an oxidizing furnace at 1020°C. The gases from the combustion were passed through a reduction furnace at 650°C and a chemical water trap, followed by a gas chromatograph, which separated the evolved carbon dioxide from the nitrogen gas. These pulses of combustion gases were isotopically assessed following calibration of the mass spectrometer with pulses of laboratory gases of known isotopic composition.

As an auxiliary activity, sulfur isotopes were also being examined. For these determinations, the furnace temperature was higher (1030°C), and the gas chromatographic separation was accomplished at a higher temperature. A total of 5 to 6 mg of sample was required for sample analysis. The evolved sulfur dioxide was analyzed versus a laboratory tank of calibrated gas and corrected for cross mass overlap of oxygen. Typical precision of the measurements was 0.2‰.

The isotope compositions will be reported relative to standard material and follow the same procedure for all stable isotopic measurements, as follows:

$$\delta^x E = [(^x E/^y E)_{sample}/(^x E/^y E)_{standard}] - 1) * 1000 \qquad (8.6\text{-}1)$$

where E is the element analyzed (carbon, nitrogen or sulfur), x is the atomic weight of the heavier isotope, and y the lighter isotope (x = 13, 15, 34 and y = 12, 14, 32 for carbon, nitrogen, and sulfur, respectively). The standard materials to which the samples are compared are PDB (Pee Dee Belemnite) for carbon, air ($N^2$) for nitrogen, and CDT (Canyon Diablo Triolite) for sulfur. Reproducibility of all measurements is typically better than 0.3‰ for $\delta^{34}S$, and 0.2‰ for $\delta^{13}C$ and $\delta^{15}N$.

**Immunoassay.** Immunoassay, or serological assay, can be a reliable means of identifying ingested tissues when tissue cropping, mastication, and digestion have rendered stomach contents otherwise unrecognizable. Application of this technique to the identification of prey-predator links in the marine benthos has been extensively developed by Dr. Robert Feller of the University of South Carolina (Feller *et al.* 1979). The technique is based on the fact that immune systems create antibodies to foreign proteins (antigens). This process is exploited as an analytical tool by taking possible prey tissue and injecting it into lab rabbits to trigger antibiotic creation. These antibodies are then extracted and purified. If successful, the resulting antibody will be highly specific to the prey species and the antigen-antibody reaction used as an assay when unknown tissues are encountered. In the current task, immunoassay was attempted only on a trial, or proof of method, basis. The main limitation in this approach is that the antibodies produced may lack the required species specificity. When this is the case, the antibody may give false positive reactions to potential prey tissue (Feller and Gallagher 1982). While it is hoped that mussels, tubeworms, and bacteria are sufficiently unrelated and that highly specific antibodies will be produced, this must first be confirmed.

### 8.6.5 Results

**General sampling results.** The collection methods described above were tested and refined during the 1997 cruise. Most importantly, it was shown that traps could be deployed and recovered in over 500 m of water from the surface ship with minimal gear requirement. Three traps were deployed by the submersible in separate seep sites – GC185, GC233, and GC234. Off-site deployments made use of a hydraulic pot hauler. The use of a commercial pot-hauling line proved to be a simple operation requiring approximately 1 hour from start to finish to deploy or recover. Operations of such short duration did not conflict with inter-site steaming or dive-support use of the ship.

In the following year, many short-duration deployments around GC185, GC233, and GC234 were planned in order to sample as much of the spatial variation as possible. Unfortunately, the highly effective line hauler used in 1997 was not available, and hauling was done on a berthing-line capstan, requiring 2.5 hours to haul. Including positioning, the time needed from start to finish in a retrieval was about four hours. This proved far too long to allow for the planned deployments. As a result only seven deployments were made with longer soak times ranging from two to seven days (Table 8.6.1).

Table 8.6.1. Deployments and recovery of large surface-deployed traps.

| Date | Latitude | Longitude | Station | Site | Action |
|------|----------|-----------|---------|------|--------|
| 7/10/97 | 27°47.19 | 91°31.05 | BHR1 | GC185 | Deployed |
| 7/11/97 | 27°47.19 | 91°31.05 | BHR1 | GC185 | Recovered |
| 7/11/97 | 27°44.35 | 91°16.74 | BPR2 | GC233 | Deployed |
| 7/13/97 | 27°44.35 | 91°17.74 | BPR2 | GC233 | Recovered |
| 7/13/97 | 27°44.8 | 91°14.6 | GCR1 | GC234 | Deployed |
| 7/16/97 | 27°44.8 | 91°14.6 | GCR1 | GC234 | Recovered |
| 7/3/98 | 27°47.20 | 91°29.000 | BHTP1 | GC185 | Deployed |
| 7/5/98 | 27°47.20 | 91°29.000 | BHTP1 | GC185 | Recovered |
| 7/5/98 | 27°47.17 | 91°30.032 | BHTP2 | GC185 | Deployed |
| 7/12/98 | 27°47.173 | 91°30.032 | BHTP2 | GC185 | Recovered |
| 7/12/98 | 27°47.173 | 91°30.032 | BHTP3 | GC185 | Deployed |
| 7/16/98 | 27°47.173 | 91°30.032 | BHTP3 | GC185 | Recovered |
| 7/6/98 | 27°45.900 | 91°11.60 | CGTP1 | GC234 | Deployed |
| 7/10/98 | 27°45.900 | 91°11.60 | GCTP1 | GC234 | Recovered |
| 7/10/98 | 27°46.330 | 91°13.480 | GCTP2 | GC234 | Deployed |
| 7/15/98 | 27°46.330 | 91°13.480 | GCTP2 | GC234 | Recovered |
| 7/9/98 | 27°43.430 | 91°16.624 | BPTP1 | GC233 | Deployed |
| 7/13/98 | 27°43.340 | 91°16.624 | BPTP1 | GC233 | Recovered |
| 7/13/98 | 27°43.860 | 91°16.400 | BPTP2 | GC233 | Deployed |
| 7/16/98 | 27°43.869 | 91°16.400 | BPTP2 | GC233 | Recovered |

An unexpected benefit of the fewer settings with longer soak times may have been larger catches. The planned one- and two-day deployments may have produced very few specimens. The possibility exists, however, that predation and scavenging by *Bathynomus giganteus* and *Eptatretus* sp. in the traps may have removed soft tissue animals when traps were deployed for several days. The very low catch of fish other than hagfish may be due to this cause.

On-site small trap deployments proved feasible but complicated by shifting dive sites and equipment priorities. As a matter of policy, traps were not deployed unless it was highly likely that the site would be revisited and the trap recovered. Traps were deployed at GC233, GC185, and GC234 (Table 6.6.2). However, only the GC233 trap with nine specimens was recovered while the task participants were on board. Workers retrieved the other traps as a matter of course near the end of the dive, but faunal samples were not logged.

Table 8.6.2. Small within-site traps deployed and
recovered by submersible.

| Dive | Site | Date | Action |
|------|------|------|--------|
| 2851 | GC233 | 7/9/97 | Deploy |
| 2854 | GC233 | 7/11/97 | Recover |
| 2857 | GC185 | 7/12/97 | Deploy |
| 2860 | GC233 | 7/13/97 | Deploy |
| 2878 | GC233 | 7/24/97 | Recover |
| 2862 | GC234 | 7/14/97 | Deploy |
| 2881 | GC234 | 7/25/97 | Recover |
| 4025 | GC185 | 7/4/98 | Deploy |
| 4027 | GC185 | 7/5/98 | Recover |
| 4029 | GC234 | 7/6/98 | Deploy |
| 4032 | GC234 | 7/7/98 | Recover |
| 4043 | GC234 | 7/12/98 | Deploy |
| 4052 | GC234 | 7/16/98 | Recover |
| 4039 | GC233 | 7/10/98 | Deploy |
| 4054 | GC233 | 7/17/98 | Recover |

**General isotope results.** An overall summary of isotope results is presented species-by-species in Table 8.6.3. The following sections present this same information on an isotope-by-isotope and a site-by-site basis.

**General isotope results–carbon.** $\delta^{13}C$ determinations were made for 86 producer organisms in six taxa, 155 resident consumers in 23 taxa, and 76 vagrant species in 15 taxa. Figure 8.6.1 illustrates the single-isotope results. The results replicate those obtained in previous studies. The $\delta^{13}C$ values in the chemosynthetic producers range from close to that of background deep-sea organisms to very distinctive values. This range mimics two-food source mixing and severely limits the utility of $\delta^{13}C$ alone in trophic studies of these systems. *Bathymodiolus childressi* from multiple sites show a broad range of values (minimum = -68.96‰, average = -46.23‰, maximum = -26.19‰) consistent with the site-varying sources of methane. The much rarer thiotrophic mussel *Tamu fisheri* was collected at a single site and had a narrower range and less depleted values (minimum = -38.68‰, average = -37.04‰, maximum = -35.75‰). The thiotrophic tubeworms *Lamellibrachia* sp. and *Escarpia* sp. showed even less depletion (*Lamellibrachia*, minimum = -24.76‰, average = -21.32‰, maximum = -18.18‰; *Escarpia*, minimum = -35.59‰, average = -25.73‰, maximum = -21.71‰).

Table 8.6.3.  Summary table for stable isotope analyses from program study sites.

| Faunal Element | Site | δ¹³C | | | | δ¹⁵N | | | | δ³²S | | | |
|---|---|---|---|---|---|---|---|---|---|---|---|---|---|
| | | n | min. | average | max. | n | min. | average | max. | n | min. | average | max. |
| **Chemosynthetic-host fauna** | | | | | | | | | | | | | |
| *Bathymodiolus childressi* | GB425 | 3 | -59.0 | -53.6 | -43.1 | 3 | -9.2 | -2.0 | 4.3 | 1 | 4.3 | 4.3 | 4.3 |
| *Bathymodiolus childressi* | GC185 | 26 | -44.5 | -38.6 | -26.2 | 26 | 0.3 | 3.9 | 8.3 | 17 | -24.2 | -3.8 | 3.3 |
| *Bathymodiolus childressi* | GC233 | 11 | -69.0 | -63.6 | -60.8 | 11 | -20.9 | -16.6 | -14.0 | 7 | 5.8 | 11.8 | 14.6 |
| *Bathymodiolus childressi* | GC234 | 6 | -45.5 | -43.7 | -41.2 | 6 | 1.8 | 3.1 | 4.1 | 1 | 6.7 | 6.7 | 6.7 |
| *Bathymodiolus childressi* | | | | | | | | | | | | | |
| *Escarpia sp.* | GC185 | 5 | -22.5 | -22.1 | -21.7 | 5 | 2.5 | 3.2 | 3.8 | 3 | -35.1 | -32.8 | -29.4 |
| *Escarpia sp.* | GC234 | 3 | -35.6 | -31.8 | -29.7 | 3 | 2.5 | 3.6 | 5.4 | | | | |
| *Lamellabrachia sp.* | GC185 | 15 | -23.2 | -20.9 | -18.2 | 15 | -0.5 | 1.5 | 2.7 | 9 | -35.1 | -26.1 | -21.9 |
| *Lamellabrachia sp.* | GC234 | 2 | -24.8 | -24.5 | -24.2 | 2 | 3.2 | 3.5 | 3.7 | | | | |
| *Lamellabrachia sp.* | | | | | | | | | | | | | |
| *Tamu fisheri* | GC185 | 14 | -40.3 | -37.3 | -35.8 | 14 | -1.6 | 2.0 | 6.6 | 10 | -29.0 | -19.6 | -1.2 |
| *Tamu fisheri* | | | | | | | | | | | | | |
| Lucinid clam | GC185 | 1 | -31.6 | -31.6 | -31.6 | 1 | 1.9 | 1.9 | 1.9 | 1 | -20.8 | -20.8 | -20.8 |
| **Seep-dwelling heterotrophic fauna** | | | | | | | | | | | | | |
| **Mobile taxa** | | | | | | | | | | | | | |
| *Bathynerita naticoidea* | GB425 | 1 | -46.9 | -46.9 | -46.9 | 1 | -3.1 | -3.1 | -3.1 | 1 | 6.4 | 6.4 | 6.4 |
| *Bathynerita naticoidea* | GC185 | 8 | -31.5 | -28.0 | -20.3 | 8 | 5.8 | 7.8 | 10.7 | 6 | -7.8 | -3.3 | 0.5 |
| *Bathynerita naticoidea* | GC233 | 2 | -52.4 | -51.9 | -51.4 | 2 | -6.5 | -6.0 | -5.6 | 5 | 6.6 | 8.9 | 11.2 |
| *Provanna sculpta* | GC185 | 3 | -32.3 | -31.4 | -30.6 | 3 | 3.4 | 4.0 | 4.5 | 1 | -9.9 | -9.9 | -9.9 |
| *Cataegis meroglypta* | GC185 | 1 | -28.5 | -28.5 | -28.5 | 1 | 4.1 | 4.1 | 4.1 | | | | |
| *Munidopsis sp. type1* | GC185 | 34 | -41.0 | -31.5 | -23.3 | 34 | 0.1 | 6.1 | 8.9 | 5 | -13.0 | -7.2 | -2.1 |
| *Munidopsis sp. type1* | GC233 | 2 | -52.3 | -50.2 | -48.2 | 2 | -10.7 | -9.6 | -8.4 | 1 | 17.3 | 17.3 | 17.3 |
| *Munidopsis sp. type1* | GC234 | 3 | -36.1 | -33.1 | -30.2 | 3 | 5.8 | 6.3 | 7.0 | | | | |
| *Munidopsis sp. type2* | GC185 | 2 | -28.9 | -28.7 | -28.6 | 2 | 9.2 | 9.3 | 9.3 | | | | |
| *Munidopsis sp. type2* | GC234 | 2 | -27.4 | -27.1 | -26.7 | 2 | 6.7 | 8.2 | 9.6 | 1 | 6.1 | 6.1 | 6.1 |
| *Alvinocaris sp.* | GC185 | 1 | -20.6 | -20.6 | -20.6 | 1 | 5.4 | 5.4 | 5.4 | 1 | -0.4 | -0.4 | -0.4 |
| *Alvinocaris stactophilia* | GC185 | 14 | -38.5 | -28.6 | -21.3 | 14 | 2.2 | 5.9 | 9.1 | 5 | -6.4 | 1.3 | 10.1 |
| *Alvinocaris stactophilia* | GC233 | 8 | -51.3 | -43.7 | -36.5 | 8 | -9.2 | -7.7 | -4.4 | 4 | 16.1 | 17.1 | 19.5 |
| *Alvinocaris stactophilia* | GC234 | 3 | -30.0 | -29.1 | -28.5 | 3 | 6.8 | 8.3 | 10.1 | | | | |
| *Buccina canatae* | GC233 | 3 | -53.7 | -52.6 | -50.5 | 3 | -11.5 | -10.6 | -9.8 | 1 | 7.4 | 7.4 | 7.4 |
| *Buccina canatae* | GC234 | | | | | | | | | 1 | -3.5 | -3.5 | -3.5 |

Table 8.6.3. Continued.

| Faunal Element | Site | δ¹³C n | min. | average | max. | δ¹⁵N n | min. | average | max. | δ³²S n | min. | average | max. |
|---|---|---|---|---|---|---|---|---|---|---|---|---|---|
| *Buccina canatae* | GC185 | 2 | -35.6 | -29.2 | -22.8 | 2 | 5.0 | 6.2 | 7.3 | 4 | -9.6 | -4.5 | 3.8 |
| ScotchBonnet-like gastropod | GC185 | 6 | -23.4 | -14.8 | 22.4 | 6 | 3.2 | 4.0 | 4.8 | 4 | -4.3 | 4.6 | 11.3 |
| *Sclerasterias tanneri* | GB425 | | | | | 0 | | | | 1 | 10.7 | 10.7 | 10.7 |
| *Sclerasterias tanneri* | GC185 | 5 | -36.3 | -34.4 | -32.5 | 5 | 0.7 | 4.6 | 5.6 | 1 | 4.2 | 4.2 | 4.2 |
| orbinid worm | GC233 | 4 | -62.6 | -61.4 | -60.0 | 4 | -10.4 | -9.4 | -9.0 | 9 | 12.6 | 16.5 | 21.1 |
| orbinid worm | GC234 | 1 | -41.0 | -41.0 | -41.0 | 1 | 4.2 | 4.2 | 4.2 | | | | |
| sipunculid | GC185 | 14 | -41.1 | -30.0 | -27.3 | 14 | -5.9 | 4.5 | 8.9 | 9 | -12.3 | -3.0 | 4.5 |
| sipunculid | GC234 | 3 | -31.1 | -29.9 | -28.2 | 3 | 7.0 | 7.4 | 7.8 | 1 | 1.5 | 1.5 | 1.5 |
| Atelecylidae crab | GC185 | 1 | -24.8 | -24.8 | -24.8 | 1 | 9.7 | 9.7 | 9.7 | | | | |
| *Nephropsis sp.* | GC185 | 1 | -35.2 | -35.2 | -35.2 | 1 | 3.1 | 3.1 | 3.1 | | | | |
| White shrimp | GC185 | 1 | -31.0 | -31.0 | -31.0 | 1 | 3.0 | 3.0 | 3.0 | | | | |
| Axiidae | GC185 | 1 | -33.2 | -33.2 | -33.2 | 1 | 2.6 | 2.6 | 2.6 | | | | |
| Nereiid polychaete | GC185 | 2 | -31.2 | -30.6 | -29.9 | 1 | 5.4 | 5.4 | 5.4 | 2 | -9.8 | -9.5 | -9.3 |
| *Nicomache sp.* | GC185 | 1 | -28.5 | -28.5 | -28.5 | 1 | 7.5 | 7.5 | 7.5 | 1 | -3.4 | -3.4 | -3.4 |
| polychaete unidentified | GC185 | 5 | -36.4 | -29.1 | -23.7 | 5 | 3.4 | 4.1 | 4.9 | | | | |
| polychaete unidentified | GC234 | 2 | -30.9 | -30.4 | -29.8 | 2 | 8.9 | 9.7 | 10.6 | | | | |
| *Harmothoe sp.* | GC185 | 2 | -23.7 | -23.6 | -23.5 | 2 | 4.3 | 5.7 | 7.0 | 2 | -12.6 | -10.5 | -8.5 |
| *Harmothoe sp.* | GC233 | | | | | | | | | 2 | 15.6 | 16.0 | 16.5 |
| *Eurythoe sp.* | GC185 | 1 | -40.6 | -40.6 | -40.6 | 1 | 8.1 | 8.1 | 8.1 | 3 | -12.0 | -9.8 | -7.1 |
| Nemertean | GC185 | 5 | -29.0 | -25.5 | -22.2 | 5 | 1.1 | 4.4 | 7.5 | 2 | -9.6 | -7.9 | -6.1 |
| Nemertean | GC234 | 2 | -40.1 | -40.0 | -39.9 | 2 | 5.1 | 5.4 | 5.8 | | | | |
| Platyhelmenthes | GC233 | | | | | | | | | 1 | 15.9 | 15.9 | 15.9 |
| Pycnogonia | GC185 | 1 | -26.1 | -26.1 | -26.1 | 1 | 6.7 | 6.7 | 6.7 | | | | |
| Ophiuroid | GC185 | | | | | | | | | 1 | 21.9 | 21.9 | 21.9 |
| *Bellottia sp.* | GC234 | 2 | -27.4 | -27.3 | -27.1 | 2 | 9.6 | 9.9 | 10.1 | | | | |
| Bellotia sp. gut content | GC185 | 1 | -21.7 | -21.7 | -21.7 | 1 | 8.7 | 8.7 | 8.7 | | | | |
| Unidentified eel | GC185 | 1 | -30.4 | -30.4 | -30.4 | 1 | 7.4 | 7.4 | 7.4 | | | | |
| *Diodora sp.* | GC185 | 2 | -31.8 | -30.2 | -28.6 | 2 | 9.2 | 9.6 | 10.0 | 1 | 4.9 | 4.9 | 4.9 |
| **Sessile taxa** | | | | | | | | | | | | | |
| sponge | GC185 | 4 | -34.2 | -31.4 | -25.3 | 4 | 3.4 | 6.7 | 8.7 | 1 | 3.6 | 3.6 | 3.6 |
| Hydroid | GC185 | 5 | -32.6 | -28.4 | -26.2 | 5 | 1.9 | 4.7 | 7.3 | 2 | -18.5 | -8.4 | 1.8 |
| Hydroid | GC234 | 1 | -24.5 | -24.5 | -24.5 | 1 | 8.5 | 8.5 | 8.5 | 0 | 0.0 | 0.0 | 0.0 |
| Scalpellid barnacle | GC185 | 1 | -19.5 | -19.5 | -19.5 | 1 | 9.9 | 9.9 | 9.9 | 1 | 14.3 | 14.3 | 14.3 |

Table 8.6.3. Continued.

| Faunal Element | Site | δ $^{13}$C | | | | δ $^{15}$N | | | | δ $^{32}$S | | | |
|---|---|---|---|---|---|---|---|---|---|---|---|---|---|
| | | n | min. | average | max. | n | min. | average | max. | n | min. | average | max. |
| Scalpellid barnacle | GC234 | 1 | -17.7 | -17.7 | -17.7 | 1 | 12.7 | 12.7 | 12.7 | 1 | 20.6 | 20.6 | 20.6 |
| Verrucamorph barnacle | GC234 | | | | | | | | | 1 | 18.8 | 18.8 | 18.8 |
| *Acesta bullisi* | GC233 | | | | | | | | | 1 | -5.6 | -5.6 | -5.6 |
| **Vagrant taxa** | | | | | | | | | | | | | |
| *Synaphobranchus sp.* | GC185 | 1 | -33.4 | -33.4 | -33.4 | 1 | 7.1 | 7.1 | 7.1 | 1 | -13.3 | -13.3 | -13.3 |
| *Synaphobranchus sp.* | GC233 | 1 | -42.5 | -42.5 | -42.5 | 1 | -3.0 | -3.0 | -3.0 | | | | |
| *Synaphobranchus sp.* | GC234 | 1 | -24.9 | -24.9 | -24.9 | 1 | 8.5 | 8.5 | 8.5 | | | | |
| Nezumia | GC233 | 1 | -32.7 | -32.7 | -32.7 | 1 | 2.2 | 2.2 | 2.2 | | | | |
| *Urophycis cf. cirratus* | GC234 | 1 | 12.3 | 12.3 | 12.3 | 1 | -17.5 | -17.5 | -17.5 | 1 | 20.0 | 20.0 | 20.0 |
| *Bathynomus giganteus* | GC185 | 7 | -18.4 | -16.0 | -14.2 | 7 | 12.3 | 14.0 | 15.8 | 9 | 15.9 | 17.5 | 18.9 |
| *Bathynomus giganteus* | GC233 | 5 | -16.7 | -15.9 | -14.4 | 5 | 11.4 | 14.6 | 16.3 | 7 | 9.3 | 18.0 | 20.4 |
| *Bathynomus giganteus* | GC234 | 3 | -15.9 | -15.1 | -14.0 | 3 | 13.4 | 14.1 | 14.6 | 7 | 18.3 | 20.0 | 21.6 |
| gut contents | GC233 | 3 | -30.6 | -21.8 | -15.6 | 3 | 3.7 | 8.2 | 13.4 | 1 | 20.5 | 20.5 | 20.5 |
| gut contents | GC234 | | | | | | | | | 4 | 16.3 | 19.8 | 22.4 |
| *Eptatretus sp.* | GC185 | 5 | -28.3 | -23.3 | -19.6 | 5 | 7.8 | 9.9 | 11.5 | 29 | -8.8 | 17.6 | 21.9 |
| *Eptatretus sp.* | GC233 | 7 | -28.6 | -21.1 | -17.7 | 7 | 8.2 | 10.4 | 13.3 | 1 | 18.4 | 18.4 | 18.4 |
| *Eptatretus sp.* | GC234 | 7 | -18.3 | -17.0 | -15.8 | 7 | 7.3 | 10.4 | 12.2 | 12 | 12.1 | 16.2 | 18.5 |
| gut contents | GC233 | 2 | -62.8 | -42.1 | -21.4 | 2 | -15.5 | -2.6 | 10.4 | 1 | 19.1 | 19.1 | 19.1 |
| gut contents | GC234 | | | | | | | | | 6 | 12.7 | 16.3 | 18.5 |
| *Rochinia crassa* | GC185 | 14 | -22.9 | -18.6 | -16.4 | 14 | 9.2 | 10.3 | 13.2 | 12 | -12.0 | 13.4 | 19.9 |
| *Rochinia crassa* | GC233 | 1 | -26.2 | -26.2 | -26.2 | 1 | 5.1 | 5.1 | 5.1 | 1 | 12.8 | 12.8 | 12.8 |
| *Rochinia crassa* | GC234 | 3 | -18.8 | -18.0 | -17.3 | 3 | 10.1 | 10.5 | 11.0 | 3 | 20.1 | 20.3 | 20.5 |
| gut contents | GC185 | 5 | -20.4 | -19.1 | -17.8 | 5 | 6.5 | 9.5 | 11.1 | 3 | 12.7 | 18.3 | 24.3 |
| **Background taxa** | | | | | | | | | | | | | |
| meso-pelagic fish | GC233 | 3 | -18.9 | -18.5 | -18.3 | 3 | 6.5 | 7.8 | 9.5 | | | | |
| Shark | GC233 | 6 | -19.9 | -18.3 | -17.4 | 6 | 6.7 | 9.7 | 12.9 | 4 | 17.5 | 18.5 | 19.7 |
| *Chaceon sp.* | GC185 | | | | | | | | | 1 | 19.7 | 19.7 | 19.7 |
| **Miscellaneous** | | | | | | | | | | | | | |
| Sediment | GC185 | 2 | -26.8 | -26.6 | -26.5 | 2 | 11.7 | 13.0 | 14.4 | 1 | 1.3 | 1.3 | 1.3 |
| Sediment | GC234 | 2 | -35.9 | -31.1 | -26.3 | 2 | 3.1 | 5.5 | 7.9 | | | | |
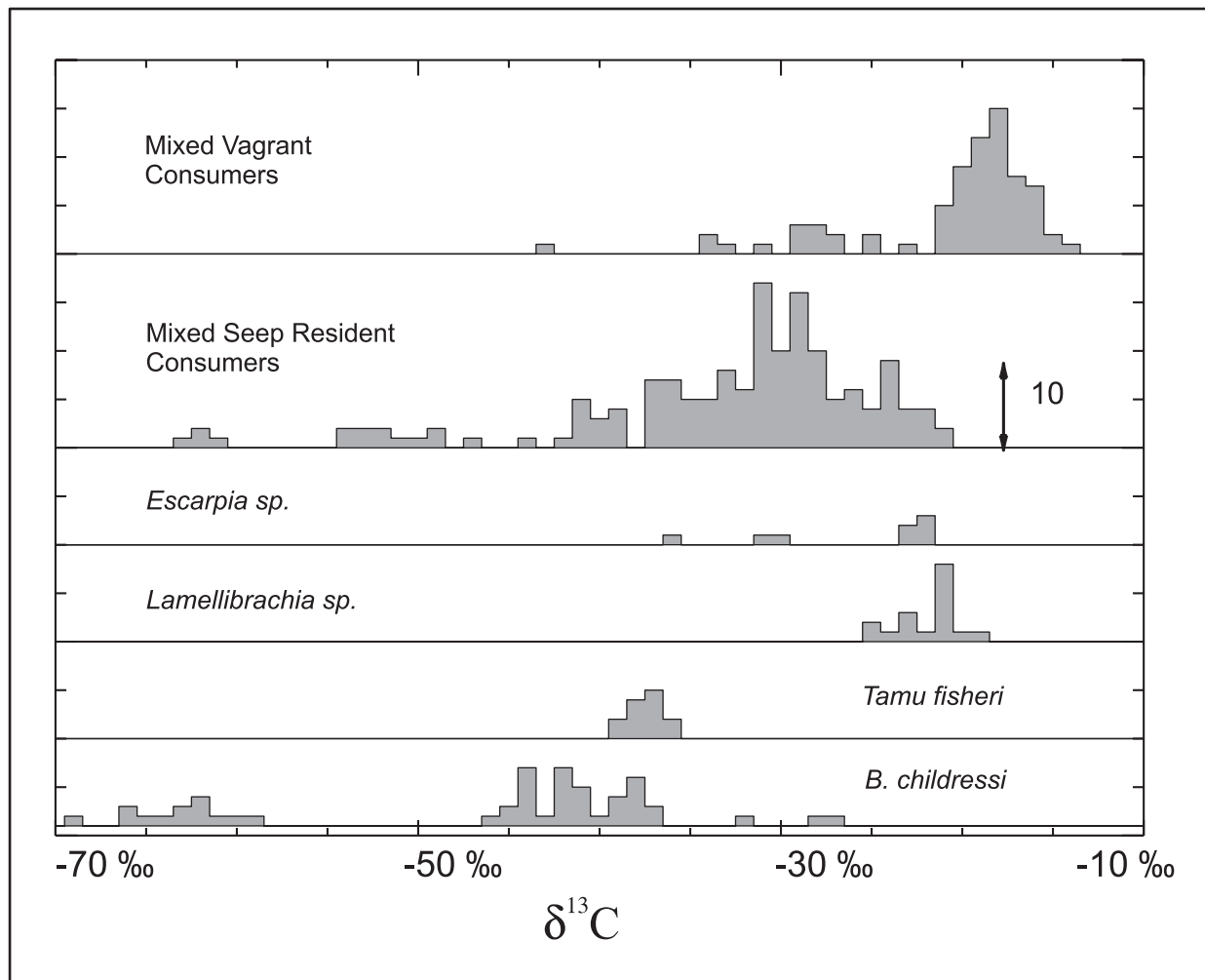
Figure 8.6.1.    Univariate histograms of $\delta^{13}$C determinations for faunal groups.

All 39 taxa of seep-resident consumers showed depleted carbon values relative to typical deep Gulf fauna. The most depleted values were found in an orbinid worm from GC233 (-62.55‰) and the least depleted from a nerite snail at GC185 (-20.30‰). Such a range could be explained by consumption of chemosynthetic production or a mixed diet incorporating typical deep-sea phytodetritus material. In effect, $\delta^{13}$C alone is ambiguous. There is less ambiguity in the case of vagrant consumers. The eight taxa considered vagrants showed dramatically different results. All except the eel, *Synaphobranchus* sp., showed values on average indistinguishable from background deep-sea fauna, in spite of close association with seeps. Scattered individuals of the hagfish *Eptatretus* and the crab *Rochinia crassa* had depleted values consistent with seep feeding.

**General isotope results–nitrogen.**   $\delta^{15}$N determinations were paired with $\delta^{13}$C, and the same number and distribution of values were obtained. Figure 8.6.2 illustrates the single-isotope results. The results largely          mirror          those          for          $\delta^{13}$C          with          some          informative          differences.
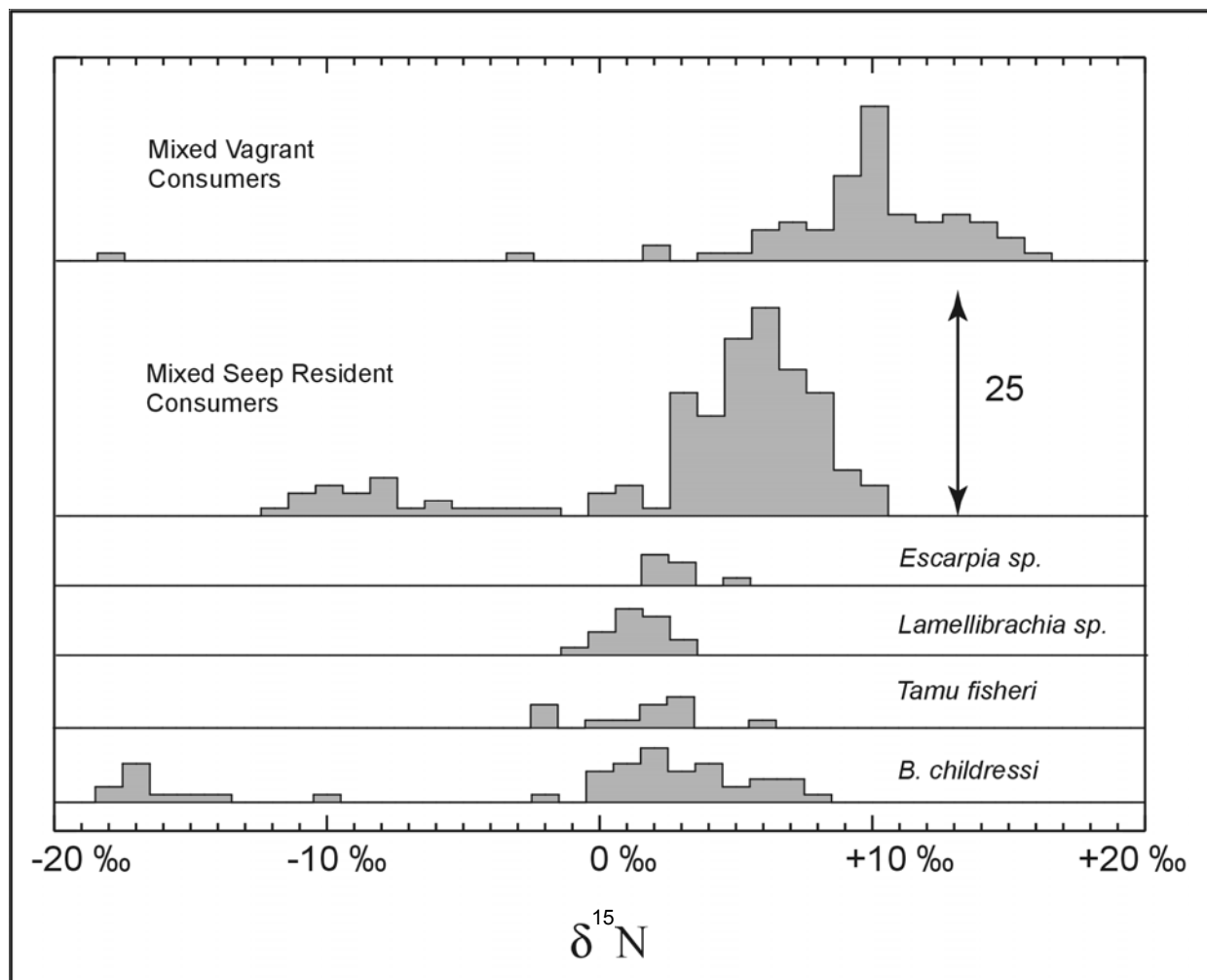
Figure 8.6.2.    Univariate histograms of $\delta^{15}N$ determinations for faunal groups.

*Bathymodiolus childressi* shows a large range (minimum = -20.92, average = -1.51, maximum = 8.30) directly caused by the distinctly low values at GC233. Rather than having a progression of values as in the case of $\delta^{13}C$, all three thiotrophs showed a consistent range of values centered at about 2.0‰. Resident consumers appeared to be bimodal with a mode of -11‰ and less depleted mode at about +6‰. As with carbon, the lower values coincided with GC233 (19 out of the 24 samples in the lower mode were from GC233). Vagrant consumers showed additional shifts to less depleted values and had a modal value (+10‰) consistent with typical deep Gulf benthos. Again, scattered individuals of *Eptatretus* and *Rochinia crassa* had values indicative of seep feeding. A shift to less depleted values is expected in consumers due to trophic effects or could be due to a diet incorporating tissue from the background. This possibility of confounding trophic shifts with mixed food sources reduces the utility of $\delta^{15}N$.

**General isotope results–sulfur.** $\delta^{34}S$ determinations were made as a developmental effort. For 143 specimens, $\delta^{34}S$ was determined in conjunction with $\delta^{13}C$ and $\delta^{15}N$. An additional 91 determinations of $\delta^{34}S$ alone were made. Figure 8.6.3 illustrates the single-isotope results. $\delta^{34}S$ values proved to be

extremely informative and less affected by the ambiguities associated with $\delta^{15}N$ and $\delta^{13}C$. Chemosynthetic producers showed a species-specific shift with thiotrophs being more depleted than methanotrophic mussels. This is directly opposite the case for $\delta^{13}C$ and $\delta^{15}N$. Resident consumers had values more easily interpreted, coming from a diet of mussel tissue rather than tubeworm. Again, vagrant consumers formed a much narrower group with most values reflecting the deep Gulf background food web.
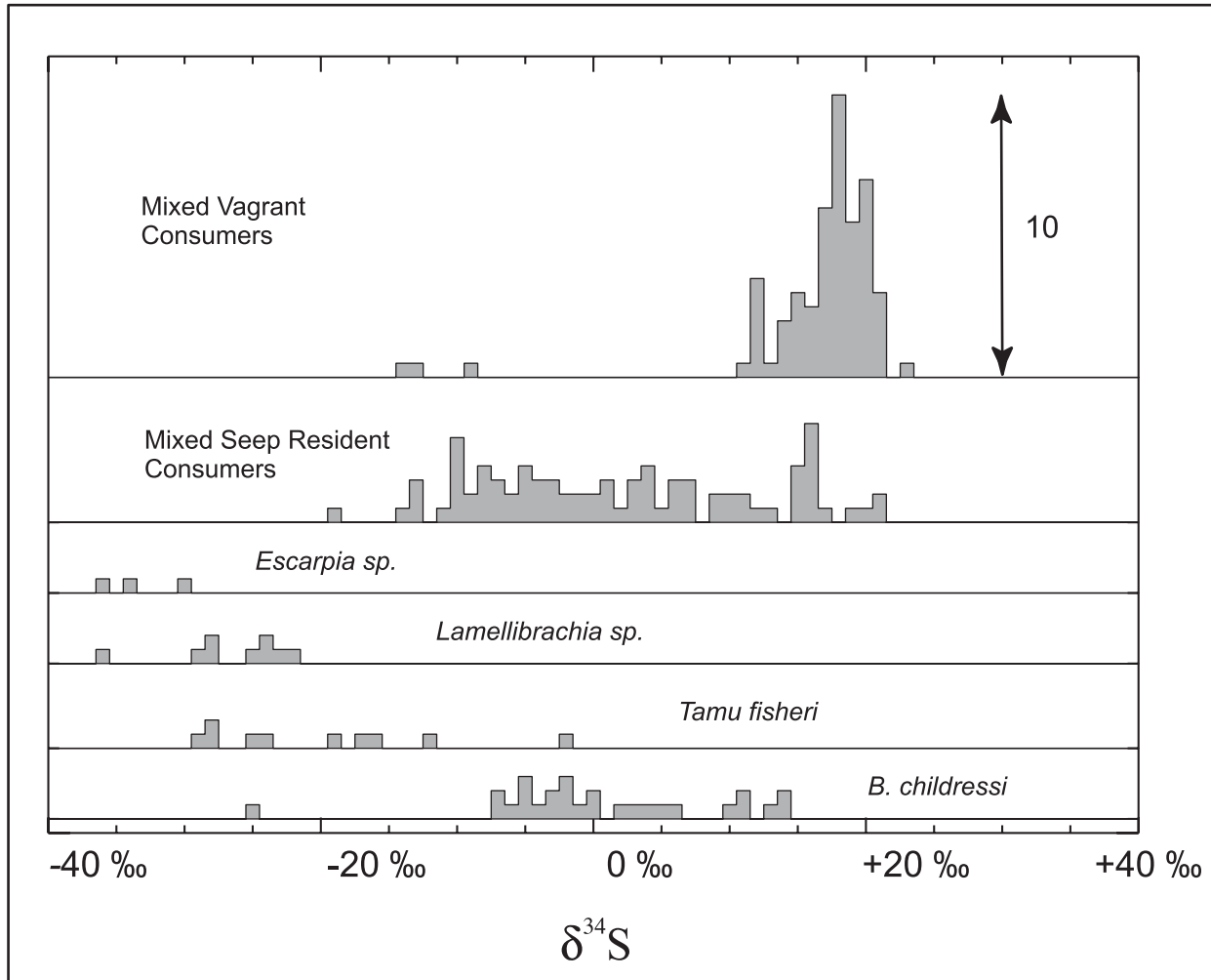


Figure 8.6.3.    Univariate histograms of $\delta^{34}S$ determinations for faunal groups.

**General isotope results–carbon, nitrogen and sulfur.** When bivariate isotope data, $\delta^{13}C$ and $\delta^{15}N$, are collected from a wide variety of organisms in an ecosystem, two non-exclusive relationships can be expected. The first is produced by a system with isotopically homogenous food sources in which isotope partitioning produces a shift at each trophic level. This shift is usually in the form of a line passing through the food source and extending along a slope of (+3‰ N)/(+1‰C). Position along this trophic-shift line can be used to assess the number of levels in a given system. The second expected pattern in $\delta^{13}C$ and $\delta^{15}N$ data is produced by a system in which the food sources are isotopically heterogeneous. Consumers with a mixed diet will fall on lines between the sources describing mixing.

8-83

Mixed results were obtained with respect to a definitive determination of whether Gulf hydrocarbon seep systems act as single food source systems with trophic shifts or complex food-source systems in which mixing obscures determination of trophic levels (Figure 8.6.4). In the case of the dominant mussel, the methanotroph *Bathymodiolus childressi*, carbon again proved to be a definite marker. Nitrogen, however, proved unexpectedly variable in this chemosynthetic producer. The great range of values (-20.92‰ to 8.3‰) can completely mask the trophic shifts that might be produced by an improbable ten trophic levels. Within a given site the variance in nitrogen is less, but the range seen at GC233 underscores the difficulty of interpreting trophic structure. When carbon alone was used in previous studies, tubeworm values overlapped typical deep-sea phytodetritus values making it impossible to discern the food source of associated fauna. It was hoped that the addition of nitrogen would provide better resolution. Unfortunately, this objective was only partially met. Nitrogen values associated with tubeworms were distinct from those associated with the background fauna. The combined carbon and nitrogen values for tubeworms did, however, fall close to background values and directly upon an ambiguous line that might equally as well describe trophic shifting by tubeworm consumers or mixing of food sources.

**Multiple isotope considerations.** Ideally, determination of three or more isotopes will lead to a multivariate model of food webs. Such a model cannot be developed from the current study because the dynamics of nitrogen and sulfur fractionation remain poorly understood, and the sampling was unbalanced with respect to the number of samples per species. Nevertheless, the considerable potential for such a model is evident from examination of inter-isotope correlation (Table 8.6.4). Correlation or covariance matrices are the starting point for a wide range of multivariate analyses such as principal components and factor analysis.

Table 8.6.4. Product-moment correlation of isotope
pairs as an indication of utility in any future multivariate model.

| Correlation Pair | All Data n = 144 | Producers n = 42 | Resident Consumers n = 50 | Vagrant Consumers n = 52 |
|---|---|---|---|---|
| $\delta^{13}C$ vs $\delta^{34}S$ | + 0.23 | - 0.84 | - 0.54 | + 0.78 |
| $\delta^{13}C$ vs $\delta^{15}N$ | +0.77 | + 0.50 | + 0.78 | + 0.59 |
| $\delta^{15}N$ vs $\delta^{34}S$ | +0.39 | - 0.33 | - 0.46 | + 0.34 |

For $\delta^{34}S$ and $\delta^{13}C$, the results were unexpected. The strong negative correlation in producers must reflect unknown linked geochemical processes in the sources or linked metabolic chemistry in the producers. The weaker negative correlation in resident consumers reflects retention of this seep food-source signal with some effect of mixing. The strong correlation of reversed sign in the vagrant consumers indicates that food-source mixing has completely obscured the relationship in the original seep source. For $\delta^{13}C$ versus $\delta^{15}N$, the correlations are as expected. There is limited positive linkage in the producer population that is increased in the resident consumers due to an unresolvable combination of trophic shifts and food-source mixing. This positive correlation remains in vagrant consumers due to trophic effects but declines as mixing reaches its endpoint, and the signal of the seep source becomes

obscured. For $\delta^{15}N$ versus $\delta^{34}S$, the correlation is low and less informative than the other two pairings. The sign of the correlation indicates that variation in sulfur is the dominant component.

The most informative combination of isotopes for food web tracing proved to be $\delta^{34}S$ and $\delta^{13}C$. The utility of this pair has three causes. First, unlike $\delta^{15}N$ these are minimally influenced by trophic shift. Second, there is a linear or nearly linear relationship between the two isotopes in chemosynthetic organisms. Third, the slope of the linear relationship is such as to minimize ambiguity. The $\delta^{34}S$ shift going from methanotroph-thiotroph-background is opposite in direction from the $\delta^{13}C$ shift. As a result, in specimens where $\delta^{13}C$ cannot distinguish food sources, $\delta^{34}S$ can, and visa versa.

**Trapped fauna results.** Trapping on- and off-site was a qualified success in spite of the logistical inability to carry out the number of deployments planned. The principal organisms collected were a spider-like crab *Rochinia crassa*, a hagfish *Eptatretus* sp., and the giant isopod *Bathynomus giganteus*. The results on a species basis are presented in Table 8.6.1. On a per-site basis, the data were plotted as vagrant species in Figures 8.6.5 through 8.6.6.

At GC233, a number of different predator species were trapped on-site. In addition to the three most common vagrants, *Bathynomus giganteus* (seven specimens), *Eptatretus* (four specimens), and *Rochinia* (three specimens), the rattail fish *Nezumia* sp. (one specimen) was captured. Direct collection by the submersible produced two additional vagrants, the eel *Synaphobranchus* sp. and a small demersal shark, as well as an additional specimen of *Eptratretus*. Eight specimens have markedly depleted $\delta^{13}C$ values indicating heavy usage of the chemoautotrophic production, while the remaining 15 reflected greatest reliance on photosynthetic food sources.

The off-site trap, deployed approximately two km from GC233, caught eleven *Bathynomus* and one *Rochinia*. The *Rochinia* was distinct, being depleted in $^{13}C$ relative to typical ocean predators and to the same species collected off-site at GC234. *Rochinia* captured on-site at GC233 were more depleted than those captured off-site at GC233. These values, as well as depleted $\delta^{34}S$, were indicative of consumer-utilizing chemosynthetically fixed sulfur. Based on the $\delta^{34}S$ values, the *Rochinia* had derived approximately 48% of its sulfur from methanotrophic material. There was no statistical difference in $\delta^{13}C$ or $\delta^{15}N$ between the *Bathynomus* caught on- and off-site at GC233; however, those caught off-site were significantly more enriched in $^{34}S$ (p = .03) relative to those on-site, indicating less reliance on seep food sources.

At GC234, two species of vagrant predators were captured in the small on-site trap– *Bathynomus giganteus* (two specimens) and *Eptatretus* sp. (11 specimens)–along with a single specimen of the predatory gastropod *Buccinum canetae*, which is likely a seep colonist rather than a vagrant (Figure 8.6.2). The on-site vagrants yielded values more reflective of heavy reliance on photosynthetically derived foods than the surrounding chemoautotrophic production. The relatively large sample size for *Eptatretus* did, however, reveal a pattern for $\delta^{13}C$ and $\delta^{34}S$ consistent with limited consumption of chemoautotrophic tissue. The range of values for captured *Eptatretus* $\delta^{13}C$, $\delta^{15}N$, and $\delta^{34}S$ was -18.3 to -16.3‰, 7.3 to 12.2‰, 12.1 to 18.5‰, respectively, with a trend toward depletion in $^{13}C$ and $\delta^{34}S$. Several of the *Eptatretus* have $\delta^{34}S$ values that were quite depleted relative to ocean sulfate (20‰) or animals utilizing ocean sulfate, 19 to 20‰ (Peterson and Howarth, 1987). A simple regression of $\delta^{13}C$ with $\delta^{34}S$ was significant (p = 0.02). The two *Bathynomus giganteus* were significantly more enriched in $^{13}C$ and $^{15}N$ (p = .05 and .03, respectively) than the *Eptatretus* and were isotopically similar to "typical" ocean fauna.

Three species of vagrant predators were caught off-site in Z-frame traps approximately 2 km from a known seep community at GC234. In addition to *Rochinia* (three specimens) and *Bathynomus* (two specimens*)*, one hake (*Urophycis*) was captured. All individuals had isotope values similar to those seen in other pelagic Gulf of Mexico predators (Roelke and Cifuentes 1997). Due to the small sample size and mismatch of species captured, statistical comparison within the off-site specimens had limited power. *Bathynomus* on-site was the more enriched in $^{13}$C and $^{15}$N than off-site, although not significantly so (p= .08). Off-site, there was no statistical difference between the $\delta^{34}$S of *Bathynomus* and *Rochinia*. As a group, the predators collected off-site in the Z-frame trap were significantly more enriched in $\delta^{34}$S compared to those caught in the small on-site trap (p = .0002). It is unlikely that these off-site vagrants consumed any appreciable amount of chemosynthetically derived food.

Samples at GC185 were limited to numerous off-site specimens of *Eptatretus*, *Rochinia*, and *Bathynomus* collected at 27°47.173' N, 91°30.032' W. The relatively large sample sizes for the three species allowed a more thorough analysis of the data. For *Eptatretus*, the mean off-site $\delta^{13}$C at GC185 was equal to that on-site at GC233 consistent with incorporation of chemosynthetic organic matter. The same extent of incorporation at both sites, however, cannot be assumed due to the site-specific differences in the isotopic signatures of the food sources. The chemosynthetic fauna at GC185 are not as depleted in $^{13}$C (or $^{15}$N) as the GC233 fauna for two reasons. First, the GC233 population of *Bathymodiolus childressi* utilizes biogenic methane ($\delta^{13}$C < 55‰), while the *Bathymodiolus childressi* population at GC185 utilizes thermogenic methane and has more $\delta^{13}$C enriched values (around -40‰). Second, there is a substantial community of *Lamellibrachia* and *Escarpia* tubeworms at GC185 that harbor thiotrophic bacteria and have $\delta^{13}$C values of approximately 21‰. Additionally, the thiotrophic bivalves *Tamu fisheri* and lucinid clams are present at GC185 and have much more depleted $\delta^{13}$C values than the tubeworms.

*Rochinia* were also depleted in $^{13}$C and $^{34}$S (to a greater extent) relative to background ocean isotopic values. Their $\delta^{13}$C and $\delta^{15}$N values overlap the range observed for the *Eptatretus* (Figure 8.6.4), but their $\delta^{34}$S values are significantly depleted relative to *Eptatretus* (p = .002). The relatively low $\delta^{34}$S (substantially lower than that of marine plankton) combined with $\delta^{13}$C values that seldom fall below -22‰ suggests that tubeworm material or organisms that feed on tubeworms contribute to the diet of the *Rochinia*. The fact that the *Rochinia* are approximately 8‰ higher in $\delta^{15}$N than tubeworms strongly suggests that they are not directly grazing upon tubeworms but are consuming tubeworm predators.
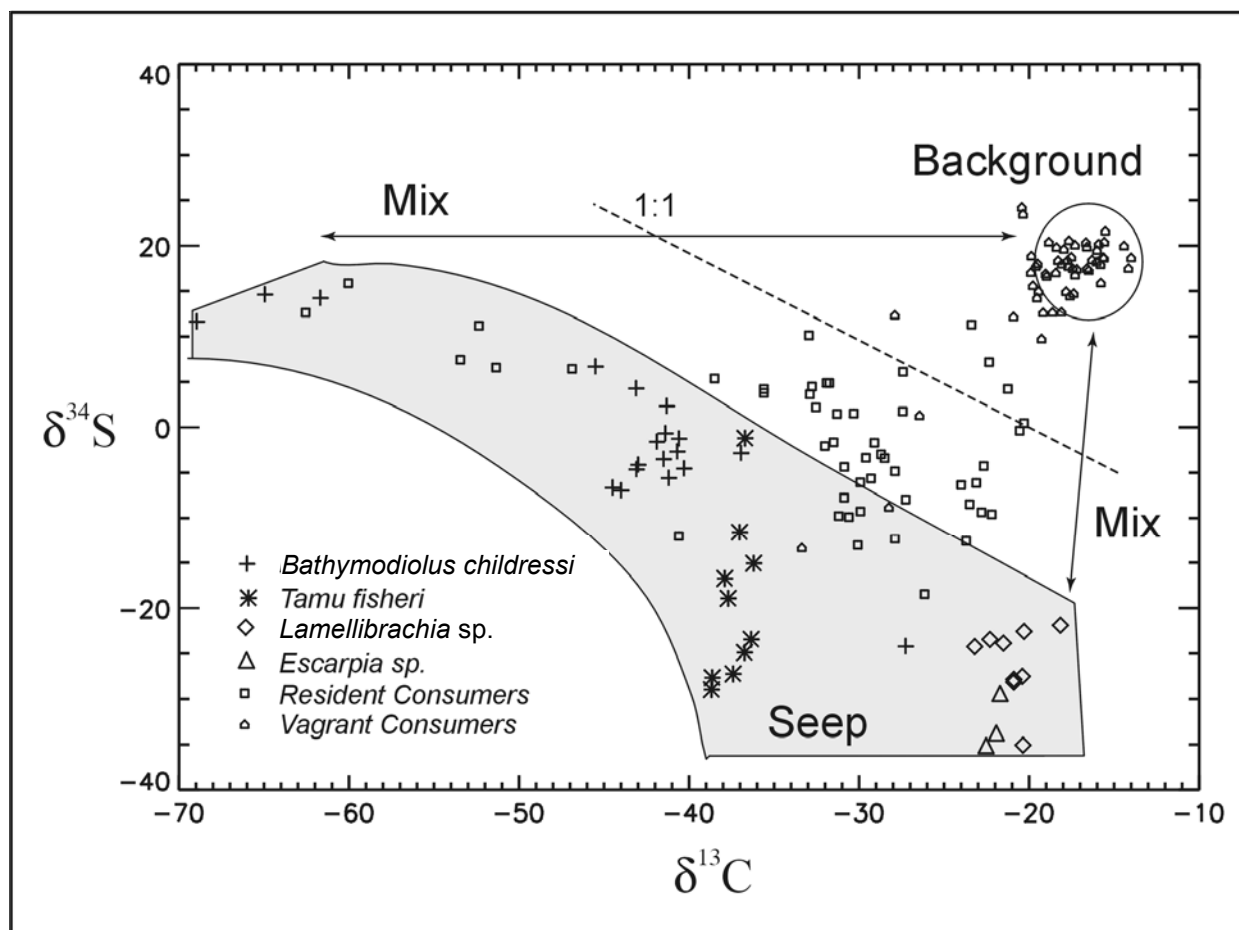
Figure 8.6.4.    Apparent utility of $\delta^{13}C$ and $\delta^{34}S$ for elimination of food source ambiguity in seep and background systems.


**Site-specific community results.**

**GC234 and GC233.** Principal sampling at GC233 consisted of mussel ring collections, trapping on- and off-site, and supplemental discretionary sampling with the submersible manipulator. Tissue from 284 specimens was frozen in 1997 and 105 additional were frozen in 1998. Isotopic determinations were made on 81 samples. Of these, 55 had both carbon and nitrogen determined, and 19 had carbon and sulfur determined (Figure 8.6.5). Within the immediate area of GC233, *Bathymodiolus childressi* is the sole producer with a very distinctive isotope signature ($\delta^{13}C$ = -63.59 ±16.58, $\delta^{15}N$ = -16.58 ±1.87, n = 11). The associated fauna is comparatively simple with only five taxa analyzed. These consumers showed the distinctive depletion of the site ($\delta^{13}C$ = -50.35 ±7.76, $\delta^{15}N$ = 8.55 ±1.79, n = 19) but were clearly shifted towards background values. Seven species of background organisms were analyzed ($\delta^{13}C$ = -20.66 ±6.25, $\delta^{15}N$ = 9.64 ±4.42, n = 24), posing a definite contrast to the producers.

Figure 8.6.5 illustrates that the data are an excellent example of the processes discernable from isotopic testing. The scatter of points suggests that both in the seep and in the background there is trophic enrichment of nitrogen producing the expected "T" line. Far more of the data variance, however, is

associated with the mixing "Mix" line caused by feeding on two endpoints. Examination of the $\delta^{13}$C and $\delta^{34}$S data produces an unexpected result in spite of the limited number of analyses. The consumers tend to be more depleted in sulfur than the *Bathymodiolus childressi*. This suggests multiple food sources at GC233.

**GC185**. Contrasted to the simplicity of the trophically open GC233, GC185 is a more complex system (Figure 8.6.6). Principal sampling at GC185 consisted of bushmaster, mussel ring collections, trapping on- and off-site, and supplemental discretionary sampling with the submersible manipulator. Tissues from 230 specimens were frozen in 1997, and 98 additional specimens were frozen in 1998. Isotopic determinations were made on 261 samples. Thirty-eight taxa were collected with substantial producer populations represented by mixed populations of thiotrophs, *Lamellibrachia*, *Escarpia*, and *Tamu fisheri*, as well as by the methanotroph, *Bathymodiolus childressi*. Resident consumers comprised twenty taxa, and vagrant consumers four taxa. Tubeworm tissue, as exemplified by *Lamellibrachia*, had $\delta^{13}$C values only slightly more depleted than background fauna but distinctively lower $\delta^{15}$N values ($\delta^{13}$C = -20.90 ±1.3, $\delta^{15}$N = 1.50 ±0.87, n = 15). The associated fauna from these worm clumps tended to be more depleted with respect to carbon and sometimes with respect to nitrogen, suggesting that the tubeworm tissue *per se* was not a food source. Rather, resident consumers at GC185 tended to fall within a lose cluster framed by tubeworms, *Bathymodiolus childressi* ($\delta^{13}$C = -38.7 ±4.38, $\delta^{15}$N = 3.78 ±2.48, n = 27) and background consumers (($\delta^{13}$C = -19.36 ± 3.95, $\delta^{15}$N = 10.8 ± 1.15, n = 32). This pattern is not especially informative and might be interpreted as reflective of many possible combinations of trophic effects and mixing of the three isotopic end-members.

 Despite the complexity contributed by the apparent trophic enrichment of nitrogen, $\delta^{13}$C and $\delta^{34}$S determinations added some clarity. Most resident consumers had values consistent with incorporation of mussel production, either *Bathymodiolus childressi* or *Tamu fisheri,* with background food sources. There was little indication of direct consumption of tubeworms alone or mixed with mussel or background.
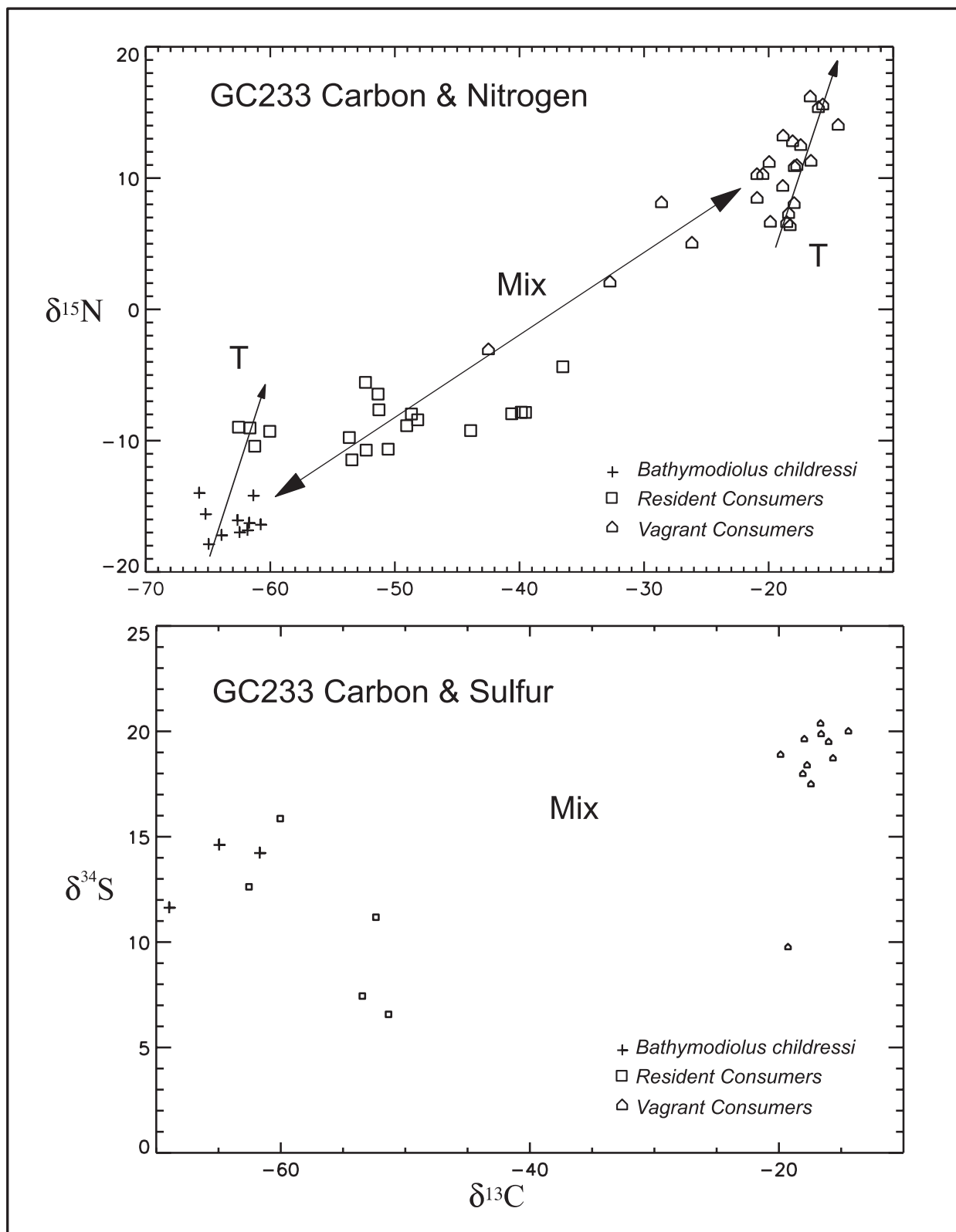
Figure 8.6.5.    GC233 $\delta^{13}C$ versus $\delta^{15}N$ and $\delta^{13}C$ versus $\delta^{34}S$ scatter plots for main faunal groups showing strong influence of mixing and minor influence of trophic shifts.
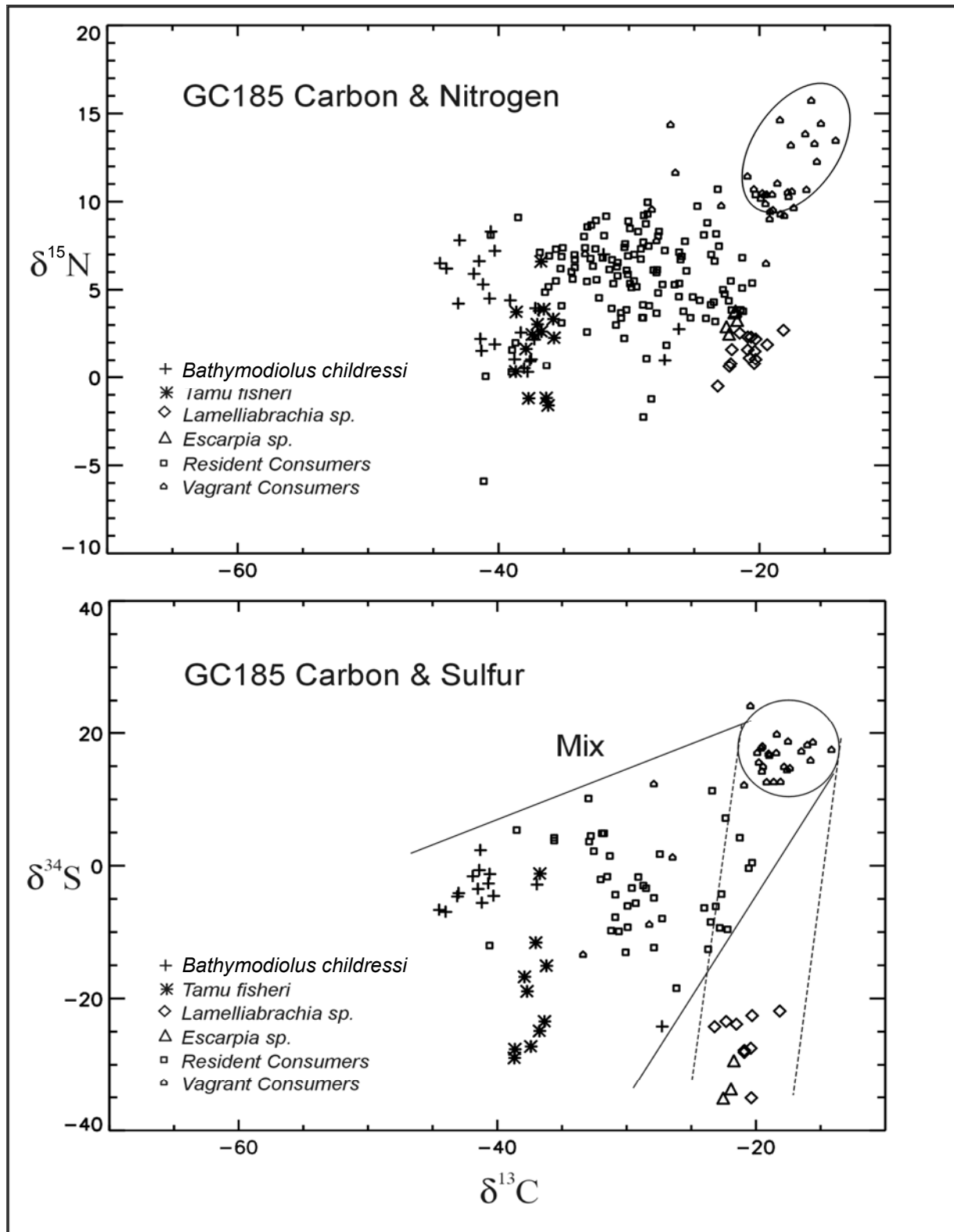
Figure 8.6.6. GC185 $\delta^{13}C$ versus $\delta^{15}N$ and $\delta^{13}C$ versus $\delta^{34}S$ scatter plots for main faunal groups showing greater indication of mixing from $\delta^{34}S$.

**GC234.** Principal sampling at GC234 consisted of bushmaster, mussel ring collections, trapping on-

and off-site, and supplemental discretionary sampling with the submersible manipulator. Tissue from 55 specimens was frozen in 1997 and 233 additional were frozen in 1998. Isotopic determinations were made on 58 samples (Figure 8.6.7). This site is similar to GC185 in that production is multi source with three species having been sampled: *Lamellibrachia*, *Escarpia* and *Bathymodiolus childressi*. Resident consumers comprised only five taxa due to limited sampling, and vagrant consumers five taxa. Tubeworm tissue, *Lamellibrachia* and *Escarpia*, combined had $\delta^{13}$C values distinctly more depleted than background fauna and distinctively lower $\delta^{15}$N values ($\delta^{13}$C = -28.89 ±4.64, $\delta^{15}$N = 3.11 ± 0.88, n = 5). The second potential food source, *Bathymodiolus childressi* ($\delta^{13}$C = -43.66 ± 1.56, $\delta^{15}$N = 3.11 ± 0.88, n = 6) formed a distinct cluster and background consumers ($\delta^{13}$C = -17.29 ± 2.37, $\delta^{15}$N = 11.32 ± 2.00, n = 16) a third. The associated fauna ($\delta^{13}$C = -31.11 ± 4.81, $\delta^{15}$N = 7.62 ± 1.85, n = 19) produced an ambiguous pattern consistent with both mixing of mussel and background sources, or exclusive use of tubeworms followed by trophic shifts. Analysis of sulfur was too limited to improve upon the interpretation.

**Immunoassay results.** A modest trial program was initiated to determine the utility of immunoassay to confirm sub-lethal predation (cropping) by seep heterotrophic consumers. This effort did not conform to the overall sampling design but assumed that given species had the same trophic role at all sites. Intended prey species included *Beggiatoa*, *Escarpia*, and *Bathymodiolus*. Intended predators included ten each of the dominant seep associates. The complete results of the immunoassay component are presented in the appendix volume. The material presented here is intended as a summary (Table 8.6.5).

The effort was generally successful with only minor departures from the original proposal. Antisera were successfully developed and tests for specificity were run against a variety of marine invertebrates. Antisera for tubeworms were usable but showed lower specificity. Analyses were run on stomach contents for 54 specimens. With respect to prey, antisera for *Beggiatoa* were not made, while 13 taxa were analyzed rather than four with a total of 54 specimens being suitable for assay.

All taxa assayed had indications of having eaten *Escarpia* and/or *Bathymodiolus*. There appears to be no feeding specialization in the taxa examined. On a specimen level, 26 animals had neither in the gut (using a low sensitivity test) indicating an alternate diet. Most of these 26 were hagfish or crustaceans. *Buccina* contributed the majority of 13 specimens that showed evidence of both *Escarpia* and *Bathymodiolus* in the stomach contents.
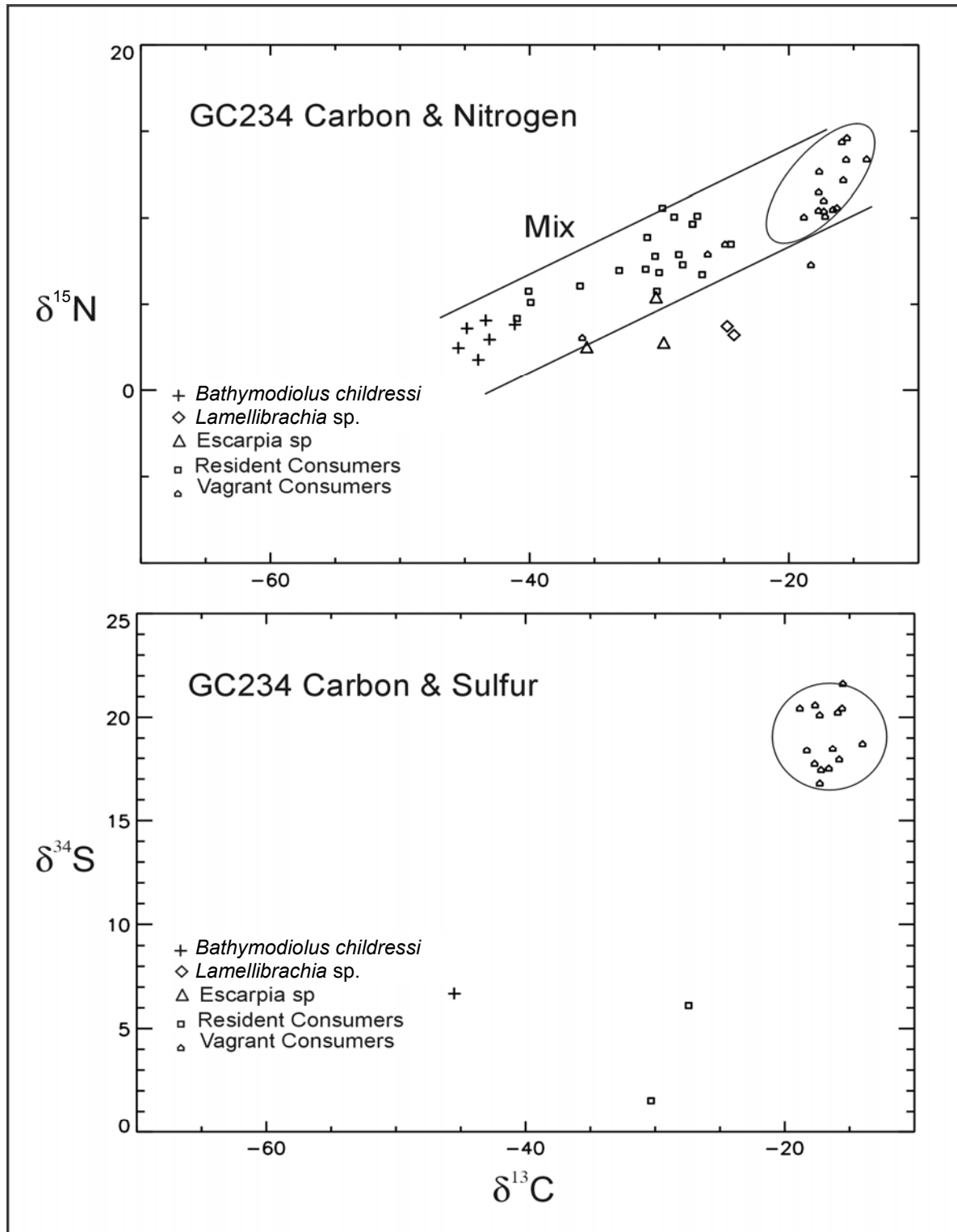
Figure 8.6.7.    GC234 $\delta^{13}C$ versus $\delta^{15}N$ and $\delta^{13}C$ versus $\delta^{34}S$ scatter plots for main faunal groups showing indication of mixing but with insufficient $\delta^{34}S$ determinations for more definitive statements.

Table 8.6.5. Summary of immunoassays.

| Species Assayed | n | Tubeworm Feeding Responses to Test Sensitivity | | Mussel Feeding Responses to Test Sensitivity | |
|---|---|---|---|---|---|
| | | Low | High | Low | High |
| *Eptatretus* sp. | 11 | 2 | 3 | 2 | 9 |
| *Bathynomus* | 7 | 0 | 6 | 1 | 7 |
| *Munidopsis I* | 7 | 3 | 4 | 3 | 3 |
| *Buccina* | 5 | 4 | 3 | 5 | 5 |
| *Alvinocaris* | 5 | 2 | 2 | 4 | 3 |
| *Atelecylida* | 4 | 1 | 2 | 1 | 2 |
| *Bathyneritia* | 4 | 0 | 1 | 4 | 3 |
| *Synaphobranchus* | 2 | 1 | 0 | 2 | 1 |
| *Munidopsis II* | 3 | 0 | 3 | 0 | 2 |
| Nereid worms | 2 | 1 | 0 | 2 | 0 |
| *Rochinia* | 1 | 1 | 1 | 1 | 1 |
| *Chaceon* | 2 | 0 | 0 | 0 | 1 |

## 8.6.6 Discussion

**Seep residents–evidence of a two-way open system.** Since seeps are known to have very high biomass and are assumed to have very high productivity, it is easy to assume that they would be exploited by the food-limited background species. Indeed, the more relevant question is not whether the background exploits seeps, but why so few background species are apparently active in this exploitation. As found in this study, this exploitation with transfer into the background is indicated by a faint but distinct seep isotope signature in trap-collected scavengers and predators. A far more unexpected result was the finding of seep-associated consumers such as the galatheid crabs and nerite gastropods with signatures of a diet-mixing seep and background production. At the site, GC233, where the determinations were most distinctive, some seep endemics may have consumed as much as 50% of their assimilated diet from the background.

The presence of an apparent isotope signature for a mixed seep-background diet in animals thought to be intimately associated with seeps has other explanations that cannot be refuted from the data at hand.

1. Wide foraging–The intimacy of the seep association may be more apparent than real, with significant foraging into the background an event so far unobserved during submersible dives. In effect, seep consumers may range and forage widely.

2. Bacterial mimics–Seep detritus may contain bacteria that produce a biomass that exactly mimics the mixed diet signal.

3. Mixed detrital pool–Seep detritus may be the location of the diet mixing containing both seep production and organic detritus from the background.

**Conflicting evidence of direct predation.** The full immunoassay component is presented in the appendix volume. The discussion here is limited to apparent conflicts concerning the extent to which tubeworms serve as prey to resident and vagrant consumers. Isotopic tracing indicates that tubeworm-associated fauna can have an apparent thiotrophic $^{13}$C and $^{34}$S signature but is not consistent with consumption of tubeworm tissue *per se*. Immunoassay indicates the contrary, with gut contents commonly testing positive for tubeworm tissue. The difference in results cannot be resolved from the data on hand but could be due to three factors.

1. It simply reflects the actual feeding history of the individual organisms sampled. Some had recently eaten tubeworms while others had not. The sample size was too small to establish the general pattern.

2. It reflects a difference between ingestion and assimilation with the worm tissue in the gut not being assimilated.

3. The test for tubeworm tissue in the gut gave false positives due to cross-reactions with polychaete tissue noted in the cross-reaction study.

### 8.6.7 Conclusion – scientific questions and regulatory consequences

Seep systems interact with the background, posing two questions.

**Scientific.** What role does predation by background species play in determining the establishment, species composition, persistence, and ultimate stability of seep systems?

1. Disruption background predators exert a predatory pressure on (a) the browsing, (b) resident predator population, and (c) substrate producing organisms. Similar predation is generally accepted as an important factor in biodiversity preservation in other systems and may play a similar role in the seep systems. Alteration of this predation due to environmental impacts in the background may have a detrimental effect upon seep systems as a whole.

2. Disruption of seep predation on background will eliminate a food source that may be critical to sustaining the full biodiversity of seep communities during times of reduced chemosynthetic production.

3. Contamination of background detritus that is then transported and mingles with the seep detritus pool may result in food-web amplification and toxic effects upon seep fauna.

**Regulatory.** What should the appropriate scales and nature of restrictions on development be to protect both local seeps and the larger area of the bottom with which they interact? Present regulations of offshore oil and gas consider environmental impact within a region one kilometer in diameter a likely consequence of development but acceptable when weighed against the vastness of the soft-bottom benthic environment. Present regulations governing protection of seep communities view seep communities as isolated systems threatened only by local physical disruption.

**8.7 Mussel and Vestimentiferan Population Ecology**[*]

**8.7.1. Objectives**

Molecular genetic methods provide a powerful tool with which to infer the evolutionary history of populations. Each of the major evolutionary forces—mutation, recombination, natural selection, and migration—leaves a characteristic signature on the genomic DNA carried by an organism. The evolutionary history of individuals within and between populations as well as relationships among species can be inferred with molecular genetic methods. The chemosynthetic communities that live at the cold seeps of the Gulf of Mexico provide a unique opportunity to examine the role that dispersal plays in the evolution of the dominant hydrocarbon seep organisms.

The vestimentiferan tubeworms and mussels, in association with their endosymbiotic bacteria, are the main ecosystem structuring organisms at the cold seeps (Fisher *et al.* 1997). The tubeworms are sessile organisms that lack a mouth, gut, and anus, but thrive at the cold seeps through their association with endosymbiotic bacteria that live a specialized tissue known as the trophosome. Two aspects of the vestimentiferan life history are not clearly understood and can be clarified with molecular genetic approaches. First, how are endosymbionts acquired each generation? Male and female tubeworms issue their gametes into the water column where fertilization takes place. Whether the endosymbionts are transmitted with the egg or acquired later in development is not known. Efforts to detect endosymbionts in the egg have failed to find evidence for vertical transmission of the bacteria (Cary *et al.* 1993), yet newly settled juveniles always have endosymbionts. Thus, it appears that the endosymbionts are acquired each generation. Second, the distance that larvae can travel to colonize new seep habitats has profound implications for the long-term stability of these communities. Limited dispersal ability of seep fauna would suggest that the chemosynthetic communities are fragile where biodiversity is at risk. Genetic variation is the raw material of the evolutionary process that allows populations to change in response to environmental flux. Destruction of seep habitats, in this model, causes a profound loss of genetic diversity and may lead to an uncertain future for these fragile communities. Extensive dispersal ability of vestimentiferans and mussels would indicate that chemosynthetic communities are genetically robust to disturbance. This model of genetic exchange suggests that loss of a single community may be overcome through recolonization of seep sites from other localities within the Gulf of Mexico. Under this scenario, the main limitation to the survival of global chemosynthetic communities is the availability of suitable habitat for new communities to be established.

In this study, appropriate types of DNA variation were used to investigate the following:

1) the migratory history of three seep species found in chemosynthetic communities, two vestimentiferan tubeworms (*Escarpia* sp. and *Lamellibrachia* sp.) and one mussel (*Bathymodiolus childressi*);

2) the phylogenetic history of tubeworms from cold seeps and hydrothermal vents;

3) the phylogenetic history of tubeworm endosymbionts. These data are used to address the robustness of the chemosynthetic communities to disturbance.

---

[*] This section was authored by Steve Schaeffer.

## 8.7.2. Materials and laboratory methods

**Mussel and tubeworm samples.** Tubeworms and mussels were collected from four hydrocarbon seeps during the summer of 1997 (see Tables 8.7.1-8.7.3). For each species, individuals were sampled from each of four populations to examine short, intermediate, and long range movement of larvae among seep communities. Gene flow among local aggregations of tubeworms and mussels within GC185 were used to estimate short distance dispersal where sampled localities were separated by less than one kilometer. Gene flow among the three Green Canyon populations were used to estimate intermediate distance dispersal where sampled sites were separated by 4 to 25 kilometers. Finally, gene flow between GB425 and the Green Canyon populations was used to estimate long distance dispersal where sampled localities were separated by over 100 kilometers.

Table 8.7.1. Samples of *Escarpia spicata* collected from four localities in the Gulf of Mexico.

| Sampling Site | Latitude, Longitude | Depth (m) | Station ID | Individuals Sampled |
|---|---|---|---|---|
| GC185 {Bush Hill (BH)} | 27°46.9' N, 91°30.4' W | 550-580 | JT1 | 10 |
| | | | JT2 | 10 |
| | | | JT5 | 10 |
| | | | AT1 | 10 |
| | | | AT5 | 10 |
| | | | TT6 | 10 |
| GC233 {Brine Pool (BP)} | 27°43.4' N, 91°16.8' W | 525-560 | AT1 | 10 |
| GC234 {Green Canyon (GC)} | 27°44.1' N, 91°15.3' W | 640 | NM1 | 10 |
| GB425 {Garden Banks (GB)} | 27°33.2' N, 92°32.4' W | 600 | | 10 |

Table 8.7.2. Samples of *Lamellibrachia* sp. collected from four localities in the Gulf of Mexico.

| Sampling Site | Latitude, Longitude | Depth (m) | Station ID | Individuals Sampled |
|---|---|---|---|---|
| GC185 {Bush Hill (BH)} | 27°46.9' N, 91°30.4' W | 550-580 | JT1 | 10 |
| | | | JT2 | 10 |
| | | | JT5 | 10 |
| | | | AT1 | 10 |
| | | | AT5 | 10 |
| | | | TT6 | 10 |
| GC233 {Brine Pool (BP)} | 27°43.4' N, 91°16.8' W | 525-560 | AT1 | 10 |
| | | | | 10 |
| GC234 {Green Canyon (GC)} | 27°44.1' N, 91°15.3' W | 640 | NM1 | 10 |
| | | | | 10 |
| GB425 {Garden Banks (GB)} | 27°33.2' N, 92°32.4' W | 600 | | 10 |

Table 8.7.3. Samples of *Bathymodiolus childressi* collected from four localities in the Gulf of Mexico.

| Sampling Site | Latitude, Longitude | Depth (m) | Station ID | Individuals Sampled |
|---|---|---|---|---|
| GC185 {Bush Hill (BH)} | 27°46.9' N, 91°30.4' W | 550-580 | M1 | 10 |
| | | | M2 | 10 |
| | | | M3 | 10 |
| | | | M4 | 10 |
| | | | M5 | 10 |
| | | | M6 | 10 |
| GC233 {Brine Pool (BP)} | 27°43.4' N, 91°16.8' W | 525-560 | M1 | 10 |
| | | | M2 | 10 |
| GC234 {Green Canyon (GC)} | 27°44.1' N, 91°15.3' W | 640 | M1 | 10 |
| | | | M2 | 10 |
| GB425 {Garden Banks (GB)} | 27°33.2' N, 92°32.4' W | 600 | M1 | 10 |
| | | | M2 | 17 |

**Microsatellite isolation and statistical analysis.** The study of dispersal and gene flow in tubeworms and mussels utilizes highly variable genetic loci that are likely to be different among individuals. The rationale for choosing these loci was that genetic markers that can change each generation are likely to give an accurate reflection of how much gene flow occurs on intermediate time scales. For this work, microsatellite loci, which are di-, tri-, and tetranucleotide sequences that change rapidly among individuals of the same species, were used to estimate levels of gene flow among four seep populations (from samples at sites GB425, GC185, GC233, and GC234).

Microsatellite loci were cloned with standard genetic engineering methods (Armour *et al.* 1994; Sambrook *et al.* 1989). Genomic DNA was purified with standard methods (Ausubel *et al.* 1989). The genomic DNA was partially digested with the restriction enzyme *Sau*3A and size separated on a 2% agarose gel. Digested DNA were size selected for fragments between 200 and 800 base pairs. These fragments were cloned either into the Blue Script (Stratagene) cloning vector directly or were subject to a procedure that enriched the sequences for microsatellite repeats and then cloned them into the Blue Script vector (Armour *et al.* 1994). The plasmid vector was moved into the bacterial host *Escherichia coli* via the process of transformation to create a genomic library for the species. The genomic library was screened nonisotopically with probes that contained di-, tri-, and tetranucleotide repeats. Nucleotide sequences of clones that hybridized strongly to the microsatellite repeat probes were determined with polymerase chain reaction (PCR) mediated sequencing (Saiki *et al.* 1988). Clones that contained a valid microsatellite whose position was near the middle of the recombinant DNA insert were used to design PCR primers that could be used to test organisms from the sample collections for repeat polymorphisms. Microsatellites that were shown to be identical among all individuals tested in the tubeworms or mussels were not investigated further. Polymorphic microsatellite loci were used to screen all individuals collected from the four populations.

The frequencies of each microsatellite allele within each locus were estimated with standard population genetic methods (Nei 1987). The microsatellite allele frequencies were used to estimate $F_{st}$, the probability that two alleles from two subpopulations will be identical by descent (Nei 1987). The neutral migration parameter, $4N_em$, is estimated directly from $F_{st}$ (Slatkin 1985), where $N_e$ is the

effective population size and *m* is the migration rate. This value is interpreted as the number of migrants exchanged between populations per generation (Wright 1931, 1943).

**Nucleotide sequencing of a new escarpid species.** The morphological identification of tubeworms from bushmaster collections of entire vestimentiferan communities revealed a new species of *Escarpia*. To clarify the relationship of this new vestimentiferan species, the cytochrome oxidase I (COI) gene from the mitochondrial DNA molecule was used to establish what affinity this escarpid-like species showed toward previously identified species of tubeworms from the Gulf of Mexico and the Pacific Ocean. Genomic DNA was prepared with standard procedures (Ausubel *et al.* 1989). The COI was amplified from the new escarpid species with the polymerase chain reaction (Saiki *et al.* 1988) using the vestimentiferan specific COI gene primers (Black *et al.* 1997). The COI gene was sequenced on an ABI 373 and a Beckman CEQ2000 automated sequencers. The gene was sequenced on both DNA strands and the complete sequence was assembled with the SEQMAN II program with the LASERGENE package of DNA analysis software (DNAStar, Inc.). The sequences were aligned with the MEGALIGN program within the LASERGENE package using Clustal V (Higgins *et al.* 1992). The nucleotide sequence alignments were adjusted manually to allow for the placement of insertions and deletions in the alignment.

Molecular evolutionary relationships among sequences were examined by the neighbor-joining method of tree construction (Saitou and Nei 1987), based on pairwise genetic distances estimated from the proportion of differences and corrected for multiple substitutions by the Jukes and Cantor formula (Jukes and Cantor 1969). The significance of the branching order was evaluated by bootstrap analysis of 1000 computer-generated trees. All analyses were performed with MEGA (Kumar *et al.* 1994).

An *Alu*I restriction endonuclease assay of the COI gene was designed to discriminate between the "spiked" morph of *Escarpia* and the "normal" Gulf of Mexico *Escarpia*. The COI gene of each species had three DNA fragments when digested with *Alu*I, but DNA fragments in the "spiked" morph were shorter than the "normal" morph of *Escarpia*. This analysis was performed on all tubeworms collected during the 1997 field season to insure that the genomic libraries used to isolate microsatellites came from the dominant *Escarpia* species and to insure that collected tubeworms used in the gene flow study were identified correctly.

**Nucleotide sequencing to determine host-endosymbiont relationships.** Vestimentiferan tubeworms were collected by manned submersibles DSV ALVIN and the Johnson SEA-LINK II from the following deep-sea hydrothermal vent and cold seep sites:

1) Middle Valley, Northeast Pacific (NEP), 2420 m, *Lamellibrachia barhami*, n = 1; *Ridgeia piscesae*, n = 1;

2) Gorda Ridge, NEP, 2720 m, *Ridgeia piscesae*, n = 1;

3) 90N, East Pacific Rise (EPR), 2500 m, *Oasisia alvinae*, n = 1; *Riftia pachyptila*, n = 2; *Tevnia jerichonana*, n = 2.;

4) Alaminos Canyon, Gulf of Mexico, 2020 m, *Escarpia laminata*, n = 2; *Lamellibrachia sp*. nov. 1., n = 1;

5) GC185, Gulf of Mexico, 545 m, "escarpid-like", n = 1; *Lamellibrachia sp*. nov. 2., n = 1; and Green

Canyon 234, Gulf of Mexico, 540 m, "escarpid-like", n = 1; *Lamellibrachia sp*. nov. 2., n = 1 (GC185 and Green Canyon 234 are separated by approximately 10 km.);

6) Florida Escarpment, Gulf of Mexico, 3700 m, *Escarpia laminata*, n = 2.

Total nucleic acids were extracted from the symbiont-containing trophosome tissue by previously described methods (Nelson and Selander 1994). Most of the bacterial small subunit ribosomal gene (SSU rDNA) was amplified by PCR with primers (fD1 and rP1) that are highly conserved among eubacteria (Weisburg *et al.* 1991). The sequence of the 3' end of the SSU rDNA was obtained by amplification with primers (1406f and 242r) located in the 3' end of the SSU rDNA and the 5' end of the large subunit rDNA, respectively (Lane 1991).

Nearly complete SSU rDNA sequences (exclusive of the 5' primer site) were obtained by Taq cycle-sequencing, and the resulting products were analyzed on an ABI 373 automated sequencer. Internal primers for Taq cycle sequencing were selected from a list of conserved eubacterial primers (Lane 1991). For each symbiont, 1515-1516 base pairs (bp) of the SSU rDNA gene were completely sequenced with multiple overlapping sequences on both strands, with the exception of the approximately 30 bp near the 5' most primer, which was single-stranded. Individual sequencing runs were assembled and edited by the use of SEQMAN and SEQMANED (DNASTAR, Inc.). Final symbiont sequences were aligned and compared with the Eyeball Sequence Editor (Cabot and Beckenbach 1989).

To establish host relationships for five of the tube worm taxa, a portion of the mitochondrial cytochrome oxidase I gene (COI) was sequenced and compared with published data for other vestimentiferans (Black *et al.* 1997; Kojima *et al.* 1997). For these studies, total nucleic acids were extracted from vestimentum tissue. The COI gene was amplified by PCR with primers designed from conserved sequences of other invertebrates:

> COIf: TC(CA)ACTAATCA(CT)AA(GA)GA(CT)ATTGG(ATGC)AC, and     (8.7-1)
> COIr: CC(ATG)CTTAG(TA)CCTA(GA)(GA)AA(GA)TGTTG(ATCG)GG.

These primers amplified an approximately 1250-bp segment, and from this segment 350 bp were sequenced as described above. Sequences were obtained from the following individuals and localities:

1) *Lamellibrachia barhami*, Middle Valley, site 1;

2) *Escarpia laminata*, Alaminos Canyon, site 4;

3) "escarpid-like", GC185, site 5;

4) *Lamellibrachia* sp. nov. 2., GC185, site 5;

5) *Escarpia laminata*, Florida Escarpment, site 6.

Molecular evolutionary relationships among sequences were examined by the neighbor-joining method of tree construction (Saitou and Nei 1987), based on pairwise genetic distances estimated from the proportion of differences and corrected for multiple substitutions by the Jukes and Cantor formula

(Jukes and Cantor 1969). The significance of the branching order was evaluated by bootstrap analysis of 1000 computer-generated trees. All analyses were performed with MEGA (Kumar *et al.* 1994).

To determine the branching pattern of the deep phylogenetic relationships, we utilized four-cluster analysis (Rzhetsky *et al.* 1995). This method may be used to infer the relationships among groups of species, of which each group may contain many species.

### 8.7.3 Results

**Overview of the microsatellite work.** The proposed use of DNA microsatellites for this project was based on the use of these hypervariable loci in model organisms, where they were used for DNA forensics, for population genetic studies, and for human disease gene localization (Rubinsztein *et al.* 1995). Three unexpected observations in the collections of tubeworms and mussels initially impeded progress in isolating microsatellite loci. First, early in the second year, the histopathology study of mussels from GC185 (Section 8.5) revealed a high infection rate with metazoa parasites. DNA isolation procedures from these parasite-infested mussels do not discriminate between the DNAs of the two organisms. The organismal origin of any microsatellites isolated from the GC185 mussels could be from either mussel or parasite. Therefore, the mussel microsatellite project had to start anew using *B. childressi* from the GC233 Brine Pool site where parasites had not been detected. Second, the discovery of a second *Escarpia* morph in year two set back the microsatellite project because it was unclear how many individuals of each species had been collected. A molecular biological identification procedure was developed to screen all sampled tubeworms in our collections before the microsatellite isolation project could continue. Finally, the screens of microsatellites in the studies of tubeworms and mussels suggest that while these species do have microsatellites, the number of polymorphic loci may be quite small as has been observed in a variety of species (Rubinsztein *et al.* 1999; Samadi *et al.* 1999).

**Vestimentiferan tubeworms microsatellites.** The screen for microsatellites in *Lamellibrachia* sp. yielded 104 positive clones that hybridized strongly to the repetitive DNA probes out of ~1,000 total clones that were screened. Of the 104 positive clones, 45 clones had an insert size greater than 200 base pairs, the minimum size capable of containing a viable insert for microsatellite primer design. Of the 45 clones that were sequenced, nine microsatellite clones could be used to design PCR primers for screening *Lamellibrachia* populations. Two of these nine microsatellite loci, 1-2B and JW7, were polymorphic and could be used for studies of gene flow (Table 8.7.4).

A second screen of this species has been conducted on a DNA library that was not pre-enriched for microsatellite sequences. This second screen has generated 70 positive clones out of roughly 500, 20 of which have been sequenced. Five of these 20 clones contained microsatellites and one PCR primer have been designed to test for levels of variability. The JW7 microsatellite locus shows that 2.0 *Lamellibrachia* larvae are estimated to be exchanged among the three Green Canyon populations each generation (Table 8.7.5). A total of 3.6 *Lamellibrachia* larvae are estimated to be exchanged between GB425 and the three Green Canyon populations each generation (Table 8.7.5). The 1-2E microsatellite locus is currently being run on all of the *Lamellibrachia* sp. samples.

Table 8.7.4. PCR primers for nine microsatellite loci in *Lamellibrachia* sp. from the Gulf of Mexico.

| Name | Size (bp) | PCR Primers | Variability | Temp (°C) | Repeat |
|---|---|---|---|---|---|
| A10 | 75 | f 5' CAA TTA CGA GTC AGT GTG AG 3' | N | 65 | $(GA)_{12}$ |
| | | r 5' CGC AAT GAT GGT GAA TGT C 3' | | | |
| JW1 | 130 | f 5' CGC TAG CCA CGA CTA CCG AT 3' | N | 51 | $(GGA)_6$ |
| | | r 5' ACG CGG GAG CGA ATA CGA GT 3' | | | |
| JW8 | 320 | f 5' GGC AAT TGT TGA GGA CGT GT 3' | N | 51 | $(GAC)_{20}+(CA)_{30}$ |
| | | r 5' GGA AGT GAA CCA ATG CTC TG 3' | | | |
| JW3 | 160 | f 5' CAT CAC CAA GAC CAA AGC AG 3' | N | 55 | $(GGA)_5$ |
| | | r 5' ATA GTG AGC CAG TCT CGA TG 3' | | | |
| JW4 | 250 | f 5' CGC TTT ACT CAT CCA CAG TT 3' | N | 55 | $(CCAGA)_6$ |
| | | r 5' GCT GGC ACT GAC GTA ATC AA 3' | | | |
| JW5 | 50 | f 5' CTC GAC GAA GCC CTC AAA GA 3' | N | 57 | $(GGA)_9$ |
| | | r 5' CTT CAC TCA TCA TCG CTT TC 3' | | | |
| L3.7B | 270 | f 5' CAG CAG AAT GAG GTG TGG AT 3' | N | 55 | $(CCT)_{48}$ |
| | | r 5' CCT ACG TGG AAG ATG GTT GA 3' | | | |
| JW2 | 160 | f 5' GAT GGT AAT GAA ATG TCT GC 3' | P | 51 | $(CT)_{20}$ |
| | | r 5' ATG ACA GTA CCC AAT TAC GA 3' | | | |
| JW7 | 300 | f 5' GCA GAG CAT TGG TTC ACT TC 3' | P | 53 | $(CACG)_{13}$ |
| | | r 5' GAA TCG TGC AAC TGG TTG AC 3' | | | |
| 1-2E | 250 | f 5' TGT TGA GGA CGT GTT ACA AG 3' | P | | $(CACG)_{15}$ |
| | | r 5' ACG TGC ATG TGT TTA CTA GC 3' | | | |

f, forward PCR primer; r, reverse PCR primer; N, PCR primers could not be developed for the microsatellite locus; P, microsatellite locus was polymorphic; Temp, annealing temperature for the PCR reactions; and Repeat, length of the original microsatellite clone.

Table 8.7.5.  Estimates of the number of migrants
exchanged between four populations of
*Lamellibrachia* sp.

|       | GC185 | GC233 | GC234 |
|-------|-------|-------|-------|
| GB425 | 2.06  | 2.43  | 2.33  |
| GC185 |       | 1.55  | 6.79  |
| GC233 |       |       | 1.63  |

Two screens have been conducted for microsatellite DNA in *Escarpia* sp.  The first screen was of a library constructed using repeat-enriched DNA and it generated 75 positive clones out of roughly 150. Of the 75 positive clones, 56 had inserts larger than 150 base pairs, and were sequenced.  Of the 56 clones that were sequenced, only 17 were suitable for PCR primer design.  Four of these primers successfully amplified the target microsatellite sequence.  Two of the four were invariant and were not useful for estimating levels of gene flow among *Escarpia* populations.  Three primers, 4-10d, 3-2d, and 2-2A, were polymorphic and were used in a population screen on this species.  A second screen of this species has been conducted on a DNA library that was not pre-enriched for microsatellite sequences. This second screen has generated 110 positive clones out of roughly 1000, 45 of which have been sequenced.  Eighteen of these 45 clones contained microsatellites and four PCR primers have been designed to test for levels of variability.  Table 8.7.6 shows the primers designed for the microsatellite loci found in our genomic library screens of *Escarpia* sp.

Table 8.7.6. PCR primers for 25 microsatellite loci in *Escarpia* sp. from the Gulf of Mexico.

| Name | Size (bp) | PCR primers | Var | Temp (°C) | Repeat |
|------|-----------|-------------|-----|-----------|--------|
| 4-8H | 200 | f 5' CAA TAT TTG ACA GCT CGG AC 3'<br>r 5' CTG TAC GCA TCA TGT TTG AC 3' | N | | $(GT)_{30}$ |
| 1-4d | 77 | f 5' GAT CCT GCC ATG CAA ACG TG 3'<br>r 5' CCA TAA CTG ACT AAC GTC TC 3' | N | | $(GT)_{10}$ |
| 1-5d | 180 | f 5' GTA AAC ATT GTC TAT ACA G 3'<br>r 5' CCT ATT GGA TCA ATA TTT AC 3' | N | | $(GT)_{20}$ |
| 3-2e | 220 | f 5' GAT CTA CCG TAC CTA TAA TG 3'<br>r 5' GAT CAA GGT AAA CGT GGA TG 3' | N | | $(GT)_{50}$? |
| 3-1a | 190 | f 5' GAT CGG CAC AAT AAT GTA AGA G 3'<br>r 5' TAG TGG ATC ACG CGC GCA AGT A 3' | N | | $(GT)_{40}$ |
| 1-2g | 180 | f 5' GCG TGC GTG CGT AAG TGA GT 3'<br>r 5' GGA TCA CAA CAC GCC TGG GT 3' | N | | $(CGTG)_8$ |
| 1-2g#2 | 180 | f 5' TCG CTG CGT AAG TGA GTG TA 3'<br>r 5' CAC AAC ACG CCC TGG TAT CAC AAC | N | | $(CGTG)_8$ |
| 1-3b | 150 | f 5' CAT TAT GTG TGA GTG CGT CC 3'<br>r 5' CTG TAA GAA GAC ACC CAA CC 3' | N | | $(GT)_{40}$ |
| 1-3b#2 | 150 | f 5' CAT TAT GTG TGA GTG CGT CC 3'<br>r 5' CTA TCT GTA AGA AGA CAC CCA ACC | N | | $(GT)_{40}$ |
| 1-3g | 300 | f 5' TCC GGT GTA CTA TGA GGT CG 3'<br>r 5' TAG TGG ATC ACA CAC GCA CG 3' | N | | $(GT)_{80}$? |
| 3-5f | 225 | f 5' GGA TCA GCA GCA CAG TCT TA 3'<br>r 5' TCA CCA TAC GCA CGT ATG AA 3' | N | | $(GT)_{50}$? |
| 3-1h | 150 | f 5' CTC AGT GTG ACA GGT ATG TG 3'<br>r 5' GGA TCA TGA CTG TAG GAG TG 3' | N | | $(GT)_{26}$ |
| 3-5h | 120 | f 5' TGG TAT TAG CAT TTG TCC CA 3'<br>r 5' TCC ATA ACT GAC CAA CGT CT 3' | N | | $(GT)_{15}$ |
| 3-6b | 170 | f 5' GGA TCT TGG CAC AAA TGT CT 3'<br>r 5' GGA TCA CAT CAC ATA CAC AC 3' | N | | $(GT)_{45}$ |
| 1-2H#2 | 209 | f 5' ACA TAC ATG ACC GAC TAA CG 3'<br>r 5' ATC AGG GT TGA ACG AGA TA 3' | N | | $(GT)_{35}$ |
| 4-10E | 200 | f 5' TCT TAA ATA TGC GAC TGC CT 3'<br>r 5' TCA ACC ATG AGT GAT GTG TA 3' | N | | $(GT)_{22}$ |
| 3-3h | 120 | f 5' TGG TAT TAG CAT TTG TCC CA 3'<br>r 5' TCC ATA ACT GAC CAA CGT CT 3' | M | | $(GT)_{18}$ |
| 1-2H | 185 | f 5' GAC TAA CGT CTC TGT ACC GA 3'<br>r 5' GGT TGA ACG AGA TAG GTT GC 3' | M | | $(GT)_{35}$ |

Table 8.7.6. Continued.

| | | | | |
|---|---|---|---|---|
| 3-2D | 150 | f 5' GAT CTC TTC TGG CAG GCG TT 3'<br>r 5' CTC CAT TGC ATC TAC GGG TC 3' | P | $(CGTG)_{10}$ |
| 4-10D | 200 | f 5' GGA CAA GGA TGA GAG CAA CA 3'<br>r 5' TCG CTC CAC TAC TCA CAC AA 3' | P | $(GT)_{26}$ |
| E2-2A | 150 | f 5' CAG TGT CAT ACA GCG GGC TT 3'<br>r 5' ATC CGC CTC TGC CTA CGT TT 3' | P | (GCGG)9 |
| 2-7E | 550 | f 5' GAT AAA CTG CAA GCC TCA GAG<br>r 5' GGT AAG AGT GGT TTC ATT CG 3' | P | (CA)40 |
| 2-9E | 400 | f 5' CAC AAC TGC TGT TAT TGG AA 3'<br>r 5' ACA GAG TGC GTG CAT ATG TG 3' | M | (CACG)5 |
| 2-9H | 450 | f 5' GTA TTA GCT CGT GAA CGC CA 3'<br>R 5' GGT CTA TAG TTA TCG GAC TG 3' | N | (TATT)5,(TAA |

f, forward PCR primer; r, reverse PCR primer; N, PCR primers could not be developed for the microsatellite locus; M, microsatellite locus was monomorphic; P, microsatellite locus was polymorphic; Temp, annealing temperature for the PCR reactions; and Repeat, length of the original microsatellite clone.

Figures 8.7.1 and 8.7.2 show the allele frequencies of the two variable microsatellite loci (4-10D and 3-2D) in *Escarpia* sp. collected from four hydrocarbon seeps. The allele frequencies of these three microsatellites are currently being collected for the stations within GC185. A total of 11.3 *Escarpia* larvae are estimated to be exchanged among the three Green Canyon populations each generation (Table 8.7.7). A total of 1.4 *Escarpia* larvae are estimated to be exchanged between GB425 and the three Green Canyon populations each generation (Table 8.7.7).

Table 8.7.7. Estimates of the number of migrants
exchanged between four populations of *Escarpia* sp.

| | GC185 | GC233 | GC234 |
|---|---|---|---|
| GB425 | 2.0 | 1.8 | 0.5 |
| GC185 | | 12.7 | 1.0 |
| GC233 | | | 21.2 |

**Mussel microsatellites.** Three screens have been or are being conducted for microsatellite DNA in *Bathymodiolus childressi*. The first screen for microsatellites yielded five positive clones out of 1000 total clones that were tested. One of the five positive clones that were nucleotide sequenced, gA3C, had a large (GA) repeat and had an insert size sufficient to design PCR primers for further analysis. This microsatellite locus was highly polymorphic and was used to screen the individuals in the four seep populations for genetic diversity. The microsatellite locus has been run on all of the *B. childressi* samples from the four Gulf of Mexico populations.

The second microsatellite screen yielded 30 positive clones out of 850 total recombinant clones that hybridized strongly to the repetitive DNA clones. Of the 30 positive clones, 20 clones had an insert size greater than 200 base pairs, the minimum size capable of containing a viable insert for microsatellite primer design. Of the 20 clones that were sequenced, three microsatellite clones could be used to design PCR primers for screening *B. childressi* populations. The three microsatellite loci from the second screen were monomorphic and could not be used for studies of gene flow (Table 8.7.8). A third screen for microsatellites is currently underway.
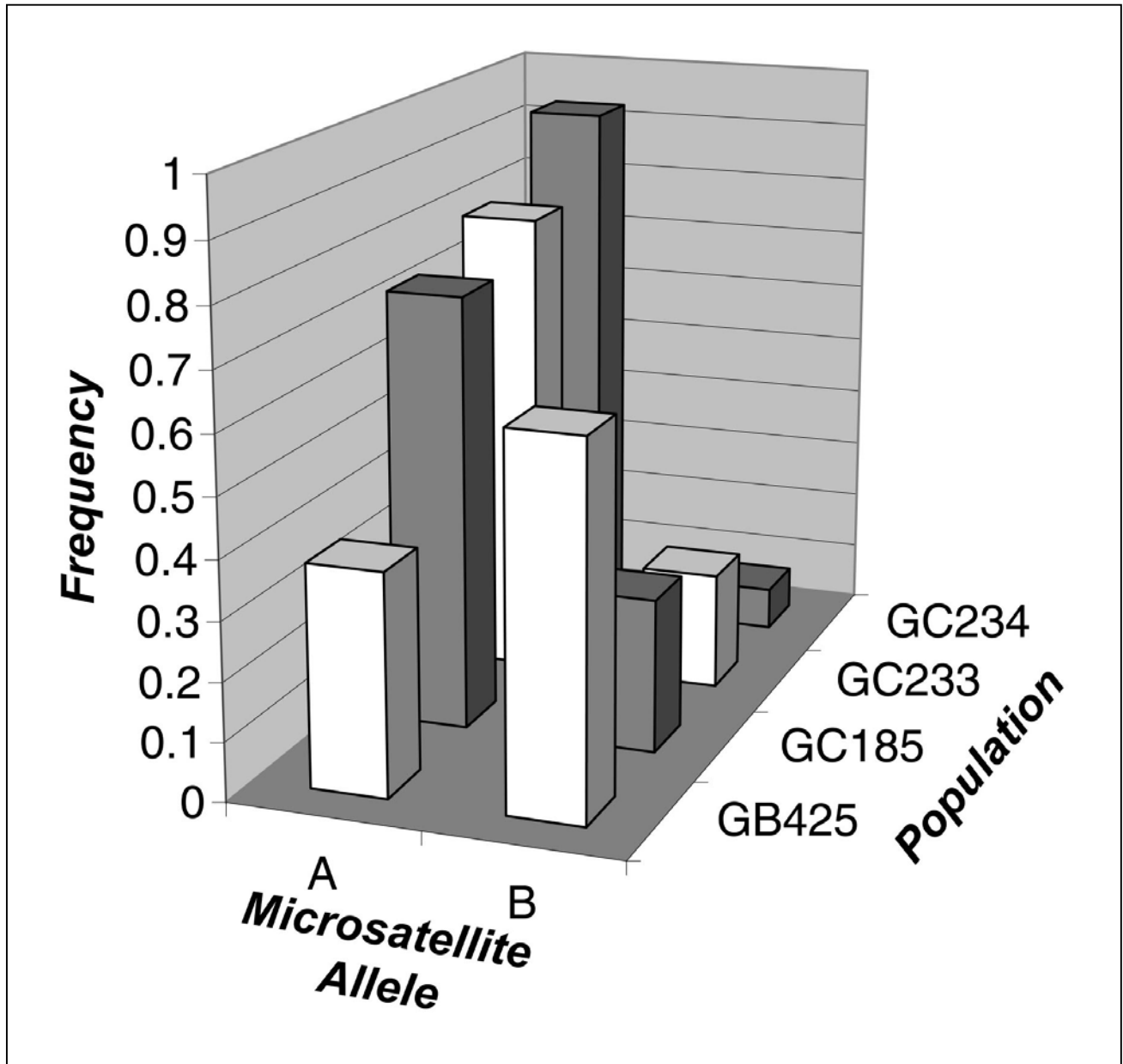


Figure 8.7.1.   Frequency distribution of microsatellite alleles for the 4-10D microsatellite locus in *Escarpia* sp. collected from four hydrocarbon seeps in the Gulf of Mexico.
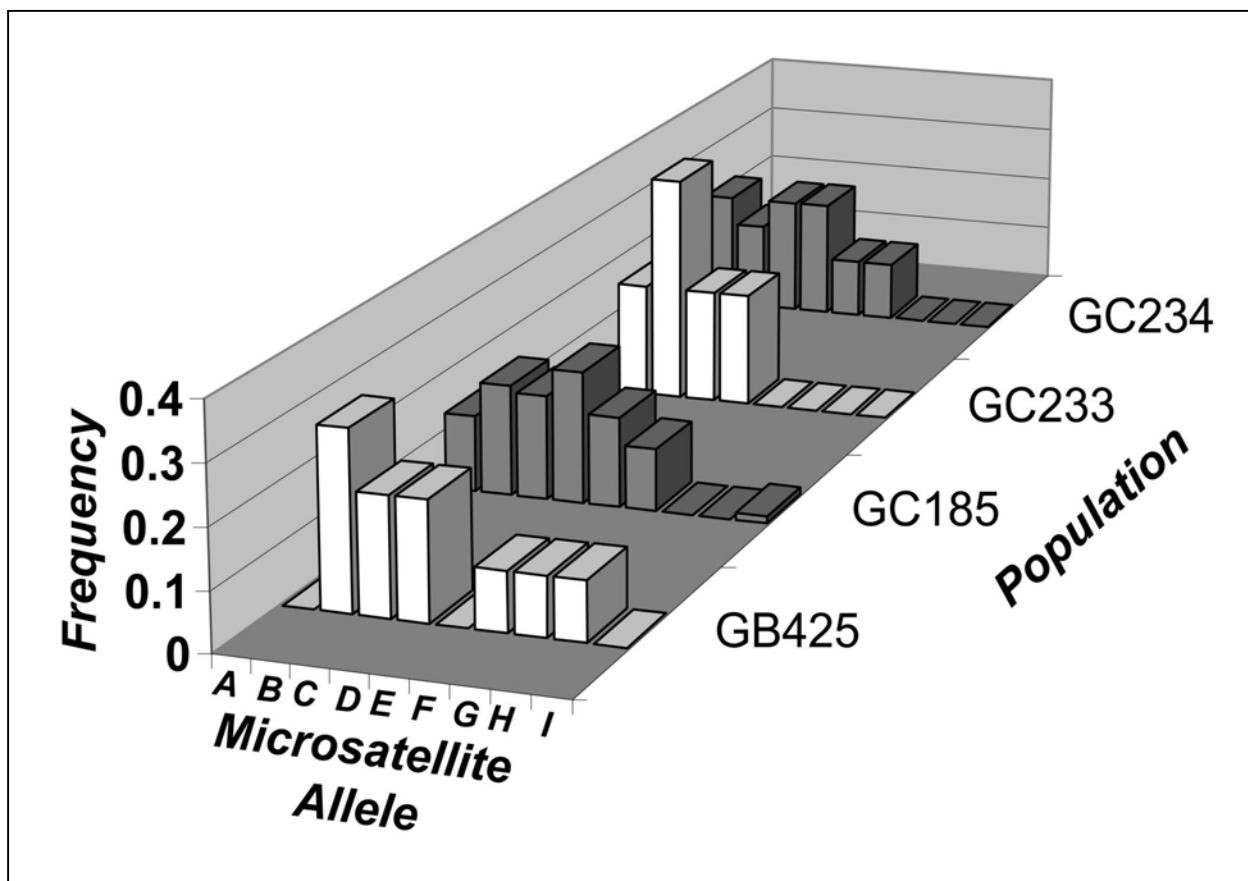
Figure 8.7.2. Frequency distribution of microsatellite alleles for the 3-2D microsatellite locus in *Escarpia* sp. collected from four hydrocarbon seeps in the Gulf of Mexico.

Table 8.7.8. PCR primers for four microsatellite loci in *Bathymodiolus childressi* from the Gulf of Mexico.

| Name | Size (bp) | PCR Primer | Variab ility | Temp (°C) | Repeat |
|------|-----------|------------|--------------|-----------|--------|
| gA3C | | f 5' TAT TAA CAC GAC GCG TGG CA 3' | P | 55 | $(GA)_{28}$ |
| | | r 5' TTC GCG ACA ACT ACC AGA GA 3' | | | |
| B8-01 | 157 | f 5'  GGC TTC CTC CAC CAC TAA TA 3' | M | 60 | $(TCAA)_4$ |
| | | r 5' TGA GCG TGG CAG TAA TGA GA 3' | | | |
| C9-2 | 119 | f 5' GGT ACG CAA TCT TCA ACG TC 3' | M | 55 | $(GAA)_5$ |
| | | r 5' ACG AGT TGG TCA AGG TAC GA 3' | | | |
| 2C9-2 | 117 | f 5' GGT ACG CAA TCT TCA ACG TC 3' | M | 50 | $(GAA)_5$ |
| | | r 5' ACG AGT TGG TCA AGG TAC GA 3' | | | |

f, forward PCR primer; r, reverse PCR primer; M, microsatellite locus was monomorphic; P, microsatellite locus was polymorphic; Temp, annealing temperature for the PCR reactions; and Repeat, length of the original microsatellite clone.

A total of 23 microsatellite alleles were observed at the gA3C locus in *B. childressi*. The allele frequencies of gA3C in the six collection stations at GC185 are found in Figure 8.7.3. Most microsatellite alleles are shared among the six collection stations. The allele frequencies of gA3C at the four collection localities are found in Figure 8.7.4. Again, although there are frequencies differences in gA3C microsatellite alleles among populations, the alleles that are present in the five populations are similar. A total of 2.47 *B. childressi* larvae are estimated to be exchanged among the GC185 mussel stations. A total of 8.7 *B. childressi* larvae are estimated to be exchanged among the three GC234 populations each generation (Table 8.7.9). A total of 14.5 *B. childressi* larvae are estimated to be exchanged between GB425 and the three GC234 populations each generation (Table 8.7.9).
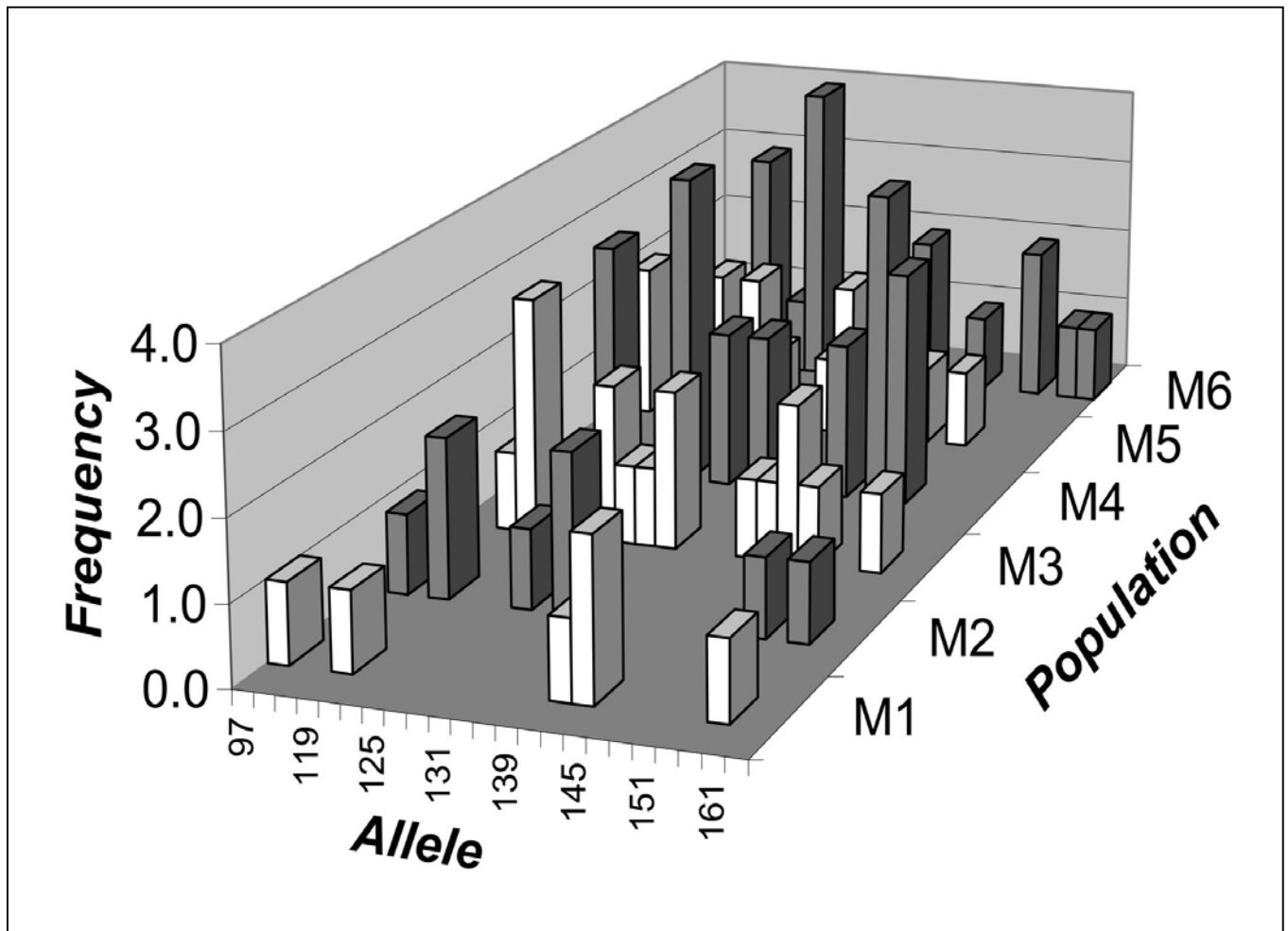


Figure 8.7.3. Frequency distribution of microsatellite alleles for the gA3C microsatellite locus in *B. childressi* collected from six stations within the GC185 hydrocarbon seep in the Gulf of Mexico.
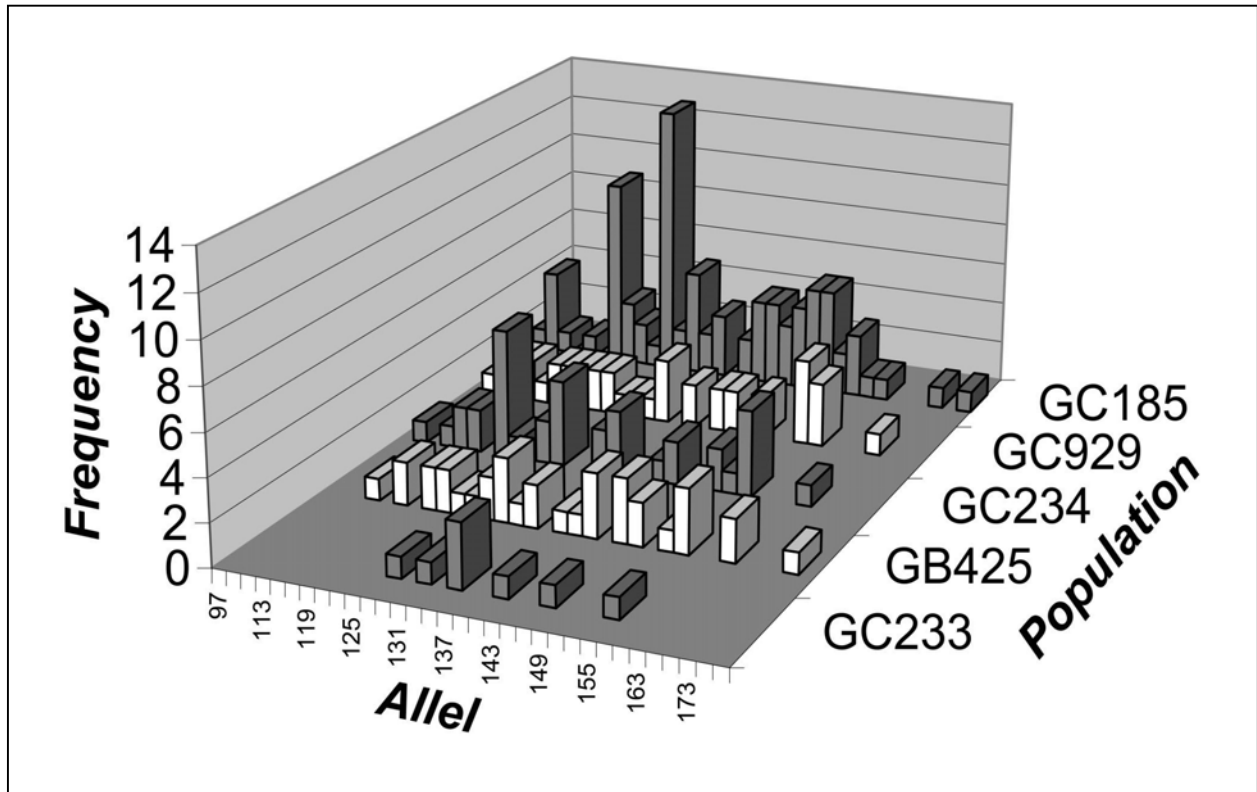
Figure 8.7.4. Frequency distribution of microsatellite alleles for the gA3C microsatellite locus in *B. childressi* collected from five hydrocarbon seeps in the Gulf of Mexico.

Table 8.7.9. Estimates of the number of migrants exchanged
between four populations of *Bathymodiolus childressi*.

|  | GC185 | GC233 | GC234 |
|---|---|---|---|
| GB425 | 20.3 | 9.4 | 13.8 |
| GC185 |  | 16.9 | 13.2 |
| GC233 |  |  | 6.7 |

**Phylogenetics of vestimentiferans.** The phylogenetic relationships of the vestimentiferan tubeworms based on the COI sequences are shown Figure 8.7.5. The newly discovered "spiked morph" of *Escarpia* is closely related to other escarpid species that are found in the Gulf of Mexico where this new morph clusters with an escarpid collected at GC234. The genetic distance between

the "spiked" escarpid and the "normal" escarpid from GC234 is similar to that which separates a *Lamellibrachia* from the Gulf of Mexico and that of Pacific Ocean species of *Lamellibrachia*.
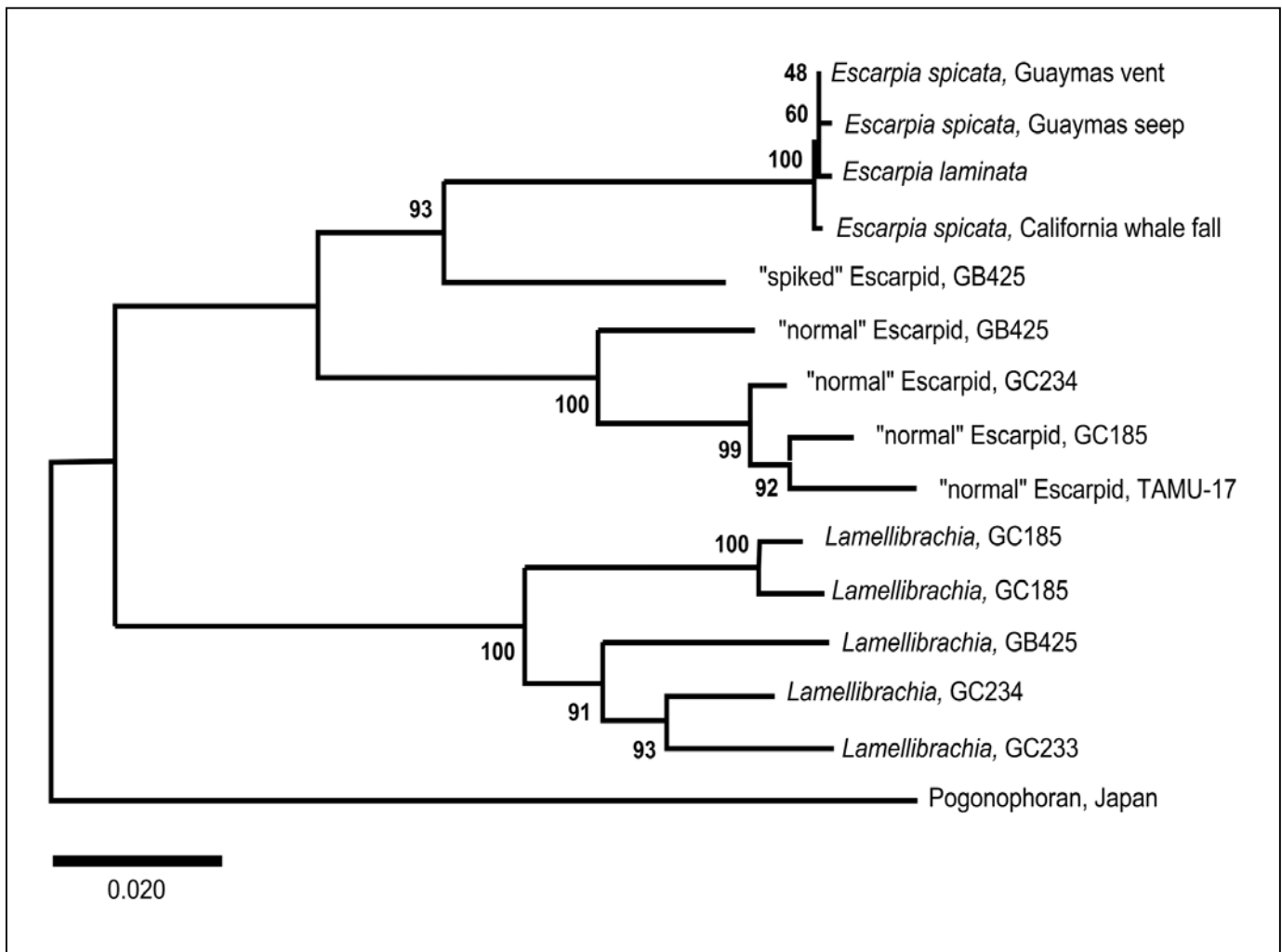
Figure 8.7.5. Phylogenetic relationships among vestimentiferan tubeworms from the hydrocarbon seeps and hydrothermal vents. Note the two species of Escarpid-like tubeworms from the MMS study sites are different from each other and from the other described Escarpids

**Phylogenetic relationships of vestimentiferan endosymbionts.** Nelson and Fisher (2000) in a paper supported by the MMS contract showed that the seep vestimentiferans fall into two easily distinguishable groups. One group consists entirely of species in the genus *Lamellibrachia*. The other includes all of the described species in the genus *Escarpia* and an undescribed "escarpid-like" species, which is distantly related to the named species of *Escarpia* (Figure 8.7.6; S. Gardiner personal communication). *Lamellibrachia* and *Escarpia* (or the "escarpid-like" species) co-occur at many seep sites in the Gulf of Mexico as well as at several locations around Japan (Kojima *et al.* 1993).

In contrast to the evolutionary relationships among the hosts, the present findings identified three groups of symbionts from seep vestimentiferans that do not correlate with host taxonomic classification (Figure 8.7.7). The first group includes the symbionts from *Lamellibrachia* sp. nov. 2. and the "escarpid-like" tube worms from shallow seep sites in the Gulf of Mexico. In fact, sequence differences between symbionts from two individuals of the same host species are the same or greater than the differences between the sequences of symbionts of the two different host species sampled from the same site (Figure 8.7.6). Average divergence (5.8 sites, 0.38%) among the symbionts in four host individuals from the shallow seep sites in the Gulf of Mexico is approximately three times the divergence (2.1 sites, 0.14%) found among all vent symbionts analyzed.

A second group of cold seep symbionts is found in vestimentiferans collected from Alaminos Canyon, a seep site that occurs in the deeper waters of the Gulf of Mexico (Brooks *et al.* 1990) Similar to the
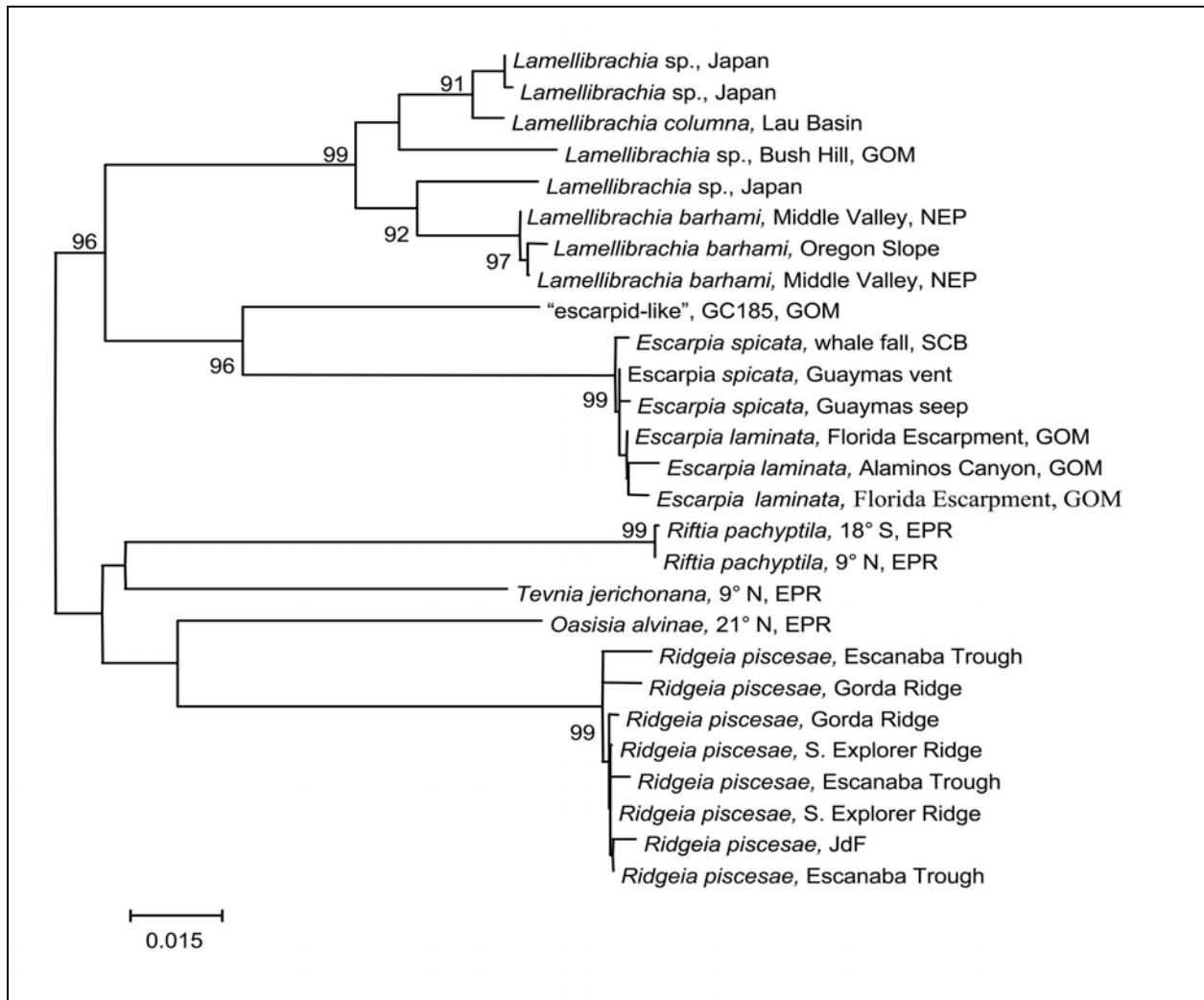


Figure 8.7.6. Phylogenic tree of tubeworms based on the COI gene of the mitochondrial DNA. This tree is based on data collected by Nelson and Fisher (2000), Feldman *et al*. (1997), Black *et al*. (1997).

shallow sites, two species of tube worms, *Lamellibrachia* sp. nov. 1. and *Escarpia laminata*, occur at the site and harbor symbionts from the same population. Only a single nucleotide difference was found among the three symbiont sequences analyzed from Alaminos Canyon tube worms. These sequences differed from those of the shallow Gulf of Mexico species by an average of 19 nucleotide differences (1.3%).

*Escarpia laminata* was collected from 3,700 meters on the Florida Escarpment in the Gulf of Mexico. The SSU rDNA sequences of the symbionts from the two individuals analyzed from this site were quite similar (99.9%) but differed by 1.8% from symbionts of the other Gulf of Mexico sites (Figure 8.7.7).
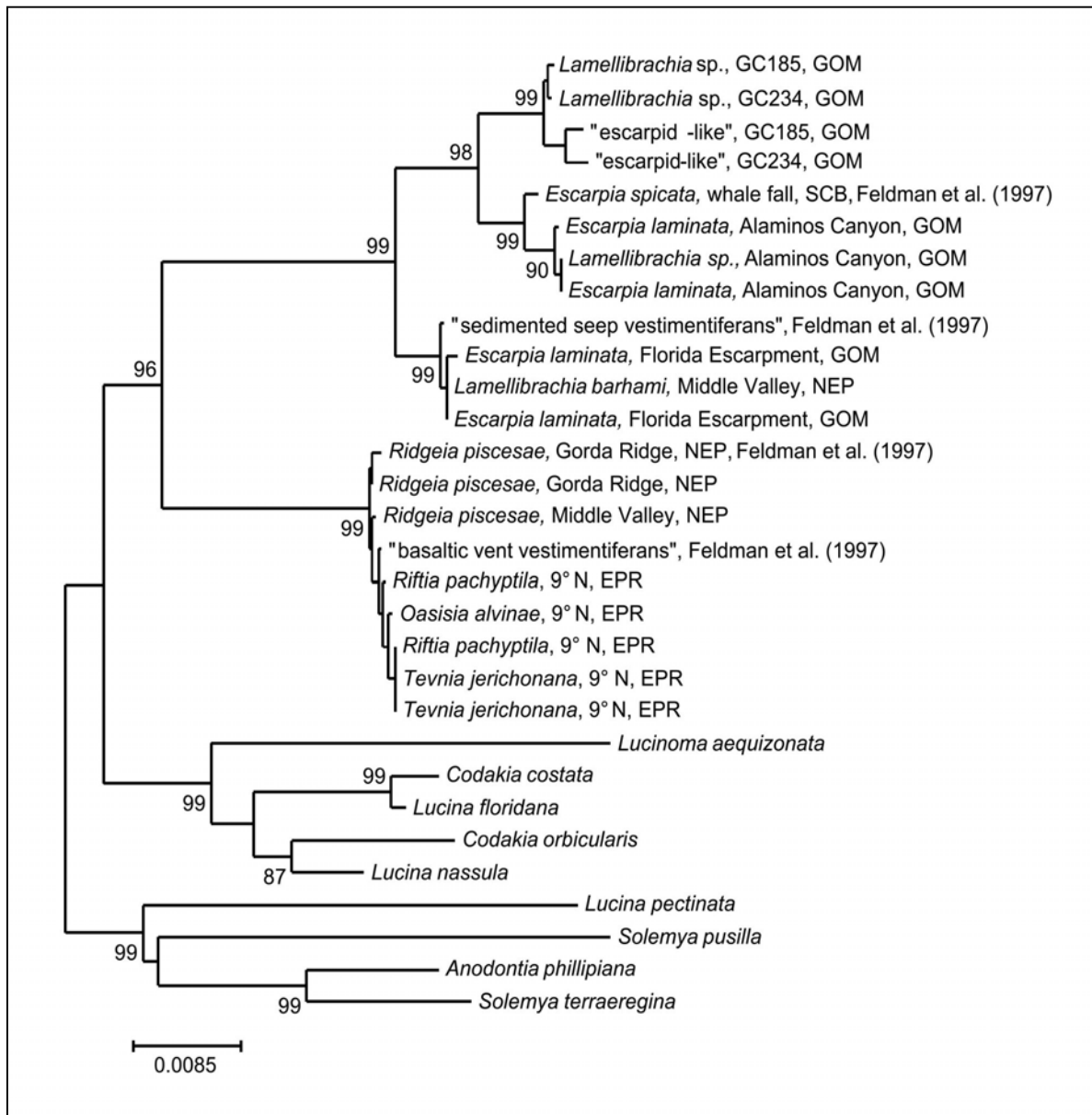


Figure 8.7.7. Phylogenetic relationships among sulfur-oxidizing endosymbionts based on 16S rDNA sequences. Included results presented in Feldman et al. (1997).

The large divergence (27.1 nucleotide differences) between the symbionts of *Escarpia laminata* from the Florida Escarpment and *Escarpia laminata* from Alaminos Canyon is not reflected in the evolutionary relationships of the hosts, which show few differences in the COI gene (Figure 8.7.6, 2.5 sites). Clearly, the seep symbiont phylogeny is not congruent with that of the hosts, but rather with geography.

### 8.7.4. Discussion

**Gene flow in vestimentiferans.** Wright's (1931, 1943) mathematical model of migration shows that one migrant per generation is sufficient to homogenize gene frequencies among populations. The data from *Lamellibrachia* and *Escarpia* sp. collected from four seeps in the Gulf of Mexico show that microsatellite alleles are largely not restricted to a single habitat, but are shared among the tube worm populations examined in this study (Tables 8.7.5 and 8.7.7). These data suggest that disturbance of a local community will not have a profound effect on genetic diversity within the communities in the Gulf of Mexico. There is potential for large amounts of gene flow provided there are sufficient habitats for the tubeworms to settle. Thus, the amount of suitable habitat in the Gulf of Mexico will limit how many chemosynthetic communities that can be established not the biological ability of the tubeworms to disperse. The estimates of gene flow in *Lamellibrachia* and *Escarpia* are consistent with those found for the tubeworms that inhabit the hydrothermal vents of the Pacific Ocean (Black *et al.* 1994).

**Gene flow in mussels.** The single variable microsatellite for *Bathymodiolus childressi* indicates that the migration parameters are greater than one for all comparisons between study sites (Table 8.7.9). This is evidence that this species is capable of extensive gene flow over short, intermediate, and long ranges. Again, this level of exchange is capable of homogenizing gene frequencies among mussel populations and that mussels have the potential to recolonize new seep sites in the Gulf of Mexico. These results are quite striking given the variation in the growth abilities and condition of the mussels in the different populations. The migration data suggest that the condition of endemic mussels is not controlled genetically, but by the selective constraints of the local environment.

**Phylogenetics of vestimentiferans.** The relationship of the newly discovered "spiked morph" of *Escarpia* to vestimentiferans from the Gulf of Mexico and the Pacific Ocean suggest that this morph is a new species of escarpid-like tubeworm. These results should be viewed with caution because our conclusion is based on a single genetic locus that resided within the mitochondrial DNA; however, the molecular differentiation of the COI genes in the two morphs of *Escarpia* is substantiated by the extensive morphological characterization of these tubeworms (Stephen Gardner; Bryn Mar, unpublished data). This new escarpid-like species was rare in our collections of tubeworms taken with the Bushmaster suggesting that this new type should be considered fragile because of its low abundance.

**Phylogenetics of vestimentiferan endosymbionts.** The lack of concordance between the evolutionary relationships of the seep lineages of hosts and symbionts argues strongly against vertical transmission of symbionts from one generation to the next. Although this lack of congruence stands in contrast to other deep-sea metazoan endosymbioses that have been studied to date (Cary *et al.* 1993; Distel *et al.* 1994; Kreuger *et al.* 1996; Peek *et al.* 1998), it is not without precedence. An environmental transmission of the sulfur-oxidizing gill symbiont of the shallow water lucinid bivalve has been proposed (Durand *et al.* 1996; Gros *et al.* 1996). However, a strategy that requires the *de-novo* acquisition of symbionts each generation would seem risky for a host that is absolutely dependent on the symbiont for its nutritional needs as an adult, and for a host that occupies a habitat that is as patchy

and ephemeral as the hydrothermal vents. Thus, there must be some mechanism of host-symbiont recognition that assures the uptake and establishment of a symbiont population within larval or early juvenile tubeworms.

An unexpected finding was the close relationship between the *Escarpia laminata* symbionts from the Florida Escarpment and *Lamellibrachia barhami* from Middle Valley in the northeast Pacific. Not only are the two locations separated by land masses, but Middle Valley is a hydrothermal vent site located on a mid-ocean ridge. However, Middle Valley is a sedimented site with some areas of very low flow (Southward *et al.* 1996). Thus, in some ways, areas of Middle Valley may be very similar to a cold seep environment. The same species, *L. barhami*, is found at the cold seep sites (400 km distant) on the continental margins off the coast of Oregon and California (Southward *et al.* 1996; Suess *et al.* 1985; Webb 1969). At the Middle Valley site where these collections were made, the hydrothermal vent species, *Ridgeia piscaesae*, appeared emaciated, apparently reflecting the relatively inactive status of this site (J.J. Childress personal communication), and harbored the expected vent symbiont and not the seep symbiont hosted by *L. barhami*. This site is only one that we know of where two taxa of tube worms co-occur but do not host the same species of symbiont. (At Guyamas Basin, *Riftia pachyptila* and *Escarpia spicata* co-occur, and we predict that the symbionts from these two species would also be very different.) The fact that they house very divergent symbionts argues for host/symbiont co-evolution at least at the level of the divergence into the two very different habitats.

**Overall Conclusions.** This effort has improved our understanding of the genetic structure of seep communities and has implications for protection of these environments. The currents in the Gulf of Mexico are sufficient to allow transport of mussel and tube worm larvae among the four seep communities sampled for this study. This would suggest that the seep communities are robust to disturbance, but gene flow data provides no insights into the number of suitable habitats that the tubeworms and mussels can colonize. The microsatellite loci developed in this study will provide useful tools for further examination of tubeworm and mussel populations to further refine how these chemosynthetic organisms are transported around the Gulf of Mexico. Each depth community supports a unique form of free-living bacterial endosymbiont for the tubeworms that is likely to be transmitted environmentally to the host. The movement of hosts from different seep habitats may or may not be allowed because of the unique bacterial flora present in each habitat.

# 9.0 Inorganic Biogeochemistry of Cold Seep Sediments[*]

## 9.1 Overview

This component of the program was designed to provide a more detailed examination of the inorganic biogeochemistry occurring in cold seep sediments. The primary focus of the research was on understanding the processes influencing the carbon dioxide and sulfide systems. A review of the basic marine chemistry of these systems is given below. The sections of this chapter have been divided according to major activity and are synthesized at the end of this chapter.  The topic areas for each section are as follows:

## 9.2  Pore water and solid phase chemistry

This section uses a "classical" approach in which cores were sectioned to establish depth profiles of dissolved and solid phase chemical components of interest.

## 9.3  Stable isotope chemistry

Fractionation of the stable isotopes of carbon, oxygen and sulfur occurs by both biotic and abiotic processes. Stable isotope ratios of these elements were determined at selected sites for both dissolved and authigenic mineral phases to aid in the interpretation of the processes occurring in cold seep sediments.

## 9.4   Microelectrode profiling

An "emerging" new technology was utilized to obtain very detailed depth profiles of dissolved sulfide near the sediment-water interface. This was done in order to obtain better estimates of fluxes across the sediment-water interface and behavior of sulfide in the highly dynamic region.

## 9.5  Synthesis

In this section the findings made in the above sections are integrated to establish more general relationships among these parameters. This is the first step toward  the overall project integration and modeling of research results.

## 9.2 Pore Water and Solid Phase Chemistry*

### 9.2.1   Introduction

The biogeochemistry of hydrocarbon seeps is fundamentally related to the concentration, fluxes, sources, and sinks of dissolved gases. Gases, such as methane and other hydrocarbon

---

[*] This section was authored by John Morse and Rolf Aruitsm.

components, which migrate from depth or are supplied by disassociating methane hydrate located close to the sediment-water interface, may represent a major source of reduced carbon in these environments. Carbon dioxide ($CO_2$) and hydrogen sulfide ($H_2S$) play critical roles as metabolic products of microbial sulfate reduction and exert a major influence on critical environmental variables such as pH and oxidation-reduction potential ($pe$/Eh). The reoxidation of reduced sulfur also plays a critical role as an energy source for benthic organisms.

The speciation systematics of carbon dioxide and hydrogen sulfide in natural waters share some important similarities. Both behave as acids that dissolve via stepwise hydration and diprotic dissociation reactions, producing components whose relative concentrations vary as a function of pH. $CO_2$ dissolves in water according to the following reactions:

$$CO_{2(g)} \overset{K_H}{=} CO_{2(aq)} \tag{9-1a}$$

$$CO_{2(aq)} + H_2O \overset{K_1}{=} HCO_3^- + H^+ \tag{9-1b}$$

$$HCO_3^- \overset{K_2}{=} H^+ + CO_3^{2-} \tag{9-1c}$$

Because seawater pH is ~ 8, roughly the average of $pK_1$ (6.4) and $pK_2$ (10.3) at 25°C, bicarbonate ion is the primary dissolved inorganic carbon component. In similar fashion, hydrogen sulfide dissolves as

$$H_2S_{(g)} \overset{K_H}{=} H_2S_{(aq)} \tag{9-2a}$$

$$H_2S_{(aq)} \overset{K_1}{=} HS^- + H^+ \tag{9-2b}$$

$$HS^- \overset{K_2}{=} H^+ + S^{2-} \tag{9-2c}$$
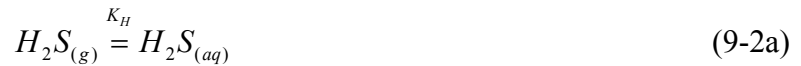
Bisulfide ion is also the most common component at seawater pH. $CO_2$ and $H_2S$ are both produced when sulfate is used as an electron acceptor in the remineralization of simple organic matter,

$$2CH_2O + SO_4^{2-} = HS^- + 2HCO_3^- + H^+ \tag{9-3}$$
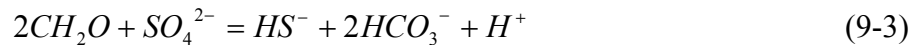
or methane (here written as the complete oxidation of $CH_4$ to $CO_2$),

$$CH_4 + SO_4^{2-} = HS^- + HCO_3^- + H_2O \tag{9-4}$$
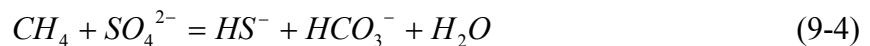
The bisulfide and bicarbonate produced in these reactions may react further to form sulfide and carbonate minerals within the sediment.

Important sulfide minerals consist of pyrite (FeS$_2$) and the metastable, so-called acid-volatile sulfides (AVS: i.e., amorphous FeS, mackinawite, and possibly greigite). The abundance of pyrite + AVS (total reduced sulfur, or TRS) is limited by the availability of sulfide and/or iron (Canfield 1989). These minerals are thus important in terms of buffering dissolved sulfide and may also serve to sequester toxic metals (Morse 1994) and thus control their bioavailability. Carbonate minerals such as calcite and aragonite (CaCO$_3$), and more rarely, dolomite (CaMg(CO$_3$)$_2$) form via reactions represented as

$$2HCO_3^- + Ca^{2+} = CaCO_3 + H_2O + CO_2 \qquad (9\text{-}5)$$
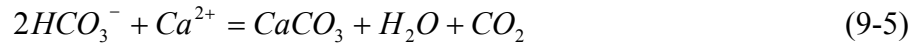
and may act as inorganic cements in binding of primary sedimentary particles or, in the case of carbonate mounds, form important sedimentary structures themselves.

In the presence of reactive iron oxides, reactions (9-3) and (9-5) may combine to yield both carbonates and AVS as products,

$$\frac{9}{4} CH_2O + SO_4^{2-} + Ca^{2+} + FeOOH = FeS + CaCO_3 + \frac{5}{4} CO_2 + \frac{11}{4} H_2O \qquad (9\text{-}6)$$
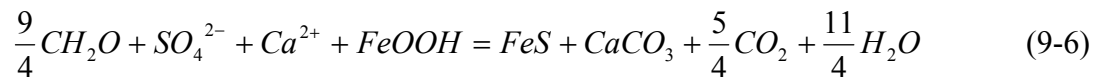
In oxic regimes, remineralization of organic matter may also lead to the dissolution of carbonate minerals,

$$O_2 + CH_2O + CaCO_3 = 2HCO_3^- + Ca^{2+} \qquad (9\text{-}7)$$
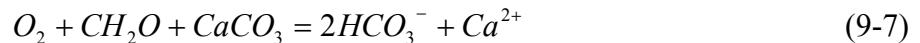
Dissolved sulfide produced in reaction (9-3) may also be reoxidized to sulfate by oxygen, nitrate, Fe(III) or Mn(IV) compounds, depending on their availability.

Sulfide may be used as an electron donor by microbial sulfide oxidizers yielding sulfate, intermediate thiosulfate, or elemental sulfur as metabolic products. Thus sulfide is important both as a waste product of sulfate reduction, and as a substrate itself for new energy production.

In addition, despite the important differences in geometry that distinguish chemosynthetic seep systems from other benthic habitats, it is not clear what limitation is imposed on these systems in terms of the supply of metabolizable organic matter. Evidence of bacterial oxidation of both crude oil hydrocarbons (Sassen *et al.* 1994a) and methane hydrates (Sassen *et al.* 1999a) suggests a complex relationship between the organic matter pools and their relative lability, sulfate reducing bacteria, and sulfide oxidizers.

The production and remineralization of organic matter in chemosynthetic seep communities are thus intimately linked to the cycling of inorganic CO$_2$ and H$_2$S via reactions such as those described above. A practical understanding of the location and distribution, productivity, and dynamics of seep populations cannot be made without careful measurement of pore water and solid phase carbon and sulfur components. These measurements were undertaken with the following objectives:

1. Identification of carbon dioxide and hydrogen sulfide sources: Variations in CO$_2$ and H$_2$S concentrations may derive entirely from local reactions occurring within the sediment. It is

also possible, however, that deep-seated fluids migrating to the surface may deliver these gases. For example, if seep fluids are a significant source of sulfide, these chemosynthetic communities might be reasonably compared with those associated with seafloor hydrothermal vent systems. It will thus be determined whether pore waters reflect extra local sources of these inorganic gases.

2. Quantification of sulfate reduction rates: Understanding the dynamics of sulfur and carbon cycling in these chemosynthetic ecosystems, particularly with respect to sulfide oxidizers, is not possible without measurement of the rate of microbial sulfate reduction. This parameter serves as a basic discriminator between sites that are biologically "active" and those that are in relatively quiescent or in decline, and as a means of general comparison of these communities with "normal" marine systems.

3. Understanding of the relationship between supply of organic components and electron acceptors (sulfate), and identification of limiting components: Despite apparent widespread abundance of organic material in the form of both hydrocarbon gases and crude oil components, chemosynthetic communities are localized and heterogeneously distributed. A critical step to understanding these systems thus lies in identifying those components (organic, inorganic, physical-chemical, sedimentologic, etc.) responsible for overall limitation and localization of these systems.

4. Determination of the role of brines in mineral formation: Because brines can possess solute concentrations much greater than seawater, their arrival from depth and mixing with pore water could substantially alter solute concentrations and form an important source of components for mineral formation. It is thus important to determine the end member composition of brine fluids and what component they represent in pore water.

5. Quantification of sulfide and carbonate mineral formation: Diagenetic processes such as precipitation and dissolution of sedimentary mineral phases also buffer concentrations of pore water sulfide and carbon. These phases (AVS/TRS, calcite, reactive iron oxides) act as sources and sinks for dissolved components and thus affect their bioavailability as well as physical sediment properties.

### 9.2.2 Results

Complete results of all solid phase and pore water work are tabulated in the Appendix and organized in the following manner: pH, DIC, sulfide, sulfate, and chloride (Table A.9.1); major cations (Table A.9.2); nutrients and dissolved organic carbon (Table A.9.3); solid phase properties (Table A.9.4); and sulfate reduction rates (Tables A.9.5 and Table 9.1). Stable isotope data are presented later in this chapter. The results of organic geochemistry appear in a separate chapter. In these tables, any differences in coverage with respect to the various analytical components at each station reflect the difficulties imposed by undertaking a large number of analyses from a relatively small number of cores. Cores that showed obvious evidence of upset during retrieval were discarded. Missing data arise from inadequate core material or pore water sample volume to accommodate analysis of all components (many deeper intervals yielded less than 5 mL), differences in depth of core penetration, and infrequently due to poor analyses; blank

cells indicate these. In addition, certain analyses (e.g., sulfate reduction assays, dissolved organic carbon, carbon and sulfur isotopes) focused only on specific cores and intervals therein.

### 9.2.3 Discussion

The following discussion will focus on key aspects of the inorganic geochemistry that relate to biotic relationships and activities. The most important reaction in these communities is dissimulatory sulfate reduction. As will be seen below, the overall vigor of sulfate reduction serves as a principle discriminator in the geochemical characterization of these highly dynamic chemosynthetic communities.

Table 9.1.  Porewater pH, carbon, sulfur, and anions.

| Dive Number | Site | Station | Depth (cm) | pH | Dissolved Inorganic Carbon (mM) | Total Dissolved Sulfide (µM) | Sulfate (mM) | Chloride (mM) |
|---|---|---|---|---|---|---|---|---|
| 2871 | GC234 | GCST1 | 0–2 | 7.948 | 2.845 | .0 | – | 560.82 |
|  |  |  | 2–4 | 7.979 | 3.998 | .0 | 28.189 | 563.11 |
|  |  |  | 4–6 | 8.076 | 3.995 | .0 | 22.414 | 565.41 |
|  |  |  | 6–8 | 8.119 | 4.434 | .0 | 27.271 | 567.70 |
|  |  |  | 8–10 | – | – | – | – | – |
|  |  |  | 10–12 | 8.080 | 4.103 | .0 | 27.465 | 565.47 |
|  |  |  | 12–14 | 8.088 | 4.323 | .0 | 27.865 | 565.24 |
|  |  |  | 14–16 | 8.014 | 3.914 | .0 | 26.948 | 544.05 |
|  |  |  | 16–18 | 7.956 | 3.682 | – | 25.804 | 522.86 |
|  |  |  | 18–20 | 7.937 | – | .0 | 26.837 | 571.06 |
| 2873 | GC235 | BHAT1 | 0–2 | 7.976 | 3.349 | .0 | 27.161 | 537.13 |
|  |  |  | 2–4 | 7.949 | 4.056 | .0 | 26.473 | 534.66 |
|  |  |  | 4–6 | 8.010 | 4.396 | .0 | 25.353 | 552.15 |
|  |  |  | 6–8 | 7.978 | 5.186 | 2.1 | 26.017 | 551.08 |
|  |  |  | 8–10 | 7.879 | 4.134 | 28.4 | 25.983 | 542.77 |
|  |  |  | 10–12 | 8.011 | 4.517 | 6.6 | 25.687 | 544.65 |
|  |  |  | 12–14 | 7.890 | 4.187 | 30.0 | 24.649 | 533.51 |
|  |  |  | 14–16 | 7.872 | 4.148 | 28.1 | 26.459 | 555.78 |
| 2873 | GC235 | BHM4 | 0–2 | 7.809 | – | 2784.4 | 17.585 | 569.72 |
|  |  |  | 2–4 | 7.826 | 7.478 | 5026.9 | 11.086 | 575.74 |
|  |  |  | 4–6 | 7.724 | 8.893 | 5300.4 | 1.983 | 591.39 |
|  |  |  | 6–8 | 7.919 | 12.015 | 6519.0 | .0 | 577.48 |
|  |  |  | 8–10 | 7.940 | 10.770 | 5322.6 | .0 | 572.96 |
|  |  |  | 10–12 | 7.939 | 12.854 | 5352.2 | .0 | 606.34 |
|  |  |  | 12–14 | 7.860 | 13.336 | 5248.7 | .0 | 577.64 |
|  |  |  | 14–16 | 7.878 | 12.621 | 5300.4 | .0 | 580.95 |
|  |  |  | 16–18 | 7.936 | 11.875 | 5359.6 | 0.037 | 559.62 |
|  |  |  | 18–20 | 7.895 | 10.212 | 5307.8 | .0 | 580.03 |
| 2874 | GC235 | BHST1 | 0–2 | 8.024 | – | .0 | 28.435 | 600.92 |
|  |  |  | 2–4 | 7.953 | 4.527 | 48.2 | 25.668 | 549.51 |
|  |  |  | 4–6 | 7.834 | – | 276.4 | 24.411 | 546.77 |
|  |  |  | 6–8 | 7.893 | 6.263 | 1219.7 | 23.240 | 557.81 |
|  |  |  | 8–10 | 7.800 | 6.002 | 1931.9 | 22.138 | 546.00 |
|  |  |  | 10–12 | 7.825 | 7.000 | 1948.4 | 21.572 | 545.01 |
|  |  |  | 12–14 | 7.886 | 6.693 | 1828.0 | 21.606 | 571.14 |
|  |  |  | 14–16 | – | – | – | – | – |
|  |  |  | 16–18 | 7.875 | 8.674 | 1866.3 | 20.630 | 564.13 |
| 2875 | GC235 | BHST2 | 0–2 | 7.963 | 3.531 | 0.8 | 26.202 | 546.57 |
|  |  |  | 2–4 | 7.912 | 4.371 | 0.9 | 25.753 | 536.27 |
|  |  |  | 4–6 | 7.907 | 4.484 | 0.6 | 26.609 | 545.08 |
|  |  |  | 6–8 | 7.992 | 3.814 | .0 | 22.627 | 453.56 |
|  |  |  | 8–10 | 7.911 | 3.440 | .0 | 26.625 | 539.69 |
|  |  |  | 10–12 | 7.879 | 4.088 | .0 | 27.212 | 552.15 |
| 2875 | GC235 | BHUN1 | 0–2 | 7.941 | 2.927 | .0 | 27.246 | 558.07 |
|  |  |  | 2–4 | 7.869 | 2.421 | .0 | 27.217 | 555.83 |
|  |  |  | 4–6 | 7.877 | 3.093 | .0 | 27.372 | 553.59 |
|  |  |  | 6–8 | 8.052 | 3.429 | .0 | 26.837 | 551.34 |

Table 9.1. Porewater pH, carbon, sulfur, and anions. (Continued)

| Dive Number | Site | Station | Depth (cm) | pH | Dissolved Inorganic Carbon (mM) | Total Dissolved Sulfide (µM) | Sulfate (mM) | Chloride (mM) |
|---|---|---|---|---|---|---|---|---|
| | | | 8–10 | 8.067 | 3.060 | .0 | 26.972 | 549.10 |
| | | | 10–12 | 8.095 | 3.322 | .0 | 27.618 | 548.77 |
| | | | 12–14 | 8.121 | 3.268 | .0 | 26.988 | 548.44 |
| | | | 14–16 | 8.104 | 3.259 | .0 | 26.765 | 548.11 |
| | | | 16–18 | 8.083 | 3.537 | .0 | 26.614 | 547.78 |
| | | | 18–20 | 8.081 | 2.823 | .0 | 26.904 | 547.45 |
| | | | 22–24 | 8.044 | 3.584 | .0 | 26.739 | 546.79 |
| | | | 26–28 | 8.019 | 3.186 | 1.0 | 27.765 | 554.97 |
| 2876 | GC233 | BPR2 | 0–2 | 7.932 | 3.244 | .0 | 26.198 | 597.77 |
| | | | 2–4 | 7.841 | 3.165 | .0 | 23.584 | 492.36 |
| | | | 4–6 | 7.993 | 3.626 | 2.0 | 23.638 | 498.75 |
| | | | 6–8 | 7.771 | 4.163 | .0 | 22.907 | 491.77 |
| | | | 8–10 | 7.734 | 5.186 | 2.0 | 24.933 | 518.49 |
| | | | 10–12 | 7.958 | 4.088 | 17.9 | 26.569 | 550.64 |
| 2880 | GC234 | GCB1@GCAT1 | 0–2 | 7.920 | 4.295 | 0.9 | 27.426 | 559.46 |
| | | | 2–4 | 7.852 | 6.314 | 452.4 | 24.936 | 560.40 |
| | | | 4–6 | 7.905 | 9.668 | 1186.2 | 22.838 | 561.34 |
| | | | 6–8 | 7.839 | 7.119 | 1247.7 | 22.559 | 562.28 |
| | | | 8–10 | 7.856 | 9.059 | 1242.1 | 21.863 | 563.22 |
| | | | 10–12 | 7.815 | 8.725 | 1257.5 | 21.998 | 564.16 |
| | | | 12–14 | 7.755 | 8.490 | 2126.1 | 21.035 | 559.20 |
| | | | 14–16 | 7.773 | 8.306 | 2153.5 | 19.526 | 554.23 |
| | | | 16–18 | 7.758 | 8.553 | 2142.5 | 18.888 | 549.27 |
| | | | 18–20 | 7.667 | 6.912 | 2139.8 | 17.663 | – |
| | | | 22–24 | 7.695 | 10.360 | 3418.2 | 16.482 | – |
| 2882 | GB425 | GBB1@GBM2 | 0–2 | 7.544 | 6.069 | 1407.0 | 18.482 | 640.49 |
| | | | 2–4 | 7.437 | 6.399 | 2012.5 | 8.992 | 799.65 |
| | | | 4–6 | 7.343 | 6.936 | 870.8 | 2.954 | 1079.00 |
| | | | 6–8 | 7.371 | 7.342 | 724.6 | 0.729 | 1284.56 |
| | | | 8–10 | 7.300 | 8.114 | 824.4 | 0.526 | 1439.06 |
| | | | 10–12 | 7.367 | 9.403 | 338.2 | 0.848 | 1533.00 |
| | | | 12–14 | 7.385 | 15.895 | 21.7 | 0.391 | 1621.28 |
| | | | 14–16 | 7.358 | 9.826 | 25.8 | 0.390 | 1629.44 |
| | | | 16–18 | 7.383 | 10.278 | 2.1 | 0.341 | 1607.36 |
| | | | 18–20 | 7.348 | 9.763 | 1.6 | 0.344 | 1698.21 |
| | | | 22–24 | 7.418 | 7.987 | 1.7 | 0.246 | 1697.65 |
| | | | 26–28 | 7.497 | 9.134 | 1.7 | 0.473 | 1669.09 |
| 2883 | GB425 | GBM1 | 0–2 | 7.957 | 3.623 | .0 | 27.678 | – |
| | | | 2–4 | 7.746 | 4.524 | .0 | – | – |
| | | | 4–6 | 7.806 | 3.699 | .0 | 27.002 | – |
| | | | 6–8 | 7.901 | – | .0 | 27.285 | – |
| | | | 8–10 | 7.867 | 4.245 | 1.0 | 26.720 | 576.33 |
| | | | 10–12 | – | 4.140 | 0.0 | 26.518 | – |
| | | | 12–14 | 7.886 | 4.512 | 24.8 | 26.716 | – |
| | | | 14–16 | 7.849 | 4.516 | 20.7 | 25.818 | – |
| | | | 16–18 | 7.724 | 4.318 | 2.1 | 26.979 | – |
| 2885 | GB425 | GBM2 | 0–2 | 7.725 | 10.613 | 374.3 | 16.226 | 779.66 |
| | | | 2–4 | 7.488 | 15.378 | 719.6 | 2.425 | 1139.57 |

Table 9.1. Porewater pH, carbon, sulfur, and anions. (Continued)

| Dive Number | Site | Station | Depth (cm) | pH | Dissolved Inorganic Carbon (mM) | Total Dissolved Sulfide (µM) | Sulfate (mM) | Chloride (mM) |
|---|---|---|---|---|---|---|---|---|
| | | | 4–6 | 7.513 | 12.747 | 364.8 | 0.419 | 1497.99 |
| | | | 6–8 | 7.346 | 14.565 | 359.2 | 0.103 | 1367.35 |
| | | | 8–10 | 7.415 | 10.095 | – | 0.385 | 992.21 |
| | | | 10–12 | 7.444 | 11.811 | 42.0 | – | – |
| | | | 12–14 | 7.446 | 11.033 | 39.1 | 0.324 | 1562.10 |
| | | | 14–16 | 7.569 | 8.546 | – | – | – |
| | | | 16–18 | 7.521 | – | 3.6 | – | – |
| 2886 | GC234 | GCAT2 | 0–2 | 7.741 | 5.825 | 4585.7 | 18.961 | 571.15 |
| | | | 2–4 | 7.777 | 7.508 | 6832.9 | 13.816 | 564.66 |
| | | | 4–6 | 7.818 | 4.379 | 7810.8 | 12.106 | 568.64 |
| | | | 6–8 | 7.779 | 10.943 | 10157.7 | 5.472 | 568.15 |
| | | | 8–10 | 7.807 | 11.034 | 10018.0 | 0.384 | 568.65 |
| | | | 10–12 | 7.819 | 18.914 | | .0 | 557.18 |
| | | | 12–14 | 7.787 | 13.098 | 10353.3 | .0 | 451.04 |
| | | | 14–16 | 7.820 | 14.172 | 10618.8 | .0 | 573.10 |
| | | | 16–18 | 7.797 | 11.915 | 11191.5 | .0 | 562.83 |
| | | | 18–20 | 7.822 | 12.770 | 10297.4 | .0 | 588.10 |
| | | | 20–22 | 7.793 | 18.469 | – | – | – |
| 2888 | GC234 | GCAT1 | 0–2 | 7.918 | 3.956 | 0.7 | 27.146 | 572.59 |
| | | | 2–4 | 7.803 | 4.576 | 4.7 | 26.217 | 551.83 |
| | | | 4–6 | 7.730 | 4.661 | 51.5 | 26.344 | 548.12 |
| | | | 6–8 | 7.792 | 4.204 | 44.9 | 25.531 | 564.32 |
| | | | 8–10 | 7.530 | 4.867 | 47.2 | 25.997 | 551.32 |
| | | | 10–12 | 7.770 | 5.119 | 18.8 | – | – |
| | | | 12–14 | 7.736 | 5.302 | 19.8 | – | – |
| 2891 | GC235 | BHAT2 | 0–2 | 7.776 | 4.027 | 1.5 | 26.080 | 567.65 |
| | | | 2–4 | 7.609 | 3.403 | 0.8 | 24.232 | 567.87 |
| | | | 4–6 | 7.628 | 2.779 | 0.6 | 26.324 | 535.49 |
| | | | 6–8 | 7.857 | 3.817 | 1.9 | 26.441 | 543.78 |
| | | | 8–10 | 8.019 | 4.320 | 1.1 | 26.264 | 546.95 |
| | | | 10–12 | 8.654 | 4.215 | 1.5 | 26.595 | 567.82 |
| | | | 12–14 | – | – | – | – | – |
| | | | 14–16 | 7.972 | 4.706 | 32.7 | 26.505 | 559.51 |
| box | GC235 | BHBC2 | 0–2 | 7.986 | 2.803 | .0 | 27.638 | 567.27 |
| | | | 2–4 | 7.854 | 2.756 | .0 | 27.719 | 553.30 |
| | | | 4–6 | 7.868 | 3.601 | .0 | 27.433 | 555.71 |
| | | | 6–8 | 7.988 | 2.833 | .0 | 27.166 | 563.94 |
| | | | 8–10 | 8.046 | 3.244 | .0 | 26.735 | 549.69 |
| | | | 10–12 | 8.145 | 3.574 | .0 | 26.319 | 538.95 |
| | | | 12–14 | 8.140 | 3.454 | – | 26.319 | 546.00 |
| | | | 14–16 | 7.870 | 3.504 | .0 | 25.669 | 530.73 |
| | | | 16–18 | 8.002 | 3.860 | .0 | 25.533 | 528.43 |
| | | | 18–20 | 7.976 | 4.328 | 1.8 | 25.808 | 532.11 |
| | | | 22–24 | 8.007 | 3.124 | 0.9 | 25.663 | 537.35 |
| 4025 | GC185 | BHAT1 | 0–2 | 7.272 | 4.521 | .0 | 27.085 | 551.42 |
| | | | 2–4 | 7.551 | 4.654 | .0 | 27.359 | 552.05 |
| | | | 4–6 | 7.570 | 5.044 | .0 | 26.979 | 558.44 |
| | | | 6–8 | 7.477 | 4.686 | .0 | 27.646 | 561.54 |

Table 9.1. Porewater pH, carbon, sulfur, and anions. (Continued)

| Dive Number | Site | Station | Depth (cm) | pH | Dissolved Inorganic Carbon (mM) | Total Dissolved Sulfide (µM) | Sulfate (mM) | Chloride (mM) |
|---|---|---|---|---|---|---|---|---|
| | | | 8–10 | 7.465 | 6.468 | .0 | 27.526 | 559.80 |
| | | | 12–14 | 7.516 | – | .0 | 27.840 | 588.32 |
| 4027 | GC185 | BHST1 | 0–2 | 7.229 | 3.582 | .0 | 27.674 | 557.98 |
| | | | 2–4 | 7.718 | 2.960 | .0 | 27.333 | 555.98 |
| | | | 4–6 | 7.933 | 4.101 | .0 | 27.362 | 554.56 |
| | | | 6–8 | 8.072 | 3.637 | 1.3 | 27.485 | 548.95 |
| | | | 8–10 | 7.959 | 4.448 | 0.0 | 27.500 | 552.22 |
| | | | 10–12 | 7.903 | 3.975 | 25.3 | 27.798 | 555.46 |
| | | | 12–14 | 7.918 | 3.346 | 20.1 | 28.406 | 571.24 |
| | | | 16–18 | 7.742 | 3.385 | 34.9 | 27.614 | 552.74 |
| | | | 20–22 | 7.592 | 5.037 | 123.3 | 27.438 | 559.31 |
| 4028 | GC185 | BHB3 | 0–2 | 7.409 | 9.414 | 457.5 | 23.883 | 564.10 |
| | | | 2–4 | 7.433 | 13.225 | 5296.3 | 13.223 | 573.05 |
| | | | 4–6 | 7.532 | 28.631 | – | 2.260 | 560.16 |
| | | | 6–8 | 7.443 | – | 10598.0 | .0 | 556.26 |
| | | | 8–10 | 7.459 | 27.117 | 9756.0 | .0 | – |
| | | | 10–12 | 7.399 | 34.952 | 8390.0 | .0 | 560.84 |
| | | | 12–14 | 7.310 | – | 9175.9 | .0 | – |
| | | | 14–16 | 7.517 | 11.617 | 4759.8 | – | 560.27 |
| 4029 | GC234 | GCAT2 | 0–2 | 7.812 | 4.050 | 0.0 | 22.345 | 552.63 |
| | | | 2–4 | 7.783 | 5.655 | 386.1 | 22.025 | 553.81 |
| | | | 4–6 | 7.516 | 6.789 | 892.1 | 18.362 | 550.31 |
| | | | 6–8 | 7.468 | 12.821 | 791.0 | 14.294 | 556.91 |
| | | | 8–10 | 7.437 | 20.076 | 6090.7 | 7.368 | 561.71 |
| | | | 10–12 | 7.304 | 24.289 | 5073.3 | 3.824 | 584.54 |
| | | | 12–14 | – | – | – | 2.338 | – |
| | | | 14–16 | 7.390 | 20.136 | 2843.5 | 1.382 | – |
| | | | 16–18 | – | – | – | .0 | – |
| | | | 18–20 | 7.366 | 24.338 | 2634.5 | .0 | – |
| | | | 22–24 | 7.509 | 23.305 | 3958.4 | .0 | 576.48 |
| 4031 | GC234 | GCST1 | 0–2 | 7.464 | 4.078 | 0.0 | 27.982 | 558.34 |
| | | | 2–4 | 7.625 | 4.486 | 0.0 | 27.702 | 556.57 |
| | | | 4–6 | 7.826 | 5.231 | 3.4 | 27.602 | 564.75 |
| | | | 6–8 | 7.913 | 4.889 | 100.1 | 27.529 | – |
| | | | 8–10 | 7.754 | 3.569 | 247.5 | 27.403 | 553.26 |
| | | | 10–12 | 8.015 | 5.859 | 87.3 | 27.355 | 542.09 |
| | | | 12–14 | 7.964 | – | 113.2 | 27.486 | 559.87 |
| | | | 14–16 | 8.019 | 5.048 | 48.8 | 27.684 | 555.40 |
| | | | 18–20 | 8.017 | 7.304 | 34.9 | 27.829 | 555.82 |
| | | | 22–24 | 7.870 | 4.669 | 39.4 | 27.959 | 569.33 |
| 4031 | GC234 | GCST1 | 0–2 | – | – | .0 | – | – |
| | | | 2–4 | – | – | .0 | – | – |
| | | | 4–6 | – | – | .0 | – | – |
| | | | 6–8 | – | – | .0 | – | – |
| | | | 8–10 | – | – | .0 | – | – |
| | | | 10–12 | – | – | .0 | – | – |
| | | | 12–14 | – | – | .0 | – | – |
| | | | 14–16 | – | – | 11.2 | – | – |

Table 9.1. Porewater pH, carbon, sulfur, and anions. (Continued)

| Dive Number | Site | Station | Depth (cm) | pH | Dissolved Inorganic Carbon (mM) | Total Dissolved Sulfide (μM) | Sulfate (mM) | Chloride (mM) |
|---|---|---|---|---|---|---|---|---|
| | | | 18–20 | – | – | 42.7 | – | – |
| | | | 20–22 | – | – | 67.6 | – | – |
| 4032 | GC234 | GCAT1 | 0–2 | 7.372 | 3.733 | .0 | 27.899 | 553.83 |
| | | | 2–4 | 7.541 | 3.158 | .0 | 27.699 | 557.84 |
| | | | 4–6 | 7.829 | 4.413 | .0 | 27.556 | 555.81 |
| | | | 6–8 | 8.026 | 4.751 | .0 | 27.405 | 549.04 |
| | | | 8–10 | 8.144 | 4.865 | .0 | 27.291 | 542.55 |
| | | | 10–12 | 8.132 | 2.395 | .0 | 27.079 | 551.90 |
| | | | 12–14 | 7.898 | 4.946 | 24.3 | 27.833 | 597.08 |
| | | | 14–16 | 7.675 | 3.636 | 98.5 | 27.374 | – |
| 4036 | GC234 | GCJT1 | 0–2 | 7.324 | 3.810 | .0 | 27.223 | 556.27 |
| | | | 2–4 | 7.171 | 3.692 | .0 | 27.352 | 588.80 |
| | | | 4–6 | 7.309 | 4.551 | .0 | 27.363 | 557.10 |
| | | | 6–8 | 7.334 | 6.826 | .0 | 28.238 | 574.86 |
| | | | 8–10 | 7.648 | 4.168 | .0 | 28.484 | 583.98 |
| | | | 10–12 | 7.804 | 4.034 | .0 | 27.975 | 573.88 |
| | | | 12–14 | 7.585 | 3.710 | 52.7 | 27.577 | 523.17 |
| | | | 16–18 | 7.683 | 3.963 | .0 | 28.798 | 564.26 |
| 4037 | GC233 | BPAT1 | 0–2 | 7.306 | 4.067 | .0 | 28.847 | 577.69 |
| | | | 2–4 | 7.234 | 3.913 | .0 | 28.873 | 599.75 |
| | | | 4–6 | 7.601 | 1.793 | .0 | 28.059 | 546.25 |
| | | | 6–8 | 7.771 | 3.980 | .0 | 28.425 | 600.49 |
| | | | 8–10 | 7.986 | 3.724 | .0 | 28.977 | 580.26 |
| | | | 10–12 | 7.936 | 3.276 | .0 | 28.618 | 567.77 |
| | | | 12–14 | 7.878 | 4.361 | .0 | 25.459 | – |
| 4038 | GC233 | BPB2 | 0–2 | 7.579 | 5.525 | 638.4 | 25.564 | 641.13 |
| | | | 2–4 | 7.555 | 4.810 | 811.7 | 21.759 | 743.96 |
| | | | 4–6 | 7.304 | 7.833 | 2175.4 | 19.127 | 741.15 |
| | | | 6–8 | 7.318 | 7.900 | 1901.3 | 18.092 | 783.13 |
| | | | 8–10 | 7.263 | 8.307 | 2565.2 | 15.220 | 840.98 |
| | | | 10–12 | 7.077 | 11.975 | 4656.0 | 1.774 | – |
| | | | 12–14 | – | – | 4496.9 | – | – |
| 4040 | GB425 | GBUN1 | 0–2 | 7.397 | 2.285 | .0 | 28.929 | 585.36 |
| | | | 2–4 | 7.414 | 3.575 | .0 | 28.136 | 567.02 |
| | | | 4–6 | 7.547 | | .0 | 27.574 | 587.10 |
| | | | 6–8 | 7.710 | 4.411 | .0 | 27.302 | 577.89 |
| | | | 8–10 | 7.731 | 4.008 | 6.6 | 27.188 | 593.64 |
| | | | 10–12 | 7.747 | | 4.5 | – | – |
| | | | 12–14 | 7.436 | 3.681 | 250.9 | 27.806 | 606.73 |
| | | | 14–16 | 7.634 | 4.034 | .0 | 27.058 | 575.50 |
| | | | 16–18 | 7.641 | 3.788 | 17.2 | 26.450 | 638.28 |
| | | | 18–20 | – | – | – | – | – |
| 4042 | GC185 | BHM3 | 0–2 | 7.317 | 4.968 | 123.7 | 28.121 | 587.19 |
| | | | 2–4 | 7.503 | 5.443 | 300.0 | 26.184 | 703.06 |
| | | | 4–6 | 7.480 | 4.415 | 378.3 | 26.440 | 626.02 |
| | | | 6–8 | 7.416 | 6.123 | 572.9 | 26.941 | – |
| | | | 8–10 | 7.416 | 4.076 | 572.9 | 26.446 | 593.45 |
| | | | 10–12 | 7.411 | 5.034 | 481.3 | 26.042 | 676.85 |

Table 9.1. Porewater pH, carbon, sulfur, and anions. (Continued)

| Dive Number | Site | Station | Depth (cm) | pH | Dissolved Inorganic Carbon (mM) | Total Dissolved Sulfide (µM) | Sulfate (mM) | Chloride (mM) |
|---|---|---|---|---|---|---|---|---|
| | | | 14–16 | 7.532 | 5.088 | 355.4 | 25.979 | 576.14 |
| | | | 18–20 | 7.690 | 4.340 | 124.8 | 28.385 | 561.10 |
| 4043 | GC234 | GCB3 orange *Beggiatoa* | 0–2 | 7.431 | 6.415 | 992.6 | 26.619 | 565.32 |
| | | | 2–4 | 7.395 | 8.700 | 2893.3 | 21.209 | 558.91 |
| | | | 4–6 | 7.400 | 7.297 | 3863.6 | 22.107 | – |
| | | | 6–8 | 7.539 | 6.065 | 2244.9 | 24.543 | 606.71 |
| | | | 8–10 | 7.443 | 8.921 | 2533.4 | 22.277 | 576.81 |
| | | | 10–12 | 7.535 | 7.806 | 2500.9 | 21.322 | 573.50 |
| | | | 12–14 | 7.508 | 7.902 | 2528.9 | 20.438 | 559.46 |
| | | | 14–16 | 7.631 | 4.800 | 2368.5 | 21.139 | – |
| | | | 16–18 | 7.568 | 5.638 | 2006.0 | 24.489 | 473.32 |
| | | | 20–22 | 7.624 | 7.286 | 2079.2 | 23.413 | 600.58 |
| 4043 | GC234 | GCB3 off mat | 0–2 | 7.501 | 3.322 | .0 | 25.193 | 589.99 |
| | | | 2–4 | 7.766 | 4.729 | .0 | 26.121 | 628.57 |
| | | | 4–6 | 7.892 | 3.705 | .0 | 25.428 | 601.37 |
| | | | 6–8 | 8.037 | – | .0 | 25.614 | 574.05 |
| | | | 8–10 | 8.132 | 4.218 | .0 | 25.186 | 578.05 |
| | | | 10–12 | 8.083 | 7.117 | 6.5 | 26.935 | 596.32 |
| | | | 14–16 | 7.756 | 4.884 | 251.6 | 25.869 | 567.14 |
| | | | 18–20 | 7.547 | 3.550 | 409.5 | 26.958 | 613.84 |
| | | | 22–24 | 7.810 | 6.342 | 229.6 | 26.477 | – |
| | | | 26–28 | 7.527 | 5.211 | 306.0 | 27.464 | 677.01 |
| 4043 | GC234 | GCB3 white *Beggiatoa* | 0–2 | 7.410 | 6.849 | 515.7 | 29.067 | 558.71 |
| | | | 2–4 | 7.614 | 4.519 | 1097.0 | 25.401 | 567.54 |
| | | | 4–6 | 7.356 | 8.049 | 1712.9 | 25.523 | 586.51 |
| | | | 6–8 | 7.468 | – | – | – | – |
| | | | 8–10 | 7.538 | 4.802 | 1992.2 | 24.729 | 605.03 |
| | | | 10–12 | 7.250 | 7.795 | 2158.6 | 24.234 | 554.39 |
| | | | 12–14 | 7.487 | 9.913 | 2579.9 | 24.638 | 573.37 |
| | | | 14–16 | 7.532 | 8.514 | 2382.6 | 23.734 | 561.92 |
| | | | 16–18 | 7.525 | 7.255 | 2063.2 | 23.405 | 553.71 |
| | | | 18–20 | 7.545 | 7.168 | 1383.7 | 23.706 | 556.21 |
| 4044 | GC185 | BHAT2 | 0–2 | 7.204 | 4.368 | .0 | 28.380 | 680.18 |
| | | | 2–4 | 7.099 | 4.907 | .0 | 27.605 | 604.20 |
| | | | 4–6 | 7.298 | 4.452 | .0 | 27.803 | 637.58 |
| | | | 6–8 | 7.571 | 7.458 | .0 | 27.521 | 557.04 |
| | | | 8–10 | 7.731 | 5.284 | .0 | 28.358 | 677.69 |
| | | | 10–12 | 7.712 | 4.256 | .0 | 28.757 | 597.19 |
| | | | 12–14 | 7.895 | 5.070 | .0 | 28.209 | 597.50 |
| | | | 14–16 | 7.796 | 5.533 | .0 | 28.482 | 618.21 |
| | | | 18–20 | 7.739 | 5.186 | .0 | 28.268 | – |
| | | | 22–24 | 7.539 | 3.522 | 29.0 | 28.042 | 627.28 |

Table 9.1. Porewater pH, carbon, sulfur, and anions. (Continued)

| Dive Number | Site | Station | Depth (cm) | pH | Dissolved Inorganic Carbon (mM) | Total Dissolved Sulfide (µM) | Sulfate (mM) | Chloride (mM) |
|---|---|---|---|---|---|---|---|---|
| 4046 | GC185 | BHM4 | 0–2 | 7.287 | 5.138 | 1675.5 | 19.359 | 634.32 |
| | | | 2–4 | 7.528 | 24.715 | 7255.3 | 9.300 | 613.08 |
| | | | 4–6 | 7.462 | 17.071 | 3980.9 | 7.302 | 565.59 |
| | | | 6–8 | 7.437 | 29.688 | 10918.2 | 2.670 | 567.45 |
| | | | 8–9 | 7.552 | 27.497 | 4947.9 | 0.664 | 665.26 |
| 4047 | GC234 | GCJT2 | 0–2 | 7.917 | 6.100 | 427.9 | 27.659 | 663.92 |
| | | | 2–4 | 7.810 | 4.535 | 672.1 | 26.624 | 588.61 |
| | | | 4–6 | 7.737 | 5.771 | 584.3 | 27.508 | 595.70 |
| | | | 6–8 | 7.579 | 6.683 | 1656.5 | 25.078 | 575.78 |
| | | | 8–10 | 7.884 | 7.735 | 1580.2 | 24.515 | 588.20 |
| | | | 10–12 | 7.797 | 11.748 | 1931.8 | 23.408 | 595.25 |
| | | | 12–14 | 7.858 | 5.821 | 1901.3 | 24.200 | 623.18 |
| 4047 | GC234 | GCJT2 | 16–18 | 7.804 | 9.252 | 1992.9 | 23.846 | 620.93 |
| | | | 20–22 | 7.493 | 14.098 | 4831.7 | 15.013 | 612.62 |
| | | | 22–24 | 7.629 | 15.575 | 4600.6 | 11.481 | 738.28 |
| 4048 | GC234 | GCAT2 | 0–2 | 7.585 | 6.293 | 0.4 | 27.984 | 597.10 |
| | | | 2–4 | 7.902 | 4.818 | 6.3 | 27.896 | 605.84 |
| | | | 4–6 | 7.957 | 6.640 | 204.7 | 26.409 | 902.69 |
| | | | 6–8 | 7.604 | 8.949 | 2328.0 | 22.999 | 577.19 |
| | | | 8–10 | 7.380 | 13.103 | 4460.1 | 15.363 | 597.57 |
| | | | 10–12 | 7.453 | 22.202 | 9272.3 | 6.604 | 661.53 |
| | | | 12–14 | – | – | – | 3.569 | – |
| | | | 14–16 | 7.423 | 24.515 | 12672.5 | 1.006 | 570.93 |
| | | | 16–18 | – | – | – | 0.401 | – |
| | | | 18–20 | 7.428 | 26.595 | 9641.8 | .0 | 595.71 |
| | | | 20–22 | – | – | – | .0 | – |
| | | | 22–24 | 7.413 | 27.196 | 7942.1 | .0 | 579.04 |
| | | | 24–26 | 7.404 | 26.900 | 10205.5 | – | 595.38 |
| 4053 | GB425 | GBM2 | 0–2 | 7.435 | 11.637 | 2921.7 | 22.525 | 601.31 |
| | | | 2–4 | 7.438 | 18.448 | 8012.8 | .0 | – |
| | | | 4–6 | 7.604 | 18.561 | 8808.3 | – | 608.80 |
| | | | 6–8 | 7.564 | 11.602 | 7530.4 | .0 | – |
| | | | 8–10 | 7.486 | 16.109 | – | .0 | 695.04 |
| | | | 10–12 | 7.364 | 4.555 | 8819.6 | .0 | – |
| | | | 14–16 | 7.154 | 14.083 | 4455.5 | .0 | 951.52 |
| | | | 18–20 | 6.978 | 13.287 | 3055.3 | .0 | 870.30 |
| | | | 22–24 | 6.998 | 11.662 | 2541.9 | .0 | 1189.27 |
| | | | 28–30 | 7.116 | 13.137 | 2940.7 | .0 | 1044.96 |
| box | GC185 | BHBXC1 | 0–2 | 8.096 | 3.656 | 1.3 | 28.339 | 570.15 |
| | | | 2–4 | 7.933 | 4.223 | .0 | 27.881 | 558.15 |
| | | | 4–6 | 7.921 | 3.681 | .0 | 27.689 | 558.09 |
| | | | 6–8 | 7.846 | 2.609 | .0 | 27.177 | 549.63 |
| | | | 8–10 | 7.881 | 4.110 | .0 | 27.712 | 556.50 |
| | | | 10–12 | 7.845 | 4.138 | .0 | 27.238 | 552.69 |
| | | | 14–16 | 7.843 | 4.126 | .0 | 26.801 | 547.97 |
| | | | 18–20 | 7.775 | 3.332 | .0 | 26.785 | 551.69 |
| | | | 22–24 | 7.588 | 4.872 | .0 | 26.588 | – |

Table 9.1. Porewater pH, carbon, sulfur, and anions. (Continued)

| Dive Number | Site | Station | Depth (cm) | pH | Dissolved Inorganic Carbon (mM) | Total Dissolved Sulfide (µM) | Sulfate (mM) | Chloride (mM) |
|---|---|---|---|---|---|---|---|---|
| box | GC185 | BHUN2 | 0–2 | 7.466 | 11.382 | 961.3 | 23.552 | 629.35 |
| | | | 2–4 | 7.473 | 15.324 | 7018.2 | 12.955 | 759.90 |
| | | | 4–6 | 7.507 | 18.954 | 6988.2 | 11.112 | 638.97 |
| | | | 6–8 | 7.532 | 24.270 | 2783.3 | 7.486 | 556.55 |
| | | | 8–10 | 7.517 | 28.919 | 11070.8 | .0 | 565.28 |
| | | | 10–12 | 7.473 | 28.444 | 9697.2 | – | 619.89 |
| | | | 12–14 | 7.536 | 26.824 | 8819.6 | .0 | 658.24 |
| | | | 14–16 | 7.546 | 35.647 | 11304.9 | .0 | 562.09 |
| | | | 18–20 | 7.485 | 26.122 | 9907.0 | – | 611.22 |
| | | | 20–22 | 7.486 | 26.900 | 12710.4 | .0 | 616.33 |
| box | GC234 | GCBX2 | 0–2 | 7.367 | 3.941 | .0 | 29.425 | – |
| | | | 2–4 | 7.290 | 3.598 | .0 | 26.881 | – |
| | | | 4–6 | 7.348 | 4.332 | .0 | 27.206 | – |
| | | | 6–8 | 7.441 | 4.168 | .0 | 27.994 | – |
| | | | 8–10 | 7.484 | 3.834 | .0 | 24.480 | 603.77 |
| | | | 10–12 | 7.492 | 4.569 | .0 | 25.715 | 559.29 |
| | | | 14–16 | – | – | – | – | – |
| | | | 18–20 | 7.806 | 4.648 | .0 | – | – |
| | | | 22–24 | 7.952 | 4.569 | .0 | – | – |
| | | | 26–28 | 7.707 | 4.411 | .0 | – | – |
| box | GC234 | GCBXC1 | 0–2 | 7.907 | 4.676 | .0 | 27.252 | 554.19 |
| | | | 2–4 | 8.030 | | 577.8 | 26.047 | 550.44 |
| | | | 4–6 | 7.902 | 3.740 | 630.8 | 26.725 | 555.21 |
| | | | 6–8 | 7.856 | 4.701 | 275.8 | 26.885 | 556.82 |
| | | | 8–10 | 8.026 | 6.248 | 320.3 | 28.017 | 573.35 |
| | | | 10–12 | 7.958 | 4.137 | 131.6 | 27.639 | 556.79 |
| | | | 14–16 | 8.009 | 4.404 | 69.1 | 28.060 | 566.86 |
| | | | 18–20 | 7.897 | 4.521 | 218.7 | 27.551 | – |
| | | | 22–24 | 7.870 | 3.759 | 206.9 | 27.420 | 564.79 |
| | | | 28–30 | 7.427 | 3.184 | 192.4 | 27.707 | – |
| box | GC234 | GCBXC1 | 0–2 | – | – | .0 | – | – |
| | | | 2–4 | – | – | – | – | – |
| | | | 4–6 | – | – | 299.9 | – | – |
| | | | 6–8 | – | – | 154.5 | – | – |
| | | | 8–10 | – | – | 304.3 | – | – |
| | | | 10–12 | – | – | 129.0 | – | – |
| | | | 14–16 | – | – | 149.1 | – | – |
| | | | 18–20 | – | – | 293.4 | – | – |
| | | | 22–24 | – | – | 346.4 | – | – |
| | | | 28–30 | – | – | 363.2 | – | – |

As described in the Introduction, hydrogen sulfide and dissolved bicarbonate produced by bacterially mediated reduction reactions, Equations (9-3) and (9-4), can be in turn consumed in sulfide and carbonate mineral formation. The relationship of these processes determines the availability of dissolved sulfide, for example, for use as a reductant in the fixation of $CO_2$ by chemolithoautotrophic bacteria such as *Beggiatoa* and other sulfide oxidizers. Carbonate mineral formation within the surface sediment also creates a hard substrate for attached biota such as vestimentiferan tubeworms. Because of the central importance of sulfate reduction in these processes, most of this discussion describes how reduction rates vary throughout the study area and how this variation relates to other measured pore water and sediment properties.

**Limitation of sulfate reductor.** As can be seen from reaction (9-3), the extent of sulfate reduction is limited by two factors: the supply of metabolizable organic matter and/or seawater sulfate. One of the critical differences between seep and normal benthic marine environments is the overall abundance of organic matter in the form of liquid hydrocarbons and dissolved methane gas. At most stations in which extensive sulfate reduction was observed (stations classified as active, see below), gas was also observed freely bubbling from cores during recovery. This indicates super saturation under surface conditions. Organic carbon concentrations are substantially higher and more variable than elsewhere in the northern Gulf of Mexico. Continental shelf and slope transects by Linn and Morse (1991) showed organic carbon to vary between 0.3 and 1.5 wt %, with an overall mean of 0.71 ± 0.27 wt %. In contrast, organic carbon concentrations here (see Table 9.1) ranged from 0.2 to 13.1 wt %. Organic carbon data are presented in Figure 9.1. Figure 9.1A shows the asymmetric frequency distribution of organic carbon, in which the greatest frequency of samples contained between 1 and 1.5 wt % organic carbon. Mean values for 1997 and 1998 cruises were 4.4 ± 2.6 and 3.9 ± 2.7 wt %, respectively. Figure 9.1B also indicates that these sediments are predominantly fine-grained, with the greatest frequency having a mass fraction less than 65 μm in diameter of approximately 90% (mean 84±12%). Furthermore, Figure 9.1C also suggests that samples with decreasing grain sizes tended to be richer in organic carbon. DOC concentrations vary widely throughout the study area (range 5.8-42289 μM, mean 10105 ± 7701 μM), but do not correlate well with other measured parameters. Nutrients concentrations also do not tend to show any obvious relationship to other pore water or solid phase data. However, concentrations do tend to be higher at "M" (mussel) stations, and ammonia levels at GBM2 are more than an order of magnitude higher than elsewhere (3940 μM versus a mean of 286 μM).

**Stations classified by sulfate reduction rates.** The variation in the extent and intensity of sulfate reduction is large, as quantified both by measured sulfate reduction rates and the relative distribution of sulfate versus sulfide. These parameters are used here to distinguish between stations that are either active or inactive; they are summarized in Table 9.2. The variation in integrated sulfate reduction rates is also shown graphically in Figure 9.2. The choice of these terms is somewhat arbitrary, the important distinction being that active areas show clear evidence of intense sulfate reduction, either in terms of a high integrated sulfate reduction rate (SRR > 50 mmoles-sulfate m$^{-2}$ day$^{-1}$), or in terms of depleted sulfate and calcium and elevated concentrations of sulfide and DIC. By comparison, inactive areas lack evidence of significant
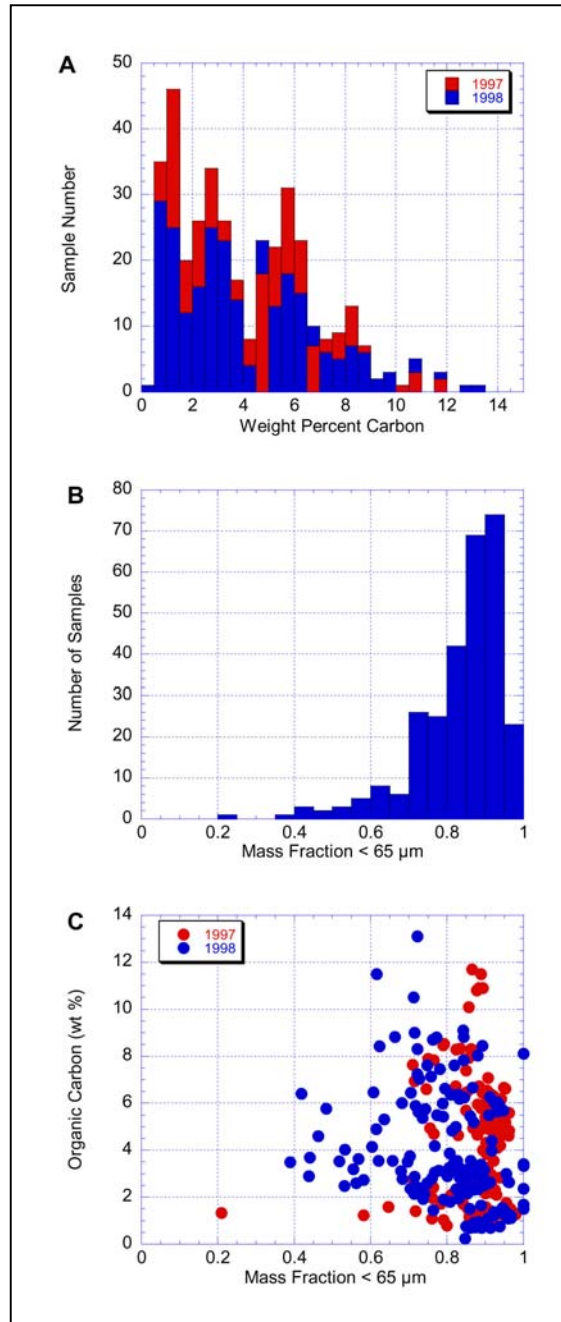
Figure 9.1.  Organic carbon and grain size distributions. (A) *Organic carbon frequency distribution.* Note here that the distribution for both years is similar and distinctly asymmetric, with the greatest number of samples falling between 1 and 1.5 wt % organic carbon. Mean values for 1997 and 1998 cruises were 4.4±2.6 and 3.9±2.7 wt %, respectively. These sediments are thus richer in organic carbon than is typical: Lin and Morse (1991) reported a mean of 0.71±0.27 wt % for Mississippi River delta and adjacent continental shelf and slope sediments. (B) *Grain size distribution.* These sediments are predominantly fine-grained. The largest number of sediment samples have a mass fraction less than 65 μm in diameter of ~90%, with a mean of 84±12%. (C) *Relationship of organic carbon and grain size distributions.* As sediments become more fine-grained (increasing mass fraction of grains < 65 μm in diameter), organic carbon content increases as well. This may reflect dilution of seep sediment by influx of coarser-grained material relatively poor in organic carbon.

Table 9-2.  Summary of sulfate reduction

| | Dive | Site | Station | integrated SRR[3] mmoles/m²/day | Excess Chloride | >10% calcium depletion | >10% sulfate depletion | DIC > 4 mM | H$_2$S >1000 M |
|---|---|---|---|---|---|---|---|---|---|
| **inactive** | 4043 | GC234 | GCB3 off mat | — | | | | | |
| | 2876 | GC233 | BPR2 | — | | | | | |
| | box | GC234 | GCBX2 | — | | | | | |
| | box | GC185 | BHBC2 | — | | | | | |
| | box | GC234 | GCBXC1 | — | | | | | |
| | 4040 | GB425 | GBUN1 | — | | | | | |
| | 4037 | GC233 | BPAT1 | — | | | | | |
| | 2873 | GC185 | BHAT1 | 13.8 | | | | | |
| | 4025 | GC185 | BHAT1 | — | | | | | |
| | 4027 | GC185 | BHST1 | 14.4 | | | | | |
| | 2888 | GC234 | GCAT1 | 16.5 | | | | | |
| | 4032 | GC234 | GCAT1 | — | | | | | |
| | 2875 | GC185 | BHST2 | 19.7 | | | | | |
| | box | GC185 | BHUN2 (1997) | 20.0 | | | | | |
| | 2875 | GC185 | BHUN1 | 20.7 | | | | | |
| | 2871 | GC234 | GCST1 | 21.3 | | | | | |
| | 4042 | GC185 | BHM3 | — | | | | | |
| | 2873 | GC185 | BHM4 | 22.1 | | | | | |
| | 2874 | GC185 | BHST1 | 23.0 | | | | | |
| | box | GC185 | BHBXC1 | — | | | | | |
| | 4031 | GC234 | GCST1 | 28.6 | | | | | |
| | box | GC185 | BHBC2 | 29.8 | | | | | |
| | 2891 | GC185 | BHAT2 | 32.2 | | | | | |
| | 4044 | GC185 | BHAT2 | — | | | | | |
| | 2883 | GB425 | GBM1 | 55.0 | | | | | |
| **brines** | 2882 | GB425 | GBM2 (GBB1@GBM2) | 1541.2[2] | x | 2 | x | x | 2 |
| | 2885 | GB425 | GBM2 | — | x | 2 | x | x | 2 |
| | 4053 | GB425 | GBM2 | 348.0 | x | 2 | x | x | 2 |
| | 4038 | GC233 | BPB2 | 57.7 | x | 2 | x | x | 2 |
| **active** | 4028 | GC185 | BHB3 | 8.2 | x | x | x | x |
| | 4043 | GC234 | GCB3 white *Beggiatoa* | 13.7 | x | x | x | x |
| | 2880 | GC234 | GCAT1 (GCB1@GCAT1) | 13.8 | x | x | x | x |
| | 4047 | GC234 | GCJT2 | 23.4 | x | x | x | x |
| | 4046 | GC185 | BHM4 | 6.0 | x | x | x | x |
| **high** | 4043 | GC234 | GCB3 orange *Beggiatoa* | 244.3 | x | x | x | x |
| | box | GC185 | BHUN2 (1998) | 374.5 | x | x | x | x |
| | 4048 | GC234 | GCAT2 | 458.5 | x | x | x | x |
| **extreme** | 4029 | GC234 | GCAT2 | 1585.2[1] | x | x | x | x |
| | 2886 | GC234 | GCAT2 | 1635.9 | x | x | x | x |
| | 2872 | GC234 | GCAT2 | 2452.5 | x | x | x | x |

*Notes*
[1] Indicates a maximum value; incubations of shorter duration gave lower integrated rates.
[2] Sulfate reduction (and resulting sulfide accumulation and calcium depletion) associated with brines is limited to the mixing zone between seawater and the brine end member. Brine end member is Na-Ca-Cl in composition, and contains essentially no sulfide or sulfate.
[3] Integrated rates were calculated by summing the area under the sulfate reduction rate curve with respect to depth. Missing data (–) indicate that no sulfur-35 core was available, or no extraction was done due to negligible sulfide concentrations observed in porewater sample core.
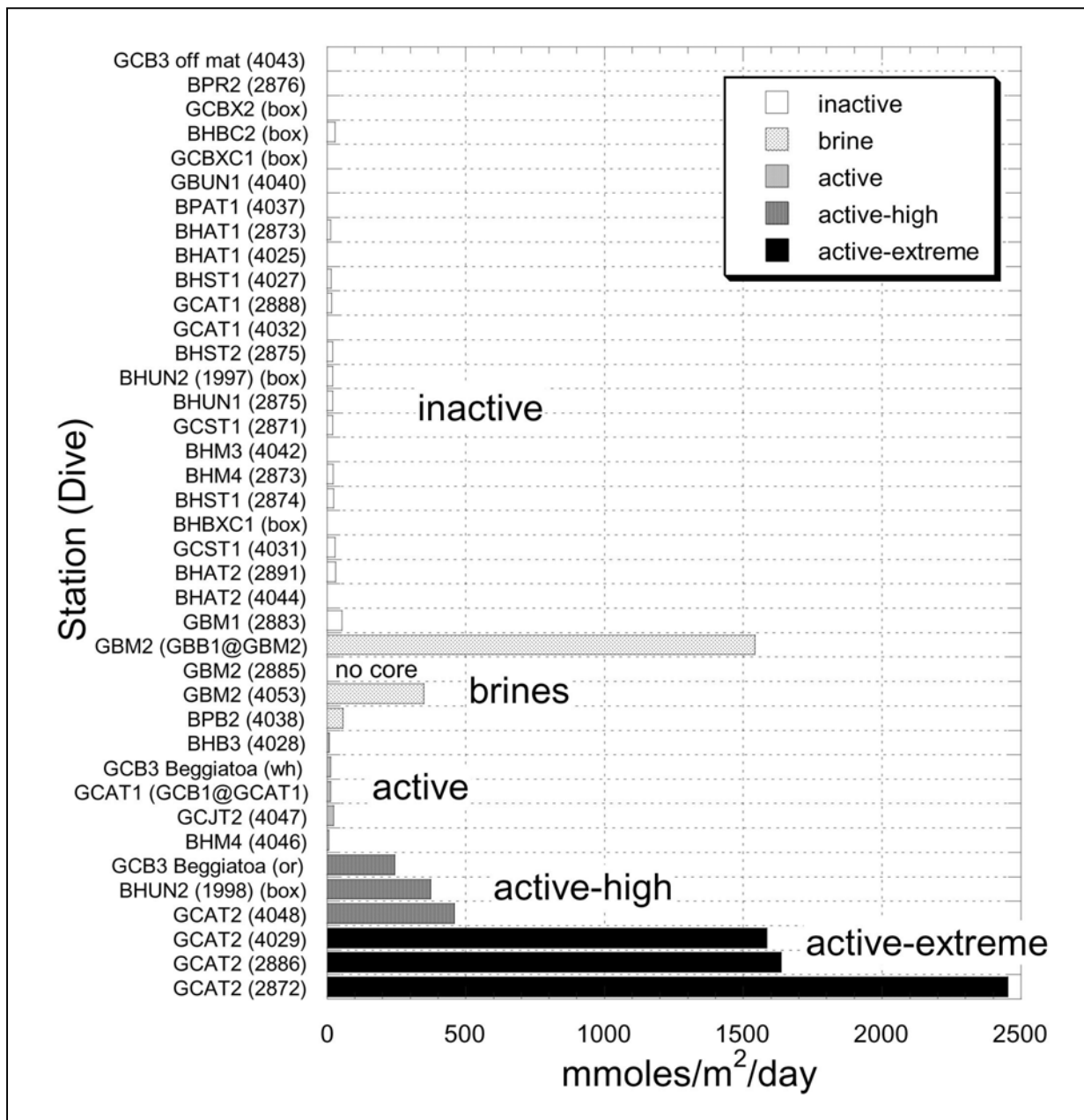
Figure 9.2.    Characterization of chemosynthetic sample stations by sulfate reduction. Stations are categorized as *active* or *inactive* according to overall evidence of sulfate reduction, either in terms of a high integrated sulfate reduction rate (SRR > 50 mM-sulfate $m^{-2}$ $day^{-1}$) or depleted sulfate and calcium and elevated concentrations of sulfide and DIC. Inactive areas lack evidence of significant sulfate reduction in terms of low integrated reduction rates (<10 to 50 mmoles-sulfate $m^{-2}$ $day^{-1}$) and porewater compositions that are only slightly modified from normal seawater (sulfide concentrations less than ~250 μM, negligible depletion of sulfate, DIC concentrations less than two times seawater). Although not all active stations showed high measured sulfate reduction rates, they clearly exhibit significant production of sulfide at the expense of sulfate. *Active-high* stations record integrated rates from 50 to 1000 mM-sulfate $m^{-2}$ $day^{-1}$), and rates at *active-extreme* stations exceed >1000 mM-sulfate $m^{-2}$ $day^{-1}$. *Brines* stations may show high measured sulfate reduction rates confined to the shallow interval where brine mixing is minimal.

9-17

sulfate reduction. Inactive areas have low integrated reduction rates (<10 to 50 mmoles-sulfate $m^{-2}$ $day^{-1}$) and pore water compositions that are only slightly modified from normal seawater. Furthermore, sulfide concentrations at inactive stations are typically less than approximately 250 µM with negligible depletion of sulfate, DIC concentrations that are less than two times seawater, and the chloride and major ion compositions that are more or less invariant with respect to standard seawater. This group comprises the largest number of stations, and with the possible exception of bacterial mats, does not distinguish itself biologically in any obvious way. According to the station descriptors (AT, JT, ST, M, etc.), it is variously dominated by tubeworms (adult, juvenile, senescent) and mussels. Although the discrimination between active and inactive is an operational one, sulfate reduction rates measured at inactive stations agree with the averages of (non-seep) rates measured in the northern Gulf of Mexico (Table 9.3).

Active stations include BHUN2 (1998 core), BHM4 (dive 4046), BHB3, GCAT1 (dive 2880), GCAT2, GCB3, and GCJT2. Note that although not all active stations showed high measured sulfate reduction rates (SRR), they clearly exhibit significant production of sulfide at the expense of sulfate. In addition, integrated rates at certain active sites are so high as to merit further division of this category to high (50 to 1000 mmoles-sulfate $m^{-2}$ $day^{-1}$) and extreme (>1000 mmoles-sulfate $m^{-2}$ $day^{-1}$). Active-high stations thus include BHUN2 (1998 core), GCAT2-dive 4048 and GCB3 (orange *Beggiatoa* mat); active-extreme stations are limited to GCAT2 (dives 2872, 2886, 4029). The most important station in terms of defining the relationship between SRR and other measured parameters is GCAT2. In addition, SRR experiments using cores recovered during dive 4029 used variable incubation times of 4.1, 8.5, and 13.3 hours and gave integrated rates of 1585, 86, and 84 mmols/$m^2$/d, respectively. This behavior of increasing apparent rate with decreasing reaction time suggests that these rates probably represent minimum values, although it is also possible (but unlikely) that this variation reflects lateral heterogeneity as well.

These rates probably constitute the highest ever measured in marine sediments. Comparison with data compiled from various sources in Table 9.3 indicates that they exceed the highest rates measured in the Gulf of Mexico (which agree well with those of inactive stations) by at least two orders of magnitude (Lin and Morse 1991). In addition, certain stations show clear evidence of mixing between seawater and a sodium-calcium-chloride brine end member, and these stations (GBM2 and BPB2) form a separate category in Table 9.2. Sulfate reduction in these stations may also be very high but is limited to the shallow interval just below the sediment-water interface. Brine mixing is only locally important and is discussed below.

The observed co-variations in sulfate, DIC, sulfide, and calcium at active sites can be understood by recognizing the essential stoichiometric relationships among these components. As sulfate reduction proceeds according to Equations (9-3) or (9-4), DIC and sulfide are produced at the expense of sulfate and organic material. These relationships may be used to calculate an apparent extent of sulfate reduction, by comparing the amount of so-called reduced sulfate with excess DIC. Reduced sulfate is calculated as the difference between an initial seawater concentration of sulfate and the sulfate concentration observed in pore fluid. This difference is normalized to chloride to remove any differences in overall salinity. If there is no sulfate reduction, the reduced sulfate value will be zero. If sulfate reduction is completed, the reduced sulfate value will be 28.898 mM/L (the standard concentration at a salinity of 35 psu). Excess DIC concentrations are

Table 9.3.  Major cations.

| Dive Number | Site | Station | Depth (cm) | Ba (µM) | Ca (mM) | Mg (mM) | K (mM) | Na (mM) | Sr (mM) | Fe (µM) | Mn (µM) |
|---|---|---|---|---|---|---|---|---|---|---|---|
| 2871 | GC234 | GCST1 | 0-2 | .0 | 12.266 | 59.447 | 12.899 | 498.75 | 0.1100 | 19.3 | 1.2 |
| | | | 2-4 | 2.96 | 10.927 | 50.937 | 12.419 | 454.16 | 0.0946 | 21.1 | 1.2 |
| | | | 4-6 | .0 | 9.033 | 40.883 | 9.095 | 354.45 | 0.0637 | 21.3 | 3.2 |
| | | | 6-8 | .0 | 10.038 | 49.873 | 11.841 | 454.33 | 0.0839 | 19.7 | 2.2 |
| | | | 10-12 | .0 | 16.224 | 50.751 | 12.139 | 452.29 | 0.0884 | 19.5 | 1.7 |
| | | | 12-14 | .0 | 9.983 | 50.349 | 11.671 | 444.70 | 0.0855 | 21.2 | 1.7 |
| | | | 14-16 | .0 | 10.061 | 49.724 | 11.722 | 441.31 | 0.0874 | – | – |
| | | | 16-18 | 3.02 | 8.968 | 40.087 | 10.700 | 357.56 | 0.0798 | – | – |
| | | | 18-20 | .0 | 10.140 | 50.239 | 11.914 | 449.33 | 0.0842 | 37.9 | 3.7 |
| 2873 | GC235 | BHAT1 | 0-2 | 4.20 | 10.758 | 49.410 | 11.493 | 437.40 | 0.0998 | 22.9 | 1.7 |
| | | | 2-4 | .0 | 9.804 | 48.717 | 10.695 | 431.25 | 0.0819 | 24.3 | 1.2 |
| | | | 4-6 | .0 | 9.903 | 49.542 | 11.092 | 438.38 | 0.0817 | 17.6 | 1.7 |
| | | | 6-8 | .0 | 10.798 | 49.183 | 10.944 | 428.04 | 0.0837 | 25.0 | 1.2 |
| | | | 8-10 | .0 | 10.229 | 48.707 | 11.543 | 436.93 | 0.0883 | 21.0 | 1.7 |
| | | | 10-12 | .0 | 9.629 | 49.411 | 10.862 | 448.46 | 0.0788 | 21.7 | 1.7 |
| | | | 12-14 | .0 | 9.539 | 47.497 | 10.663 | 424.45 | 0.0783 | 19.3 | 1.2 |
| | | | 14-16 | .0 | 9.877 | 49.202 | 11.272 | 438.15 | 0.0825 | 17.8 | 3.2 |
| 2873 | GC235 | BHM4 | 0-2 | 4.58 | 9.175 | 54.916 | 12.329 | 505.02 | 0.0844 | 20.9 | 1.7 |
| | | | 2-4 | 5.05 | 7.782 | 50.042 | 10.992 | 450.41 | 0.0660 | 22.0 | 1.2 |
| | | | 4-6 | .0 | 1.560 | 52.628 | 11.983 | 474.26 | 0.0178 | 16.5 | 1.2 |
| | | | 6-8 | 6.67 | 5.312 | 53.839 | 13.374 | 495.71 | 0.0465 | 4.5 | .0 |
| | | | 8-10 | 4.25 | 4.803 | 48.034 | 11.509 | 445.84 | 0.0419 | 4.1 | 4.8 |
| | | | 10-12 | .0 | 0.620 | 68.180 | 16.112 | 642.92 | 0.0000 | 2.4 | 5.6 |
| | | | 12-14 | 4.78 | 5.157 | 49.042 | 12.765 | 457.27 | 0.0486 | 6.4 | 1.8 |
| | | | 14-16 | 5.75 | 5.473 | 49.610 | 12.476 | 462.03 | 0.0505 | 18.6 | 1.7 |
| | | | 16-18 | 5.43 | 4.357 | 48.101 | 12.722 | 445.97 | 0.0504 | 2.8 | 1.0 |
| | | | 18-20 | 4.17 | 2.664 | 51.575 | 13.242 | 479.82 | 0.0327 | 2.1 | 1.4 |
| 2874 | GC235 | BHST1 | 0-2 | 3.06 | 11.291 | 54.740 | 12.747 | 471.77 | 0.0850 | 19.3 | 1.4 |
| | | | 2-4 | 2.68 | 10.346 | 48.773 | 11.933 | 440.29 | 0.0894 | 21.1 | – |
| | | | 4-6 | .0 | 9.214 | 48.138 | 11.154 | 443.04 | 0.0773 | – | – |
| | | | 6-8 | .0 | 9.656 | 50.020 | 11.379 | 450.46 | 0.0733 | 15.8 | 1.0 |
| | | | 8-10 | .0 | 9.246 | 48.528 | 10.876 | 437.34 | 0.0762 | 17.6 | 1.2 |
| | | | 10-12 | .0 | 9.054 | 47.697 | 11.492 | 437.31 | 0.0765 | 17.6 | 1.2 |
| | | | 12-14 | 4.19 | 9.710 | 51.365 | 12.257 | 477.49 | 0.0834 | 20.8 | 1.7 |
| | | | 14-16 | .0 | 9.978 | 50.451 | 10.454 | 440.29 | 0.0823 | 20.6 | 1.2 |
| | | | 16-18 | .0 | 8.904 | 49.718 | 11.935 | 454.79 | 0.0761 | 6.1 | .0 |

Table 9-3. Major cations. (continued)

| Dive Number | Site | Station | Depth (cm) | Ba (µM) | Ca (mM) | Mg (mM) | K (mM) | Na (mM) | Sr (mM) | Fe (µM) | Mn (µM) |
|---|---|---|---|---|---|---|---|---|---|---|---|
| 2875 | GC235 | BHST2 | 0-2 | .0 | 9.898 | 49.156 | 11.102 | 433.33 | 0.0797 | 18.2 | .0 |
| | | | 2-4 | .0 | 9.550 | 47.743 | 10.723 | 428.57 | 0.0783 | 21.4 | 1.7 |
| | | | 4-6 | .0 | 10.191 | 48.843 | 11.511 | 441.20 | 0.0875 | 19.4 | 1.2 |
| | | | 6-8 | .0 | 8.041 | 41.856 | 8.909 | 379.19 | 0.0612 | 19.2 | 1.2 |
| | | | 8-10 | 2.57 | 10.402 | 48.816 | 12.009 | 438.95 | 0.0914 | 21.1 | 1.2 |
| | | | 10-12 | .0 | 10.011 | 49.797 | 11.269 | 445.67 | 0.0857 | 19.4 | 1.2 |
| 2875 | GC235 | BHUN1 | 0-2 | .0 | 9.909 | 50.012 | 10.485 | 446.22 | 0.0838 | 15.8 | 2.1 |
| | | | 2-4 | .0 | 10.083 | 49.807 | 11.072 | 446.20 | 0.0866 | 12.3 | 1.8 |
| | | | 4-6 | .0 | 9.813 | 50.060 | 11.451 | 452.05 | 0.0812 | 12.2 | 1.8 |
| | | | 6-8 | .0 | 9.689 | 49.048 | 11.415 | 439.74 | 0.0808 | 12.3 | 1.0 |
| | | | 8-10 | .0 | 9.757 | 48.756 | 11.670 | 442.13 | 0.0825 | 19.3 | 1.0 |
| | | | 10-12 | 2.33 | 10.583 | 49.674 | 12.809 | 454.84 | 0.0932 | 13.8 | 1.0 |
| | | | 12-14 | .0 | 9.769 | 48.887 | 11.907 | 444.79 | 0.0816 | 15.9 | 1.0 |
| | | | 14-16 | .0 | 9.759 | 48.236 | 12.086 | 447.71 | 0.0828 | 14.1 | 1.0 |
| | | | 16-18 | .0 | 9.701 | 48.827 | 11.261 | 431.86 | 0.0772 | 14.0 | 1.4 |
| | | | 18-20 | .0 | 9.724 | 48.606 | 11.825 | 441.30 | 0.0820 | 12.2 | 1.4 |
| | | | 22-24 | .0 | 9.848 | 48.041 | 11.705 | 434.99 | 0.0821 | 36.3 | 1.0 |
| | | | 26-28 | .0 | 9.965 | 49.684 | 12.541 | 454.58 | 0.0851 | 21.2 | 1.4 |
| 2876 | GC233 | BPR2 | 0-2 | .0 | 9.514 | 47.688 | 10.648 | 423.96 | 0.0785 | 21.1 | 1.2 |
| | | | 2-4 | .0 | 8.598 | 43.345 | 9.860 | 385.70 | 0.0755 | 14.7 | 1.6 |
| | | | 4-6 | .0 | 8.654 | 43.163 | 10.541 | 393.69 | 0.0756 | 15.8 | 1.4 |
| | | | 6-8 | .0 | 8.488 | 41.899 | 10.483 | 386.95 | 0.0738 | 16.8 | 1.0 |
| | | | 8-10 | .0 | 9.393 | 45.633 | 11.381 | 421.72 | 0.0813 | 14.0 | 2.1 |
| | | | 10-12 | 2.23 | 10.289 | 48.801 | 12.492 | 446.92 | 0.0951 | 15.9 | 1.0 |
| 2880 | GC234 | GCB1@GCAT1 | 0-2 | .0 | 10.336 | 51.522 | 11.309 | 466.32 | 0.0883 | 15.9 | 3.1 |
| | | | 2-4 | .0 | 9.562 | 49.290 | 11.328 | 450.56 | 0.0816 | 14.0 | 2.1 |
| | | | 4-6 | .0 | 9.615 | 48.501 | 11.534 | 432.61 | 0.0893 | 0.8 | .0 |
| | | | 6-8 | .0 | 8.981 | 49.417 | 12.061 | 451.85 | 0.0838 | 4.2 | .0 |
| | | | 8-10 | .0 | 8.293 | 47.883 | 10.957 | 431.80 | 0.0794 | 1.8 | .0 |
| | | | 10-12 | .0 | 8.811 | 49.134 | 11.243 | 441.55 | 0.0852 | 3.7 | .0 |
| | | | 12-14 | 2.66 | 9.274 | 49.326 | 12.593 | 446.48 | 0.0946 | 1.6 | 2.5 |
| | | | 14-16 | .0 | 8.944 | 48.521 | 11.491 | 435.75 | 0.0889 | 3.4 | .0 |
| | | | 16-18 | .0 | 8.093 | 47.970 | 11.126 | 433.53 | 0.0776 | 8.8 | 1.4 |
| | | | 18-20 | .0 | 7.891 | 47.382 | 11.242 | 427.08 | 0.0778 | – | 2.9 |
| | | | 22-24 | .0 | 8.373 | 48.096 | 11.529 | 435.59 | 0.0849 | 13.9 | 1.8 |

Table 9.3. Major cations. (continued)

| Dive Number | Site | Station | Depth (cm) | Ba (μM) | Ca (mM) | Mg (mM) | K (mM) | Na (mM) | Sr (mM) | Fe (μM) | Mn (μM) |
|---|---|---|---|---|---|---|---|---|---|---|---|
| 2882 | GB425 | GBB1@GBM2 | 0-2 | .0 | 12.851 | 44.241 | 10.006 | 504.87 | 0.1420 | 3.2 | 1.8 |
| | | | 2-4 | 5.91 | 18.180 | 40.523 | 12.236 | 642.02 | 0.2377 | 17.9 | .0 |
| | | | 4-6 | 87.35 | 27.644 | 38.123 | 14.160 | 894.70 | 0.6063 | 18.2 | .0 |
| | | | 6-8 | 1555.48 | 35.978 | 36.776 | 15.683 | 1070.21 | 0.9585 | 21.1 | .0 |
| | | | 8-10 | .0 | 43.669 | 36.873 | 17.428 | 1267.27 | 1.2258 | 18.0 | .0 |
| | | | 10-12 | .0 | 43.939 | 35.419 | 17.059 | 1292.72 | 1.2119 | 17.9 | .0 |
| | | | 12-14 | .0 | 44.246 | 36.038 | 17.532 | 1359.84 | 1.2011 | – | – |
| | | | 14-16 | .0 | 43.527 | 36.029 | 17.618 | 1403.87 | 1.1662 | – | – |
| | | | 16-18 | .0 | 46.415 | 35.227 | 18.934 | 1352.86 | 1.2439 | – | – |
| | | | 18-20 | .0 | 49.776 | 37.044 | 20.277 | 1437.00 | 1.3139 | – | – |
| | | | 22-24 | .0 | 48.540 | 36.604 | 20.163 | 1434.48 | 1.2886 | – | – |
| | | | 26-28 | .0 | 45.231 | 36.664 | 22.988 | 1417.89 | 1.2349 | – | – |
| 2883 | GB425 | GBM1 | 0-2 | .0 | 10.432 | 50.306 | 11.111 | 456.16 | 0.0876 | 12.1 | 1.4 |
| | | | 2-4 | – | – | – | – | – | – | 12.3 | 1.0 |
| | | | 4-6 | 2.92 | 11.040 | 49.558 | 11.742 | 442.40 | 0.1014 | 14.0 | 1.4 |
| | | | 6-8 | .0 | 10.398 | 50.188 | 11.683 | 461.64 | 0.0923 | – | – |
| | | | 8-10 | 2.71 | 11.103 | 49.388 | 12.053 | 452.64 | 0.1096 | 1.7 | .0 |
| | | | 10-12 | .0 | 10.887 | 49.288 | 11.548 | 460.28 | 0.1108 | – | – |
| | | | 12-14 | .0 | 11.114 | 49.719 | 11.979 | 479.38 | 0.1098 | 17.4 | 1.4 |
| | | | 14-16 | .0 | 11.455 | 48.027 | 11.796 | 464.76 | 0.1207 | 12.3 | 1.4 |
| | | | 16-18 | 3.51 | 11.969 | 49.972 | 13.270 | 473.06 | 0.1174 | – | – |
| 2885 | GB425 | GBM2 | 0-2 | .0 | 16.302 | 45.588 | 9.460 | 615.22 | 0.1147 | 16.3 | .0 |
| | | | 2-4 | 40.99 | 27.457 | 38.365 | 8.914 | 982.14 | 0.4249 | 19.6 | 2.9 |
| | | | 4-6 | .0 | 33.038 | 32.922 | 9.270 | 1253.33 | 1.0885 | 17.9 | 1.7 |
| | | | 6-8 | .0 | 37.910 | 34.763 | 10.985 | 1363.76 | 1.2961 | 17.8 | .0 |
| | | | 8-10 | .0 | 34.624 | 31.983 | 9.641 | 1348.74 | 1.1705 | – | – |
| | | | 10-12 | – | – | – | – | – | – | – | – |
| | | | 12-14 | .0 | 37.636 | 31.817 | 10.201 | 1335.30 | 1.1885 | – | – |
| | | | 14-16 | – | – | – | – | – | – | 50.8 | .0 |
| | | | 16-18 | – | – | – | – | – | – | 16.4 | 1.2 |
| 2886 | GC234 | GCAT2 | 0-2 | 3.30 | 9.070 | 49.006 | 11.578 | 445.33 | 0.0884 | 16.6 | .0 |
| | | | 2-4 | .0 | 7.819 | 47.891 | 10.331 | 444.55 | 0.0727 | 18.6 | .0 |
| | | | 4-6 | .0 | 8.371 | 47.831 | 10.734 | 436.58 | 0.0796 | 18.4 | .0 |
| | | | 6-8 | .0 | 4.916 | 47.836 | 11.087 | 445.10 | 0.0684 | 16.4 | .0 |
| | | | 8-10 | .0 | 5.034 | 47.636 | 11.181 | 446.64 | 0.0684 | 18.7 | .0 |
| | | | 10-12 | .0 | 3.976 | 45.752 | 10.626 | 431.99 | 0.0638 | – | – |

Table 9.3. Major cations. (continued)

| Dive Number | Site | Station | Depth (cm) | Ba (µM) | Ca (mM) | Mg (mM) | K (mM) | Na (mM) | Sr (mM) | Fe (µM) | Mn (µM) |
|---|---|---|---|---|---|---|---|---|---|---|---|
| | | | 12-14 | .0 | 2.554 | 48.955 | 11.916 | 473.15 | 0.0601 | 20.7 | .0 |
| | | | 14-16 | 4.90 | 5.098 | 47.011 | 10.832 | 439.90 | 0.0658 | 17.1 | .0 |
| | | | 16-18 | 5.24 | 5.107 | 46.166 | 10.730 | 431.02 | 0.0666 | – | – |
| | | | 18-20 | 5.37 | 2.312 | 48.279 | 11.505 | 451.28 | 0.0636 | 3.5 | .0 |
| | | | 20-22 | 4.77 | 5.213 | 47.774 | 11.546 | 451.02 | 0.0680 | 5.6 | 2.1 |
| 2888 | GC234 | GCAT1 | 0-2 | .0 | 9.285 | 50.285 | 9.981 | 452.12 | 0.0786 | 12.3 | 1.5 |
| | | | 2-4 | .0 | 9.703 | 48.879 | 10.963 | 439.56 | 0.0848 | 14.5 | – |
| | | | 4-6 | .0 | 9.768 | 49.175 | 10.816 | 435.48 | 0.0867 | 16.5 | 1.7 |
| | | | 6-8 | .0 | 9.236 | 47.526 | 10.195 | 425.45 | 0.0810 | 17.2 | 1.2 |
| | | | 8-10 | .0 | 9.807 | 47.985 | 11.175 | 441.86 | 0.0833 | – | – |
| | | | 12-14 | – | – | – | – | – | – | – | 1.7 |
| 2891 | GC235 | BHAT2 | 0-2 | .0 | 9.587 | 47.764 | 10.216 | 425.22 | 0.0831 | 16.4 | 4.4 |
| | | | 2-4 | .0 | 9.484 | 46.492 | 10.269 | 419.95 | 0.0805 | 29.6 | 5.2 |
| | | | 4-6 | .0 | 9.788 | 47.961 | 11.014 | 434.47 | 0.0834 | 18.5 | 1.7 |
| | | | 6-8 | .0 | 9.800 | 48.183 | 11.175 | 438.94 | 0.0849 | – | 1.2 |
| | | | 8-10 | .0 | 9.567 | 48.184 | 11.546 | 445.21 | 0.0829 | 18.2 | 1.7 |
| | | | 10-12 | .0 | 9.691 | 48.827 | 11.720 | 451.38 | 0.0845 | – | 1.2 |
| | | | 14-16 | .0 | 9.840 | 49.745 | 12.253 | 445.53 | 0.0866 | – | – |
| box | GC235 | BHBC2 | 0-2 | .0 | 10.043 | 49.930 | 12.121 | 454.87 | 0.0890 | 12.3 | 1.8 |
| | | | 2-4 | .0 | 9.717 | 49.780 | 11.018 | 451.77 | 0.0861 | 13.3 | 1.6 |
| | | | 4-6 | .0 | 9.800 | 49.264 | 11.853 | 457.31 | 0.0840 | 14.1 | 1.8 |
| | | | 6-8 | .0 | 9.910 | 49.466 | 12.072 | 450.85 | 0.0857 | 13.9 | 1.4 |
| | | | 8-10 | .0 | 10.356 | 48.580 | 12.271 | 438.90 | 0.0926 | 14.2 | 1.4 |
| | | | 10-12 | .0 | 9.671 | 47.740 | 11.881 | 434.04 | 0.0831 | 12.3 | 1.8 |
| | | | 12-14 | .0 | 9.619 | 47.429 | 11.848 | 439.58 | 0.0826 | 12.1 | 1.8 |
| | | | 14-16 | .0 | 9.242 | 46.354 | 11.068 | 422.76 | 0.0779 | 12.8 | 1.8 |
| | | | 16-18 | .0 | 9.837 | 46.455 | 11.619 | 421.74 | 0.0865 | 12.2 | 1.8 |
| | | | 18-20 | .0 | 9.028 | 46.899 | 10.694 | 436.74 | 0.0724 | 12.2 | 1.4 |
| | | | 22-24 | .0 | 9.710 | 46.811 | 11.541 | 422.85 | 0.0852 | 12.3 | 1.4 |
| 4025 | GC185 | BHAT1 | 0-2 | 0.43 | 10.048 | 51.486 | 11.010 | 455.74 | 0.0908 | .0 | .0 |
| | | | 2-4 | 0.36 | 10.206 | 51.250 | 11.129 | 455.07 | 0.0900 | 36.7 | .0 |
| | | | 4-6 | 0.32 | 10.283 | 51.701 | 11.266 | 456.24 | 0.0916 | 23.5 | .0 |
| | | | 6-8 | 0.37 | 10.596 | 52.553 | 11.459 | 469.44 | 0.0922 | 24.1 | .0 |
| | | | 8-10 | 0.34 | 10.704 | 52.664 | 12.105 | 469.75 | 0.0964 | 33.9 | 4.7 |
| | | | 12-14 | 0.31 | 10.689 | 52.202 | 11.829 | 471.96 | 0.0934 | 21.2 | .0 |

Table 9.3. Major cations. (continued)

| Dive Number | Site | Station | Depth (cm) | Ba (μM) | Ca (mM) | Mg (mM) | K (mM) | Na (mM) | Sr (mM) | Fe (μM) | Mn (μM) |
|---|---|---|---|---|---|---|---|---|---|---|---|
| 4027 | GC185 | BHST1 | 0-2 | 0.49 | 10.279 | 52.200 | 11.635 | 460.63 | 0.0914 | .0 | .0 |
| | | | 2-4 | 0.39 | 9.945 | 50.716 | 11.032 | 462.76 | 0.0853 | 25.8 | 0.4 |
| | | | 4-6 | 0.34 | 9.835 | 49.776 | 11.271 | 454.36 | 0.0875 | 15.5 | .0 |
| | | | 6-8 | 0.40 | 10.194 | 51.384 | 11.715 | 459.26 | 0.0883 | 29.3 | 0.4 |
| | | | 8-10 | 0.39 | 9.936 | 50.143 | 11.493 | 458.54 | 0.0897 | 12.0 | .0 |
| | | | 10-12 | 0.37 | 9.984 | 50.289 | 11.655 | 460.29 | 0.0900 | 18.9 | .0 |
| | | | 12-14 | 0.41 | 10.120 | 51.265 | 11.766 | 469.76 | 0.0904 | 14.9 | .0 |
| | | | 16-18 | 0.45 | 9.868 | 49.829 | 11.741 | 461.51 | 0.0884 | 9.8 | .0 |
| | | | 20-22 | 0.51 | 9.838 | 49.890 | 11.961 | 463.91 | 0.0905 | .0 | .0 |
| 4028 | GC185 | BHB3 | 0-2 | 0.86 | 9.572 | 51.405 | 11.009 | 462.13 | 0.0871 | 6.3 | .0 |
| | | | 2-4 | 1.18 | 6.908 | 50.066 | 11.280 | 458.85 | 0.0759 | 13.8 | 5.3 |
| | | | 4-6 | 1.15 | 3.811 | 48.544 | 11.083 | 444.85 | 0.0599 | 11.5 | .0 |
| | | | 6-8 | 0.24 | 0.880 | 47.560 | 11.110 | 445.40 | 0.0113 | 12.0 | .0 |
| | | | 8-10 | 1.41 | 1.930 | 48.112 | 11.304 | 448.33 | 0.0392 | 24.1 | .0 |
| | | | 10-12 | 2.71 | 2.648 | 48.010 | 11.414 | 462.89 | 0.0531 | 9.8 | 1.1 |
| | | | 12-14 | 3.43 | 3.795 | 46.488 | 12.117 | 467.02 | 0.0642 | 3.4 | 0.2 |
| | | | 14-16 | 5.71 | 3.999 | 44.310 | 10.834 | 401.62 | 0.0568 | 13.2 | 3.6 |
| 4029 | GC234 | GCAT2 | 0-2 | 0.39 | 9.866 | 47.820 | 11.362 | 428.83 | 0.0880 | 11.5 | .0 |
| | | | 2-4 | 0.38 | 9.791 | 48.047 | 11.311 | 434.19 | 0.0872 | 10.9 | .0 |
| | | | 4-6 | 0.04 | 9.497 | 48.010 | 11.470 | 430.84 | 0.0858 | 10.9 | .0 |
| | | | 6-8 | 0.42 | 8.754 | 47.675 | 11.493 | 443.47 | 0.0862 | 2.3 | .0 |
| | | | 8-10 | 0.08 | 0.889 | 47.784 | 11.484 | 440.89 | 0.0099 | 8.0 | .0 |
| | | | 10-12 | 0.13 | 1.779 | 47.605 | 11.069 | 438.19 | 0.0321 | 13.2 | .0 |
| | | | 14-16 | 0.54 | 5.404 | 47.850 | 11.237 | 439.17 | 0.0751 | 13.2 | .0 |
| | | | 18-20 | 0.69 | 5.340 | 48.274 | 11.310 | 443.94 | 0.0731 | 19.6 | 3.2 |
| | | | 22-24 | 1.04 | 4.297 | 46.003 | 12.026 | 436.70 | 0.0708 | 24.2 | 2.6 |
| 4031 | GC234 | GCST1 | 0-2 | 0.42 | 10.266 | 50.697 | 10.483 | 454.25 | 0.0857 | 18.4 | .0 |
| | | | 2-4 | 0.52 | 10.186 | 51.323 | 10.733 | 458.79 | 0.0881 | 11.5 | .0 |
| | | | 4-6 | 0.36 | 9.996 | 50.455 | 11.511 | 456.64 | 0.0869 | 13.8 | 0.6 |
| | | | 6-8 | 0.29 | 10.113 | 51.329 | 11.135 | 472.87 | 0.0886 | 12.7 | 1.3 |
| | | | 8-10 | 0.24 | 10.117 | 52.117 | 10.708 | 469.83 | 0.0846 | – | 2.6 |
| | | | 10-12 | 0.26 | 10.198 | 51.730 | 11.593 | 470.81 | 0.0893 | 9.2 | 1.9 |
| | | | 12-14 | 0.27 | 9.926 | 50.331 | 11.746 | 462.82 | 0.0928 | 12.1 | 0.6 |
| | | | 14-16 | 0.24 | 10.201 | 51.710 | 11.560 | 470.99 | 0.0900 | 14.4 | 0.6 |
| | | | 18-20 | 0.26 | 10.308 | 52.533 | 11.429 | 476.86 | 0.0894 | 19.0 | 0.6 |
| | | | 22-24 | 0.26 | 10.217 | 50.931 | 11.463 | 467.39 | 0.0886 | 12.7 | 2.6 |

Table 9.3. Major cations. (continued)

| Dive Number | Site | Station | Depth (cm) | Ba (μM) | Ca (mM) | Mg (mM) | K (mM) | Na (mM) | Sr (mM) | Fe (μM) | Mn (μM) |
|---|---|---|---|---|---|---|---|---|---|---|---|
| 4032 | GC234 | GCAT1 | 0-2 | 0.34 | 10.257 | 52.030 | 10.910 | 464.37 | 0.0904 | 26.5 | .0 |
| | | | 2-4 | 0.35 | 10.094 | 51.762 | 11.334 | 469.12 | 0.0903 | 21.3 | .0 |
| | | | 4-6 | 0.36 | 10.125 | 52.106 | 11.335 | 468.05 | 0.0886 | 12.1 | 0.6 |
| | | | 6-8 | 0.27 | 9.859 | 51.116 | 11.821 | 467.56 | 0.0908 | 16.1 | 0.6 |
| | | | 8-10 | 0.25 | 9.984 | 51.463 | 11.680 | 462.34 | 0.0884 | 25.3 | .0 |
| | | | 10-12 | 0.26 | 9.691 | 50.047 | 11.575 | 461.36 | 0.0895 | 12.1 | .0 |
| | | | 12-14 | 0.32 | 10.109 | 52.322 | 12.301 | 485.29 | 0.0939 | – | .0 |
| | | | 14-16 | 0.30 | 10.042 | 51.308 | 11.721 | 466.50 | 0.0906 | 15.5 | 0.6 |
| 4036 | GC234 | GCJT1 | 0-2 | 0.37 | 10.693 | 53.782 | 11.436 | 483.89 | 0.0942 | .0 | .0 |
| | | | 2-4 | 2.60 | 10.458 | 52.929 | 11.349 | 473.19 | 0.0909 | .0 | 0.6 |
| | | | 4-6 | 0.23 | 10.269 | 51.693 | 11.567 | 473.23 | 0.0910 | .0 | 0.6 |
| | | | 6-8 | 0.21 | 10.458 | 52.551 | 11.955 | 482.74 | 0.0939 | .0 | 0.6 |
| | | | 8-10 | 0.23 | 10.542 | 52.779 | 12.307 | 482.68 | 0.0958 | .0 | 2.5 |
| | | | 10-12 | 0.39 | 10.543 | 53.237 | 11.872 | 482.38 | 0.0932 | .0 | 1.9 |
| | | | 12-14 | 0.03 | 10.329 | 52.174 | 11.754 | 472.72 | 0.0921 | .0 | 1.2 |
| | | | 16-18 | 0.42 | 10.074 | 51.173 | 11.801 | 464.06 | 0.0916 | .0 | 1.2 |
| 4037 | GC233 | BPAT1 | 0-2 | 0.44 | 10.458 | 53.381 | 12.067 | 484.65 | 0.0966 | 42.6 | 0.6 |
| | | | 2-4 | 0.53 | 10.419 | 53.200 | 12.056 | 479.51 | 0.0966 | 35.7 | 1.2 |
| | | | 4-6 | 0.45 | 10.245 | 51.931 | 11.884 | 470.11 | 0.0937 | 16.1 | 1.2 |
| | | | 6-8 | 0.70 | 10.308 | 51.624 | 12.376 | 476.49 | 0.0977 | 43.2 | 1.2 |
| | | | 8-10 | 0.59 | 12.430 | 52.600 | 12.203 | 475.57 | 0.0974 | 5.8 | 1.9 |
| | | | 10-12 | 4.89 | 12.702 | 52.697 | 12.210 | 486.33 | 0.0976 | 12.1 | 3.1 |
| | | | 12-14 | 9.04 | 11.879 | 47.586 | 10.870 | 423.73 | 0.0861 | 5.8 | 2.5 |
| 4038 | GC233 | BPB2 | 0-2 | 13.40 | 14.272 | 47.895 | 11.272 | 436.99 | 0.0911 | 0.2 | 1.2 |
| | | | 2-4 | 3.16 | 12.675 | 49.499 | 11.374 | 585.82 | 0.2030 | 0.5 | 0.6 |
| | | | 4-6 | 5.48 | 14.079 | 48.068 | 11.138 | 643.65 | 0.2588 | 0.6 | 0.6 |
| | | | 6-8 | 3.41 | 13.619 | 47.534 | 10.319 | 658.97 | 0.2663 | 11.8 | .0 |
| | | | 8-10 | 2.34 | 13.370 | 45.540 | 10.810 | 712.97 | 0.3092 | .0 | 0.7 |
| | | | 10-12 | 11.86 | 17.016 | 44.561 | 10.052 | 870.64 | 0.4048 | .0 | .0 |
| | | | 12-14 | 18.75 | 15.877 | 41.796 | 10.488 | 842.05 | 0.4377 | .0 | .0 |
| 4040 | GB425 | GBUN1 | 0-2 | 5.98 | 11.153 | 52.741 | 11.172 | 465.14 | 0.0979 | 1.2 | 0.7 |
| | | | 2-4 | 3.34 | 10.441 | 50.022 | 11.266 | 453.11 | 0.0949 | 3.0 | 1.4 |
| | | | 4-6 | 2.57 | 10.816 | 51.352 | 11.138 | 467.74 | 0.0837 | 2.4 | 0.7 |
| | | | 6-8 | 5.22 | 10.888 | 50.541 | 10.725 | 469.78 | 0.0952 | 0.6 | 1.4 |
| | | | 8-10 | 0.27 | 10.684 | 51.714 | 11.663 | 477.23 | 0.1008 | 1.2 | 1.4 |
| | | | 12-14 | 4.85 | 11.138 | 51.467 | 11.087 | 480.47 | 0.1035 | .0 | .0 |

Table 9.3. Major cations. (continued)

| Dive Number | Site | Station | Depth (cm) | Ba (μM) | Ca (mM) | Mg (mM) | K (mM) | Na (mM) | Sr (mM) | Fe (μM) | Mn (μM) |
|---|---|---|---|---|---|---|---|---|---|---|---|
| | | | 14-16 | 3.93 | 10.738 | 51.163 | 11.984 | 471.42 | 0.1138 | 7.7 | 0.7 |
| | | | 16-18 | 3.46 | 11.174 | 52.819 | 12.644 | 510.42 | 0.1199 | 4.7 | 0.7 |
| 4042 | GC185 | BHM3 | 0-2 | 2.00 | 11.108 | 53.556 | 11.511 | 470.73 | 0.0923 | 1.8 | 0.7 |
| | | | 2-4 | 1.19 | 10.831 | 53.795 | 11.987 | 479.26 | 0.0945 | .0 | .0 |
| | | | 4-6 | 5.07 | 10.916 | 52.412 | 11.225 | 467.29 | 0.0880 | 3.6 | .0 |
| | | | 6-8 | 2.97 | 11.249 | 54.901 | 12.202 | 490.04 | 0.0959 | 4.1 | .0 |
| | | | 8-10 | 1.53 | 10.569 | 52.482 | 11.467 | 462.72 | 0.0880 | 2.4 | .0 |
| | | | 10-12 | 2.43 | 10.905 | 53.483 | 11.525 | 471.98 | 0.0904 | 1.8 | 0.7 |
| | | | 14-16 | 2.22 | 11.187 | 54.530 | 12.347 | 483.82 | 0.0937 | .0 | .0 |
| | | | 18-20 | 1.66 | 10.490 | 51.808 | 11.889 | 465.71 | 0.0915 | 3.6 | .0 |
| 4043 | GC234 | GCB3 orange *Beggiota* | 0-2 | 2.47 | 10.597 | 51.965 | 11.301 | 473.29 | 0.0943 | 0.6 | .0 |
| | | | 2-4 | 1.31 | 7.185 | 37.454 | 8.448 | 342.87 | 0.0669 | .0 | .0 |
| | | | 4-6 | 2.55 | 9.931 | 51.278 | 11.615 | 471.73 | 0.0923 | 0.6 | .0 |
| | | | 6-8 | 3.03 | 10.288 | 52.800 | 11.548 | 481.76 | 0.0874 | 0.6 | .0 |
| | | | 8-10 | 1.62 | 9.484 | 51.620 | 11.512 | 467.92 | 0.0885 | 0.6 | .0 |
| | | | 10-12 | 1.88 | 9.021 | 50.048 | 11.536 | 466.00 | 0.0885 | .0 | .0 |
| | | | 12-14 | 1.65 | 8.841 | 50.386 | 10.576 | 458.04 | 0.0810 | 5.9 | .0 |
| | | | 14-16 | 0.87 | 8.630 | 50.276 | 11.221 | 454.32 | 0.0863 | 2.4 | .0 |
| | | | 16-18 | 1.07 | 9.343 | 51.276 | 11.629 | 467.35 | 0.0888 | 3.0 | .0 |
| | | | 20-22 | 1.29 | 9.119 | 51.097 | 11.701 | 467.76 | 0.0900 | .0 | .0 |
| 4043 | GC234 | GCB3 off mat | 0-2 | 0.95 | 10.191 | 51.860 | 11.401 | 465.30 | 0.0927 | 0.6 | .0 |
| | | | 2-4 | 1.82 | 10.649 | 53.293 | 12.114 | 484.81 | 0.0937 | .0 | .0 |
| | | | 4-6 | 1.41 | 10.436 | 51.866 | 11.981 | 476.23 | 0.0927 | 0.6 | 0.7 |
| | | | 6-8 | 1.34 | 10.287 | 50.980 | 11.805 | 463.63 | 0.0910 | 4.7 | .0 |
| | | | 8-10 | 1.90 | 10.076 | 49.475 | 11.866 | 452.05 | 0.0895 | 1.2 | 0.7 |
| | | | 10-12 | 0.19 | 11.067 | 53.147 | 12.039 | 476.96 | 0.0923 | .0 | 1.4 |
| | | | 14-16 | 2.86 | 10.726 | 49.928 | 10.856 | 456.24 | 0.0845 | 12.0 | 2.2 |
| | | | 18-20 | 2.52 | 11.113 | 51.802 | 11.170 | 474.08 | 0.0885 | .0 | .0 |
| | | | 22-24 | 1.60 | 10.453 | 49.184 | 11.426 | 453.11 | 0.0853 | .0 | .0 |
| | | | 26-28 | 1.98 | 10.827 | 50.186 | 11.893 | 465.38 | 0.0935 | 2.4 | .0 |
| 4043 | GC234 | GCB3 white *Beggiota* | 0-2 | 1.56 | 10.206 | 50.937 | 10.412 | 457.18 | 0.0874 | 0.6 | .0 |
| | | | 2-4 | 1.51 | 9.931 | 50.568 | 11.114 | 457.18 | 0.0893 | 1.2 | .0 |
| | | | 4-6 | 1.83 | 10.685 | 54.034 | 11.717 | 489.43 | 0.0947 | .0 | .0 |

Table 9.3. Major cations. (continued)

| Dive Number | Site | Station | Depth (cm) | Ba (μM) | Ca (mM) | Mg (mM) | K (mM) | Na (mM) | Sr (mM) | Fe (μM) | Mn (μM) |
|---|---|---|---|---|---|---|---|---|---|---|---|
| | | | 8-10 | 1.01 | 9.841 | 50.819 | 11.363 | 463.36 | 0.0901 | .0 | .0 |
| | | | 10-12 | 1.32 | 9.881 | 51.459 | 11.448 | 466.54 | 0.0916 | .0 | .0 |
| | | | 12-14 | 0.96 | 9.619 | 50.195 | 11.793 | 468.48 | 0.0932 | .0 | .0 |
| | | | 14-16 | 1.14 | 9.635 | 51.045 | 11.963 | 466.70 | 0.0940 | 1.8 | .0 |
| | | | 16-18 | 0.84 | 9.794 | 51.323 | 11.570 | 468.83 | 0.0913 | 1.2 | .0 |
| | | | 18-20 | 0.83 | 9.852 | 50.806 | 11.589 | 463.06 | 0.0929 | 1.2 | .0 |
| 4044 | GC185 | BHAT2 | 0-2 | 1.81 | 10.725 | 53.079 | 11.209 | 474.85 | 0.0970 | 3.5 | 1.5 |
| | | | 2-4 | 1.46 | 10.678 | 52.721 | 11.747 | 469.12 | 0.0945 | 78.0 | .0 |
| | | | 4-6 | 0.95 | 10.344 | 51.343 | 11.981 | 471.16 | 0.0955 | 17.0 | .0 |
| | | | 6-8 | 0.83 | 9.933 | 49.506 | 12.118 | 467.56 | 0.0949 | 5.3 | .0 |
| | | | 8-10 | 0.92 | 10.350 | 51.700 | 13.289 | 485.29 | 0.1027 | 5.3 | .0 |
| | | | 10-12 | 1.53 | 10.451 | 51.919 | 12.511 | 485.23 | 0.0985 | 7.0 | .0 |
| | | | 12-14 | 1.17 | 10.214 | 51.392 | 12.472 | 480.93 | 0.0979 | 2.3 | 2.3 |
| | | | 14-16 | 1.31 | 10.271 | 51.344 | 12.594 | 483.37 | 0.0983 | 2.9 | .0 |
| | | | 18-20 | 0.95 | 10.299 | 52.044 | 12.626 | 491.52 | 0.1000 | 16.4 | 2.3 |
| | | | 22-24 | 1.27 | 10.410 | 51.871 | 12.718 | 488.40 | 0.0989 | 0.6 | .0 |
| 4046 | GC185 | BHM4 | 0-2 | 1.83 | 8.512 | 43.124 | 9.302 | 376.48 | 0.0754 | .0 | 0.8 |
| | | | 2-4 | 16.66 | 9.773 | 54.831 | 11.195 | 479.80 | 0.0838 | 0.6 | .0 |
| | | | 4-6 | 45.61 | 5.922 | 49.136 | 11.324 | 445.34 | 0.0757 | 1.2 | 4.6 |
| | | | 6-8 | 49.66 | 7.903 | 49.961 | 11.790 | 445.70 | 0.0795 | 2.9 | 0.8 |
| | | | 8-9 | 41.63 | 7.862 | 50.542 | 11.717 | 460.45 | 0.0733 | – | – |
| 4047 | GC234 | GCJT2 | 0-2 | 1.61 | 10.278 | 54.068 | 11.247 | 478.59 | 0.0923 | .0 | 0.8 |
| | | | 2-4 | 1.46 | 9.914 | 53.107 | 11.422 | 471.50 | 0.0904 | 2.3 | .0 |
| | | | 4-6 | 1.74 | 10.176 | 53.774 | 10.938 | 478.40 | 0.0885 | 1.8 | 1.5 |
| | | | 6-8 | 1.18 | 9.911 | 51.674 | 11.581 | 471.26 | 0.0896 | 3.5 | 1.5 |
| | | | 8-10 | 1.12 | 9.572 | 51.406 | 11.809 | 474.00 | 0.0893 | 3.5 | .0 |
| | | | 10-12 | 1.07 | 10.203 | 54.952 | 12.477 | 505.37 | 0.0947 | .0 | .0 |
| | | | 12-14 | 1.36 | 6.092 | 32.508 | 7.423 | 294.98 | 0.0546 | 2.3 | .0 |
| | | | 16-18 | 1.28 | 9.485 | 51.918 | 12.137 | 482.48 | 0.0900 | .0 | 1.4 |
| | | | 20-22 | 1.41 | 7.600 | 50.955 | 12.146 | 476.12 | 0.0857 | .0 | 0.7 |
| | | | 22-24 | 1.35 | 3.975 | 51.813 | 12.550 | 486.24 | 0.0718 | 13.5 | 0.7 |
| 4048 | GC234 | GCAT2 | 0-2 | 1.59 | 9.941 | 49.374 | 10.289 | 438.03 | 0.0864 | 85.2 | .0 |
| | | | 2-4 | 1.64 | 10.692 | 55.105 | 12.135 | 495.24 | 0.0953 | 85.2 | 2.6 |
| | | | 4-6 | 1.65 | 11.410 | 59.292 | 13.333 | 534.08 | 0.1033 | 0.7 | 0.0 |
| | | | 6-8 | 1.58 | 9.528 | 51.431 | 11.771 | 470.37 | 0.0898 | 8.2 | 1.4 |
| | | | 8-10 | 2.81 | 9.272 | 52.179 | 11.235 | 468.60 | 0.0851 | 71.0 | 1.4 |

Table 9.3. Major cations. (continued)

| Dive Number | Site | Station | Depth (cm) | Ba (μM) | Ca (mM) | Mg (mM) | K (mM) | Na (mM) | Sr (mM) | Fe (μM) | Mn (μM) |
|---|---|---|---|---|---|---|---|---|---|---|---|
| | | | 10-12 | 3.72 | 7.474 | 51.978 | 11.850 | 475.45 | 0.0839 | 4.1 | 0.7 |
| | | | 14-16 | 4.77 | 6.832 | 50.123 | 11.856 | 463.74 | 0.0819 | 4.1 | 0.7 |
| | | | 18-20 | 4.56 | 6.319 | 50.558 | 11.615 | 467.31 | 0.0778 | 2.9 | 1.4 |
| | | | 22-24 | 5.24 | 5.925 | 49.739 | 11.498 | 462.35 | 0.0751 | 2.3 | 0.7 |
| | | | 24-26 | 4.77 | 5.765 | 49.491 | 11.659 | 465.11 | 0.0738 | 1.8 | 1.4 |
| 4053 | GB425 | GBM2 | 0-2 | 5.54 | 8.434 | 52.338 | 12.180 | 469.85 | 0.0958 | .0 | 2.2 |
| | | | 2-4 | 18.53 | 5.493 | 51.487 | 12.012 | 492.58 | 0.0936 | 7.0 | 0.7 |
| | | | 4-6 | 7.45 | 4.436 | 48.544 | 11.172 | 490.60 | 0.0850 | 1.8 | 1.4 |
| | | | 6-8 | 9.70 | 5.604 | 48.517 | 11.645 | 523.99 | 0.1190 | 2.9 | 0.7 |
| | | | 8-10 | 10.86 | 6.632 | 54.697 | 13.483 | 590.95 | 0.1384 | 1.8 | 0.7 |
| | | | 10-12 | 2.30 | 1.686 | 51.639 | 12.894 | 622.34 | 0.0380 | 4.7 | 1.4 |
| | | | 14-16 | 91.55 | 11.550 | 44.662 | 12.886 | 809.55 | 0.4630 | 21.7 | 1.4 |
| | | | 18-20 | .0 | 17.772 | 38.667 | 11.693 | 920.12 | 0.6621 | 1.8 | 0.7 |
| | | | 22-24 | .0 | 21.495 | 41.126 | 11.571 | 972.91 | 0.6626 | 1.8 | 1.4 |
| | | | 28-30 | .0 | 15.510 | 43.155 | 12.972 | 898.18 | 0.5602 | 2.3 | 2.9 |
| box | GC185 | BHBXC1 | 0-2 | 0.46 | 10.072 | 51.256 | 11.378 | 471.04 | 0.0897 | 2.3 | 0.7 |
| | | | 2-4 | 0.42 | 9.916 | 50.333 | 11.559 | 462.87 | 0.0888 | 21.8 | .0 |
| | | | 4-6 | 0.41 | 10.123 | 52.100 | 11.437 | 461.04 | 0.0903 | 7.5 | .0 |
| | | | 6-8 | 0.45 | 9.834 | 50.201 | 11.407 | 449.05 | 0.0873 | 18.4 | 0.7 |
| | | | 8-10 | 0.45 | 10.045 | 51.220 | 11.691 | 457.40 | 0.0897 | 6.9 | .0 |
| | | | 10-12 | 0.50 | 10.130 | 51.295 | 11.650 | 459.94 | 0.0901 | 38.4 | .0 |
| | | | 14-16 | 0.52 | 9.940 | 50.136 | 11.404 | 453.34 | 0.0879 | 28.1 | .0 |
| | | | 18-20 | 0.46 | 9.704 | 49.802 | 11.814 | 456.90 | 0.0893 | 18.4 | 0.7 |
| | | | 22-24 | 0.43 | 9.820 | 50.471 | 11.340 | 457.26 | 0.0888 | 37.3 | 0.7 |
| box | GC185 | BHUN2 | 0-2 | 2.19 | 8.923 | 51.911 | 11.877 | 476.18 | 0.0877 | .0 | 0.8 |
| | | | 2-4 | 1.64 | 6.008 | 56.631 | 12.311 | 513.07 | 0.0765 | 1.8 | 0.8 |
| | | | 4-6 | 1.52 | 6.005 | 50.655 | 11.782 | 465.25 | 0.0757 | .0 | .0 |
| | | | 6-8 | 1.56 | 5.666 | 48.951 | 12.838 | 503.52 | 0.0795 | .0 | .0 |
| | | | 8-10 | 1.77 | 5.999 | 49.047 | 11.297 | 448.02 | 0.0713 | 8.2 | .0 |
| | | | 10-12 | 2.35 | 6.784 | 50.115 | 12.435 | 471.76 | 0.0799 | .0 | 0.8 |
| | | | 12-14 | 1.80 | 2.320 | 49.712 | 12.117 | 469.89 | 0.0586 | .0 | 1.5 |
| | | | 14-16 | 2.74 | 1.732 | 47.447 | 12.006 | 460.72 | 0.0562 | 0.6 | 0.8 |
| | | | 18-20 | 5.23 | 4.514 | 50.556 | 14.999 | 568.08 | 0.0785 | .0 | .0 |
| | | | 20-22 | 2.26 | 2.065 | 47.517 | 11.506 | 436.55 | 0.0482 | 2.9 | 0.8 |

Table 9.3. Major cations. (continued)

| Dive Number | Site | Station | Depth (cm) | Ba (μM) | Ca (mM) | Mg (mM) | K (mM) | Na (mM) | Sr (mM) | Fe (μM) | Mn (μM) |
|---|---|---|---|---|---|---|---|---|---|---|---|
| box | GC234 | GCBX2 | 0-2 | 1.99 | 11.313 | 56.913 | 11.969 | 508.61 | 0.1040 | 2.3 | 2.9 |
| | | | 2-4 | 4.00 | 10.474 | 52.664 | 11.533 | 484.48 | 0.0995 | 10.6 | 0.7 |
| | | | 4-6 | 2.16 | 10.109 | 52.115 | 11.593 | 475.58 | 0.0941 | 3.5 | 5.0 |
| | | | 6-8 | 1.81 | 10.251 | 54.452 | 12.571 | 509.25 | 0.1018 | 18.8 | 1.4 |
| | | | 8-10 | 4.16 | 10.044 | 53.576 | 11.779 | 483.37 | 0.0950 | 20.5 | 3.6 |
| | | | 10-12 | 1.77 | 9.554 | 52.193 | 11.215 | 485.97 | 0.0879 | 21.7 | 1.4 |
| | | | 14-16 | – | – | – | – | – | – | – | – |
| | | | 18-20 | 0.49 | 8.699 | 52.525 | 11.702 | 471.74 | 0.0884 | 4.6 | – |
| | | | 22-24 | 0.57 | 8.799 | 53.194 | 12.508 | 494.34 | 0.0936 | 7.5 | – |
| | | | 26-28 | – | – | – | – | – | – | 1.2 | .0 |
| box | GC234 | GCBXC1 | 0-2 | 0.52 | 9.972 | 51.736 | 11.558 | 467.42 | 0.0911 | 9.2 | 0.6 |
| | | | 2-4 | 0.27 | 9.545 | 50.612 | 11.920 | 462.09 | 0.0903 | 9.8 | .0 |
| | | | 4-6 | 0.24 | 9.576 | 50.454 | 11.885 | 463.62 | 0.0892 | 17.8 | 0.6 |
| | | | 6-8 | 0.21 | 9.629 | 50.250 | 11.652 | 460.11 | 0.0889 | 9.2 | 0.6 |
| | | | 8-10 | 0.22 | 10.023 | 51.706 | 12.215 | 480.79 | 0.0918 | .0 | 0.0 |
| | | | 10-12 | 0.21 | 9.823 | 50.446 | 12.129 | 466.83 | 0.0909 | 10.4 | 0.6 |
| | | | 14-16 | 0.19 | 10.064 | 51.824 | 11.708 | 476.01 | 0.0896 | 17.8 | 0.6 |
| | | | 18-20 | 0.21 | 10.087 | 51.471 | 12.252 | 475.91 | 0.0907 | 1.7 | 0.6 |
| | | | 22-24 | 0.03 | 10.059 | 51.661 | 11.835 | 472.76 | 0.0905 | .0 | 0.6 |
| | | | 28-30 | 0.26 | 10.063 | 51.801 | 12.076 | 477.69 | 0.0921 | 2.9 | 1.2 |

calculated as the difference between the observed concentration and a nominal seawater concentration (2.400 mols/L). Excess DIC is also affected by calcium carbonate precipitation (Equation 9-5) and dissolution. This effect can be corrected by calculating the difference between a standard seawater calcium concentration 10.512 mM/L at S = 35‰) and the observed value. Positive and negative differences indicate net precipitation and dissolution, respectively.

These relationships are important because they constrain the source of the carbon undergoing oxidation. Figure 9.3 shows excess DIC versus reduced sulfate for the following stations: GCAT2 (dives 4029 and 4048), BHB3, BHM4 (dive 4046), BHUN2, GCB3, GCBXC1, and GCJT2. These data are compared in each station with the two reaction paths that would result from sulfate reduction involving either a simple organic matter ($CH_2O$) or methane ($CH_4$). The complete data set from both the 1997 and 1998 cruises, less those stations showing brine compositions, is shown in Figure 9.4. Where the extent of reduction is less than ~30%, excess DIC values tend to scatter between these two bounding slopes. In contrast, where reduction varies from less than 30% to approximately 100%, excess DIC concentrations are consistent with methane oxidation. The fact that sulfide concentrations shown in Figure 9.3 do not show the same stoichiometric relationship with DIC as they do with sulfate suggests that sulfide is either consumed by sulfide, or possibly reacts to form solid phase AVS, as discussed below.

**Solid-phase buffers**. Although the concentrations of dissolved carbon and sulfide clearly reflect the intensity of biogenic sulfate reduction, they also reflect mineral precipitation reactions. The DIC that is produced promotes the non-organic precipitation of calcium carbonate. Increases in DIC should thus be correlated to increases in solid phase inorganic carbon. This pattern is well illustrated in Figure 9.5A, which shows a steep rise in inorganic $CaCO_3$ with pore water DIC up to approximately 10 mM DIC (calcium concentrations significantly greater than seawater reflect the addition of Ca-rich brines). Over this region, DIC concentrations are well buffered by $CaCO_3$ precipitation. However, extensive $CaCO_3$ precipitation also brings about significant depletion in calcium concentration. This depletion is shown in Figure 9.5B, which shows that dissolved calcium falls to approximately 10% of its nominal seawater value (10 mM) at the very elevated DIC concentrations. Thus the scatter of points at very high DIC concentrations (associated with methane oxidation) in Figure 9.5A reflects the limitations of DIC buffering by $CaCO_3$ as calcium is removed from the system.

The formation of solid-phase sulfides is an important buffer to dissolved $H_2S$ concentrations. It is important to recognize that a dearth of dissolved sulfide does not necessarily imply a low rate of sulfate reduction, but may instead reflect excess reactive iron to form iron sulfide minerals. Conversely, high pore water sulfide concentrations may reflect a limitation in the availability of reactive iron. High sulfate reduction rates, low concentrations of solid phase sulfide minerals (acid-volatile sulfide, or AVS, and pyrite), and low concentrations of reactive iron suggests that the very high pore water sulfide concentrations in these seep sediments indicates constraints to sulfide mineral formation. Compared with $CaCO_3$ mineral formation, precipitation of solid phase sulfides is substantially more complex. It involves the reduction of sedimentary iron oxides by dissolved $H_2S$, and reaction paths that lead to formation of either AVS and/or pyrite. Moreover, substantial differences exist in the reactivity of various iron oxides phases, and analyses of "total" sedimentary iron, which may involve contributions from iron silicate phases,
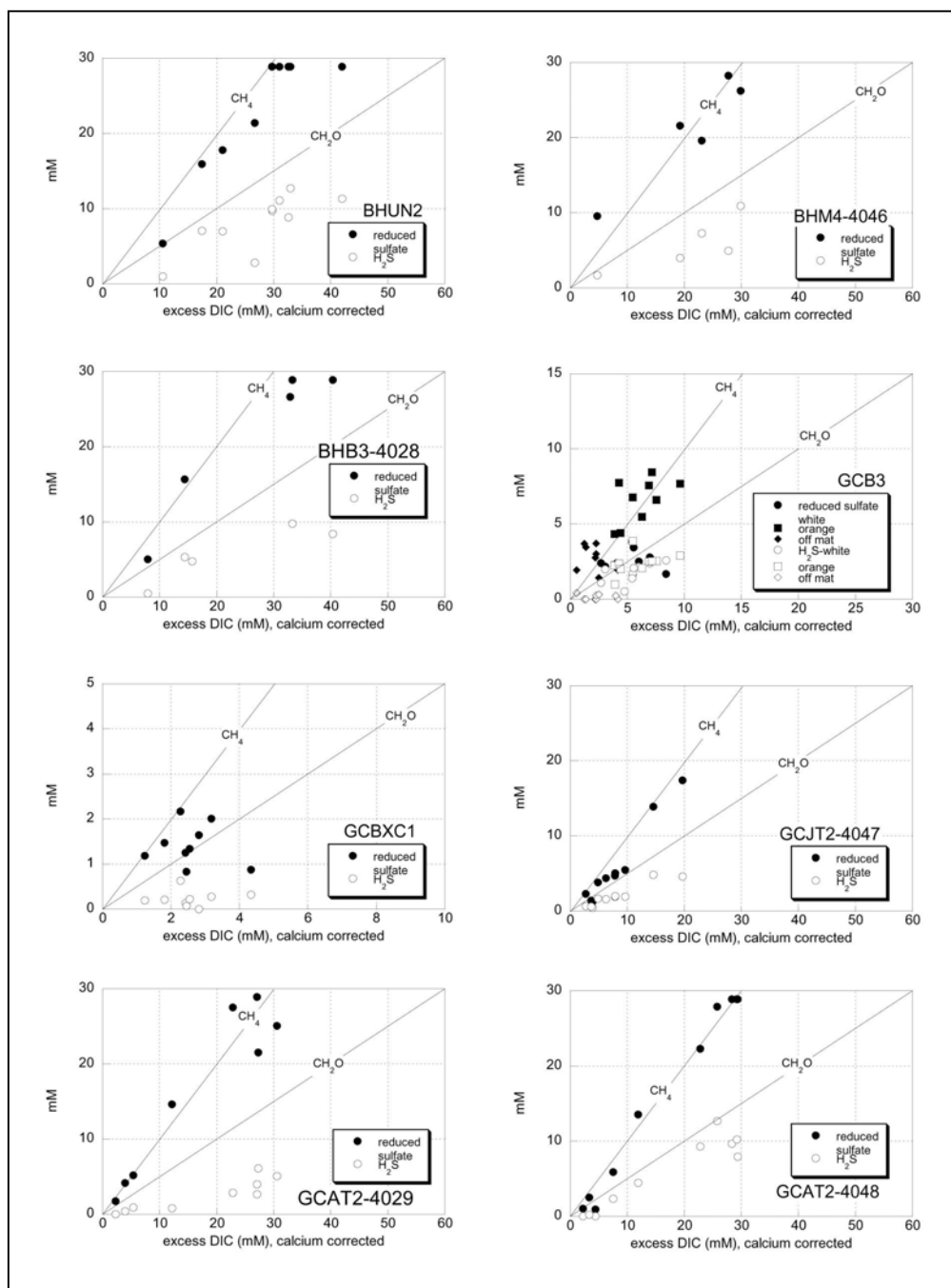
Figure 9.3. Sulfate reduction stoichiometry by station. Reduced sulfate (solid symbols) is plotted versus excess DIC for stations GCAT2 (dives 4029 and 4048), BHB3, BHM4 (dive 4046), BHUN2, GCB3, GCBXC1, and GCJT2, and is used to constrain the source of the carbon undergoing oxidation. These data are compared in each station with the reaction paths that would result from sulfate reduction involving either a simple organic matter ($CH_2O$) or methane ($CH_4$). Dissolved sulfide (open symbols) is also shown for comparison.
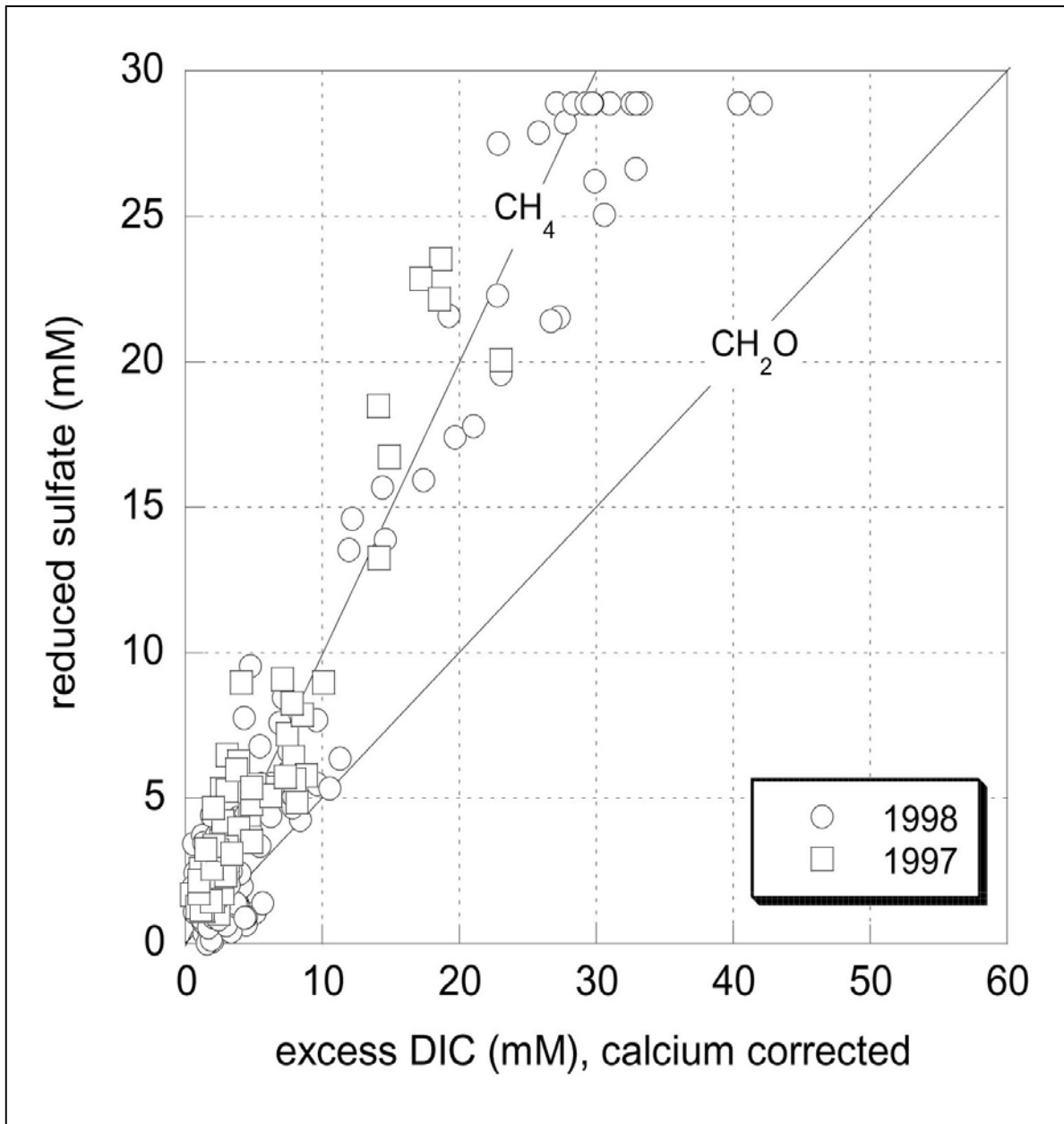
Figure 9.4.    Sulfate reduction stoichiometry, all stations by year. Reduced sulfate versus excess DIC is plotted for 1997 (squares) and 1998 (circles) stations, excluding those classified as brines in Figure 9.2. Data for both years tend to scatter between the bounding reaction paths for simple organic matter such as crude oil or detritus and methane (see Figure 9.3) for those stations showing less than ~30% extent of reduction. Where reduction varies from >30 to ~100%, excess DIC concentrations are consistent with a methane oxidation reaction path.
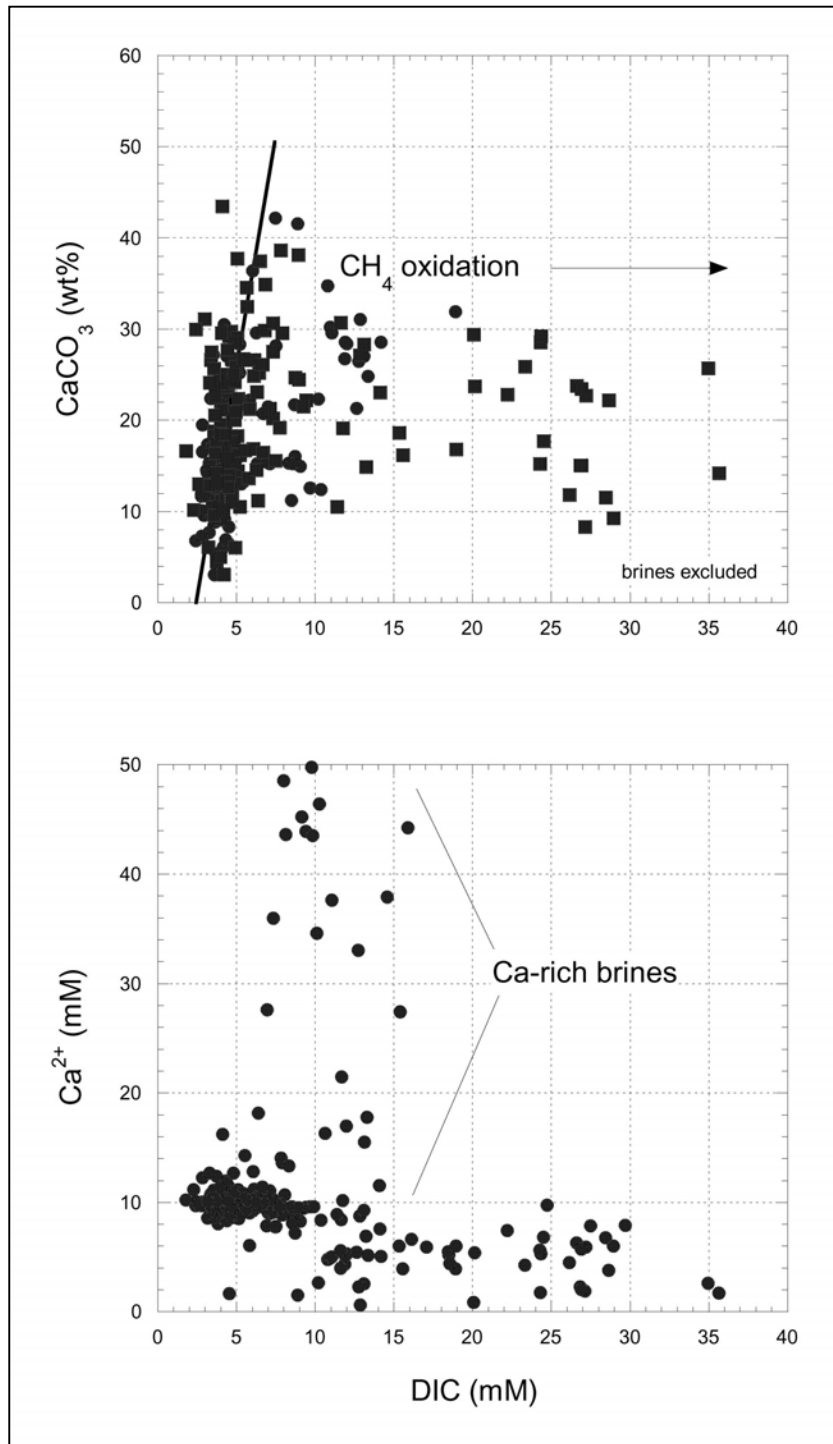
Figure 9.5. Carbonate mineral precipitation. (A) *Inorganic carbon (as CaCO₃) versus porewater DIC.* Up to about 10 mM DIC, increases in porewater concentration correlate strongly with increases in solid phase $CaCO_3$. Above 10 mM DIC, depletion of dissolved calcium limits $CaCO_3$ formation. (B) *Porewater calcium.* Concentrations above ~10 mM record influence of calcium-rich brines. Precipitation of $CaCO_3$ at high DIC concentrations brings about calcium depletion to ~10% of its nominal seawater value (10 mM).

may overestimate the iron that is potentially available for incorporation as sulfide. This variability has led to the notion of "reactive" Fe, and is the motivation for using buffered citrate dithionite (CD) versus HCl for metal extractions (see Methods). The differences in the effect of these solvents are easily seen in Figure 9.6, which plots HCl- and CD-extracted iron versus grain size. The important point here is that CD-Fe concentrations are substantially less than those of HCl-Fe, and may be a more accurate reflection of the iron that is available for sulfide mineral formation.

These relationships between dissolved sulfide, Pyrite-S (TRS) concentrations (mean 111.8±35.4 µmol/g), greatly exceed those of AVS (mean 4.3 ± 4.9 µmol/g) in these sediments. Thus, AVS represents a very minor fraction of the reduced sulfur present in these sediments, particularly in comparison to the $H_2S$ present in the pore water. AVS and TRS are compared in Figure 9.7, which plots both these values versus dissolved sulfide (Figure 9.7A) and organic carbon (Figure 9.7B). TRS also shows little variation with respect to $H_2S$, which implies that pyrite-S generation may be largely decoupled in time or space from the process of sulfate reduction.

In much the same way that reduced sulfate was compared to excess DIC as a way of constraining the stoichiometry of the reacting organic matter, iron concentrations determined from CD extracts can be compared with AVS concentrations to constrain the composition of the sulfide forming in these sediments. This is shown in Figure 9.8A, which also includes the reaction paths for two AVS minerals, mackinawite and greigite. Points which lie to the left of the greigite line suggest that greigite is incompletely dissolved in citrate dithionite buffer (Morse 1994) but completely liberated by the AVS distillation. However, the fact that the data also tend to scatter to the right of the mackinawite line implies incomplete sulfidization of "reactive" iron and is problematic in the face of high $H_2S$ concentrations. CD-Fe and $H_2S$ are plotted in Figure 9.8B (bottom), which does show a crude inverse relationship between these two parameters, but only when relatively high concentrations of CD-Fe are included in the dataset, at slightly less than 20 µmol/g CD-Fe, $H_2S$ concentrations rapidly exceed 1 mM.

Resolution of this apparent paradox of reactive iron limitation (low AVS and high pore water sulfide) with "excess" reactive iron may come about through consideration of the kinetics of iron oxide mineral dissolution and sulfidization. Using data from (Crill and Martens, 1987), Figure 9.9 tabulates the reactivity of iron phases by their first order "decay" constant, $k$. If we assume that CD must extract all iron having a $k$ greater than $10^{-4}$, this iron would have a half-life of approximately 7000 years. This implies that the maximum age of the as-yet unsulfidized reactive iron in this system is on the order of $10^4$ years. This time span is long compared with the apparent dynamics of this environment; for example, substantial changes in near surface sulfide concentrations were noted between 1997 and 1998 at GCAT2.

In summary, the observation of high dissolved sulfide reflects both the high rates of sulfate reduction and low availability of reactive sedimentary iron. Although sedimentary iron is present, it is apparently not reactive in sufficiently brief time scales as to effectively buffer dissolved sulfide. Sulfide that is not incorporated as AVS and pyrite is then available for biological consumption by sulfide oxidizers. Because sulfide oxidizers may play critical roles in chemosynthetic communities, a low concentration of sedimentary reactive iron may be an
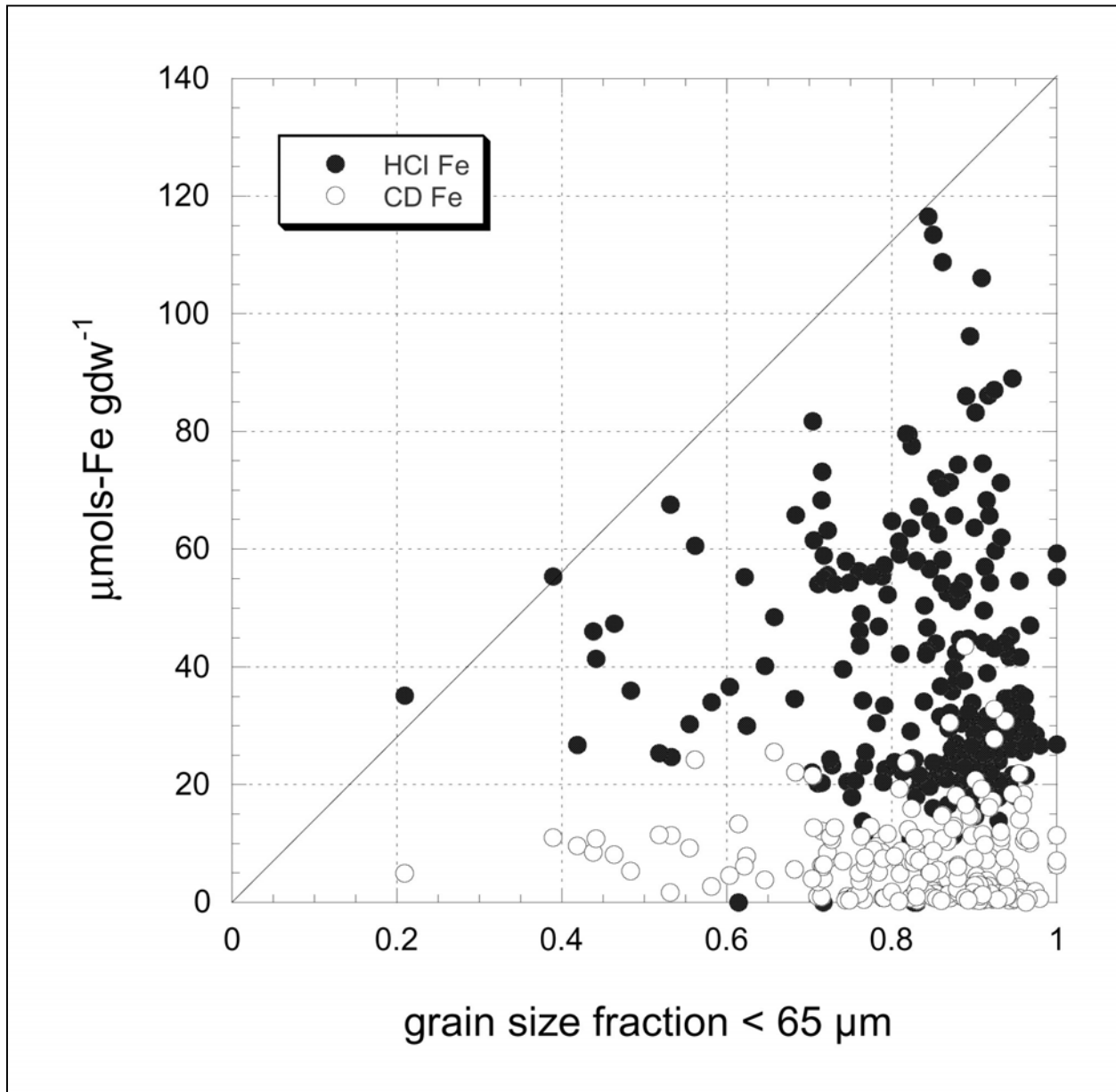
Figure 9.6    Sedimentary reactive iron. Iron extracted from sediments using citrate dithionite (CD, open circles) and HCl (closed circles) increases qualitatively as a function of grain size. However, CD-Fe concentrations are substantially less than those of HCl-Fe and are probably a more accurate reflection of the iron that is available for sulfide mineral formation.
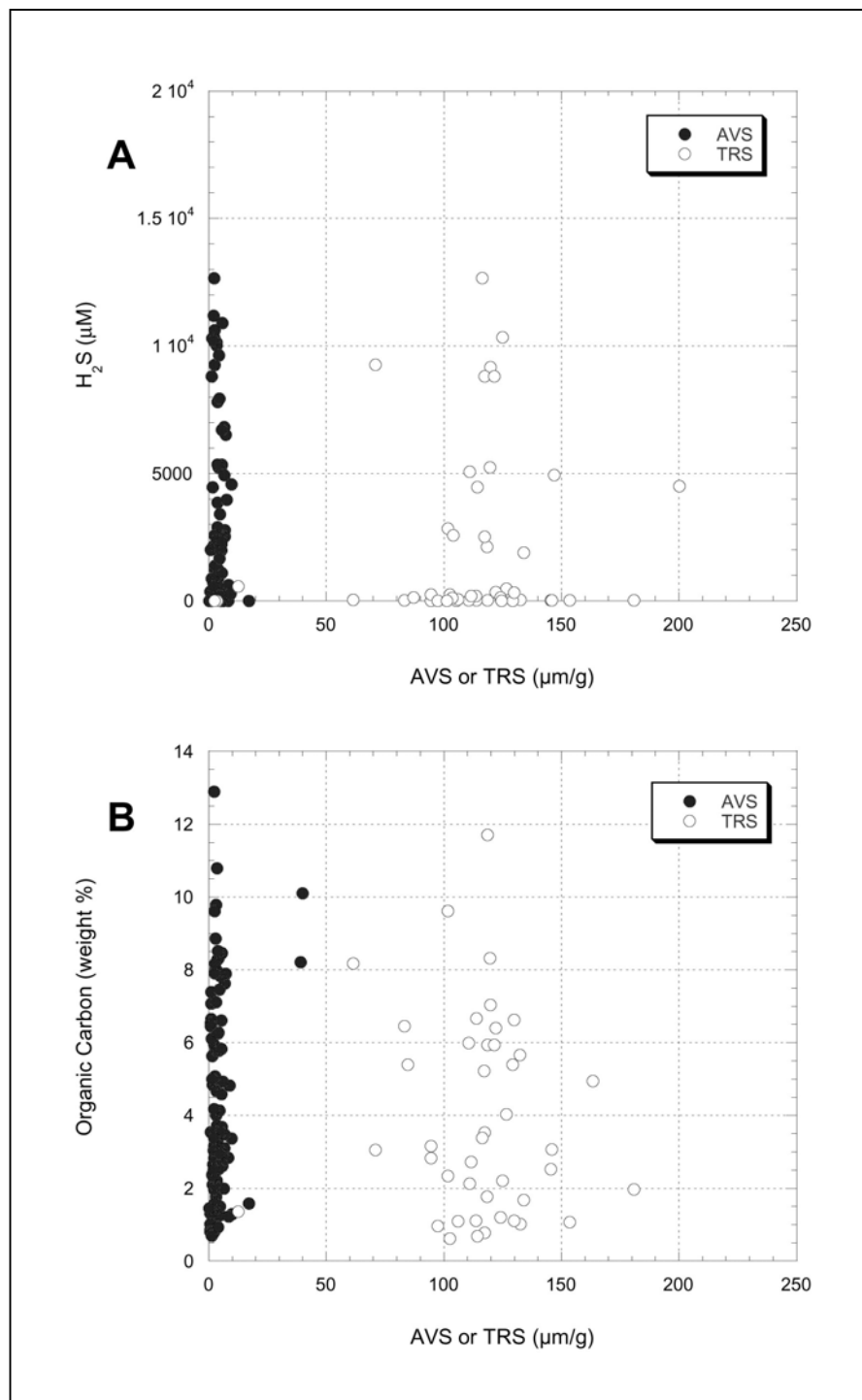
Figure 9.7.    Sedimentary sulfide (TRS and AVS). (A) *Dissolved versus solid phase sulfide.* Pyrite sulfur (TRS, open circles) is substantially greater (mean 111.8±35.4 µmol/g) than metastable, iron monosulfide (AVS, closed circles, mean 4.3±4.9 µmol/g) in these sediments. Although the TRS concentrations are largely invariant with respect to dissolved sulfide, there is some suggestion that AVS concentrations are lowest in those samples having very high dissolved sulfide concentrations, consistent with iron limitation. (B) *Organic carbon and solid phase sulfide.* AVS (closed circles) and TRS (closed circles) show little control by organic carbon concentration.
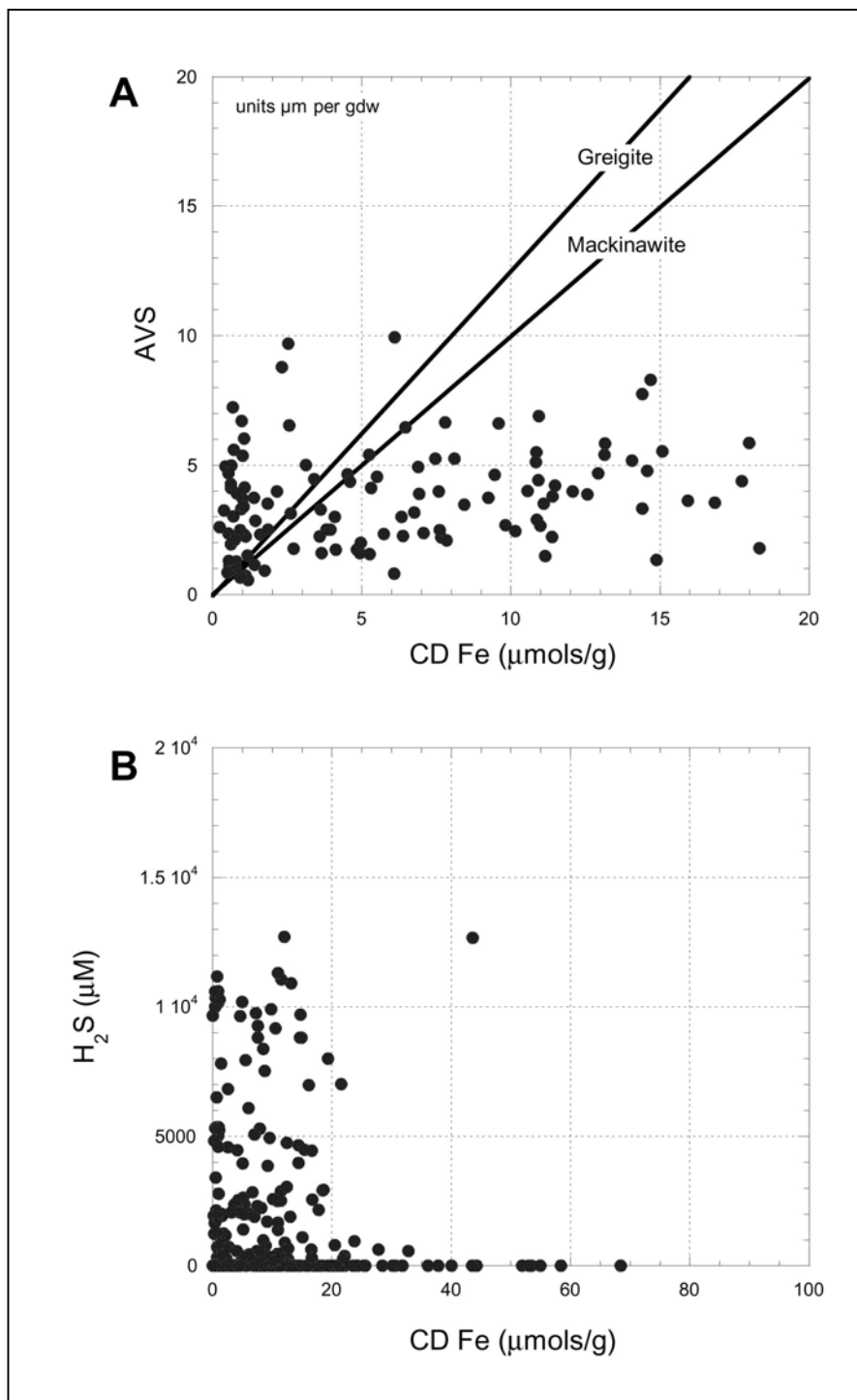
Figure 9.8. Reactive iron availability. (A) *Reactive iron versus AVS*. Data are cast relative to reaction paths for AVS minerals mackinawite and greigite. Data which lie to the left of the greigite line suggest this phase is incompletely dissolved in citrate dithonite buffer (Morse 1994) but completely liberated by the AVS distillation. Conversely, data that scatter to the right of the mackinawite line implies incomplete iron sulfidization. This latter result points to variations in iron reactivity with respect to sulfide that may reflect kinetic controls discussed in text. (B) *CD-Fe and dissolved $H_2S$*. Iron limitation is consistent with an inverse relationship, albeit crude, between these two parameters: dissolved sulfide is negligible at relatively high concentrations of CD-Fe, whereas at less than ~20 µmol/g CD-Fe, $H_2S$ concentrations rapidly exceed 1 mM.

$$\frac{\partial}{\partial t}[\text{Fe}] = -ak\,[\text{Fe}]$$

$$t_{1/2} = \frac{\ln 2}{k}$$
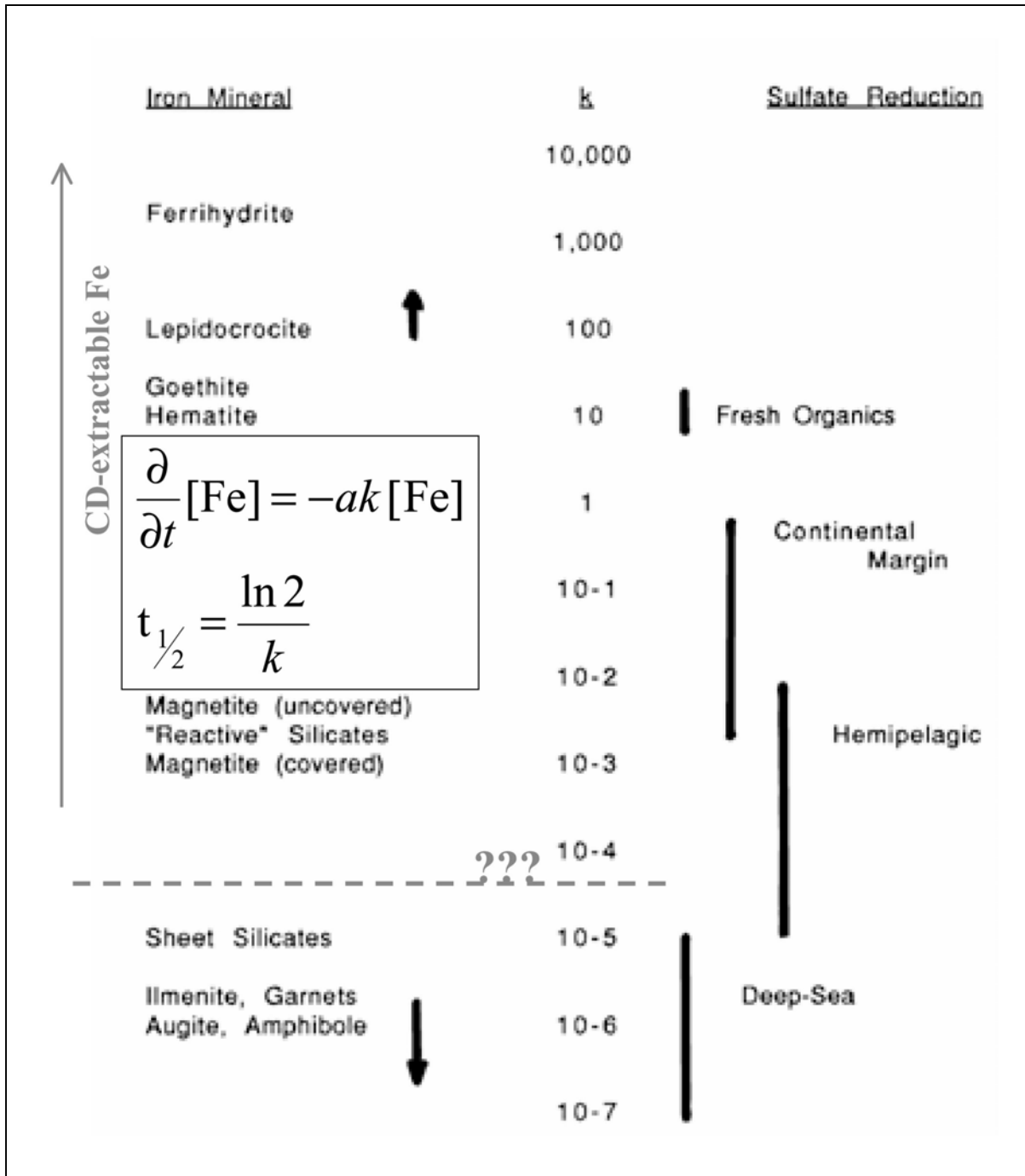
Figure 9.9. Iron reactivity towards sulfide. The variation in the reactivity of iron phases is reflected by the first order "decay" constant, $k$, which spans many orders of magnitude. If $k \sim 10^{-4}$ is set as a lower limit for CD-extractable Fe, this iron would have a half-life of ~7000 years, implying that the *maximum* age of the unsulfidized reactive iron is on the order of $10^4$ years. This time span is long compared with the apparent dynamics of this environment; for example, substantial changes in near surface sulfide concentrations were noted between 1997 and 1998 at GCAT2. After Canfield *et al.* (1992).

important feature of these environments. In addition, the excess DIC produced during sulfate reduction promotes extensive precipitation of calcium carbonate. This must in turn produce critical environmental changes in terms of substrate stability, permeability, and related physical sediment characteristics. Moreover, because the observed extent of sulfide mineralization is low, the development of calcium carbonate cements and hardgrounds may be the only truly physically durable signature of ancient seeps where no extant community is detectable.

**Sulfate depletion.** In addition to variations in the overall intensity of sulfate reduction discussed above, the depth at which sulfate was quantitatively depleted also varied at active sites. This variation is shown in Figure 9.10 in sulfate versus depth profiles for stations GCAT2, BHB3, and BHUN2 (1998). These profiles show production of DIC and $H_2S$ for comparison. At BHB3, sulfate depletion is essentially complete at 7 cms; at BHUN2 this occurs at approximately 9 cms. At GCAT2 (dives 4029 and 4048) depletion is not complete until 17 to 19 cms. There are also apparent temporal changes in this depth. Comparison of the 1997 data for GCAT (dive 2886) with that of the 1998 dives (4029 and 4048) shows a relaxation of the sulfate gradient and an expansion of the zone of sulfate reduction over this one-year period, with sulfate persisting to deeper depths in the later dives. This change is also reflected in the presence of high concentrations of sulfide (> 5 mM) within 2 cm of the surface in 1997. These levels are not encountered until 9-10 cms in the 1998 cores.

Despite variation in the depth at which sulfate depletion is complete, all of the above stations show greater than 50% depletion by 10 cm. This pattern is in contrast with that observed of the bacterial mat transect at GCB3. Three cores were taken here: one from the interior of a mixed orange and white *Beggiatoa* mat, one from the outer perimeter of the mat consisting of white *Beggiatoa* only, and a control core taken outside the mat entirely. This transect shows a clear influence of pore water chemistry by the mat itself. For example, comparison of on- and off-mat profiles in Figure 9.11A shows a development of a shallow pH maximum in the off-mat profile that is absent in the on-mat cores. The off-mat core contains negligible sulfide concentrations, whereas both the orange and white mats have sulfide concentrations over 2.5 mM (Figure 9.11B). However, although the orange *Beggiatoa* mat core shows a high-integrated sulfate reduction rate (Table 9.2), all the cores collected at GCB3 exhibit a pattern of sulfate depletion with respect to depth that is distinctly different from that seen at other stations of comparable productivity (Figure 9.11C). GCB3 contains only modest overall depletions in sulfate, with orange *Beggiatoa* showing greater reduction (<30%) than white. This is in contrast to other active sites that show more extensive shallow sulfate depletion. In addition, the depletion profile for the orange mat shows considerable scatter. Although GCB3 is a significant site because it is dominated by *Beggiatoa*, the weak and noisy sulfate depletion curves coupled with relatively high integrated rates (at least in the case of the orange mat) are difficult to reconcile and suggest that these bacteria may significantly influence transport of pore water sulfate.

**Brines.** Brines were clearly distinguished on the basis of elevated chloride concentrations. In these stations (GBM2 and BPB2), pore waters directly below the sediment-water interface typically exhibit chloride values close to seawater values. With increasing depth, there is a shallow zone of variable thickness with chloride concentrations intermediate between those of seawater and the brine end member. Because of its variable thickness, this zone can best be seen by calculating a mixing line between seawater and brine end members, with the latter having
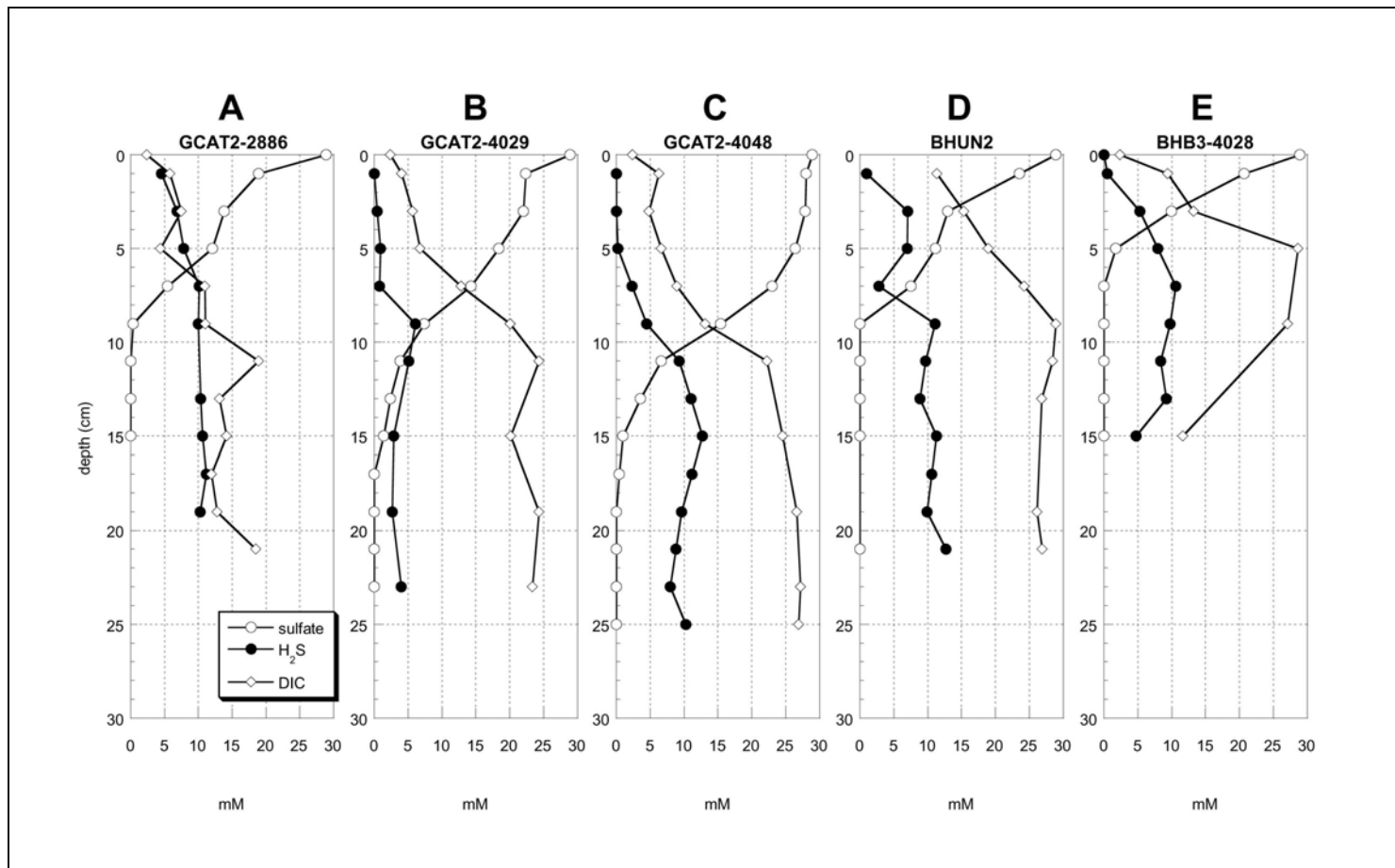
Figure 9.10.    Sulfate depletion depth.  Depth profiles of dissolved sulfate (open circles), sulfide (closed circles), and DIC (diamonds). Variations in the depth at which sulfate was quantitatively depleted varies at active stations GCAT2 (A-C), BHUN2 (1998 core, D), and BHB3 (E). At BHB3, sulfate depletion is essentially complete at 7 cms; at BHUN2 this occurs at ~ 9 cms, and at GCAT2 (dives 4029 and 4048) depletion is not complete until 17 to 19 cms. Comparison of the 1997 data for GCAT (dive 2886) with that of the 1998 dives (4029 and 4048) also shows a relaxation of the sulfate gradient and an expansion of the zone of sulfate reduction, with sulfate persisting to deeper depths in the later dives. Sulfide concentrations are also higher (> 5 mM) within 2 cm of the surface in 1997 at GCAT2 compared to the 1998 GCAT2 cores.
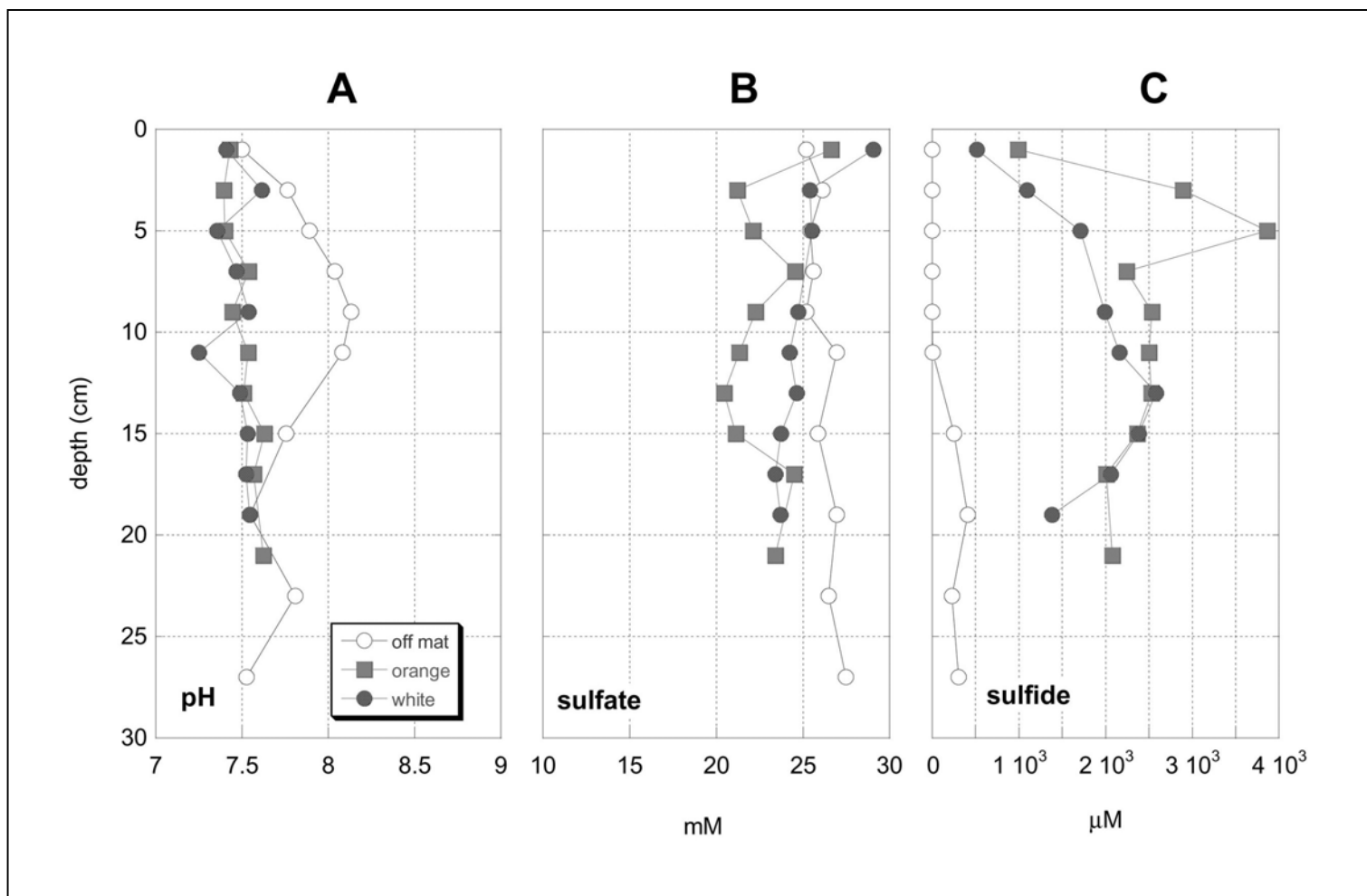
Figure 9.11.    *Beggiatoa* mat transect (GCB3). Depth profiles at GCB3 of pH (A), dissolved sulfate (B), and sulfide (C) differ both within-transect and from profiles at other stations. Open circles are off-mat, filled circles are orange mat, and filled squares denote orange mat cores. Off-mat pH shows a mid-depth maximum with is absent in the on-mat cores. The off-mat core contains negligible sulfide concentrations, whereas both the orange and white mats have sulfide concentrations over 2.5 mM.  Sulfate shows a noisy and mild depletion in the on-mat cores that differs from the pattern of sulfate depletion seen at other stations of comparable productivity.

maximum chloride values three times that of standard seawater, negligible sulfide and sulfate, elevated calcium, strontium, and sodium, and depleted magnesium concentrations relative to standard seawater. The pattern of chloride, sulfide, sulfate, and DIC concentrations with extent of mixing for GBM2 (dives 2882 and 4053) is shown in Figure 9.12. The pattern of rapid sulfate depletion with mixing clearly reflects the absence of sulfate in the end member brine, and confines the entire zone of sulfate reduction to a thin zone less than approximately 5 cm ($<$ ~50 % brine) in thickness at GBM2. Despite being limited to a relatively thin depth interval, sulfate reduction rates at GBM2 were among the highest measured (Table 9.2). There is considerably less brine dilution at BPB2, also shown for comparison in Figure 9.12.

## 9.3 Stable Isotope Geochemistry[*]

### 9.3.1 Introduction

Carbon, sulfur, and oxygen each have more than one stable isotope. By use of a mass spectrometer it is possible to measure the ratio of the stable isotopes for a given element. These ratios are then reported relative to a standard using the "$\delta$" notation, which is in ‰ because the differences are usually small. The isotope ratios of these elements vary depending on their source and as a result of chemical and biological processes that cause fractionation of the isotopes. Therefore, they are often good indicators of sources and tracers of biogeochemical processes.

A modest effort was made in this study to use carbon and oxygen isotopes to investigate the $CO_2$ system and sulfur isotopes to investigate the $H_2S$ system. Stable isotope ratios of dissolved components (DIC and $H_2S$) and solids ($CaCO_3$ and TRS) were determined on selected samples from sites of particular interest.

### 9.3.2 Results

Analytical results are reported in Tables 9.4 and 9.5.

Carbon and oxygen stable isotope ratios for DIC and $CaCO_3$ were plotted against each other and against other components including sulfur isotope ratios and concentrations of dissolved and solid components. In many cases, no relationships were observed, and those results are not presented here. However, interesting relationships were apparent. A good ($R^2 = 0.85$) linear relationship was observed (Figure 9.13) between carbon and oxygen isotope ratios in $CaCO_3$. However, virtually no ($R^2 = 0.08$) relationship occurred between the carbon isotope ratios in DIC and $CaCO_3$ or between the DIC concentration and its stable isotope ratio ($R^2 = 0.006$).

There were generally no good correlations between sulfur stable isotope ratios in TRS and $H_2S$ and with other components. For example, $R^2$s are 0.06 for TRS $\delta^{34}S$ vs. $SO_4$, 0.11 for TRS $\delta^{34}S$ vs. TRS, 0.19 for $H_2S$-$\delta^{34}S$ vs. DIC, and 0.30 for $H_2S$-$\delta^{34}S$ vs. $H_2S$. Figure 9.14 shows that with the exception of two TRS samples, TRS has a large range of quite negative $\delta^{34}S$ values at both low and high (low $SO_4$ concentrations) extents of sulfate reduction. In contrast, many $H_2S$-$\delta^{34}S$ values are close to zero with an increasingly large scatter to high positive values with increasing extent of sulfate reduction.

---

[*] This section was authored by John W. Morse and Steven Macks.
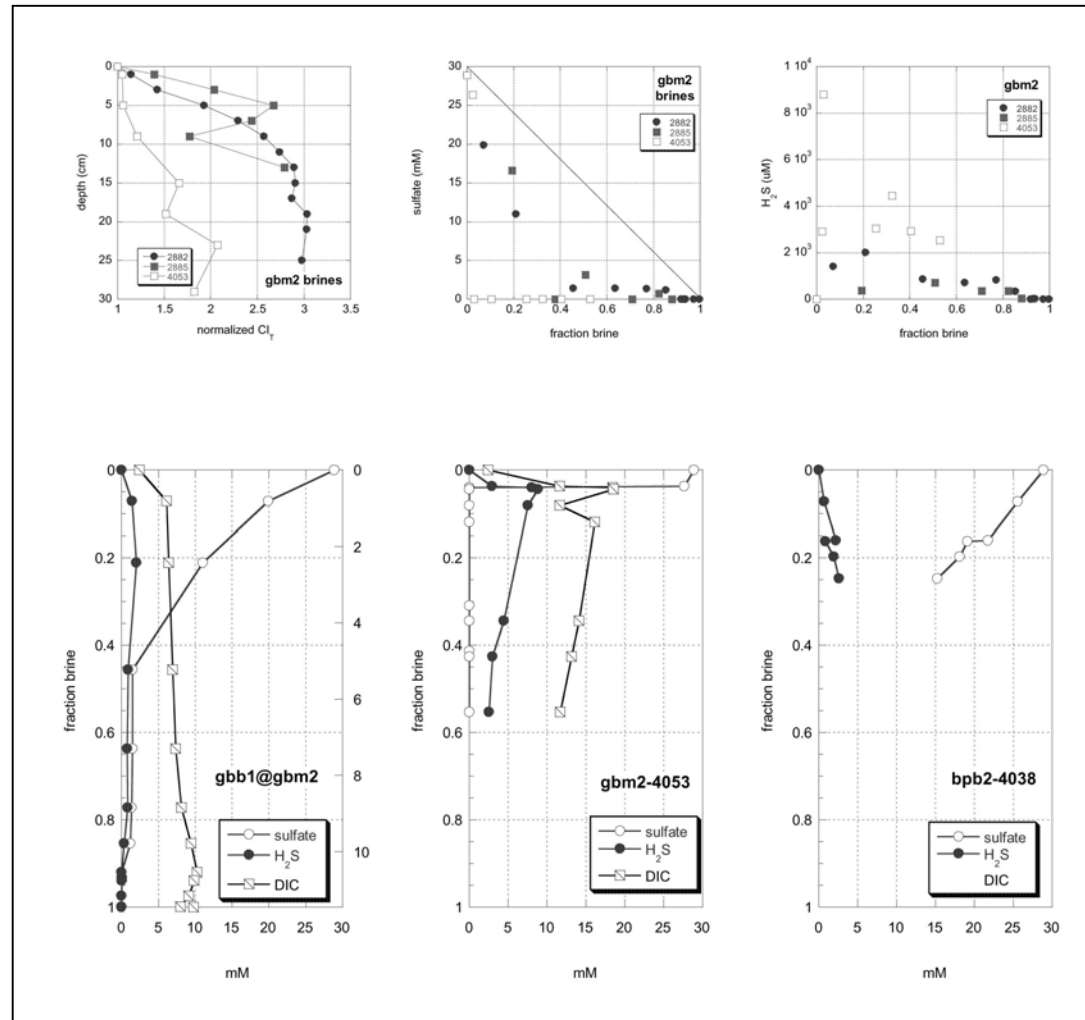
Figure 9.12.   Brine geochemisty. (A) Variation in chloride concentration as a function of depth at GBM2, normalized with respect to standard seawater. Open circles are dive 2882, closed squares are 2885, and open squares are 4053 data. (B) Sulfate concentrations at GBM2 brines, expressed as fraction brine. (C) Sulfide concentrations at GBM2 brines, expressed as fraction brine. (D-F) Variations with respect to depth at GBB1@GMB2 (D), GBM2 (dive 4053), and BPB2 (dive 4038). Open circles are sulfate, closed circles are sulfide, and open squares are DIC data. Note variation in the sulfate depletion with respect to fraction of brine mixing.

Table 9.4. Dissolved organic carbon and nutrients.

| Dive Number | Site | Station | Depth (cm) | Dissolved Organic Carbon (μM) | NH$_4$ (μM) | PO$_4$ (μM) | Urea (μM) | NO$_3$ (μM) | NO$_2$ (μM) | SiO$_3$ (μM) |
|---|---|---|---|---|---|---|---|---|---|---|
| 2871 | GC234 | GCST1 | 0-2 | 6262 | 135.39 | 10.45 | 2.91 | 12.79 | 1.94 | 96.16 |
| | | | 2-4 | 8417 | 158.12 | 9.66 | 4.15 | 11.30 | 2.63 | 89.65 |
| | | | 4-6 | 8272 | 186.18 | 9.70 | 8.30 | 8.45 | 2.01 | 91.38 |
| | | | 6-8 | 8425 | 190.50 | 9.13 | 10.38 | 6.78 | 1.99 | 88.99 |
| | | | 8-10 | 9070 | 217.38 | 8.72 | 5.81 | 7.40 | 1.48 | 78.37 |
| | | | 10-12 | 8892 | 228.05 | 9.43 | 17.44 | 2.54 | 1.08 | 81.12 |
| | | | 12-14 | 9157 | 264.43 | 8.34 | 8.30 | 2.11 | 1.60 | 77.70 |
| | | | 14-16 | 10275 | 229.91 | 7.48 | 9.55 | 2.24 | 1.59 | 73.26 |
| | | | 16-18 | – | – | – | – | – | – | – |
| | | | 18-20 | – | – | – | – | – | – | – |
| 2873 | GC235 | BHAT1 | 0-2 | 7181 | 244.83 | 53.75 | 9.55 | 0.00 | 0.46 | 155.95 |
| | | | 2-4 | 9044 | 322.13 | 71.57 | 34.04 | 0.12 | 0.44 | 187.59 |
| | | | 4-6 | 7850 | 330.95 | 78.38 | 9.55 | 0.24 | 0.42 | 191.38 |
| | | | 6-8 | 9556 | 337.45 | 82.89 | 9.55 | 0.37 | 0.40 | 198.28 |
| | | | 8-10 | 9995 | 299.10 | 52.29 | 10.38 | 0.40 | 1.36 | 148.42 |
| | | | 10-12 | 11768 | 268.47 | 34.42 | 12.45 | 0.72 | 0.26 | 126.45 |
| | | | 12-14 | 13289 | 239.01 | 39.96 | 16.19 | 0.54 | 1.43 | 114.80 |
| | | | 14-16 | – | – | – | – | – | – | – |
| 2873 | GC235 | BHM4 | 0-2 | 18310 | 472.90 | 146.42 | 22.47 | 1.78 | 3.91 | 208.12 |
| | | | 2-4 | 18285 | 454.56 | 120.24 | 27.51 | 2.48 | 2.43 | 182.47 |
| | | | 4-6 | 18318 | 431.84 | 72.15 | 21.38 | 1.76 | 1.20 | 132.48 |
| | | | 6-8 | – | – | – | – | – | – | – |
| | | | 8-10 | – | – | – | – | – | – | – |
| | | | 10-12 | – | 398.05 | 30.64 | 16.96 | 0.62 | 2.31 | 80.77 |
| | | | 12-14 | – | 390.70 | 30.26 | 21.52 | 4.31 | 2.50 | 89.26 |
| | | | 14-16 | – | 391.39 | 31.62 | 16.80 | 3.53 | 1.33 | 84.55 |
| | | | 16-18 | – | 408.18 | 38.31 | 14.39 | 1.71 | 1.20 | 97.21 |
| | | | 18-20 | – | 397.89 | 22.45 | 12.92 | 2.69 | 1.76 | 70.95 |
| 2874 | GC235 | BHST1 | 0-2 | 6011 | 152.52 | 5.03 | 24.49 | 1.94 | 1.03 | 75.39 |
| | | | 2-4 | 5391 | 145.63 | 12.19 | 9.55 | 0.95 | 1.23 | 101.78 |
| | | | 4-6 | 4016 | 109.33 | 10.81 | 8.72 | 0.00 | 0.50 | 96.30 |

Table 9.4. Dissolved organic carbon and nutrients. (continued)

| Dive Number | Site | Station | Depth (cm) | Dissolved Organic Carbon (µM) | NH₄ (µM) | PO₄ (µM) | Urea (µM) | NO₃ (µM) | NO₂ (µM) | SiO₃ (µM) |
|---|---|---|---|---|---|---|---|---|---|---|
| | | | 6-8 | 7448 | 95.86 | 10.54 | 4.57 | 1.14 | 1.25 | 106.25 |
| | | | 8-10 | 5945 | 80.99 | 8.93 | 4.57 | 0.08 | 0.63 | 93.58 |
| | | | 10-12 | 3056 | 107.72 | 7.39 | 7.47 | 0.39 | 1.32 | 91.18 |
| | | | 12-14 | 5670 | 101.81 | 9.15 | 12.04 | 1.07 | 1.63 | 94.96 |
| | | | 14-16 | 4229 | 106.87 | 8.89 | 12.45 | 1.14 | 1.66 | 82.29 |
| | | | 16-18 | – | 106.11 | 7.88 | 16.19 | 1.61 | 2.19 | 116.93 |
| 2875 | GC235 | BHST2 | 0-2 | 12064 | 291.60 | 64.94 | 25.75 | 4.02 | 0.45 | 250.31 |
| | | | 2-4 | 12287 | 209.80 | 39.51 | 23.61 | 0.05 | 0.63 | 170.09 |
| | | | 4-6 | 18979 | 187.83 | 33.17 | 22.28 | 0.68 | 0.55 | 148.14 |
| | | | 6-8 | – | – | – | – | – | – | – |
| | | | 8-10 | – | – | – | – | – | – | – |
| | | | 10-12 | – | – | – | – | – | – | – |
| 2875 | GC235 | BHUN1 | 0-2 | 2398 | 78.86 | 7.46 | 6.23 | 10.58 | 0.48 | 90.87 |
| | | | 2-4 | 2150 | 79.82 | 7.50 | 7.47 | 1.82 | 0.41 | 88.48 |
| | | | 4-6 | 2339 | 88.69 | 8.14 | 5.40 | 0.99 | 0.44 | 80.95 |
| | | | 6-8 | 2609 | 93.77 | 8.62 | 7.06 | 1.11 | 0.42 | 80.62 |
| | | | 8-10 | 3999 | 99.53 | 8.66 | 7.89 | 1.34 | 0.30 | 94.68 |
| | | | 10-12 | 3814 | 90.19 | 7.86 | 5.29 | 0.62 | 0.65 | 69.89 |
| | | | 12-14 | 3939 | 98.98 | 7.68 | 7.23 | 0.65 | 1.18 | 86.61 |
| | | | 14-16 | – | – | – | – | – | – | – |
| | | | 16-18 | – | – | – | – | – | – | – |
| | | | 18-20 | – | – | – | – | – | – | – |
| | | | 22-24 | – | – | – | – | – | – | – |
| | | | 26-28 | – | – | – | – | – | – | – |
| 2876 | GC233 | BPR2 | 0-2 | 6725 | 176.48 | 6.05 | 8.76 | 0.63 | 0.79 | 87.97 |
| | | | 2-4 | 3462 | 196.53 | 6.30 | 10.29 | 0.49 | 0.53 | 97.04 |
| | | | 4-6 | 4301 | 232.62 | 6.19 | 15.94 | 0.88 | 0.69 | 84.93 |
| | | | 6-8 | 4846 | 230.06 | 5.36 | 7.97 | 0.51 | 0.67 | 82.45 |
| | | | 8-10 | – | – | – | – | – | – | – |
| | | | 10-12 | – | – | – | – | – | – | – |
| 2880 | GC234 | GCB1@GCAT1 | 0-2 | 4433 | 278.70 | 19.11 | 7.43 | 0.19 | 0.59 | 121.47 |

Table 9.4. Dissolved organic carbon and nutrients. (continued)

| Dive Number | Site | Station | Depth (cm) | Dissolved Organic Carbon (µM) | NH$_4$ (µM) | PO$_4$ (µM) | Urea (µM) | NO$_3$ (µM) | NO$_2$ (µM) | SiO$_3$ (µM) |
|---|---|---|---|---|---|---|---|---|---|---|
| | | | 2-4 | 9483 | 96.60 | 28.77 | 11.85 | 1.76 | 1.48 | 159.89 |
| | | | 4-6 | 4400 | 70.57 | 12.51 | 5.12 | 2.64 | 1.16 | 131.99 |
| | | | 6-8 | 6134 | 83.85 | 14.44 | 1.68 | 4.11 | 1.20 | 153.86 |
| | | | 8-10 | 10005 | 70.93 | 13.09 | 1.56 | 4.86 | 1.00 | 126.00 |
| | | | 10-12 | 8223 | 61.78 | 12.91 | 3.50 | 1.09 | 0.55 | 119.62 |
| | | | 12-14 | 5402 | 55.75 | 12.29 | 3.79 | 1.54 | 0.65 | 120.99 |
| | | | 14-16 | – | – | – | – | – | – | – |
| | | | 16-18 | 4134 | 57.30 | 11.45 | 2.84 | 1.22 | 0.57 | 110.74 |
| | | | 18-20 | 3969 | 63.69 | 12.21 | 2.30 | 1.90 | 1.40 | 131.52 |
| | | | 22-24 | 7198 | 54.21 | 11.44 | 0.93 | 0.39 | 1.57 | 127.07 |
| 2882 | GB425 | GBB1@GBM2 | 0-2 | 34392 | 1970.00 | 169.43 | 81.09 | 15.66 | 1.96 | 387.25 |
| | | | 2-4 | 38426 | 2610.00 | 89.86 | 91.90 | 10.38 | 2.06 | 324.09 |
| | | | 4-6 | 29993 | 2820.00 | 43.99 | 68.66 | 6.13 | 1.13 | 273.89 |
| | | | 6-8 | 14992 | 3040.00 | 4.47 | 86.80 | 5.94 | 0.93 | 259.23 |
| | | | 8-10 | 7751 | 3250.00 | 10.50 | 67.42 | 0.74 | 0.40 | 287.06 |
| | | | 10-12 | 6038 | 3540.00 | 8.63 | 77.07 | 2.52 | 0.26 | 283.49 |
| | | | 12-14 | 5385 | 3690.00 | 5.32 | 64.73 | 3.22 | 0.12 | 267.65 |
| | | | 14-16 | 5358 | 3910.00 | 6.44 | 67.46 | 2.00 | 0.80 | 252.83 |
| | | | 16-18 | 5874 | 3940.00 | 6.09 | 55.14 | 3.09 | 1.36 | 262.56 |
| | | | 18-20 | 5105 | 3900.00 | 4.25 | 44.47 | 4.92 | 0.08 | 221.17 |
| | | | 22-24 | – | – | – | – | – | – | – |
| | | | 26-28 | – | – | – | – | – | – | – |
| 2883 | GB425 | GBM1 | 0-2 | 6740 | 220.73 | 33.26 | 29.02 | 0.62 | 1.17 | 121.09 |
| | | | 2-4 | 8517 | 198.39 | 47.93 | 29.71 | 0.04 | 1.23 | 167.57 |
| | | | 4-6 | 12577 | 242.14 | 80.13 | 29.99 | 0.67 | 1.15 | 197.73 |
| | | | 6-8 | 10744 | 242.04 | 95.73 | 26.63 | 0.91 | 0.38 | 248.34 |
| | | | 8-10 | 11770 | 309.52 | 112.94 | 26.92 | 0.78 | 1.06 | 319.44 |
| | | | 10-12 | 11208 | 364.76 | 103.53 | 35.68 | 1.35 | 1.05 | 310.76 |
| | | | 12-14 | 12127 | 406.47 | 52.93 | 25.06 | 4.53 | 0.60 | 202.89 |
| | | | 14-16 | – | – | – | – | – | – | – |
| | | | 16-18 | – | – | – | – | – | – | – |

Table 9.4. Dissolved organic carbon and nutrients. (continued)

| Dive Number | Site | Station | Depth (cm) | Dissolved Organic Carbon (µM) | NH$_4$ (µM) | PO$_4$ (µM) | Urea (µM) | NO$_3$ (µM) | NO$_2$ (µM) | SiO$_3$ (µM) |
|---|---|---|---|---|---|---|---|---|---|---|
| 2885 | GB425 | GBM2 | 0-2 | 6056 | 224.23 | 14.46 | 26.55 | 5.23 | 0.46 | 80.84 |
| | | | 2-4 | 8257 | 303.86 | 46.94 | 28.85 | 4.71 | 0.45 | 153.86 |
| | | | 4-6 | 10208 | 334.01 | 98.38 | 21.47 | 6.43 | 0.37 | 246.37 |
| | | | 6-8 | 11562 | 367.10 | 115.48 | 18.92 | 6.49 | 0.87 | 257.12 |
| | | | 8-10 | 11871 | 361.34 | 79.51 | 23.64 | 6.47 | 0.35 | 205.50 |
| | | | 10-12 | 11321 | 340.06 | 68.13 | 23.12 | 8.13 | 0.34 | 176.39 |
| | | | 12-14 | – | – | – | – | – | – | – |
| | | | 14-16 | – | – | – | – | – | – | – |
| | | | 16-18 | – | – | – | – | – | – | – |
| 2886 | GC234 | GCAT2 | 0-2 | 23204 | 313.91 | 97.45 | 21.38 | 21.88 | 0.20 | 263.80 |
| | | | 2-4 | 24558 | 321.55 | 73.48 | 5.56 | 15.98 | 0.13 | 234.67 |
| | | | 4-6 | 21681 | 292.64 | 40.37 | 0.21 | 0.76 | 0.68 | 192.26 |
| | | | 6-8 | 11149 | 277.82 | 25.43 | 10.14 | 10.59 | 0.10 | 161.11 |
| | | | 8-10 | 23291 | 250.45 | 19.36 | 4.39 | 12.06 | 0.28 | 140.18 |
| | | | 10-12 | 15209 | 222.47 | 15.08 | 7.89 | 10.32 | 0.39 | 124.36 |
| | | | 12-14 | – | – | – | – | – | – | – |
| | | | 14-16 | – | – | – | – | – | – | – |
| | | | 16-18 | – | – | – | – | – | – | – |
| | | | 18-20 | – | – | – | – | – | – | – |
| | | | 20-22 | – | – | – | – | – | – | – |
| 2888 | GC234 | GCAT1 | 0-2 | 8415 | 198.04 | 29.07 | 18.23 | 9.81 | 0.38 | 156.55 |
| | | | 2-4 | 6488 | 201.07 | 26.20 | 12.87 | 10.50 | 0.24 | 133.58 |
| | | | 4-6 | 9846 | 204.75 | 18.73 | 8.96 | 5.43 | 0.75 | 102.68 |
| | | | 6-8 | 8357 | 209.47 | 13.10 | 7.95 | 5.87 | 0.69 | 83.37 |
| | | | 8-10 | – | – | – | – | – | – | – |
| | | | 10-12 | – | – | – | – | – | – | – |
| | | | 12-14 | – | – | – | – | – | – | – |
| 2891 | GC235 | BHAT2 | 0-2 | 5473 | 136.61 | 9.50 | 26.46 | 9.44 | 7.97 | 75.87 |
| | | | 2-4 | 6657 | 145.72 | 15.47 | 8.72 | 4.97 | 1.18 | 69.77 |
| | | | 4-6 | 7517 | 153.73 | 13.85 | 6.32 | 3.63 | 0.57 | 71.31 |
| | | | 6-8 | 6637 | 145.64 | 13.10 | 8.09 | 3.52 | 1.06 | 103.44 |

Table 9.4. Dissolved organic carbon and nutrients. (continued)

| Dive Number | Site | Station | Depth (cm) | Dissolved Organic Carbon (µM) | $NH_4$ (µM) | $PO_4$ (µM) | Urea (µM) | $NO_3$ (µM) | $NO_2$ (µM) | $SiO_3$ (µM) |
|---|---|---|---|---|---|---|---|---|---|---|
| | | | 8-10 | 4233 | 132.43 | 11.48 | 10.80 | 3.16 | 0.63 | 62.58 |
| | | | 10-12 | – | – | – | – | – | – | – |
| | | | 12-14 | – | – | – | – | – | – | – |
| | | | 14-16 | – | – | – | – | – | – | – |
| box | GC235 | BHBC2 | 0-2 | 5618 | 130.18 | 14.40 | 18.98 | 0.43 | 1.12 | 151.84 |
| | | | 2-4 | 5446 | 140.33 | 12.46 | 17.20 | 1.31 | 0.80 | 162.03 |
| | | | 4-6 | 4855 | 111.62 | 8.28 | 15.02 | 0.81 | 0.90 | 95.38 |
| | | | 6-8 | 4659 | 104.91 | 7.30 | 11.18 | 1.26 | 1.00 | 95.79 |
| | | | 8-10 | 3568 | 122.98 | 7.26 | 10.23 | 1.55 | 0.31 | 90.41 |
| | | | 10-12 | 3967 | 132.44 | 7.51 | 11.34 | 1.11 | 0.36 | 87.93 |
| | | | 12-14 | 3754 | 148.08 | 7.55 | 13.28 | 0.96 | 1.06 | 88.33 |
| | | | 14-16 | 3919 | 147.91 | 8.31 | 11.92 | 1.43 | 0.19 | 95.47 |
| | | | 16-18 | 4879 | 163.53 | 7.77 | 8.90 | 1.94 | 0.24 | 98.77 |
| | | | 18-20 | 4578 | 149.98 | 6.86 | 5.89 | 0.29 | 1.49 | 82.81 |
| 4025 | GC185 | BHAT1 | 0-2 | – | 144.46 | 30.38 | 8.4 | 122.12 | 29.34 | 88.28 |
| | | | 2-4 | – | 183.98 | 53.77 | 6.61 | 3.81 | 8.21 | 119.53 |
| | | | 4-6 | – | 228.61 | 51.86 | 7.13 | 7.28 | 2.54 | 109.34 |
| | | | 6-8 | – | 194.67 | 45.47 | 6.49 | 1.92 | 1.36 | 101.73 |
| | | | 8-10 | – | 145.92 | 23.89 | 6.43 | 1.18 | 1.33 | 57.71 |
| | | | 10-12 | – | 142.18 | 22.83 | 5.23 | 3.15 | 0.77 | 57.05 |
| | | | 12-14 | – | 116.64 | 12.82 | 5.17 | 2.16 | 0.99 | 38.96 |
| | | | 14-16 | – | 461.24 | 9.77 | 5.11 | 1.61 | 0.77 | 33.09 |
| | | | 16-18 | – | 95.41 | 9.29 | 6.19 | 2.16 | 0.9 | 28.96 |
| 4027 | GC185 | BHST1 | 0-2 | 6788 | 109.45 | 12.08 | 5.78 | 87.29 | 27.16 | 60.19 |
| | | | 2-4 | 6387 | 140.09 | 8.39 | 7.95 | 82.35 | 22.89 | 50.1 |
| | | | 4-6 | 5367 | 224.78 | 15.14 | 6.23 | 216.2 | 26.73 | 91.69 |
| | | | 6-8 | 5048 | 183.14 | 9.92 | 5.07 | 70.65 | 12.05 | 70.43 |
| | | | 8-10 | 5229 | 172.43 | 8.82 | 5.56 | 13.2 | 4.04 | 54.76 |
| | | | 10-12 | 4729 | 187.94 | 10.17 | 5.51 | 6.93 | 1.28 | 66.12 |
| | | | 12-14 | 4731 | 204.3 | 11.25 | 5.46 | 5.58 | 1.01 | 66.35 |
| | | | 14-16 | 4663 | 136.25 | 6.41 | 5.4 | 5.17 | 0.63 | 49.08 |

Table 9.4. Dissolved organic carbon and nutrients. (continued)

| Dive Number | Site | Station | Depth (cm) | Dissolved Organic Carbon (µM) | NH$_4$ (µM) | PO$_4$ (µM) | Urea (µM) | NO$_3$ (µM) | NO$_2$ (µM) | SiO$_3$ (µM) |
|---|---|---|---|---|---|---|---|---|---|---|
| | | | 16-18 | 4342 | 110.05 | 5.65 | 4.25 | 2.46 | 0.91 | 35.8 |
| | | | 18-20 | 4691 | 97.59 | 5.09 | 5.29 | 0.29 | 0.65 | 35.23 |
| | | | 20-22 | 5037 | 89.19 | 5.55 | 4.15 | 0.33 | 0.64 | 34.65 |
| | | | 22-24 | 4372 | 81.52 | 5.67 | 6.28 | 2.01 | 0.63 | 36.47 |
| | | | 24-26 | 4753 | 77.9 | 5.12 | 4.05 | 2.05 | 0.63 | 35.1 |
| | | | 26-28 | 5246 | 71.7 | 5.51 | 4.54 | 2.79 | 0.74 | 37.71 |
| | | | 28-29 | 5773 | 77.99 | 4.48 | 5.57 | 2.16 | 0.59 | 29.98 |
| 4028 | GC185 | BHB3 | 0-2 | 8930 | 195.9 | 23.72 | 7.3 | 109.2 | 1.29 | 63.17 |
| | | | 2-4 | 6429 | 57.64 | 7.31 | 4.43 | 25.29 | 1.65 | 51.41 |
| | | | 4-6 | 7031 | 37.39 | 5.11 | 1.04 | 5.07 | 0.42 | 46.5 |
| | | | 6-8 | 6666 | 38.76 | 4.69 | 0.98 | 4.83 | 0.61 | 45.01 |
| | | | 8-10 | 6419 | 29.91 | 5.03 | 1.49 | 1.93 | 0.5 | 62.25 |
| | | | 10-12 | 5666 | 35.5 | 5.15 | 0.88 | 1.45 | 0.19 | 50.56 |
| | | | 12-14 | 6216 | 47.49 | 8.03 | 0.28 | 1.57 | 0.02 | 61.8 |
| | | | 14-16 | 7494 | 75.39 | 10.83 | 4.1 | 1.91 | 0.38 | 61.15 |
| 4029 | GC234 | GCAT2 | 0-2 | 7718 | 159.61 | 12.34 | 6.63 | 264.34 | 24.19 | 39.39 |
| | | | 2-4 | 6311 | 167.08 | 7.5 | 3.73 | 154.18 | 7.66 | 45.93 |
| | | | 4-6 | 9748 | 114.26 | 5.33 | 3.68 | 110.67 | 1.33 | 41.42 |
| | | | 6-8 | 7140 | 104.92 | 4.78 | 6.46 | 103.83 | 0.6 | 47.17 |
| | | | 8-10 | 10127 | 105.36 | 7.33 | 1.32 | 60.45 | 0.45 | 64.00 |
| | | | 10-12 | 7351 | 68.29 | 4.48 | 3.52 | 15.56 | 0.47 | 43.67 |
| | | | 12-14 | 7419 | 83.08 | 7.37 | 1.22 | 52.76 | 0.67 | 73.97 |
| | | | 14-16 | 5797 | 66.2 | 5.6 | 3.42 | 22.08 | 0.63 | 59.15 |
| | | | 16-18 | 7554 | 45.45 | 3.37 | 1.13 | 15.12 | 0.16 | 43.55 |
| | | | 18-20 | 10256 | 83.95 | 9.36 | 0.52 | 21.54 | 0.39 | 90.56 |
| | | | 20-22 | 10640 | 80.39 | 10.03 | 1.03 | 13.68 | 0 | 95.57 |
| | | | 22-24 | 9835 | 73.2 | 7.98 | 2.1 | 15.96 | 0.23 | 104.57 |
| | | | 24-26 | 11755 | 66.02 | 6.54 | 0.38 | 13.6 | 0.14 | 93.67 |
| | | | 26-28 | 11323 | 41.94 | 5.79 | 0.34 | 6.3 | 0.04 | 70.05 |
| | | | 28-30 | 13368 | 40.51 | 5.23 | 0.29 | 2.16 | 0.1 | 60.76 |
| 4031 | GC234 | GCST1 | 0-2 | 5516 | 144.91 | 11.48 | 9.05 | 75.97 | 23.93 | 66.93 |

Table 9.4. Dissolved organic carbon and nutrients. (continued)

| Dive Number | Site | Station | Depth (cm) | Dissolved Organic Carbon (µM) | $NH_4$ (µM) | $PO_4$ (µM) | Urea (µM) | $NO_3$ (µM) | $NO_2$ (µM) | $SiO_3$ (µM) |
|---|---|---|---|---|---|---|---|---|---|---|
| | | | 2-4 | 6238 | 117.15 | 13.68 | 5.62 | 18.84 | 1.68 | 73.65 |
| | | | 4-6 | 4575 | 104.32 | 11.58 | 3.56 | 119.94 | 1.24 | 81.24 |
| | | | 6-8 | 11543 | 88.96 | 9.4 | 3.87 | 21.24 | 0.86 | 89.7 |
| | | | 8-10 | 6018 | 74.2 | 8.15 | 2.14 | 33.11 | 0.6 | 81.64 |
| | | | 10-12 | 5769 | 64.86 | 8 | 3.81 | 8.37 | 1.47 | 95.53 |
| | | | 12-14 | 9660 | 59.31 | 8.74 | -4.74 | 29.11 | 0.65 | 96.62 |
| | | | 14-16 | 10886 | 48.27 | 7.97 | -5.11 | 4.1 | 1.2 | 89.53 |
| | | | 16-18 | 11378 | 45.01 | 8.23 | -8.21 | 1.83 | 1.75 | 104.19 |
| | | | 18-20 | 21224 | 42.85 | 8.97 | -91.76 | 10.09 | 0.1 | 94.44 |
| | | | 20-22 | 10866 | 35.6 | 7.24 | -4.16 | 3.33 | 1.25 | 78.25 |
| 4032 | GC234 | GCAT1 | 0-2 | 7516 | 147.36 | 6.62 | 8.83 | 301.91 | 13.95 | 30.48 |
| | | | 2-4 | 6940 | 170.14 | 6.21 | 9.98 | 78.3 | 11.25 | 24.88 |
| | | | 4-6 | 5795 | 166.4 | 3.91 | 8.68 | 66.04 | 7.8 | 21.87 |
| | | | 6-8 | 5503 | 147.55 | 3.76 | 7.38 | 18.73 | 3.42 | 24.01 |
| | | | 8-10 | 5183 | 124.87 | 4.56 | 7.93 | 34.63 | 3.01 | 25.29 |
| | | | 10-12 | 4548 | 115.34 | 4.01 | 8.47 | 14.42 | 1.33 | 33.45 |
| | | | 12-14 | 4489 | 81.68 | 3.26 | 7.17 | 9.12 | 1 | 22.7 |
| | | | 14-16 | 4568 | 80.65 | 3.04 | 6.48 | 8.65 | 0.76 | 30.01 |
| | | | 16-18 | 4845 | 71.78 | 3.1 | 7.02 | 9.31 | 0.8 | 26.13 |
| | | | 18-20 | 4797 | 71.47 | 3.16 | 6.95 | 9.15 | 0.96 | 36.87 |
| | | | 20-22 | 5328 | 85.09 | 3.55 | 6.88 | 6.56 | 0.75 | 26.98 |
| 4036 | GC234 | GCJT1 | 0-2 | – | 117.25 | 16.47 | 10.8 | 14.88 | 12.79 | 60.38 |
| | | | 2-4 | – | 136.89 | 14.45 | 11.36 | 6.56 | 10.22 | 52.06 |
| | | | 4-6 | – | 141.23 | 9.5 | 11.35 | 3.04 | 2.99 | 42.89 |
| | | | 6-8 | – | 123.28 | 6.17 | 11.34 | 0.78 | 1.15 | 42.78 |
| | | | 8-10 | – | 108.71 | 6.17 | 11.33 | 1.08 | 0.81 | 45.15 |
| | | | 10-12 | – | 94.24 | 5.76 | 10.75 | 1.07 | 0.8 | 44.22 |
| | | | 12-14 | – | 88.45 | 5.48 | 11.31 | 1.67 | 0.98 | 44.12 |
| | | | 14-16 | – | 86.61 | 5.41 | 9.59 | 1.82 | 0.81 | 48.14 |
| | | | 16-18 | – | 83.34 | 5.34 | 10.71 | 1.83 | 0.76 | 51.34 |
| | | | 18-20 | – | 85.45 | 5.54 | 10.14 | 2.07 | 1.29 | 45.46 |

Table 9.4. Dissolved organic carbon and nutrients. (continued)

| Dive Number | Site | Station | Depth (cm) | Dissolved Organic Carbon (µM) | NH$_4$ (µM) | PO$_4$ (µM) | Urea (µM) | NO$_3$ (µM) | NO$_2$ (µM) | SiO$_3$ (µM) |
|---|---|---|---|---|---|---|---|---|---|---|
| | | | 20-22 | – | 82.54 | 5.61 | 11.26 | 2.27 | 1.06 | 48.66 |
| | | | 22-23 | – | 82.51 | 5.74 | 11.26 | 1.41 | 1.11 | 49.37 |
| 4037 | GC233 | BPAT1 | 0-2 | – | 112.38 | 10.77 | 24.53 | 42.61 | 10.9 | 52.86 |
| | | | 2-4 | – | 108.33 | 11.09 | 8.57 | 13.35 | 12.26 | 44.74 |
| | | | 4-6 | – | 105.1 | 10.54 | 5.17 | 5.67 | 3.64 | 36.64 |
| | | | 6-8 | – | 102.69 | 13.02 | 6.1 | 44.41 | 8.62 | 48.29 |
| | | | 8-10 | – | 98.3 | 11.79 | 8.36 | 16.12 | 3.04 | 46.2 |
| | | | 10-12 | – | 95.91 | 8.64 | 6.62 | 4.08 | 2.69 | 43.27 |
| 4038 | GC233 | BPB2 | no frozen core available | | | | | | | |
| 4040 | GB425 | GBUN1 | 0-2 | 3950 | 47.76 | 6.47 | 5.55 | 123.08 | 3.41 | 47.17 |
| | | | 2-4 | 7015 | 121.09 | 20.13 | 8.47 | 66.27 | 2.96 | 50.2 |
| | | | 4-6 | 3589 | 69.9 | 4.83 | 7.41 | 19.19 | 2.2 | 34.53 |
| | | | 6-8 | 3412 | 88.39 | 7.22 | 4.01 | 10.04 | 0.91 | 55.38 |
| | | | 8-10 | 3083 | 88.76 | 5.01 | 1.6 | 3.33 | 0.3 | 26.21 |
| | | | 10-12 | 2850 | 91.09 | 4.55 | 2.2 | 6.43 | 0.21 | 28.41 |
| | | | 12-14 | 3078 | 80.59 | 4.04 | 2.79 | 1.78 | 1.23 | 41.58 |
| 4042 | GC185 | BHM3 | 0-2 | 9331 | 11.39 | 2.38 | 0.62 | 1.28 | 0.27 | 8.16 |
| | | | 2-4 | 13046 | 282.15 | 46.17 | 6.97 | 17.52 | 1.45 | 129.84 |
| | | | 4-6 | 10601 | 240.5 | 34.28 | 5.8 | 6.21 | 0.91 | 121.73 |
| | | | 6-8 | 11014 | 225.58 | 29.68 | 6.96 | 4.72 | 1.46 | 119.24 |
| | | | 8-10 | 10826 | 213.38 | 25.52 | 5.79 | 1.42 | 1.13 | 90.9 |
| | | | 10-12 | 9873 | 213.69 | 29.7 | 5.78 | 3.19 | 1.12 | 118.28 |
| | | | 12-14 | 9757 | 201.93 | 23.68 | 5.78 | 3.16 | 1.11 | 81.8 |
| | | | 14-16 | 10056 | 194.72 | 17.42 | 6.93 | 1.37 | 1.1 | 106.83 |
| | | | 16-18 | 10939 | 186.79 | 16.89 | 6.35 | 1.36 | 1.08 | 83.24 |
| | | | 18-20 | 21325 | 183.36 | 14.95 | 5.76 | 0.47 | 1.07 | 82.34 |
| | | | 20-22 | 25818 | 178.82 | 14.62 | 10.97 | 1.27 | 1.12 | 129.16 |
| | | | 22-24 | 25104 | 155 | 13.14 | 8.64 | 1.9 | 1.33 | 56.85 |
| 4043 | GC234 | GCB3 orange *Beggiotoa* | 0-2 | 8797 | 291.35 | 37.51 | 9.79 | 9.65 | 7.47 | 83.69 |
| | | | 2-4 | 9458 | 193.21 | 21.99 | 5.74 | 10.15 | 1.68 | 80.34 |

Table 9.4. Dissolved organic carbon and nutrients. (continued)

| Dive Number | Site | Station | Depth (cm) | Dissolved Organic Carbon (μM) | NH₄ (μM) | PO₄ (μM) | Urea (μM) | NO₃ (μM) | NO₂ (μM) | SiO₃ (μM) |
|---|---|---|---|---|---|---|---|---|---|---|
| | | | 4-6 | 10577 | 137.53 | 12.27 | 5.16 | 6.93 | 1.38 | 78.62 |
| | | | 6-8 | 24492 | 126.86 | 11.74 | 2.86 | 6.4 | 1 | 96.43 |
| | | | 8-10 | 31250 | 121.71 | 11.2 | 0.57 | 4.94 | 0.7 | 64.54 |
| | | | 10-12 | 39172 | 119.47 | 10.99 | 4.57 | 4.19 | 0.56 | 64.45 |
| | | | 12-14 | 42289 | 98.4 | 11.06 | 2.28 | 2.64 | 0.39 | 69.26 |
| | | | 14-16 | 15743 | 87.91 | 16.52 | 2.85 | 0.95 | 1.2 | 88.76 |
| | | | 16-18 | 17545 | 83.91 | 20.35 | 2.84 | 1.22 | 0.9 | 77.25 |
| | | | 18-20 | 17966 | 75.99 | 13.76 | 1.14 | 0.92 | 0.34 | 73.88 |
| | | | 20-22 | 17692 | 56.73 | 11.06 | 0.57 | 1.74 | 0.33 | 71.33 |
| | | | 22-24 | 17110 | 48.55 | 5.78 | 0 | 0.07 | 0.32 | 87.58 |
| | | | 24-26 | 16816 | 42.17 | 6.11 | 2.83 | 0.06 | 1.13 | 89.94 |
| 4043 | GC234 | GCB3 off mat | 0-2 | 3485 | 65.17 | 8 | 7.42 | 204.35 | 7.56 | 44.58 |
| | | | 2-4 | 3609 | 85.54 | 8.46 | 7.35 | 135.8 | 9.12 | 56.14 |
| | | | 4-6 | 3724 | 98.96 | 6.64 | 6.66 | 33.5 | 11.99 | 38.56 |
| | | | 6-8 | 5142 | 107.03 | 8.71 | 7.82 | 11.14 | 12.8 | 51.85 |
| | | | 8-10 | 5107 | 125.13 | 5.81 | 5.9 | 9.98 | 7.71 | 41.13 |
| | | | 10-12 | 5174 | 111.9 | 5.73 | 6.44 | 5.13 | 4.95 | 28.66 |
| | | | 12-14 | 5428 | 111.22 | 5.58 | 5.75 | 1.71 | 3.53 | 53.98 |
| | | | 14-16 | 5451 | 103.95 | 5.57 | 7.54 | 2.83 | 1.73 | 52.69 |
| | | | 16-18 | 5186 | 89.47 | 4.14 | 7.46 | 2.57 | 1.31 | 29.94 |
| | | | 18-20 | 6329 | 89.88 | 4.54 | 4.3 | 2.94 | 0.95 | 33.8 |
| | | | 20-22 | 5869 | 89.57 | 4.53 | 7.32 | 1.94 | 0.58 | 41.96 |
| | | | 22-24 | 5641 | 95.77 | 5.26 | 7.87 | 1.98 | 0.56 | 41.53 |
| | | | 24-26 | 6230 | 95.82 | 4.71 | 7.79 | 1.98 | 0.56 | 52.25 |
| | | | 26-28 | 6813 | 96.96 | 5.52 | 5.86 | 1.77 | 0.78 | 46.67 |
| | | | 28-30 | 7035 | 98.83 | 5.85 | 6.41 | 1.96 | 0.6 | 40.22 |
| | | | 30-32 | 6854 | 91.95 | 4.68 | 6.95 | 3.35 | 0.58 | 46.65 |
| 4043 | GC234 | GCB3 white *Beggiotoa* | no frozen core available | | | | | | | |

Table 9.4. Dissolved organic carbon and nutrients. (continued)

| Dive Number | Site | Station | Depth (cm) | Dissolved Organic Carbon (μM) | NH$_4$ (μM) | PO$_4$ (μM) | Urea (μM) | NO$_3$ (μM) | NO$_2$ (μM) | SiO$_3$ (μM) |
|---|---|---|---|---|---|---|---|---|---|---|
| 4045 | GC185 | BHAT2 | 0-2 | – | 198.43 | 25.06 | 13.22 | 144.35 | 7.78 | 64.02 |
| | | | 2-4 | – | 220.11 | 26.85 | 8.28 | 65.94 | 10.52 | 65.42 |
| | | | 4-6 | – | 230.48 | 23.64 | 7.42 | 20.93 | 10.64 | 59.11 |
| | | | 6-8 | – | 206.37 | 21.7 | 5.96 | 12.24 | 5.39 | 60.51 |
| | | | 8-10 | – | 179.9 | 15.3 | 5.09 | 8.43 | 1.83 | 52.49 |
| | | | 10-12 | – | 164.17 | 10.67 | 5.38 | 3.95 | 1.4 | 46.17 |
| | | | 12-14 | – | 168.07 | 8.97 | 6.31 | 2.26 | 1.2 | 22.09 |
| | | | 14-16 | – | 133.72 | 6.83 | 5.73 | 1.73 | 1.85 | 23.45 |
| | | | 16-18 | – | 131.42 | 6.55 | 5.73 | 8.73 | 2.85 | 21.51 |
| | | | 18-20 | – | 140.07 | 7.11 | 6.3 | 1.5 | 1.34 | 21.22 |
| | | | 20-22 | – | 142.47 | 8.29 | 7.44 | 1.06 | 1.89 | 25.07 |
| | | | 22-24 | – | 122.62 | 6.34 | 5.72 | 1.29 | 0.8 | 25.6 |
| | | | 24-26 | – | 121.11 | 6.55 | 5.71 | 1.11 | 2.1 | 22.01 |
| | | | 26-28 | – | 123.47 | 6.62 | 7.43 | 3.53 | 0.78 | 15.95 |
| 4046 | GC185 | BHM4 | no frozen core available | | | | | | | |
| 4047 | GC234 | GCJT2 | 0-2 | 10372 | 13.54 | 1.3 | 0.54 | 5.41 | 1.89 | 3.84 |
| | | | 2-4 | 8519 | 7.95 | 0.62 | 0.51 | 1.8 | 0.26 | 3.22 |
| | | | 4-6 | 7962 | 4.95 | 0.42 | 0.54 | 2.64 | 0.13 | 2.9 |
| | | | 6-8 | 12063 | 6.86 | 0.75 | 0.46 | 1.81 | 0.05 | 3.89 |
| | | | 8-10 | 24608 | 6.45 | 0.96 | 0.28 | 1.37 | 0.06 | 3.92 |
| | | | 10-12 | 22034 | 2.33 | 0.32 | 0.23 | 0.72 | 0.03 | 2.69 |
| | | | 12-14 | 23805 | 1.9 | 0.31 | 0.2 | 0.58 | 0.01 | 3.07 |
| | | | 14-16 | 29024 | 1.69 | 0.32 | 0.02 | 0.34 | 0.05 | 3.75 |
| | | | 16-18 | 29398 | 2.08 | 0.83 | 0.03 | 0.26 | 0.14 | 5.58 |
| | | | 18-20 | 34789 | 1.92 | 0.36 | 0.2 | 0.3 | 0.01 | 3.95 |
| | | | 20-22 | 32307 | 2.04 | 0.41 | 0.03 | 0.07 | 0.04 | 5.47 |
| | | | 22-24 | 26844 | 1.78 | 0.27 | 0.03 | 0.1 | 0.01 | 3.7 |
| | | | 24-26 | 26030 | 1.95 | 0.41 | 0.01 | 0.05 | 0.02 | 4.29 |
| | | | 26-27 | 25609 | 1.65 | 0.31 | 0.04 | 0.02 | 0.01 | 3.68 |
| 4048 | GC234 | GCAT2 | 0-2 | 9251 | 201.46 | 59.93 | 8.04 | 148.31 | 0.71 | 153.67 |
| | | | 2-4 | 12334 | 125.35 | 20.73 | 2.65 | 32.04 | 0.42 | 91.23 |

Table 9.4. Dissolved organic carbon and nutrients. (continued)

| Dive Number | Site | Station | Depth (cm) | Dissolved Organic Carbon (μM) | NH₄ (μM) | PO₄ (μM) | Urea (μM) | NO₃ (μM) | NO₂ (μM) | SiO₃ (μM) |
|---|---|---|---|---|---|---|---|---|---|---|
| | | | 4-6 | 11173 | 72.13 | 15.11 | 1.92 | 14.72 | 1.41 | 69.85 |
| | | | 6-8 | 26860 | 76.32 | 14.96 | 1.84 | 12.71 | 0.38 | 72.79 |
| | | | 8-10 | 9950 | 43.41 | 10.07 | -4.9 | 6.37 | 0.15 | 76.55 |
| | | | 10-12 | 27003 | 45.24 | 10.38 | -6.65 | 7.51 | 0.17 | 89.45 |
| | | | 12-14 | 24415 | 35.8 | 10.24 | -10.74 | 3.17 | 0.36 | 95.65 |
| | | | 14-16 | 22517 | 29.35 | 9.96 | -5.11 | 6.27 | 0.19 | 86.91 |
| | | | 16-18 | 11497 | 29.37 | 11.99 | -10.88 | 6.31 | 0.13 | 106.33 |
| | | | 18-20 | 18385 | 27.24 | 11.51 | -9.61 | 12.14 | 0.12 | 104.21 |
| | | | 20-22 | 23185 | 29.39 | 14.83 | -8.34 | 6.36 | 0.62 | 126.79 |
| | | | 22-24 | 23705 | 27.98 | 12.8 | -17.47 | 7.95 | 0.16 | 125.47 |
| | | | 24-26 | 24085 | 32.63 | 12.98 | -12.17 | 6.72 | 0.21 | 116.76 |
| | | | 26-28 | 25253 | 33.36 | 12.83 | -29.77 | 2.18 | 0.12 | 123.64 |
| | | | 28-30 | 7829 | 36.24 | 11.5 | -22.4 | 3.32 | 0.12 | 106.79 |
| | | | 30-32 | 8798 | 43.84 | 10.83 | -14.05 | 2.69 | 0.17 | 94.07 |
| | | | 32-34 | 9178 | 55.2 | 12.12 | -83.66 | 5.4 | 0.3 | 87.1 |
| 4053 | GB425 | GBM2 | 0-2 | 9860 | 288.8 | 59.06 | 5.5 | 114.26 | 0.77 | 151.67 |
| | | | 2-4 | 10070 | 276.83 | 43.49 | -8.23 | 49.34 | 0.97 | 142.22 |
| | | | 4-6 | 8853 | 335.27 | 21.11 | -80.02 | 15.5 | 0.34 | 107.69 |
| | | | 6-8 | 7456 | 646 | 7.59 | 1.9 | 11.71 | 0.11 | 67.71 |
| | | | 8-10 | 6195 | 1040 | 3.24 | 0.97 | 9.74 | 0.05 | 84.89 |
| | | | 10-12 | 5814 | 1244 | 2.78 | 2.64 | 4.15 | 0.16 | 80.87 |
| | | | 12-14 | 5253 | 1604 | 2.82 | 30.37 | 8.1 | 0.39 | 109.77 |
| | | | 14-16 | 3687 | 1940 | 4.51 | 40.34 | 9.63 | 0.28 | 115 |
| | | | 16-18 | 3689 | 2165 | 2.78 | 29.36 | 2.23 | 0.1 | 136.15 |
| | | | 18-20 | 3122 | 2508 | 2.64 | 37.01 | 2.15 | 0.22 | 135.44 |
| | | | 20-22 | 3913 | 2686 | 2.78 | 41.32 | 3.2 | 0.59 | 154 |
| | | | 22-24 | 3203 | 3116 | 3.08 | 40.32 | 3.52 | 0.3 | 159 |
| | | | 24-26 | 3714 | 3461 | 2.74 | 40.31 | 5.63 | 0.3 | 157.5 |
| | | | 26-28 | 3546 | 3683 | 3.28 | 20.33 | 105.9 | 24.77 | 99.25 |

Table 9.4. Dissolved organic carbon and nutrients. (continued)

| Dive Number | Site | Station | Depth (cm) | Dissolved Organic Carbon (µM) | NH$_4$ (µM) | PO$_4$ (µM) | Urea (µM) | NO$_3$ (µM) | NO$_2$ (µM) | SiO$_3$ (µM) |
|---|---|---|---|---|---|---|---|---|---|---|
| box | GC185 | BHBXC1 | 0-2 | – | 61.36 | 9.55 | 3.45 | 364.83 | 0.76 | 83.75 |
| | | | 2-4 | – | 51.07 | 10.87 | 2.6 | 76 | 0.56 | 74.82 |
| | | | 4-6 | – | 49.02 | 10.34 | 2.88 | 41.18 | 0.48 | 68.46 |
| | | | 6-8 | – | 46.71 | 11.64 | 4.09 | 24.87 | 0.56 | 68.14 |
| | | | 8-10 | – | 53.77 | 10.53 | 5.3 | 31.67 | 0.54 | 67.82 |
| | | | 10-12 | – | 60.56 | 13.96 | 8.48 | 72.86 | 0.57 | 71.81 |
| | | | 12-14 | – | 59.98 | 22.91 | 5.74 | 23.09 | 0.57 | 68.05 |
| | | | 14-16 | – | 66.13 | 23.02 | 2.35 | 14.65 | 0.54 | 66.01 |
| | | | 16-18 | – | 65.9 | 21.52 | 3.56 | 19.54 | 0.71 | 69.99 |
| | | | 18-20 | – | 76.06 | 25.5 | 4.76 | 33.73 | 0.76 | 79.96 |
| | | | 20-22 | – | 76.92 | 22.83 | 4 | 33.71 | 0.73 | 71.93 |
| | | | 22-24 | – | 81.04 | 14.79 | 7.83 | 16.96 | 0.73 | 74.18 |
| | | | 24-26 | – | 80.08 | 13.61 | 2.81 | 7.12 | 0.54 | 73 |
| | | | 26-28 | – | 89.85 | 14.56 | 5.39 | 7.8 | 0.71 | 82.07 |
| | | | 28-30 | – | 97.94 | 13.77 | 3.37 | 12.89 | 0.62 | 74.07 |
| | | | 30-32 | – | 102.02 | 14.25 | 13.49 | 6.7 | 1.01 | 66.91 |
| box | GC185 | BHUN2 | 0-2 | 23872 | 388 | 90.81 | 28.24 | 34.2 | 2.09 | 429.49 |
| | | | 2-4 | 10351 | – | – | – | – | – | – |
| | | | 4-6 | 9095 | 166.53 | 24.3 | 13.91 | 55.8 | 1.02 | 112.49 |
| | | | 6-8 | 8539 | 138.7 | 21.71 | 10.49 | 74.98 | 0.76 | 104.36 |
| | | | 8-10 | 8640 | 97.76 | 15.39 | 11.18 | 51.13 | 0.72 | 121.21 |
| | | | 10-12 | 9028 | 121.26 | 8.68 | 11.19 | 10.37 | 0.73 | 101.47 |
| | | | 12-14 | 9589 | 79.73 | 23.86 | 4.37 | 12.55 | 0.2 | 164.65 |
| | | | 14-16 | 10332 | 62.77 | 25.05 | 0.97 | 6.69 | 1.17 | 193.66 |
| | | | 16-18 | 12641 | 44.65 | 19.25 | 0.31 | 8.05 | 0.01 | 131.85 |
| | | | 18-20 | 26398 | 33.89 | 14.76 | 0.34 | 8.24 | 0.02 | 108.11 |
| | | | 20-22 | 22148 | 150.69 | 8.21 | 11.21 | 27.81 | 8.61 | 49.87 |
| | | | 22-24 | 29285 | 36.29 | 13.37 | 1.08 | 1.17 | 0.09 | 99.48 |
| box | GC234 | GCBX2 | 0-2 | – | 29.11 | 6.88 | 6.01 | 18.44 | 1.53 | 101.46 |
| | | | 2-4 | – | 23.76 | 8.72 | 4.63 | 6.07 | 1.3 | 85.88 |
| | | | 4-6 | – | 30.61 | 8.23 | 5.62 | 9.3 | 1.29 | 81.41 |

Table 9.4. Dissolved organic carbon and nutrients. (continued)

| Dive Number | Site | Station | Depth (cm) | Dissolved Organic Carbon (μM) | NH₄ (μM) | PO₄ (μM) | Urea (μM) | NO₃ (μM) | NO₂ (μM) | SiO₃ (μM) |
|---|---|---|---|---|---|---|---|---|---|---|
| | | | 6-8 | – | 41.5 | 6.97 | 5.93 | 3.33 | 0.65 | 78.81 |
| | | | 8-10 | – | 56.21 | 6.82 | 2.5 | 1.32 | 0.42 | 72.47 |
| | | | 10-12 | – | 56.24 | 8.39 | 6.89 | 1.12 | 0.56 | 74.56 |
| | | | 12-14 | – | 63.33 | 14.81 | 4.49 | 4.76 | 0.71 | 85.94 |
| | | | 14-16 | – | 70.84 | 7.4 | 7.86 | 3.93 | 0.94 | 87.06 |
| | | | 16-18 | – | 74.26 | 6.14 | 3.41 | 2.73 | 0.44 | 77.05 |
| | | | 18-20 | – | 90.24 | 6.75 | 0.66 | 1.12 | 0.35 | 88.37 |
| | | | 20-22 | – | 82.65 | 6.05 | 3.02 | 0.51 | 0.35 | 79.32 |
| | | | 22-24 | 3689 | 83.45 | 5.2 | 7.07 | 0.43 | 0.38 | 75.81 |
| | | | 24-26 | – | 91.11 | 6.02 | 4.32 | 0.35 | 0.41 | 74.16 |
| box | GC234 | GCBXC1 | 0-2 | 10203 | 195.49 | 26.23 | 8.74 | 119.34 | 65.51 | 102 |
| | | | 2-4 | 9475 | 226.1 | 24.75 | 9.39 | 11.68 | 7.29 | 92.26 |
| | | | 4-6 | 5071 | 173.96 | 11.22 | 2.57 | 2.53 | 1.33 | 56.8 |
| | | | 6-8 | 3469 | 83.65 | 9.71 | 5.26 | 8.55 | 0.84 | 56.1 |
| | | | 8-10 | 2679 | 61.48 | 6.35 | 1.49 | 9.35 | 0.55 | 55.4 |
| | | | 10-12 | 2988 | 50.41 | 6.47 | 2.49 | 3.1 | 0.6 | 51 |
| | | | 12-14 | 2674 | 45.3 | 6.53 | 0.08 | 3.49 | 0.72 | 50.3 |
| | | | 14-16 | 2704 | 37.67 | 5.2 | 1.41 | 3.57 | 1.15 | 51.46 |
| | | | 16-18 | 2580 | 42.44 | 5.67 | 0.02 | 2.58 | 0.4 | 49.84 |
| | | | 18-20 | 2798 | 35.92 | 6.28 | 15.93 | 2.45 | 0.48 | 50.07 |
| | | | 20-22 | 2798 | 34.14 | 5.72 | 2.69 | 2.98 | 0.45 | 48.46 |
| | | | 22-24 | 3136 | 33.81 | 5.29 | 2.66 | 3.52 | 0.42 | 49.66 |

Table 9.5.  Solid phase properties.

| Dive Number | Site | Station | Depth (cm) | Porosity (Φ) | Grain Size >65 μm | Sulfur (μmols/g) | | Carbon (weight percent) | | | Extractable Metals (μmols/g) | | | |
|---|---|---|---|---|---|---|---|---|---|---|---|---|---|---|
| | | | | | | Acid Volatile AVS | Total Reduced TRS | Total | Organic | Inorganic (as CaCO₃) | Fe | | Mn | |
| | | | | | | | | | | | HCl | Citrate Dithonite | HCl | Citrate Dithonite |
| 2871 | GC234 | GCST1 | 0-2 | 0.799 | 0.909 | | | 8.25 | 5.91 | 19.50 | 19.24 | 1.76 | 0.69 | 0.15 |
| | | | 2-4 | 0.776 | 0.851 | | | 9.04 | 6.47 | 21.42 | 20.94 | 0.85 | 0.49 | 0.09 |
| | | | 4-6 | 0.760 | 0.908 | 1.0 | | 9.67 | 7.07 | 21.67 | 19.75 | 0.54 | 0.47 | 0.06 |
| | | | 6-8 | 0.751 | 0.911 | | | 8.73 | 6.20 | 21.08 | 20.18 | 0.39 | 0.48 | 0.00 |
| | | | 8-10 | 0.739 | 0.831 | | | 9.07 | 6.40 | 22.25 | 18.93 | 0.37 | 0.45 | 0.08 |
| | | | 10-12 | 0.742 | 0.947 | | | 7.89 | 5.22 | 22.25 | 21.69 | 0.36 | 0.46 | 0.05 |
| | | | 12-14 | 0.736 | 0.898 | | 118.5 | 7.60 | 5.94 | 13.83 | 15.73 | 0.41 | 0.37 | 0.07 |
| | | | 14-16 | 0.736 | 0.922 | | | 7.76 | 6.31 | 12.08 | 19.80 | 0.40 | 0.46 | 0.07 |
| | | | 16-18 | 0.000 | 0.942 | | | 8.14 | 6.19 | 16.25 | 20.06 | 0.38 | 0.44 | 0.06 |
| | | | 18-20 | 0.000 | 0.903 | | | 7.64 | 5.55 | 17.42 | 24.47 | 0.52 | 0.50 | 0.00 |
| 2873 | GC185 | BHAT1 | 0-2 | 0.809 | 0.873 | 39.0 | | 10.90 | 8.21 | 22.42 | 24.46 | 2.96 | 0.48 | 0.09 |
| | | | 2-4 | 0.795 | 0.857 | 40.0 | | 13.00 | 10.10 | 24.17 | 21.97 | 1.88 | 0.41 | 0.09 |
| | | | 4-6 | 0.775 | 0.878 | 3.5 | | 14.10 | 10.80 | 27.50 | 27.00 | 1.85 | 0.45 | 0.09 |
| | | | 6-8 | 0.745 | 0.889 | | | 14.90 | 11.50 | 28.33 | 23.08 | 1.54 | 0.43 | 0.07 |
| | | | 8-10 | 0.764 | 0.885 | | | 13.70 | 10.90 | 23.33 | 20.73 | 1.11 | 0.39 | 0.08 |
| | | | 10-12 | 0.776 | 0.894 | | | 13.90 | 10.90 | 25.00 | 17.91 | 0.65 | 0.37 | 0.05 |
| | | | 12-14 | 0.763 | 0.866 | | 118.7 | 13.80 | 11.70 | 17.50 | 20.97 | 0.60 | 0.37 | 0.07 |
| | | | 14-16 | 0.000 | 0.864 | | | 10.90 | 8.30 | 21.67 | 23.03 | 0.66 | 0.46 | 0.05 |
| 2873 | GC185 | BHM4 | 0-2 | 0.813 | 0.710 | 6.7 | | 11.80 | 7.63 | 34.75 | 20.22 | 0.97 | 0.31 | 0.00 |
| | | | 2-4 | 0.809 | 0.715 | | | 12.00 | 6.94 | 42.17 | 20.29 | 0.89 | 0.33 | 0.00 |
| | | | 4-6 | 0.814 | 0.746 | 5.4 | | 11.60 | 6.61 | 41.58 | 20.51 | 1.01 | 0.35 | 0.08 |
| | | | 6-8 | 0.768 | 0.751 | 7.2 | | 11.30 | 7.89 | 28.42 | 17.91 | 0.68 | 0.33 | 0.00 |
| | | | 8-10 | 0.781 | 0.766 | 5.0 | | 12.00 | 7.83 | 34.75 | 23.20 | 0.42 | 0.43 | 0.00 |
| | | | 10-12 | 0.761 | 0.789 | 5.6 | | 12.20 | 8.47 | 31.08 | 20.60 | 0.70 | 0.41 | 0.00 |
| | | | 12-14 | 0.772 | 0.835 | 4.1 | 119.6 | 11.30 | 8.32 | 24.83 | 20.08 | 1.07 | 0.36 | 0.00 |
| | | | 14-16 | 0.754 | 0.857 | 4.1 | | 10.50 | 7.94 | 21.33 | 23.44 | 0.62 | 0.40 | 0.00 |
| | | | 16-18 | 0.757 | 0.825 | 3.7 | | 11.50 | 8.29 | 26.75 | 24.54 | 1.01 | 0.42 | 0.09 |
| | | | 18-20 | 0.757 | 0.792 | | | 11.20 | 8.52 | 22.33 | 22.61 | 0.82 | 0.40 | 0.00 |
| 2874 | GC185 | BHST1 | 0-2 | 0.791 | 0.903 | | | 6.61 | 4.33 | 19.00 | 30.76 | 4.47 | 0.45 | 0.08 |
| | | | 2-4 | 0.765 | 0.944 | | | 6.27 | 4.64 | 13.58 | 45.39 | 3.96 | 0.57 | 0.08 |
| | | | 4-6 | 0.742 | 0.883 | 8.8 | | 6.81 | 4.83 | 16.50 | 44.66 | 2.32 | 0.55 | 0.08 |
| | | | 6-8 | 0.731 | 0.961 | | | 8.16 | 4.61 | 29.58 | 28.65 | 1.84 | 0.74 | 0.07 |
| | | | 8-10 | 0.734 | 0.884 | | | 11.10 | 6.73 | 36.42 | 30.42 | 1.54 | 0.61 | 0.07 |
| | | | 10-12 | 0.724 | 0.873 | | | 10.80 | 8.22 | 21.50 | 26.08 | 0.99 | 0.52 | 0.11 |
| | | | 12-14 | 0.727 | 0.823 | | | 9.21 | 6.72 | 20.75 | 29.12 | 0.77 | 0.51 | 0.08 |
| | | | 14-16 | 0.000 | 0.953 | | 129.8 | 9.01 | 6.62 | 19.92 | 31.72 | 1.06 | 0.52 | 0.05 |
| | | | 16-18 | 0.000 | 0.915 | | | 8.99 | 6.38 | 21.75 | 31.66 | 0.64 | 0.51 | 0.07 |
| 2875 | GC185 | BHST2 | 0-2 | 0.764 | 0.765 | | | 7.96 | 4.69 | 27.25 | 13.82 | 3.32 | 0.30 | 0.14 |
| | | | 2-4 | 0.777 | 0.829 | | | 7.41 | 4.64 | 23.08 | 17.98 | 1.92 | 0.30 | 0.13 |
| | | | 4-6 | 0.777 | 0.756 | 2.3 | | 6.88 | 4.93 | 16.25 | 20.67 | 1.07 | 0.36 | 0.13 |
| | | | 6-8 | 0.000 | 0.891 | | | 7.96 | 5.03 | 24.42 | 16.71 | 2.07 | 0.31 | 0.11 |
| | | | 8-10 | 0.000 | 0.850 | | | 7.32 | 5.69 | 13.58 | 16.00 | 1.92 | 0.30 | 0.14 |
| | | | 10-12 | 0.000 | 0.868 | | 163.4 | 7.76 | 4.94 | 23.50 | 16.55 | 3.86 | 0.29 | 0.14 |
| 2875 | GC185 | BHUN1 | 0-2 | 0.811 | 0.922 | | | 4.69 | 3.54 | 9.58 | 30.62 | 17.19 | 2.06 | 3.75 |
| | | | 2-4 | 0.799 | 0.932 | | | 4.93 | 4.11 | 6.83 | 20.56 | 9.92 | 0.71 | 1.25 |
| | | | 4-6 | 0.779 | 0.916 | 1.6 | | 6.58 | 4.84 | 14.50 | 22.27 | 3.65 | 0.40 | 0.42 |
| | | | 6-8 | 0.769 | 0.918 | | | 6.11 | 4.84 | 10.58 | 20.07 | 2.74 | 0.34 | 0.24 |
| | | | 8-10 | 0.743 | 0.953 | | | 6.40 | 5.20 | 10.00 | 28.19 | 2.60 | 0.37 | 0.29 |
| | | | 10-12 | 0.741 | 0.930 | | | 6.54 | 4.99 | 12.92 | 13.83 | 1.36 | 0.21 | 0.17 |
| | | | 12-14 | 0.735 | 0.931 | | 117.13 | 6.15 | 5.22 | 7.75 | 29.60 | 1.33 | 0.38 | 0.15 |
| | | | 14-16 | 0.000 | 0.930 | | | 6.36 | 4.67 | 14.08 | 20.54 | 1.30 | 0.33 | 0.14 |
| | | | 16-18 | 0.000 | 0.941 | | | 6.28 | 4.84 | 12.00 | 26.11 | 3.13 | 0.35 | 0.19 |
| | | | 18-20 | 0.000 | 0.930 | | | 6.12 | 4.91 | 10.08 | 28.45 | 1.46 | 0.36 | 0.18 |
| | | | 22-24 | 0.000 | 0.962 | | | 5.95 | 5.58 | 3.08 | 21.63 | 1.21 | 0.36 | 0.16 |
| | | | 26-28 | 0.000 | 0.891 | | | 6.30 | 4.90 | 11.67 | 22.35 | 1.69 | 0.28 | 0.19 |
| 2876 | GC233 | BPR2 | 0-2 | 0.797 | 0.878 | | | 4.29 | 2.45 | 15.33 | 42.40 | 18.16 | 0.54 | 0.43 |

Table 9.5. Solid phase properties. (continued)

| Dive Number | Site | Station | Depth (cm) | Porosity (Φ) | Grain Size >65 μm | Acid Volatile AVS | Total Reduced TRS | Total | Organic | Inorganic (as CaCO$_3$) | Fe HCl | Fe Citrate Dithonite | Mn HCl | Mn Citrate Dithonite |
|---|---|---|---|---|---|---|---|---|---|---|---|---|---|---|
| | | | 2-4 | 0.794 | 0.938 | | | 4.92 | 2.84 | 17.33 | 34.67 | 30.87 | 0.54 | 0.66 |
| | | | 4-6 | 0.773 | 0.898 | 8.3 | | 4.35 | 2.84 | 12.58 | 33.97 | 14.68 | 0.44 | 0.40 |
| | | | 6-8 | 0.739 | 0.916 | | | 4.66 | 2.96 | 14.17 | 39.01 | 7.17 | 0.55 | 0.23 |
| | | | 8-10 | 0.000 | 0.839 | | | 5.57 | 2.54 | 25.25 | 34.15 | 8.21 | 0.45 | 0.48 |
| | | | 10-12 | 0.000 | 0.873 | | 145.4 | 6.07 | 2.52 | 29.58 | 35.95 | 5.52 | 0.76 | 0.57 |
| 2880 | GC234 | GCB1@GCAT1 | 0-2 | 0.802 | 0.901 | 17.0 | | 3.05 | 1.59 | 12.17 | 83.24 | 20.79 | 1.99 | 0.15 |
| | | | 2-4 | 0.794 | 0.943 | 10.0 | | 3.12 | 1.29 | 15.25 | 41.69 | 6.10 | 0.76 | 0.08 |
| | | | 4-6 | 0.767 | 0.955 | 4.0 | | 2.76 | 1.25 | 12.58 | 41.69 | 2.15 | 1.05 | 0.16 |
| | | | 6-8 | 0.742 | 0.974 | 2.5 | | 3.17 | 1.34 | 15.25 | 28.51 | 1.86 | 0.80 | 0.08 |
| | | | 8-10 | 0.729 | 0.961 | 2.6 | | 3.00 | 1.20 | 15.00 | 31.72 | 0.23 | 0.77 | 0.08 |
| | | | 10-12 | 0.726 | 0.945 | 3.9 | | 3.17 | 1.24 | 16.08 | 26.06 | 0.81 | 0.74 | 0.08 |
| | | | 12-14 | 0.732 | 0.955 | 3.0 | 118.5 | 3.12 | 1.77 | 11.25 | 30.53 | 0.69 | 0.81 | 0.05 |
| | | | 14-16 | 0.724 | 0.979 | 4.3 | | 3.10 | 1.26 | 15.33 | 26.65 | 0.62 | 0.76 | 0.07 |
| | | | 16-18 | 0.729 | 0.948 | 5.0 | | 3.09 | 1.26 | 15.25 | 32.95 | 0.63 | 0.84 | 0.11 |
| | | | 18-20 | 0.724 | 0.933 | 2.0 | | 3.14 | 1.29 | 15.42 | 31.32 | 0.61 | 0.91 | 0.06 |
| | | | 22-24 | 0.721 | 0.966 | 4.7 | | 2.99 | 1.50 | 12.42 | 28.19 | 0.53 | 0.83 | 0.07 |
| 2882 | GB425 | GBB1@GBM2 | 0-2 | 0.744 | 0.784 | | | 4.54 | 1.73 | 23.42 | 46.94 | 5.11 | 0.93 | 0.04 |
| | | | 2-4 | 0.636 | 0.761 | | | 4.43 | 1.09 | 27.83 | 46.14 | 1.44 | 1.27 | 0.08 |
| | | | 4-6 | 0.637 | 0.874 | 1.2 | | 3.79 | 1.03 | 23.00 | 39.83 | 1.41 | 1.07 | 0.16 |
| | | | 6-8 | 0.686 | 0.791 | | | 3.49 | 1.03 | 20.50 | 33.45 | 0.71 | 1.39 | 0.08 |
| | | | 8-10 | 0.661 | 0.859 | | | 3.18 | 1.16 | 16.83 | 31.59 | 1.22 | 1.53 | 0.08 |
| | | | 10-12 | 0.643 | 0.871 | | | 2.65 | 1.17 | 12.33 | 32.30 | 0.76 | 1.20 | 0.05 |
| | | | 12-14 | 0.620 | 0.859 | | 153.5 | 2.86 | 1.07 | 14.92 | 36.76 | 0.80 | 1.27 | 0.16 |
| | | | 14-16 | 0.610 | 0.879 | | | 2.74 | 1.00 | 14.50 | 37.71 | 1.83 | 1.33 | 0.24 |
| | | | 16-18 | 0.575 | 0.893 | | | 4.00 | 0.99 | 25.11 | 32.25 | 1.64 | 1.26 | 0.24 |
| | | | 18-20 | 0.580 | 0.853 | | | 2.94 | 1.52 | 11.83 | 43.98 | 1.50 | 1.55 | 0.18 |
| | | | 22-24 | 0.000 | 0.912 | | | 2.94 | 1.43 | 12.58 | 44.24 | 1.67 | 1.83 | 0.27 |
| | | | 26-28 | 0.000 | 0.843 | | | 2.92 | 1.70 | 10.17 | 42.84 | 1.45 | 1.60 | 0.25 |
| 2883 | GB425 | GBM1 | 0-2 | 0.761 | 0.810 | 1.7 | | 3.16 | 2.10 | 8.83 | 42.23 | 4.83 | 1.04 | 0.33 |
| | | | 2-4 | 0.744 | 0.839 | 6.7 | | 4.56 | 3.11 | 12.08 | 50.43 | 7.79 | 1.24 | 0.42 |
| | | | 4-6 | 0.692 | 0.823 | 4.9 | | 4.19 | 3.54 | 5.42 | 63.56 | 6.89 | 1.50 | 0.36 |
| | | | 6-8 | 0.667 | 0.842 | 6.5 | | 5.79 | 2.00 | 31.58 | 42.20 | 6.46 | 1.02 | 0.37 |
| | | | 8-10 | 0.619 | 0.710 | 4.5 | | 3.86 | 2.76 | 9.17 | 54.07 | 3.40 | 1.47 | 0.18 |
| | | | 10-12 | 0.538 | 0.764 | 1.6 | | 3.14 | 2.41 | 6.08 | 34.35 | 5.26 | 0.95 | 0.30 |
| | | | 12-14 | 0.476 | 0.761 | 2.3 | 180.9 | 2.96 | 1.96 | 8.33 | 43.68 | 3.58 | 1.24 | 0.34 |
| | | | 14-16 | 0.000 | 0.646 | 2.5 | | 2.37 | 1.59 | 6.50 | 40.18 | 3.81 | 1.07 | 0.40 |
| | | | 16-18 | 0.000 | 0.718 | 2.5 | | 2.23 | 1.40 | 6.92 | 58.88 | 3.94 | 1.70 | 0.44 |
| 2885 | GB425 | GBM2 | 0-2 | 0.674 | 0.209 | 1.6 | | 4.27 | 1.32 | 24.58 | 35.21 | 4.94 | 1.96 | 0.23 |
| | | | 2-4 | 0.684 | 0.581 | 1.8 | | 3.62 | 1.22 | 20.00 | 33.99 | 2.71 | 1.34 | 0.16 |
| | | | 4-6 | 0.661 | 0.800 | 0.9 | | 4.04 | 0.79 | 27.10 | 64.76 | 1.75 | 3.40 | 0.45 |
| | | | 6-8 | 0.661 | 0.887 | 0.8 | | 3.60 | 1.30 | 19.17 | 54.49 | 1.11 | 3.04 | 0.49 |
| | | | 8-10 | 0.611 | 0.911 | 2.3 | | 2.95 | 0.81 | 17.87 | 49.62 | 1.11 | 2.06 | 0.30 |
| | | | 10-12 | 0.604 | 0.885 | 0.7 | | 2.78 | 0.86 | 16.00 | 52.07 | 0.96 | 2.34 | 0.28 |
| | | | 12-14 | 0.000 | 0.919 | 0.6 | 132.6 | 2.63 | 1.02 | 13.42 | 54.44 | 1.19 | 2.33 | 0.33 |
| | | | 14-16 | 0.000 | 0.914 | 0.7 | | 2.51 | 0.81 | 14.18 | 68.30 | 0.92 | 2.81 | 0.30 |
| | | | 16-18 | 0.000 | 0.926 | 1.3 | | 2.52 | 0.79 | 14.42 | 59.69 | 0.78 | 2.23 | 0.22 |
| 2886 | GC234 | GCAT2 | 0-2 | 0.774 | 0.887 | 9.7 | | 6.04 | 3.37 | 22.25 | 37.67 | 2.53 | 0.81 | 0.07 |
| | | | 2-4 | 0.800 | 0.913 | 6.6 | | 6.18 | 2.80 | 28.17 | 30.19 | 2.56 | 0.72 | 0.07 |
| | | | 4-6 | 0.965 | 0.868 | 3.7 | | 6.02 | 2.77 | 27.08 | 29.56 | 1.39 | 0.71 | 0.07 |
| | | | 6-8 | 0.769 | 0.916 | 3.3 | | 6.14 | 2.51 | 30.25 | 24.47 | 0.96 | 0.63 | 0.09 |
| | | | 8-10 | 0.749 | 0.900 | 3.3 | | 5.72 | 2.17 | 29.58 | 26.60 | 0.39 | 0.77 | 0.06 |
| | | | 10-12 | 0.742 | 0.920 | 3.4 | | 6.04 | 2.21 | 31.92 | 23.54 | 1.04 | 0.78 | 0.07 |
| | | | 12-14 | | 0.916 | 2.4 | 124.9 | 5.45 | 2.20 | 27.08 | 27.14 | 0.53 | 0.90 | 0.08 |
| | | | 14-16 | | 0.930 | 2.5 | | 5.52 | 2.09 | 28.58 | 24.07 | 0.93 | 0.75 | 0.09 |
| | | | 16-18 | | 0.926 | 2.1 | | 5.72 | 2.29 | 28.58 | 25.14 | 0.73 | 0.86 | 0.07 |
| | | | 18-20 | | 0.918 | 1.5 | | 5.54 | 2.36 | 26.50 | 25.84 | 1.17 | 0.86 | 0.16 |
| | | | 20-22 | | | | | | | | | | | |

Table 9.5. Solid phase properties. (continued)

| Dive Number | Site | Station | Depth (cm) | Porosity (Φ) | Grain Size >65 μm | Sulfur (μmols/g) Acid Volatile AVS | Total Reduced TRS | Carbon (weight percent) Total | Organic | Inorganic (as CaCO$_3$) | Fe HCl | Fe Citrate Dithonite | Mn HCl | Mn Citrate Dithonite |
|---|---|---|---|---|---|---|---|---|---|---|---|---|---|---|
| 2888 | GC234 | GCAT1 | 0-2 | 0.829 | 0.917 | 2.9 | | 7.66 | 5.77 | 15.75 | 25.42 | 1.43 | 0.47 | 0.06 |
| | | | 2-4 | 0.802 | 0.881 | 2.3 | | 7.47 | 5.95 | 12.67 | 23.51 | 1.60 | 0.41 | 0.07 |
| | | | 4-6 | 0.796 | 0.949 | 1.1 | | 8.84 | 6.65 | 18.25 | 18.13 | 0.57 | 0.34 | 0.06 |
| | | | 6-8 | 0.794 | 0.850 | 1.1 | | 8.92 | 7.39 | 12.75 | 23.78 | 0.80 | 0.42 | 0.07 |
| | | | 8-10 | | 0.926 | 1.3 | | 8.06 | 6.11 | 16.25 | 17.70 | 0.55 | 0.33 | 0.06 |
| | | | 10-12 | | 0.906 | 0.9 | | 8.46 | 6.54 | 16.00 | 19.83 | 0.55 | 0.35 | 0.00 |
| | | | 12-14 | | 0.892 | 0.9 | 83.3 | 8.02 | 6.45 | 13.08 | 20.95 | 0.50 | 0.29 | 0.00 |
| 2891 | GC185 | BHAT2 | 0-2 | 0.815 | 0.920 | | | 7.18 | 5.13 | 17.08 | 21.96 | 1.43 | 0.53 | 0.07 |
| | | | 2-4 | 0.795 | 0.908 | | | 6.75 | 5.17 | 13.17 | 23.34 | 2.07 | 0.40 | 0.00 |
| | | | 4-6 | 0.784 | 0.941 | 6.0 | | 6.33 | 4.93 | 11.67 | 33.00 | 1.05 | 0.36 | 0.00 |
| | | | 6-8 | 0.767 | 0.962 | | | 6.56 | 4.83 | 14.42 | | | 0.35 | 0.00 |
| | | | 8-10 | 0.767 | 0.942 | | | 6.89 | 5.47 | 11.83 | 34.65 | 2.32 | 0.38 | 0.00 |
| | | | 10-12 | | 0.940 | | | 7.86 | 4.20 | 30.50 | 28.79 | 0.97 | 0.39 | 0.00 |
| | | | 12-14 | | 0.929 | | 132.4 | 7.43 | 5.66 | 14.75 | 17.84 | 0.42 | 0.23 | 0.00 |
| | | | 14-16 | | 0.906 | | | 7.97 | 5.89 | 17.33 | 20.36 | 0.26 | 0.30 | 0.00 |
| box | GC185 | BHBC2 | 0-2 | 0.846 | 0.903 | | | 4.70 | 3.82 | 7.33 | 24.40 | 3.55 | 1.22 | 0.40 |
| | | | 2-4 | 0.867 | 0.906 | | | 4.71 | 3.28 | 11.92 | 24.16 | 2.91 | 0.77 | 0.18 |
| | | | 4-6 | 0.759 | 0.894 | 3.1 | | 5.76 | 4.01 | 14.58 | 16.83 | 2.62 | 0.32 | 0.12 |
| | | | 6-8 | 0.748 | 0.879 | | | 6.65 | 4.66 | 16.58 | 18.27 | 2.33 | 0.34 | 0.07 |
| | | | 8-10 | 0.740 | 0.901 | | | 7.09 | 5.36 | 14.42 | 14.61 | 2.84 | 0.32 | 0.08 |
| | | | 10-12 | 0.738 | 0.906 | | | 6.77 | 4.91 | 15.50 | 27.10 | 1.12 | 0.54 | 0.06 |
| | | | 12-14 | 0.727 | 0.900 | | 84.6 | 7.45 | 5.40 | 17.08 | 28.74 | 1.11 | 0.56 | 0.07 |
| | | | 14-16 | 0.711 | 0.899 | | | 7.88 | 5.75 | 17.75 | 23.00 | 1.59 | 0.42 | 0.06 |
| | | | 16-18 | 0.719 | 0.907 | | | 7.99 | 5.87 | 17.67 | 25.75 | 1.06 | 0.46 | 0.00 |
| | | | 18-20 | 0.736 | 0.910 | | | 8.16 | 5.86 | 19.17 | 25.25 | 1.29 | 0.45 | 0.07 |
| | | | 22-24 | | 0.888 | | | 7.50 | 5.78 | 14.33 | 25.70 | 0.76 | 0.48 | 0.08 |
| 4025 | GC185 | BHAT1 | 0-2 | 0.845 | | | 4.2 | 11.10 | 7.59 | 29.25 | 52.38 | 14.47 | 1.38 | 0.47 |
| | | | 2-4 | 0.813 | | | 3.7 | 10.50 | 6.93 | 29.75 | 124.1 | 16.36 | 1.10 | 0.62 |
| | | | 4-6 | 0.799 | | | 5.8 | 11.60 | 8.52 | 25.67 | 9.24 | 7.58 | 0.14 | 0.54 |
| | | | 6-8 | 0.789 | | | 3.5 | 13.00 | 9.79 | 26.75 | 35.94 | 6.76 | 0.42 | 0.43 |
| | | | 8-10 | 0.789 | | | 1.7 | 17.40 | 12.90 | 37.50 | 41.00 | 5.74 | 0.72 | |
| | | | 10-12 | 0.793 | | | 2.9 | 105.8 | 14.30 | 9.96 | 36.17 | 18.12 | 7.40 | 0.71 | 0.44 |
| | | | 12-14 | 0.804 | | | | | 15.20 | 9.61 | 46.58 | 40.60 | | 1.12 | |
| | | | 14-16 | 0.808 | | | | | 15.80 | 10.80 | 41.67 | | | | |
| | | | 16-18 | 0.805 | | | | | 15.30 | 8.25 | 58.75 | | | | |
| 4027 | GC185 | BHST1 | 0-2 | 0.867 | 0.870 | | | 7.46 | 5.20 | 18.83 | 71.31 | 30.58 | 1.96 | 0.86 |
| | | | 2-4 | 0.819 | 0.810 | | | 10.10 | 6.36 | 31.17 | 59.04 | 19.31 | 0.93 | 1.36 |
| | | | 4-6 | 0.812 | 0.781 | 4.6 | | 10.00 | 7.46 | 21.17 | 30.51 | 9.45 | 0.66 | 0.37 |
| | | | 6-8 | 0.813 | 0.833 | | | 8.91 | 6.19 | 22.67 | 67.16 | 3.16 | 1.23 | 0.12 |
| | | | 8-10 | 0.792 | 0.830 | | | 9.21 | 6.37 | 23.67 | 0.00 | 8.64 | 1.19 | |
| | | | 10-12 | 0.761 | 0.868 | | 113.8 | 9.01 | 6.66 | 19.58 | 52.59 | 10.36 | 0.93 | 0.38 |
| | | | 12-14 | 0.802 | 0.788 | | 110.5 | 9.19 | 5.99 | 26.67 | 55.40 | 8.49 | 0.91 | 0.86 |
| | | | 14-16 | 0.796 | 0.748 | | | 9.73 | 7.61 | 17.67 | | | | |
| | | | 16-18 | 0.777 | 1.000 | | | 11.40 | 8.10 | 27.50 | 59.27 | 6.34 | 1.18 | |
| | | | 18-20 | 0.769 | 0.616 | | | 12.00 | 11.50 | 4.17 | | | | |
| | | | 20-22 | 0.768 | 0.715 | | | 11.20 | 9.00 | 18.33 | 68.29 | 6.23 | 1.05 | 0.84 |
| | | | 22-24 | 0.780 | 0.844 | | | 10.80 | 8.83 | 16.42 | | | | |
| | | | 24-26 | 0.819 | 0.722 | | | 10.40 | 7.23 | 26.42 | | | | |
| | | | 26-28 | 0.775 | 0.713 | | | 11.90 | 10.50 | 11.67 | | | | |
| | | | 28-30 | 0.780 | 0.773 | | | 12.20 | 8.81 | 28.25 | | | | |
| 4028 | GC185 | BHB3 | 0-2 | 0.821 | 0.844 | | | 10.50 | 7.83 | 22.25 | 116.6 | 10.87 | 1.26 | 0.46 |
| | | | 2-4 | 0.790 | 0.843 | | | 10.90 | 9.11 | 14.92 | 46.74 | 7.91 | 1.25 | 2.84 |
| | | | 4-6 | 0.793 | 0.880 | 3.0 | | 10.70 | 8.03 | 22.25 | 51.24 | 6.32 | 0.55 | |
| | | | 6-8 | 0.787 | 0.893 | | | 11.80 | 8.45 | 27.92 | 44.85 | 0.39 | 1.01 | |
| | | | 8-10 | 0.790 | 0.722 | | | 14.10 | 13.10 | 8.33 | 55.57 | 7.22 | 1.13 | |

# Table 9.5. Solid phase properties. (continued)

| Dive Number | Site | Station | Depth (cm) | Porosity (Φ) | Grain Size >65 µm | Sulfur (µmols/g) Acid Volatile AVS | Total Reduced TRS | Carbon (weight percent) Total | Organic | Inorganic (as CaCO$_3$) | Extractable Metals (µmols/g) Fe HCl | Citrate Dithonite | Mn HCl | Citrate Dithonite |
|---|---|---|---|---|---|---|---|---|---|---|---|---|---|---|
| | | | 10-12 | 0.784 | 0.722 | | | 11.40 | 8.31 | 25.75 | 63.15 | 8.44 | 0.57 | 0.48 |
| | | | 12-14 | 0.783 | 0.728 | | 119.9 | 10.00 | 7.03 | 24.75 | 23.31 | 10.58 | 0.88 | 0.43 |
| | | | 14-16 | 0.789 | 0.820 | | | 11.30 | 7.61 | 30.75 | 79.46 | 12.42 | 1.22 | |
| 4029 | GC234 | GCAT2 | 0-2 | 0.830 | 0.562 | | | 6.15 | 2.60 | 29.58 | 60.49 | 24.25 | 0.93 | 1.95 |
| | | | 2-4 | 0.775 | 0.683 | | | 6.68 | 2.78 | 32.50 | 65.72 | 22.08 | 1.48 | 0.41 |
| | | | 4-6 | 0.785 | 0.716 | 4.0 | | 6.47 | 2.88 | 29.92 | 73.13 | 12.06 | 1.44 | 0.77 |
| | | | 6-8 | 0.783 | 0.778 | | | 6.39 | 3.13 | 27.17 | 56.02 | 8.88 | 1.27 | 0.58 |
| | | | 8-10 | 0.769 | 0.717 | | | 6.03 | 2.50 | 29.42 | 0.00 | 6.06 | | 1.23 |
| | | | 10-12 | 0.732 | 0.741 | | 110.9 | 5.56 | 2.13 | 28.58 | 39.68 | 7.00 | 1.19 | 1.05 |
| | | | 12-14 | 0.764 | 0.801 | | | 6.02 | 2.90 | 26.00 | | | | |
| | | | 14-16 | 0.754 | 0.827 | | 101.7 | 5.18 | 2.33 | 23.75 | 0.00 | 6.70 | 0.00 | 0.92 |
| | | | 16-18 | 0.746 | 0.807 | | | 6.06 | 3.87 | 18.25 | | | | |
| | | | 18-20 | 0.742 | 0.846 | | | 6.41 | 2.90 | 29.25 | 56.66 | 5.08 | 0.74 | 1.03 |
| | | | 20-22 | 0.767 | 0.737 | | | 5.70 | 1.92 | 31.50 | | | | |
| | | | 22-24 | 0.736 | 0.760 | | | 5.90 | 2.79 | 25.92 | 56.28 | 5.04 | 1.73 | 1.12 |
| | | | 24-26 | 0.751 | 0.680 | | | 6.11 | 3.11 | 25.00 | | | | |
| | | | 26-28 | 0.748 | 0.714 | | | 6.55 | 2.13 | 36.83 | | | | |
| | | | 28-30 | 0.750 | 0.824 | | | 5.90 | 2.34 | 29.67 | | | | |
| 4031 | GC234 | GCST1 | 0-2 | 0.828 | 0.657 | | | 4.90 | 3.55 | 11.25 | 48.47 | 25.58 | 1.17 | 0.47 |
| | | | 2-4 | 0.862 | 0.614 | | | 6.77 | 4.90 | 15.58 | 0.00 | 13.34 | | 0.47 |
| | | | 4-6 | 0.840 | 0.725 | 1.5 | | 8.25 | 5.63 | 21.83 | 24.34 | 11.14 | 0.60 | 0.51 |
| | | | 6-8 | 0.832 | 0.795 | | | 9.03 | 6.62 | 20.08 | 52.37 | 11.64 | 0.90 | |
| | | | 8-10 | 0.825 | 0.705 | | | 8.64 | 6.44 | 18.33 | 61.45 | 12.68 | 0.82 | |
| | | | 10-12 | 0.804 | 0.774 | | | 8.70 | 5.50 | 26.67 | 55.50 | 12.86 | 0.99 | |
| | | | 12-14 | 0.798 | 0.763 | | | 8.95 | 8.70 | 2.08 | 49.10 | 11.21 | 1.13 | 0.27 |
| | | | 14-16 | 0.796 | 0.717 | | | 9.37 | 5.88 | 29.08 | 54.99 | 6.46 | 1.43 | |
| | | | 16-18 | 0.809 | 0.758 | | | 9.30 | 7.13 | 18.08 | | | | |
| | | | 18-20 | 0.805 | 0.744 | | | 8.18 | 5.75 | 20.25 | 57.91 | 0.37 | 1.28 | 0.02 |
| | | | 20-22 | 0.799 | 0.682 | | | 8.29 | 6.01 | 19.00 | 34.61 | 5.54 | | 0.40 |
| | | | 22-24 | 0.788 | | | | 8.61 | 5.45 | 26.33 | 57.67 | 12.94 | 1.12 | |
| 4032 | GC234 | GCAT1 | 0-2 | 0.881 | | | | 5.01 | 3.69 | 11.00 | 62.79 | 15.63 | 2.24 | 1.59 |
| | | | 2-4 | 0.874 | | | | 4.88 | 3.32 | 13.00 | 48.09 | 7.00 | 1.51 | 1.02 |
| | | | 4-6 | 0.845 | | 3.5 | | 5.83 | 3.73 | 17.50 | 36.80 | 11.10 | 0.83 | 0.38 |
| | | | 6-8 | 0.841 | | | | 8.62 | 5.42 | 26.67 | 53.06 | 4.02 | 1.12 | 0.74 |
| | | | 8-10 | 0.827 | | | | 7.02 | 3.59 | 28.58 | 48.95 | 2.61 | 1.46 | 1.33 |
| | | | 10-12 | 0.813 | | | | 6.71 | 3.11 | 30.00 | 44.46 | 4.11 | 0.90 | 0.60 |
| | | | 12-14 | 0.820 | | | 145.9 | 5.57 | 3.06 | 20.92 | 28.94 | 5.95 | 1.26 | 0.86 |
| | | | 14-16 | 0.821 | | | | 5.27 | 2.80 | 20.58 | 44.23 | 2.46 | 1.28 | 0.63 |
| 4036 | GC234 | GCJT1 | 0-2 | 0.810 | | 4.2 | | 8.38 | 6.28 | 17.50 | 58.70 | 22.11 | | 0.44 |
| | | | 2-4 | 0.810 | | 3.6 | | 7.57 | 5.77 | 15.00 | 0.00 | 16.84 | | 0.50 |
| | | | 4-6 | 0.802 | | 3.3 | | 6.75 | 4.66 | 17.42 | 60.50 | 14.40 | 0.74 | 0.64 |
| | | | 6-8 | 0.796 | | 2.7 | | 9.27 | 5.08 | 34.92 | 50.74 | 9.82 | 1.72 | 0.42 |
| | | | 8-10 | 0.808 | | 2.5 | | 8.29 | 7.91 | 3.17 | 0.00 | | | |
| | | | 10-12 | 0.797 | | 2.9 | | 10.20 | 8.86 | 11.17 | 61.15 | | 1.88 | 0.63 |
| | | | 12-14 | 0.795 | | 2.6 | 61.5 | 8.72 | 8.17 | 4.58 | 26.27 | | 1.16 | |
| | | | 16-18 | 0.799 | | 3.1 | | 7.73 | 7.12 | 5.08 | 34.88 | 20.03 | 1.14 | 0.87 |
| 4037 | GC233 | BPAT1 | 0-2 | 0.862 | | | | 5.05 | 3.13 | 16.00 | 88.80 | | 2.82 | |
| | | | 2-4 | 0.879 | | | | 4.57 | 2.68 | 15.75 | 58.45 | 25.31 | 0.99 | 0.63 |
| | | | 4-6 | 0.786 | | 5.9 | | 4.61 | 2.61 | 16.67 | 42.85 | 17.99 | 1.15 | 0.48 |
| | | | 6-8 | 0.754 | | | | 4.69 | 2.46 | 18.58 | 72.88 | 21.59 | 0.89 | 1.05 |
| | | | 8-10 | 0.774 | | | | 4.61 | 2.54 | 17.25 | 57.90 | 20.88 | 0.96 | 0.61 |
| | | | 10-12 | 0.746 | | | | 5.31 | 2.41 | 24.17 | 75.89 | 17.53 | 1.51 | 0.69 |
| | | | 12-14 | | | | 105.4 | | | | 35.64 | 20.66 | 1.07 | 0.48 |
| 4040 | GB425 | GBUN1 | 0-2 | 0.753 | | | | 2.35 | 1.12 | 10.25 | 57.29 | | 1.42 | |
| | | | 2-4 | 0.729 | | | | 2.37 | 1.11 | 10.50 | 58.82 | | 1.42 | |
| | | | 4-6 | 0.684 | | 3.9 | | 1.97 | 0.94 | 8.58 | 45.64 | 12.57 | 0.55 | 0.32 |
| | | | 6-8 | 0.615 | | | | 2.04 | 0.62 | 11.80 | | 9.13 | | |

Table 9.5. Solid phase properties. (continued)

| Dive Number | Site | Station | Depth (cm) | Porosity (Φ) | Grain Size >65 μm | Sulfur (μmols/g) Acid Volatile AVS | Total Reduced TRS | Carbon (weight percent) Total | Organic | Inorganic (as CaCO₃) | Fe HCl | Citrate Dithonite | Mn HCl | Citrate Dithonite |
|---|---|---|---|---|---|---|---|---|---|---|---|---|---|---|
| | | | 8-10 | 0.616 | | | | 1.86 | 0.59 | 10.58 | 45.28 | 0.26 | 1.07 | 0.02 |
| | | | 10-12 | 0.607 | | | | 2.36 | 0.80 | 12.97 | 49.45 | 4.40 | 1.40 | 0.41 |
| | | | 12-14 | 0.601 | | | 102.5 | 2.14 | 0.62 | 12.66 | | 5.23 | | 0.20 |
| | | | 14-16 | | | | | | | | | 0.23 | | 0.02 |
| | | | 16-18 | | | | | | | | 18.76 | 0.19 | 0.76 | 0.03 |
| | | | 18-20 | | | | | | | | 1.82 | 0.32 | 0.10 | 0.10 |
| 4042 | GC185 | BHM3 | 0-2 | 0.857 | | | | 9.29 | 6.18 | 25.92 | 20.23 | 8.33 | 0.62 | 0.47 |
| | | | 2-4 | 0.816 | 0.812 | | | 9.58 | 6.37 | 26.75 | 23.16 | 8.77 | 0.43 | 0.47 |
| | | | 4-6 | 0.806 | 0.846 | 3.9 | | 9.58 | 6.25 | 27.75 | 19.71 | 6.92 | | 0.28 |
| | | | 6-8 | 0.804 | 0.790 | | | 8.62 | 5.42 | 26.67 | 20.44 | 7.41 | 0.42 | |
| | | | 8-10 | 0.760 | 0.703 | | | 8.97 | 3.75 | 43.50 | 22.09 | 3.99 | 0.46 | 0.24 |
| | | | 10-12 | 0.760 | 0.533 | | 126.5 | 8.56 | 4.03 | 37.75 | 24.67 | 11.42 | | 0.68 |
| | | | 12-14 | 0.792 | 0.636 | | | 8.90 | 5.31 | 29.92 | | | | |
| | | | 14-16 | 0.771 | 0.419 | | 122.1 | 9.09 | 6.40 | 22.42 | 26.75 | 9.57 | 0.78 | 0.51 |
| | | | 16-18 | 0.781 | 0.664 | | | 9.33 | 8.82 | 4.25 | | | | |
| | | | 18-20 | 0.789 | 0.624 | | | 11.30 | 8.42 | 24.00 | 29.99 | 7.79 | 0.58 | 0.44 |
| | | | 20-22 | 0.791 | 0.608 | | | 11.20 | 6.46 | 39.50 | | | | |
| | | | 22-24 | 0.769 | 0.736 | | | 8.38 | 5.38 | 25.00 | | | | |
| 4043 | GC234 | GCB3 orange *Beggiatoa* | 0-2 | 0.840 | 0.438 | 3.5 | | 5.92 | 2.89 | 25.25 | 46.09 | 8.44 | 1.67 | 0.48 |
| | | | 2-4 | 0.794 | 1.000 | 3.8 | | 6.31 | 3.34 | 24.75 | 55.27 | 11.40 | 1.39 | 1.50 |
| | | | 4-6 | 0.789 | 0.555 | 3.7 | | 6.87 | 3.19 | 30.67 | 30.29 | 9.24 | 0.79 | 0.39 |
| | | | 6-8 | 0.785 | 0.464 | 5.3 | | 6.62 | 4.59 | 16.92 | 47.34 | 8.11 | 1.42 | 0.39 |
| | | | 8-10 | 0.761 | 0.389 | 6.9 | | 8.06 | 3.48 | 38.17 | 55.38 | 10.94 | 1.63 | 1.79 |
| | | | 10-12 | 0.764 | 0.441 | 5.5 | | 8.33 | 3.69 | 38.67 | 41.46 | 10.85 | 1.11 | 1.25 |
| | | | 12-14 | 0.758 | 0.518 | 4.2 | 117.3 | 7.08 | 3.53 | 29.58 | 25.38 | 11.47 | 1.03 | 0.90 |
| | | | 14-16 | 0.756 | 0.484 | 4.1 | | 7.95 | 5.77 | 18.17 | 36.02 | 5.31 | 1.53 | 1.12 |
| | | | 16-18 | 0.754 | 0.621 | 0.8 | | 7.69 | 3.54 | 34.58 | 55.26 | 6.09 | 1.46 | 0.95 |
| | | | 18-20 | 0.755 | 0.581 | | | 6.32 | 2.74 | 29.83 | | | | |
| | | | 20-22 | 0.756 | 0.603 | 4.7 | | 7.45 | 4.14 | 27.58 | 36.62 | 4.53 | 0.99 | 0.66 |
| | | | 22-24 | 0.753 | 1.000 | | | 6.80 | 3.41 | 28.25 | | | | |
| | | | 24-26 | 0.677 | 0.569 | | | 7.53 | 3.63 | 32.50 | | | | |
| 4043 | GC234 | GCB3 off ma*t* | 0-2 | 0.862 | 0.960 | 1.8 | | 4.50 | 2.66 | 15.33 | 25.51 | 18.32 | 1.23 | 1.03 |
| | | | 2-4 | 0.847 | 0.955 | 5.2 | | 5.12 | 3.00 | 17.67 | 35.51 | 14.06 | 1.54 | 0.95 |
| | | | 4-6 | 0.842 | 0.963 | 4.0 | | 4.61 | 2.64 | 16.42 | 26.54 | 10.55 | 1.00 | 0.49 |
| | | | 6-8 | 0.806 | 0.827 | 2.9 | | 5.75 | 3.20 | 21.25 | 24.37 | 10.86 | 1.24 | 0.46 |
| | | | 8-10 | 0.805 | 0.827 | 2.2 | | 5.75 | 3.54 | 18.42 | 10.95 | 7.67 | 0.00 | 0.37 |
| | | | 10-12 | 0.814 | 0.897 | 2.2 | 94.6 | 5.72 | 3.16 | 21.33 | 26.53 | 11.37 | 1.12 | 0.44 |
| | | | 12-14 | 0.772 | 0.871 | | | 5.91 | 3.14 | 23.08 | | | | |
| | | | 14-16 | 0.778 | 0.833 | 2.4 | 94.6 | 5.74 | 2.83 | 24.25 | 21.62 | 7.06 | 1.19 | 0.45 |
| | | | 16-18 | 0.759 | 0.805 | | | 6.38 | 3.24 | 26.17 | | | | |
| | | | 18-20 | 0.747 | 0.768 | 2.3 | | 7.26 | 4.18 | 25.67 | 25.59 | 6.38 | 1.08 | |
| | | | 20-22 | 0.756 | 0.808 | | | 6.61 | 3.13 | 29.00 | | | | |
| | | | 22-24 | 0.757 | 0.823 | 1.5 | | 6.34 | 4.99 | 11.25 | 10.82 | | 0.00 | |
| | | | 24-26 | 0.767 | 0.858 | | | 6.33 | 3.22 | 25.92 | | | | |
| | | | 26-28 | 0.749 | 0.813 | | | 6.79 | 4.84 | 16.25 | 22.16 | | 0.94 | |
| | | | 28-30 | 0.747 | 0.836 | | | 6.27 | 3.22 | 25.42 | | | | |
| | | | 30-32 | 0.749 | 0.697 | | | 7.08 | 3.51 | 29.75 | | | | |
| 4045 | GC185 | BHAT2 | 0-2 | 0.857 | | | | 8.81 | 5.80 | 25.08 | 56.09 | 31.70 | 1.00 | 1.24 |
| | | | 2-4 | 0.819 | | | | 8.07 | 7.34 | 6.08 | 0.00 | 28.46 | 0.00 | 0.49 |
| | | | 4-6 | 0.821 | | 5.4 | | 7.26 | 5.83 | 11.92 | 35.38 | 13.13 | 0.73 | 0.44 |
| | | | 6-8 | 0.812 | | | | 7.24 | 5.37 | 15.58 | 53.46 | 19.95 | 0.72 | |
| | | | 8-10 | 0.791 | | | | 7.18 | 5.56 | 13.50 | 62.72 | 17.71 | 0.50 | 0.44 |
| | | | 10-12 | 0.806 | | | | 7.41 | 5.42 | 16.58 | 59.19 | 17.17 | 0.58 | 0.50 |
| | | | 12-14 | 0.811 | | | 129.2 | 7.14 | 5.40 | 14.50 | 30.68 | 7.08 | 0.60 | 0.48 |
| | | | 14-16 | 0.802 | | | | 7.24 | 5.23 | 16.75 | 58.65 | 12.38 | 0.39 | 0.48 |

Table 9.5. Solid phase properties. (continued)

| Dive Number | Site | Station | Depth (cm) | Porosity (Φ) | Grain Size >65 μm | Sulfur (μmols/g) Acid Volatile AVS | Total Reduced TRS | Carbon (weight percent) Total | Organic | Inorganic (as CaCO$_3$) | Extractable Metals (μmols/g) Fe HCl | Citrate Dithonite | Mn HCl | Citrate Dithonite |
|---|---|---|---|---|---|---|---|---|---|---|---|---|---|---|
| | | | 16-18 | 0.792 | | | | 7.38 | 5.83 | 12.92 | | | | |
| | | | 18-20 | 0.786 | | | | 7.11 | 5.84 | 10.58 | 53.19 | 9.56 | 0.45 | 0.49 |
| | | | 20-22 | 0.789 | | | | 7.15 | 5.54 | 13.42 | | | | |
| | | | 22-24 | 0.783 | | | | 7.22 | 5.67 | 12.92 | 56.92 | 10.91 | 0.76 | |
| | | | 24-26 | 0.775 | | | | 6.89 | 5.63 | 10.50 | | | | |
| | | | 26-28 | 0.786 | | | | 7.11 | 6.01 | 9.17 | | | | |
| 4047 | GC234 | GCJT2 | 0-2 | 0.833 | 0.532 | | | 5.47 | 2.48 | 24.92 | 67.58 | 1.62 | 1.71 | 0.08 |
| | | | 2-4 | 0.814 | 0.731 | | | 5.31 | 2.38 | 24.42 | 54.14 | 12.69 | 1.34 | 0.50 |
| | | | 4-6 | 0.825 | 0.804 | 2.1 | | 4.68 | 3.04 | 13.67 | 23.85 | 7.84 | 0.61 | 0.70 |
| | | | 6-8 | 0.812 | 0.749 | | | 4.58 | 2.60 | 16.50 | 54.43 | 0.32 | 1.06 | 0.03 |
| | | | 8-10 | 0.767 | 0.791 | | | 4.21 | 1.90 | 19.25 | 57.24 | | 1.94 | 0.00 |
| | | | 10-12 | 0.746 | 0.809 | | | 4.11 | 1.81 | 19.17 | 61.27 | 0.18 | 1.42 | 0.02 |
| | | | 12-14 | 0.730 | 1.000 | | 134.0 | 4.23 | 1.68 | 21.25 | 26.89 | 7.04 | 1.37 | 0.86 |
| | | | 14-16 | 0.711 | 0.870 | | | 4.45 | 2.32 | 17.75 | | | | |
| | | | 16-18 | 0.739 | 0.854 | | | 4.76 | 2.17 | 21.58 | 72.01 | 0.67 | 1.38 | 0.08 |
| | | | 18-20 | 0.749 | 0.764 | | | 4.00 | 1.44 | 21.33 | | | | |
| | | | 20-22 | 0.754 | 0.860 | | | 4.27 | 1.50 | 23.08 | 54.18 | 0.27 | 1.15 | 0.03 |
| | | | 22-24 | 0.765 | 0.830 | | | 3.90 | 1.95 | 16.25 | 58.06 | 0.95 | 1.62 | 0.07 |
| | | | 24-26 | 0.754 | 0.889 | | | 3.80 | 1.64 | 18.00 | | | | |
| | | | 26-28 | 0.765 | 1.000 | | | 3.68 | 1.51 | 18.08 | | | | |
| 4048 | GC234 | GCAT2 | 0-2 | 0.864 | 0.875 | 4.7 | | 5.72 | 2.94 | 23.17 | 65.71 | 12.92 | 1.28 | |
| | | | 2-4 | 0.809 | 0.824 | 3.6 | | 6.14 | 3.13 | 25.08 | 77.54 | 15.93 | 1.36 | 0.45 |
| | | | 4-6 | 0.790 | 0.862 | 5.1 | | 6.68 | 3.54 | 26.17 | 58.21 | 10.83 | 1.11 | 0.54 |
| | | | 6-8 | 0.778 | 0.900 | 5.3 | | 5.63 | 2.69 | 24.50 | 63.63 | 7.47 | 1.53 | 0.52 |
| | | | 8-10 | 0.776 | 0.880 | 1.8 | | 5.74 | 2.34 | 28.33 | 53.17 | 4.13 | 1.54 | |
| | | | 10-12 | 0.778 | 0.767 | 2.5 | 71.0 | 5.79 | 3.05 | 22.83 | 11.82 | 7.61 | 0.71 | 1.06 |
| | | | 12-14 | 0.770 | 0.870 | | | | | 0.00 | | | | |
| | | | 14-16 | 0.763 | 0.889 | 2.3 | 116.4 | 5.52 | 3.39 | 17.75 | 22.94 | 43.54 | 0.97 | 1.01 |
| | | | 16-18 | 0.761 | 0.897 | | | 5.51 | 2.49 | 25.17 | | | | |
| | | | 18-20 | 0.766 | | 4.4 | | 5.40 | 2.54 | 23.83 | 66.03 | 4.60 | 0.82 | 0.43 |
| | | | 20-22 | 0.763 | 0.904 | | | 5.64 | 2.56 | 25.67 | | | | |
| | | | 22-24 | 0.765 | 0.857 | 4.6 | | 5.68 | 2.95 | 22.75 | 62.51 | 5.51 | 1.44 | 0.47 |
| | | | 24-26 | 0.768 | 0.847 | 2.0 | | 5.33 | 2.51 | 23.50 | 64.72 | 4.97 | 1.37 | 0.42 |
| | | | 26-28 | 0.767 | 0.913 | | | 5.03 | 2.63 | 20.00 | | | | |
| | | | 28-30 | 0.771 | 0.888 | | | 5.06 | 2.45 | 21.75 | | | | |
| | | | 30-32 | 0.745 | 0.866 | | | 5.48 | 2.45 | 25.25 | | | | |
| | | | 32-34 | 0.739 | 1.000 | | | 5.25 | 2.36 | 24.08 | | | | |
| 4053 | GB425 | GBM2 | 0-2 | 0.863 | 0.946 | | | 2.68 | 1.55 | 9.42 | 89.05 | 18.45 | 2.29 | 1.07 |
| | | | 2-4 | 0.740 | 0.909 | | | 3.10 | 1.10 | 16.67 | 106.1 | 19.30 | 3.72 | 1.64 |
| | | | 4-6 | 0.662 | 0.861 | 1.4 | | 3.03 | 0.70 | 19.45 | 108.8 | 14.89 | 4.73 | 2.91 |
| | | | 6-8 | 0.635 | 0.850 | | | 2.68 | 0.74 | 16.13 | 113.5 | 8.71 | 4.91 | 1.11 |
| | | | 8-10 | 0.616 | 0.880 | | | 2.50 | 0.83 | 13.95 | 74.39 | 6.03 | 3.36 | 0.56 |
| | | | 10-12 | 0.598 | 0.895 | | 117.3 | 2.35 | 0.78 | 13.12 | 96.17 | 14.61 | 4.25 | 2.21 |
| | | | 12-14 | 0.594 | 0.876 | | | 2.38 | 0.77 | 13.46 | | | | |
| | | | 14-16 | 0.629 | 0.890 | | 114.4 | 2.50 | 0.69 | 15.09 | 86.00 | 16.57 | 4.11 | 2.30 |
| | | | 16-18 | 0.619 | 0.913 | | | 2.30 | 0.69 | 13.40 | | | | |
| | | | 18-20 | 0.607 | 0.874 | | | 2.33 | 0.71 | 13.49 | 11.29 | 12.46 | 0.38 | 0.49 |
| | | | 20-22 | 0.624 | 0.883 | | | 2.39 | 0.94 | 12.06 | | | | |
| | | | 22-24 | 0.645 | 0.938 | | | 2.25 | 0.75 | 12.53 | 42.89 | 4.31 | 1.41 | 0.97 |
| | | | 24-26 | 0.626 | 0.871 | | | 2.18 | 0.91 | 10.62 | | | | |
| | | | 26-28 | 0.611 | 0.847 | | | 2.39 | 0.23 | 18.00 | | | | |
| | | | 28-30 | | | | | | | | 98.47 | 18.54 | 4.77 | 1.80 |
| box | GC185 | BHBXC1 | 0-2 | 0.851 | | | | 2.82 | 0.85 | 16.38 | 36.54 | 23.53 | 2.80 | 2.20 |
| | | | 2-4 | 0.838 | | | | 2.69 | 0.93 | 14.68 | 64.67 | 19.83 | 3.25 | 1.65 |
| | | | 4-6 | 0.827 | | | | 2.69 | 0.94 | 14.55 | 36.25 | 31.83 | 3.46 | 2.87 |
| | | | 6-8 | 0.808 | | | | 2.56 | 0.99 | 13.06 | 78.74 | 17.48 | 3.58 | 1.75 |
| | | | 8-10 | 0.802 | | | | 2.79 | 1.04 | 14.58 | 79.18 | 19.24 | 3.56 | 1.73 |

Table 9.5. Solid phase properties. (continued)

| Dive Number | Site | Station | Depth (cm) | Porosity (Φ) | Grain Size >65 μm | Acid Volatile AVS | Total Reduced TRS | Total | Organic | Inorganic (as CaCO₃) | Fe HCl | Fe Citrate Dithonite | Mn HCl | Mn Citrate Dithonite |
|---|---|---|---|---|---|---|---|---|---|---|---|---|---|---|
| | | | | | | **Sulfur (μmols/g)** | | **Carbon (weight percent)** | | | **Extractable Metals (μmols/g)** | | | |
| | | | 10-12 | 0.804 | | | 97.5 | 2.69 | 0.96 | 14.40 | 41.51 | 4.50 | 2.11 | 0.41 |
| | | | 12-14 | 0.805 | | | | 2.83 | 0.98 | 15.43 | | | | |
| | | | 14-16 | 0.804 | | | | 2.59 | 1.01 | 13.17 | 50.63 | 21.17 | 9.45 | 7.17 |
| | | | 16-18 | 0.798 | | | | 2.46 | 0.92 | 12.88 | | | | |
| | | | 18-20 | 0.804 | | | | 2.53 | 0.98 | 12.91 | 50.25 | 30.18 | 5.04 | 3.78 |
| | | | 20-22 | 0.802 | | | | 2.64 | 0.98 | 13.88 | | | | |
| | | | 22-24 | 0.804 | | | | 2.81 | 0.98 | 15.28 | 42.43 | 11.44 | 4.72 | 0.78 |
| | | | 24-26 | 0.797 | | | | 2.59 | 0.93 | 13.88 | | | | |
| | | | 26-28 | 0.800 | | | | 2.46 | 0.92 | 12.87 | | | | |
| | | | 28-30 | 0.776 | | | | 2.46 | 1.02 | 12.00 | | | | |
| | | | 30-32 | 0.771 | | | | 2.68 | 0.90 | 14.86 | | | | |
| box | GC185 | BHUN2 | 0-2 | 0.812 | 0.818 | | | 4.71 | 3.44 | 10.58 | 79.56 | 23.80 | 0.94 | 0.69 |
| | | | 2-4 | 0.785 | 0.704 | | | 4.60 | 2.36 | 18.67 | 81.75 | 21.55 | 1.03 | 0.61 |
| | | | 4-6 | 0.812 | 0.918 | | | 6.00 | 3.98 | 16.83 | 65.70 | 16.12 | 0.00 | 0.53 |
| | | | 6-8 | 0.795 | 0.917 | | | 6.23 | 4.40 | 15.25 | 86.13 | | 1.05 | 0.53 |
| | | | 8-10 | 0.792 | 0.910 | | | 6.61 | 5.49 | 9.33 | 74.54 | 11.52 | 1.11 | 0.51 |
| | | | 10-12 | 0.787 | 0.861 | | | 6.85 | 5.46 | 11.58 | 70.46 | 14.68 | 1.04 | 0.55 |
| | | | 12-14 | 0.778 | 0.937 | | 121.6 | 7.74 | 5.93 | 15.08 | 44.12 | 7.54 | 0.00 | 0.43 |
| | | | 14-16 | 0.777 | 0.933 | | | 7.35 | 5.64 | 14.25 | 61.96 | 10.98 | 0.94 | 0.49 |
| | | | 16-18 | 0.790 | 0.948 | | | 7.06 | 5.68 | 11.50 | | | | |
| | | | 18-20 | 0.787 | 0.913 | | | 7.69 | 6.27 | 11.83 | 57.01 | 9.76 | 0.57 | 1.65 |
| | | | 20-22 | 0.758 | 0.932 | | | 7.85 | 6.04 | 15.08 | 71.27 | 12.00 | 0.86 | 0.94 |
| | | | 22-24 | 0.792 | 0.925 | | | 8.15 | 6.01 | 17.83 | | | | |
| box | GC234 | GCBX2 | 0-2 | 0.908 | | | | 2.59 | 1.49 | 9.17 | 77.36 | 40.03 | 40.89 | 25.24 |
| | | | 2-4 | 0.872 | | | | 2.68 | 1.53 | 9.58 | 64.95 | 68.42 | 28.30 | 50.96 |
| | | | 4-6 | 0.835 | | 0.2 | | 2.83 | 1.45 | 11.50 | 47.70 | 51.89 | 3.41 | 4.83 |
| | | | 6-8 | | | | | | | | 95.11 | 36.08 | 3.18 | 2.19 |
| | | | 8-10 | | | | | | | | 66.44 | 54.94 | 1.35 | 2.13 |
| | | | 10-12 | | | | 3.5 | | | | 44.28 | 44.24 | 2.76 | 1.90 |
| | | | 14-16 | | | | 2.4 | | | | 39.07 | 37.82 | 1.42 | 1.79 |
| | | | 18-20 | 0.792 | | | | 2.86 | 1.53 | 11.08 | 125.0 | 53.45 | 3.10 | 1.86 |
| | | | 22-24 | 0.778 | | | | 2.89 | 1.21 | 14.00 | 112.3 | 58.38 | 2.21 | 3.33 |
| | | | 26-28 | 0.796 | | | | 3.24 | 1.33 | 15.92 | 89.19 | 53.03 | 2.24 | 1.88 |
| box | GC234 | GCBXC1 | 0-2 | 0.859 | | | | 3.15 | 1.82 | 11.08 | 56.64 | 43.46 | 1.35 | 0.81 |
| | | | 2-4 | 0.816 | 0.924 | | 12.6 | 2.98 | 1.36 | 13.50 | 43.16 | 32.81 | 1.51 | 0.49 |
| | | | 4-6 | 0.814 | 0.924 | 8.4 | | 2.94 | 1.23 | 14.25 | 87.01 | 27.78 | 1.52 | 0.92 |
| | | | 6-8 | 0.808 | 0.955 | | | 2.76 | 1.34 | 11.83 | 54.72 | 21.88 | 1.46 | 0.89 |
| | | | 8-10 | 0.786 | 0.959 | | 130.0 | 2.86 | 1.11 | 14.58 | 1.71 | 16.60 | 0.03 | 0.96 |
| | | | 10-12 | 0.762 | 0.967 | | 124.1 | 2.43 | 1.20 | 10.25 | 47.16 | 10.03 | 1.41 | 0.44 |
| | | | 12-14 | 0.793 | 0.964 | | | 2.60 | 1.14 | 12.17 | | | | |
| | | | 14-16 | 0.797 | 0.961 | | 106.0 | 2.69 | 1.09 | 13.33 | 34.94 | 10.45 | 1.32 | 0.44 |
| | | | 16-18 | 0.781 | 0.953 | | | 3.28 | 1.24 | 17.00 | | | | |
| | | | 18-20 | 0.776 | 0.962 | | | 2.72 | 1.20 | 12.67 | 32.22 | 11.07 | 0.74 | 0.46 |
| | | | 20-22 | 0.768 | 0.958 | | | 3.05 | 1.11 | 16.17 | | | | |
| | | | 22-24 | 0.773 | 0.967 | | 113.8 | 2.68 | 1.10 | 13.17 | 29.26 | 10.58 | 1.35 | 0.57 |
| | | | 24-26 | 0.776 | | | | 2.90 | 1.14 | 14.67 | | | | |
| | | | 26-28 | 0.765 | | | | 3.03 | 1.24 | 14.92 | | | | |
| | | | 28-30 | 0.755 | | | 111.6 | 3.46 | 2.72 | 6.17 | 39.10 | 10.22 | 1.42 | |
| | | | 30-32 | 0.755 | | | | 2.86 | 1.18 | 14.00 | | | | |
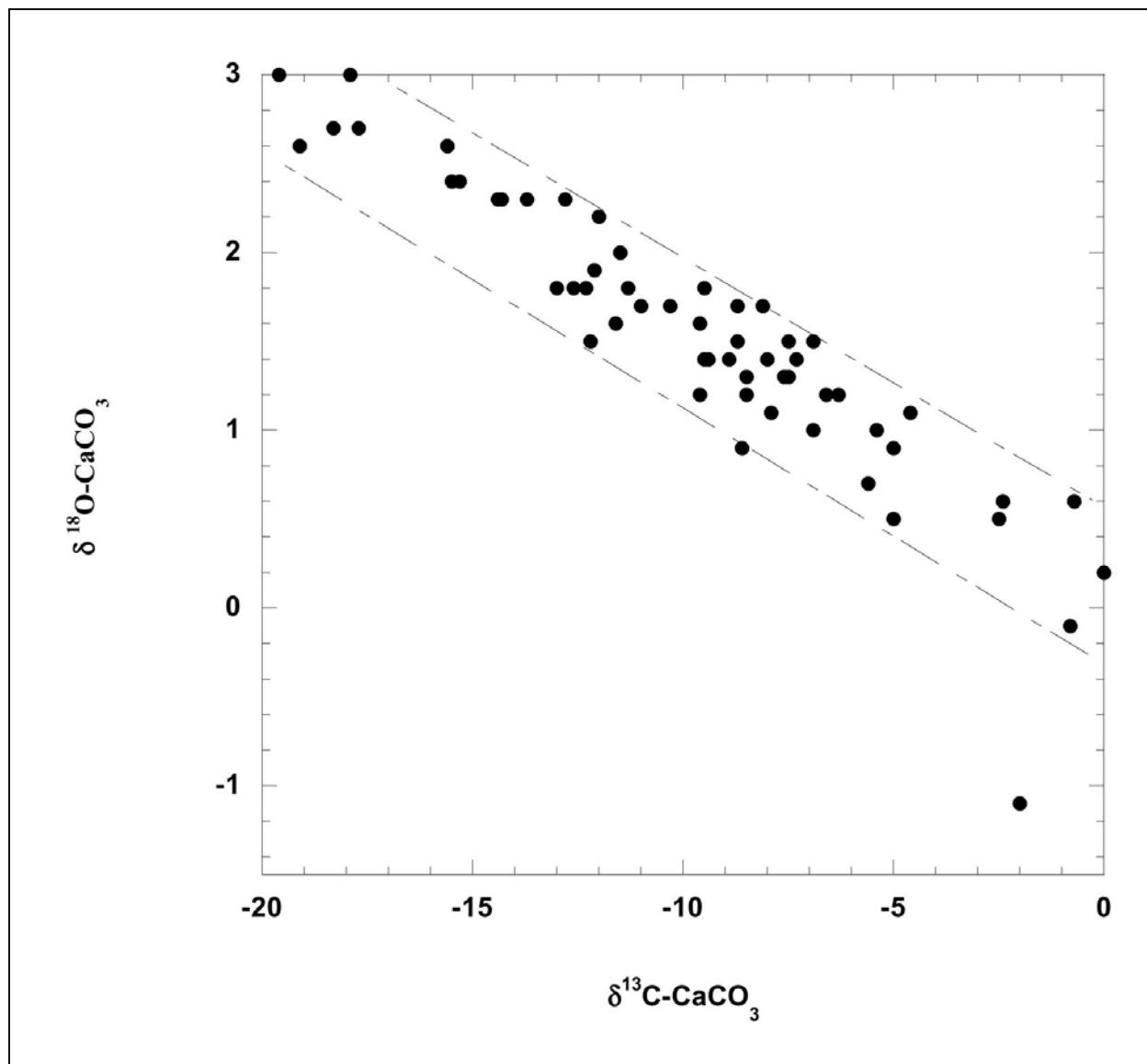
Figure 9.13.    Stable isotopes in carbonates.  The relationship between $\delta^{18}O$ and $\delta^{13}C$ ($^0/_{00}$ vs PDB standard) in CaCO$_3$.
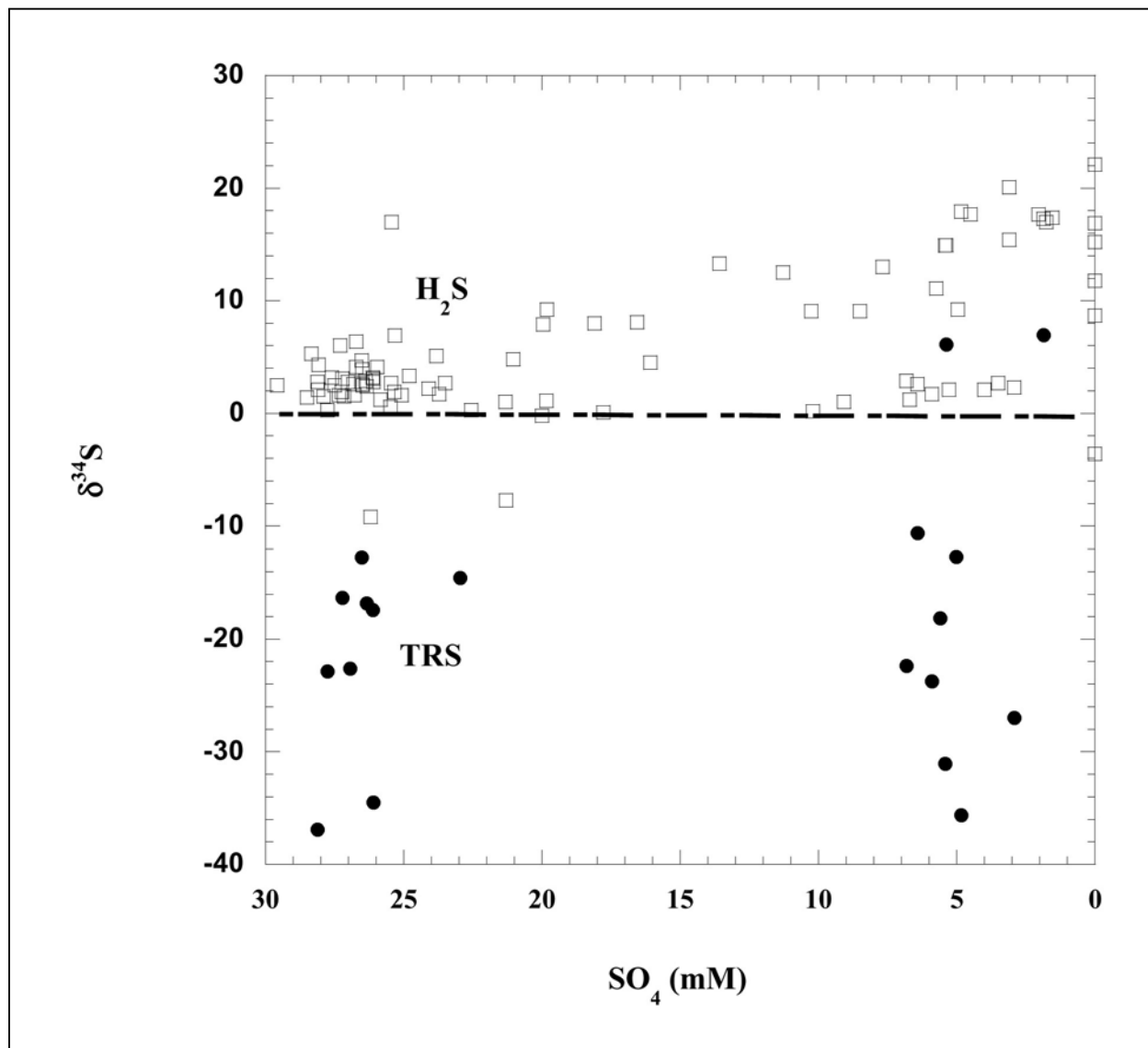
Figure 9.14.   Sulfur stable isotopes in H$_2$S and TRS.  Sulfur stable isotopes in H$_2$S and TRS in $^0/_{00}$ plotted against dissolved sulfate concentration.

### 9.3.3 Discussion

The probable explanation for the observed relationship between $CaCO_3$ $\delta^{13}C$ and $\delta^{18}O$ is that it represents a mixture of biogenic $CaCO_3$, largely from pelagic organisms, and $CaCO_3$, which is being formed authigenically in the sediments. Support of this hypothesis is made by the increasingly negative $\delta^{13}C$ values and increasingly positive $\delta^{18}O$ values with increasing $CaCO_3$ concentration (Figure 9.15A), and an increasing $CaCO_3$ content with increasing organic matter concentration (Figure 15B). Further evidence of extensive precipitation in these sediments is the major loss of dissolved calcium from pore waters. Figure 9.16 shows the relationship between DIC concentrations and $\delta^{13}C$-DIC. It includes an approximate line for the trend that would be expected if oxidation of marine organic matter were the primary source of added DIC. Although many points fall close to this line, many others fall both to the right and left of the line. A possible explanation, for the $\delta C^{13}$-DIC data falling to the negative side of the line, is that a more isotopically negative source of organic matter is being oxidized (e.g., thermogenic methane). In cases where the $\delta C^{13}$-DIC is on the positive side of the line, methane formation is likely, leaving behind isotopically heavier DIC.

The sulfur isotope ratios in TRS are, while relatively wide ranging, well within the range observed for marine muds for over a quarter of a century. Thus, even though the sedimentary geochemistry and extremely high sulfate reduction rates at the active sites are not typical for marine sediments, the sulfur stable isotopes do not indicate anything unusual is occurring in the sulfur system. The explanation for the causes of the strong positive sulfur stable isotope ratios in $H_2S$ is not certain. A major factor influencing sulfur stable isotope ratios is how "open or closed" the system is with respect to the sulfate that is the source for sulfide. The situation is further confounded by sulfur cycling within the sediment where sulfides can be oxidized to sulfate, which may then again be reduced to sulfide. Certainly, one way to produce positive sulfide values is to have a system that approaches being closed as is evidenced by reduction of almost all dissolved sulfate. As this occurs, the sulfate must become more positive, and the resulting $H_2S$ that is produced from the residual sulfate will also become more positive. The scatter to higher stable isotope ratios with increasing extent of sulfate reduction (Figure 9.14) is consistent with this explanation but does not necessarily prove it is the only possibility. Since there is vastly more solid-phase sulfide than dissolved sulfide, this "end member" affect will not be readily observed in TRS sulfur isotope ratios.

## 9.4 Microelectrode profiling[*]

### 9.4.1 Introduction

As discussed in the first section of this chapter, the biogeochemical cycling of sulfur, mainly sulfate reduction, $H_2S$ mineral formation and $H_2S$ oxidation, fuels important heterotrophic (sulfate reduction coupled to organic carbon oxidation) and autotrophic ($H_2S$ oxidation coupled to $CO_2$ reduction) processes in Gulf of Mexico hydrocarbon seep chemosynthetic communities. Solid-state gold-mercury (Au-Hg) amalgam microelectrodes and square and cyclic wave voltammetry were used to acquire millimeter scale concentration profiles of dissolved $H_2S$ in the

---

[*] This section was authored by Samatha Joye, Susan Escortia and John W. Morse.
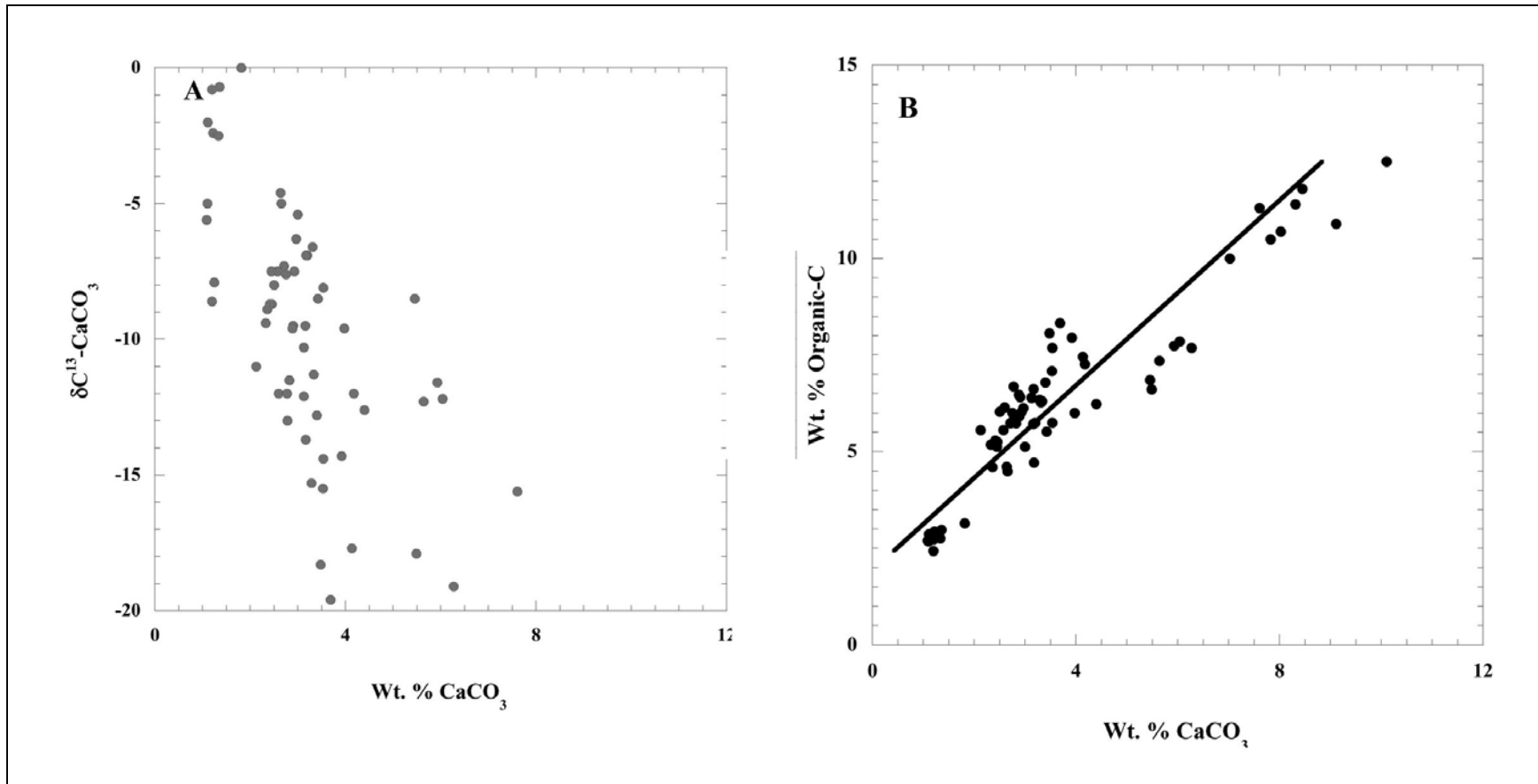
Figure 9.15.    Calcium carbonate concentration.  The relationship between calcium carbonate concentration and (A) $\delta^{13}C$ and (B) organic-C concentration.
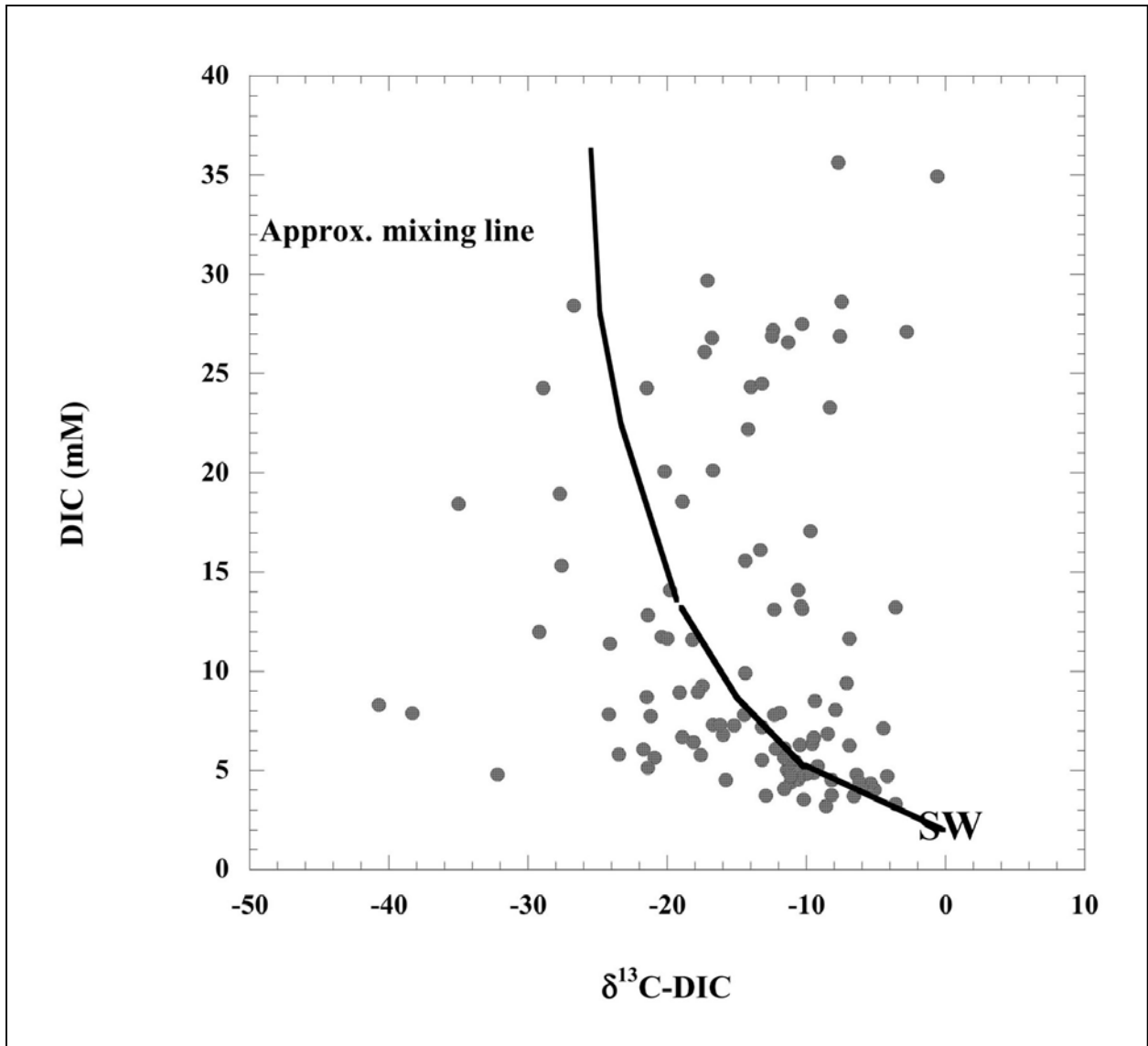
Figure 9.16. DIC stable carbon isotopes. The concentration of DIC versus its $\delta^{13}C$ ($^o/_{oo}$) value.

upper six centimeters of sediment (Brendel 1995; Brendel and Luther 1995) with the goal of constraining sediment-water fluxes of $H_2S$. The dissolved species profiles obtained using microelectrodes can easily document the steep, mm-scale concentration gradients that are either obscured or erased by more traditional scale-sampling techniques, such as squeezing or centrifuging cm-scale core sections, used to collect pore water for chemical analyses. While solid-state Au-Hg microelectrodes have clear advantages over traditional membrane-diffusion microelectrodes (mainly they are easier and less expensive to fabricate), they are prone to technical difficulties under harsh environmental conditions (Brendel 1995). Performance must be carefully documented when conditions are sub-optimal, particularly if the goal is to micro profile sediments characterized by high concentrations of DOC and/or $H_2S$.

The objectives of the microelectrode work were as follows:

1. Acquire mm-scale depth profiles of dissolved $H_2S$ in sediment pore water: The upper six centimeters of the sediment is a region of active material cycling and represents the region where aerobic and anaerobic processes may be coupled as oxygen diffuses into the sediment from the overlying water column. Documenting the $H_2S$ profiles within this region allowed us to calculate sediment-water interface exchange (i.e., fluxes) of $H_2S$.

2. Calculate sediment-water fluxes of $H_2S$: The sediment-water flux of $H_2S$ may serve as a means to group chemosynthetic community types (bacterial mat versus tubeworm, etc.) and provide insight to the mechanisms by which different chemosynthetic communities cycle $H_2S$ in the upper reaches of the sediment.

### 9.4.2 Results

Despite precautions and monitoring of the electrode performance, saturation of the electrode surface was frequently inescapable. Thus, the concentrations obtained using microelectrodes sometimes underestimated concentrations determined using traditional (colorimetric) techniques (Escorcia 2000). On some occasions, no usable data were obtained, e.g., when the detectable range was exceeded (Escorcia 2000). These results present the internally consistent findings from a selected subset of the data.

Micro profiles of $H_2S$ concentration in cores collected from *Beggiatoa* mats (Figures 9.17 and 9.18) and tubeworm bushes (Figure 9.19). The strategy in 1997 was to collect cores from representative environments (i.e., tubeworm bushes, bacterial mats, mussel beds, and control sites) to document the pore-water $H_2S$ distribution in different community types. After examining the 1997 results, the sampling strategy was altered in 1998 to collect cores from transects crossing from white to orange bacterial mats (Figure 9.18) and from the drip line and periphery of tubeworm bushes (Figure 20B and C). Cores were classified by macro community type following confirmation via video or the dive log. Table 9.6 summarizes the sediment-water interface fluxes of $H_2S$ calculated using Fick's First Law of Diffusion, $H_2S$ concentrations from the core water overlying and a depth of 0.4 cm, and diffusion constants for $H_2S$ described earlier in this chapter. Table 9.7 summarizes the sediment oxygen demand estimated from measured sulfate reduction rates (see Tables A.9.5 and 9.1) and underscores the inherent problem associated with microelectrode profiling aboard ship (as opposed to *in situ* micro profiling with a benthic lander).
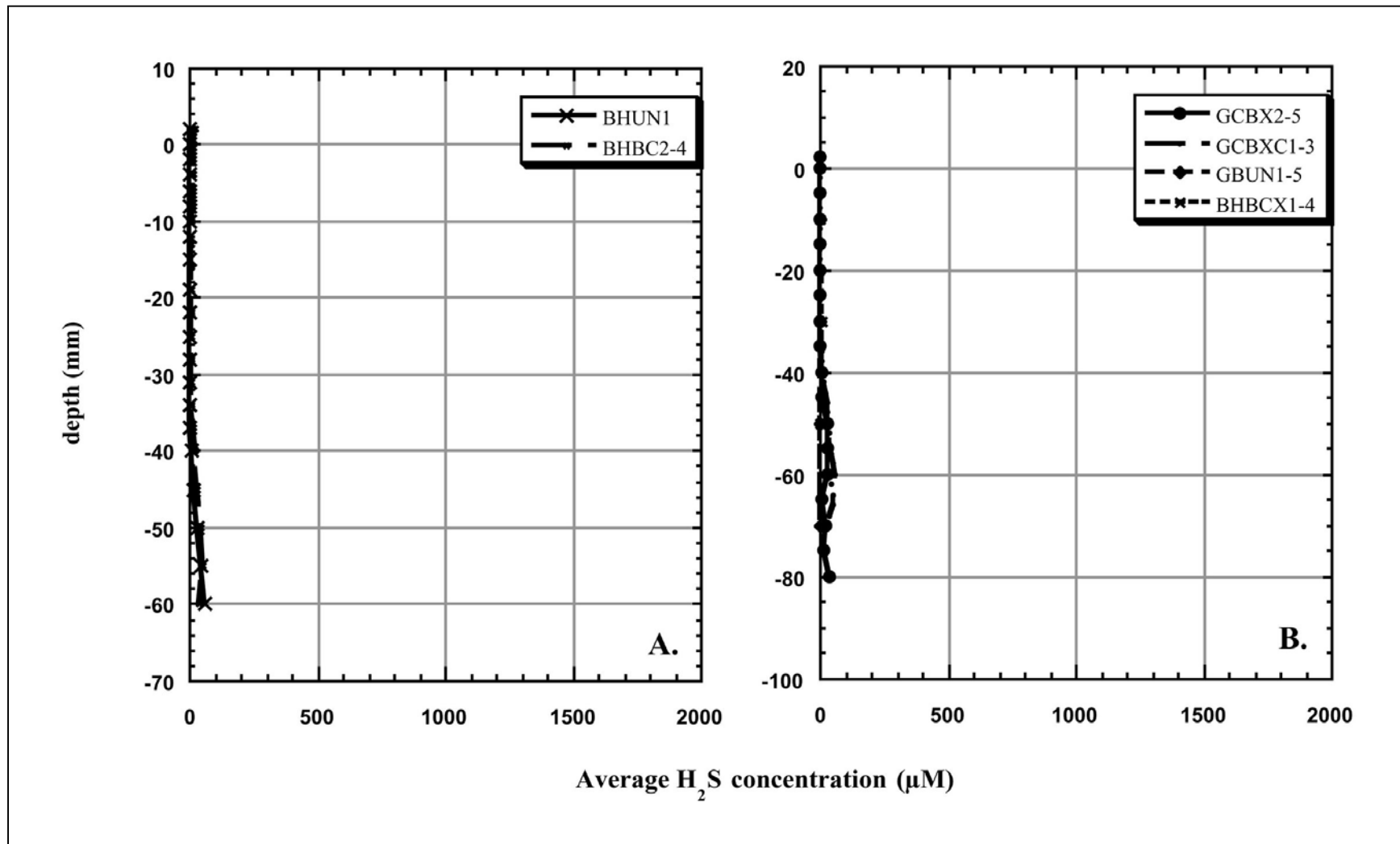
Figure 9.17. Control H$_2$S profiles. Microelectrode profiles of the average pore water H$_2$S concentration in control cores from 1997 (A) and 1998 (B).
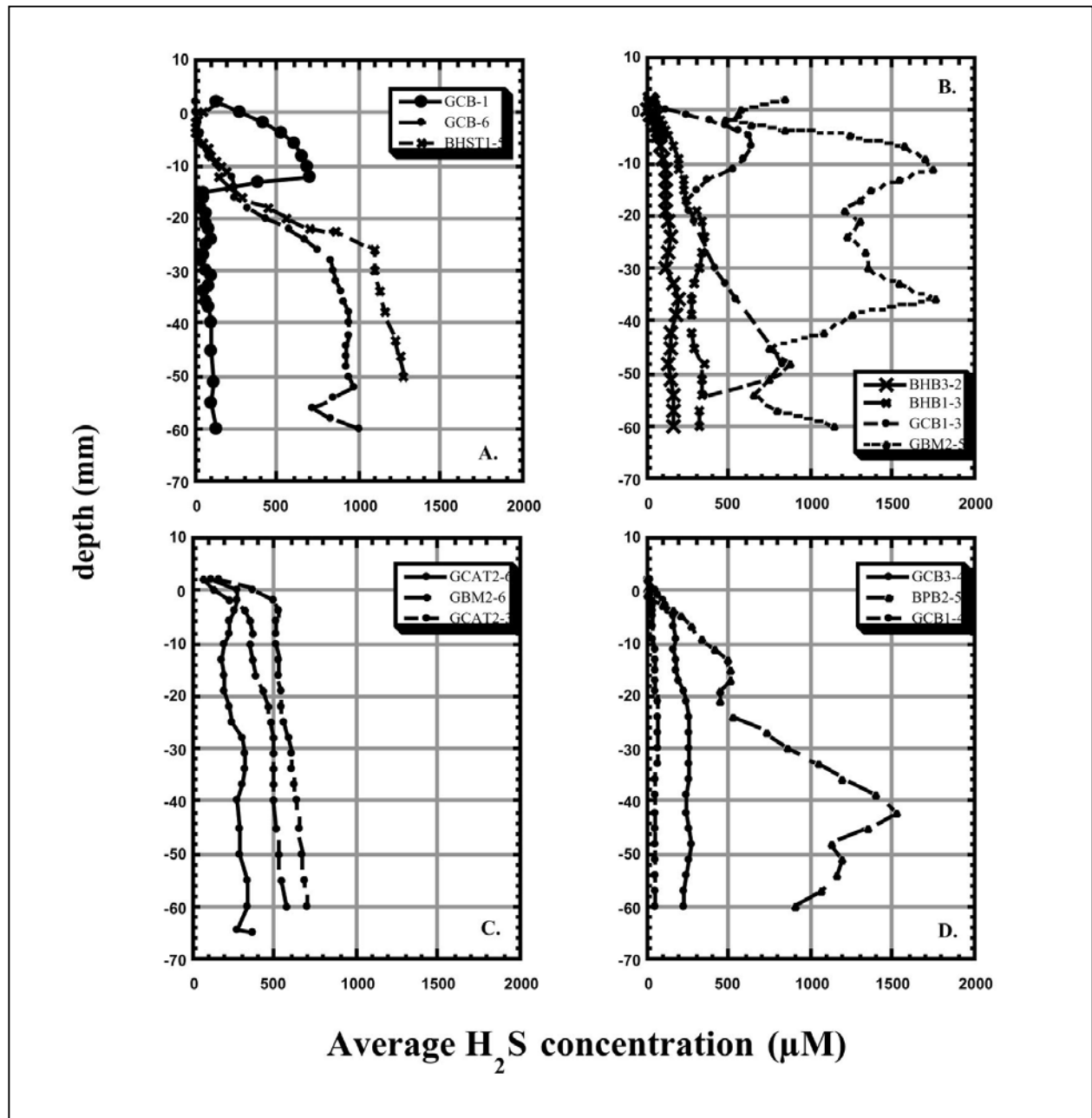
Figure 9.18.    *Beggiatoa* H$_2$S profiles. Microelectrode profiles of the average pore water H$_2$S concentration in cores from white Beggiatoa mats in 1997 (A) and 1998 (B) and orange Beggiatoa mats in 1997 (C) and 1998 (D).
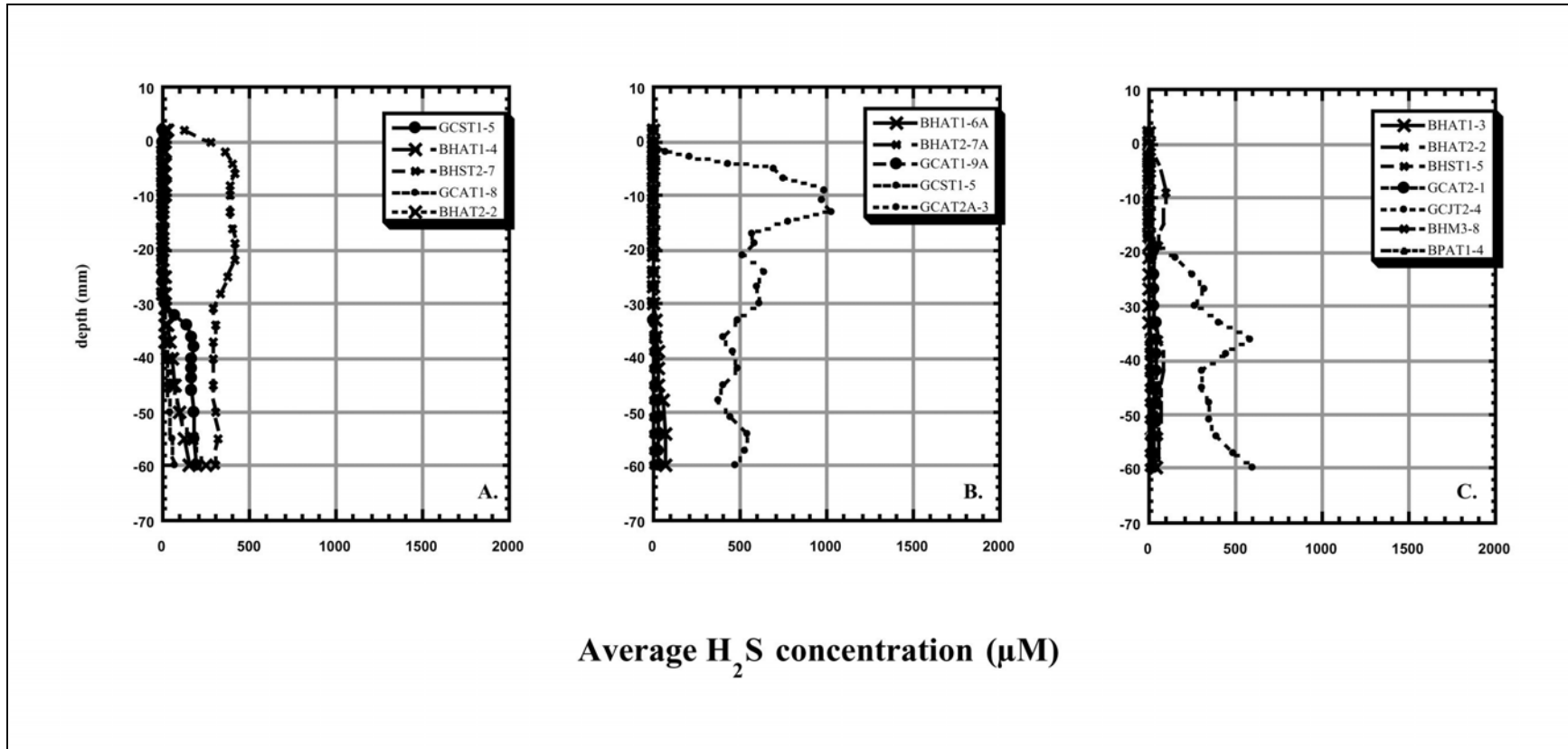
Figure 9.19.    Tubeworm H₂S profiles. Microelectrode profiles of the average pore water H₂S concentration in cores from tubeworm bushes in 1997 (A) and 1998 (B: > 1m from bush and C: at the bush dripline).
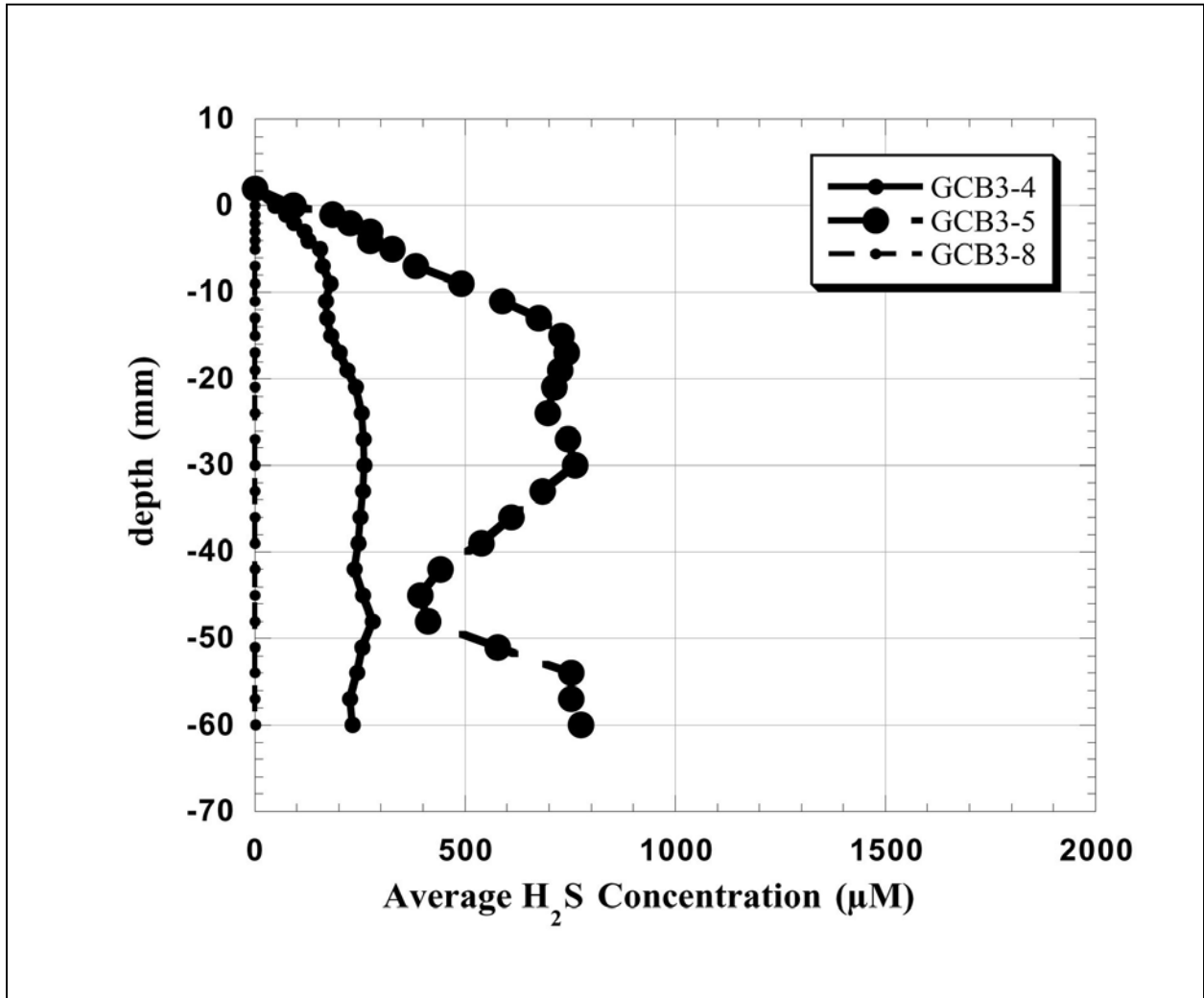
Figure 9.20.   Transect $H_2S$ profiles. Microelectrode profiles of the average pore water $H_2S$ concentration in cores collected along a transect from no mat (small circles), to orange/white mat (medium circles), to orange mat (large circles).

Table 9.6.  Sulfate reduction rate ($^{35}$S).

| Dive Number | Site | Station | Core | Incubation Time (h) | Injection Depth (cm) | Sulfate Reduction Rate (mmols/cm$^3$/sec x 10$^9$) |
|---|---|---|---|---|---|---|
| 2871 | GC234 | GCST1 | 5 | 11.3 | 1 | 2.21 |
| | | | | | 3 | 2.78 |
| | | | | | 5 | 1.95 |
| | | | | | 7 | 1.70 |
| | | | | | 9 | 1.92 |
| | | | | | 11 | 1.22 |
| | | | | | 13 | 2.22 |
| 2872 | GC234 | GCAT2 (SO$_4$ data from dive 2886) | 3 | 11.0 | 1 | 647.05 |
| | | | | | 3 | 157.21 |
| | | | | | 5 | 382.91 |
| | | | | | 7 | 387.22 |
| | | | | | 9 | 10.58 |
| | | | | | 17 | 2.66 |
| 2873 | GC185 | BHM4 | 6 | 10.6 | 1 | 3.85 |
| | | | | | 3 | 9.13 |
| | | | | | 5 | 1.47 |
| | | | | | 17 | 0.03 |
| 2873 | GC185 | BHAT1 | 4 | 9.8 | 1 | 1.94 |
| | | | | | 3 | 2.63 |
| | | | | | 5 | 1.48 |
| | | | | | 7 | 1.72 |
| | | | | | 9 | 1.38 |
| 2874 | GC185 | BHST1 | 5 | 11.5 | 1 | 1.18 |
| | | | | | 3 | 2.15 |
| | | | | | 5 | 1.10 |
| | | | | | 7 | 2.51 |
| | | | | | 9 | 1.79 |
| | | | | | 11 | 0.81 |
| | | | | | 13 | 1.74 |
| | | | | | 15 | 1.65 |
| | | | | | 17 | 1.33 |
| 2875 | GC185 | BHST2 | 4 | 12.0 | 1 | 1.65 |
| | | | | | 3 | 1.78 |
| | | | | | 5 | 2.86 |
| | | | | | 7 | 2.14 |
| | | | | | 9 | 2.18 |
| | | | | | 11 | 2.46 |
| 2875 | GC185 | BHUN1 | 5 | 18.0 | 1 | 0.44 |
| | | | | | 3 | 0.75 |
| | | | | | 5 | 1.49 |
| | | | | | 7 | 0.90 |
| | | | | | 9 | 1.30 |
| | | | | | 11 | 0.76 |
| | | | | | 13 | 1.02 |
| | | | | | 15 | 1.87 |
| | | | | | 17 | 1.24 |
| | | | | | 19 | 1.31 |
| | | | | | 21 | 0.70 |
| | | | | | 23 | 0.67 |

Table 9.6. Sulfate reduction rate ($^{35}$S). (continued)

| Dive Number | Site | Station | Core | Incubation Time (h) | Injection Depth (cm) | Sulfate Reduction Rate (mmols/cm$^3$/sec x 10$^9$) |
|---|---|---|---|---|---|---|
| box | GC185 | BHBC2 | 1 | 18.0 | 1 | 246.59 |
| | | | | | 3 | 431.15 |
| | | | | | 5 | 15.63 |
| | | | | | 7 | 2.33 |
| | | | | | 9 | 1.58 |
| | | | | | 11 | 1.12 |
| | | | | | 13 | 1.05 |
| | | | | | 17 | 1.43 |
| | | | | | 19 | 1.37 |
| | | | | | 21 | 2.26 |
| 2880 | GC234 | GCAT1 (GCB1@GCAT1) | 5 | 10.0 | 1 | 1.94 |
| | | | | | 3 | 1.33 |
| | | | | | 5 | 1.35 |
| | | | | | 7 | 0.72 |
| | | | | | 9 | 1.12 |
| | | | | | 11 | 1.29 |
| | | | | | 13 | 0.19 |
| | | | | | 15 | 1.03 |
| 2882 | GB425 | GBM2 (GBB1@GBM2) | 8 | 17.0 | 1 | 83.15 |
| | | | | | 3 | 791.97 |
| | | | | | 5 | 17.10 |
| | | | | | 7 | 10.32 |
| | | | | | 9 | 20.53 |
| 2883 | GB425 | GBM1 | 8 | 9.7 | 1 | 12.61 |
| | | | | | 5 | 11.85 |
| | | | | | 9 | 5.33 |
| | | | | | 15 | 5.18 |
| 2886 | GC234 | GCAT2 | 6 | 12.0 | 1 | 26.94 |
| | | | | | 3 | 171.81 |
| | | | | | 5 | 273.98 |
| | | | | | 7 | 443.53 |
| | | | | | 9 | 74.36 |
| 2888 | GC234 | GCAT1 | 8 | 12.0 | 1 | 1.57 |
| | | | | | 3 | 5.04 |
| | | | | | 7 | 1.46 |
| | | | | | 11 | 1.86 |
| 2891 | GC185 | BHAT2 | | 7.8 | 1 | 12.73 |
| | | | | | 3 | 2.33 |
| | | | | | 7 | 3.79 |
| | | | | | 11 | 2.95 |
| 4027 | GC185 | BHST1 | 1 | 14.3 | 1 | 1.72 |
| | | | | | 3 | 1.65 |
| | | | | | 5 | 1.36 |
| | | | | | 7 | 1.18 |
| | | | | | 9 | 0.75 |
| | | | | | 11 | 0.75 |
| | | | | | 13 | 0.60 |
| | | | | | 17 | 0.77 |
| 4028 | GC185 | BHB3 | 6 | 12.0 | 1 | 4.20 |
| | | | | | 3 | 2.50 |
| | | | | | 5 | 0.33 |

Table 9.6. Sulfate reduction rate ($^{35}$S). (continued)

| Dive Number | Site | Station | Core | Incubation Time (h) | Injection Depth (cm) | Sulfate Reduction Rate (mmols/cm$^3$/sec x 10$^9$) |
|---|---|---|---|---|---|---|
| 4029 | GC234 | GCAT2 | 5A | 4.1 | 1 | 10.10 |
| | | | | | 3 | 12.21 |
| | | | | | 5 | 45.55 |
| | | | | | 7 | 40.85 |
| | | | | | 9 | 176.75 |
| | | | | | 11 | 291.48 |
| | | | | | 13 | 0.00 |
| | | | | | 15 | 47.69 |
| 4029 | GC234 | GCAT2 | 5B | 8.5 | 1 | 4.62 |
| | | | | | 3 | 7.22 |
| | | | | | 5 | 7.27 |
| | | | | | 7 | 9.58 |
| | | | | | 9 | 8.43 |
| | | | | | 11 | 6.87 |
| | | | | | 13 | 5.23 |
| | | | | | 15 | 3.64 |
| 4029 | GC234 | GCAT2 | 8A | 13.3 | 1 | 7.57 |
| | | | | | 3 | 10.30 |
| | | | | | 5 | 11.76 |
| | | | | | 7 | 7.67 |
| | | | | | 9 | 7.22 |
| | | | | | 11 | 3.82 |
| | | | | | 13 | 1.69 |
| | | | | | 15 | 0.89 |
| 4031 | GC234 | GCST1 | 8 | 11.8 | 1 | 0.60 |
| | | | | | 3 | 3.13 |
| | | | | | 5 | 2.44 |
| | | | | | 7 | 1.62 |
| | | | | | 9 | 1.47 |
| | | | | | 11 | 1.84 |
| | | | | | 13 | 1.57 |
| | | | | | 15 | 1.65 |
| | | | | | 17 | 1.82 |
| | | | | | 19 | 1.16 |
| 4038 | GC233 | BPB2 | 7 | 12.0 | 1 | 10.01 |
| | | | | | 3 | 9.06 |
| | | | | | 5 | 6.22 |
| | | | | | 7 | 5.20 |
| | | | | | 9 | 4.56 |
| | | | | | 11 | 1.70 |
| 4043 | GC234 | GCB3 orange *Beggiatoa* | 1 | 13.1 | 1 | 12.25 |
| | | | | | 3 | 10.88 |
| | | | | | 5 | 13.34 |
| | | | | | 7 | 19.49 |
| | | | | | 9 | 28.53 |
| | | | | | 11 | 20.34 |
| | | | | | 13 | 29.89 |
| | | | | | 15 | 19.45 |
| 4043 | GC234 | GCB3 white *Beggiatoa* | 9 | 12.4 | 1 | 3.21 |
| | | | | | 3 | 2.44 |
| | | | | | 5 | 2.39 |
| | | | | | 7 | 1.78 |

Table 9.6. Sulfate reduction rate ($^{35}$S). (continued)

| Dive Number | Site | Station | Core | Incubation Time (h) | Injection Depth (cm) | Sulfate Reduction Rate (mmols/cm$^3$/sec x 10$^9$) |
|---|---|---|---|---|---|---|
| box | GC185 | BHUN2 | 1 | 12.1 | 1 | 70.04 |
| | | | | | 3 | 79.71 |
| | | | | | 5 | 65.75 |
| | | | | | 7 | 37.49 |
| 4046 | GC185 | BHM4 | 5 | 4.2 | 1.5 | 2.74 |
| | | | | | 2.5 | 1.79 |
| | | | | | 3.5 | 1.30 |
| | | | | | 4.5 | 1.55 |
| 4047 | GC234 | GCJT2 | 3 | 13.7 | 1 | 3.24 |
| | | | | | 3 | 1.39 |
| | | | | | 5 | 1.70 |
| | | | | | 7 | 1.70 |
| | | | | | 9 | 1.25 |
| | | | | | 11 | 1.41 |
| | | | | | 13 | 0.52 |
| | | | | | 15 | 0.85 |
| | | | | | 17 | 0.78 |
| | | | | | 19 | 0.99 |
| | | | | | 21 | 0.67 |
| | | | | | 23 | 0.45 |
| 4048 | GC234 | GCAT2 | 5 | 11.9 | 1 | 37.11 |
| | | | | | 3 | 57.86 |
| | | | | | 5 | 75.52 |
| | | | | | 7 | 48.35 |
| | | | | | 9 | 27.03 |
| | | | | | 11 | 17.77 |
| | | | | | 13 | 7.27 |
| | | | | | 15 | 3.18 |
| | | | | | 17 | 1.01 |
| 4053 | GB425 | GBM2 | 5 | 12.3 | 1 | 186.89 |

Table 9.7.  Comparative sulfate reduction rates

| Locality | water depth (m) | Integrated SO$_4$ Reduction rate (mmoles-SO$_4$/m$^2$/day) |
|---|---|---|
| Great Sippewissett Marsh, Massachusetts[1] | ~ | 107- 420 |
| Cape Lookout Bight, North Carolina[2] | 8 | 149.9 |
| Black Hole, Long Island Sound *(i)* | 10 | 35.6 |
| Saanich Inlet, British Columbia *(ii)* | 225 | 16.5 |
| Gulf of Mexico shelf, Mississippi delta *(iii)* | 59 | 13.8 |
| Skagerrak, Danish coast *(iv)* | 200 | 12.4 |
| Gulf of Mexico shelf, Texas *(reference)* | 151 | 2.11 |
| MANOP, Station M, Pacific *(v)* | 3100 | 0.004 |

i.   J. T. Westrich, Ph.D. dissertation, Yale University (1983).

ii.  A. H. Devol, J. J. Anderson, K. Kuivia, J. W. Murray, *Geochim. Cosmochim. Acta* **48**, 993 (1984).

iii. S. Lin and J. W. Morse, *Amer. J. Sci.* **291**, 55 (1991).

iv. N. Iversen and B. B. Jørgensen, *Limnol. Ocean.* **30**, 945 (1985).

v.  This rate is not obtained from direct measurement but from a model calculation in B. Bender and D. T. Heggie, *Geochim. Cosmochim. Acta* **48**, 977 (1984).

Though the microelectrode system we used is capable of simultaneous quantification of dissolved oxygen and dissolved H$_2$S concentration, we never documented any dissolved oxygen in the water overlying sediment cores or in the sediment pore water. The lack of dissolved oxygen in these cores probably reflects an artifact stemming from the unavoidable time delay between core collection and microelectrode profiling. On a typical day, approximately 4-8 hours elapsed between core collection using the JSL submersible and initiation of micro profiling. An additional 2-3 hours elapsed between the completion of the first micro profile and the initiation of the second micro profile in a given core. These delays were unavoidable.

Submarine dives lasted 2-4 hours, retrieval and cataloging of cores required 1-2 hours, and preparing the cores and microelectrodes (repeated standardization) required an additional 1-2 hours. Approximately 4-6 hours were required to complete two 6-cm deep profiles in one core, meaning that there was an addition 2-3 hour lag between replicate profiles in a given core. We hypothesized that during this time, dissolved oxygen in the overlying water was rapidly consumed given the (predicted) high sediment oxygen demand. We attempted to remedy this artifact in 1998 by aerating the overlying waters with an aquarium pump once the cores were on deck; however, aeration for one hour did not restore oxygen to detectable levels. To evaluate the potential oxygen demand associated with H$_2$S oxidation, we used the integrated sulfate reduction

---

[1]  Higher rates are reported by R. W. Howarth and J. M. Teal, *Limnol. Ocean.* **24**, 999 (1979); Lower rates are from G. M. King, B. L. Howes, J. W. H. Dacey, *Geochim. Cosmochim. Acta* **49**, 1561 (1985).

[2]  A maximum sulfate reduction rate is taken from July 1983 data reported in P. M. Crill and C. S. Martens, *Geochim. Cosmochim. Acta* **51**, 1175 (1987).

rates to estimate oxygen consumption due to complete oxidation of $H_2S$ oxidation to sulfate. This calculation does not consider the oxygen demand associated with other metabolic processes, such as aerobic respiration or methane oxidation, so should be considered a conservative estimate of the sediment oxygen demand. This calculation requires the following assumptions:

1. The sediment surface area in a core was flat and averaged 38.5 $cm^2$;

2. Two moles of oxygen were consumed per mole of $H_2S$ oxidized completely to $SO_4^{2-}$;

3. The overlying water was saturated with oxygen at bottom water temperature (7°C) and salinity (35‰), i.e., the concentration of dissolved oxygen was ≈ 300 μM (Pilson 1998);

4. A 100 mL water phase was present above the core.

For example, consider a core having a daily depth-integrated sulfate reduction rate (SRR) of 232 mmol S $m^{-2}$ $d^{-1}$ (this value represents the average rate at sites with high SRR; Tables A.9.5 and 9.1), the hourly SRR was 9.7 mmol S $m^{-2}$ $hr^{-1}$. Reoxidation of the generated $H_2S$ resulted in an oxygen demand of 19.3-mmol $m^{-2}$ $hr^{-1}$. Given a surface area of 38.5 $cm^2$, the total sediment oxygen demand in the core was 0.074-mmol $hr^{-1}$ or 74-μmol $hr^{-1}$. A 100 mL overlying water phase saturated with oxygen when the core was collected would have contained only approximately 30 μmoles of oxygen. At the calculated oxygen consumption rate (74 μmol $hr^{-1}$), this oxygen (~ 30 μmoles) would have been consumed in approximately 25 minutes. Values of the oxygen consumption due to $H_2S$ oxidation in sediments exhibiting low, high, and extremely high SRR rates are shown in Table 9.7. In all cases, complete consumption of oxygen from the overlying water would have occurred by the time micro profiling began. This calculation considers only one sink for oxygen (i.e., $H_2S$ oxidation) so actual oxygen consumption rates are likely to be even faster. Even sites characterized by 'low' rates of SRR (i.e., low for CHEMO communities) were prone to rapid oxygen depletion. Once oxygen was depleted, sediment oxygen consumption could have maintained oxygen concentrations below detectable levels, even if the water column was aerated with an aquarium pump. The oxygen demand in CHEMO sediments is extreme. For comparison, the oxygen demand in sediments of the South Atlantic and Danish coastal regions are 0.07 to 0.2 and 0.6 to 0.8-mmol $m^{-2}$ $hr^{-1}$, respectively (Glud *et al.* 1994; Gundersen and Jorgensen 1990). The oxygen demand in sediments from Galveston Bay, Texas, was 0.3-mmol $m^{-2}$ $h^{-1}$ (An 1999; An and Joye 2000). The rates from deep-sea sediments are two orders of magnitude lower than those typical of low SRR GOM hydrocarbon seep sites, while the rates from estuarine environments are approximately half of that estimated at "low" SRR GOM hydrocarbon sites.

### 9.4.3 Discussion

Sediment micro profiles of $H_2S$ concentration revealed significant differences between chemosynthetic community types. The following section presents the average $H_2S$ concentration profiles for cores collected from control sites, within *Beggiatoa* mats and near tubeworm bushes. Cores from mussel beds were not profiled with microelectrodes, because it was difficult to collect viable cores. However, several cores from *Beggiatoa* mats adjacent to mussel beds were collected and sampled (these are classified as *Beggiatoa* cores). From these profiles, sediment-water interface $H_2S$ fluxes were calculated for each year and community type. The most striking

and consistent conclusion based on the microelectrode data is that *Beggiatoa* mats exploit regions characterized by high $H_2S$ flux.

Average $H_2S$ profiles in cores collected from white (A, B) and orange (C, D) *Beggiatoa* mats in 1997 (A, C) and 1998 (B, D) are presented in Figure 9.17. Profiles of $H_2S$ concentration obtained from *Beggiatoa* mats exhibit sharp concentration gradients near sediment water interface (SWI). In one core from 1997 (GCB-1), a large drop in concentration was observed at approximately 1.5 cm (Figure 9.17A). We attribute this to a loss of sensitivity in the microelectrode (most likely due to amalgam degradation). This feature did not reflect the actual pore water concentration. Oxygen was never documented in the water overlying these cores; however, $H_2S$ was commonly present in the overlying water (at concentrations up to 170 μM), suggesting that our assumption of high sediment oxygen demand and rapid oxygen consumption is valid. Concentration changes were most obvious within the upper two cm; below that depth, concentrations increased gradually.

Three cores collected along a transect grading from an uninhabited sediment to sediment dominated by orange and/or white *Beggiatoa* were micro profiled in 1998 (Figure 9.18). The core collected from the area without a visible *Beggiatoa* mat exhibited negligible $H_2S$ concentrations (< 2 μM). The core from the center of the mat, which was dominated by orange *Beggiatoa*, exhibited $H_2S$ concentrations ranging from negligible (in overlying water) to 280 μM (at 5 cm). The transition zone between orange *Beggiatoa* and no *Beggiatoa* mat was a mixture of white and orange *Beggiatoa*. This region exhibited the highest $H_2S$ concentrations (745 μM at 3 cm). Both cores collected from *Beggiatoa* inhabited sediments exhibited sharp increases in $H_2S$ concentration near the SWI.

Pore water $H_2S$ profiles from sediment cores collected near tubeworm bushes are presented in Figure 20. In 1997 (Figure 9.20A), profiles from cores (n = 4) collected at the drip line of tubeworm bushes exhibited $H_2S$ depletion in the upper 3 cm. Below this depth, $H_2S$ concentration gradually increased. One core was collected approximately 0.5 m away from the bush drip line (BHST2-7) and higher $H_2S$ concentration were observed in this core. To investigate the hypothesis that sediments adjacent to the tubeworm bush (i.e., at the drip line) exhibited lower $H_2S$ concentration, we collected sets of cores at the drip line (Figure 9-19C) and away from the drip line (> 1 m, Figure 9.20B) in 1998. In 10 of 12 cores, $H_2S$ was depleted throughout the upper 3.5 (or more) cm. In the remaining two cores (GCAT1-9A on Figure 9-19B and GCJT2-4 on Figure 9.20C), higher $H_2S$ concentrations were observed but there was no consistent pattern over depth. Data from 1997 and 1998 support the hypothesis of Julian *et al.* (1999a) that tubeworm roots actively take up $H_2S$ from the sediment contributing to $H_2S$ depletion, particularly within the upper 4 cm.

Sediment-water interface fluxes of $H_2S$ were compared between community types to identify distinguishing community features (Table 9.6). Negative values predict a flux from the sediment to the overlying water while positive values predict a flux from the overlying water to the sediment. However, we do not believe that $H_2S$ fluxes from the overlying water into the sediment. Our large geochemical database shows clearly that large reservoirs of $H_2S$ are found at depths greater than 6 cm in these sediments. We believe that (calculated) positive fluxes are an artifact related to the depletion of oxygen from the overlying water during core processing. Oxygen depletion could restrict $H_2S$ oxidation, thereby shifting the $H_2S$ profile up into the water

column. Microbially-mediated $H_2S$ oxidation coupled to nitrate reduction within upper sediment layers could consume $H_2S$ in the absence of oxygen, yielding profiles that suggest an $H_2S$ flux from the overlying water into the sediment. Explanation of these profiles requires an active $H_2S$ oxidant (other than oxygen) at the sediment-water interface, which is entirely feasible based on the known ability of some microorganisms to couple $H_2S$ oxidation with $NO_3$ reduction.

Fluxes from *Beggiatoa* mats were not related to mat coloration. Negative fluxes (from the sediment to the water column) were consistently documented for both mat types and fluxes ranged from 0 to -200 mmol $m^{-2}d^{-1}$. In cores collected along a transect grading from no mat (outside) to orange/white mat (transition) to orange mat (interior), fluxes varied from 0 (outside) to -137 (transition) and -44 (interior) mmol $m^{-2}$ $day^{-1}$. Because of the variability between replicate profiles, the calculated fluxes in the transition zone were not significantly different from those observed in the interior. In 1997, both positive and negative fluxes were calculated from $H_2S$ profiles in cores collected near tubeworm bushes. Positive fluxes (i.e., a sediment sink) of $H_2S$ within the top cm were observed in some sites (0-6 mmol $m^{-2}d^{-1}$), while large gradient supported negative fluxes were observed at one site (BHST2-7). In 1998, only 2 of 13 profiles supported an $H_2S$ flux (an efflux). Fluxes from the remaining cores were insignificant (not distinguishable from zero).

Hydrogen sulfide concentrations and distribution in sediment collected from within *Beggiatoa* mats were distinct from those obtained in sediment associated with tubeworm bushes. Sediment beneath *Beggiatoa* mats was characterized by sharp gradients in $H_2S$ concentrations and increasing concentrations with depth. In contrast, sediment from areas inhabited by tubeworm bushes exhibited $H_2S$ deletion within the upper 2-3 centimeters and slight increases in $H_2S$ concentrations with depth. While calculated fluxes from *Beggiatoa* cores were similar in 1997 and 1998, fluxes from tubeworm were not detectable (in 11 of 13 cores) in 1998. This difference probably arose because of our effort to reestablish oxygen concentrations in the overlying water in 1998. By aerating the overlying water for 1 hour, we prevented upward migration of the $H_2S$ profiles. Thus, a 'zero' sediment-water interface $H_2S$ flux is probably more representative of cores collected from tubeworm bushes than the "positive" fluxes we calculated in 1997.

However, pore water $H_2S$ concentrations in sediment associated with tubeworm bushes were lower at depths greater than 3 cm in 1998 compared to 1997, suggesting that hydrocarbon seepage rates may have declined between 1997 and 1998. Short-term (annual) variations in seepage rates are difficult to document, but would not be surprising. Since tubeworms are sessile organisms, they must cope with environmental variability. Changes in tubeworm "condition" and in the organic geochemistry of the sediments associated with tubeworm environments may provide more definitive proof of inter-annual variability in hydrocarbon seepage rate. $H_2S$ profiles from tubeworm bushes support the theory that tubeworm roots consume $H_2S$ from sediments (Julian *et al.* 1999a), as the upper sediments consistently exhibit $H_2S$ depletion. Though our microelectrode $H_2S$ profiles only penetrated to 6 cm, additional $H_2S$ measurements to depths of 20 cm confirm an increase in $H_2S$ concentration below the average depth of the root ball (Table A.9.1).

No reduction in pore water $H_2S$ concentration was observed in cores collected from *Beggiatoa* mats in 1998. *Beggiatoa* mats have the ability to exploit their environment by gliding into favorable chemical positions under their own locomotion. These microorganisms may "colonize"

other areas following disturbance via gas or oil ebullition or bottom currents. *Beggiatoa* mats are not found in regions where there is no significant sedimentary $H_2S$ source (e.g., Figure 9.20), suggesting *Beggiatoa* do not proliferate in regions where the $H_2S$ flux is insignificant. This feature explains the apparent insensitivity of these *Beggiatoa* mats to changes in hydrocarbon seepage rates. Rather, *Beggiatoa* are opportunistic and occur only where environmental conditions are optimal.

## 9.5 Conclusion

The observations discussed above can be summarized as follows:

SRR is a strong discriminator. The overall geochemistry of chemosynthetic communities is strongly controlled by the rate and extent of sulfate reduction, and SRR in concert with coupled reactions serves to characterize stations as active versus inactive. Maximum measured sulfate reduction rates are extremely high at certain stations, and are associated with quantitative reduction of sulfate to sulfide. Comparison of the corrected DIC concentrations with sulfate depletion calculations implies methane oxidation. However, this activity is highly focused and localized, and represented only by a minority of the stations visited. The majority of sites appear to have sulfate reduction rates that are typical of the northern Gulf of Mexico.

Elemental distributions reflect sulfate reduction and iron limitation. Consumption of sulfate is balanced by $H_2S$ production, and the extent of reaction reflects local dynamics. Production of bicarbonate during sulfate reduction serves to precipitate $CaCO_3$ – this reaction is detectable both as TIC and by depletion of dissolved calcium. Production of AVS appears to be limited by low quantities of reactive iron. Of the total solid phase sulfide pool, well over 95% is present as pyrite (TRS). Iron limitation gives rise to the very high dissolved sulfide concentrations observed at these stations. Reactive (citrate-dithonite) iron probably varies considerably in reactivity, and substantial "excess" iron apparently remains unsulfidized despite high $H_2S$ concentrations. Constraints imposed by kinetic rate constants suggest that this iron has been available no longer than approximately $10^4$ years, fixing an approximate maximum age for this system.

The depth of sulfate depletion probably reflects a localized balance between activities of near-surface sulfide oxidizers and sulfide reducing bacteria (SRB) at depth. The pattern of sulfate depletion with respect to depth is variable and possibly related to specific habitat. *Beggiatoa* mats, although located over high rates of sulfate reduction, appear to exert strong control on profiles of pore water sulfate, which show only modest depletion. This pattern stands in contrast with profiles observed at GCAT, which may thus reflect both tubeworm and bacterial mat influences. Observations of freely bubbling gas and high methane concentrations, particularly at GCAT2, suggest that organic matter is not limiting, and it is likely that methane fluxes are high enough that even intense activity by SRB brings about little depletion. However, these conditions are strongly localized: methane concentrations are also observed to be highly variable, and the flow of gas from depth may be focused along preferred avenues of escape. Rapid decomposition of shallowly buried methane hydrate could also modify sedimentary structure and introduce methane fluxes that are very high but also transient and short lived.

Brines are localized influences only, appear to be Na-Ca-Cl in composition with a salinity roughly three times seawater, and are depleted in Mg and Sr. Brine fluids lack sulfate and sulfide. Significant sulfate reduction at these sites is thus confined to the shallow, near-surface mixing zone.

Carbon and oxygen stable isotope ratios strongly support the formation of authigenic carbonates, which can frequently quantitatively dominate over carbonates from biogenic sources in the upper water column.

Sulfur stable isotope ratios are consistent with the highly complex biogenic sulfur system present in many of the sediments. This results in considerable variability in their ratios that does not reflect simple relationships to other chemical parameters.

The microelectrode studies demonstrated the difficulties associated with working in sediments where high concentrations of DOC are present and dissolved sulfide concentrations vary by orders of magnitude. The considerable time period between core collection and when the cores became available for study also made precise determinations of interfacial gradients difficult. In spite of these difficulties clearly different patterns of near-interfacial dissolved sulfide were observed in association with different types of benthic biota. Data from 1997 and 1998 support the hypothesis of Julian *et al.* (1999a) that tubeworm roots actively take up $H_2S$ from the sediment contributing to $H_2S$ depletion, particularly within the upper 4 cm. Fluxes from *Beggiatoa* mats were not related to mat coloration. Some data are consistent with the hypothesis that significant changes in gas/hydrocarbon input at a site can change within a year.

# 10.0 Hydrocarbon Geochemistry of Gulf of Mexico Chemosynthetic Communities[*]

## 10.1 Introduction

In an ecological sense, stability connotes the ability of a community to return to a prior condition following perturbation (May 1973). Unique complex chemosynthetic communities were first discovered in the Gulf of Mexico during trawling in areas characterized by sediments containing free hydrocarbon gases, gas hydrates, and bacterially oxidized crude oil rich in toxic aromatic hydrocarbons at water depths in the 600 to 700 meter range (Kennicutt $et$ $al.$ 1985). These low-temperature complex chemosynthetic communities derive energy from reduced carbon, mainly hydrocarbon gases and bacterial $H_2S$. Later research confirmed that a number of complex chemosynthetic communities are spatially associated with hydrocarbon production (Sassen $et$ $al.$ 1993a). Hence, an important issue is whether or not hydrocarbon production in the Gulf of Mexico slope will impact the stability of complex chemosynthetic communities.

It is important to recognize that the impact of seepage on biologic communities in the Gulf of Mexico is not restricted to the present time (i.e., the Holocene). The geologic record of hydrocarbon seepage in the Gulf of Mexico Salt Basin spans tens of millions of years as successive waves of hydrocarbon migration have impacted the sea floor. Salt and faults have served as conduits for vertical migration in the Gulf of Mexico during much of the Tertiary Era, impacting the sediments and fauna immediately above shallow salt domes. One well-documented example is Damon Mound, an exposed salt dome cap rock onshore in Brazoria County, Texas, where seepage of hydrocarbons was active from the Late Oligocene to Early Miocene Epochs, roughly 20 to 30 million years before present.

The geochemical literature on salt dome cap rocks shows that complex biogeochemical processes in the Gulf of Mexico tens of millions of years ago had already assumed the general pattern that we observe today (Sassen 1980; Sassen $et$ $al.$ 1994a). Bacterial activity in sea floor seeps encompasses oxidation of oil and gas to generate $CO_2$. Geologically enormous volumes of authigenic carbonate rock occur as disk-shaped deposits over most shallow oil-productive salt domes that have been drilled in the northern Gulf of Mexico Salt Basin. The authigenic carbonate rock is strongly depleted in $^{13}C$, a clear indication of an origin from bacterial hydrocarbon oxidation (Posey $et$ $al.$ 1987; Prikryl 1990; Sassen 1980). The same can be said for the enormous economic reserves of elemental sulfur in the Gulf of Mexico. There is general agreement that bacterial sulfate reduction to produce $H_2S$, and bacterial oxidation of $H_2S$ to elemental sulfur have been the main factors in formation of the Gulf Coast's reserves of elemental sulfur (Sassen 1980; Sassen $et$ $al.$ 1994a; Sassen $et$ $al.$ 1994b). When we look at the biogeochemical processes that drive the chemosynthetic communities of the present day Gulf of Mexico slope, we see the continuation of a basic biogeochemical pattern over a long span of geologic time.

---

[*] This section was authored by Roger Sassen.

## 10.2 Petroleum source rocks

Understanding the Gulf slope subsurface hydrocarbon system over time and space is necessary to address community stability. A large structural complex formed during the Tertiary Era across much of the Gulf slope by syndepositional loading of an unstable salt substrate, creating temperature conditions within salt withdrawal basins that generate enormous volumes of oil and gas from deeply buried petroleum source rocks (Sassen *et al.* 1999b). Biomarker analysis of oil from the GC185 area, plus numerous unpublished biomarker analyses performed at GERG, is consistent with a single petroleum source rock of varying lithology and maturity. Upper Jurassic source rocks are thought to be the main source of hydrocarbons across much of the upper Gulf slope from Garden Banks (GB) east to southern Mississippi Canyon (Gross *et al.* 1995). Actively moving salt bodies and concomitant faulting are the migration conduits from depth where oil and gas reservoirs occur and to the sea floor upon which chemosynthetic communities are found (Sassen *et al.* 1993a). The main conclusion is that the occurrence of chemosynthetic communities of the Gulf slope is largely related to a single Upper Jurassic hydrocarbon system in which hydrocarbon generation is ongoing or geologically recent. This source rock has probably been generating oil and feeding hydrocarbon seeps since the Miocene Epoch, leading to the assumption that we are looking at a geologically long-term process.

## 10.3 Oil in chemosynthetic communities

Upper Jurassic-sourced oil is found in anomalous amounts in sediments at or near four of our chemosynthetic community sites (GC185, GC234, GC233, GB425). The mean of 108 measurements of oil concentration performed on the four study sites is about 11,778 ppm by sediment weight. The range between individual measurements is large, however, from 6 ppm to 46,834 ppm. This wide range is expected in sediments of hydrocarbon seeps and even within single piston cores of seep sediments. Although oil is normally absent or present in low abundance in most Gulf slope sediments (<10 ppm), three of our sites are clearly anomalous in terms of oil concentration. Differences in concentration of oil between three sites (GC185, GC234, GB425) are not thought to be meaningful. In contrast, our new data and previous studies (Sassen *et al.* 1994b) do not demonstrate that crude oil is as widely distributed in sediments adjacent to the GC233 brine pool site. This, however, could be an artifact of sampling.

$C_{15+}$ chromatography of crude oil from chemosynthetic communities as part of the present and previous studies shows a common pattern of alteration. If in significant concentration, all oils are heavily impacted by bacterial oxidation that did not necessarily occur within surficial sediments of chemosynthetic communities. Bacteria selectively oxidize the *n*-alkanes and isoprenoid hydrocarbons originally present in the oil, eventually leaving only an elevated baseline on chromatograms called the unresolved complex mixture (UCM) (Sassen *et al.* 1994b). The work of Sassen (1980) implies that the lack of a continuous alteration series from altered to unaltered oil shows that the process of bacterial oxidation of oil is either inactive or only active at a low rate. Thus, slow bacterial oxidation of increasingly toxic crude oil could have a minor effect on

driving geomicrobiologic processes but cannot be assumed as a major driving force driving bacterial activity at present in shallow sediments (<20 cm) of our study areas. This uniformly advanced bacterial oxidation of oil was also observed in studies of three of the same localities in previous years (Sassen *et al.* 1993a; Sassen *et al.* 1994b; Sassen *et al.* 1993b). Other areas not part of the present study (i.e., the GC142 mud volcano) show the continuous alteration series in oil samples but such areas are generally not occupied by chemosynthetic communities (Sassen *et al.* 1994a). This bias is inherent to our study based on our choice of sampling sites.

Hydrocarbon gas is concluded to be more effective at driving bacterial processes at all of our study sites (GC185, GC234, GC233, GB425). Molecular and isotopic properties provide abundant evidence of the classic bacterial alteration series of hydrocarbon gases commonly observed in geologic environments, particularly at GC185 and GC234 (Sassen *et al.* 1999a). This bacterial alteration series is observed in subsurface oil reservoirs, (James and Burns 1984; Winters and Williams 1969), in cap rocks of Gulf Coast salt domes (Sassen 1980), and in laboratory simulations (Stahl 1980).

Relatively unaltered thermogenic hydrocarbon gases from the subsurface hydrocarbon system were sampled at the vent sites of GC185 and GC234 as shown in Table 10.1 and 10.2 (Sassen *et al.* 1999a; Sassen *et al.* 1998). These gases resemble the gases from subsurface reservoirs of nearby Jolliet Field on GC184 (Kennicutt *et al.* 1988a). The sites are complex chemosynthetic communities including various species of tubeworms, mussels, clams, and other organisms. The bulk of thermogenic gases and $CO_2$ from the subsurface hydrocarbon system bypass shallow sediments and exit by venting to the water column (Sassen *et al.* 1999a).

An extensive interpretation of the molecular and isotopic properties of vent gases and gas hydrates at the GC185 and GC234 localities of the present study is given by Sassen *et al.* (1999a, 1998). The present report provides additional summary data. We studied $C_1$-$C_5$ hydrocarbon gases using a new analytical procedure for gas chromatography developed at GERG starting in 1994. See Sassen *et al.* (1999a) for analytical details.

We subjected less than 164 samples of gas from sites of chemosynthetic communities to $C_1$-$C_5$ gas chromatography, including gas-hydrate associated samples. The analysis included methane plus thermogenic hydrocarbon gases including ethane, propane, isobutane, normal butane, isopentane, normal pentane, and neopentane. No previous studies have included neopentane, a compound that was not previously known to occur in chemosynthetic communities. In addition, we looked at distinct bacterial hydrocarbon gases including ethylene and propylene.

Background in the Gulf slope of $C_1$-$C_5$ hydrocarbons is low. Methane is generally present in sediments (at concentrations of <10 ppm) but the higher hydrocarbon gases are generally absent or in low abundance (<1 ppm). The concentrations we see in our sample suite from chemosynthetic communities are anomalous, linking hydrocarbon gases to chemosynthetic communities of all sites. The mean total concentration of $C_1$-$C_5$ hydrocarbons from 164 samples is 200,518 ppm. The range is from 4 ppm to 1,047,626 ppm. The wide range is typical of seeps in natural geologic settings.

Table 10.1.  Molecular and isotopic properties of vent gases and gas hydrates.

| Station | Location | Sample | JSL Dive | $\delta^{13}C$ $C_1$ | $\delta D$ $C_1$ | % $C_1$ | $\delta^{13}C$ $C_2$ | % $C_2$ | $\delta^{13}C$ $C_3$ | % $C_3$ | $\delta^{13}C$ $i\text{-}C_4$ | % $i\text{-}C_4$ | $\delta^{13}C$ $n\text{-}C_4$ | % $n\text{-}C_4$ | $\delta^{13}C$ $i\text{-}C_5$ | % $i\text{-}C_5$ | $\delta^{13}C$ $n\text{-}C_5$ | % $n\text{-}C_5$ | $\delta^{13}C$ $CO_2$ |
|---|---|---|---|---|---|---|---|---|---|---|---|---|---|---|---|---|---|---|---|
| BHHYD-1 | GC185 | Vent Gas* | 2874 | -46.0 | -198 | 95.9 | -29.7 | 2.4 | -25.0 | 1.2 | | <0.1 | -22.6 | 0.3 | -26.1 | 0.2 | | <0.1 | -4.9 |
| BHHYD-1 | GC185 | Vent Gas* | 2875 | -44.1 | -200 | 90.4 | -30.2 | 4.5 | -26.3 | 3.7 | -27.9 | 0.6 | -23.3 | 0.6 | -26.1 | 0.2 | | <0.1 | -5.4 |
| BHHYD-1 | GC185 | Gas Hydrate* | 2892 | -42.9 | -163 | 83.1 | -28.6 | 7.6 | -24.9 | 8.1 | -27.2 | 0.9 | -22.1 | 0.2 | | 0.0 | | 0.0 | -27.8 |
| BHHYD-1 | GC185 | Gas Hydrate* | 2637 | -42.2 | -190 | 71.7 | -29.0 | 10.6 | -25.5 | 12.6 | -27.6 | 2.6 | -22.8 | 1.7 | -26.2 | 0.8 | | 0.0 | -20.0 |
| BHHYD-1 | GC185 | Gas Hydrate* | 2637 | -43.5 | -177 | 80.2 | -29.7 | 9.4 | -25.5 | 7.3 | -27.9 | 1.6 | -23.0 | 1.2 | -24.8 | 0.3 | | 0.0 | -23.7 |
| BHHYD-1 | GC185 | Gas Hydrate* | 2637 | -42.5 | -193 | 72.1 | -29.2 | 12.4 | -25.7 | 11.4 | -27.8 | 2.3 | -22.7 | 1.6 | -24.7 | 0.3 | | 0.0 | -21.6 |
| BHHYD-2 | GC185 | Gas Hydrate | 2891 | -42.9 | -115 | 85.7 | -28.6 | 6.3 | -25.6 | 6.1 | -26.8 | 1.1 | | 0.8 | | 0.0 | | 0.0 | |
| GCHYD-1 | GC234 | Vent Gas | 2881 | -48.7 | -203 | 93.7 | -29.2 | 2.4 | -26.4 | 2.4 | -27.9 | 0.5 | -25.2 | 0.6 | -26.5 | 0.2 | -25.0 | 0.1 | +2.9 |
| GCHYD-1 | GC234 | Gas Hydrate | 2881 | -48.4 | -203 | 73.8 | -29.4 | 12.6 | -26.4 | 9.9 | -28.4 | 1.6 | -24.9 | 1.8 | | 0.2 | | 0.1 | |
| BPRN-1 | GC233 | Vent Gas | 2876 | -64.3 | -165 | 97.8 | | 0.1 | | 2.1 | | 0.0 | | 0.0 | | 0.0 | | 0.0 | -25.3 |
| BPRN-1 | GC233 | Vent Gas | 2860 | -65.5 | -200 | 97.4 | | 0.1 | | 2.5 | | 0.0 | | 0.0 | | 0.0 | | 0.0 | |

* Data from Sassen *et al.* (1998)

Table 10.2.  Molecular and isotopic properties of hydrocarbons and carbon dioxide in selected sediment samples.

| Station | Location | Sample | JSL Dive | $C_1\text{-}C_5$ ppm | $\delta^{13}C$ $C_1$ | $\delta D$ $C_1$ | % $C_1$ | $\delta^{13}C$ $C_2$ | % $C_2$ | $\delta^{13}C$ $C_3$ | % $C_3$ | $\delta^{13}C$ $i\text{-}C_4$ | % $i\text{-}C_4$ | $\delta^{13}C$ $n\text{-}C_4$ | % $n\text{-}C_4$ | $\delta^{13}C$ $i\text{-}C_5$ | % $i\text{-}C_5$ | $\delta^{13}C$ $n\text{-}C_5$ | % $n\text{-}C_5$ | $\delta^{13}C$ $CO_2$ |
|---|---|---|---|---|---|---|---|---|---|---|---|---|---|---|---|---|---|---|---|---|
| BHHYD-1 | GC185 | Sediment* | 2637 | 241,808 | -45.4 | -140 | 61.0 | -29.5 | 16.4 | -24.7 | 13.7 | -28.5 | 3.3 | -21.5 | 3.7 | -24.9 | 1.9 | | 0.0 | -17.5 |
| BHHYD-1 | GC185 | Sediment* | 2641 | 88,687 | -42.4 | -134 | 57.1 | -28.8 | 30.7 | -20.3 | 2.4 | -31.0 | 0.7 | -19.6 | 3.4 | -25.3 | 5.7 | | 0.0 | -21.8 |
| BHHYD-1 | GC185 | Sediment* | 2641 | 107,902 | -42.3 | -158 | 61.5 | -29.6 | 25.4 | -20.5 | 5.6 | -28.5 | 5.8 | -20.4 | 0.6 | -21.3 | 1.1 | | 0.0 | -18.2 |
| BHHYD-1 | GC185 | Sediment* | 2651 | 225,079 | -51.0 | -136 | 71.5 | -29.3 | 17.4 | -22.9 | 4.6 | -28.4 | 1.1 | -20.6 | 1.6 | -18.1 | 0.3 | | 0.0 | -19.7 |
| BHST-2 | GC185 | Sediment** | 2875 | 137,631 | -41.6 | -125 | 90.8 | -24.7 | 9.2 | | 0.0 | | 0.0 | | 0.0 | | 0.0 | | 0.0 | -27.3 |
| GCHYD-1 | GC234 | Sediment* | 2881 | 138,864 | -49.3 | -121 | 60.5 | -26.7 | 24.5 | -22.1 | 5.7 | -27.8 | 2.7 | -19.8 | 3.1 | -23.7 | 3.5 | | 0.0 | -28.3 |
| GCAT-2 | GC234 | Sediment** | 2886 | 75,249 | -53.1 | -125 | 85.2 | -27.7 | 1.4 | -19.3 | 0.9 | -28.3 | 1.8 | -21.9 | 2.9 | -22.4 | 7.3 | | 0.5 | -28.0 |
| GCAT-2 | GC234 | Sediment** | 2886 | 46,530 | -53.9 | -119 | 80.8 | -27.2 | 1.3 | -20.5 | 0.7 | -28.2 | 1.8 | -22.4 | 1.0 | -25.2 | 13.4 | -22.4 | 1.0 | -29.4 |
| GCAT-2 | GC234 | Sediment** | 2886 | 12,960 | -54.2 | -104 | 73.3 | | 1.4 | | 0.6 | -26.5 | 2.0 | -22.8 | 3.5 | -25.1 | 13.8 | -23.3 | 1.4 | -34.4 |

*Hydrate mound  ** Tubeworm

There are some similarities between sites that contain abundant tubeworms and mussels, sites GC185 and GC234 (e.g. Figure 10.1). These sites also contain abundant gas hydrates impacting the geochemistry of hydrocarbon gases. Figure 10.2 shows results of $C_1$-$C_5$ hydrocarbon gases from 23 samples associated with tubeworms at GC185 (mean = 38,408 ppm). Methane is the single most abundant light hydrocarbon, at concentrations up to 666,642 ppm (mean = 36,538 ppm). Sassen *et al*. (1999a) used carbon and hydrogen isotopes to show that methane in GC185 sediments is a complex mixture of both thermogenic and bacterial methane that has been subjected to intense bacterial oxidation. Hydrogen isotopes are diagnostic in this regard (Sassen *et al*. 1994b). Ethane (mean = 1603 ppm), propane (mean = 0.5 ppm), isobutane (mean = 18.4 ppm), normal butane (mean = 90.2 ppm), isopentane (mean = 76.9 ppm), normal pentane (mean = 3.8 ppm), and neopentane (0.4 ppm) are present. Carbon isotopes suggest that bacteria show some preference for oxidation of straight-chain compounds such as propane, normal butane, and normal pentane. Ethylene and propane are very minor components (means = <1 ppm).
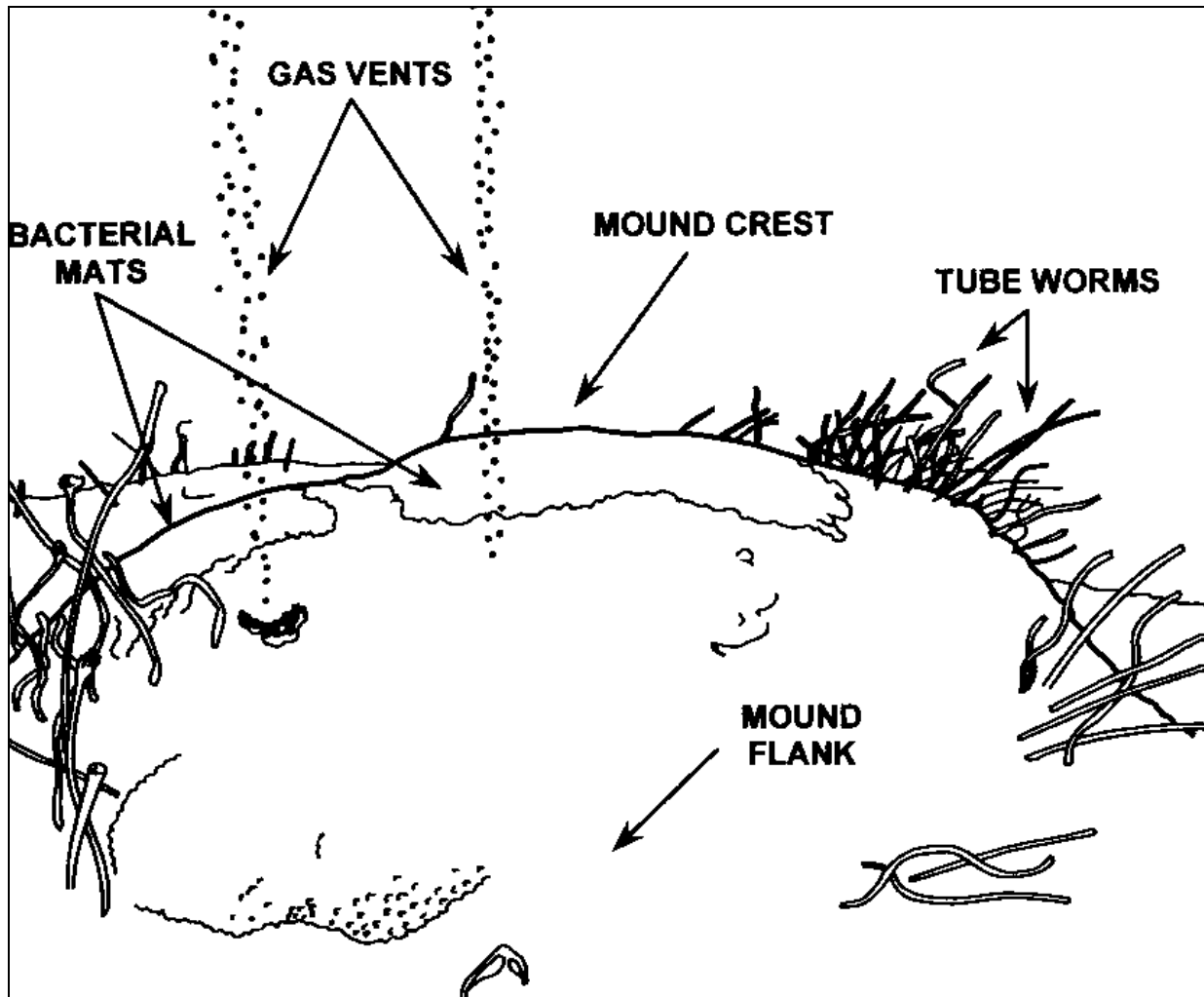


Figure 10.1   Sketch of typical gas hydrate mound (~1-3 m across) modeled after the Bush Hill site including sampling stations BHHYD-1 (gas hydrate and mound sediment cover) and BHST-2 (nearby tube worm sediments).  From photograph in Sassen *et al*. (1998).

**A**

**Carbon and Hydrogen Isotopes**

$\delta^{13} C \ (\delta D^*) \ ^0/_{00}$

Sediments
Tube Worm ●
Hydrate Mound ▲

25
-25
-75
-125
-175
-225

*$C_1$   $C_1$   $C_2$   $C_3$   i-$C_4$   n-$C_4$   i-$C_5$   n-

**B**

**Molecular Compositions**

Normalized $C_1$ to $C_5$

100%
75%
50%
25%
0%

$C_1$   $C_2$   $C_3$   i-$C_4$   n-$C_4$   i-$C_5$   n-$C_5$

Figure 10.2. Diagrams summarizing isotopic (A) and molecular (B) properties of sediments overlying gas hydrate mounds and from near tube worm colonies at GC133 (BHST-2) and GC234 (GCAT-2) sampling stations.

$C_1$-$C_5$ hydrocarbon gases from 21 samples associated with tubeworms at GC234 (mean = 21,906 ppm) were analyzed. Methane is the single most abundant light hydrocarbon, at concentrations up to 94,030 ppm (mean = 18,557 ppm). Carbon and hydrogen isotopes show the methane in GC185 sediments is a complex mixture of both thermogenic and bacterial methane that has been subjected to intense bacterial oxidation (Sassen *et al.* 1999a). Ethane (mean = 326 ppm), propane (mean = 155.6 ppm), isobutane (mean = 332 ppm), normal butane (mean = 551 ppm), isopentane (mean = 1665 ppm), normal pentane (mean = 211 ppm), and neopentane (12.1 ppm) are present. Carbon isotopes suggest that bacteria show some preference for oxidation of straight-chain compounds such as propane, normal butane, and normal pentane. Possibly because of its molecular structure, causing its exclusion during gas hydrate crystallization, the branched-chain isopentane molecule appears to be preferentially preserved in some sediment samples. Ethylene and propane are very minor components (means = <1 ppm).

$C_1$-$C_5$ hydrocarbon gases from six samples associated with mussels at GC185 (mean = 341,593 ppm) were analyzed. Methane is the single most abundant light hydrocarbon, at concentrations up to 885,790 ppm (mean = 296,791 ppm). Ethane is in significant abundance (mean = 23338 ppm), along with propane (mean = 6945 ppm), isobutane (mean = 2498 ppm), normal butane (mean = 1389 ppm), isopentane (mean = 10,542 ppm), normal pentane (mean = 29 ppm), and neopentane (12.1 ppm). Carbon isotopes suggest that bacteria show some preference for oxidation of straight-chain compounds such a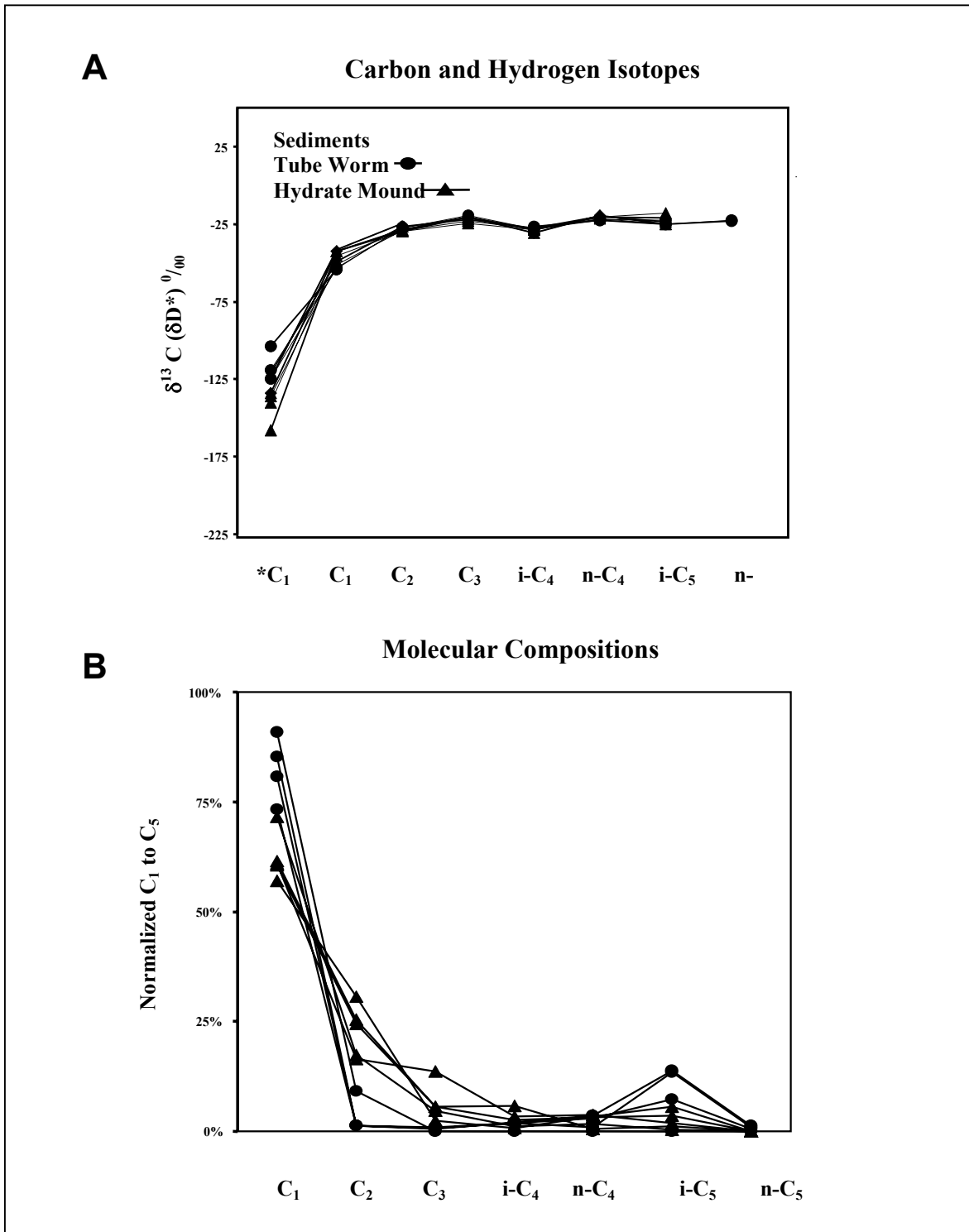s propane, normal butane, and normal pentane (Sassen *et al.* 1999a), but bacteria do not heavily oxidize these gases. Possibly because of its molecular structure, causing its exclusion during gas hydrate crystallization, the branched-chain isopentane molecule appears to be preferentially preserved in some sediment samples. Ethylene and propane are very minor components (means = <1 ppm). Only one sample of sediment from a mussel site at GC234 was obtained during sampling and analyzed.

The tubeworms at GC185 and GC234 are associated with abundant gas hydrate masses and share a geochemical environment in sediments with high concentrations of $C_1$-$C_5$ hydrocarbon gases that are heavily altered by bacterial oxidation. Bacterial hydrocarbon oxidation is geochemically associated with bacterial sulfate reduction. The hydrocarbon gases at tubeworm sites show evidence of being involved in progressive gas hydrate crystallization. The relative abundance of isopentane as a free gas, which is excluded during crystallization of gas hydrate, serves as a marker for the gas hydrate crystallization process. In contrast, the concentrations of $C_1$-$C_5$ hydrocarbon gases at GC234 mussel sites are about an order of magnitude higher than at tubeworm sites and consequently higher concentrations of less altered hydrocarbons are present. Mussel sites in complex chemosynthetic communities are interpreted to be directly associated with high-flux vent sites. Video records of mussel sites at complex communities could show a relation to visible gas bubble trains in the water column.

## 10.4 Gas Hydrates

Vent gas undergoes a rapid phase change under ambient temperature and pressure and crystallizes as abundant solid gas hydrate at the GC185 and GC234 localities. Conclusions cannot be extended to all chemosynthetic communities but, where present in abundance, gas

hydrates can have a profound localized effect on diverse bacterially mediated geochemical processes in complex chemosynthetic communities dependent on hydrocarbon gases and $H_2S$ (Sassen *et al.* 1999a). Gas hydrates occur physically as vein-fillings in hemipelagic muds near gas vents and are surrounded by chemosynthetic organisms such as tubeworms at GC185.

Molecular and isotopic properties of the gas hydrate forming $C_1$-$C_5$ hydrocarbons and $CO_2$ provide key insight to bacterially mediated processes (Figure 10.3). Hydrate-bound methane is altered by bacterial oxidation at GC185, as indicated by enrichment of $^{13}C$ and deuterium (D) and by hydrate-bound $CO_2$ depleted in $^{13}C$ (Sassen *et al.* 1998). Results suggest that the degree of gas hydrate alteration is related to duration of exposure of gas hydrate at the sea floor (Sassen *et al.* 1999a). On this basis, we speculated that gas hydrates could play a role in initiation and development of complex chemosynthetic communities and in the presence of abundant tubeworms.

## 10.5 Hydrocarbon Oxidation Rates

The rate of hydrocarbon gas oxidation is high in the sediments associated with gas hydrates at GC185 and GC234. In sediments associated with gas hydrates, bacterial oxidation of a mixed pool of $C_1$-$C_5$ hydrocarbon gases yields a net production of $CO_2$ highly depleted in $^{13}C$ (Sassen *et al.* 1999a, Table 2). The bacterial oxidation rate is assumed to be rapid based on molecular and isotopic evidence, suggesting concomitant bacterial sulfate reduction and precipitation of authigenic carbonate in sediments are also rapid. The rate of bacterial oxidation is such that it could destabilize gas hydrates by removing the free hydrocarbon gases necessary to maintain their stability (Sassen *et al.* 1999a).

Sediments at both GC185 and GC234 often contain methane depleted in $^{13}C$ relative to both thermogenic vent gases and gas hydrates (Sassen *et al.* 1999a). This is strong geochemical evidence that thermogenic carbon in sediments (i.e., mainly gaseous *n*-alkanes) can be recycled via methanogenesis to yield a net production of bacterial methane depleted in $^{13}C$ at chemosynthetic communities (Sassen *et al.* 1999a). This observation has significance to life in extreme environments (Sassen *et al.* 1999a) and also to the geochemistry of the dominant hydrocarbon gas at our other study sites (GC233 and GB425).

# A

## Carbon and Hydrogen Isotopes

$\delta^{13}$ C ($\delta$D*) $^0/_{00}$

25

-25

-75

-125

-175

-225

*$C_1$   $C_1$   $C_2$   $C_3$   i-$C_4$   n-$C_4$   i-$C_5$   n-$C_5$

# B

## Molecular Compositions

Normalized $C_1$ to $C_5$

100%

75%

50%

25%

0%

$C_1$   $C_2$   $C_3$   i-$C_4$   n-$C_4$   i-$C_5$   n-$C_5$
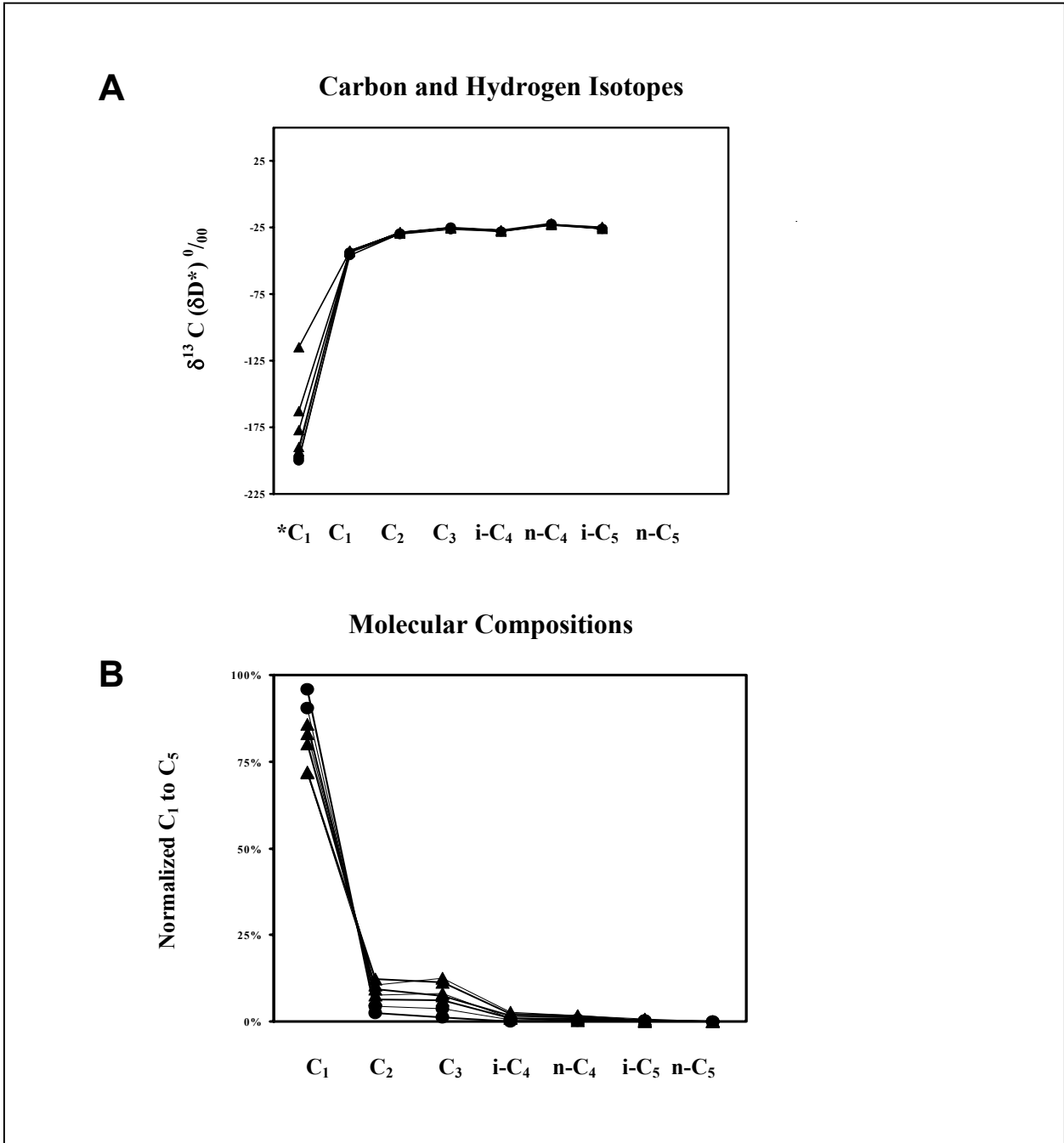
Figure 10.3. Diagrams summarizing isotopic (A) and molecular (B) properties of vent gas and gas hydrate samples at the BHHYD-1 and -2 sample stations, GC133.

## 10.6 Brine Pools

The origin of flowing methane at brine pools at GB425 and GC233 provides a key example of bacterial recycling of thermogenic carbon. Measurements of both $\delta^{13}C$ and $\delta D$ unambiguously identify thermogenic methane and bacterial methane of varying origin (Coleman *et al.* 1996). Isotopic properties identify the volumetrically significant methane at brine pool sites as mainly from reduction of $CO_2$ via bacterial methanogenesis (Sassen *et al.* 1999a and references therein).

The molecular geochemistry of $C_1$-$C_5$ hydrocarbons at the GC233 and GB425 brine pool sites is surprisingly similar. No intact gas hydrate has been recovered and analyzed from either site. We conclude that gas hydrates are probably less abundant at these sites because of gas composition (dominantly methane) and suppression of gas hydrate crystallization by high salinity.

The gas at both sites is typically less than 99% methane. We analyzed 30 samples from the GC233 site for $C_1$-$C_5$ hydrocarbons. Concentration of bacterial methane at GC233 is as much as 999,515 ppm (mean = 422,374 ppm). We analyzed 14 samples from the GB425 site. At GB425, concentration of bacterial methane is as much as 940,402 ppm (mean = 125,662 ppm). Ethane and other higher hydrocarbon gases in the carbon number range we studied are relatively minor components. These mussels are associated with high flux bacterial methane, and the same could be said of mussel sites studied at GC234. There, as noted above, the methane is more thermogenic in origin. The mussels appear to be adventitious to high flux methane vents and brine pools.

The main source of $CO_2$ at the brine pool sites is assumed to be bacterial oxidation of thermogenic hydrocarbons (gas and oil), reinforcing the relationship of the Upper Jurassic source system even to some simple chemosynthetic communities of mussels on the Gulf slope. The $\delta^{13}C$ and $\delta D$ values of some methane from adjacent sediments are consistent with the atypically high rates of bacterial oxidation, suggesting that concomitant bacterial sulfate reduction rates are also high, tending to increase alkalinity and to drive precipitation of abundant authigenic carbonate rock.

## 10.7 Biogeochemical Synthesis

The hydrocarbon geochemist looks at starting and ending products of chemical reactions in a natural environment; the task is then to infer the reactions most likely to explain complex observations (Sassen 1980). The biogeochemical cycles at chemosynthetic communities are not unique. Instead, they appear to be similar to those long observed in salt dome cap rocks of the Gulf Coast. However, this study leads to an improvement of the old models, as summarized in Figure 10.4. Hydrocarbons are oxidized to bicarbonate or $CO_2$, and some oxidized carbon precipitates as authigenic carbonate rock. Sassen (1980) suggested that this net accumulation of authigenic carbonate rock is a perturbation in the carbon cycle. However, the present work diminishes that emphasis because much thermogenic carbon (gas and oil) is apparently cycled to bacterial methane via $CO_2$ reduction. This also explains the common observation of bacterially altered oil and gas from subsurface reservoirs in association with bacterial methane (James and Burns 1984). The sulfur cycle appears to involve bacterial sulfate reduction, $H_2S$ oxidation, accumulation of elemental sulfur, and then bacterial oxidation back to sulfate (Figure 10.4).
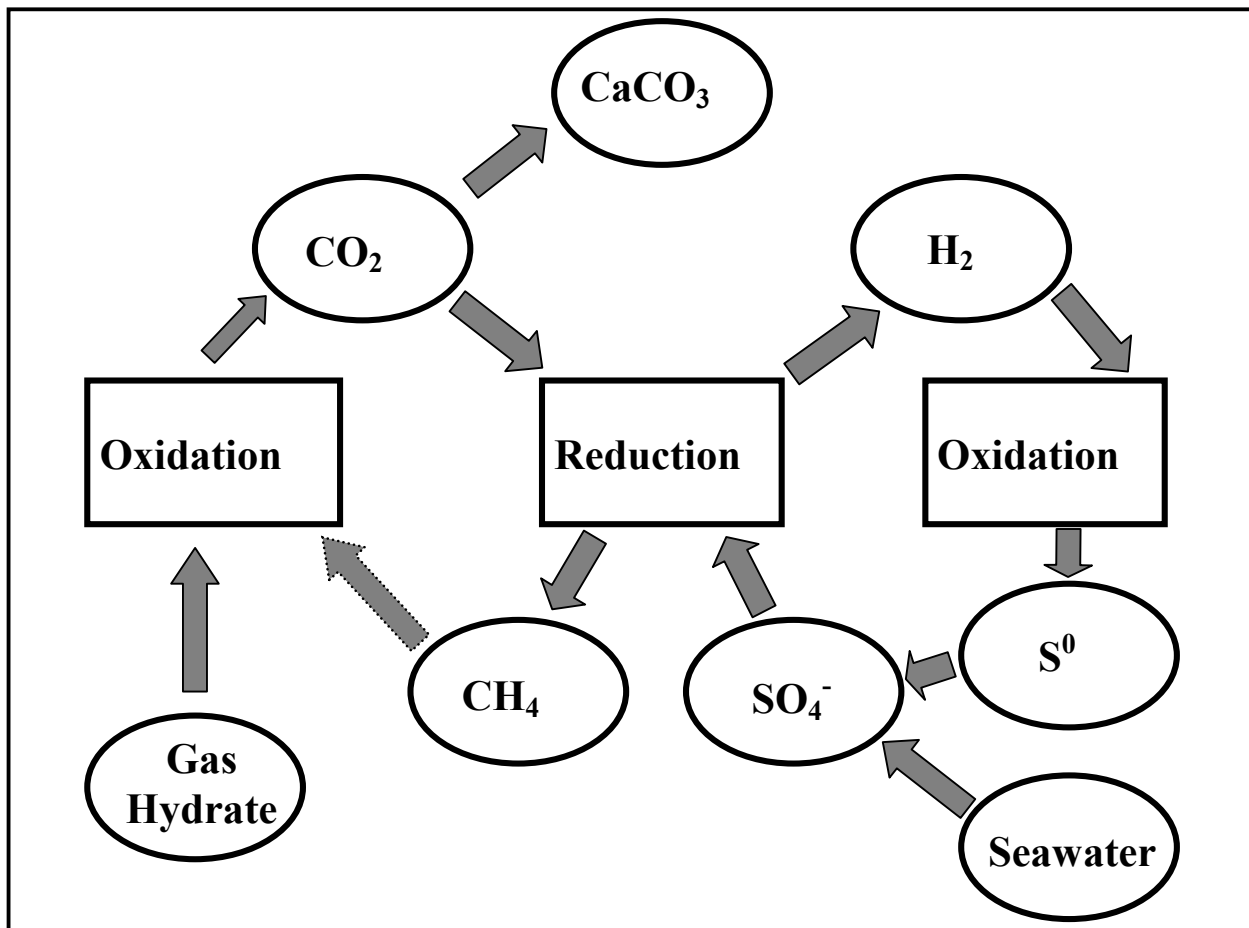
Figure 10. 4. Geochemical overview of the gas hydrate environment.

## 10.8 Conclusions

All study sites share the presence of hydrocarbons that drive multiple bacterial processes including bacterial hydrocarbon oxidation to produce $CO_2$, sulfate reduction to produce $H_2S$, and methanogenesis to produce methane, fueling the chemosynthetic communities. However, gas hydrocarbon geochemistry differs.

GC185 and GC234 represent active seep environments with ongoing charge of thermogenic gas at obvious vent sites related to deep subsurface reservoirs. Thermogenic gas hydrates are present in abundance and impact sediment geochemistry. Thermogenic hydrocarbon gas is bacterially oxidized. Bacterial gas oxidation promotes bacterial sulfate reduction and concomitant precipitation of authigenic carbonate rock. GC185 and GC234 host complex communities where tubeworms are important elements. Mussel sites within complex communities are associated with very localized high-flux methane-rich thermogenic gas.

In contrast, at the GC233 and GB425 sites, the main hydrocarbon gas is bacterial methane, and thermogenic hydrocarbon gases are minor constituents. The bacterial methane is speculated to be

the result of recycling of thermogenic hydrocarbons (gas and oil) largely destroyed by bacterial activity in the past. Mussels dominate at the GC233 and GB425 sites. It could be argued that mussels are adventitious and merely prefer high-flux vents and brine pools where methane is abundant. Origin of methane (i.e., bacterial versus thermogenic) is not a preference. Geologically, the brine pool sites at GC233 and GB425 might appear to be more active than the GC185 and GC234 sites. However, geochemically, thermogenic hydrocarbon charge to GC233 and GB425 occurred in the geologic past, and the GC185 and GC234 sites are more active receiving thermogenic gas at present.

Given the prolific volumetrics of the Upper Jurassic source system, hydrocarbon charge to migration conduits can be expected to continue on a scale of millions of years. Oil and gas production is unlikely to significantly affect overall flow of hydrocarbons to the sea floor or the stability of communities.

# 11.0 Synthesis of Results and Recommendations for Future Study

## 11.1 Introduction

The program obtained results from an extensive program of field collections and laboratory analyses. Under the direction of the Geochemical and Environmental Research Group of Texas A&M University, sixteen investigators, associates, and students from seven separate institutions collaborated to formulate and carry out the work. During the course of two ambitious field seasons, program investigators collected samples from over fifty stations, which were distributed among four principal sampling sites with use of the submarine Johnson SEA-LINK. Extensive additional collections were made with use of the R/V GYRE and the US Navy Submarine NR-1. The primary geochemical samples included more than fifty sediment cores, which were extensively sub-sampled by sediment depth. Extensive collections of chemosynthetic and heterotrophic animals were obtained for investigations to determine, among other objectives, growth rates, health, genetic diversity, and food-web structure. A regional context for the targeted sampling was established through geophysical survey, sediment coring, and layered comparisons between community and regional-scale data with use of geographic information system (GIS) tools. Valuable time-series records of current, water temperature, and fluid discharge properties of the seep environment were obtained from targeted deployments of in-situ instruments and moorings. Satellite remote sensing records were obtained through cooperation with industry to examine large-scale variation in seepage rates. This section reiterates the study objectives as specified by the Mineral Management Service's Request for Proposal and outline how they were addressed by the separate work efforts that were completed during the program. It concludes by synthesizing major finding as descriptive models for geochemical and ecological processes at Gulf of Mexico hydrocarbon seeps and outlining knowledge gaps for future study.

## 11.2 Objectives and Basic Study Design

The request for proposal that initiated this program specified the following objectives for study (taken *verbatim* from solicitation number 3813):

Review biotic and a biotic features of existing conceptual models of chemosynthetic communities which explain observed patterns of distribution and abundance, in order to develop an effective, refined plan for continued research.

Further evaluate the physical-chemical factors (e.g., depth, temperature, water chemistry, sediment types, and dissolved gasses) which influence, limit, enhance, or control the distribution, abundance, and growth of chemosynthetic communities.

Further investigate the sources (e.g., deep versus shallow or petrogenic versus biogenic) of any necessary dissolved gasses and the likelihood that petroleum production may ultimately deprive the animals of an energy source.

Further determine if chemosynthetic communities are robust or fragile, and whether they are essentially permanent or ephemeral; characterize age, growth rate, turnover rates, reproduction and recruitment, and patterns of senescence and death in the dominant chemosynthetic animals;

further examine recovery rates of communities damaged by physical disturbance.

Further determine the reliability of methods for detecting chemosynthetic communities using remote acoustic and/or geophysical devices, imaging instrumentation, hydrocarbon measurements, and/or other available technologies.

To address Objective One, a thorough review of published literature and reports was completed. Two principal conclusions were reached. First, it was evident that the chemosynthetic fauna from Gulf of Mexico hydrocarbon seeps (tubeworms and mussels) were taxonomically and functionally similar what is found at hydrothermal vents at mid-ocean ridges, but included important differences. They are all dependent on symbiosis with bacteria that can utilize chemical energy. Tubeworms in both settings use hydrogen sulfide ($H_2S$) to nourish their symbionts. Seep mussels have symbionts that can oxidize methane ($CH_4$) from natural gas, while vent mussels rely only on $H_2S$. However, communities at hydrothermal vents are attached a rocky substratum; they obtain needed $H_2S$ directly from vent fluids and are frequently disturbed by volcanic eruptions and other catastrophic events. Vent communities are often separated from each other by hundreds of miles of inhospitable habitat. Seep communities thrive on soft marine sediments where elemental cycling by microbial and chemical processes strongly influence the environment. Importantly, the $H_2S$ is produced by microbial consumption of seep organics—i.e. oil and gas. Many seeps appear to be stable features, in which colonies can persist for decades or longer without major natural disruptions. Seep also appear to be much more numerous and widespread than vents within comparable seafloor areas. This means that there is more opportunity for interaction between neighboring seeps (e.g. exchange of recruits) and a greater scope for non-seep fauna to utilize the productivity of seep animals as a food supply. It was concluded that new conceptual models of colonization, persistence, and interaction would have to be developed to describe seep chemosynthetic communities.

The second finding of the review and study design process was that two styles of seepage have been described at Gulf of Mexico hydrocarbon seeps and contribute to habitat formation. In *sediment diffusion* habitats, mussels, clams, and tubeworms utilize reduced compounds – $CH_4$ and $H_2S$ – by extending body parts into the sediment or by bathing their brachia (gills or plumes) in the steep gradients immediately above the sediment/water interface. *Brine pooling* habitats are found where concentrated brines are associated with petroleum migration and seepage. Because brines are much denser than sea water brine discharge can form distinct pools on the seafloor. The brines contain high concentrations of $CH_4$, which supports dense beds of mussel and associated species. The study hypothesizes that much of the community-level diversity in cold seep communities can be explained by examining the environmental consequences of these two styles of seepage. Although there was a clear interest in exploring the Gulf of Mexico slope for new communities, this was balanced against the need for intense sampling to answer process questions. The program proceeded with four representative sampling sites for process studies and the shallow and deep mega-sites for studies of regional distribution and remote sensing investigations.

## 11.3 Physical Factors and the Distribution and Abundance of Chemosynthetic Communities

Two factors in the physical oceanography of the Gulf of Mexico slope have the potential to

control the distribution and abundance of chemosynthetic communities: the temperature range at depths where the communities occur and the water circulation patterns that disperse larvae among communities or potential communities.

Temperature tolerances of the dominant tubeworms and mussels are relatively narrow. As noted in Chapter 4, collections made for the physiology and growth experiments during the program made use of an insulated container to preserve living specimens at near *in-situ* temperatures. Observations of seep mussels under laboratory conditions show that exposure to temperatures over 10° C was sufficient to cause mussels to slough their symbionts (Fisher, 1990). The mean temperature recorded at 550m by the thermistor deployed at GC185 was 7.2° C, with occasional excursions approaching a maximum temperature of 9° C. The historic record, reproduced from thermistor deployments made prior to this program, indicates that temperature spikes as high as 11° C are a regular occurrence at these localities on the Gulf slope. At no time, however, were temperatures above 9° C sustained for more than a few hours. From this information, one can infer that temperature stresses are a routine component of the seep mussel's habitat in this depth range. Although systematic comparisons are lacking, there is general agreement that the upper depth limit for chemosynthetic communities in the Gulf of Mexico seems to occur between 400 m and 500 m. This upper limit corresponds to the approximate isotherm above which sustained exposures (days rather than hours?) to temperature >10° C will occur. Seep mussel aggregations at lesser depths would have to endure regular episodes of temperatures that would produce extreme stress in laboratory populations.

The case for a depth-temperature limit in the range of vestimentiferan tubeworms is less straight–forward than for the mussels, but available information on behavior of larvae from seep vestimentiferans does indicate a mechanism that would affect this life stage. Observations of seep vestimentiferans spawned under laboratory conditions Young et al. (1996) showed that the larvae will swim or float upward in the water column for approximately eight days prior to settlement. Larvae spawned at shallower depths might therefore be carried into warm surface waters where temperature would be stressful. What is the upward rate of motion and how far up in the water column could a larva get in 8 days from 500 m? This mechanism would not preclude colonization from tubeworm populations that were established at greater depths, but could limit the genetic viability of populations on the upper slope.

Regardless of how the mechanism of temperature effect plays out to limit or enhance chemosynthetic community viability, temperature fluctuations are correlated with circulation events, which in turn have the potential to affect larval transport between communities. Current meter records from GC185 indicate a weak but non-random positive correlation (statistics?) between the magnitude of temperature change over time (*dT/dt*) and the strength of currents (Figure 11.1). During the deployment, most of this movement (which movement?) was in a northerly (*v*) direction. Ecologically, the implication is that temperature stress indicates increased current speed.

Many invertebrates, including seep fauna, respond to temperature spikes by spawning (C. Young, personnel communication). One can conjecture that rapid change in water temperature is sensed by seep mussels and tubeworms. Gametes released in response to this signal be advected away from the immediate vicinity of the seep community and could potentially colonize new sites or provide migrants to other communities.
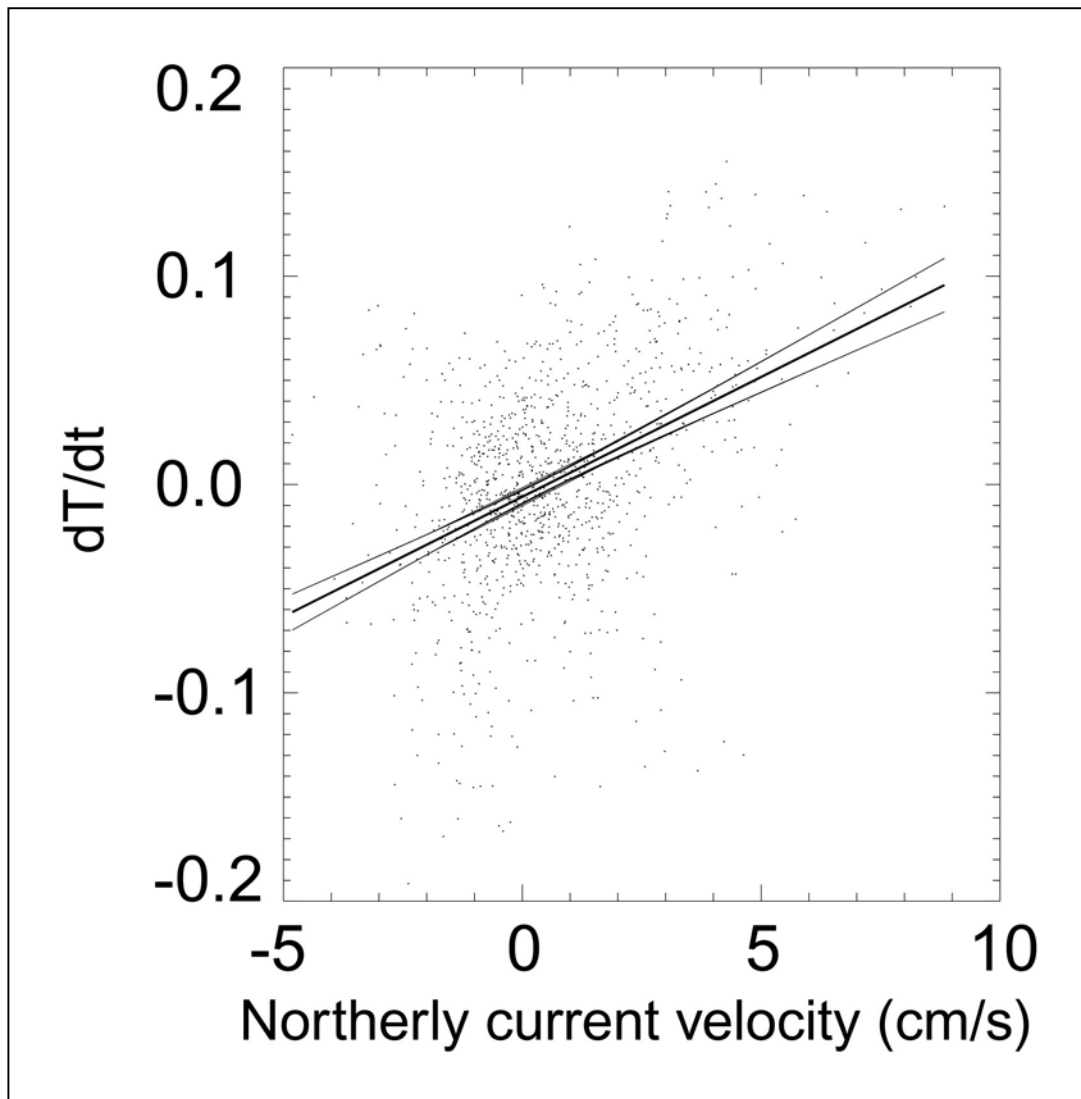
Figure 11.1   Plot of the rate of change of bottom water temperature (dT/dt) versus the northerly component of the current velocity shows a weak, but non-random correlation ($R^2 = 0.17$).

Results from the DNA fingerprinting of seep mussels and tubeworms clearly show that larval exchange among sites takes place with sufficient frequency to maintain gene pools for seep mussels (*Bathymodiolus childressi*) and two species of tubeworms (Escarpid and *Lamellibrachia sp.*) that are integrated among the four study sites (see Section 8.7). There is no evidence that any populations of these species are isolated from the others to the extent that divergence would occur at the species level. The metric of genetic exchange is the number of migrants per generation exchanged between pairs of populations (Tables 8.7.7, 8.7.8, and 8.7.9). The higher the rate of exchange, in theory, the greater the larval transport between sites. Comparing genetic exchange with distance between sites (Figure 3.1), it is apparent that physical separation does not act to limit exchange over the distance scales that separate chemosynthetic communities. This pattern is consistent with a mechanism in which larvae that migrate to the upper layers of the water column are transported over greater distance due to the more energetic water movement in these strata. The ability of larvae to survive transport and remain viable will also be limited by temperature-induced stresses.

## 11.4 Regional and Local Geophysical Signatures of Chemosynthetic Communities

Classification systems proposed by Reilly et al. (1996) and Roberts and Carney (1997) as a means of locating chemosynthetic communities from remotely sensed data sets were reviewed at the mega-site and local scales during the course of the program. Comparison of known chemosynthetic organism sites with side-scan sonar and other data types highlights the difficulty in attempting to find a diagnostic geophysical signature that will identify inhabited seep sites. Several localities in the data are characterized by large, focused-flow fluid discharges—also called mud volcanoes. The data from mud volcanoes (i.e. the GB425 site, the Bush Lite site located in the southern half of GC185, and the TAMU-6 and TAMU-17 sites discovered in lease blocks GC191 and GC233) indicate extensive and recent discharges of mud, which are evident as flow patterns on the edges of mounds. The GB185 study site, continuously vents oil and gas, but shows no evidence of recent sediment expulsion. In contrast, the GC234 and GC233 sites are seeps that support significant chemosynthetic communities, but are not evident (resolvable) in either the side-scan sonar or multi-channel seismic data. Both occur in areas of high acoustic backscatter, but the locations of the chemosynthetic communities do not stand out against the complex anomalies located along fault zones in the vicinity.

Several different types of mound character have been noted in the geophysical data. The side-scan sonar data show three types: 1) nearly homogeneous high backscatter, 2) high-backscatter center with a halo of lesser backscatter ("bulls-eye"), and 3) high backscatter with a "dead spot" from which the sonar receives no return ("dead-eye"). The GC185 study site is an example of type 1, and this appears to be a result of a mound charged with gas and gas hydrate but without an obvious fluid expulsion vent. Bulls-eye mounds (type 2) are characterized in chirp sonar surveys by a central hard-bottom, surrounded by a region of acoustic wipeout likely caused by gas charged sediments. These mounds were not inhabited by chemosynthetic organisms and appeared to be senescent or dormant. Dead-eye mounds (type 3) were all highly active mud volcanoes with brine pools or brine vents. We speculate that the central dead spots are caused by specular reflection of the sonar signal away from the sonar (i.e., no backscatter) or nearly complete absorption of the sonar signal by an extremely gas- charged, sediment/fluid slurry in

the vent region.

MCS data shows that seafloor amplitude anomalies associated with known chemosynthetic sites and mounds are variable. The GC185 site has a negative reflection coefficient, implying a reduction of seismic velocity within the mound and a reversal of the signal polarity, probably as a result of gas-charged sediments. In contrast, the Garden Banks 425 mound shows a ring of slightly greater reflection around the mound perimeter, with the mound center showing no anomaly. This type of perimeter signature was noted on several other mounds. The TAMU-17 mound, a highly active mud volcano with abundant tubeworm clusters, displays a positive amplitude anomaly. The GC233 and GC234 sites were difficult to detect with MCS amplitude anomaly data.

Two geological features identified in the combined remote-sensing survey and ground-truth studies played critical roles in establishment of chemosynthetic communities. These features were standing pools of hyper-saline brine formed in the craters of mud volcanoes and shallow deposits of gas hydrate overlying actively venting faults. Both features have the capacity to trap large volumes of hydrocarbons at the seafloor. Both should be considered diagnostic of chemosynthetic communities. That is, a brine pool or a shallow deposit of gas hydrate would have a very high likelihood of being colonized by a significant concentration of chemosynthetic fauna. The exception would be possible cases where sediment discharge was so vigorous or so recent that colonization was impeded. The prospects for detecting colonization in MCS data are slight, although associated attributes such as mounds, faulting, and wipe-out zones will be evident. Satellite remote sensing can be used to confirm active oil discharge, but significant seeps could go undetected in satellite data due to highly episodic discharge. Shallow gas hydrate is readily collected by coring and analysis of surface geochemistry. There is no single characteristic geophysical signature that will allow an interpreter to find all of the known chemosynthetic organism sites in our study areas. Geophysical data can be used to define areas affected by seepage, and these generally make up only a small fraction (about 11%) of the total survey area (although the percentage can be much higher within a localized area, such as a single lease block). Whether chemosynthetic organisms inhabit a given locality can ultimately be determined only by direct observations, such as submersible observations, camera sled, or ROV photos. However, the likelihood of chemosynthetic organism occurrence can be inferred by using a number of geologic and geophysical observations to build a case for their occurrence and to screen out false positives (Table 6.1).

## 11.5 Program-wide Hypotheses

Objectives two and three required and examination of the chemical factors that may control the distribution, abundance, and growth of chemosynthetic communities. Physiological requirements for chemosynthesis require availability of chemical substrates, $CH_4$ and $H_2S$, at localities where tubeworms and mussels form stable aggregations. However, as we have seen in the course of this program, the spatial and temporal gradients of chemical compounds at seeps tend to be abrupt and heterogeneous over small space and time scales (see Chapter 7). Moreover, biogeochemical processes that produce, maintain, or consume chemical substrates—particularly $H_2S$—exhibit a wide range of activity (see Chapter 9). Thus, although we know that tubeworms require $H_2S$, and can measure high concentrations of $H_2S$, in association with tubeworms, and can demonstrate that the $H_2S$ is produced by reduction of seawater $SO_4$ driven by oxidation of

methane the specific temporal and spatial availability of $H_2S$ needed to support and tubeworm bush has not yet been determined. The sampling program was designed to examine whether there is a predictable relationship between the prominent chemosynthetic fauna (primarily tubeworms) and sediment geochemistry. A further refinement was to compare tubeworm aggregations that were in different stages of development (juvenile, adult, senescent). Basically, there appear to be two possibilities: 1) There is a robust threshold level of $H_2S$ (or some other chemical variable) in the sediments next to all tubeworm bushes; so that the distribution of tubeworms in a seep community mirrors the availability of hydrocarbon gas and $H_2S$. Or, 2) chemical concentrations were not consistent in the sediments next to tube worm bushes; implying that a high degree of spatial and temporal haphazardness.

The approach to the integrated statistical analysis was to merge data sets from various geochemical and biological components to characterize environments and test hypotheses on distribution patterns gleaned from the sampling design. First we examine the variability of geochemical variables alone, then we test for correlation between geochemistry and the biological community. Principal components analysis (PCA) was used to characterize environmental patterns by grouping stations along two axes of a PCA plot. PCA is a variable reduction technique with three important characteristics: Because it is a transformation of data, there are as many components as there are variables, the components are mutually orthogonal (i.e., the components are uncorrelated), and the components are extracted in order of decreasing variance. Therefore, the new variables resulting from the PCA contain most of the variance and none of the redundancy of the original data set. The sampling plan can be thought of as simply a spatial surrogate for environmental heterogeneity due to geochemical differences in the chemosynthetic habitats. A PCA of all the geochemical variables was used to reduce this large number of variables to two new variables, which are uncorrelated and contain most of the variance in the data set. These new variables can then be used as dependent variables to assess biological relationships between tubeworms and the geochemical environment (Green and Montagna 1996; Carr *et al.* 2000).

Three different PCAs were performed. Most geochemical variables were measured at different depths in sediment to create a vertical profile of the chemical within the sediment. These profiles were converted to integrated values over the sediment horizons to a depth of 11 cm to reduce the profile data to one number (Arvidsson, personal communication). The second analysis was performed on surface sediments only. A third analysis was performed by using the average surface values over both sampling years at a station to create a data set to compare with the tubeworm data set. All data were log transformed prior to PCA treatment. Patterns of the PCA scores from the analyses allow us to test the program-wide hypotheses that there are no differences or changes in chemosynthetic communities over time, sites, habitats, and subhabitats. The hypotheses are tested by looking for groupings on the PCA scores from the sampling design.

## 11.5.1 Integrated geochemistry

The first two principal components for the integrated geochemical data set explained 55% of the variance. Sr, Na, and Cl had the highest positive loadings on PC1, whereas TOC, $SO_4$ and Mg had the most negative loadings on PC1 (Figure 11.2). The total C1 - C5 gases, DIC, and $H_2S$ also loaded highly on PC1. The PC1 axis represents the major geochemical process of brine seepage (high salt) and high sulfate reduction due to seeping gases and sulfide production. Interestingly,

brine seepage does not appear to be separating from hydrocarbon seepage. Because of the lack of separation of indicators of brine and hydrocarbon seepage (Figure 11.2), it is not surprising that sites do not separate when scores are examined (Figure 11.3). There is overlap in patterns for all habitats (Figure 11.2), and stations and years (Figure 11.4). This lack of a pattern among scores for elements of the sampling design indicates there are no differences in integrated values of geochemical variables among sites, habitats, stations, and years. The only outliers are values taken from GB425 in 1997, where the two samples group together along PC2. The second major axis, PC2, had high positive values for Ca, pH, and K.

## 11.5.2 Surface geochemistry

The first two principal components for the surface sediment geochemical data set explained 49% of the variance. More hydrocarbon and inorganic values could be retained for this data set, and nutrient values were added. In some respects the results are different, but the major outcome is the same. Again Na, Cl, methane, total C2 - C5 gases, DIC, and $H_2S$ loaded highly on PC1. However, Sr loaded negatively on PC1. The most negative loadings on PC1 were TOC, $SO_4$, Ca and $NO_2$ (Figure 11.5). PC2 was very different from the integrated analysis, containing mostly high positive values for nutrients $NH_4$, Urea, $PO_4$, and $SIO_3$. The PC 1 axis again represents the major geochemical process of brine seepage (high salt) and high sulfate reduction due to seeping gases and sulfide production. Once again brine seepage does not appear to be separating from hydrocarbon seepage. The lack of separation of indicators of brine and hydrocarbon seepage (Figure 11.5) again made it difficult to distinguish sites and habitats or stations and years (Figure 11.6). Again, no pattern among scores for elements of the sampling design indicates there are no differences in integrated values of geochemical variables among sites, habitats, stations, and years.

Slight patterns do exist in the PCA scores. Three of the GB station had the highest PC1 loadings (Figures 11.5), indicating they were the most active seeping sites. No clear pattern emerges among any of the other sites. The three highest PC1 scores were all for mussel stations (Figures 11.5). One other mussel station also had a positive score, but the remaining two stations were close to zero. All of the senescent tubeworm stations (ST) were close to the origin (0, 0), indicating these were likely among the least active stations.

The lack of clear patterns for sites, stations, and habitats can be caused by two mechanisms. First, chemosynthetic communities are broadly homogeneous. Second, the variance at individual sites is so great that the sites and habitats appear homogeneous when they are in fact heterogeneous and the appearance of homogeneity is simply a function of small sample sizes. The most likely explanation is probably a combination of both mechanisms. There is a great deal of variance from core to core, or sample to sample. There is also likely a great similarity of geochemical processes across broad areas of the chemosynthetic communities.

## 11.5.3 Comparison of geochemistry with tubeworms.

The tubeworm data was by station, so a third analysis was run by averaging the temporal samples by site. The analysis of means by stations was similar to the previous analysis, which included years. The total C1 - C5 gases, DIC, and $H_2S$ had the highest positive loadings on PC1, whereas TOC, $SO_4$ and Ca had the most negative loadings on PC1 (Figure 11.7). PC2 again contained high positive values for nutrients $NH_4$, Urea, $PO_4$, and $SIO_3$. One difference was that

Na and Cl had intermediately high values for both PC1 and PC2, thus falling between both axes.

The PC scores for stations were correlated to the growth and condition scores for tubeworms (Table 11.1). There was no significant correlation between geochemical properties and *Lamellibrachia* condition, growth, or length. Escarpid condition did correlate to both PC1 and PC2, indicating that better tubeworm condition was found where higher seepage activity occurred.

Table 11.1. Tubeworm condition and growth data correlated to chemical (by station) principal components (PC1 and PC2). Pearson correlation coefficients (*r*), probability *r*=0, and number of observations (N).

| Species Metric | Chemical PC1 $r$ N | Chemical PC2 $r$ N |
|---|---|---|
| *Lamellibrachia* Condition | 0.32 0.4368 8 | -0.44 0.2743 8 |
| Escarpid Condition | 0.99 0.0013 5 | -0.87 0.0554 5 |
| *Lamellibrachia* Growth | -0.02 0.9542 8 | -0.34295 0.4056 8 |
| *Lamellibrachia* Length | 0.47 0.2356 8 | -0.08 0.8538 8 |

In summary, we have not been able to demonstrate a predictable relationship between tubeworm bushes and the concentrations of chemical forms in the nearby surface sediments. This provides very important guidance for study design in ecological investigations of chemosynthetic communities. The results demonstrate an overwhelming heterogeneity at the level of individual aggregations of tubeworms, bacterial mats, and seep mussels. In the face of this variability and the proven longevity of tubeworms and mussels, the importance of colonization history is paramount. A seep community—at least in a sediment diffusion habitat similar to GC185 and GC234—comprises a mosaic of individual colonies, active gas vents, and shallow hydrate deposits (Figure 11.8). Within this array, the intensity of venting and the geochemical response to hydrocarbons is highly variable. Large numbers of unbiased samples would be required to reduce the variance of sample means. In practical terms, the number of samples exceeds what is

possible for a program operating from a submarine with limited time on bottom and sampling payload. A further complication is the problem of collection bias. Locations for sediment collection were chosen in a non-random manner. Although this sample choice was clearly necessary to establish the ecological context for geochemical analyses, the statistical power of the study design was compromised. Consequently, the results are most useful for setting the upper and lower bounds for relevant processes such as sulfate reduction.
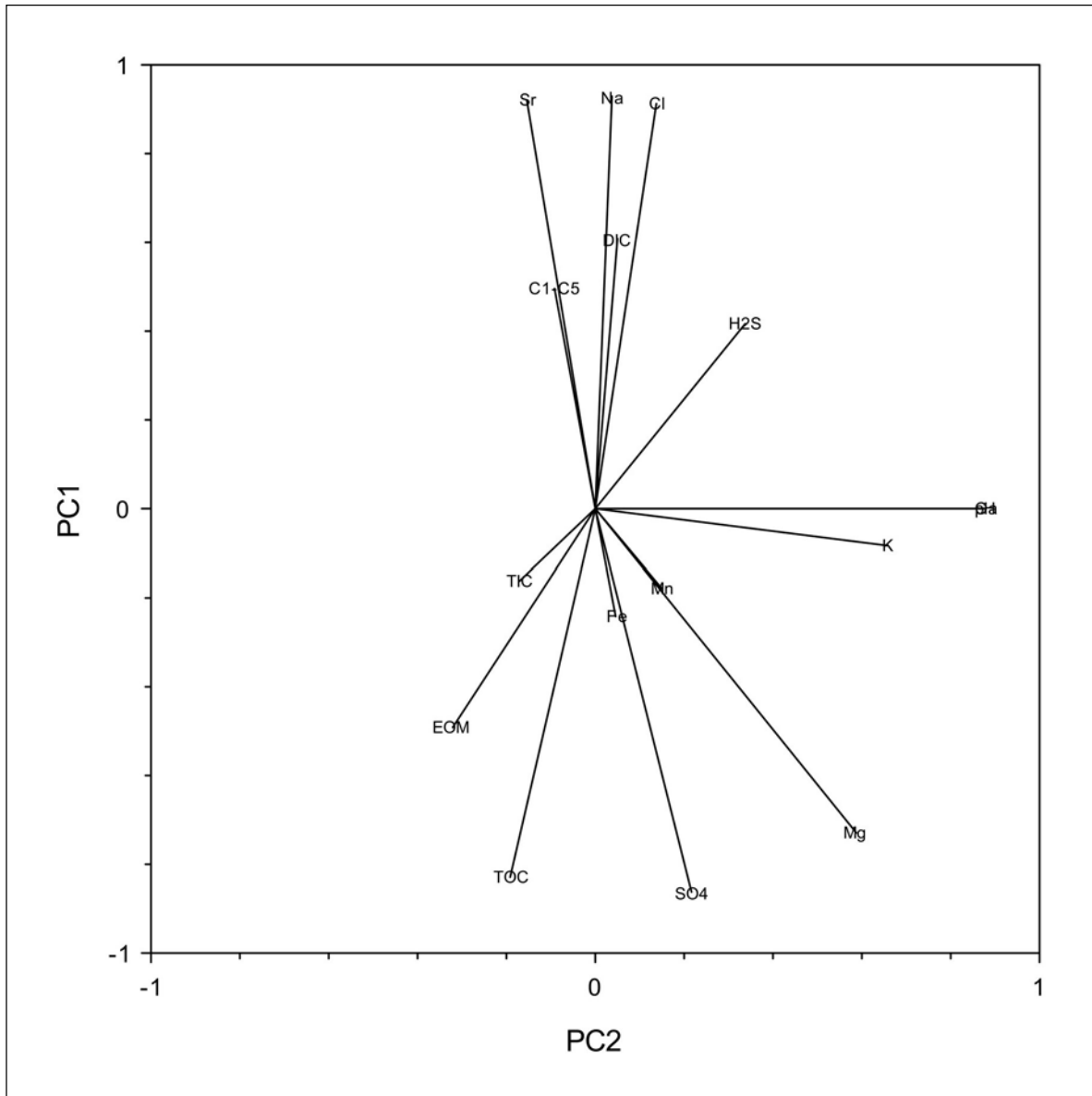


Figure 11.2. Variable loadings on principal component axes (PC1 and PC2) for inorganic and organic chemicals integrated over a depth range of 11 cm. Variables are abbreviated as follows: calcium (Ca), chlorine (Cl), dissolved inorganic carbon (DIC), extractable organic material (EOM), hydrocarbon gases methane through pentane (C1-C5), sulfate (SO4), hydrogen sulfide (H2S), iron (Fe), manganese (Mn), magnesium (Mg), potassium (K), strontium (Sr), sodium (Na), total inorganic carbon (TIC), total organic carbon (TOC), and pH. For a discussion of variables see Chapter 9.

Figure 11.3.  Variable scores for elements in the experimental design for inorganic and organic chemicals integrated over a depth range of 11 cm. Sites and program years are plotted as symbols. See Chapter 3 for site descriptions.
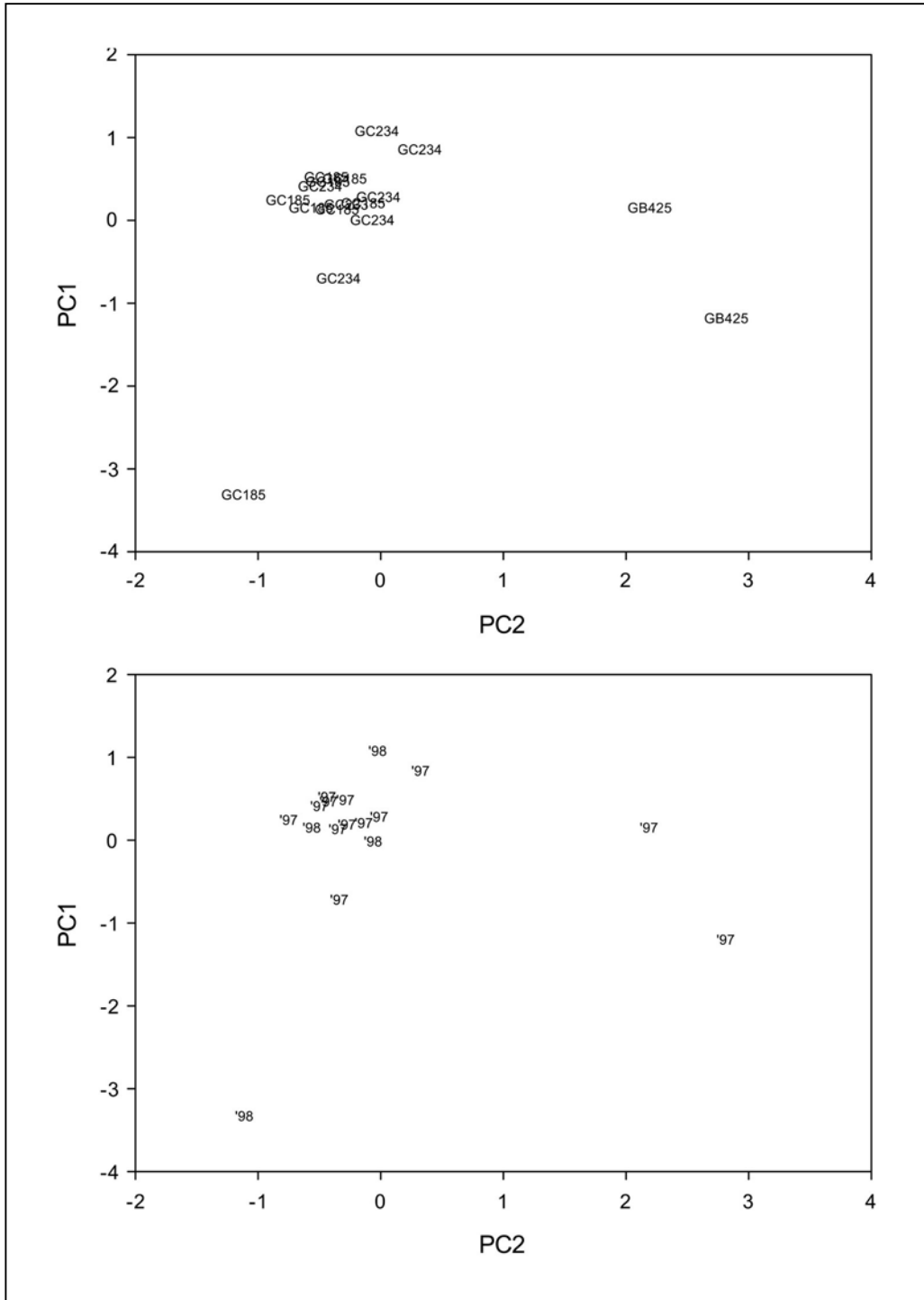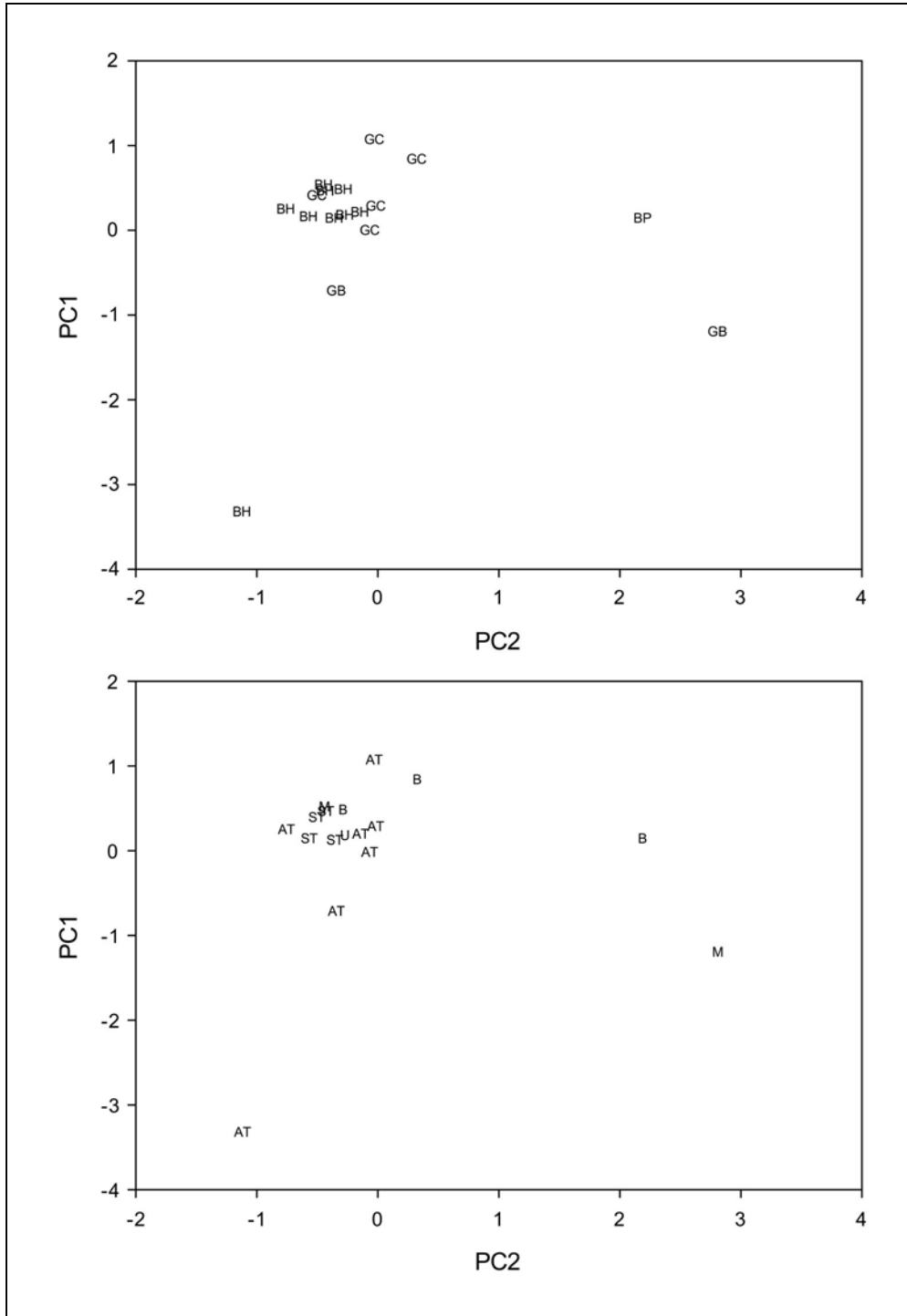
Figure 11.4. Variable scores for elements in the experimental design for inorganic and organic chemicals integrated over a depth range of 11 cm. Sites and habitats are plotted as symbols. Habitats are abbreviated as follows: adult tubeworm (AT), bacterial mat (B), mussel bed (M), senescent tubeworm (ST), unoccupied seep station (U).
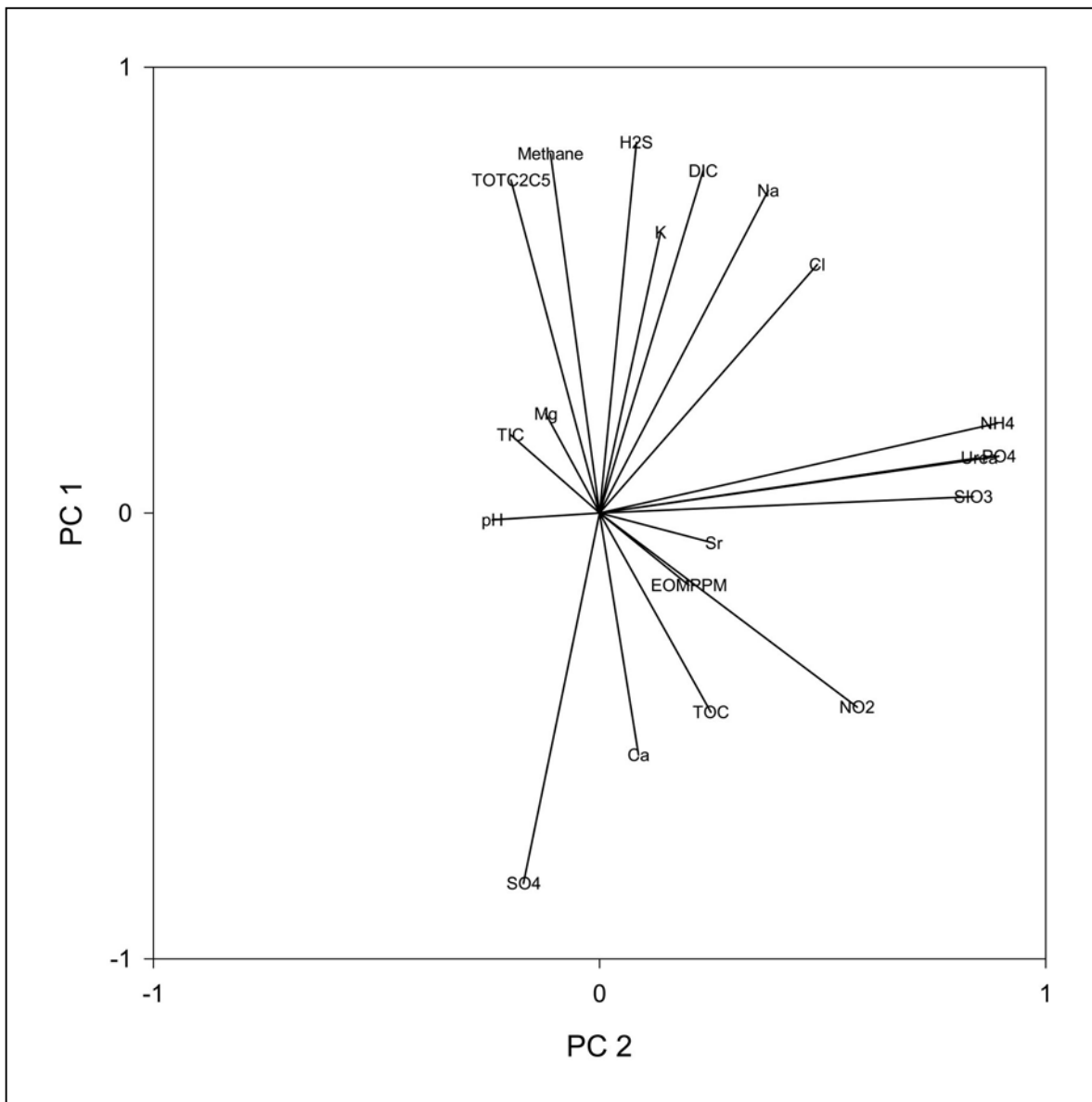
Figure 11.5. Variable loadings for inorganic and organic chemicals in upper-most layers of surface sediments (2 - 4 cm). Variables abbreviated as in Figure 11.1 and as follows: ammonia (NH4), hydrocarbon gases ethane through pentane (TOTC2C5), nitrite (NO2), phosphate (PO4), and silicate (SIO3).
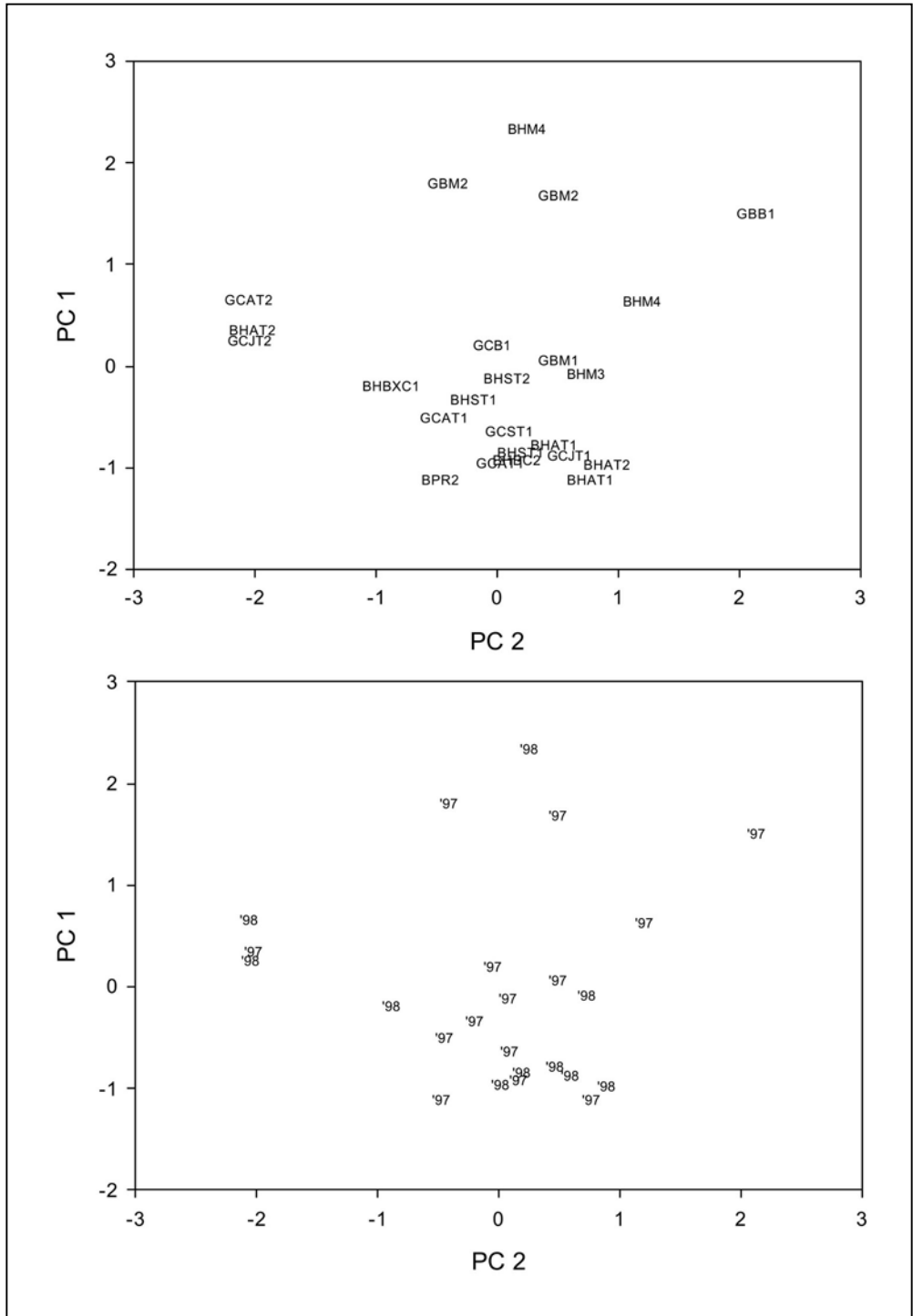
Figure 11.6. Variable scores for elements in the experimental design for inorganic and organic chemicals in surface sediments (upper 2 - 4 cm). Upper panel shows stations (see Table 3.3 for station definitions), lower panel show program years 1997 and 1998.
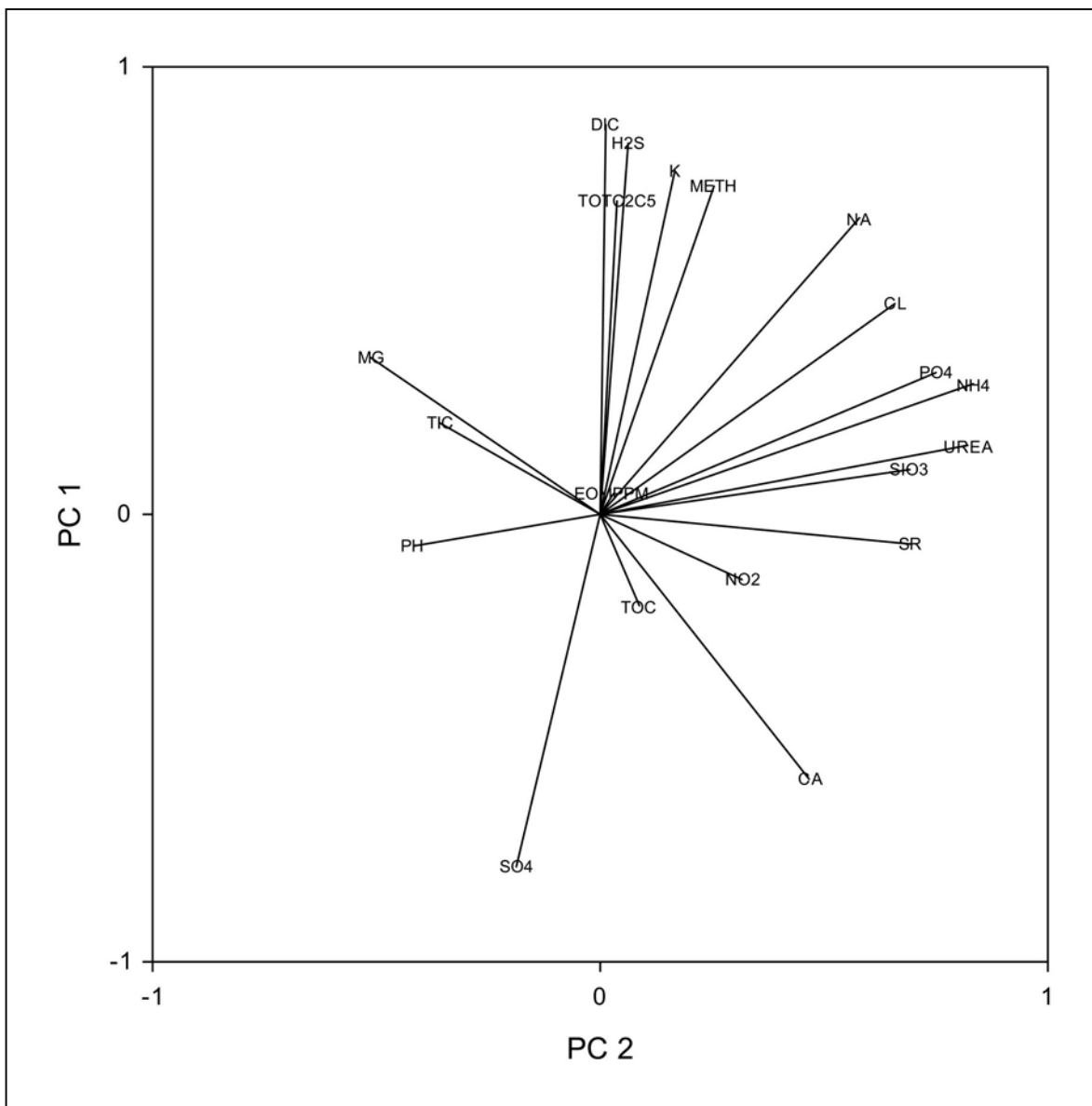
Figure 11.7.  Variable loadings for inorganic and organic chemicals in surface sediments only (2 - 4 cm) averaged over both sampling years. Calculated for comparison to tubeworm condition and growth.
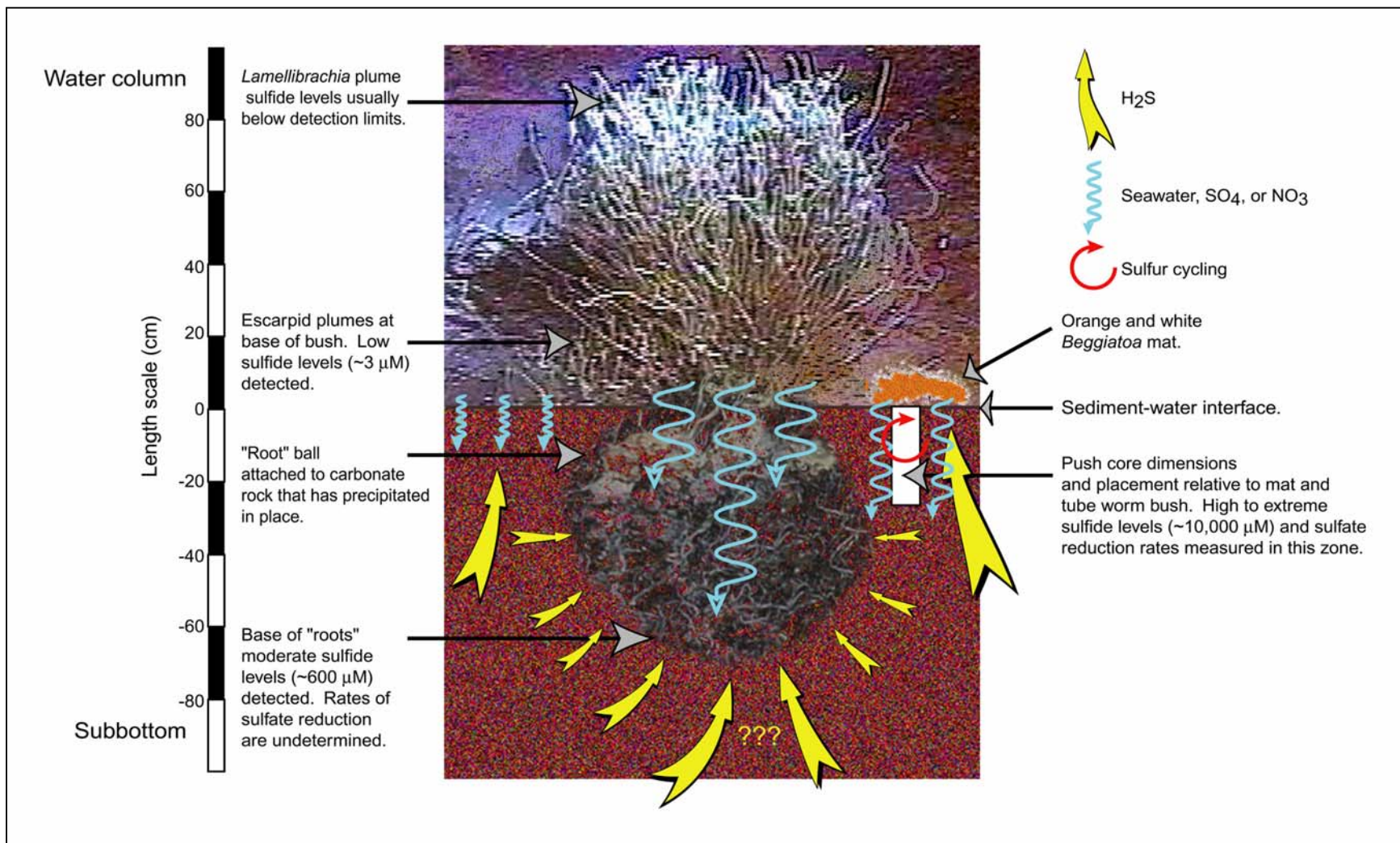
Figure 11.8. Schematic of the tubeworm bush and bacterial mat habitats sampled during the program. The bush shown is a photograph of the tubeworms at the BHAT1 station. The root ball was recovered following a collection with the bushmaster and is superimposed to show its approximate *in situ* position. Proximity of push core sediment samples to tubeworm bushes was limited by the physical barrier of the tubes and roots. The highest concentrations of $H_2S$ and rates of sulfate reduction were measured beneath *Beggiatoa* mats adjacent to tubeworm bushes (e.g., GCAT2 station). Sulfide production is presumed to be enhanced by biologically mediated transport of oxidants into the sediments and cycling of sulfur species.

## 11.6 Geochemical Dependence of Tube Worm and *Beggiatoa* Colonies

Sulfide-based chemoautotrophy, as exhibited by the tubeworm symbiosis and by *Beggiatoa,* plays a central role in the seep ecosystem. The program examined this overall process from two semi-distinct perspectives. Tubeworm growth, condition, and habitat geochemistry were studied through methods described in Chapters 4 and 8.4. Notably, a unique sample set of pore fluids from within the so-called "root ball" of several tubeworms bushes was collected with a wand that routinely penetrated 50 cm or more into the subbottom. Results reported by Julian *et al.* (1999) demonstrated that the roots, which are slender extensions of the worm tubes buried in the sediments beneath the bush, are the site of sulfide uptake in *Lamellibrachia* and Escarpids. The geochemistry of seep sediments was extensively studied based on samples collected in push cores. A sub-set of the geochemical sediment samples were cross-compared with collections of *Beggiatoa*. As the schematic in Figure 11.8 illustrates, these tubeworm and sediment geochemistry samples are only partially comparable. The geochemical samples were taken from a shallower subbottom depth adjacent to the tubeworm bushes while the wand-collected fluids from the root balls were small-volume samples on which only a limited suite of analyses could be performed. A synthesis of these studies provides a better delineation of seep geochemistry, but leaves details of the process to be resolved by future study.

With their high biomass and evident impact on seafloor topography, the large colonies (bushes) of tubeworms exert a strong influence on seep ecology. Consumption of sulfide by the aggregation of individual tubeworms and symbionts in a large bush must be substantial over time. Given their extremely long life spans (hundreds of years) the persistence of a tubeworm bush must mark a stable supply of sulfide in its immediate locality; however, as the mapping efforts undertaken by the program have shown, the distribution of tubeworms within a seep complex is notably patchy and discontinuous. The *Beggiatoa,* in contrast, are ubiquitous. All cores collected from seep stations contained visible filaments of *Beggiatoa*. The *Beggiatoa* filaments concentrate into conspicuous mats on surface sediments where conditions are optimal. The sulfide is produced through reduction of seawater sulfate in an undetermined consortium of bacteria and is a byproduct of hydrocarbon consumption. Based on the observed variability in the distribution of mats, these optimal conditions are presumed to be ephemeral and spatially transient. Beneath *Beggiatoa* mats, infiltration of bacterial filaments ten or more centimeters into the sediment and transport of $NO_3$ in filament vacuoles enhance consumption of sulfide (large arrows in Figure 11.8).

Where tubeworms or *Beggiatoa* are lacking, the supply of seawater sulfate at depth in the subbottom is limited by molecular diffusion (small arrows in Figure 11.8) and the rates of sulfate reduction are comparatively low. Many of the stations classified as inactive in Figure 9.2 fall into this category. However, these mechanisms specifically do not address sulfide production and consumption at the root level beneath tubeworm bushes. The wand-collected samples consistently found moderate to high sulfide concentrations in this zone. The probable effect of the root mass upon the diffusion of seawater into the subbottom is significant. A tangle assembly of tubes displaces sediment and greatly increases its permeability to seawater. The highest sulfate reduction rates were seen beneath mats adjacent to tubeworm bushes. The following sections develop a model for how *Beggiatoa* and possibly tubeworms can enhance sulfate reduction rates as well as mediate overall sulfide concentrations.

**11.6.1 Model contribution of *Beggiatoa* to maintenance of extreme rates of sulfate reduction**

In geochemical studies, transport fluxes are typically calculated from observed gradients. In the seep sites investigated during this program, we find a conundrum: sulfate gradient profiles and sulfate reduction rates indicate that the sulfate flux into the sediment porewaters needed to sustain the observed sulfate-reduction rates greatly exceeds the sulfate flux calculated from the gradients. What is the mechanism for enhanced supply of sulfate? Because sulfur plays a central role in the biological productivity in seep communities, the mechanisms by which sulfate reduction rates are enhanced are critical.

Insight into the possible importance of transport can also be had through comparison of the sulfate depletion and reduction rate curves in the context of a simple diagenetic model. By Fick's law, the gradient expressed in the sulfate depletion curve at a given depth is proportional to the diffusive flux of sulfate occurring over this interval. By making the assumption that sulfate reduction is the only sink for sulfate, the flux of sulfate required to sustain the measured reduction rate can be compared with that implied by the depletion curve. This has been done for station GCAT (dive 4029) in Figure 9.12, by fitting the sulfate concentration curve and comparing the apparent rate diffusion with the reduction rate according to the diagenetic equation [Berner, 1980 #382],

$$\frac{\partial(\phi C)}{\partial t} = \frac{\partial}{\partial z}\left(\phi(D_S + D_I)\frac{\partial C}{\partial z}\right) - \frac{\partial(\phi\omega C)}{\partial z} - R \qquad (11.1)$$

Here $C$ is the concentration of sulfate, $\phi$ is porosity, $D_S$ and $D_I$ are the sediment diffusion and irrigation coefficients, respectively, $\omega$ is the depositional rate, and $R$ is the reduction rate. This equation essentially states that the change in concentration at a fixed depth per unit time is the sum of diffusive, advective, and reaction processes. Assuming that the depositional rate is negligible compared to diffusion, and that the profile reflects a steady state condition (i.e., that the sum of the right hand terms is zero), the ratio of the reduction rate and the second derivative of concentration ($R / \{\partial^2 C(z)/ \partial z^2\}$) should approximate the sum $D_S + D_I$. The average value of this ratio over the fitted part of the curve shown in Figure 11.9 is 236 x $10^6$ cm$^2$ sec$^{-1}$. The accepted value for $D_S$ is ~ 5 x $10^{-6}$ cm$^2$ sec$^{-1}$ [Berner, 1980 #382]. This implies that the diffusive flux of sulfate to the zone of maximum sulfate reduction (10-12 cm) is relatively minor, and thus that transport via other processes (described generally as bioirrigation) is a critical feature in sustaining these very high reduction rates. The fact that highest rates also occur in areas in which there is a high abundance of *Beggiatoa* mats and tubeworms are found together suggests that tubeworms and *Beggiatoa* may interact to increase the rate of sulfate reduction.

It is possible that surface-bound sulfide oxidizers such as tubeworms and *Beggiatoa* may play a critical role in sustaining the observed high sulfate reduction rates. What follows is speculative, but it is at least consistent with the biotic distributions and the overall pattern of 1) sulfate reduction rates, 2) depletion of sulfate at depth, and (3) the association of bacterial mats. Figure 11.10 depicts a possible temporal sequence in which the interaction between methane flux, sulfate reduction rate, and the depth at which sulfate is depleted (i.e., the thickness of the zone of sulfate reduction, and thus the magnitude of the integrated rate) is mediated by the activities of surface-bound sulfide oxidizers. Assuming an unlimited methane supply, sulfate reduction rates are limited by the diffusive supply of sulfate to the zone of sulfate reduction (stage 1 in Figure 11.10). Sulfate depletion gradients here are very high, with sulfate typically depleted within

$$\frac{\partial \phi C}{\partial t} = \underbrace{\frac{\partial}{\partial z}\left\{\phi(D_S^o + D_S^*)\frac{\partial C}{\partial z}\right\}}_{\text{diffusion+recycling}} - \underbrace{\frac{\partial}{\partial z}\phi\omega C}_{\text{advection}} - \underbrace{R}_{\text{reaction}}$$

$$= 0$$
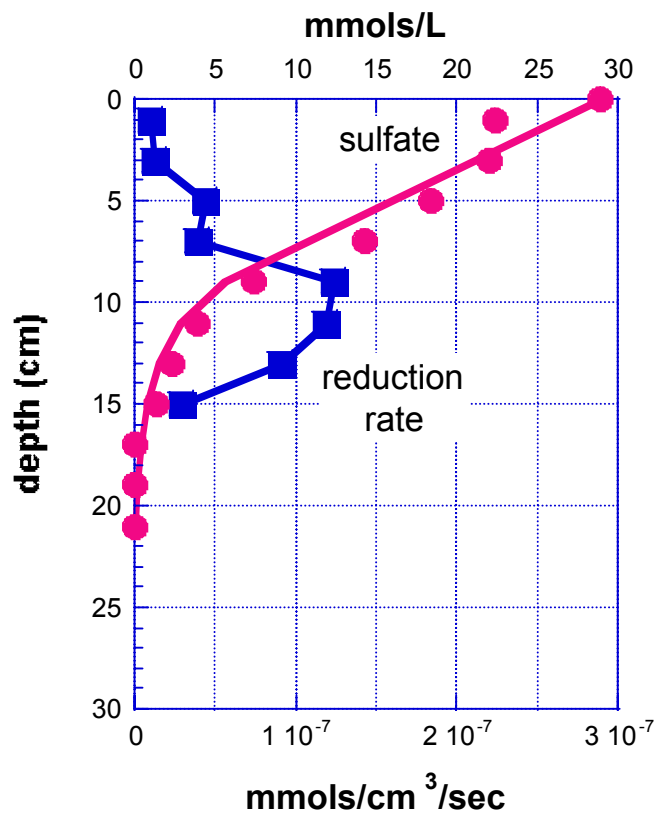


$$(D_S^o + D_S^*) = 236 \times 10^{-6}\ cm^2\ sec^{-1}$$

$$\therefore D_S^* \ggg (D_S^o \simeq 5 \times 10^{-6}\ cm^2\ sec^{-1})$$

Figure 11.9. Apparent diffusion coefficients. Diffusion coefficients computed from sulfate reduction rate and sulfate depletion profile data are composed of a molecular component and an "excess" term. In cases where this excess term is large, enhanced transport or recycling of sulfate is indicated.

5 cms. The gradient may approach zero concentration axis asymptotically as shown in Figure 11.10, or linearly. Convex-upward curvature indicates consumption of sulfate through the entire zone; no curvature indicates consumption at the base. As sulfate cycling is progressively enhanced, reduction rates increase, sulfate gradients relax in the near-surface section and decrease the second derivative of the concentration curve, thus increasing the apparent diffusion coefficient. The zone of sulfate reduction increases in depth, and the integrated rate increases proportionally (stage 2 in Figure 11.10).

With increased reduction rate, sulfide concentrations (poorly buffered by reactive iron) increase as well. However, *Beggiatoa* may be unable to maintain sulfide gradients under very high sulfide concentrations, and thus may be forced to confine their activities to progressively shallower depths in the sediment. As this trend continues, enhanced sulfate cycling decays, and the zone of sulfate reduction progressively shrinks (stage 3 in Figure 11.10). As *Beggiatoa* are ultimately forced out, the system ultimately returns to its initial diffusion-limited state.

Alternatively, ebullition of methane gas could displace sulfate-depleted porewater, which would then be replaced by seawater from the sediment-water interface. This transport mechanism was suggested by Fossing *et al.* [, 2000 #375] as a means of reconciling measured high sulfate reduction rates with sulfate depletion profiles, and has also been discussed by O'Hara *et al.* [, 1995 #379]. It is noteworthy that the cores from GCAT2 were characterized by extensive gas fractures to a degree not seen in most sediment samples. This indicates that gas venting was extremely active at this station and may have contributed to the apparent high diffusion rates.

These speculations may be inaccurate and require extensive microbiological data for corroboration. In particular, if *Beggiatoa* utilize nitrate as an intermediate electron acceptor, they must be shown to be capable of sustaining rates of nitrate reduction close to the measured "excess" sulfate reduction (see Section 8.2). In addition, stage 2 profiles are typical of those seen at adult tubeworm station GCAT2 (dives 2886, 4029, and 4048). This station is also significant in having a dripline *Beggiatoa* mat. In Figure 11.11, the apparent diffusion coefficient ($D_S + D_I$ computed from equation 11.1) is plotted against the sulfate reduction rate measured at that depth. "Pure" bacterial mats (those having no immediate association with tubeworms) and, similarly, tubeworms unassociated with bacterial mats both tend to plot at the lower end of enhanced coefficients and rates. However, it is where tubeworms and mats are closely associated that extreme enhancements of rates is seen. This may indicate some interaction between mats and tubeworms: e.g., if tubeworms sequester sulfur and do not return it as sulfate to the porewater, they may be able to buffer sulfide to levels that *Beggiatoa* mats can tolerate. Lastly, it must be noted that sulfate-reducing bacteria have not been observed to oxidize methane (or other hydrocarbons) directly. There is field evidence that anaerobic methane oxidation occurs close to or at the base of the sulfate reduction zone [Reeburgh, 1976 #380; Reeburgh, 1980 #381; Martens, 1977 #378; Devol, 1981 #374; Iversen, 1985 #377; Blair, 1995 #373]. Hoehler *et al.* [, 1994 #376] have hypothesized that this process may be accomplished by methanogenic bacteria who oxidize methane through a "reversed" methanogenic reaction:

$$CH_4 + 3H_2O = 4H^+ + HCO_3^- \tag{11.2}$$

The H$_2$ produced in this reaction can then be utilized directly by sulfate-reducing bacteria, who apparently are able to out-compete methanogens for this substrate and maintain it at low concentrations:
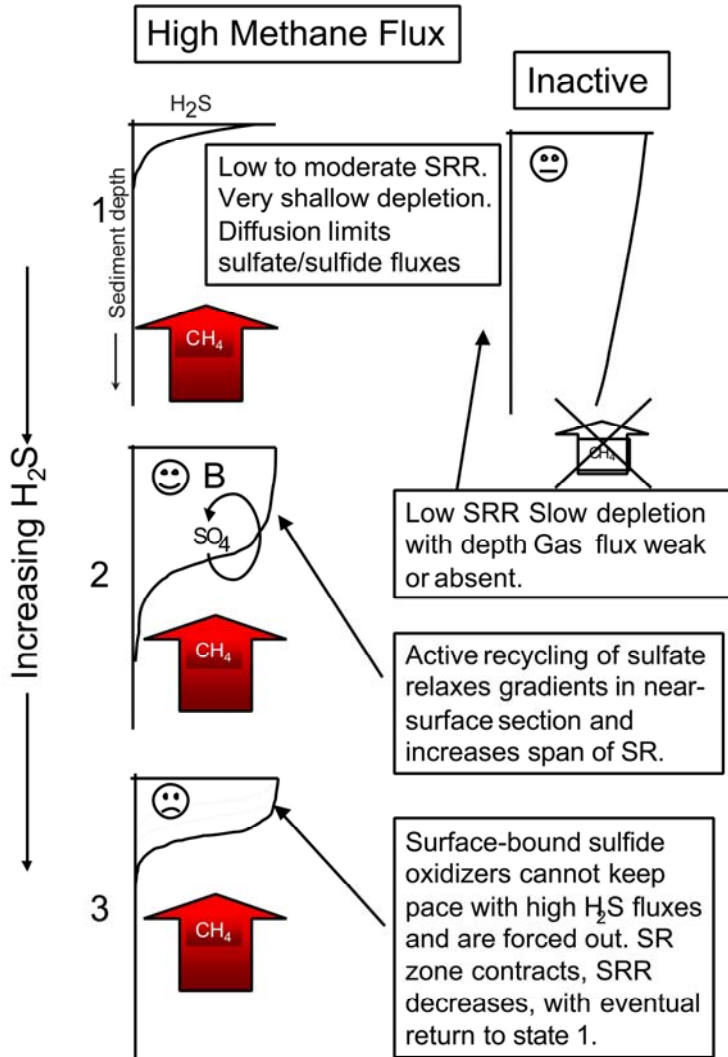


Figure 11.10. Temporal cycle of sulfate reduction and enhanced sulfate supply. Cartoon shows a possible sequence in which sulfate reduction rate is mediated by the activities of surface-bound sulfide oxidizers. Left-hand panel, unlimited methane supply; right-hand panel, organic matter limitation. Stage 1: sulfate reduction rates are limited by the diffusive supply of sulfate to the zone of sulfate reduction. Stage 2: sulfate cycling is progressively enhanced by activities of sulfide oxidizers, giving rise to increasing reduction rates increase. Stage 3: sulfide oxidizers cannot keep pace with sulfide flux at extreme SR rates and are gradually forced out, resulting in an eventual return to initial diffusion-limited state.

11-21
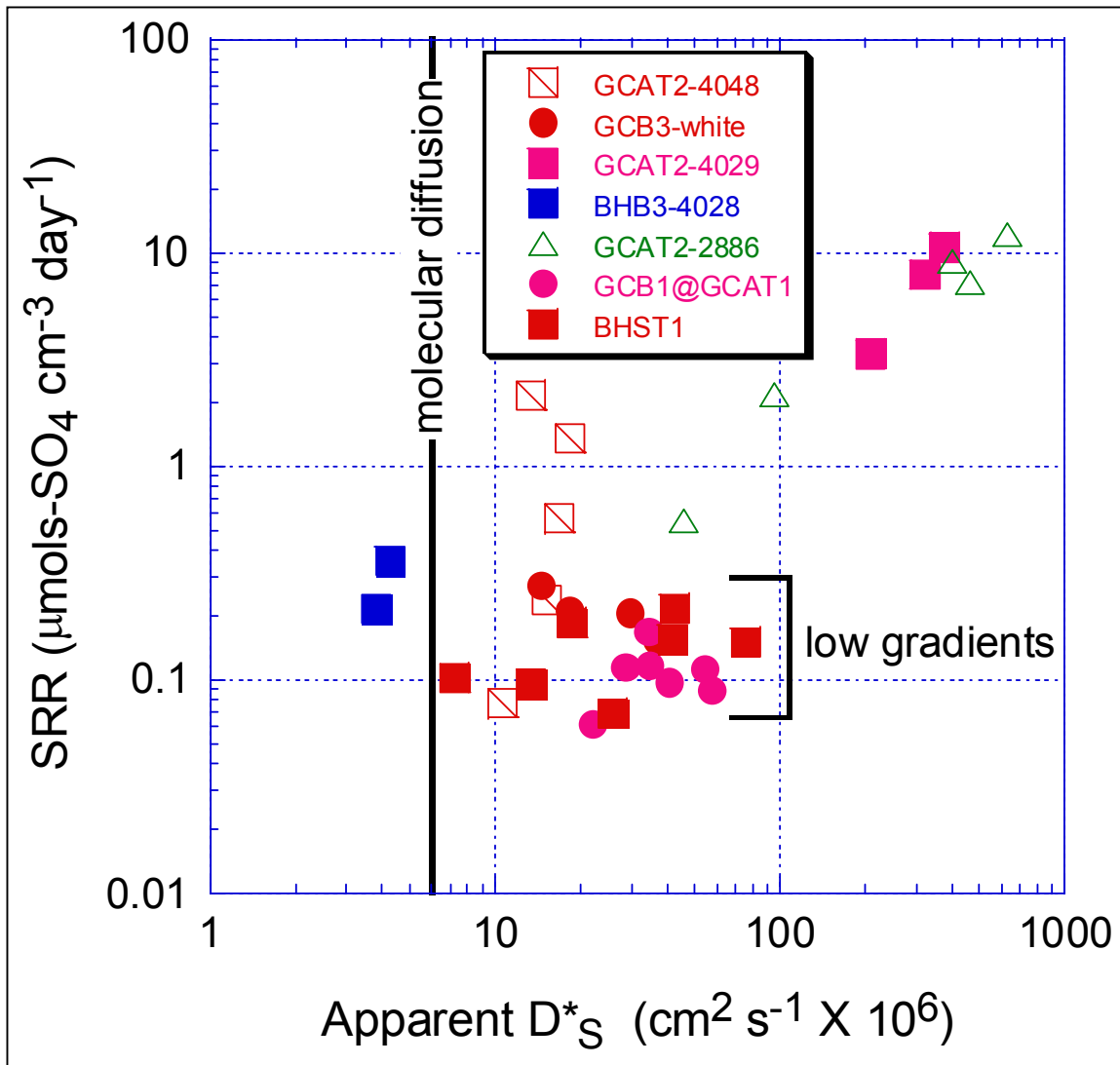
Figure 11.11. Comparison of apparent diffusion coefficients and sulfate reduction rates. Although there is evidence of enhanced cycling of sulfate in both tubeworm and mat habitats, extreme rates are dominated by GCAT2, where tubeworm and mats are found in close proximity.

$$4H_4 + SO_4^{2-} + H^+ = 4H_2O\ HS^- \tag{11.2}$$

The net reaction above is equivalent to reaction (9-4). A sulfate reduction peak located close (or at least within) the interval over which sulfate is being depleted (e.g., at GCAT2) is consistent with observations of anaerobic methane oxidation in other environments.

## 11.7 A Conceptual Model of Seep Community Establishment, Growth, and Evolution

Objective fours required and examination of the life history and ecology of chemosynthetic species and their community components.  How long do the tubeworms live and individual aggregations persist?  A variety of observations suggest that they may live much longer even than we have previously suggested (Fisher *et al.* 1997; Bergquist *et al.* 2000). The empirical data on growth rates of the vestimentiferans indicates that most are 170 – 250 years old by the time they reach a length of 2 m. It also indicates that their growth rate slows down dramatically at this time. However, we often collect animals in excess of 2 m in length, sometimes as much as 3 m in length. The oldest aggregations sampled contained animals in good health, with no signs of increased mortality. Occasional sightings of aggregations of very large individuals of the Escarpid-like species and the total absence of monospecific aggregations of *L.* cf *luymesi* in these areas suggest that the Escarpid-like species may outlive *L.* cf *luymesi* by a considerable margin. When all of the above observations and data are taken into consideration, it is not unrealistic to suggest that present estimates of longevity up to 250 years may be low by a factor of at least two.

The following model has been developed from size-based classification of tubeworms or mussels as juveniles and from geochemical analyses of fluids associated with physiological uptake by these species. New seep communities normally develop in specific areas where active surface expression of seepage results in deposition of carbonate substrate for the larvae to settle upon in an environment enriched in methane or sulfide or both. Bacterial mats may proliferate during the early stages before significant carbonate deposition has occurred. Mussel or tubeworm larvae settle on the solidifying carbonate substrate, and the tubes and shells of the young animals provide additional substrate for further settlement. Mussel communities will continue to flourish as long as methane is released in substantial quantities from the sediments. In some cases this can last for periods measured in hundreds of years at least, such as at the GC233 site and perhaps over methane hydrate deposits. Parasitism can radically alter the reproductive capability of mussel communities such that, even though individuals are living and contributing to community structure, they are unable to reproduce. In most cases, deposition of carbonate slows down and channels seepage over a period of decades, such that the release of seep fluid from that point on the ocean floor is greatly diminished. During the early decades while the high level of seepage is maintained, the carbonate upon which the first recruits have settled may continue to grow. Recruitment of tubeworms or mussels to this point continues as long as sulfide and/or methane is released from the seafloor and the carbonate remains exposed. The majority of recruits are derived from established colonies in the immediate vicinity, but significant recruitment occurs from communities that are tens of kilometers distant. Because the young communities are in microhabitats of very active seepage, only fauna that can tolerate this chemistry are associated with the young communities. Mussels cannot bind and accumulate methane (as tubeworms do sulfide), and therefore only occur in the areas of most active seepage. As a result, associated fauna found in mussel beds is completely dominated by endemic seep animals that can tolerate these conditions (the highest species richness documented in any mussel bed was 8, and a total of only 16 species was found in all mussel beds sampled). However, these well-adapted endemic species occur in large numbers with significant biomass. During this time, the very young tubeworms obtain sulfide across their plumes and may begin to grow a posterior extension of their tubes (a "root") to supplement their sulfide uptake from interstitial pools. Young tubeworm aggregations support not only large numbers and biomasses of endemic animals like the mussel beds, but significant numbers of non-endemic animals as well.

Over the next century or two, the tubeworms continue to grow while seepage of sulfide from the sediment into the water column progressively decreases because 1) the tubeworms absorb it at depth in the sediment and 2) the accumulation of carbonates and the "root ball" impede seepage. The tubeworms continue to expand their "roots" into the sediment and at least *Lamellibrachia* cf *luymesi* increases its dependence on this source of sulfide. The Escarpid-like species continues to take up significant amounts of sulfide across its plume which is maintained near the sediment-water interface. During this period, there is sufficient primary production associated with the aggregation to maintain a moderately high biomass community while the toxicity of the habitat has decreased to the point that a much wider variety of non-endemic fauna colonizes or visits the aggregations. At this point, the analogy between the tubeworms and long-lived ecosystem-structuring plants (e.g., trees) is quite strong. Although the tubeworms are not a food source for most of the associated fauna, they provide a habitat for numerous species that are supported by seep primary production. During this time we infer that significant primary production by free-living bacteria associated with tubeworm tubes is supporting the diverse community of associated fauna.

As the aggregation ages, flow of sulfide into the water column continues to decrease and some thinning of the aggregation occurs. "Roots" are the primary route of sulfide acquisition by all remaining tubeworms. Non-endemic and non-mobile fauna often colonize the tubes heavily; primary production by free-living bacteria associated with the aggregation decreases significantly, and the biomass of the associated faunal community drops significantly. This stage in their life history may also last a very long time, because the tubeworms in these less dense old aggregations continue to grow and are in very good condition, presumably in part because of reduced competition from the remaining vestimentiferans.

Clearly program results have contributed substantially to understanding of the seep fauna. However, there are still very significant and important questions to be addressed concerning this fauna that would provide essential information for management decisions. This includes furthering understanding of the relatively shallow slope communities, and determining the general applicability of findings to the functionally similar but taxonomically distinct, deeper-water communities. The latter may be especially critical to the MMS as energy company activities continue to expand into the deep-water environment. Some examples of key questions that remain to be addressed are summarized as follows:

1. What is the source of the sulfide that sustains the vestimentiferan tubeworm communities over centuries?
   1a. If it is sulfide produced by reduction of seawater sulfate, then how does it reach the roots of the tubeworms, 0.5 m and more below the seawater-sediment surface?
   1b. What rate of sulfide flux is required to sustain a typical old tubeworm aggregation?
   1c. What rate of sulfide flux is required to sustain the very large aggregations?

2. Is transfer of seep organic production to the surrounding deep sea even more extensive than documented to date?
   2a. Is transfer through zooplankton significant?
   2b. Is transfer through as yet untrapped mobile predators significant? For example we observe large sharks and fishes—even swordfish—at seeps. Do these animals obtain a food supply at seeps?

3. Is the working model of faunal succession correct?
   3a. Is diversity and biomass inversely correlated with each other and both correlated with toxicity and production?
   3b. Does this model hold in other biogeographical settings with different species filling similar roles?

4. What is the total biodiversity in the tubeworm ecosystems in these relatively well known sites?
   4a. What is the biodiversity of the ecosystems at much more poorly sampled sites where quick looks suggest differences, such as sites 100 – 200 miles west and barite hosted mussel beds?

5. Do any of our findings apply to the taxonomically distinct communities at deeper sites?
   5a. What and who is there? (biodiversity)
   5b. Are the sites and species long-lived?
   5c. Are roots a universal feature of seep tubeworms?
   5d. Do the mussels with two types of symbionts (at places like Alaminos Canyon and the Florida Escarpment) compete with and eventually overgrow the tubeworms as mussels do at hydrothermal vents on the East Pacific Rise?
   5e. Are these sites more productive as some photographs seem to suggest?
   5e. Do our successional models for the associated fauna hold in the context of a much reduced surrounding biota?
   5f. Is the importance of seep production to the surrounding fauna enhanced in deeper (and more nutrient limited) settings?

## 11.8 Model of seep-background trophic interaction.

The principal finding of the trophic interaction study was that hydrocarbon seep systems are to some degree trophically linked to the surrounding background system (Figure 11.12). Since the beginning of deep chemosynthetic community studies, there has been an implicit assumption based in dramatically different biomass and species composition that such systems were largely isolated from the surrounding background benthic system. Reinforcing this assumption has been the considerable depth and remoteness from coastal productivity of hydrothermal sites, which place them within comparatively food-limited background regions.

The typical background deep-sea phytoplankton-derived detritus fuels the system that accumulates as newly arrived material at the sediment-water interface. As this labile material is consumed by detritivores, it is also mixed downward into the sediment by their action and diluted with mineral components of the sediment. Over time, a residue of old refractory detritus builds up in the sediment mixed layer, which may reenter the food web via a microbial intermediary. Determination of the exact importance of old versus new detritus is an active area of deep-sea research. Collectively, old and new carbon supports an extremely diverse but low biomass detritivore community on all size scales (meiofauna to megafauna). These, in turn, support predator and scavenger populations on the same size scale. Although meager compared to the influx of detritus from the photic zone, both detritivores and the predators that prey upon them contribute via a fecal route to the detritus pool in the sediments. Isotopically, this phytodetritus-based system displays quite narrow ranges in isotope values.

Seep systems differ from the background in many obvious respects. First and foremost, they are

a bioherm in the sense of having a biogenic structure comprised of shells, tubes of the metazoan hosts for thiotrophic and methanotrophic bacteria, and cementing authigenic carbonates. Most of the associated consumer fauna can be effectively categorized as browsers, opportunistically consuming mucous films, free-living bacteria, and bits of tissue from the substrate-forming mussels, tubeworms, and clams. Within this browser group, there is probably a continuum from strict detritivores such as orbinid polychaetes and sipunculids through film grazers such as nerite and limpet gastropods to non-lethal predators that can feed on either snips of tissue or detritus, such as the *Munidopsis* species. At the highest trophic level are resident predator/scavengers such as the seastar *Sclerasterias tanneri* and the gastropod *Buccina canatae* that feed opportunistically on both the substrate formers and the browsers.
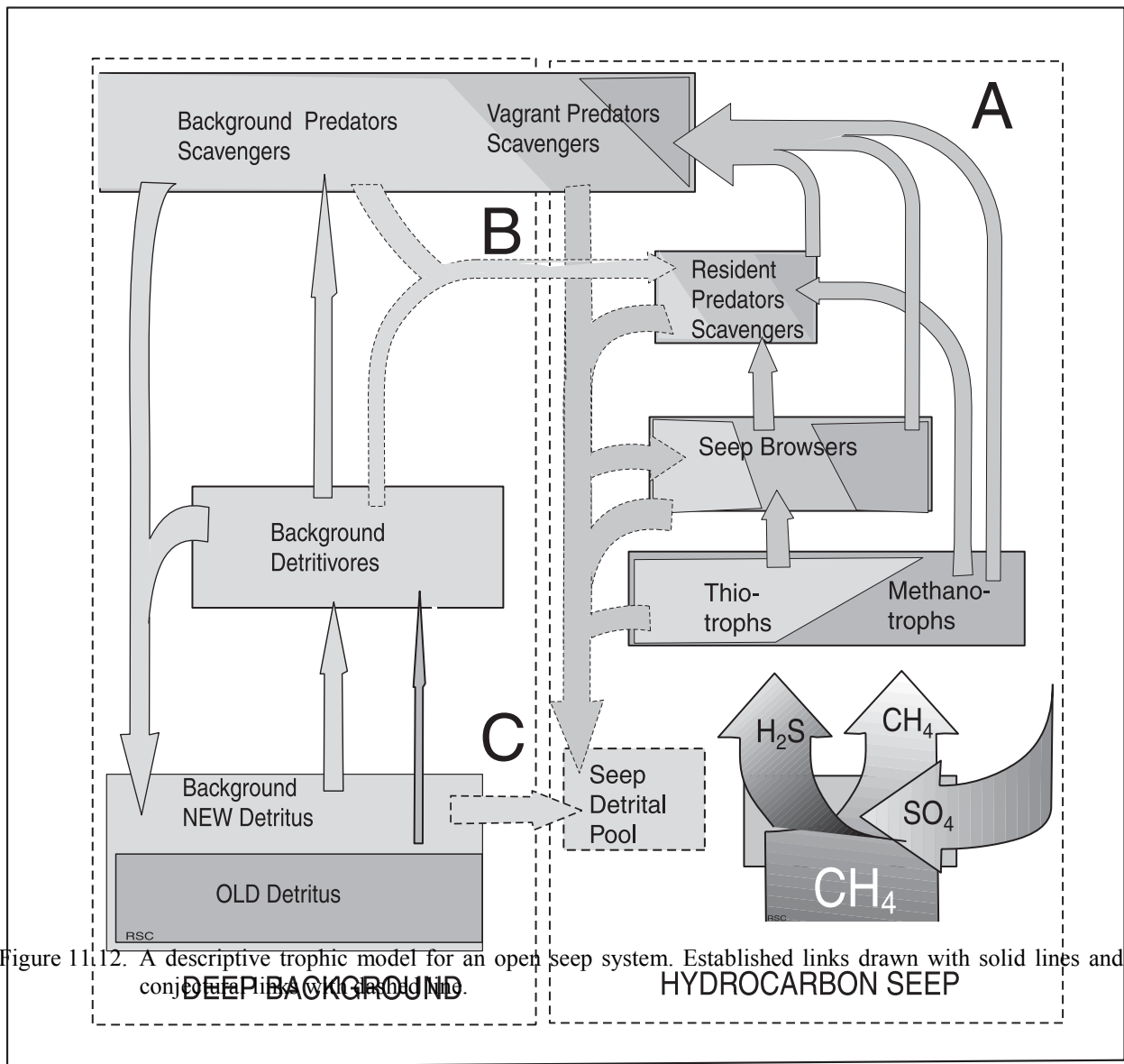


Figure 11.12. A descriptive trophic model for an open seep system. Established links drawn with solid lines and conjectural links with dashed lines.

The present work has confirmed one seep-background link and provided evidence of possibly three more. Explanation of why seep browsers and resident predator/scavengers seem to have various amounts of phytodetritus-derived tissue may depend on the existence of three other links flowing from the background into the seep.

**Link A: Predation on seep fauna by background vagrants.** The proven link is trophic flow from the seeps to the background in the form of predation by the vagrant fauna. Our results indicate that this takes place but at a relatively low level. Analyses of stable isotope ratios, immunoassays, gut content examinations, and direct observations prove that species from the background prey upon all three major species in the seep system.

**Link B: Predation on the background by seep residents.** Simple predation by the seep residents upon background fauna would introduce a background isotope signature into the seep. Such predation or scavenging could involve wide-area foraging episodes but would most likely be due to background fauna entering the seep community. Such an inflow of tissue would be aided by mortality caused by the toxicity of the environment.

**Link C: Mingling of the detritus pool.** The browser component of the seep fauna is composed of detritivores exploiting thin films of detritus rather than the sediment-mixed detritus exploited by the background. If the spatially vast detritus pool of the background mingles with the on-site detritus pool of the seep systems, the isotope signal of the background would be introduced to all consumers. As with all benthic systems, the detritus of seeps is the most poorly defined and sampled ecosystem component. Given the lack of knowledge of both background and seep detritus, it is easier to delineate expected differences than to describe each separately. Unlike other bioherms in which the substrate organisms are heterotrophic filter feeders, seep mussels, tubeworms, and clams should produce no fecal contribution to a detritus pool. There may, however, be an unmeasured contribution of mucous pseudofeces associated with gill and plume cleaning. Seep consumers will contribute fecal material to the detritus pool. Unlike the background detritus pool, seep detritus is unaffected by bioturbation and is available to browsers on the surface of the biogenic substrate.

The detrital pool in the seep may be open to import from the background, thus explaining the apparent food source mixing seen in the browser component. Such import may be of two forms. Biological import occurs because when background vagrants visit the seep sites, they will make a fecal contribution to the local detritus pool, which will carry the isotopic signature of the background. If the topography of the seeps serves as fish attractors, this fecal influx may be appreciable. Physical import may occur because seeps experience net influx by being a passive trap for re-suspended material, even though the area of a seep site is too small to receive much direct vertical influx of phytodetritus. The mesh of tubeworm bushes and the pumping of mussels both produce elevated local sedimentation, drawing laterally transported detritus from the benthic boundary layer. While not a food source for the substrate forming organisms, the seep browsers along with its background isotope signature consume this imported detritus.

## 11.9 Recommended Approach to Sampling Design for Future Efforts

The following recommendations for future study have been developed in consultation with

program investigators, members of the scientific review committee, and MMS representatives. They are based on a review of program results, assessment of future needs, and appraisal of available technology. The recommendations fall into two basic categories: 1) Expanded survey and enumeration of individual seeps and seep communities to measure the effect of regional variables upon community composition and abundance, and 2) studies focused on processed-related questions germane to seep communities. Specific suggestions are grouped under these respective headings.

### 11.9.1 Survey, characterization, and enumeration of seeps and seep communities

**Extend the investigation of Gulf of Mexico chemosynthetic communities to the entire slope.** The results of the present program are qualified in light of the relatively narrow depth and geographic range of study sites. Essentially, existing data comprised findings from the mid-slope (500 to 700 m) and a single site at the 2250 m base of the escarpment (Alaminos Canyon). As the deep megasite sonar data clearly show, the slope between 1000 and 2000 m comprises sedimentary regimes that are very different from the deeper or shallower slope. Because bottom water temperatures are colder in the deep slope, gas hydrate stability will presumably be enhanced at the expense of active gas venting. The abundance of ecosystem forming species such as tubeworms may be radically altered. The consequence for community formation and composition on the deep slope needs to be investigated because the regulatory model is based on mid-slope and shallow slope models for the most part. Likewise, the geographic range of known communities is too selective. Most of the work to date has focused on a narrow range of the central slope. Rates of sedimentation, heat flow, and salt tectonism differ to the east or west of the Mississippi Fan. These factors will impact the development of chemosynthetic communities.

**Employ cost-effect sampling methodologies and analytical suites.** The use of submarines for further investigation of the deep slope beyond the 1000 m limit of the SEA-LINK submarines will be sharply constrained by vessel availability. The national facility for deep submergence, submarine ALVIN, is typically occupied in other marine regions. Consequently, expanded sampling from surface ships and ROVs should be utilized to expand regional coverage. Use of standard methods of box coring and piston coring proved very effective during the program and can be a cost-effective component of future studies. The numbers of inorganic chemical species measured can be safely reduced to a few key parameters, e.g. $H_2S$, sulfate reduction, chlorinity. However, depth profiles are important and should be extended at least to the ~1 m subbottom depths where tubeworm roots interact with the sulfur cycle. What is envisioned is a two or three stage process for investigating the deep slope. First, potential sites are identified by use of regional geological and geophysical characters; seep-affected zones within the sites can be further defined by review of MCS data to identify areas of low seismic amplitude and by using piston coring to screen for thermogenic gas and high-molecular weight hydrocarbons. The result should define broad zones as active seeps, marginal, or non-seep areas. Second, a more intensive program of sediment collection from surface ships can stratify sampling within the identified zones. The resulting collections from each could match the sample numbers achieved during the present program at a fraction of the cost. Ultimately, investigations of chemosynthetic communities require direct observation and sampling from the seafloor. By accomplishing the bulk of the sediment collection for site characterization from the surface ship, seafloor operations can be focused on photodocumentation of biomass, fine-scale mapping, and tissue collection for molecular genetics.

**Extend the database of DNA fingerprints for seep tubeworms and mussels.** Work accomplished during the program has established a powerful set of tools for further defining rates of genetic exchange, speciation, and population stability among Gulf of Mexico chemosynthetic fauna. The present results demonstrate a mixed gene pool and robust populations for the four study sites, but do not go far enough to address cross-slope and along-slope exchange. Consequently, it remains undetermined whether there are geographic- or depth-related barriers to population migrants or genetically isolated communities that might be of special management concern. The DNA fingerprinting technique is cost-effective because the sample collection can be accomplished with an ROV without requirements for specialized collection equipment. Collections can be accomplished in conjunction with regional survey expeditions.

**Continue histopathology and host-parasite modeling.** Like DNA fingerprinting, mussel histopathology provides very useful data on community health without the need for elaborate collection equipment. In fact, the same specimens can be analyzed for both purposes. The most important consideration is to determine to what extent parasite epizootics are responsible for local extinctions of mussels. The extent to which PAH exposure facilitates the development of epizootics must be considered as well. The possibility that other seep mollusks are severely impacted by parasites should also be considered. In shallow water, gastropods usually have higher trematode body burdens than bivalves. This, by analogy, would mean that gastropods at seeps are heavily impacted. In shallow water, clams tend to be somewhat less impacted than mussels, on the average. A check of the lucinids and vesicomyids would seem in order. A host-parasite model should be developed to provide some predictive capability with respect to epizootic generation. The management of shallow water molluscan keystone species now often involves numerical modeling. Hard clams, mussels and oysters are good examples. The influence of disease is now a topic of active research. Coupled host-disease models are being developed and routinely used now in the case of oysters. One of the realizations is that small changes in environment can destabilize host-parasite population dynamics leading to widespread epizootics. Only a numerical model can investigate this phenomenon.

**Continue to compile and maintain a GIS database for Gulf of Mexico chemosynthetic communities.** Because of the success of the investigations to date, continued applied and basic research at seeps will generate ever more data that is potentially important for effective management. Gas hydrate research, for example, promises to produce a diverse array of results over the next decade. The collective aggregate results will be multi-disciplinary and coordination will be sporadic. A central database utilizing GIS tools should be established and actively maintained. A common set of descriptors for Gulf of Mexico chemosynthetic communities should be developed and periodically reviewed and expanded. Efforts should be made to incorporate non-standard indicators on seep numbers and activity such as have been obtained from satellite remote sensing.

### 11.9.2 Process-related studies

**Examine rate-limiting processes at the sediment-water interface and at the level of tubeworm roots.** Results during the program indicated that extreme fluxes of sulfide species occur at seeps. These rates are calculated from measurements of sulfate reduction and assumptions regarding sediment porosity and molecular diffusion. Solid state instruments such as micro-electrodes and benthic flux chambers are becoming proven tools for making direct, *in-situ* measurements. This work would be directed from a human-occupied submarine.

11-29

Deployment of this type of instrument would be a valuable component of a submersible or ROV expedition that focused on process-related questions at the existing study sites or similar habitats on the mid-slope.

**Characterize the guild of sulfate-reducing micro-organisms.** Reduction of seawater sulfate to $H_2S$ as a byproduct of microbial hydrocarbon consumption is the key process supporting the lush communities of chemosynthetic communities at Gulf of Mexico seeps. However, the consortium of taxa which carry out this process, their distribution within surface sediments, and the intermediate chemical markers produced remain undetermined. A significant first step toward answering these questions would be to conduct phylogenetic studies with use of 16-S RNA probes or similar molecular techniques. Automated sample processing facilities have become more widely available and could analyze depth profiles from sediment cores.

**Extend collections of the tubeworm epifauna.** The bushmaster collection device, which was perfected during the present program, should be used to collect tubeworm bushes and associated fauna at other seep sites. This work would provide important information concerning variation in the species diversity of the tubeworm fauna.

**Focus on gas hydrate interaction with seep ecology.** The role of gas hydrate deposits in formation or maintenance of chemosynthetic communities has not been clearly defined. The evidence to date is often anecdotal concerning biological interactions with hydrate. The stability characteristics of gas hydrate change significantly over the depth range on the Gulf of Mexico slope. Its ecological role may also change. The ice worm (*Hesiocaeca methanicola*) increases the surface area of exposed hydrate by forming an extensive network of burrows. This may significantly affect persistence of shallow hydrate deposits. However, the functional relationship of the polychaete with hydrate has not been determined.

**12.0    Data Management**

**12.1    Data Management**

Data management plays a key role in complex environmental programs. It is an important component of the program because it serves as the central node for the flow of data. As this central node, data management monitors, controls and facilitates data flow, ensuring the integrity of the data through each phase of the program.

Data management initially prepared a detailed summary of the planned data and sample collections for the initial phase of the program (Table 12.1). Using this summary, a unique sample designation was assigned to each planned sample collection element.  These sample designators were then incorporated into the sample tracking system. This sample designation scheme formed the central component for the sample tracking system and the basis for documenting the collection and labeling of samples in the field, monitoring their progress through the laboratories, and submission of analytical results.

Appropriate forms for sample collection and data transmittal were developed prior to collection (Figure 12.1). The uniformity gained by preparation of standardized forms facilitated documentation and ensured the completeness of data entered into the program database. As each field effort was completed, collection information was entered into the database.

As the project investigators completed their sample analysis, they submitted their data on task specific electronic data submission forms. Before an investigator's data file was incorporated into the program database, it was subjected to a data screening analysis; a quality control procedure designed to minimize errors.

**12.2    The Project Database**

A computerized relational database management system (DBMS) is invaluable for effective search and retrieval of data to support project management and to provide data products and analyses to report authors. Relational systems insulate the end-user from the physical links in the database and allow the relationships between data to be easily restructured, thus responding quickly to changing needs. The program database is an integrated repository for all information relevant to the study.

Table 12.1.  Sampling summary at each site.

| Site | Habitat | Sub- habitat | Stations |
|---|---|---|---|
| GC185 (BH) Oily diffusion | Tubeworm | Adult | AT1, AT2, AT3, AT4, AT5 |
| | | Senescent | ST1, ST2 |
| | | Juvenile | JT1, JT2, JT4, JT5, JT6 |
| | Mussel | | M1, M2, M3, M4, M5 |
| | Bacterial Mat | White Mat | B1 |
| | | Red Mat | B2 |
| | Reference | | Boxcore |
| GC234 (GC) Oily diffusion | Tubeworm | Adult | AT1, AT2, AT3, AT4 |
| | | Senescent | ST1, ST2 |
| | | Juvenile | JT1, JT2, JT4, JT5 |
| | Mussel | | M1, M2 |
| | Bacterial Mat | | B |
| GC233 (BP) Brine dissolution | Tubeworm | Adult | AT1 |
| | Mussel | Inner edge | M1, M4, M7 |
| | | Outer edge | M2, M3, M5 |
| GB425 (GC) Brine dissolution | Mussel | | M1, M2 |



Figure 12.1. Example of data collection form used for CTD casts.

The central component of a relational DBMS is the table and was the first design step in constructing a database. A table is a set of information concerning a given topic. By definition, a properly designed relational database contains multiple tables.

The project database contains reference tables (e.g., Dive Log, Dive Activities, samples sediment, etc.) and tables for each sampling activity (e.g., Brine Samples, Hydrate Samples, Boxcores, etc.) and the relationship among each of the tables (Figure 12.2). The DBMS contains tables for each of the research component results (e.g., PAH, Histo, etc.)0 is shown in (Figure 12.3). Tables are in turn broken down into records, which give information about a certain item in a table, and fields, which contain discrete pieces of information about each record. As an example, the sediment sample table is organized into records (rows), with each record representing a dive, and fields (columns) named dive number, station, sample type, etc. and disposition of the sample (Figure 12.4).

## 12.3    Data Entry

Having designed the database tables, the database was then populated with data from the various program components. Forms for data entry standardized the data files. Forms that are more complex were created with lookup boxes that allowed a selection from acceptable values for entry into a given field. List boxes were also used. These permit more than one item to be associated with a given record, as is the case when one station contains multiple samples (Figure 12.5).

The program database is divided into two modules. The first module is sample/data status inventory. It consists of the files necessary to track the status and custody of all data and samples collected during the program.

The second module of the database contains the analytical results of the samples. The merging of these two modules results in the project database, as represented in (Figure 12.6).

A summary of the samples collected over the course of the program is shown in (Table 12.2). Many of the samples for a particular matrix were sub-sampled and distributed among the researchers. As results arrived from the researchers, a tracking table was populated with information on the source, analysis type and disposition of the data (Table 12.3).
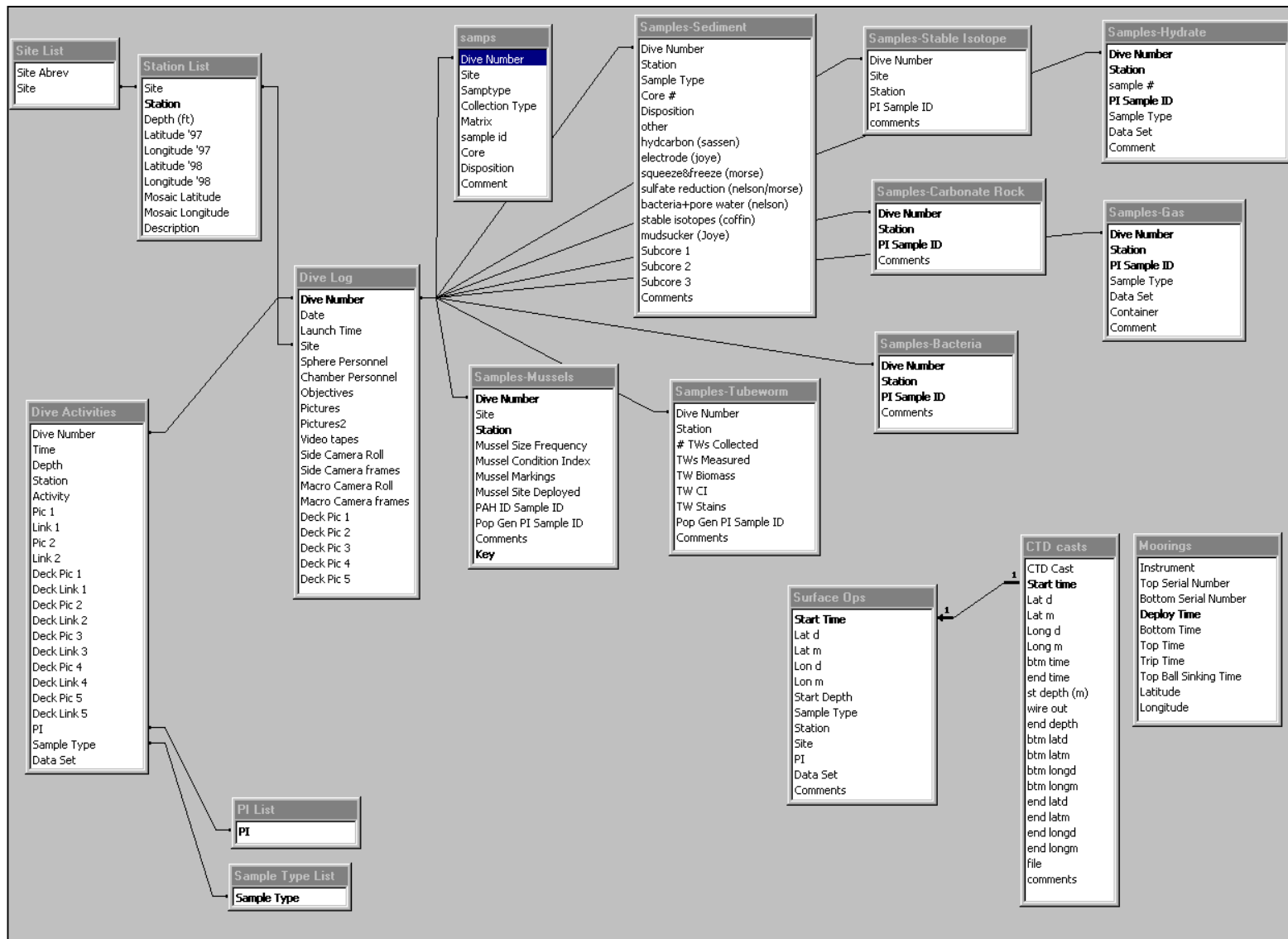
Figure 12.2. Table and relationships in the program DBMS.

Figure 12.3. Table listing of the program DBMS.

Microsoft Access - [Samples-Sediment : Table]

File  Edit  View  Insert  Format  Records  Tools  Window  Help

| Dive Num | Station | Sample Typ | Core # | Disposition | hydcarbon (sassen) | electrode (joye) | squeeze&freeze (morse) |
|---|---|---|---|---|---|---|---|
| 2875 | BHST2 | Push Core | 6 | IM can | BHST2-6a | | |
| 2885 | GBM2 | Push Core | 5 | IM can | GBM2-5 | | |
| 2881 | GCHYD1 | Scoop | | IM can | GCHYD1-2 | | |
| 2881 | GCHYD1 | Scoop | | IM can | GCHYD1-4 | | |
| 2881 | GCHYD1 | Scoop | | IM can | GCHYD1-5 | | |
| 2882 | GBM2 | Push Core | 7 | IM can | GBM2-7-2 | | |
| 2875 | BHST2 | Push Core | 6 | IM can | BHST2-6b | | |
| 2882 | GBM2 | Push Core | 7 | IM can | GBM2-7-3 | | |
| 2888 | GCAT1 | Push Core | 7 | IM can | GCAT1-7-1 | | |
| 2881 | GCHYD1 | Scoop | | IM can | GCHYD1-6 | | |
| 2881 | GCHYD1 | Scoop | | IM can | GCHYD1-7 | | |
| 2876 | BPR2 | Push Core | 2 | IM can | BPR2 | | |
| 2882 | GBM2 | Push Core | 7 | IM can | GBM2-7-1 | | |
| 2881 | GCHYD1 | Scoop | | IM can | GCHYD1-3 | | |
| 2891 | BHM3 | Mudsucker | | IM | BHM3-D2 | | |
| 2891 | BHM3 | Mudsucker | | IM | BHM3-D1 | | |
| 2882 | GBM2 | Mudsucker | | IM | GBM2-D6 | | |
| 2882 | GBM2 | Mudsucker | | IM | GBM2-D5 | | |
| 2882 | GBM2 | Mudsucker | | IM | GBM2-D1 | | |
| 2882 | GBM2 | Mudsucker | | IM | GBM2-D3 | | |
| 2882 | GBM2 | Mudsucker | | IM | GBM2-D4 | | |
| 2891 | BHM3 | Mudsucker | | IM | BHM3-D3 | | |
| 2882 | GBM2 | Mudsucker | | IM | GBM2-D2 | | |
| 0 | BHBXc1 | Box Core | 9 | IM | BHBXc1-8b | | |
| 2891 | BHM3 | Mudsucker | | IM | BHM3-D5 | | |
| 2891 | BHM3 | Mudsucker | | IM | BHM3-D6 | | |
| 0 | BHBXc1 | Box Core | 8 | IM | BHBXc1-8t | | |
| 2891 | BHM3 | Mudsucker | | IM | BHM3-D4 | | |
| 4029 | GCAT2 | Push core | 4b | hydrocarbon (Sassen) | GCAT2-4b | | |
| 0 | GCBxc1 | Box core | 8a | hydrocarbon (Sassen) | | | |
| 0 | GCBxc1 | Box core | 8b | hydrocarbon (Sassen) | | | |
| 4032 | GCAT1 | Push core | 3 | hydrocarbon (Sassen) | | | |
| 4031 | GCAT2a | Push core | 9b | hydrocarbon (Sassen) | GCAT2a-9b | | |
| 4027 | BHST1 | Push core | 9 | hydrocarbon (Sassen) | BHST1-9 | | |
| 4032 | GCAT1 | Push core | 5 | hydrocarbon (Sassen) | | | |
| 4031 | GCAT2a | Push core | 9a | hydrocarbon (Sassen) | GCAT2a-9a | | |
| 4029 | GCAT2 | Push core | 2a | hydrocarbon (Sassen) | GCAT2-2a | | |
| 4029 | GCAT2 | Push core | 2b | hydrocarbon (Sassen) | GCAT2-2b | | |
| 4031 | GCST1 | Push core | 7 | hydrocarbon (Sassen) | GCST1-7 | | |
| 4032 | GCAT1a | Push core | 7 | hydrocarbon (Sassen) | | | |
| 4029 | GCAT2 | Push core | 4a | hydrocarbon (Sassen) | GCAT2-4a | | |
| 4025 | BHAT1 | Push core | 8 | hydrocarbon | BHAT1-8 | | |
| 4031 | GCST1 | Push core | 2 | freeze (Morse) | | | |
| 4027 | BHST1 | Push core | 7 | freeze (Morse) | | | BHST1-7 |
| 4032 | GCAT1 | Push core | 1 | freeze (Morse) | | | |
| 4025 | BHAT1 | Push core | 1 | freeze | | | BHAT1-1 |
| 4025 | BHAT1 | Push core | 3 | electrode and sqeeze | | BHAT1-3 | BHAT1-3 |
| 4031 | GCAT2a | Push core | 3 | electrode (joye) and squeeze (morse | | GCAT2a-3 | GCAT2a-3 |
| 4026 | BHAT1 | Push core | 6A | electrode (joye) | | BHAT1-6A | |
| 4031 | GCST1 | Push core | 5 | electrode (joye) | | GCST1-5 | |
| 4027 | BHST1 | Push core | 5 | electrode (joye) | | BHST1-5 | |
| 4032 | GCAT1a | Push core | 9 | electrode (joye) | | | |
| 4029 | GCAT2 | Push core | 1 | electrode (joye) | | GCAT2-1 | |
| 2875 | BHST2 | Push Core | 4 | DN; CC | | | BHST2-4b |
| 2880 | GCAT1 | Push Core | 5 | DN; CC | | | GCAT1-5a |

Record: I◄ ◄ 1 ► ►I ►* of 432

Figure 12.4. Sediment sample table.

12-6

Figure 12.5.  Form designed to record surface operations with pull down menus for selecting site.

| Dive | Site | Station | Core | Sample id | Lab_no | Comments | METHANE | ETHANE | ETHYLENE | PROPANE |
|---|---|---|---|---|---|---|---|---|---|---|
| 4025 | GC185 | BHAT1 | 8 | BHAT1-8 | C31028 | | 415.4 | 2.1 | 0.9 | 1.3 |
| 4026 | GC185 | BHAT1a | 1b | BHAT1a-1b | C31029 | | 787.3 | 3.5 | 0.7 | 0.7 |
| 4026 | GC185 | BHAT1a | 2a | BHAT1a-2a | C31030 | | 150.6 | 1.3 | 0.6 | 0.6 |
| 4026 | GC185 | BHAT1a | 2a | BHAT1a-2a | C31030 | | 150.6 | 1.3 | 0.6 | 0.6 |
| 4026 | GC185 | BHAT1a | 2a | BHAT1a-2a | C31030 | | 154.2 | 1.4 | 0.7 | 0.7 |
| 4026 | GC185 | BHAT1a | 2a | BHAT1a-2a | C31030D | | 154.2 | 1.4 | 0.7 | 0.7 |
| 4026 | GC185 | BHAT1a | 2b | BHAT1a-2b | C31031 | | 5887.4 | 105.9 | 0 | 71.6 |
| 4044 | GC185 | BHAT2 | 3a | BHAT2-3a | C31049 | | 78.1 | 1.3 | 0.4 | 0.6 |
| 4044 | GC185 | BHAT2 | 3b | BHAT2-3b | C31050 | Broken Jar | | | | |
| NA | GC185 | BHBXc1 | 8b | BHBXc1-8 bottom | C31017 | Bush Hill Box Core | 182.1 | 2.5 | 0 | 0.8 |
| NA | GC185 | BHBXc1 | 8t | BHBXc1-8 top | C31016 | Broken Jar | | | | |
| 40? | GC185 | BHM3 | 7a | BHM3-7a | C31047 | | 297.1 | 3.7 | 0.5 | 1.2 |
| 40? | GC185 | BHM3 | 7b | BHM3-7b | C31048 | | 207.5 | 3.7 | 0.4 | 0.6 |
| 4046 | GC185 | BHM4 | 9 | BHM4-9 | C31057 | ST1 instead of M4 | 71049.4 | 86086.4 | 0 | 27680.8 |
| 4045 | GC185 | BHST1 | 8a | BHST1-8a | C31053 | Broken Jar | | | | |
| 4045 | GC185 | BHST1 | 8b | BHST1-8b | C31054 | | 42.5 | 0.8 | 0.4 | 0.3 |
| 4027 | GC185 | BHST1 | 9 | BHST1-9 | C31032 | | 5837.5 | 34.7 | 0.3 | 0.6 |
| 4045 | GC185 | BHST1 | 9a | BHST1-9a | C31055 | | 320.6 | 2.4 | 0.7 | 0.5 |
| 4045 | GC185 | BHST1 | 9b | BHST1-9b | C31056 | Broken Jar | | | | |
| 4045 | GC185 | BHST1a | 1a | BHST1a-1a | C31051 | Broken Jar | | | | |
| 4045 | GC185 | BHST1a | 1b | BHST1a-1b | C31052 | a = away from mar | 183.4 | 3.3 | 0.4 | 1.3 |
| NA | GC185 | BHBXc5 | 2a | BHUN1-2a | C31020 | No Sample | | | | |
| NA | GC185 | BHBXc5 | 2b | BHUN1-2b | C31021 | No Sample | | | | |
| NA | GC185 | BHBXc5 | 5a | BHUN1-5a | C31022 | Broken Jar | | | | |
| NA | GC185 | BHBXc5 | 5b | BHUN1-5b | C31023 | | 18155.6 | 64.3 | 0.1 | 25.3 |
| NA | GC185 | BHBXc5 | 2a | BHUN2-2a | C31018 | | 309 | 1.8 | 0 | 0 |
| NA | GC185 | BHBXc5 | 2b | BHUN2-2b | C31019 | Broken Jar | | | | |
| 4038 | GC233 | BPB2 | 8 | BPB2-8 | C31046 | Broken Jar | | | | |
| 4053 | GB425 | GBM2 | 3 | GBM2-3 | C31062 | | 30545.5 | 256.9 | 0 | 58.5 |
| 4032 | GC234 | GCAT1 | 3 | GCAT1-3 | C31040 | | 15.4 | 0.4 | 0.3 | 0 |
| 4032 | GC234 | GCAT1 | 5 | GCAT1-5 | C31041 | | 26 | 0.8 | 0.3 | 0 |
| 4032 | GC234 | GCAT1a | 7a | GCAT1a-7a | C31042 | Broken Jar | | | | |
| 4032 | GC234 | GCAT1a | 7a (b) | GCAT1a-7a(b) | C31043 | a = 1m away from | 29.5 | 0.4 | 0.4 | 0 |
| 4029 | GC234 | GCAT2 | 2a | GCAT2-2a | C31033 | | 94029.7 | 1728.2 | 0 | 384.8 |
| 4029 | GC234 | GCAT2 | 2b | GCAT2-2b | C31034 | | 53099.4 | 971 | 0 | 652.2 |
| 4029 | GC234 | GCAT2 | 4b | GCAT2-4 bottom | C31036 | | 66333.5 | 1288.3 | 0 | 685.5 |
| 4029 | GC234 | GCAT2 | 4a | GCAT2-4 top | C31035 | | 46320.5 | 731.3 | 0 | 367.6 |
| 4031 | GC234 | GCAT2a | 9a | GCAT2a-9a | C31038 | a = 1m away from | 428.2 | 6.1 | 1.1 | 11.5 |
| 4031 | GC234 | GCAT2a | 9b | GCAT2a-9b | C31039 | a = 1m away from | 2154.3 | 23.9 | 0.3 | 6.9 |
| 4036 | GC234 | GCB2 | 6 | GCB2-6 | C31045 | A-site - location of | 2168.1 | 12 | 0.8 | 1 |
| NA | GC234 | GCBXc1 | 8b | GCBXc1-8 bottom | C31025 | Broken Jar | | | | |
| NA | GC234 | GCBXc1 | 8a | GCBXc1-8 top | C31024 | Broken Jar | | | | |
| NA | GC234 | GCBXc2 | 6a | GCBXc2-6a | C31026 | Broken Jar | | | | |
| NA | GC234 | GCBXc2 | 6b | GCBXc2-6b | C31027 | | 55.8 | 0.4 | 0.3 | 0.3 |
| 4036 | GC234 | GCJT1 | 5 | GCJT1-5 | C31044 | | 286.4 | 3.9 | 0.8 | 1.7 |
| 4047 | GC234 | GCJT2 | 1 | GCJT2-1 | C31058 | | 70753.8 | 74828.9 | 0 | 25314.6 |
| 4047 | GC234 | GCJT2 | 1 | GCJT2-1 | C31058 | | 1563.5 | 16.7 | 0.5 | 1.8 |
| 4047 | GC234 | GCJT2 | 2t | GCJT2-2a | C31059 | | 3.3 | 0.4 | 0.4 | 0 |
| 4047 | GC234 | GCJT2 | 2b | GCJT2-2b | C31060 | Broken Jar | | | | |
| 4048 | GC234 | GCM2 | 1 | GCM2 | C31061 | | 17479.9 | 21358.2 | 0 | 23547.1 |
| 4031 | GC234 | GCST1 | 7 | GCST1-7 | C31037 | Broken Jar | | | | |

Record: |◄ ◄ | 1 | ► ►| ►* | of 52

Datasheet View

Figure 12.6. Merged modules forming a database file for headspace.

Table 12.2. Summary of the samples collected.

| Year | Site | Matrix | Sample |
|------|------|--------|--------|
| All | GB425 | Gas | 19 |
| All | GB425 | Hydrate | 19 |
| All | GB425 | Sed | 64 |
| 1 | GB425 | Mussels | 83 |
| All | GC185 | Gas | 31 |
| All | GC185 | Hydrate | 31 |
| All | GC185 | Sed | 157 |
| 1 | GC185 | Mussels | 1002 |
| 1 | GC185 | Tubeworm | 1162 |
| All | GC233 | Gas | 29 |
| All | GC233 | Hydrate | 29 |
| All | GC233 | Sed | 38 |
| 1 | GC233 | Mussels | 187 |
| All | GC234 | Gas | 41 |
| All | GC234 | Hydrate | 41 |
| All | GC234 | Sed | 164 |
| 1 | GC234 | Mussels | 741 |
| 1 | GC234 | Tubeworm | 1769 |

Table 12.3.  Tracking table.

| | Matrix | Collection | Analysis | Cru1-Jun97 | Datafile | Cru2-Jun98 | Datafile |
|---|---|---|---|---|---|---|---|
| | **NOTE** - *DB file - italics*, **XLS file – bold** | | | | | | |
| **Fisher – TW** | TW CI, GROWTH, Biomass | Sub | Cond Index | | combined yr1&2 | tubeworm growth and condition data for the MMS stations collected in 1998 | **Tw_ci978.xls** |
| **Fisher – Mus** | Mussel Size , CI - Sites | Sub | | 1997 Gulf of Mexico ring collection mussel shell length and wet weight data. | **97rclwt.xls** | condition index and percent water data of mussels collected at study sites in 1998 | **Mus98_ci.xls** |
| | Mussel Site Condition Index - Ring | Sub | Cond Index | 1997 Gulf of Mexico ring collection mussel condition index and percent water data. | **97rc_ci.xls** | shell lengths, condition index, and % water in the tissue of the mussels from the two reciprocal transplant experiments initiated in 1997 and collected in 1998 | **Must98ci.xls** |
| | Mussel Summary Ring | Sub | Mussel Summary | summary information pertaining to the mussel populations at the primary study sites from the 1997 ring collections | **97rc_sum.xls** | biomass of the mussel soft tissue. | **98rc_summar.xls** |
| **Fisher – other** | Assoc. fauna | Sub | | 97 ring collection assoc. fauna | **97rc_afau.xls** | summary table for data on associated fauna from bushmaster collections of vestimentiferan aggregations 1998 | **Faun_98.xls 97rc_afau.xls,v1** |
| | Water | Sub | H2S, CH4 | Gas Chromatography measurements of Sulfide and Methane concentrations (mM) from water sampled at dive stations in 1997 H2S, CH4 only | **F_watgc1.xls** | CO2,H2S, O2, N2, CH4, CO 14 samples | **F_watgc2**, *D_wat_c2* |
| **Sassen** | Sediment Samples | Cores | EOM | 52 samples | **Eomdata**, *D_eom_c1* | 36 samples | **eomdata**, *D_eom_c2* |
| | Sediment Samples | | HS,Fl, GC | 15 samples - PISTON | **Pisco_hs, 76333_fl 76333_gc\***, *D_sager_core76333* | | |
| | Hydrate | | C15-C32, UCM | 6 samples | **hdrate**, *D_hyd_c1* | C1-C5, delC13 | **SASSHYD\***, *D_sashyd* |
| | | MudSuck | | | | | |
| | Brine/Gas Samples | brinetrap | C1-C5 | | **JSL97_hs**, *D_HS_JSL97* | C1-C5, delC13, Hydrate ; C1-C5, brinetrap | **89715_hs**, *D_89715hs*, **BRINTP2**, *D_brintp2* |
| | Sediment Samples | | C1-C5 | | | C1-C5, delC13 | **89716_hs**, *D_hs_sed_c2* |
| | Carbonate Samples | | | | | | |

Table 12.3. (Cont.)

| | Matrix | Collection | Analysis | Cru1-Jun97 | Datafile | Cru2-Jun98 | Datafile |
|---|---|---|---|---|---|---|---|
| | | | | | | | |
| **M.Joye** | Core Samples | | | | | | |
| | Mudsucker Samples | | Mn+2, S-2, Fe | 17 dives | **Mudsjoye.xls** | | |
| | | | | | *D-mudsk_joye1* | | |
| **Kennicutt** | Tissue | | PAH | 62 samples | **pah,** *D_pahc1* | 21 samples, pooled | **89735_ar,** *D_mus_ar_c2* |
| | Tissue | | %Lip, Tot PAH | 11 samples | **totpahc1** | 21 samples | **totpahc,** *D_totpah12* |
| **J.Morse** | Sediment | Core | Pore Water Metals, Core Metals, Sulf Red | | **Morse** *,D_por_mc1,* *D_so4_mc1 D_sol_mc1* | | **Cl2, DIC2, H2S, ICP2, NUTS2, PH2, Sulfate2** |
| | Sediment | Mudsuck | | | | | |
| **E.Powell** | Mussels | | Histo | Histopath | **powell.xls** | ? | **mmsbugs.xls?** |
| | | | | | *D_histo1* | | |
| **Macko** | | | | C,N,S trap fauna | **macko97.xls** | del34S corr, box and dive | **Macko.xls** |
| **Carney** | | | | del 13C, del 15N, del S (both cruises in 1 file) | | isotopic determinations on fauna collected during dives. | **Car_iso.xls** |
| **Nelson** | | bacterial | | | **ND** | | **ND** |

## 12.4 Geospatial applications

Export files were prepared from the database for inclusion into geospatial applications. Arcview/Arcmap (ESRI) was used to generate layered displays of the program results (Figure 12.7) and spatial analyses.

Metadata files, data dictionaries, data relations and all other database documentation files were produced for all data. These data products provide all the requested data documentation information for program data and follow the guidelines established by the Federal Geographical Data Committee. Spatial information, data quality and other categories of data information are provided in this document that accompanies the program data (Figure 12.8).
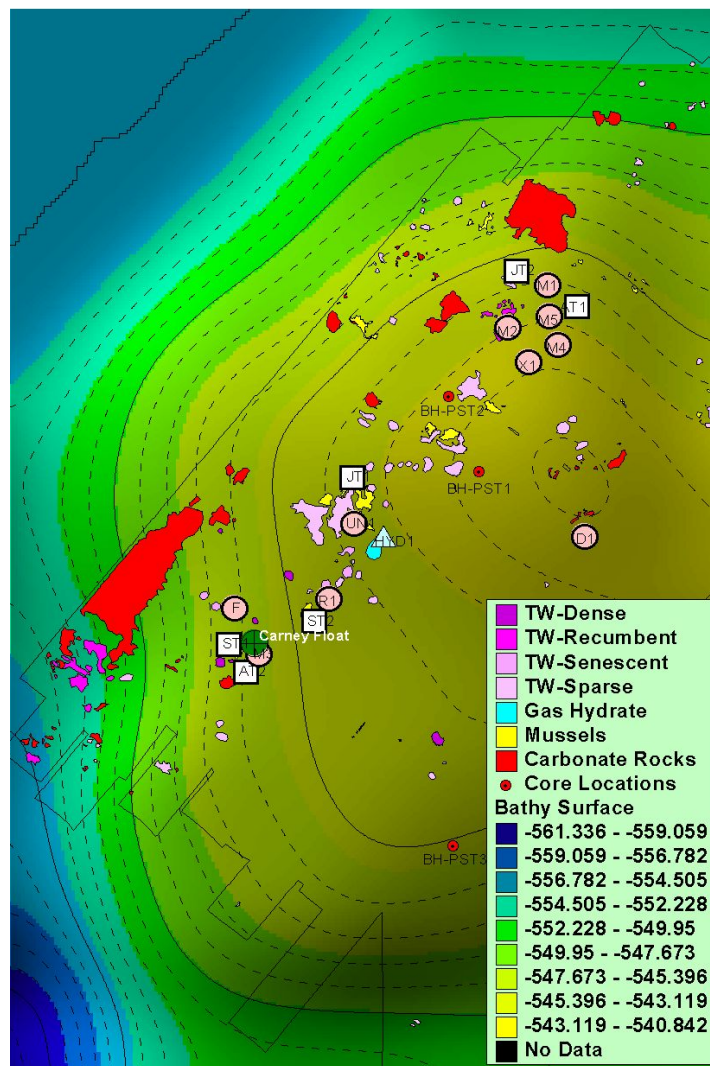


Figure 12.7. Geospatial figure with results layered over bathymetry at Bush Hill site.

**Stability and Change in the Gulf of Mexico Chemosynthetic Communities Program (CHEMO II)**

**Table of Contents**

Identification Information
Data Quality Information
Spatial Data Organization Information
Spatial Reference Information
Entity and Attribute Information
Distribution Information
Metadata Reference Information

Figure 12.8.  Metadata file and contents for program data.

# 13.0 Literature Cited

Abrams, M.A. 1996. Distribution of subsurface hydrocarbon seepage in near-surface marine sediments in Hydrocarbon Migration and Its Near-surface Expression. Edited by Schumacher, D. and M.A. Abrams. AAPG Memoir 66. Amer. Assoc. Petrol. Geol. Tulsa, OK. Pp. 1-14.

Aharon, P. 1994. Geology and biology of modern and ancient submarine hydrocarbon seeps and vents: An Introduction. Geo-Marine Letters.14: 69-73.

Ahmad, A. 1999. Phylogenetic and physiological studies of filamentous sulfur-oxidizing bacteria belonging to the genus Beggiatoa. Ph.D. dissertation thesis. University of California, Davis.

Ahmad, A., J.P. Barry, and D.C. Nelson. 1999. Phylogenetic affinity of a wide, vacuolate, nitrate-accumulating Beggiatoa sp. from Monterey Canyon, California, with Thioploca spp. Applied and Environmental Microbiology. 65(1): 270-277.

Allen, R.L. 1979. A yield model for the Foveaux Strait oyster (Ostrea lutaria) fishery. Rapports et Proces-Verbaux des Reunions Conseil International pour l'Exploration de la Mer. 175: 70-79.

Amery, G.B. 1969. Structure of Sigsbee Scarp, Gulf of Mexico. American Association of Petroleum Geologists Bulletin. 53: 2480-2482.

An, S. 1999. Nitrogen cycling and dentrification in Galveston Bay. Ph.D. dissertation thesis. Texas A&M University. College Station, TX.

An, S., and S.B. Joye. In press. Enhancement of coupled nitrification-dentrification by benthic photosynthesis in shallow estuarine sediments. Limnol. Oceanogr.

Anderson, A.L., and W.R. Bryant. 1990. Gassy sediment occurrence and properties: Northern Gulf of Mexico. Geo-Marine Letters 10: 209-220.

Anderson, R.K., R.S. Scalan, P.L. Parker, and E.W. Behrens. 1983. Seep oil and gas in Gulf of Mexico sediment. Science 222: 619-621.

Arp, A.J., J.J. Childress, and J. Fisher, C. R. 1984. Metabolic and blood gas transport characteristics of the hydrothermal vent bivalve Calyptogena magnifica. Physiological Zoology 57: 648-662.

Arp, A.J., J.J. Childress, and R.D. Vetter. 1987. The sulfide-binding protein in the blood of the vestimentiferan tube-worm, *Riftia pachyptila*, is the extracellular haemoglobin. Journal of Experimental Biology 128: 139-158.

Ausubel, F.M., R. Brent, R.E. Kingston, D.D. Moore, J.G. Seidman, J.A. Smith, and K.Strahl. 1989. Current protocols. In: Molecular Biology. John Wiley & Sons, New York.

Behrens, E. 1980. On sedimentation rates and porosity. Marine Geology 35: M11-M16.

Behrens, E.W. 1988. Geology of a continental slope oil seep, northern Gulf of Mexico. American Association of Petroleum Geologists Bulletin 72(2): 105-114.

Bergquist, D.C., C.R. fisher, and F.M. Williams. 1999. Life history characteristics and population structures of two co-occurring Vestimentiferan species at hydrocarbon seeps on the upper Louisiana Slope. EOS 80(49): OS243.

Bergquist, D.C., F.M. Williams, and C.R. Fisher. 2000. Longevity record for deep-sea invertebrate--The growth rate of a marine tubeworm is tailored to different environments. Nature 403(6769): 499-500.

Berner, R.A. 1980. Early Diagenesis: a theoretical approach. Princeton University Press, Princeton, NJ. 241 pp.

Bierbaum, R.M., and S. Ferson. 1986. Do symbiotic pea crabs decrease growth rate in mussels? Biological Bulletin 170(1): 51-61.

Biggs, D.C., and F.E. Muller-Karger. 1994. Ship and satellite observations of the chlorophyll stocks in interacting cyclone-anticyclone eddy pairs in the western Gulf of Mexico. Journal of Geophysical Research 99(C4): 2371-2384.

Black, M.B., K.M. Halanych, P.A.Y. Maas, W.R. Hoeh, J. Hashimoto, D. Desbruyeres, R.A. Lutz, and R.C. Vrijenhoek. 1997. Molecular systematics of vestimentiferan tubeworms from hydrothermal vents and cold-water seeps. Marine Biology 130(2): 141-149.

Black, M.B., R.A. Lutz, and R.C. Vrijenhoek. 1994. Gene flow among vestimentiferan tube worm (Riftia-Pachyptila) populations from hydrothermal vents of the Eastern Pacific. Marine Biology 120(1): 33-39.

Blair, N.E., and R.C. Aller. 1995. Anaerobic methane oxidation on the Amazon Shelf. Geochimica et Cosmochimica Acta 59: 3707-3715.

Blondel, P., and B.J. Murton. 1997. Handbook of seafloor sonar imagery. John Wiley and Sons, Inc. New York. 314 pp.

Boland, G.S. 1986. Discovery of co-occurring bivalve *Acesta* sp. and chemosynthetic tube worms Lamellibrachia. Nature (London) 323: 759.

Boss, K.J. 1968. New species of Vesicomyidae from the Gulf of Darien, Caribbean Sea (Bivalvia; Mollusca). Bulletin of Marine Science 18(3): 731-748.

Bouma, A.H., and W.R. Bryant. 1994. Physiographic features on the northern Gulf of mexico continental slope. Geo-Marine Letters 14: 252-263.

Bower, S.M., G.R. Meyer, and J.A. Boutillier. 1996. Stained prawn disease (SPD) of Pandalus platyceros in British Columbia, Canada, caused by a rickettsial infection. Diseases of Aquatic Organisms 24(1): 41-54.

Brendel, P.J. 1995. Development of a mercury thin film voltammetric microelectrode for the determination of biogeochemically important redox species in porewaters of marine and freshwater sediments. Ph.D. dissertation thesis. University of Delaware, Lewes, DE.

Brendel, P.J., and G.W. Luther. 1995. Development of a gold amalgam voltammetric microelectrode for the determination of dissolved Fe, Mn, O-2, and S(-Ii) in porewaters of marine and fresh water sediments. Environmental Science & Technology 29(3): 751-761.

Bright, T.J., P.A. LaRock, R.D. Lauer, and J.M. Brooks. 1980. A brine seep at the east Flower Garden Bank, northwestern Gulf of Mexico. Int. Revue Ges. Hydrobiol 65: 321-335.

Brock, T.D., and H.G. Schlegel. 1989. Introduction to autotrophic bacteria. Science and Technology Publishers, Madison, WI.

Brooks, J.M. 1984. Current and hydrographic variability in the northwestern Gulf of Mexico. Journal of Geophysical Research 89(C3): 8022-8032.

Brooks, J.M., A.L. Anderson, R. Sassen, I.R. MacDonald, M.C. Kennicutt, II, and N.L. Guinasso, Jr. 1994. Hydrate occurrence in shallow subsurface cores from continental slope sediments. In: International Conference on Natural Gas Hydrates., Annals of the New York Academy of Sciences. Pp. 381-391.

Brooks, J.M., H.B. Cox, W.R. Bryant, M.C. Kennicutt, II, R.G. Mann, and T.J. McDonald. 1986. Association of gas hydrates and oil seepage in the Gulf of Mexico. Advances in Organic Geochemistry 10: 221-234.

Brooks, J.M., M.C. Kennicutt II, C.R. Fisher, S.A. Macko, K. Cole, J.J. Childress, R.R. Bidigare, and R.D. Vetter. 1987. Deep-sea hydrocarbon seep communities: evidence for energy and nutritional carbon sources. Science 238: 1138-1142.

Brooks, J.M., M.C. Kennicutt, II, R.R. Fay, T.J. McDonald, and R. Sassen. 1984. Thermogenic gas hydrates in the Gulf of Mexico. Science 223: 696-698.

Brooks, J.M., D.A. Wiesenburg, H. Roberts, R.S. Carney, I.R. MacDonald, C.R. Fisher, J. Guinasso, N. L., W.W. Sager, S.J. McDonald, J. Burke, R., P. Aharon, and T.J. Bright. 1990. Salt, seeps, and symbiosis in the Gulf of Mexico. EOS 71: 1772-1773.

Bryant, W.R., D.A. Bean, and T.M. Dellapenna. 1999. Deep water high velocity currents and the presence of mega-furrows on the continental rise south of the Sigsbee Escarpment, northwest Gulf of Mexico. EOS, Transactions--American Geophysical Union 80: OS222.

Bryant, W.R., J.R. Bryant, M.H. Feeley, and G.R. Simmons. 1990. Physiographic and bathymetric characteristics of the continental slope, northwest Gulf of Mexico. Geo-Marine Letters 10:182-199.

Bryant, W.R., J.Y. Liu, and J. Pontheir. 1995. Engineering and geological constraints of intraslope basins and submarine canyons of the northwestern Gulf of Mexico. Transactions--Gulf Coast Association of Geological Societies 45: 95-101.

Bryant, W.R., and L.B. Roemer. 1983. Structure of the continental shelf and slope of the northern Gulf of Mexico and its geo-hazards and engineering constraints. in Handbook of Geophysical Exploration at Sea. Edited by Geyer, R.A. and J.R. Moore. CRC Press, Boca Raton, FL. Pp. 123-185.

Bryant, W.R., G.R. Simmons, and P. Grim. 1991. The morphology and evolution of basins on the continental slope, northwest Gulf of Mexico. Transactions--Gulf Coast Association of Geological Societies 51: 73-82.

Buchanan, J.S. 1978. Cytological studies on a new species of rickettsia found in association with a phange in the digestive gland of the marine bivalve mollusk, *Tellina tenius* (da Costa). Journal of Fish Diseases 1: 27-43.

Cabot, E.L., and A.T. Beckenbach. 1989. Simultaneous editing of multiple nucleic-acid and protein sequences with ESEE. Computer Applications in the Biosciences 5(3): 233-234.

Cajaraville, M.P., and E. Angulo. 1991. Chlamydia-like organisms in digestive and duct cells of mussels from the Basque Coast. Journal of Invertebrate Pathology 58(3). 381-386.

Callender, W.R., and E.N. Powell. 1997. Autochthonous death assemblages from chemoautotrophic communities at petroleum seeps: paleoproduction, energy flow and implications for the fossil record. Hist. Biol. 12: 165-198.

Callender, W.R., G.M. Staff, E.N. Powell, and I.R. MacDonald. 1990. Gulf of Mexico hydrocarbon seep communities: V. Biofacies and shell orientation of autochthonous shell beds below storm wave base. Palaios 5: 2-14.

Campbell, K.J. 1999. Deepwater geohazards: How significant are they? The Leading Edge. 18: 514-519.

Canfield, D.E. 1989. Reactive iron in marine sediments. Geochimica Et Cosmochimica Acta 53(3): 619-632.

Canfield, D.E., R. Raiswell, and S. Bottrell. 1992. The Reactivity of Sedimentary Iron Minerals Toward Sulfide. American Journal of Science 292(9): 659-683.

Carney, R.S. 1994. Consideration of the oasis analogy for chemosynthetic communities at Gulf of Mexico hydrocarbon vents. Geo-Marine Letters. 14(2-3): 149-159.

Carson, B., and E.J. Screaton. 1998. Fluid flow in accretionary prisms: evidence for focused, time-variable discharge. Rev. Geophys 36(3): 329-351.

Cary, C., B. Fry, H. Felbeck, and R.D. Vetter. 1989. Multiple trophic resources for a chemoautotrophic community at a cold water brine seep at the base of the Florida Escarpment. Marine Biology 100: 411-418.

Cary, S.C., W. Warren, E. Anderson, and S.J. Giovannoni. 1993. Identification and localization of bacterial endosymbionts in hydrothermal vent taxa with symbiont-specific polymerase-chain reaction amplification and in site hybridization. Mol. Mar. Biol. Biotechnol 2: 51-62.

Cavanaugh, C.M. 1985. Symbiosis of chemoautotrophic bacteria and marine invertebrates from hydrothermal vents and reducing sediments. Bulletin Biological Society Washington 6: 373-388.

Cavanaugh, C.M., S.L. Gardiner, M.L. Jones, H.W. Jannasch, and J.B. Waterbury. 1981. Prokaryotic cells in the hydrothermal vent tube worm Riftia pachyptila Jones: possible chemoautotrophic symbionts. Science 213: 340-341.

Cavanaugh, C.M., P.R. Levering, J.S. Maki, R. Mitchell, and M.E. Lidstrom. 1987. Symbiosis of methylotrophic bacteria and deep-sea mussels. Nature (London) 325: 346-348.

Childress, J.J., A.J. Arp, and C.R. Fisher. 1984. Metabolic and blood characteristics of the hydrothermal vent tube worm Riftia-Pachyptila. Marine Biology 83(2): 109-124.

Childress, J.J., C.R. Fisher, J.M. Brooks, M.C. Kennicutt, II, R. Bidigare, and A. Anderson. 1986. A methanotrophic marine mulluscan (Bivalvia, Mytilidae) symbiosis: mussels fueled by gas. Science 233: 1306-1308.

Clark, A.G., and L.E. Keith. 1988. Variation among extracted lines of drosophila-melanogaster in triacylglycerol and carbohydrate storage. Genetics 119(3): 595-607.

Cochrane, J.D., and F.J. Kelly. 1986. Low-frequency circulation on the Texas-Louisiana continental shelf. Journal of Geophysical Research. 91c9. 10645-10659.

Coleman, D.D., L. Chao-Li, K.C. Hackley, and S.R. Pelphrey. 1996. Isotopic identification of landfill methane. Env. Geosciences 2: 95-103.

Coleman, J.M., H.H. Roberts, and W.R. Bryant. 1991. Late quaternary sedimentation in The Gulf of Mexico Basin. Edited by A. Salvador. Geological Society of America. Boulder, CO. J: 325-352

Cook, D., and P. D'Onfro. 1991. Jolliet Field thrust fault structure and stratigraphy Green Canyon Block 184, offshore Louisiana. Transactions--Gulf Coast Association of Geological Societies. XLI. 100-121.

Corliss, J.B., J. Dymond, L. Gordon, J.M. Edmond, R.P. von Herzen, R.D. Ballard, K. Green, D. Williams, A. Bainbridge, K. Crane, and T.H. van Andel. 1979. Submarine thermal springs on the Galápagos Rift. Science 203: 1073-1083.

Corthay, J.E., II. 1997. Delineation of a massive seafloor hydrocarbon seep, overpressured acquifer sands, and shallow gas reservoirs, Louisiana continental slope, Paper OTC 8594. In: Offshore Technology Conference, Houston, TX.

Coustau, C., F. Renaud, B. Delay, I. Robbins, and M. Mathieu. 1991. Mechanisms involved in parasitic castration--invitro effects of the trematode Prosorhynchus-Squamatus on the gametogenesis and the nutrient storage metabolism of the marine bivalve mollusk Mytilus-Edulis. Experimental Parasitology 73(1): 36-43.

Cressie, N.A.C. 1991. Statistics for spatial data. John Wiley and Sons, New York. 900 pp.

Crill, P.M., and C.S. Martens. 1987. Biogeochemical cycling in an organic-rich coastal marine basin. Temporal and Spatial Variations in Sulfate Reduction Rates. Geochimica Et Cosmochimica Acta 51(5): 1175-1186.

Curtis, L.A. 1996. The probability of a marine gastropod being infected by a trematode. Journal of Parasitology 82(5): 830-833.

Curtis, L.A. 1997. Ilyanassa obsoleta (Gastropoda) as a host for trematodes in Delaware estuaries. Journal of Parasitology 83: 793-803.

Degens, E.T., M. Behrendt, B. Gottard, and E. Reppmann. 1968. Metabolic fractionation of carbon isotopes in marine plankton II. Data on samples collected off the coast of Peru and Ecuador. Deep-Sea Research 15: 11-20.

Degens, E.T., R.R.L. Guillard, W.M. Sackett, and J.A. Hellburst. 1968. Metabolic fractionation of carbon isotopes in marine plankton I: temeperature and respiration experiments. Deap-Sea Research 15: 1-9.

Desbruyeres, D., and A. Toulmond. 1998. A new species of hesionid worm, *Hesiocaeca methanicola* sp. nov. (Polychaeta: Hesionidae), living in ice-like methane hydrates in the deep Gulf of Mexico. Cah. Biol. 39 (March): 93-98.

Devol, A.H., and A. S.I. 1981. Are high rates of sulphate reduction associated with anaerobic oxidation of methane? Nature. 291: 407-408.

Dickens, G.R., C.K. Paull, P. Wallace, and O.L.S. Party. 1997. Direct measurement of in situ methane quantities in a large gas reservoir. Nature. 385: 426-428.

DiMarco, S.F. 2000. Personal communication. Dr. Steven F. DiMarco, Department of Oceanography, Texas A&M University, College Station, TX. Kindly performed the tidal calculations presented in Table 5.2, on the current meter data from GC184 using the methods described in MiMarco and Reid, 1998.

DiMarco, S.F., and R.O. Reid. 1998. Characterization of the principal tidal constituents on the Texas-Louisiana shelf. Journal of Geophysical Research. 103(C2): 3093-3109.

Distel, D.L., H. Felbeck, and C.M. Cavanaugh. 1994. Evidence for phylogenetic congruence among sulfur-oxidizing chemoautotrophic bacterial endosymbionts and their bivalve hosts. Journal of Molecular Evolution 38(5): 533-542.

Durand, P., O. Gros, L. Frenkiel, and D. Prieur. 1996. Phylogenetic characterization of sulfur-oxidizing bacterial endosymbionts in three tropical Lucinidae by 16S rDNA sequence analysis. Molecular Marine Biology and Biotechnology 5(1): 37-42.

Ellis, M.S., R.D. Barber, R.E. Hillman, Y. Kim, and E.N. Powell. 1998a. Gonadal analysis. In: Cantille, A.Y and G.C. Lauenstein, eds. Sampling and analytical methods of the national status and trends mussel watch project: 1993-1996 update. NOS ORCA 130. National Oceanic and Atmospheric Administration.

Ellis, M.S., R.D. Barber, R.E. Hillman, Y. Kim, and E.N. Powell. 1998b. Histopathology analysis. In: Cuntille, A.Y and G.C. Lauenstein, eds. "Sampling and analytical methods of the national status and trends mussel watch project: 1993-1996 update (G. C. Lauenstein and A. Y. Cantillo, eds.). NOS ORCA 130. National Oceanic and Atmospheric Administration.

Ellis, M.S., K.S. Choi, T.L. Wade, E.N. Powell, T.J. Jackson, and D.H. Lewis. 1993. Sources of local variation in polynuclear aromatic hydrocarbon and pesticide body burden in oysters (Crassostrea-Virginica) from Galveston Bay, Texas. Comparative Biochemistry and Physiology C-Pharmacology Toxicology & Endocrinology 106(3): 689-698.

Elston, R.A., and M.G. Peacock. 1984. A Rickettsiales-like infection in the Pacific Razor Clam, Siliqua-Patula. Journal of Invertebrate Pathology 44(1): 84-96.

Epping, E.H.G., and W. Helder. 1997. Oxygen budgets calculated from in situ oxygen microprofiles for Northern Adriatic sediments. Continental Shelf Research 17(14): 1737-1764.

Escorcia, S.P. 2000. Pore water sulfide distributions and sediment interface fluxes in chemosynthetic communities in the Gulf of Mexico. Masters thesis. Texas A&M University, College Station, TX.

Escorcia, S.P., I.R. MacDonald, and S.B. Joye. 1999. Spatial and inter-annual variation of sulfide fluxes in chemosynthetic communities in the Gulf of Mexico. In: Ocean Science Meeting. American Society of Limnologists and Oceanographers, Santa Fe, NM. 63 pp.

Espedal, H.A., and T. Wahl. 1999. Satellite SAR oil spill detection using wind history information. Int. J. Remote Sensing 20(1): 49-65.

Felbeck, H., J. Childress, and G. Somero. 1981. Calvin-Benson cycle and sulphide oxidation enzymes in animals from sulphide-rich habitats. Nature. 293: 291-293.

Feldman, R.A., M.B. Black, C.S. Cary, R.A. Lutz, and R.C. Vrijenhoek. 1997. Molecular phylogenetics of bacterial endosymbionts and their vestimentiferan hosts. Mol. Mar. Biol. Biotechnol. (6): 268-277.

Feller, R.J., and E.D. Gallagher. 1982. Antigenic similarities among estuarine soft-bottom benthic taxa. Oecologia 52: 305-310.

Feller, R.J., G.L. Taghon, E.D. Gallagher, G.E. Kenny, and P.A. Jumars. 1979. Immunological methods for food web analysis in a soft-bottom benthic community. Marine Biology 54: 61-74.

Fisher, C. 1993. Oxidation of methane by deepsea mytilids in the Gulf of Mexico In: Biogeochemistry of Global Change: Readiatively Active Trace Gases. In: Ormerland, R.S., ed. Chapman and Hull, New York.

Fisher, C.R. 1990. Chemoautotrophic and methanotrophic symbioses in marine invertebrates. Reviews in Aquatic Sciences. 2(3/4): 399-436.

Fisher, C.R., J.J. Childress, S.A. Macko, and J.M. Brooks. 1994. Nutritional interactions in Galapagos Rift hydrothermal vent communities--inferences from stable carbon and nitrogen isotope analyses. Marine Ecology--Progress Series. 103(1-2): 45-55.

Fisher, C.R., I.R. MacDonald, R. Sassen, C.M. Young, S.A. Macko, S. Hourdez, R.S. Carney, S. Joye, and E. McMullin. 2000. Methane ice worms: Hesiocaeca methanicola colonizing fossil fuel reserves. Naturwissenschaften. 87(4): 184-187.

Fisher, C.R., I.A. Urcuyo, M.A. Simpkins, and E. Nix. 1997. Life in the slow lane: growth and longevity of cold-seep vestimentiferans. Marine Ecology. 18(1): 83-94.

Ford, S.E., E.N. Powell, J.M. Klinck, and E.E. Hofmann. In press. Modeling the MSX parasite in eastern oyster (Crassostrea virginica) populations. I. Model development, implementation and verification. Journal of Shellfish Research.

Forristall, G.Z., K.J. Schaudt, and C.K. Cooper. 1992. Evolution and kinematics of a loop current eddy in the Gulf of Mexico during 1985. Journal of Geophysical Research 97(C2): 2173-2184.

Fossing, H., T.G. Ferdelman, and P. Berg. 2000. Sulfate reduction and methane oxidation in continental margin sediments influenced by irrigation (South-East Atlantic off Namibia). Geochimica et Cosmochimica Acta. 64: 897-910.

Friedman, C.S., M. Thomson, C. Chun, P.L. Haaker, and R.P. Hedrick. 1997. Withering syndrome of the black abalone, *Haliotis cracherodii* (Leach): water temperature, food availability, and parasites as possible causes. Journal of Shellfish Research. 16(2): 403-411.

Fries, C.R., S.B. Grau, and M.R. Tripp. 1991. Rickettsiae in the cytoplasm of gill epithelial cells of the soft-shelled clam, Mya-Arenaria. Journal of Invertebrate Pathology. 57(3): 443-445.

Friocourt, M.P., G. Bodennec, and F. Berthou. 1985. Determination of polyaromatic hydrocarbons in scallops (Pecten-Maximus) by Uv fluorescence and Hplc combined with Uv and fluorescence detectors. Bulletin of Environmental Contamination and Toxicology. 34(2): 228-238.

Fry, B. 1991. Stable isotope diagrams of fresh-water food webs. Ecology. 72(6): 2293-2297.

Gage, J.D., and P. Tyler. 1991. Deep-Sea Biology. Cambridge University Press. Cambridge, MA. 509 pp.

Gallaway, B.J. 1988. Northern Gulf of Mexico continental slope study, final report. OCS Study U.S. Dept. of the Interior, Minerals Management Service, Gulf of Mexico OCS Region, New Orleans, LA. OCS Study MMS 88-0053.

Gallaway, B.J., L.R. Martin, and G.F. Hubbard. 1990. Characterization of the chemosynthetic fauna at Viosca Knoll Block 826. Letter report to Oryx Energy, Inc. LGL Ecological Research Associates, Inc.

Gee, J.M., and J.T. Davey. 1986. Stages in the life history of Mytilicola Intestinalis Steuer, a copepod parasite of Mytilus-Edulis(L), and the effect of temperature on their rates of development. Journal Du Conseil. 42(3): 254-264.

Glud, R.N., J.K. Gundersen, B.B. Jorgensen, N.P. Revsbech, and H.D. Schulz. 1994. Diffusive and total oxygen uptake of deep-sea sediments in the eastern South Atlantic Ocean --in-situ and laboratory measurements. Deep-Sea Research, Part I--Oceanographic Research Papers. 41(11-12): 1767-1788.

Goericke, R., and B. Fry. 1994. Variations of marine plankton delta-C-13 with latitude, temperature, and dissolved CO2 in the world ocean. Global Biogeochemical Cycles. 8 (1): 85-90.

Goericke, R., J.P. Montya, and B. Fry. 1994. Physiology of isotopic fractionation in algae and cyanobacteria in Stable Isotopes In: Lajtha, K. and R.H. Michner, eds. Ecology and Environmental Sciences. Blackwell Scientific Publications. Pp. 187-221.

Gonella, J. 1972. A rotary component method for analyzing meteorological and oceanographic vector time series. Deep Sea Res. 19: 833-846.

Green, R.H., and P. Montagna. 1996. Implications for monitoring: Study designs and interpretation of results. Canadian Journal of Fisheries and Aquatic Sciences. 53(11): 2629-2636.

Gros, O., A. Darrasse, P. Durand, L. Frenkiel, and M. Moueza. 1996. Environmental transmission of a sulfur-oxidizing bacterial gill endosymbiont in the tropical lucinid

bivalve *Codakia orbicularis*. Applied and Environmental Microbiology. 62(7): 2324-2330.

Gross, O.P., K.C. Hood, L.M. Wenger, and S.C. Harrison. 1995. Seismic imaging and analysis of source and migration within an integrated hydrocarbon system study: Northern Gulf of Mexico Basin. In: First Latin American Geophysical Conference, Rio de Janeiro, Brazil. 4 pp.

Gundersen, J.K., and B.B. Jorgensen. 1990. Microstructure of diffusive boundary layers and the oxygen-uptake of the seafloor. Nature. 345(6276): 604-607.

Gustafson, R.G., R.D. Turner, R.A. Lutz, and R.C. Vrijenhoek. 1998. A new genus and five new species of mussels (Bivalvia, Mytilidae) from deep-sea sulfide/hydrocarbon seeps in the Gulf of Mexico. Malacologia. 40(1-2): 63-112.

Hecker, B. 1985. Fauna from a cold sulfur-seep in the Gulf of Mexico: comparisons with hydrothermal vent communities and evolutionary implications. Bulletin Biological Society Washington 6: 465-474.

Henry, P., X. Le Pichon, S. Lallemant, S. Lance, J.B. Martin, J.P. Foucher, A. Fiala-Médioni, F. Rostek, N. Guilhaumou, V. Pranal, and M. Castrec. 1996. Fluid flow in and around a mud volcano field seaward of the Barbados accretionary wedge: results from Manon cruise. J. Geophys. Res. 101(B9): 20297-20323.

Higgins, D.G., A.J. Bleasby, and R. Fuchs. 1992. Clustal-V: Improved software for multiple sequence alignment. Computer Applications in the Biosciences. 8(2): 189-191.

Hilde, T.W.C., R.L. Carlson, A.F. Gangi, M.C. Lee, S.F. Dwan, C.W. Kue, C.H. Herrick, P. Devall, P. Alleman, C.J. Sonnier, J. Moore, T. Richards, J. Ross, and R. Miller. 1991. [TAMU]2: New generation seafloor mapping technology. Sea Technology. 32: 45-48.

Hoehler, T.M., M.J. Alperin, D.B. Albert, and C.S. Martens. 1994. Field and laboratory studies of methane oxidation in an anoxic marine sediment; evidence for a methanogen-sulfate reducer consortium. Global Biogeochemical Cycles. 8: (451-463).

Hopkins, S.H. 1954. The American species of trematode confused with Bucephalus (Bucephalus haimeanus). Parasitology. 44: 353-370.

Hopkins, S.H. 1957. Our present knowledge of the oyster parasite Bacephalus. Proceedings of the National Shellfisheries Association. 47: 58-61.

Hopkins, S.H. 1958. Trematode parasites of *Donax variabilis* at Mustang Island, Texas. Publications of the Institute of Marine Sciences of the University of Texas. 5: 301-311.

Hovland, M., and A.G. Judd. 1988. Seabed pockmarks and seepages. Graham & Trotman, Boston, MA 293 pp.

Huhnerfuss, H., W. Alpers, and F. Witte. 1989. Layers of different thicknesses in mineral-oil spills detected by grey level textures of real aperature radar images. International Journal of Remote Sensing. 10(6): 1093-1099.

Humphris, C.C., Jr. 1979. Salt movement in continental slope, northern Gulf of Mexico. American Association of Petroleum Geologists Bulletin. 63(781-798).

Iversen, N., and B.B. Jørgensen. 1985. Anaerobic methane oxidation rates at the sulfate-methane transition in marine sediments from Kattegat and Skagerrak (Denmark). Limnology and Oceanography. 30: 944-955.

Jackson, M.P.A., and C.J. Talbot. 1986. External shapes, strain rates, and dynamics of salt structures. Geological Society America Bulletin. 97: 305-323.

Jackson, T.J., T.L. Wade, T.J. McDonald, D.L. Wilkinson, and J.M. Brooks. 1994. Polynuclear aromatic hydrocarbon contaminants in oysters from the Gulf of Mexico (1986-1990). Environmental Pollution. 83(3): 291-298.

James, A.T., and B.J. Burns. 1984. Microbial alteration of subsurface gas accumulations. AAPG Bulletin. 68: 957-960.

Jannasch, H. 1989. Chemosynthetically sustained ecosystems in the deep sea. In: Schiegel, H.G. and B. Bowien, eds. Autotrophic Bacteria. Springer-Verlag, Berlin. Pp. 147-166.

Johnson, H.P., and M. Helferty. 1990. The geological interpretation of side-scan sonar. Reviews of Geophysics. 28(4): 357-380.

Johnson, M.A., and M. Lepennec. 1995. Association between the mollusk bivalve Loripes Lucinalis and a chlamydia-like organism, with comments on its pathogenic impact, life-cycle and possible mode of transmission. Marine Biology. 123(3): 523-530.

Johnson, P.T. 1984. A rickettsia of the blue king crab, *Paralithodes platypus*. Journal of Invertebrate Pathology. 44(1): 112-113.

Jukes, T.H., and C.R. Cantor. 1969. Evolution of protein molecules. In: Munro, H.N., ed. Mammalian Protein Metabolism. 21-132. Academic Press, New York. Pp. 21-132.

Julian, D., F. Gaill, E. Wood, A.J. Arp, and C.R. Fisher. 1999a. Roots as a site of hydrogen sulfide uptake in the hydrocarbon seep vestimentiferan Lamellibrachia sp. Journal of Experimental Biology. 202(17): 2245-2257.

Julian, D., S.L. Wieting, S.L. Seto, M.R. Bogan, and A.J. Arp. 1999b. Thiosulfate elimination and permeability in a sulfide-adapted marine invertebrate. Physiological and Biochemical Zoology. 72(4): 416-425.

Juliano, S.A., and F.M. Williams. 1985. On the evolution of handling time. Evolution. 39(1): 212-215.

Jumars, P.A., L.M. Mayer, J.W. Deming, J.A. Baross, and R.A. Wheatcroft. 1990. Deep-sea deposit feeding strategies suggested by environmental and feeding constraints. Philosophical Transactions of the Royal Society of London Series A--Mathematical, Physical and Engineering Sciences. 331(1616): 85-101.

Kaluza, M.J., and E.H. Doyle. 1996. Detecting fluid migration in shallow sediments: Continental slope environment, Gulf of Mexico. In: Schumacher, D. and Abrams, M.S., Hydrocarbon Migration and its Near-surface Expression. Memoir 66 pp. 15-26. American Association of Petroleum Geologists, Tulsa, OK.Memoir 66: 15-16.

Kaluzny, S.P., S.C. Vega, T.P. Cardoso, and A.A. Shelly. 1998. S+SpatialStats user's manual for Windows and UNIX. Springer Verlag, New York.

Kennicutt, M.C., J.M. Brooks, R.R. Bidigare, R.R. Fay, T.L. Wade, and T.J. McDonald. 1985. Vent-type taxa in a hydrocarbon seep region on the Louisiana Slope. Nature. 317(6035): 351-353.

Kennicutt, M.C., J.M. Brooks, R.R. Bidigare, and G.J. Denoux. 1988a. Gulf of Mexico hydrocarbon seep communities:  I. Regional distribution of hydrocarbon seepage and associated fauna. Deep-Sea Research. 35: 1639-1651.

Kennicutt, M.C., II, J.M. Brooks, and G.J. Denoux. 1988b. Leakage of deep, reservoired petroleum to the near surface on the Gulf of Mexico continental slope. Marine Chemistry. 24: (39-59).

Kennicutt, M.C., R.A. Burke, I.R. Macdonald, J.M. Brooks, G.J. Denoux, and S.A. Macko. 1992. Stable isotope partitioning in seep and vent organisms-- chemical and ecological significance. Chemical Geology. 101(3-4): 293-310.

Kennicutt, M.C., J. Sericano, T. Wade, F. Alcazar, and J.M. Brooks. 1987. High-molecular weight hydrocarbons in the Gulf of Mexico continental slope sediment. Deep-Sea Research. 34(3): 403-424.

Kent, M.L., R.A. Elston, M.T. Wilkinson, and A.S. Drum. 1989. Impaired defense mechanisms in bay mussels, Mytilus-Edulis, with hemic neoplasia. Journal of Invertebrate Pathology. 53(3): 378-386.

Kim, Y., and E.N. Powell. 1998. Influence of climate change on interannual variation in population attributes of Gulf of Mexico oysters. Journal of Shellfish Research. 17: 265-274.

Kim, Y., E.N. Powell, T.L. Wade, B.J. Presley, and J. Sericano. 1998. Parasites of sentinel bivalves in the NOAA Status and Trends Program: Distribution and relationship to contaminant body burden. Marine Pollution Bulletin. 37: 45-55.

Kirwan, A.D., W.J. Merrell, J.K. Lewis, and R.E. Whitaker. 1984. Lagrangian observations of an anticyclonic ring in the western Gulf of Mexico.

Kojima, S., T. Hashimoto, M. Hasegawa, S. Murata, S. Ohta, H. Seki, and N. Okada. 1993. Close phylogenetic relationship between vestimentifera (tube worms) and annelida revealed by the amino-acid sequence of elongation factor-1-alpha. Journal of Molecular Evolution. 37(1): 66-70.

Kojima, S., R. Segawa, J. Hashimoto, and S. Ohta. 1997. Molecular phylogeny of vestimentiferans collected around Japan, revealed by the nucleotide sequences of mitochondrial DNA. Marine Biology 127 (3): 507-513.

Kornacki, A.S., J.W. Kendrick, and J.L. Berry. 1994. The impact of oil and gas vents and slicks on petroleum exploration in the deepwater Gulf of Mexico. Geo-Marine Letters 14(2/3): 160-169.

Krueger, D.M., R.G. Gustafson, and C.M. Cavanaugh. 1996. Vertical transmission of chemoautotrophic symbionts in the bivalve *Solemya velum* (Bivalvia: Protobranchia). Biological Bulletin 190(2): 195-202.

Kumar, S., K. Tamura, and M. Nei. 1994. MEGA: Molecular evolutionary genetics analysis software for microcomputers. Computer Applications in the Biosciences 10 (2): 189-191.

Laird, M. 1961. Microecological factors in oyster epizootics. Canadian Journal of Zoology 39: 449-485.

Lane, D.J. 1991. rDNA sequencing in nucleic acid techniques. In: Stacketbrandt, E. and M. Goodfellow, eds. Bacterial Systematics. John Wiley & Sons, New York. Pp.115-175.

Larkin, J., P. Aharon, and M.C. Henk. 1994. Beggiatoa in microbial mats at hydrocarbon vents in the Gulf of Mexico and warm mineral springs, Florida. Geo-Marine Letters. 14 (2/3): 97-103.

Larkin, J.M., and W.R. Strohl. 1983. Beggotia, thiothrix, and thioplaca. Annual Review of Microbiology. 37: 341-367.

Leben, R.R., G.H Born, and B.R. Engebreth, 2002. Operational Altimeter Data Processing for Mesoscale Monitoring, Marine Geodesy 25(1):3-18.

Leben, R.R., and G.H. Born. 1993. Tracking loop current eddies with satellite altimetry. Adv. Space Res. 13 (11): 325-333.

Leben, R.R., G.H. Born, J. Thompson, and C. Fox. 1990. Mean sea surface and variability of the Gulf of Mexico using GEOSAT altimetry data. Journal of Geophysical Research. 95 (C3): 3025-3032.

Lee, C. 1995. Geology of hydrocarbon seeps on the Northern Gulf of Mexico continental slope. Ph.D. dissertation thesis. Texas A&M University, College Station, TX.

LeGall, G.,D. Chagot, E. Mialhe, and H. Grizel. 1988. Branchial rickettsiales-like infection associated with a mass mortality of sea scallop Pecten-maximus. Diseases of Aquatic Organisms. 4(3): 229-232.

Lewis, J.K., and A.D. Kirwan. 1987. Genesis of a Gulf of Mexico ring as determined from kinematic analysis. Journal of Geophysical Research. 92(C11): 727-740.

Lin, S., and J.W. Morse. 1991. Sulfate reduction and iron sulfide mineral formation in Gulf of Mexico anoxic sediments. American Journal of Science. 291: 55-89.

Liu, J.Y. 1997. Surficial geological characteristics of the Alaminos Canyon, Gulf of Mexico. Ph.D. dissertation thesis. Texas A&M University, College Station, TX.

Lonsdale, P. 1977. Clustering of suspension-feeding macrobenthos near abyssal hydrothermal vents at oceanic spreading centers. Deep-Sea Research. 24: 857-863.

Lowrie, A. 1987. Model of upper Cenozoic geologic evolution of the Louisiana slope. Transactions--Gulf Coast Association of Geological Societies. 37: 139-151.

MacDonald, I.R. 1992. Sea-floor brine pools affect behavior, mortality, and preservation of fishes in the Gulf of Mexico: Lagerstätten in the making? Palaios. 7: 383-387.

MacDonald, I.R. 1998a. Habitat formation at Gulf of Mexico hydrocarbon seeps. Cahiers de Biologie Marine. 39(3-4): 337-340.

MacDonald, I.R. 1998b. Stability and change in Gulf of Mexico chemosynthetic communities interim report. U.S. Dept. of the Interior, Minerals Management Service, Gulf of Mexico OCS Region, New Orleans, LA.

MacDonald, I.R., G.S. Boland, J.S. Baker, J.M. Brooks, M.C. Kennicutt, II, and R.R. Bidigare. 1989. Gulf of Mexico chemosynthetic communities II: Spatial distribution of seep organisms and hydrocarbons at Bush Hill. Marine Biology. 101: 235-247.

MacDonald, I.R., W.R. Callender, R.A. Burke, Jr., and S.J. McDonald. 1990a. Fine scale distribution of methanotrophic mussels at a Louisiana slope cold seep. Progress in Oceanography. 25: 15-24.

MacDonald, I.R., J.F. Reilly, II, N.L. Guinasso, Jr., J.M. Brooks, R.S. Carney, W.A. Bryant, and T.J. Bright. 1990b. Chemosynthetic mussels at a brine-filled pockmark in the northern Gulf of Mexico. Science. 248: 1096-1099.

MacDonald, I.R., N.L. Guinasso, Jr., J.F. Reilly, J.M. Brooks, W.R. Callender, and S.G. Gabrielle. 1990a&b. Gulf of Mexico hydrocarbon seep communities: VI. Patterns of community structure and habitat. Geo-Marine Letters. 10: 244-252.

MacDonald, I.R., N.L. Guinasso, Jr., S.G. Ackleson, J.F. Amos, R. Duckworth, R. Sassen, and J.M. Brooks. 1993. Natural oil slicks in the Gulf of Mexico visible from space. Journal of Geophysical Research. 98-C9: 16351-16364.

MacDonald, I.R., N.L. Guinasso, Jr., J.M. Brooks, R. Sassen, S. Lee, and K.T. Scott. 1994. Gas hydrates that breach the seafloor and interact with the water column on the continental slope of the Gulf of Mexico. Geology. 22: 699-702.

MacDonald, I.R., J.F. Reilly, Jr. , S.E. Best, R. Venkataramaiah, R. Sassen, J. Amos, and N.L. Guinasso, Jr. 1996. A remote-sensing inventory of active oil seeps and chemosynthetic communities. In: Schumacher, R. and M.A. Abrams. The northern Gulf of Mexico in Hydrocarbon Migration and its Near-Surface Expression. Amer. Assoc. Petrol. Geol. 66: 27-37.

MacDonald, I.R., J.F. Reilly, II.J. Chu, and D. Olivier. 1997. Submarine NR-1 makes first deep-ocean use of the SM2000 laser line scanner. Sea Technology. 38(2): 59-64.

MacDonald, I.R., W.W. Schroeder, and J.M. Brooks. 1995. Chemosynthetic ecosystems studies final report. U.S. Dept. of the Interior, Minerals Management Service, Gulf of Mexico OCS Study, New Orleans, LA

Macgregor, D. 1993. Relationships between seepage, tectonics and subsurface petroleum reserves. Marine and Petroleum Geology 10: 606-619.

McBride, B.C., P. Weimer, and M.G. Rowan. 1998. The effect of allochthonous salt on petroleum systems of northern Green Canyon and Ewing Bank (offshore Louisiana), northern Gulf of Mexico. AAPG Bulletin 82 (5B): 1083-1112.

McGee, D.T., P.W. Bilinshi, P.S. Gray, D.S. Pfeiffer, and J.L. Sheiman. 1993. Geologic models and reservoir geometries of Auger Field, deepwater Gulf of Mexico. AAPG, Bull. 77 (13): 149.

McGookey, D.P. 1975. Gulf Coast Cenozoic sediments and structure: An excellent example of extra-continental sedimentation. Transactions--Gulf Coast Association of Geological Societies. 25: (104-120).

McHatton, S.C. 1998. Ecology and physiology of autotrophic sulfur bacteria from sulfide-rich seeps and marine sediments. Ph.D. dissertation thesis. University of California. Davis.

McHatton, S.C., J.P. Barry, H.W. Jannasch, and D.C. Nelson. 1996. High nitrate concentrations in vacuolate, autotrophic marine Beggiatoa spp. Applied and Environmental Microbiology. 62 (3): 954-958.

Meyers, T.R. 1979. Preliminary studies on chlamydial agent in the digestive diverticular epithelium of hard clams *Mercenaria mercenaria* (L.) from Great South Bay, New York. Journal of Fish Diseases 2: 179-189.

Mitchell, R., I.R. MacDonald, and K.K. Kvenvolden.1999. Estimates of total hydrocarbon seepage into the Gulf of Mexico based on satellite remote sensing images. In: Ocean Sciences Meeting, American Geophysical Union, San Antonio, TX. Pp. OS41I-02.

MMS. 1988. Implementation of measures to detect and protect deepwater chemosynthetic communities. U.S. Dept. of the Interior, Minnerals Management Service, Gulf of Mexico OCS Region, New Orleans, LA. 3 pp.

Morse, J.W. 1994. Interactions of trace metals with authigenic sulfide minerals--Implications for their bioavailability. Marine Chemistry. 46(1-2): 1-6.

Nei, M. 1987. Molecular evolutionary genetics. Columbia University Press, New York.

Nelson, D., and C. Fisher. 1995. Chemoautotrophic and methanotrophic endosymbiotic bacteria at deep-sea vents and seeps. In: The Microbiology of Deep-Sea Hydrothermal Vents. edited by D.M. Karl. Pp. 125-167.

Nelson, D.C., C.O. Wirsen, and H.W. Jannasch. 1989. Characterization of large, autotrophic Beggiatoa spp. abundant at hydrothermal vents of the Guaymas Basin. Applied and Environmental Microbiology. 55(11): 2909-2917.

Nelson, K., and C.R. Fisher. 2000. Absence of cospeciation in deep-sea vestimentiferan tubeworms and their bacterial endosymbionts. Symbiosis. (in press).

Nelson, K., and R.K. Selander. 1994. Analysis of genetic variation by polymerase chain reaction-based nucleotide sequencing. Bacterial Pathogenesis, Pt. A. vol. 235 pp. 174-183.

Neurauter, T.W., and W.R. Bryant. 1990. Seismic expression of sedimentary volcanism on the continental slope, northern Gulf of Mexico. Geo-Marine Letters. 10: 225-231.

Neurauter, T.W., and H.H. Roberts. 1994. Three generations of mud volcanoes on the Louisiana continental slope. Geo-Marine Letters. 14(2/3): 120-125.

Nikolaus, R.L. 1995. Determination of the tropic mode of Beggiatoa spp. found at the hydrocarbon seeps on the continental shelf of the northern Gulf of Mexico. Masters thesis. Texas A&M University, College Station, TX.

Nix, E.R., C.R. Fisher, J. Vodenichar, and K.M. Scott. 1995. Physiological ecology of a mussel with methanotrophic endosymbionts at three hydrocarbon seep sites in the Gulf of Mexico. Marine Biology. 122(4): 605-617.

Nowlin, W.D., Jr., A.E. Jochens, R.O. Reid, and S.F. DiMarco. 1998. Texas-Louisiana shelf circulation and transport processes study--synthesis report. U.S. Dept. of the Interior, Minerals Management Service, Gulf of Mexico OCS Region, New Orleans, LA. OCS Study, MMS 98-0035. 492 pp.

Otte, S., J.G. Kuenen, L.P. Nielsen, H.W. Paerl, J. Zopfi, H.N. Schulz, A. Teske, B. Strotmann, V.A. Gallardo, and B.B. Jorgensen. 1999. Nitrogen, carbon, and sulfur metabolism in natural Thioploca samples. Applied and Environmental Microbiology. 65(7): 3148-3157.

Otto, S.V., J.C. Harshbarger, and S.C. Chang. 1977. Status of selected unicellular eucaryote pathogens, and prevalence and histopathology of inclusions containing obligate procaryote parasites, in commercial bivalve mollusks from Maryland estuaries. Haliotis. 8: 285-295.

Paull, C.K., B. Hecker, R. Commeau, R.P. Freeman-Lynde, C. Neumann, W.P. Corso, S. Golubic, J.E. Hook, E. Sikes, and J. Curray. 1984. Biological communities at the Florida Escarpment resemble hydrothermal vent taxa. Science. 226: 965-967.

Paull, C.K., A.J.T. Jull, L.J. Toolin, and T. Linick. 1985. Stable isotope evidence for chemosynthesis in an abyssal seep community. Nature. 317: 709-711.

Paull, C.K., and A.C. Neumann. 1987. Continental margin brine seeps: their geological consequences. Geology. 15: 545-548.

Peek, A.S., R.A. Feldman, R.A. Lutz, and R.C. Vrijenhoek. 1998. Cospeciation of chemoautotrophic bacteria and deep-sea clams. Proceedings of the National Academy of Sciences of the United States of America. 95 (17): 9962-9966.

Pequegnat, W.E., B.J. Gallaway, and L.H. Pequegnat. 1990. Aspects of the ecology of the deep-water fauna of the Gulf of Mexico. Amer. Zool. 30: 45-64.

Perez Camacho, A., A. Villalba, R. Beiras, and U. Labarta. 1997. Absorption efficiency and condition of cultured mussels (Mytilus edulis galloprovincialis Linnaeus) of Galicia (NW Spain) infected by parasites Marteilia refringens Grizel et al. and Mytilicola intestinalis Steuer. Journal of Shellfish Research. 16: 77-82.

Peterson, B.J., and R.W. Howarth. 1987. Sulfur, carbon, and nitrogen isotopes used to trace organic matter flow in the salt-marsh estuaries of Sapelo Island, Georgia. Limnology and Oceanography. 32 (6): 1195-1213.

Pilson, M.E.Q. 1998. An introduction to the chemistry of the sea. Prentice-Hall, New Jersey. 431 pp.

Pindell, J. 1985. Alleghenian reconstruction and subsequent evolution of the Gulf of Mexico, Bahamas, and proto-Caribbean Sea. Tectonics. 4: 1-39.

Posey, H.H., P.E. Price, and J.R. Kyle. 1987. Mixed carbon sources for calcite caprocks of Gulf Coast salt domes. In: Lerche, L and J.J. O'brein, eds. Dynamical Geology of Salt and Related Structure. Academic Press, London.

Prikryl, J.D. 1990. Origin of limestone caprock at the Damon Mound salt dome. In: Schumacher, D. And B.F. Perkins, eds. Proc. Ninth Ann. Res. Conf. GCS-SEPM Foundation. Pp. 325-336.

Rainer, J.S., and R. Mann. 1992. A comparison of methods for calculating condition index in eastern oysters, *Crassostrea virginica* (Gmelin 1791). Journal of Shellfish. 11: 55-58.

Rau, G.H. 1981. Hydrothermal vent clam and tubeworm 13C/12C. Science. 213: 338-339.

Rau, G.H., and H.H. Hedges. 1979. Carbon-13 depletion in a hydrothermal vent mussel: suggestion of a chemosynthetic food source. Science. 203: 648-649.

Reeburgh, W.S. 1976. Methane consumption in Cariaco Trench waters and sediments. Earth & Planetary Science Letters. 28: 337-344.

Reeburgh, W.S. 1980. Anaerobic methane oxidation: Rate depth distributions in Skan Bay sediments. Earth and Planetary Science Letters. 47: 345-352.

Reilly, J.F., I.R. MacDonald, E.K. Biegert, and J.M. Brooks. 1996. Geologic controls on the distribution of chemosynthetic communities in the Gulf of Mexico. In: Schumacher, D. and M.A. Abrams, eds. Hydrocarbon migration and its near-surface expression. Amer. Assoc. Petrol. Geol., Tulsa, OK. Pp. 38-61.

Rice, W.R. 1989. Analyzing tables of statistical tests. Evolution. 43: 223-225.

Roberts, H.H. 1996. Surface amplitude data: 3D-seismic for interpretation of seafloor geology (Louisiana slope). Transactions of the Gulf Coast Association of Geological Societies. 46: 353-362.

Roberts, H.H., and P. Aharon. 1993. Cold seep carbonates of the northern Gulf of Mexico: A synthesis of submersible investigations. In: American Association of Petroleum Geologists Annual Convention. American Association of Petroleum Geologists, New Orleans, LA. 172 pp.

Roberts, H.H., and P. Aharon. 1994. Hydrocarbon-derived carbonate buildups of the northern Gulf of Mexico slope: A review of submersible investigations. Geo-Marine Letters. 14 (2/3): 135-148.

Roberts, H.H., P. Aharon, R. Carney, J. Larkin, and R. Sassen. 1990. Seafloor responses to hydrocarbon seeps, Louisiana continental slope. Geo-Marine Letters. 10 (4): 232-243.

Roberts, H.H., and R.S. Carney. 1997. Evidence of episodic fluid, gas, and sediment venting on the northern Gulf of Mexico continental slope. Economic Geology. 92: 863-879.

Roberts, H.H., D.J. Cook, and M.K. Sheedlo. 1992. Hydrocarbon seeps of the Louisiana continental slope: Seismic amplitude signature and seafloor response. Gulf Coast Association of Geological Societies. XLII: 349-361.

Roberts, H.H., and E.H. Doyle. 1998. Seafloor calibration of high resolution acoustic data and amplitude rendering of the "diapiric hill," GB427. In: Proceeding, 1998 Offshore Technology Conference, Houston, TX. Pp. 19-30.

Roberts, H.H., E.H. Doyle, J.R. Booth, and B.J. Clark. 1996. 3D-seismic amplitude analysis of the seafloor: An important interpretive method for improved geohazards evaluations. In: Proceedings, 1996 Offshore Technology Conference. Houston, TX. Pp. 283-292.

Roberts, H.H., and T.W. Neurauter. 1990. A direct observations of a large active mud vent on the Louisiana continental slope. American Association of Petroleum Geologists Bulletin. 74: 1508.

Roberts, H.H., R. Sassen, R. Carney, and P. Aharon. 1990b. The role of hydrocarbons in creating sediment and small-scale topography on the Louisiana continental slope. 1990. In: GCSSEPM Foundation Ninth Annual Research Conference. Pp. 311-324.

Roelke, L., and L. Cifuentes. 1997. Use of stable isotopes to assess groups of king mackerel, *Scomberomorus cavalla*, in the Gulf of Mexico and southeastern Florida. Fishery Bulletin. 93(3): 540-551.

Rosman, I., G.S. Boland, and J.S. Baker. 1987. Epifaunal aggregations of Vesicomyidae on the continental slope off Louisiana. Deep-Sea Research. 34: 1811-1820.

Rowan, M.G., M.P.A. Jackson, and B.D. Trudgill. 1999. Salt-related fault families and fault welds in the northern Gulf of Mexico. American Association of Petroleum Geologists Bulletin. 83: 1454-1484.

Rowan, M.G., and P. Weimer. 1998. Salt-sediment interaction, northern Green Canyon and Ewing Bank (offshore Louisiana), northern Gulf of Mexico. Association of American Petroleum Geologists Bulletin. 82 (5B): 1055-1082.

Rubinsztein, D.C., B. Amos, and G. Cooper. 1999. Microsatellite and trinucleotide-repeat evolution: Evidence for mutational bias and different rates of evolution in different lineages. Philosophical Transactions of the Royal Society of London, Series B--Biological Sciences. 354 (1386): 1095-1099.

Rubinsztein, D.C., W. Amos, J. Leggo, S. Goodburn, S. Jain, S.H. Li, R.L. Margolis, C.A. Ross, and M.A. Fergusonsmith. 1995. Microsatellite evolution--evidence for directionality and variation in rate between species. Nature Genetics. 10 (3): 337-343.

Rzhetsky, A., S. Kumar, and M. Nei. 1995. Four-cluster analysis: A simple method to test phylogenetic hypothesis. Molecular Biology and Evolution (12): 163-167.

Sager, W.W., C.S. Lee, I.R. MacDonald, and W.W. Schroeder. 1999. High-frequency near-bottom acoustic reflection signatures of hydrocarbon seeps on the northern Gulf of Mexico continental slope. Geo-Marine Letters. 18: 267-276.

Sager, W.W., and I.R. MacDonald. 1998. Shallow and deep acoustic mapping of hydrocarbon seep sites, northern Gulf of Mexico. In: American Geophysical Union Fall Meeting, American Geophysical Union, San Francisco, CA.

Sager, W.W., I.R. MacDonald, W.R. Bryant, R.L. Carlson, and D.B. Prior. 1998. TAMU2 digital side-scan sonar survey of Louisiana slope areas containing active oil seeps and halokinetic sediment modification. In: Proceedings, 1998 Offshore Technology Conference, Houston, TX. Pp. 57-69.

Saiki, R.K., D.H. Gelfand, S. Stoffel, S.J. Scharf, R. Higuchi, G.T. Horn, K.B. Mullis, and H.A. Erlich. 1988. Primer-directed enzymatic amplification of DNA with a thermostable DNA-polymerase. Science. 239(4839): 487-491.

Saitou, N., and M. Nei. 1987. The neighbor-joining method: A new method for reconstructing phylogenetic trees. Molecular Biology and Evolution. 4(4): 406-425.

Samadi, S., J. Mavarez, J.P. Pointier, B. Delay, and P. Jarne. 1999. Microsatellite and morphological analysis of population structure in the parthenogenetic freshwater snail Melanoides tuberculata: insights into the creation of clonal variability. Molecular Ecology. 8(7): 1141-1153.

Sambrook, J., E.F. Fritsch, and T. Maniatis. 1989. Molecular cloning: A laboratory manual. Cold Springs Laboratory Press, Cold Springs Harbor, NY.

SAS Institute. 1989. SAS/STAT user's guide, version 6. SAS Institute, Cary, NC.

Sassen, R. 1980. Biodegradation of crude oil and mineral deposition in a shallow Gulf Coast salt dome. Organic Geochemistry. 2: 153-166.

Sassen, R. 1987. Organic geochemistry of salt dome rocks, Gulf Coast salt basin. In: Lerche, I. and J.J. O'Brien, eds. Dynamic Geology of Salt and Related Structures. Pp. 631-649.

Sassen, R., and I.R. MacDonald. 1994. Evidence of structure H hydrate, Gulf of Mexico continental slope. Organic Geochemistry. 22(6): 1029-1032.

Sassen, R., J. Brooks, I.R. MacDonald, M.C. Kennicutt, II, and N.L. Guinasso, Jr. 1993. Association of oil seeps and chemosynthetic communities with oil discoveries, upper continental slope, Gulf of Mexico. Bulletin of American Association of Petroleum Geologists. 77: 1599.

Sassen, R., G.A. Cole, R. Drozd, and H.H. Roberts. 1994. Oligocene to Holocene hydrocarbon migration and salt-done carbonates, northern Gulf of Mexico. Mar. Petrol. Geol. 11: 55-65.

Sassen, R., I.R. MacDonald, N.L. Guinasso, Jr., S. Joye, A.G. Requejo, S.T. Sweet, J. Alcala-Herrera, D.A. DeFreitas, and D.R. Schink. 1998. Bacterial methane oxidation in seafloor gas hydrate: Significance to life in extreme environments. Geology. 26(9): 851-854.

Sassen, R., S. Joye, S.T. Sweet, D.A. DeFreitas, A.V. Milkov, and I.R. MacDonald. 1999. Thermogenic gas hydrates and hydrocarbon gases in complex chemosynthetic communities, Gulf of Mexico continental slope. Organic Geochemistry. 30(7): 485-497.

Sassen, R., I.R. MacDonald, A.G. Requejo, N.L. Guinasso, Jr., M.C. Kennicutt, S.T. Sweet, and J.M. Brooks. 1994. Organic geochemistry of sediments from chemosynthetic communities, Gulf of Mexico slope. Geo-Marine Letters. 14(2-3): 110-119.

Sassen, R., C. McCabe, J. Kyle, and E. Chinn. 1989. Deposition of magnetic pyrrhotite during alteration of crude oil and reduction of sulfate. Organic Geochemistry. 14: 381-392.

Sassen, R., H.H. Roberts, P. Aharon, J. Larkin, and R. Carney. 1993. Chemosynthetic bacterial mats at cold hydrocarbon seeps, Gulf of Mexico continental slope. Organic Geochemistry. 20: 77-89.

Sassen, R., S.T. Sweet, A.V. Milkov, D.A. DeFreitas, G.G. Salata, and E.C. McDade. 1999. Geology and geochemistry of gas hydrates, central Gulf of Mexico continental slope. Trans. Gulf Coast Assoc. Geol. Soc. 49: 462-468.

Saunders, G.L., E.N. Powell, and D.H. Lewis. 1993. A determination of in vivo growth rates for Perkinsus marinus, a parasite of the eastern oyster *Crassostrea virginica* (Gmelin 1791). Journal of Shellfish Research. 12: 229-240.

Schulz, H.N., T. Brinkhoff, T.G. Ferdelman, M.H. Marine, A. Teske, and B.B. Jorgensen. 1999. Dense populations of a giant sulfur bacterium in Namibian shelf sediments. Science. 284 (5413): 493-495.

Seni, S.J., and M.P.A. Jackson. 1983. Evolution of salt structures, East Texas diapir province. American Association Petroleum Geologists Bulletin. 67: 1219-1274.

Sericano, J.L., T.L. Wade, E.N. Powell, and J.M. Brooks. 1993. Concurrent chemical and histological analyses: Are they compatible? Chemistry and Ecology. 8: 41-47.

Shew, R.D., P.S. Gary, D.S. Pfeiffer, and P.W. Blinski. 1993. Evidence and importance of a pliocene, carbonate-rich deposit formed in association with a hydrocarbon seep at Auger Field. American Association of Petroleum Geologists Bulletin. 77 (13): 181.

Shipley, T.H., M.H. Houston, R.T. Buffler, F.T. Shaub, K.J. McMillen, J.W. Ladd, and J.L. Worzel. 1979. Seismic evidence for widespread possible gas hydrate horizons on continental slopes and rises. American Association of Petroleum Geologists Bulletin. 63 (12): 2204-2213.

Shokes, R.F., P.K. Trabant, B.J. Presley, and D.F. Reid. 1977. Anoxic, hypersaline basin in the northern Gulf of Mexico. Science. 196: 1443-1446.

Simpkins, M.A. 1994. Ecology of hydrocarbon seep vestimentiferans: Growth and condition in a variable environment. Masters thesis. Pennsylvania State University, State College, PA.

Slatkin, M. 1985. Gene flow in natural populations. Annual Review of Ecology and Systematics. 16: 393-430.

Sloan, E.D. 1990. Clathrate hydrates of natural gases. Marcel Drekker, Inc. New York. 641 pp.

Smith, E.B., K.M. Scott, E.R. Nix, C. Korte, and C.R. Fisher. 2000. Growth and condition of seep mussels (*Bathymodiolus childressi*) at a Gulf of Mexico brine pool. Ecology. 81: 2392-2403.

Smith, E.B., F.M. Williams, and C.R. Fisher. 1997. Effects of intrapopulation variability on von Bertalanffy growth parameter estimates from equal mark recapture intervals. Canadian Journal of Fisheries and Aquatic Sciences. 54(9): 2025-2032.

Soniat, T.M., and E.V. Kortright. 1998. Estimating time to critical levels of *Perkinsus marinus* in eastern oysters, *Crassostrea virginica*. Journal of Shellfish Research. 17: 1071-1080.

Sonnier, C., and G. Gerlach. 1999. Deepwater hazard detection with high-resolution 3D seismic. Offshore.

Sousa, W.P. 1990. Spatial scale and the processes structuring a guild of larval trematode parasites. In: Esch, G.W., A.O. Bush, and J.M. Aho, eds. Parasite Communities: Patterns and Processes. Chapman and Hall, London. Pp. 41-67.

Sparks, A.K., J.F. Morado, and J.W. Hawkes. 1985. A systemic microbial disease in the Dungeness crab, Cancer-Magister, caused by a chlamydia-like organism. Journal of Invertebrate Pathology. 45(2): 204-217.

Stahl, W.J. 1980. Compositional changes and 13C/12C fractionation during degradation of hydrocarbons by bacateria. Geochem. Cosmochim. Act. 44: 1903-1907.

Suess, E., B. Carlson, S. Ritger, J.C. Moore, M.L. Jones, L.D. Kulm, and G.R. Cochran. 1985. Biological communities at vent sites along the subduction zone off Oregon. Biol. Soc. Wash. Bull. (6): 475-484.

Teske, A., L.P. Sogin, and H.W. Jannasch. 1999. Phylogenetic relationships of large marine Beggiatoa. Systematic and Applied Microbiology. 22: 39-44.

Tunnicliffe, V., A.G. McArthur, and D. McHugh. 1998. A biogeographical perspective of the deep-sea hydrothermal vent fauna. Advances in Marine Biology. 34: 355-442.

Tusting, R.F., R.C. Tietze, K.R. Reisenbichler, D.S. Lee, I.R. MacDonald, and C.R. Fisher. 1996. Development of special purpose benthic, geochemical and biological samplers at Harbor Branch Oceanographic Institution. In: Oceans '96, Ft. Lauderdale, FL. Pp. 1019-1025.

Van den Bold, M.C., T.F. Moslow, and J.M. Coleman. 1987. Origin and timing of seafloor erosion on the Louisiana continental slope. Transactions--Gulf Coast Association of Geological Societies. 37: 487-498.

Vandover, C.L., and B. Fry. 1989. Stable isotopic compositions of hydrothermal vent organisms. Marine Biology. 102 (2): 257-263.

Vandover, C.L., and B. Fry. 1994. Microorganisms as food resources at deep-sea hydrothermal vents. Limnology and Oceanography. 39 (1): 51-57.

Vogt, P.R., G. Cherakashev, G. Ginsburg, G. Ivanov, A. Milkov, K. Crane, A. Lein, E. Sundvor, N. Pimenov, and A. Egorov. 1997. Haakon Mosby mud volcano provides unusual example of venting. EOS Transactions of the American Geophysical Union. 78: 549-557.

Wade, T.L., E.L. Atlas, J.M. Brooks, M.C. Kennicutt, R.G. Fox, J. Sericano, B. Garciaromero, and D. DeFreitas. 1988. NOAA Gulf of Mexico Status and Trends Program: Trace organic contaminant distribution in sediments and oysters. Estuaries. 11 (3): 171-179.

Wade, T.L., J.M. Brooks, M.C. Kennicutt, II, T.J. McDonald, J.L. Sericano, and T.J. Jackson. 1993. GERG trace organics contaminant analytical techniques. In: Sampling and analytical methods of the National Status and Trends Program National Benthic Surveillance and Mussel Watch Projects 1984-1992, Vol. IV. NOS ORCA 71. National Oceanic and Atmospheric Administration.

Wardle, W.J. 1990. Larval bucephalids (Trematoda, Digenea) parasitizing bivalve mollusks in the Galveston Bay area, Texas. Journal of the Helminthological Society of Washington. 57 (1): 5-11.

Webb, M. 1969. *Lamellibrachia barhami, gen. nov., sp. nov.* Bulletin of Marine Science (19): 18-47.

Weisburg, W.G., S.M. Barns, D.A. Pelletier, and D.J. Lane. 1991. 16s ribosomal DNA amplification for phylogenetic study. Journal of Bacteriology. 173 (2): 697-703.

Wilson, E.A., E.N. Powell, M.A. Craig, T.L. Wade, and J.M. Brooks. 1990. The distribution of Perkinsus-Marinus in Gulf Coast oysters--its relationship with temperature, reproduction, and pollutant body burden. Internationale Revue Der Gesamten Hydrobiologie. 75 (4): 533-550.

Wilson, E.A., E.N. Powell, T.L. Wade, R.J. Taylor, B.J. Presley, and J.M. Brooks. 1992. Spatial and temporal distributions of contaminant body burden and disease in Gulf of Mexico oyster populations--the role of local and large scale climatic controls. Helgolander Meeresuntersuchungen. 46 (2): 201-235.

Wilson-Ormond, E.A., M.S. Ellis, E.N. Powell, Y. Kim, and S. Li. In press. Effects of gas-producing platforms on continental shelf macroepifauna in the northwestern Guld of Mexico: Reproductive status and health. Internationale Revue der Gesamten Hydrobiologie.

Winters, J.C., and J.A. Williams. 1969. Microbiologic alteration of petroleum in the reservoir. In: ACS Div. Petrol. Chem. New York, NY. Pp. E22-E31.

Worrall, D.M., and S. Snelson. 1989. Evolution of the northern Gulf of Mexico, with emphasis on Cenozoic growth faulting and the role of salt. In: Bally, A.W. and A.R. Palmer, eds. The Geology of North America--An Overview. Geological Society of America, Boulder, CO. A: 97-138.

Wright, S. 1931. Evolution in mendelian populations. Genetics. 28: 97-159.

Wright, S. 1943. Isolation by distance. Genetics. 28: 114-138.

Young, C.M., E. Vazquez, A. Metaxas, and P.A. Tyler. 1996. Embryology of vestimentiferan tube worms from deep-sea methane/sulphide seeps. Nature. 381(6582): 514-516.

**The Department of the Interior Mission**

As the Nation's principal conservation agency, the Department of the Interior has responsibility for most of our nationally owned public lands and natural resources. This includes fostering sound use of our land and water resources; protecting our fish, wildlife, and biological diversity; preserving the environmental and cultural values of our national parks and historical places; and providing for the enjoyment of life through outdoor recreation. The Department assesses our energy and mineral resources and works to ensure that their development is in the best interests of all our people by encouraging stewardship and citizen participation in their care. The Department also has a major responsibility for American Indian reservation communities and for people who live in island territories under U.S. administration.

**The Minerals Management Service Mission**

As a bureau of the Department of the Interior, the Minerals Management Service's (MMS) primary responsibilities are to manage the mineral resources located on the Nation's Outer Continental Shelf (OCS), collect revenue from the Federal OCS and onshore Federal and Indian lands, and distribute those revenues.

Moreover, in working to meet its responsibilities, the **Offshore Minerals Management Program** administers the OCS competitive leasing program and oversees the safe and environmentally sound exploration and production of our Nation's offshore natural gas, oil and other mineral resources. The MMS **Minerals Revenue Management** meets its responsibilities by ensuring the efficient, timely and accurate collection and disbursement of revenue from mineral leasing and production due to Indian tribes and allottees, States and the U.S. Treasury.

The MMS strives to fulfill its responsibilities through the general guiding principles of: (1) being responsive to the public's concerns and interests by maintaining a dialogue with all potentially affected parties and (2) carrying out its programs with an emphasis on working to enhance the quality of life for all Americans by lending MMS assistance and expertise to economic development and environmental protection.